PHENOMENA BEYOND THE STANDARD MODEL: WHAT DO WE EXPECT FOR NEW PHYSICS TO LOOK LIKE?

EDITED BY: Roman Pasechnik, António Pestana Morais and Stefano Moretti
PUBLISHED IN: Frontiers in Physics

frontiers Research Topics

frontiers

ISSN 1664-8714
ISBN 978-2-88963-990-8
DOI 10.3389/978-2-88963-990-8

About Frontiers

Frontiers is more than just an open-access publisher of scholarly articles: it is a pioneering approach to the world of academia, radically improving the way scholarly research is managed. The grand vision of Frontiers is a world where all people have an equal opportunity to seek, share and generate knowledge. Frontiers provides immediate and permanent online open access to all its publications, but this alone is not enough to realize our grand goals.

Frontiers Journal Series

The Frontiers Journal Series is a multi-tier and interdisciplinary set of open-access, online journals, promising a paradigm shift from the current review, selection and dissemination processes in academic publishing. All Frontiers journals are driven by researchers for researchers; therefore, they constitute a service to the scholarly community. At the same time, the Frontiers Journal Series operates on a revolutionary invention, the tiered publishing system, initially addressing specific communities of scholars, and gradually climbing up to broader public understanding, thus serving the interests of the lay society, too.

Dedication to Quality

Each Frontiers article is a landmark of the highest quality, thanks to genuinely collaborative interactions between authors and review editors, who include some of the world's best academicians. Research must be certified by peers before entering a stream of knowledge that may eventually reach the public - and shape society; therefore, Frontiers only applies the most rigorous and unbiased reviews.
Frontiers revolutionizes research publishing by freely delivering the most outstanding research, evaluated with no bias from both the academic and social point of view. By applying the most advanced information technologies, Frontiers is catapulting scholarly publishing into a new generation.

What are Frontiers Research Topics?

Frontiers Research Topics are very popular trademarks of the Frontiers Journals Series: they are collections of at least ten articles, all centered on a particular subject. With their unique mix of varied contributions from Original Research to Review Articles, Frontiers Research Topics unify the most influential researchers, the latest key findings and historical advances in a hot research area! Find out more on how to host your own Frontiers Research Topic or contribute to one as an author by contacting the Frontiers Editorial Office: researchtopics@frontiersin.org

PHENOMENA BEYOND THE STANDARD MODEL: WHAT DO WE EXPECT FOR NEW PHYSICS TO LOOK LIKE?

Topic Editors:
Roman Pasechnik, Lund University, Sweden
António Pestana Morais, University of Aveiro, Portugal
Stefano Moretti, University of Southampton, United Kingdom

Citation: Pasechnik, R., Morais, A. P., Moretti, S., eds. (2020). Phenomena Beyond the Standard Model: What Do We Expect for New Physics to Look Like?. Lausanne: Frontiers Media SA. doi: 10.3389/978-2-88963-990-8

Table of Contents

frontiers in Physics

EDITORIAL
published: 21 July 2020
doi: 10.3389/fphy.2020.00209

Editorial: Phenomena Beyond the Standard Model: What Do We Expect for New Physics to Look Like?

António P. Morais[1], *Stefano Moretti*[2*] *and Roman Pasechnik*[3]

[1] *Departamento de Física, Universidade de Aveiro and CIDMA - Center for Research and Development in Mathematics and Applications, Aveiro, Portugal,* [2] *School of Physics and Astronomy, University of Southampton, Southampton, United Kingdom,* [3] *Department of Astronomy and Theoretical Physics, Lund University, Lund, Sweden*

Keywords: Higgs physics, grand unified theories, dark matter, baryogenesis, cosmic inflation

Editorial on the Research Topic

Phenomena Beyond the Standard Model: What Do We Expect for New Physics to Look Like?

Particle physics (PP) is a vast and active research field of contemporary theoretical and experimental physics. Measurements made at microscopic distances have started to confront the most fundamental principles of nature encoded in the structure of the Standard Model (SM) of PP. With recent observations of accelerated expansion of the universe, massive dark halos filled with invisible matter, and persistent flavour physics anomalies, the SM is entering a period of most severe phenomenological tests that could eventually lead to a revision of our current understanding of the fundamental properties of matter, interactions, and even spacetime.

While Large Hadron Collider (LHC) experiments have accessed fundamental interactions at the energy and intensity frontiers without notable discoveries so far, the demand for precision measurements is increasing. Already we are familiar with persistent inconsistencies within the SM framework, such as the absence of a viable dark matter (DM) candidate, the failure to describe the origin of dark energy, the inability to account for sufficient CP violation required for generation of the baryon asymmetry, the yet-to-be resolved hierarchy problem in the Higgs sector, and the lack of a dynamical mechanism for the natural generation of very specific observed patterns in fermion mass and mixing parameters. For instance, there is a substantial lack of first-principles understanding of the Higgs sector properties and origin of the electroweak scale, of the three quark/lepton families, of the unique neutrino features, and of the strong unexplained hierarchies in the lepton and quark sectors of the SM. The non-observation of New Physics (NP) in collider measurements remains puzzling and raises questions as to their discovery potential, methodology, precision, and sensitivity to weak signals. Conversely, with a wealth of new phenomenological information emerging from neutrino oscillation studies, astroparticle physics measurements, low-energy analyses, and, more recently, gravitational waves, can we expect the SM to remain the baseline framework of PP, or should it be replaced eventually by a more accurate and complete theory of the building blocks and symmetries of nature? What kind of NP can we expect to show up and in what particular way?

This Research Topic "Phenomena Beyond the Standard Model: What Do We Expect for New Physics to Look Like?" is devoted to highlighting selected topics in state-of-the-art theoretical

Edited and reviewed by:
J. W. F. Valle,
Consejo Superior de Investigaciones Científicas (CSIC), Spain

***Correspondence:**
Stefano Moretti
s.moretti@soton.ac.uk

Specialty section:
This article was submitted to High-Energy and Astroparticle Physics, a section of the journal Frontiers in Physics

Received: *10 May 2020*
Accepted: *18 May 2020*
Published: *21 July 2020*

Citation:
Morais AP, Moretti S and Pasechnik R (2020) Editorial: Phenomena Beyond the Standard Model: What Do We Expect for New Physics to Look Like? Front. Phys. 8:209. doi: 10.3389/fphy.2020.00209

research at the forefront of PP that explores these most fundamental questions of nature, in the quest for some Beyond the Standard Model (BSM) phenomena. A total of ten papers were submitted, covering exciting developments in the direction of uncovering some NP from both the theoretical and the experimental sides. On the one hand, two paradigms for solving the hierarchy problem of the SM, Supersymmetry and Compositeness, are considered. On the other hand, experiments from low to high energy scales are discussed, in settings ranging from colliders to ground as well as space apparatus. Delle Rose et al. address the case of potential NP signals at energies as low as 17 MeV, while Croon et al. discuss the properties of a prototypical Grand Unified Theory (GUT) at 10^{16} GeV. As two major flaws of the SM are that, therein, neutrinos are massless and there is no viable candidate for DM, it is no surprise that Shindou considers the first case while a number of other authors (Bhattacharya et al.; Belyaev; Corianò et al.; Khlopov) address the second one, including discussing the key phenomenological consequences of the corresponding BSM constructs in the aforementioned experimental settings. Finally, given the importance of the Higgs boson discovery at CERN in 2012 for the whole of PP, it is natural to also see several submissions addressing the possibility of a BSM origin of this crucial particle, within extended Higgs sectors whose motivation (as explained by Miller et al.) builds upon the Multiple Point Principle (MPP), indicating their plausibility, including both the cases of Supersymmetry (Arhrib et al.) and Compositeness (Cacciapaglia et al.). Altogether, this special issue of *Frontiers* serves to inform the reader that even though NP is currently unknown to us, we are well-equipped on both the theoretical and the experimental fronts to extract its possible manifestations, whatever these might look like.

AUTHOR CONTRIBUTIONS

All authors listed have made a substantial, direct and intellectual contribution to the work, and approved it for publication.

FUNDING

AM was supported by the COST Action CA16201, by the Center for Research and Development in Mathematics and Applications (CIDMA) through the Portuguese Foundation for Science and Technology (FCT -Fundação para a Ciência e a Tecnologia), references UIDB/04106/2020 and UIDP/04106/2020 and by national funds (OE), through FCT, I.P., in the scope of the framework contract foreseen in the numbers 4, 5, and 6 of the article 23, of the Decree-Law 57/2016, of August 29, changed by Law 57/2017, of July 19. AM is also supported by the projects PTDC/FIS-PAR/31000/2017 and CERN/FIS-PAR/0027/2019. SM was financed through the NExT Institute and the STFC Consolidated Grant No. ST/L000296/1. RP was partially supported by the Swedish Research Council, grant numbers 621-2013-4287 and 2016-05996, as well as the ERC grant agreement No. 668679.

Conflict of Interest: The authors declare that the research was conducted in the absence of any commercial or financial relationships that could be construed as a potential conflict of interest.

frontiers in Physics

MINI REVIEW
published: 14 January 2019
doi: 10.3389/fphy.2018.00159

A UV Picture of a Loop Induced Neutrino Mass Model and Its Phenomenological Consequences

*Tetsuo Shindou**

Division of Liberal-Arts, Kogakuin University, Tokyo, Japan

In this article, we review several models where tiny neutrino masses are radiatively generated via loop diagrams. In such models, additional scalar fields are often introduced so that the Standard Model Higgs sector is extended.Such an extension results in a rich phenomenology of the model. We briefly discuss such a model and its UV completion to highlight some of its phenomenological consequences.

Keywords: neutrino mass, extended Higgs sector, UV theory, SUSY model, collider phenomenology

OPEN ACCESS

Edited by:
Stefano Moretti,
University of Southampton,
United Kingdom

Reviewed by:
Chandan Hati,
UMR6533 Laboratoire de Physique de Clermont (LPC), France
Frank Franz Deppisch,
University College London,
United Kingdom

***Correspondence:**
Tetsuo Shindou
shindou@cc.kogakuin.ac.jp

Specialty section:
This article was submitted to High-Energy and Astroparticle Physics, a section of the journal Frontiers in Physics

Received: *10 October 2018*
Accepted: *20 December 2018*
Published: *14 January 2019*

Citation:
Shindou T (2019) A UV Picture of a Loop Induced Neutrino Mass Model and Its Phenomenological Consequences. Front. Phys. 6:159. doi: 10.3389/fphy.2018.00159

1. INTRODUCTION

Precise measurement of the Higgs boson property at the LHC experiments [1–6] suggests that the Standard Model (SM) provides quite a good explanation of the physics of elementary particles. However, there still are several unsolved problems in the SM. For example, there is no dark matter (DM) candidate, no successful baryogenesis scenario works, gauge hierarchy problems should be solved by some additional mechanism, and so on. An origin of tiny neutrino mass has been one of such problems for more than two decades. The neutrino oscillation data [7–12] requires that there are tiny mass squared differences among three neutrino mass eigenvalues, and the absolute value of the neutrino masses have quite a severe upper bound of $m_\nu \lesssim \mathcal{O}(0.1)$ eV [13, 14].

In many models, the tiny neutrino masses are originated from the dimension five operator $(H \cdot \bar{\ell}^c)(H \cdot \ell)$ [15] after the electroweak symmetry breaking. The question is how to provide the suppressed coefficient of the operator. There are essentially three possibilities to get such a suppression factor naturally. One idea is using a suppression by a mass scale. Since the operator is dimension five, the coefficient is suppressed by some mass scale. If such a mass scale is significantly larger than the electroweak scale, the coefficient of the dimension five operator gets a strong suppression. The necessary mass scale M in this case is naively estimated by the relation $\langle H \rangle^2 / M \sim m_\nu$, so that $m_\nu \sim 0.1$ eV suggests $M \sim 10^{15}$ GeV. The most famous mechanism of this possibility is so-called type I seesaw model [16–20], where heavy right handed neutrinos (RHNs) are introduced to the SM and the dimension five operator is suppressed by this heavy mass scale after decoupling of the RHNs. The second mechanism is that the smallness of the coefficient is naturally explained as a result of slightly broken symmetry. This idea is realized e.g., in inverse seesaw mechanism [21, 22]. The third possibility is that the operator is generated through quantum loop effect [23–34]. In this case, the suppression comes from the loop factor. For example, in a one-loop model, the coefficient gets a suppression factor of $1/(4\pi)^2$ in addition to a suppression by a particle mass in the loop. In **Figure 1**, examples of relevant diagrams for neutrino masses are shown in several models. A recent comprehensive review on the third possibility can be found, for example, in Cai et al. [35].

Comparing to the first cases (e.g., type-I seesaw mechanism), one can find that the mass scale of new particles should be much lower in the second cases. In a case that the

neutrino mass is induced via n-loop diagram, the neutrino mass can be roughly estimated as

$$m_\nu \sim \left(\frac{\lambda^2}{(4\pi)^2}\right)^n \frac{\langle H\rangle^2}{M}\ , \tag{1}$$

where λ is some coupling constant, and M is a mass scale of new particle running in the loop. For example, in a 3-loop model with $\lambda \sim 0.1$, a new particle with a mass $M \sim \mathcal{O}(100\ \text{GeV})$ is necessary. Such a new particle can be discovered by future collider experiments such as LHC.

In models where colored new particles run in the loop diagrams for the neutrino masses, these particles can also contribute to several processes in B physics [36–40]. By these new contributions, one can give an explanation of B anomalies reported by the BaBar experiment and the LHCb experiment [41–47]. From this viewpoint, models with loop induced neutrino masses have been attracting a lot of attention.

However, in many cases, such models are constructed as a phenomenological model. We strongly expect that there is a UV complete theory above a cutoff scale as a more fundamental picture of such a phenomenological model. There are a few attempts to construct such a UV picture. For example, in Doršner et al. [48], a grand unified model which leads to loop induced neutrino masses at a low energy scale is proposed. In this article, we introduce another possibility based on SUSY gauge theory with confinement [49–52]. In the low energy effective theory of this theory, the Higgs sector is extended to include necessary fields to draw loop diagrams which leads to the dimension five operator. In the model, DM candidates are included, and the electroweak phase transition is enhanced strongly enough for successful electroweak baryogenesis [53–61].

This review is organized as follows. In section 2, we introduce typical concrete examples of models with loop induced neutrino masses. In section 3, we discuss an example UV picture of such a phenomenological model. We there also discuss phenomenological consequences of the UV theory. A summary is presented in section 4.

2. RADIATIVE NEUTRINO MASS MODELS

In this section, we review typical examples of models with loop induced neutrino mass. The models are classified into two groups. In a class of models with RHNs, there should be an additional symmetry, which is a discrete symmetry in many cases, and the RHNs have a charge under that symmetry. For example, in a model with Z_2 parity, odd parity is assigned to the RHNs, since the tree level Yukawa coupling of RHNs with the lepton doublets should be forbidden. In another class of models, no RHNs are introduced.

In this review, we focus on models with RHNs [28–34], because such models has a big advantage, which is that there is a DM candidate. In order to generate the dimension five operator, the lepton number should be broken in the loop. In a model with RHNs, the Majorana mass of each RHN breaks the lepton number. As already described, a new symmetry is necessary to forbid the tree level Yukawa couplings of RHNs. To realize this with keeping the Majorana mass term of RHNs, the simplest symmetry is a Z_2 parity and the odd parity is assigned to the RHNs. In this setup, the lightest neutral Z_2-odd particle in the model can be a DM candidate, unless the Z_2 is broken.

A very well-known example of such models with one-loop induced neutrino mass is the Ma model [29], where the Z_2 odd inert doublet scalar η and three Z_2 odd RHNs N_i are introduced to the SM. The dimension five operator is generated via the one-loop diagram shown in **Figure 1A**. In this model, the lighter one among N_i and the neutral component of η can be a DM candidate.

Two-loop models with RHNs are also discussed e.g., in Aoki et al. [62], Kajiyama et al. [63]. In the model proposed in Aoki et al. [62] , the vertex corresponding to the $\eta\eta HH$ coupling in the Ma model is induced by one-loop. On the other hand, In the model proposed in Kajiyama et al. [63], the Majorana mass terms of N_i in the Ma-model are induced by one-loop.

There are examples of three loop models. Let us here introduce two examples. One is called Kraus-Nasri-Trodden model (KNT model) [28], and the other is called Aoki-Kanemura-Seto model (AKS model) [32–34]. In the KNT model, in addition to three Z_2 odd RHNs, a Z_2 even singly (electric) charged singlet scalar ω_1^- and a Z_2 odd singly charged singlet scalar ω_2^- are introduced. The three loop diagram for the dimension five operator is shown in **Figure 1B**.

In the AKS model, the discrete symmetry $Z_2 \times Z_2'$ is imposed. The Z_2 parity is assumed to be unbroken, while the Z_2' symmetry is softly broken in the Lagrangian. For the particle content, an extra scalar doublet H', three RHNs N_i, a neutral singlet scalar ζ, and a charged singlet scalar Ω^- are introduced to the SM. Under the $Z_2 \times Z_2'$, the SM particles and the new particles are charged as $q(+,+)$, $u_R(+,-)$, $d_R(+,-)$, $\ell(+,+)$, $e_R(+,+)$, $H(+,+)$, $H'(+,-)$, $\Omega^-(-,+)$, $\zeta(-,-)$, and $N_i(-,+)$. With this parity assignment, the Higgs sector of the model is nothing but the Type-X two Higgs doublet model [64]. The neutrino masses are generated by the three loop diagram shown in **Figure 1C**. In this model, the unbroken Z_2 symmetry guarantees the stability of the DM, so that the lightest neutral particle among N_i and ζ can be a DM candidate. In addition, it is nice that the electroweak phase transition is enhanced by loop contributions of Z_2-odd particles in this model. As mentioned later, such enhancement of electroweak phase transition is required for successful electroweak baryogenesis. Therefore, the AKS models has a potential to solve three big problems in the SM, neutrino mass, DM, and baryogenesis.

SUSY extension of these models are also discussed in literature. For example, the SUSY version of the Ma model is studied in e.g., [30, 31]. The SUSY version of the AKS model is provided as a low energy effective theory of a SUSY $SU(2)_H$ gauge theory with confinement, which is briefly introduced in section 3.

3. A UV PICTURE

The models discussed in the previous section are interesting as phenomenological models, since several new particles are introduced at around the TeV scale so that many new phenomena are predicted and will be tested in future experiments. However, they seem to be artificial from a view point of a fundamental theory. Here we would like to consider a example UV picture of

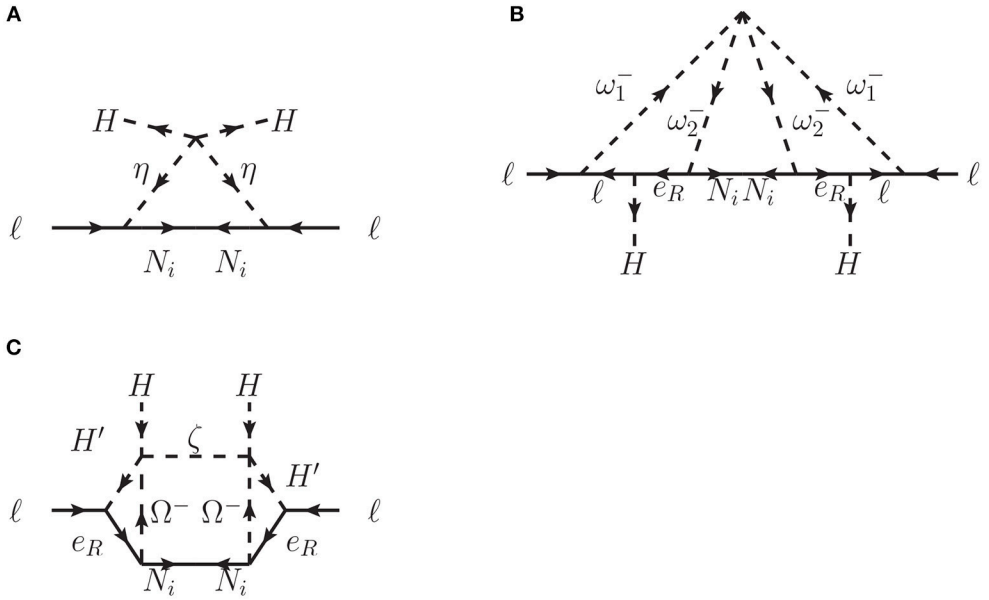

FIGURE 1 | Relevant diagrams for neutrino mass in **(A)** the Ma model [29], **(B)** the KNT model [28], and **(C)** the AKS model [32–34].

such a phenomenological model. In Kanemura et al. [49–52], an concrete example of UV theory of a loop induced neutrino mass model is proposed. The theory is based on a SUSY gauge theory with confinement.

In SUSY SU(N_c) gauge theory with $N_c + 1$ flavor fields, it is known that confinement occurs at some scale [65]. We use this setup and we consider a model with SU(2)$_H$ symmetry with three flavor fields. These three flavor fields are fundamental representations of SU(2)$_H$. Note that each of three fields has their anti-matter partner so that there are six flavor fields in total. We describe these fields as $T_i (i = 1, \cdots, 6)$. After confinement, we have fifteen mesonic fields $H_{ij} \sim T_i T_j$. The setup of this model is almost the same as in the minimal SUSY fat Higgs model [66]. In this model, additional fields are introduced in order to make only two doublets and one singlet mesonic fields light. In the model considered here, in contrast, all the mesonic fields appears in the low energy effective theory.

We here additionally introduce a RHN which is singlet under both SU(2)$_H$ and the SM gauge symmetries. We assume that the model has an unbroken discrete symmetry Z_2 which forbids tree level contributions to neutrino masses. The RHN is considered as an Z_2 odd field. **Table 1I** shows the charge assignments of T_i and the RHN N_R^c under the SM gauge symmetry, SU(2)$_H$, and the Z_2 parity, and **Table 1II** shows the fifteen mesonic fields below the confinement scale Λ_H which are canonically normalized as $H_{ij} \simeq \frac{1}{4\pi\Lambda_H} T_i T_j (i \neq j)$.

The superpotential of the Higgs sector below Λ_H is given by

$$\begin{aligned} W_{\rm eff} &= \lambda N \left(H_u H_d + \upsilon_0^2\right) + \lambda N_\Phi \left(\Phi_u \Phi_d + \upsilon_\Phi^2\right) \\ &+ \lambda N_\Omega \left(\Omega_+ \Omega_- - \zeta\eta + \upsilon_\Omega^2\right) + \lambda \left\{\zeta H_d \Phi_u + \eta H_u \Phi_d \right. \\ &- \left. \Omega_+ H_d \Phi_d - \Omega_- H_u \Phi_u - N N_\Phi N_\Omega\right\} . \end{aligned} \tag{2}$$

TABLE 1 | (I) The charge assignment of the SU(2)$_H$ doublets T_i and the RHN N_R^c under the electroweak gauge group (SU(2)$_L$ × U(1)$_Y$) and the Z_2 parity. **(II)** The field content of the extended Higgs sector in the low energy effective theory below the scale Λ_H.

Superfield	SU(2)$_H$	SU(2)$_L$	U(1)$_Y$	Z_2
(I)				
$\begin{pmatrix} T_1 \\ T_2 \end{pmatrix}$	2	2	0	+1
T_3	2	1	+1/2	+1
T_4	2	1	−1/2	+1
T_5	2	1	+1/2	−1
T_6	2	1	−1/2	−1
N_R^c	1	1	0	−1

Superfield	Z_2
(II)	
$H_d \equiv \begin{pmatrix} H_{14} \\ H_{24} \end{pmatrix}$, $H_u \equiv \begin{pmatrix} H_{13} \\ H_{23} \end{pmatrix}$ $N \equiv H_{56}$, $N_\Phi \equiv H_{34}$, $N_\Omega = H_{12}$	+1
$\Phi_d \equiv \begin{pmatrix} H_{15} \\ H_{25} \end{pmatrix}$, $\Phi_u \equiv \begin{pmatrix} H_{16} \\ H_{26} \end{pmatrix}$ $\Omega_- \equiv H_{46}$, $\Omega_+ \equiv H_{35}$ $\zeta \equiv H_{36}$, $\eta \equiv H_{45}$	−1

By the naive dimensional analysis, one expects $\lambda \simeq 4\pi$ at the confinement scale Λ_H. We here assume that the mass parameters $\mu = \lambda\langle N\rangle$, $\mu_\Phi = \lambda\langle N_\Phi\rangle$ and $\mu_\Omega = \lambda\langle N_\Omega\rangle$ are induced by the vacuum expectation values (vev's) of Z_2-even singlet fields N, N_Φ and N_Ω. The Yukawa couplings and the Majorana mass term of

the RHNs are given by

$$W_N = y_N^i N_R^c L_i \Phi_u + h_N^i N_R^c E_i^c \Omega_- + \frac{M_R}{2} N_R^c N_R^c + \frac{\kappa}{2} N N_R^c N_R^c \,. \tag{3}$$

In the low energy effective theory of this model, the dimension five operator is generated via loop contributions shown in **Figure 1** of Kanemura et al. [52] (one of the diagrams is shown in **Figure 1C** in this paper). There are both one-loop and three-loop contributions. The one-loop and three-loop diagrams correspond to the SUSY versions of the Ma model [29] and AKS model [32–34], respectively. It is worthwhile pointing out that the one-loop diagrams and three-loop diagrams are controlled by different coupling constants, i.e., one-loop diagrams are driven by the coupling y_N and the three-loop diagrams are controlled by another coupling h_N. Both one-loop and three-loop contributions can be significant if these coupling constants are hierarchical as $h_N \gg y_N$. Therefore, two different mass squared differences can be generated even if only one RHN is introduced[1].

In the $SU(2)_H$ model, not only the tiny neutrino masses but also other unsolved problems in the SM such as DM and baryogenesis may be solved. For the DM, the model contains the unbroken Z_2 symmetry as well as the unbroken R-parity. These discrete symmetries guarantee the stability of DM candidates. Since there are two different unbroken parities, there are potentially three kinds of DM candidates, *i.e.,* the lightest particles with the parity assignments of $(-,+)$, $(+,-)$, and $(-,-)$. If we consider the case that one of them is heavier than the sum of the masses of the others, the heaviest one decays into the other two DM particles so that the heaviest particle cannot be a DM.

Also, electroweak baryogenesis may work in the $SU(2)_H$ model. It is known that for successful electroweak baryogenesis, the 1st order phase transition (1stOPT) should be strong enough. This condition can be described by the inequality $\varphi_c/T_c > 1$. In addition, new CP violation phases are required in order to reproduce the correct amount of baryon asymmetry of the Universe. In this model, the 1stOPT can be enhanced by loop contributions of extra Z_2-odd scalar particles strongly enough. Though the analysis on CP phases in this model has not been done yet, it is naively expected that we can introduce several CP phases relevant to baryogenesis as in the case of MSSM [67, 68].

In Kanemura et al. [52], a benchmark scenario is provided. It reproduces the appropriate neutrino mass matrix, explains the DM relic abundance, and satisfies the 1stOPT condition as well as the constraints from the experimental data such as from lepton flavor violating processes searches. In Figure 3 of Kanemura et al. [52], the mass spectrum of the relevant particles in this benchmark scenario is shown.

The benchmark parameter point discussed above is already excluded by the direct detection experiment of the DM [69]. However, the predicted spin independent cross section can be significantly smaller, if we take into account the CP phases [70]. It is because the pseudo-scalar interaction with DM fermions are not relevant to the spin-independent cross section. Such CP phases can affect the BAU. Therefore, it may be interesting to discuss the correlation among BAU, spin-independent cross section, and other CP violating phenomena such as electric dipole moments of electron, neutron, and so on. This kind of analysis remains as a future task.

We here discuss phenomenological consequences of the benchmark scenario. The Z_2-even part of the spectrum is similar to the one in the nMSSM. In order to reproduce the relic abundance of the DM, a large mixing between doublet fields and singlet scalars are required. As a consequence, large mass splitting between the charged Higgs boson and the heavy Higgs bosons is predicted. The Z_2-even part of this scenario can be distinguished from the MSSM by looking at such a specific mass spectrum.

The condition $\varphi_c/T_c > 1$ is satisfied by loop effects of Φ_u and Ω_-. The same scalars also significantly affect the SM-like Higgs boson couplings, especially, the h-γ-γ coupling and the triple Higgs boson coupling. The prediction on the deviation of the SM-like Higgs couplings in this benchmark scenario is given by

$$\begin{aligned} \kappa_{hWW} &= 0.990\,, \quad \kappa_{hZZ} = 0.990\,, \quad \kappa_{h\bar{u}u} = 0.990\,, \\ \kappa_{h\bar{d}d} &= 0.978\,, \quad \kappa_{h\bar{\ell}\ell} = 0.978\,, \\ \kappa_{h\gamma\gamma} &= 0.88\,, \quad \kappa_{hhh} = 1.2\,, \end{aligned} \tag{4}$$

where the κ's denote the ratios between coupling constants predicted in this benchmark point and ones predicted in the SM, *i.e.*,

$$\kappa_{h\phi\phi} = \frac{g_{h\phi\phi}}{g_{h\phi\phi}^{\rm SM}} \,. \tag{5}$$

Here, in particular, the deviations in $h \to \gamma\gamma$ and the self coupling constant of the Higgs boson are as significant as 10-20%. By precise measurements of the SM-like Higgs boson couplings at future collider experiment such as the ILC [71, 72], the model can be distinguished from the nMSSM too.

Let us consider the Z_2-odd sector. By direct search for inert doublet particles [73] and inert charged singlet searches [74] at a lepton collider, we expect to get a strong hint on the Z_2-odd sector of the scenario.

4. SUMMARY

We have reviewed some models with loop induced neutrino masses. Although such models are phenomenologically quite interesting, they seems to be artificial. We have discussed an example based on SUSY $SU(2)_H$ gauge theory with confinement as a UV picture of such a phenomenological model. In the low energy effective theory, three problems in the SM namely baryogenesis, DM, and tiny neutrino mass can be solved. The 1stOPT is enhanced strongly enough for successful electroweak baryogenesis [53–61], multi-components

[1]In the ordinary type-I seesaw model, at least two RHNs are necessary for generating two different mass squared differences.

DM scenario is realized, and tiny neutrino masses [23–34] are generated via one-loop and three-loop diagrams. This model has a big advantage over the canonical type-I seesaw model. It is that new particles are required at a few TeV range so that the model will be tested at future experiments.

In models where tiny neutrino masses are radiatively generated via loop diagrams, the Higgs sector is often extended by introducing additional scalar fields. These additional scalar fields can contribute to various phenomenology. Some models can be distinguished with use of patterns of various phenomenological signals which are expected to be measured in future experiments. Then, it is expected that a UV theory which leads to a model with loop induced neutrino masses can be explored by investigating a pattern of various experimental signals. This situation is very different from a case of a grand unified theory with a grand desert such as SUSY SU(5) GUT.

AUTHOR CONTRIBUTIONS

The author confirms being the sole contributor of this work and has approved it for publication.

ACKNOWLEDGMENTS

This work was supported by JSPS KAKENHI Grant Number 17H05408 and by the Kogakuin University Grant for the project research.

REFERENCES

1. Aad G, Bentvelsenet S, Berglund E, Bobbink GJ, Bos K, Boterenbrood H, et al. Combined search for the Standard Model Higgs boson using up to 4.9 fb^{-1} of *pp* collision data at $\sqrt{s} = 7$ TeV with the ATLAS detector at the LHC. *Phys Lett.* (2012) **B710**:49–66. doi: 10.1016/j.physletb.2012.02.044
2. Chatrchyan S, Khachatryanet V, Sirunyan A, Tumasyan A, Adam W, Bergaueral T, et al. Combined results of searches for the standard model Higgs boson in *pp* collisions at $\sqrt{s} = 7$ TeV. *Phys Lett.* (2012) **B710**:26–48. doi: 10.1016/j.physletb.2012.02.064
3. Aad G, Abbott B, Abdallah J, Abdinov O, Aben R, Abolins M, et al. Study of the spin and parity of the Higgs boson in diboson decays with the ATLAS detector. *Eur Phys J.* (2015) **C75**:476. [Erratum: Eur. Phys. J.C76,no.3,152(2016)]. doi: 10.1140/epjc/s10052-015-3685-1
4. Khachatryan V, Apresyan A, Bornheim A, Bunn J, Chen Y, Duarte J, et al. Constraints on the spin-parity and anomalous HVV couplings of the Higgs boson in proton collisions at 7 and 8 TeV. *Phys Rev.* (2015) **D92**:012004. doi: 10.1103/PhysRevD.92.012004
5. Aad G, Abbott B, Abdallah J, Abdinov O, Aben R, Abolins M, et al. Measurements of the Higgs boson production and decay rates and coupling strengths using pp collision data at $\sqrt{s} = 7$ and 8 TeV in the ATLAS experiment. *Eur Phys J.* (2016) **C76**:6. doi: 10.1140/epjc/s10052-015-3769-y
6. Khachatryan V, Sirunyan AM, Tumasyan A, Adam W, Bergauer T, Dragicevic M, et al. Precise determination of the mass of the Higgs boson and tests of compatibility of its couplings with the standard model predictions using proton collisions at 7 and 8 TeV. *Eur Phys J.* (2015) **C75**:212. doi: 10.1140/epjc/s10052-015-3351-7
7. Fukuda Y,Hayakawa T, Ichihara E, Inoue K, Ishihara K, Ishino H, et al. Evidence for oscillation of atmospheric neutrinos. *Phys Rev Lett.* (1998) **81**:1562–7. doi: 10.1103/PhysRevLett.81.1562
8. Ahmad QR, Allen RC, Andersen TC, Anglin DJ, Barton JC, Beier EW, et al. Direct evidence for neutrino flavor transformation from neutral current interactions in the Sudbury Neutrino Observatory. *Phys Rev Lett.* (2002) **89**:011301. doi: 10.1103/PhysRevLett.89.011301
9. Eguchi K, Enomoto S, Furuno K, Goldman J, Hanada H, Ikeda H, et al. First results from KamLAND: evidence for reactor anti-neutrino disappearance. *Phys Rev Lett.* (2003) **90**:021802. doi: 10.1103/PhysRevLett.90.021802
10. An FP, Bai JZ, Balantekin AB, Band HR, Beavis D, Beriguete W, et al. Observation of electron-antineutrino disappearance at Daya Bay. *Phys Rev Lett.* (2012) **108**:171803. doi: 10.1103/PhysRevLett.108.171803
11. Ahn JK, Chebotaryov S, Choi JH, Choi S, Choi W, Choi Y, et al. Observation of reactor electron antineutrino disappearance in the RENO experiment. *Phys Rev Lett.* (2012) **108**:191802. doi: 10.1103/PhysRevLett.108.191802
12. Abe K, Adam J, Aihara H, Akiri T, Andreopoulos C, Aoki S, et al. Observation of electron neutrino appearance in a muon neutrino beam. *Phys Rev Lett.* (2014) **112**:061802. doi: 10.1103/PhysRevLett.112.061802
13. Otten EW, Weinheimer C. Neutrino mass limit from tritium beta decay. *Rept Prog Phys.* (2008) **71**:086201. doi: 10.1088/0034-4885/71/8/086201
14. Drexlin G, Hannen V, Mertens S, Weinheimer C. Current direct neutrino mass experiments. *Adv High Energy Phys.* (2013) **2013**:293986. doi: 10.1155/2013/293986
15. Weinberg S. Baryon and lepton nonconserving processes. *Phys Rev Lett.* (1979) **43**:1566–70. doi: 10.1103/PhysRevLett.43.1566
16. Minkowski P. $\mu \to e\gamma$ at a rate of one out of 10^9 muon decays? *Phys Lett.* (1977) **67B**:421–8.
17. Yanagida T. KEK report KEK-79-18. In: O. Sawada and A. Sugamoto, editors. *Workshop on the Unified Theory and the Baryon Number in the Universe*, Tsukuba (1979). p. 95.
18. Yanagida T. Horizontal symmetry and masses of neutrinos. *Prog Theor Phys.* (1980) **64**:1103.
19. Gell-Mann M, Ramond P, Slansky R. Complex spinors and unified theories. *Conf Proc.* (1979) **C790927**:315–21.
20. Mohapatra RN, Senjanovic G. Neutrino mass and spontaneous parity violation. *Phys Rev Lett.* (1980) **44**:912.
21. Mohapatra RN. Mechanism for understanding small neutrino mass in superstring theories. *Phys Rev Lett.* (1986) **56**:561–3.
22. Mohapatra RN, Valle JWF. Neutrino mass and Baryon number nonconservation in superstring models. *Phys Rev.* (1986) **D34**:1642.
23. Zee A. A theory of Lepton number violation, neutrino Majorana mass, and oscillation. *Phys Lett.* (1980) **93B**:389. [Erratum: Phys. Lett.95B,461(1980)].
24. Kanemura S, Shindou T, Sugiyama H. R-parity conserving supersymmetric extension of the Zee model. *Phys Rev.* (2015) **D92**:115001. doi: 10.1103/PhysRevD.92.115001
25. Zee A. Quantum numbers of Majorana neutrino masses. *Nucl Phys.* (1986) **B264**:99–110.
26. Babu KS. Model of 'Calculable' Majorana neutrino masses. *Phys Lett.* (1988) **B203**:132–6.
27. Aoki M, Kanemura S, Shindou T, Yagyu K. An R-parity conserving radiative neutrino mass model without right-handed neutrinos. *JHEP.* (2010) **7**:084. [Erratum: JHEP11,049(2010)].doi: 10.1007/JHEP07(2010)084
28. Krauss LM, Nasri S, Trodden M. A model for neutrino masses and dark matter. *Phys Rev.* (2003) **D67**:085002. doi: 10.1103/PhysRevD.67.085002
29. Ma E. Verifiable radiative seesaw mechanism of neutrino mass and dark matter. *Phys Rev.* (2006) **D73**:077301. doi: 10.1103/PhysRevD.73.077301
30. Ma E. Supersymmetric model of radiative Seesaw Majorana neutrino masses. *Annales FondBroglie.* (2006) **31**:285.
31. Ma E. Supersymmetric U(1) gauge realization of the dark scalar doublet model of radiative neutrino mass. *Mod Phys Lett.* (2008) **A23**:721–5. doi: 10.1142/S0217732308026753
32. Aoki M, Kanemura S, Seto O. Neutrino mass, dark matter and Baryon asymmetry via TeV-scale physics without fine-tuning. *Phys Rev Lett.* (2009) **102**:051805. doi: 10.1103/PhysRevLett.102.051805
33. Aoki M, Kanemura S, Seto O. A model of TeV scale physics for neutrino mass, dark matter and Baryon asymmetry and its phenomenology. *Phys Rev.* (2009) **D80**:033007. doi: 10.1103/PhysRevD.80.033007

34. Aoki M, Kanemura S, Yagyu K. Triviality and vacuum stability bounds in the three-loop neutrino mass model. *Phys Rev.* (2011) **D83**:075016. doi: 10.1103/PhysRevD.83.075016
35. Cai Y, Herrero-García J, Schmidt MA, Vicente A, Volkas RR. From the trees to the forest: a review of radiative neutrino mass models. *Front Phys.* (2017) **5**:63. doi: 10.3389/fphy.2017.00063
36. Nomura T, Okada H, Okada N. A colored KNT neutrino model. *Phys Lett.* (2016) **B762**:409–14. doi: 10.1016/j.physletb.2016.09.038
37. Cheung K, Nomura T, Okada H. Three-loop neutrino mass model with a colored triplet scalar. *Phys Rev.* (2017) **D95**:015026. doi: 10.1103/PhysRevD.95.015026
38. Doršner I, Fajfer S, Faroughy DA, Košnik N. The role of the S_3 GUT leptoquark in flavor universality and collider searches. *J High Energ Phys.* (2017) **2017**: 188. doi: 10.1007/JHEP10(2017)188
39. Guo SY, Han ZL, Li B, Liao Y, Ma XD. Interpreting the $R_{K^{(*)}}$ anomaly in the colored Zee-Babu model. *Nucl Phys.* (2018) **B928**:435–47. doi: 10.1016/j.nuclphysb.2018.01.024
40. Hati C, Kumar G, Orloff J, Teixeira AM. Reconciling *B*-meson decay anomalies with neutrino masses, dark matter and constraints from flavour violation. *JHEP.* (2018) **11**:011. doi: 10.1007/JHEP11(2018)011
41. Lees JP, Chaoet DT, Cheng CH, Echenard B, Floodal KT, Hitlin D, et al. Measurement of an excess of $\bar{B} \to D^{(*)}\tau^-\bar{\nu}_\tau$ decays and implications for charged Higgs bosons. *Phys Rev.* (2013) **D88**:072012. doi: 10.1103/PhysRevD.88.072012
42. Aaij R, Anderson J, Bernet R, Bowen E, Bursche A, Chiapolini N, et al. Measurement of the ratio of branching fractions $\mathcal{B}(\bar{B}^0 \to D^{*+}\tau^-\bar{\nu}_\tau)/\mathcal{B}(\bar{B}^0 \to D^{*+}\mu^-\bar{\nu}_\mu)$. *Phys Rev Lett.* (2015) **115**:111803. [Erratum: Phys. Rev. Lett.115,no.15,159901(2015)]. doi: 10.1103/PhysRevLett.115.111803
43. Fajfer S, Kamenik JF, Nisandzic I. On the $B \to D^*\tau\bar{\nu}_\tau$ sensitivity to new physics. *Phys Rev.* (2012) **D85**:094025. doi: 10.1103/PhysRevD.85.094025
44. Bernlochner FU, Ligeti Z, Papucci M, Robinson DJ. Combined analysis of semileptonic *B* decays to *D* and D^*: $R(D^{(*)})$, $|V_{cb}|$, and new physics. *Phys Rev.* (2017) **D95**:115008. [Erratum: Phys. Rev.D97,no.5,059902(2018)]. doi: 10.1103/PhysRevD.97.059902
45. Bigi D, Gambino P, Schacht S. A fresh look at the determination of $|V_{cb}|$ from $B \to D^*\ell\nu$. *Phys Lett.* (2017) **B769**:441–5. doi: 10.1016/j.physletb.2017.04.022
46. Hiller G, Kruger F. More model-independent analysis of $b \to s$ processes. *Phys Rev.* (2004) **D69**:074020. doi: 10.1103/PhysRevD.69.074020
47. Bordone M, Isidori G, Pattori A. On the standard model predictions for R_K and R_{K^*}. *Eur Phys J.* (2016) **C76**:440. doi: 10.1140/epjc/s10052-016-4274-7
48. Doršner I, Fajfer S, Košnik N. Leptoquark mechanism of neutrino masses within the grand unification framework. *Eur Phys J.* (2017) **C77**:417. doi: 10.1140/epjc/s10052-017-4987-2
49. Kanemura S, Machida N, Shindou T, Yamada T. A UV complete model for radiative seesaw scenarios and electroweak baryogenesis based on the supersymmetric gauge theory. *Phys Rev.* (2014) **D89**:013005. doi: 10.1103/PhysRevD.89.013005
50. Kanemura S, Senaha E, Shindou T, Yamada T. Electroweak phase transition and Higgs boson couplings in the model based on supersymmetric strong dynamics. *J High Energy Phys.* (2013) **5**:66.
51. Kanemura S, Shindou T, Yamada T. A light Higgs scenario based on the TeV-scale supersymmetric strong dynamics. *Phys Rev.* (2012) **D86**:55023. doi: 10.1103/PhysRevD.86.055023
52. Kanemura S, Machida N, Shindou T. Radiative neutrino mass, dark matter and electroweak baryogenesis from the supersymmetric gauge theory with confinement. *Phys Lett.* (2014) **B738**:178–86. doi: 10.1016/j.physletb.2014.09.013
53. Kuzmin VA, Rubakov VA, Shaposhnikov ME. On the anomalous electroweak Baryon number nonconservation in the early universe. *Phys Lett.* (1985) **155B**:36. doi: 10.1016/0370-2693(85)91028-7
54. Cohen AG, Kaplan DB, Nelson AE. Progress in electroweak baryogenesis. *Ann Rev Nucl Part Sci.* (1993) **43**:27–70. doi: 10.1146/annurev.ns.43.120193.000331
55. Quiros M. Field theory at finite temperature and phase transitions. *Helv Phys Acta.* (1994) **67**:451–583.
56. Rubakov VA, Shaposhnikov ME. Electroweak baryon number nonconservation in the early universe and in high-energy collisions. *Usp Fiz Nauk.* (1996) **166**:493–537. [Phys. Usp.39,461(1996)].
57. Funakubo K. CP violation and baryogenesis at the electroweak phase transition. *Prog Theor Phys.* (1996) **96**:475–520.
58. Trodden M. Electroweak baryogenesis. *Rev Mod Phys.* (1999) **71**:1463–500.
59. Bernreuther W. CP violation and baryogenesis. *Lect Notes Phys.* (2002) **591**:237–93.
60. Cline JM. Baryogenesis. In: *Les Houches Summer School - Session 86: Particle Physics and Cosmology: The Fabric of Spacetime Les Houches.* Paris (2006).
61. Morrissey DE, Ramsey-Musolf MJ. Electroweak baryogenesis. *New J Phys.* (2012) **14**:125003. doi: 10.1088/1367-2630/14/12/125003
62. Aoki M, Kubo J, Takano H. Two-loop radiative seesaw mechanism with multicomponent dark matter explaining the possible γ excess in the Higgs boson decay and at the Fermi LAT. *Phys Rev.* (2013) **D87**:116001. doi: 10.1103/PhysRevD.87.116001
63. Kajiyama Y, Okada H, Yagyu K. Two loop radiative seesaw model with inert triplet scalar field. *Nucl Phys.* (2013) **B874**:198–216. doi: 10.1016/j.nuclphysb.2013.05.020
64. Aoki M, Kanemura S, Tsumura K, Yagyu K. Models of Yukawa interaction in the two Higgs doublet model, and their collider phenomenology. *Phys Rev.* (2009) **D80**:15017. doi: 10.1103/PhysRevD.80.015017
65. Intriligator KA, Seiberg N. Lectures on supersymmetric gauge theories and electric-magnetic duality. *Nucl Phys Proc Suppl.* (1996) **45BC**:1–28. doi: 10.1016/0920-5632(95)00626-5
66. Harnik R, Kribs GD, Larson DT, Murayama H. The Minimal supersymmetric fat Higgs model. *Phys Rev.* (2004) **D70**:15002. doi: 10.1103/PhysRevD.70.015002
67. Dine M, Huet P, Singleton RL Jr, Susskind L. Creating the baryon asymmetry at the electroweak phase transition. *Phys Lett.* (1991) **B257**:351–56. doi: 10.1016/0370-2693(91)91905-B
68. Cohen AG, Nelson AE. Supersymmetric baryogenesis. *Phys Lett.* (1992) **B297**:111–7.
69. Akerib DS, Alsum S, Araújo HM, Bai X, Bailey AJ, Balajthy J, et al. Results from a search for dark matter in the complete LUX exposure. *Phys Rev Lett.* (2017) **118**:021303. doi: 10.1103/PhysRevLett.118.021303
70. Abe T. Effect of CP violation in the singlet-doublet dark matter model. *Phys Lett.* (2017) **B771**:125–30. doi: 10.1016/j.physletb.2017.05.048
71. Baer H, Barklow T, Fujii K, Gao Y, Hoang A, Kanemura S, et al. The international linear collider technical design report - volume 2: physics. *arXiv:1306.6352* (2013).
72. Asner DM, Barklow T, Calancha C, Fujii K, Graf N, Haber HE, et al. ILC Higgs White Paper. In: *Proceedings, 2013 Community Summer Study on the Future of U.S. Particle Physics* Minneapolis, MN:Snowmass on the Mississippi (CSS2013) (2013). Available online at: http://www.slac.stanford.edu/econf/C1307292/docs/submittedArxivFiles/1310.0763.pdf
73. Aoki M, Kanemura S, Yokoya H. Reconstruction of inert doublet scalars at the international linear collider. *Phys Lett.* (2013) **B725**:302–9. doi: 10.1016/j.physletb.2013.07.011
74. Aoki M, Kanemura S. Probing the Majorana nature of TeV-scale radiative seesaw models at collider experiments. *Phys Lett.* (2010) **B689**:28–35. doi: 10.1016/j.physletb.2010.04.024

Conflict of Interest Statement: The author declares that the research was conducted in the absence of any commercial or financial relationships that could be construed as a potential conflict of interest.

frontiers in Physics

REVIEW
published: 29 January 2019
doi: 10.3389/fphy.2019.00004

Direct and Indirect Probes for Composite Dark Matter

Maxim Y. Khlopov [1,2,3]*

[1] Institute of Physics, Southern Federal University, Rostov-on-Don, Russia, [2] Laboratory of Astroparticle Physics and Cosmology, Paris, France, [3] Center for Cosmoparticle Physics "Cosmion" and National Research Nuclear University "MEPHI", Moscow, Russia

Dark matter candidates are one of the profound signatures of new physics, reflecting existence of new stable particles. If such particles are charged they can bind with ordinary electrons, forming anomalous isotopes. Severe constraints on the anomalous hydrogen exclude new stable single charged particles, but the case of stable double charged particles is not excluded so easily. Similar to ordinary baryonic matter dark matter candidates can be in the form of neutral dark atoms in which new stable or sufficiently long living double charged particles are bound by ordinary Coulomb interaction. In the most simple case only negative double charged particles are bound in O-helium (OHe) dark atoms with primordial helium. OHe hypothesis can provide the solution for puzzles of direct dark matter searches by specifics of OHe interaction in the matter of underground detectors. OHe interaction in the matter can lead to formation of various exotic forms of O-nuclearities. Provided that the mass of the double charged particle is around 1.25 TeV OHe hypothesis can explain the observed positron annihilation line excess in the galactic bulge by pair production in de-excitation of OHe atoms colliding in this region. In the model of Walking Technicolor generation of primordial excess of negatively charged techniparticles (over their antiparticles) can be related to the baryon asymmetry of the Universe, giving proper relationship of baryonic and non-baryonic matter densities. Such primordial excess may be accompanied by a subdominant excess of longliving positively double charged techniparticles, whose decay to same sign pair of leptons can explain the high energy cosmic positron anomaly, detected by PAMELA and AMS02. This explanation should be confronted with the cosmic gamma ray background measured by FERMI/LAT, what put upper limit on the mass of a decaying double charged particle. It makes search for stable double charged particles at the LHC a direct probe for composite dark matter hypothesis.

Keywords: elementary particles, dark matter, dark atoms, stable double charged particles, composite dark matter

OPEN ACCESS

Edited by:
Roman Pasechnik,
Lund University, Sweden

Reviewed by:
Choong Sun Kim,
Yonsei University, South Korea
Alexander Merle,
Max-Planck-Institut für Physik, Germany
Giacomo Cacciapaglia,
UMR5822 Institut de Physique Nucleaire de Lyon (IPNL), France

***Correspondence:**
Maxim Y. Khlopov
khlopov@apc.univ-paris7.fr

Specialty section:
This article was submitted to High-Energy and Astroparticle Physics, a section of the journal Frontiers in Physics

Received: *19 September 2018*
Accepted: *09 January 2019*
Published: *29 January 2019*

Citation:
Khlopov MY (2019) Direct and Indirect Probes for Composite Dark Matter. Front. Phys. 7:4. doi: 10.3389/fphy.2019.00004

1. INTRODUCTION

The nature of cosmological dark matter, dominating in the matter content of the modern Universe, is related to new physics. If it consists of particles these new particles are predicted beyond the Standard model (BSM). Such particles (see [1] for review and reference) should be stable, provide the measured dark matter density and be decoupled from plasma and radiation at least before the beginning of matter dominated stage. The easiest way to satisfy these conditions is to involve neutral elementary weakly interacting massive particles (WIMPs). However negative results of WIMP searches appeal to other possible BSM solutions for the dark matter problem.

In the list of such BSM candidates the existence of heavy stable charged particles bound in neutral dark atoms is of special interest. Such atoms can be bound by various new forces, but it turns out that even stable electrically charged particles can exist hidden in such atoms and bound by ordinary Coulomb interactions (see [1] and references therein).

Stable particles with a single charge $\pm$ 1 are excluded due to overproduction of anomalous isotopes. Even very small fraction of free +1 charged particles bound with electrons leads to overproduction of anomalous hydrogen isotopes that are severely constrained by the experimental data. Frozen out free -1 charged particles are captured by primordial helium nuclei, as soon as they are produced in the Big Bang Nucleosynthesis, and the formed +1 charged ions play the same dangerous role of "nuclei" of anomalous hydrogen isotopes.

However, there doesn't appear such an evident contradiction for negatively doubly charged particles.

There exist several types of BSM particle models where heavy stable –2 charged species, O^{--}, are predicted:

(a) AC-leptons, predicted as an extension of the Standard Model, based on the approach of almost-commutative (AC) geometry [2–4].
(b) Technileptons and anti-technibaryons in the framework of Walking Technicolor (WTC) [5–11].
(c) stable "heavy quark clusters" $\bar{U}\bar{U}\bar{U}$ formed by anti-U quark of 4th generation [12]
(d) and, finally, stable charged clusters $\bar{u}_5\bar{u}_5\bar{u}_5$ of (anti)quarks $\bar{u}_5$ of 5th family can follow from the approach, unifying spins and charges[13].

It should be noted that the discovery and precise measurements of Higgs boson properties that appear to be very close to the predictions of the Standard model put severe constraints on the models (a)-(d). These constraints lead to more sophisticated WTC scenarios (see [14] for recent review) or imply strong suppression of heavy quarks to 125 GeV Higgs boson [15]. All these models also predict corresponding +2 charge particles. If these positively charged particles remain free in the early Universe, they can recombine with ordinary electrons in anomalous helium, which is not as much as hydrogen but still strongly constrained in terrestrial matter. Therefore, a cosmological scenario should provide a mechanism which suppresses anomalous helium. There are two possible mechanisms that can provide a suppression:

(i) The abundance of anomalous helium in the Galaxy may be significant, but in terrestrial matter a recombination mechanism could suppress this abundance below experimental upper limits [3]. The existence of a new U(1) gauge symmetry, causing new Coulomb-like long range interactions between charged dark matter particles, is crucial for this mechanism. This leads inevitably to the existence of dark radiation in the form of hidden photons.
(ii) Free positively charged particles are already suppressed in the early Universe and the abundance of anomalous helium in the Galaxy is negligible [12]. Such a charge asymmetric solution appeals to possible relationship between asymmetric dark matter and baryon asymmetry of the ordinary matter.

These two possibilities correspond to two different cosmological scenarios of dark atoms.

The first one is realized in the scenario with AC leptons, forming neutral AC atoms [3].

The second assumes a charge asymmetry of the O^{--} which forms the atom-like states with primordial helium [12]. If new stable species belong to non-trivial representations of the SU(2) electroweak group, sphaleron transitions at high temperatures can provide the relation between baryon asymmetry and excess of -2 charge stable species, as it was demonstrated in the case of WTC [5, 16].

After it is formed in the Standard Big Bang Nucleosynthesis (BBN), ^4He screens the O^{--} charged particles in composite ($^4He^{++}O^{--}$) *OHe* "atoms" [12]. In all the models of *OHe*, O^{--} behaves either as a lepton or as a specific "heavy quark cluster" with strongly suppressed hadronic interactions.

Dark atoms offer an interesting possibility to solve the puzzles of direct and indirect dark matter searches. Here following Khlopov [1], Bulekov et al. [17], Gani et al. [18], and Khlopov [19] we review main features of dark atom cosmology and possible direct and indirect probes for its physical basis.

2. DARK ATOM COSMOLOGY

The cosmological scenario of the OHe Universe involves only one parameter of new physics—the mass of O^{--}. Such a scenario is insensitive to the properties of O^{--} (except for its mass), since the main features of the OHe dark atoms are determined by their nuclear interacting helium shell. In the scenario of OHe Universe, presented below it is assumed that elastic processes dominate in OHe-nucleus interactions.

Due to elastic nuclear interactions of its helium constituent with nuclei in the cosmic plasma, the O-helium gas is in thermal equilibrium with plasma and radiation on the Radiation Dominance (RD) stage, while the energy and momentum transfer from plasma is effective. The radiation pressure acting on the plasma is then transferred to density fluctuations of the O-helium gas and transforms them in acoustic waves at scales up to the size of the horizon.

At temperature

$$T < T_{od} \approx 1 S_3^{2/3}\ \mathrm{eV} \tag{1}$$

the energy and momentum transfer from baryons to O-helium is not effective [5, 12] because

$$n_B \langle \sigma v \rangle (m_p/m_o) t < 1, \tag{2}$$

where m_o is the mass of the OHe atom and

$$S_3 = m_o/(1\ \mathrm{TeV}).$$

Here

$$\sigma \approx \sigma_o \sim \pi r_o^2 \approx 10^{-25}\ \mathrm{cm}^2, \tag{3}$$

and $v = \sqrt{2T/m_p}$ is the baryon thermal velocity. Then O-helium gas decouples from plasma. It starts to dominate in the Universe

after $t \sim 10^{12}$ s at $T \leq T_{RM} \approx 1$ eV, where T_{RM} is the temperature at the transition from Radiation to Matter dominated stage. At Matter dominated stage O-helium "atoms" play the main dynamical role in the development of gravitational instability, triggering the large scale structure formation. The composite nature of O-helium determines the specifics of the corresponding dark matter scenario [1].

At Radiation dominated stage, corresponding to $T > T_{RM}$, the total mass M of the OHe gas with density

$$\rho_d = (T_{RM}/T)\rho_{tot} \tag{4}$$

is equal within the cosmological horizon $l_h = t$ to

$$M = \frac{4\pi}{3}\rho_d t^3 = \frac{4\pi}{3}\frac{T_{RM}}{T}m_{Pl}(\frac{m_{Pl}}{T})^2, \tag{5}$$

In the period of decoupling $T = T_{od}$, this mass depends strongly on the O-helium mass S_3 and is given by Khlopov and Kouvaris [5]

$$M_{od} = \frac{T_{RM}}{T_{od}}m_{Pl}(\frac{m_{Pl}}{T_{od}})^2 \approx 2\cdot 10^{44}S_3^{-2}\,\mathrm{g} = 10^{11}S_3^{-2}M_\odot, \tag{6}$$

where $M_\odot$ is the solar mass. O-helium is formed only at T_o and its total mass within the cosmological horizon in the period of its creation is

$$M_o = M_{od}(T_{od}/T_o)^3 = 10^{37}\,\mathrm{g}. \tag{7}$$

On the RD stage before decoupling, the Jeans length λ_J of the OHe gas was restricted from below by the propagation of sound waves in plasma with a relativistic equation of state $p = \epsilon/3$, being of the order of the cosmological horizon and equal to

$$\lambda_J = l_h/\sqrt{3} = t/\sqrt{3}. \tag{8}$$

After decoupling at $T = T_{od}$, it falls down to $\lambda_J \sim v_o t$, where $v_o = \sqrt{2T_{od}/m_o}$. Though after decoupling the Jeans mass in the *OHe* gas correspondingly falls down

$$M_J \sim v_o^3 M_{od} \sim 3\cdot 10^{-14}M_{od}, \tag{9}$$

one should expect a strong suppression of fluctuations on scales $M < M_o$, as well as adiabatic damping of sound waves in the RD plasma for scales $M_o < M < M_{od}$. It can provide some suppression of small scale structure in the considered model for all reasonable masses of O-helium. The significance of this suppression and its effect on the structure formation needs a special study in detailed numerical simulations. In any case, it can not be as strong as the free streaming suppression in ordinary Warm Dark Matter (WDM) scenarios, but one can expect that qualitatively we deal with Warmer Than Cold Dark Matter model.

Being decoupled from baryonic matter, the OHe gas does not follow the formation of baryonic astrophysical objects (stars, planets, molecular clouds...) and forms dark matter halos of galaxies. It can be easily seen that O-helium gas is collisionless for its number density, saturating galactic dark matter. Taking the average density of baryonic matter one can also find that the Galaxy as a whole is transparent for O-helium in spite of its nuclear interaction. Only individual baryonic objects like stars and planets are opaque for it.

3. DARK ATOMS AND PUZZLES OF DIRECT DARK MATTER SEARCHES

In terrestrial matter O-helium atoms are slowed down and cannot cause significant nuclear recoil in the underground detectors, making them elusive in direct WIMP search experiments (where detection is based on nuclear recoil) such as CDMS, XENON100, LUX etc. The positive results of DAMA experiments (see [20] for review and references) can find in this scenario a nontrivial explanation due to a low energy radiative capture of OHe by intermediate mass nuclei [1].

At each underground level of the terrestrial matter local OHe concentration is determined by the equilibrium between incoming cosmic flux and OHe diffusion toward the center of Earth. Rapid adjustment (within an hour at the level of underground detectors) leads to its annual modulation due to the Earth's motion around the Sun, reflecting the annual modulation of the incoming cosmic flux, therefore the positive result of DAMA/NaI and DAMA/LIBRA experiments is explained by annual modulation in reaction of radiative capture of OHe

$$A + (^4He^{++}O^{--}) \rightarrow [A(^4He^{++}O^{--})] + \gamma \tag{10}$$

by nuclei in DAMA detector.

The crucial point in this explanation is the existence of a low lying energy level of OHe-nucleus bound state and annual modulation of energy release in OHe-nucleus capture to this level. This point needs proper quantum mechanical treatment, which appears to be not so simple due to complication of self-consistent treatment of interaction of helium shell of O-helium with the nucleus. However, in the square well and wall approximation it was shown [1] that there exists a few keV level for intermediate mass nuclei and such level doesn't exist for light and heavy nuclei. The positive result of DAMA/NaI and DAMA/LIBRA experiments follows then from annual modulation of the rate of Na capture by OHe to the 3 keV bound state of OHe-Na system.

This explains the negative results of the XENON100 and LUX experiments, since there is no such level in OHe-Xe system.

The rate of OHe capture by intermediate mass nuclei is determined by isospin violating electric dipole transition and thus proportional to the temperature. It leads to suppression of this effect in cryogenic detectors.

3.1. Inelastic Processes and *O*-Nuclearites

One should note that the nuclear physics of OHe is still in the course of development and its basic element for a successful and self-consistent OHe dark matter scenario is related to the existence of a dipole Coulomb barrier, arising in the process of OHe-nucleus interaction and providing the dominance of elastic collisions of OHe with nuclei.

Though OHe scenario seems to involve dominantly known atomic and nuclear physics, there is no small parameter in OHe-nucleus interaction. It makes the problem very complicated as compared with ordinary atoms that have electroweakly interacting electronic shells and strongly interacting nuclei of much smaller size. These two features proved small parameters in the ordinary atomic physics, which are not the case for OHe. Indeed, the size of the He shell is equal to the size of He nucleus and creation of barrier in OHe-nucleus interaction should be the result of a simultaneous action of nuclear attraction and Coulomb repulsion between He and approaching nucleus. Qualitatively, a possibility for such a solution can be illustrated by the following picture. At large distances Coulomb field of nucleus polarizes OHe so that Stark-effect attraction takes place. At some distance nuclear attraction changes the sign of polarization, but Coulomb repulsion moves it back, and then nuclear attraction moves He again toward nucleus and so on. Such oscillatory behavior can provide creation of potential barrier and this approach is now under quantitative investigation.

This problem, which implies correct quantum mechanical treatment, is the main open question of the composite dark matter [21]. The lack of such a barrier and essential contribution of inelastic OHe-nucleus processes seem to lead to inevitable overproduction of anomalous isotopes [22]. In that case one may need more sophisticated models retaining the ideas of dark atom scenario, which involve more elements of new physics, as e.g., proposed in Wallemacq [23].

On the other hand, even strongly suppressed inelastic processes inevitably lead to formation of anomalous isotopes due to O^{--} capture by nuclei. Capture by nucleus of multiple O^{--} particles can lead to existence of exotic superheavy nuclear states of O-nuclearites [18].

In the difference from early studies of bound systems of stable heavy negatively charged particles with nuclei [24–26] the approach of Gani et al. [18] is concentrated on effect of multiple O-particles capture by nuclei.

According Gani et al. [18] the most energetically favorable multi-O-particle distribution inside the nucleus with a density $n_O(r)$ is that follows the proton one, fully compensating the Coulomb field. Thereby O-particles, if their number were $N_O \geq A$, would be re-distributed to minimize the energy, and finally the density of O inside the atomic nucleus with radius R becomes

$$n_O = n_O^0 \theta(r - R) \tag{11}$$

with

$$n_O = -2n_{\rm p} = -2n_{\rm p}^0 \theta(r - R) \tag{12}$$

for O-nuclearite, that corresponds to $V = const$ for $r < R$. Here $n_{\rm p}$ is proton density in the nucleus that is assumed constant inside the nucleaus. Excessive O-particles are pushed out. Thus, constructed O-nuclearite, has the energy

$$\mathcal{E} \simeq -16{\rm MeV} \cdot A < 0 \tag{13}$$

and thereby for arbitrary A it proves to be absolutely stable (if O is considered as a stable particle), till gravity is yet unimportant. The key point here is that it is profitable to have $n_O(r) = 2n_{\rm p}(r)$, if there is a sufficient amount of O-particles.

Note that the value

$$\mathcal{E}_{\rm kin}^O < 16\,{\rm MeV} \cdot A \tag{14}$$

and thereby the matter of the nuclearite is self-bound provided $m_o > 2.3m_N$, where m_N is the mass of nucleon.

O-nuclearites can hardly be formed in the early Universe but their formation is possible in stars due to O-helium capture and the produced O-nuclearites can be released in the interstellar space after supernova explosions. If the amount of O-particles captured by star is sufficiently large, it can trigger collapse to black hole and according to de Lavallaz and Fairbairn [27] provide additional constraints on O^{--} particles. Such amount cannot be captured by neutron star owing to its small size, but can be stored at earlier stages of stellar evolution, when the star had the size of giant or supergiant [18].

4. INDIRECT EFFECTS OF COMPOSITE DARK MATTER

The existence of such form of matter as O-helium should lead to a number of astrophysical signatures, which can constrain or prove this hypothesis. One of the signatures of O-helium can be a presence of an anomalous low Z/A component in the cosmic ray flux. O-helium atoms that are present in the Galaxy in the form of the dark matter can be destroyed in astrophysical processes and free double charged particles can be accelerated as ordinary charged particles. O-helium atoms can be ionized due to nuclear interaction with cosmic rays or in the front of a shock wave in the Supernova explosions, where they were effectively accumulated during star evolution [12]. If the mechanisms of X acceleration are effective, they might be observed in AMS02 cosmic ray experiments.

4.1. Excess of Positron Annihilation Line in the Galactic Bulge

OHe collisions in the central part of the Galaxy lead to OHe excitations, and de-excitations with pair production in E0 transitions can explain the excess of the positron-annihilation line, observed by INTEGRAL in the galactic bulge [1, 16, 28].

If 2S level of O-helium is excited, its direct one-photon transition to the 1S ground state is forbidden and the de-excitation mainly goes through direct pair production. In principle this mechanism of positron production can explain the excess in positron annihilation line from the galactic bulge, measured by the INTEGRAL experiment. Due to the large uncertainty of DM distribution in the galactic bulge this interpretation of the INTEGRAL data is possible in a wide range of masses of O-helium with the minimal required central density of O-helium dark matter at [29, 30] $m_o = 1.25\,{\rm TeV}$ For the smaller values of m_o on needs larger central density to provide effective excitation of O-helium in collisions Current analysis favors lowest values of central dark matter density, making possible O-helium explanation for this excess only for a narrow window around this minimal value (see **Figure 1**).

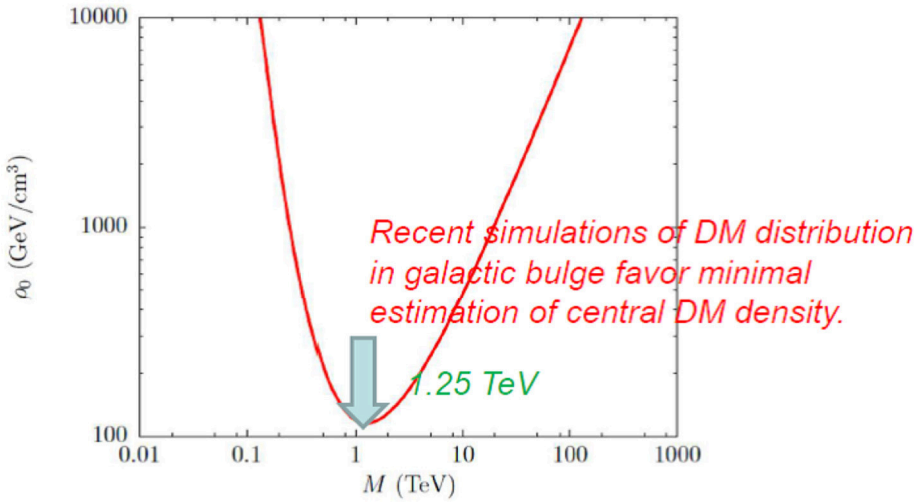

FIGURE 1 | Dark matter is subdominant in the central part of Galaxy. It strongly suppresses it dynamical effect and causes large uncertainty in dark matter density and velocity distribution. At this uncertainty one can explain the positron line excess, observed by INTERGRAL, for a wide range of m_O given by the curve with minimum at $m_O = 1.25$ TeV. However, recent analysis of possible dark matter distribution in the galactic bulge favor minimal value of its central density. The picture is taken with the according permission from Bulekov et al. [17].

4.2. Dark Atom Solution for High Energy Positron Excess

In a two-component dark atom model, based on Walking Technicolor, atom-like states, made of positive and negative doubly charged techniparticles, is present together with the dominant component of OHe dark atom. These techniparticle atoms weakly interact with matter and the upper limits from direct dark matter searches put constraints on this sparse WIMP-like dark atom component. In WTC models positively double charged particles may be very long living, but metastable and their decays to pairs of same-sign leptons can explain the excess of high-energy cosmic-ray positrons [31], found in PAMELA and AMS02 experiments [32–35]. This explanation is possible for the mass of decaying +2 charged particle below 1 TeV and depends on the branching ratios of leptonic channels (see **Figure 2**).

Since even pure lepton decay channels are inevitably accompanied by gamma radiation the important constraint on this model follows from the measurement of cosmic gamma ray background in FERMI/LAT experiment [36] (see **Figure 3**). The multi-parameter analysis of decaying dark atom constituent model determines the maximal model independent value of the mass of decaying +2 charge particle, at which this explanation is possible

$$m_o < 1 TeV.$$

One should take into account that according to Belotsky et al. [37] even in this range hypothesis on decaying composite dark matter, distributed in the galactic halo, can lead to gamma ray flux exceeding the measured by FERMI/LAT. It may favor local source of the positron component e.g., from the decays in clumps of dark matter in vicinity of the Solar system. One should also note an alternative non-dark-matter nature of such a local source as a local supernova explosion two million years ago [38].

4.3. Sensitivity of Indirect Effect of Composite Dark Matter to the Mass of Their Double Charged Constituents

We see that indirect effects of composite dark matter strongly depend on the mass of its double charged constituents.

To explain the excess of positron annihilation line in the galactic bulge mass of double charged constituent of O-helium should be in a narrow window around

$$m_o = 1.25\,\text{TeV}. \tag{15}$$

To explain the excess of high energy cosmic ray positrons by decays of constituents of composite dark matter with charge +2 and to avoid overproduction of gamma background, accompanying such decays, the mass of such constituent should be in the range

$$m_o < 1\,\text{TeV}. \tag{16}$$

These predictions should be confronted with the experimental data on the accelerator search for stable double charged particles.

5. SEARCHES FOR STABLE DOUBLE CHARGED PARTICLES

Production of pairs of elementary stable doubly charged heavy leptons is characterized by a number of distinct experimental signatures that would provide effective search for them at the experiments at the LHC and test the atom-like structure of the cosmological dark matter. Moreover, astrophysical consequences

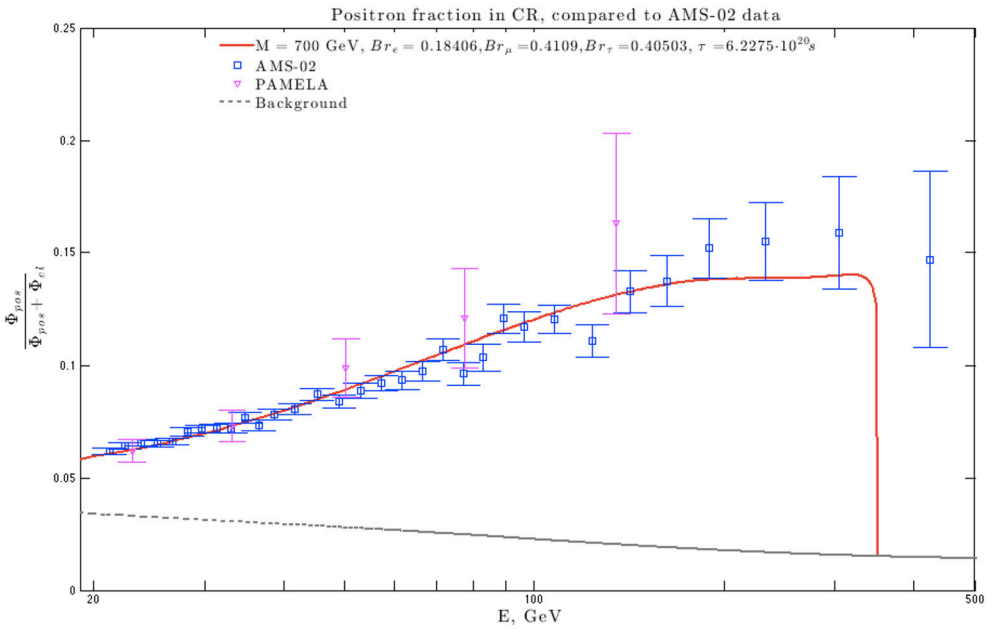

FIGURE 2 | Best fit high energy positron fluxes from decaying composite dark matter in confrontation with the results of AMS02 experiment. The picture is taken with the according permission from Bulekov et al. [17].

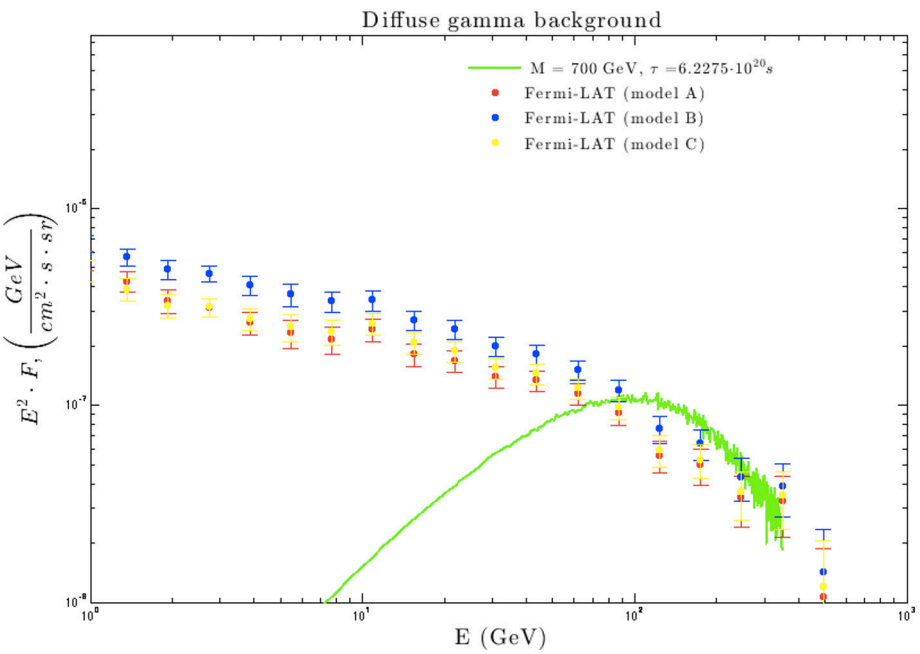

FIGURE 3 | Gamma ray flux accompanying the best fit high energy positron fluxes from decaying composite dark matter reproducing the results of AMS02 experiment, in confrontation with FERMI/LAT measurement of gamma ray background. The picture is taken with the according permission from Bulekov et al. [17].

of composite dark matter model can reproduce experimentally detected excess in positron annihilation line and high energy positron fraction in cosmic rays only if the mass of double charged O^{--} particles is in the 1 TeV range. Here we discuss following Bulekov et al. [17] confrontation of these predictions and experimental data, as well as the current status and expected progress in experimental searches for stable double charged particles as constituents of composite dark matter.

A new charged massive particle with electric charge $\neq 1e$ would represent a dramatic deviation from the predictions of

the Standard Model, and such a spectacular discovery would lead to fundamental insights and critical theoretical developments. Searches for such kind of particles were carried out in many cosmic ray and collider experiments (see for instance review in [39]).

In a tree approximation, such particles cannot decay to pair of quarks due to electric charge conservation and only decays to the same sign leptons are possible. The latter implies lepton number nonconservation, being a profound signature of new physics. In general, it makes such states sufficiently long-living in a cosmological scale.

Obviously, such experiments are limited to look only for the "long-lived" particles, which do not decay within a detector, as opposed to truly stable particles, which do not decay at all. Since the kinematics and cross sections for double charged particle production processes cannot be reliably predicted, search results at collider experiments are usually quoted as cross section limits for a range of charges and masses for well-defined kinematic models. In these early experiments, the mass limit was set at the level of up to 100 GeV (see for review [39]).

5.1. Searches at Large Hadron Collider

Significant increase of beam energy at the Large Hadron Collider (LHC) opens a new era in the high energy physics and allows accessing uncharted territories of particle masses. In this subsection the results of searches for the multi-charged particles, performed by the ATLAS and the CMS collaborations at LHC, will be described following Bulekov et al. [17].

Calculations of the cross sections assume that these particles are generated as new massive spin-1/2 ones, neutral under $SU(3)_C$ and $SU(2)_L$.

5.1.1. ATLAS Experiment at LHC

In Run 1 (2010–2012), the ATLAS [40] collaboration at LHC performed two searches for long-lived multi-charged particles, including the double charged particles: one search with 4.4 fb^{-1} of data collected in pp collisions at $\sqrt{s} = 7$ TeV [41], and another one with 20.3 fb^{-1} collected at $\sqrt{s} = 8$ TeV [42].

Both these searches feature particles with large transverse momentum values, traversing the entire ATLAS detector. An energy loss of a double charged particle is by a factor of $q^2 = 4$ higher than that of single charged particle. Such particles will leave a very characteristic signature of high ionization in the detector. More specifically, the searches look for particles with anomalously high ionization on their tracks in three independent detector subsystems: silicon pixel detector (Pixel) and transition radiation tracker (TRT) in the ATLAS inner detector, and monitoring drift tubes (MDT) in the muon system.

The estimate of the expected background originating from the SM processes and providing input into the signal region D was calculated to be $0.013 \pm 0.002(\text{stat.}) \pm 0.003(\text{syst.})$ events.

No events with double charged particles were found in neither 2011 or 2012 experimental data sets, setting the lower mass limits to 430 and 660 GeV, respectively, at 95% CL. The comparison of observed cross-section upper limits and theoretically predicted cross-sections is shown in **Figure 4**.

5.1.2. CMS Experiment at LHC

In parallel to the ATLAS experiment, the CMS [43] collaboration at LHC performed a search for double charged particles, using 5.0 fb^{-1} of data collected in pp collisions at $\sqrt{s} = 7$ TeV and 18.8 fb^{-1} collected at $\sqrt{s} = 8$ TeV [44].

Comparison between observed upper cross section limits and theoretically predicted cross section values for the 8 TeV is shown in **Figure 5**.

For the 8 TeV search, the mass limit of 665 GeV was obtained. This result (within uncertainties) is very close to the ATLAS limit of 660 GeV for the 8 TeV data set. Also, CMS treated the results obtained at 7 and 8 TeV as combined. This allowed to push the lower mass limit to 685 GeV at 95% CL. A combination of the results of two experiments for 8 TeV would mean an increase of statistics by a factor of 2. Having said that, one can conclude that the mass limit based on the results of both experiment for double charged particles can be set at the level of about 730 GeV.

5.2. What One Expects From LHC Run 2

Following the discussion of the prospects of searches for multi-charged particles in ATLAS and CMS experiments in Bulekov et al. [17], it may be concluded that each of these two experiments will be able to set a lower mass limit on the double charged particles at $m = 1000 \pm 50$ GeV. Going further and considering the data taking periods of ATLAS and CMS until the end of Run 2 (end of 2018), one can estimate according to Bulekov et al. [17] a low limit on the double charged particles mass corresponding to the Run 2 data set. Several assumptions were made in these speculations [17]:

- by the end of 2018, ATLAS and CMS will each record about 120 fb^{-1} of $\sqrt{s} = 13$ TeV data;

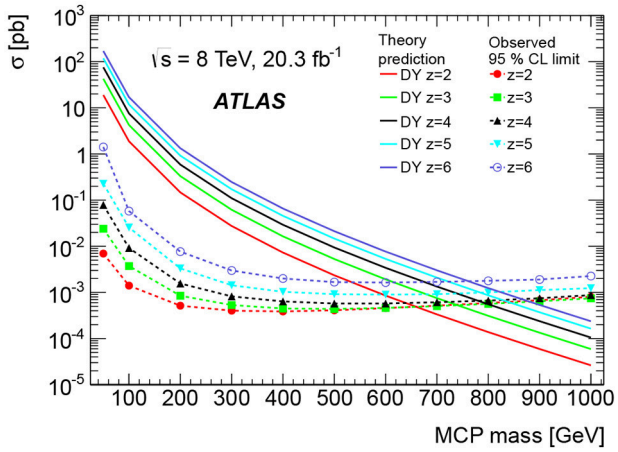

FIGURE 4 | Observed 95% CL cross-section upper limits and theoretical cross-sections as functions of the multi-charged particles mass. Again, the double charged particles are denoted as "$z = 2$" (red points and lines). The picture is taken with the according permission from Bulekov et al. [17].

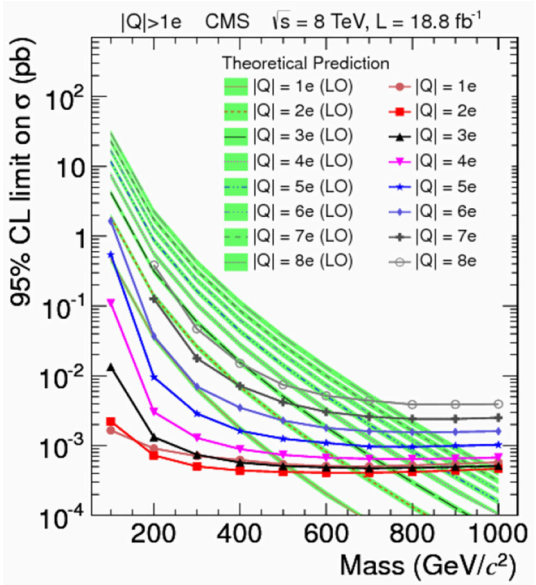

FIGURE 5 | Observed 95% CL cross-section upper limits and theoretical cross-sections as functions of the multi-charged particles mass in CMS search at the $\sqrt{s} = 8$ TeV. The double charged particles are denoted as "$|Q| = 2e$". The picture is taken with the according permission from Bulekov et al. [17].

- signal efficiency will remain at a present level in both experiments, without being compromised by high detector occupancy or any other effects;
- no double charged particle candidates will be in observed in the first place.

Considering all of the above, the ATLAS and CMS collaborations may each be expected to set the lower mass limits at the level of 1.2 TeV based on their analyses of the entire 13 TeV data set. If these two experiments combined their independently gathered statistics together for this kind of search, the limits would go as high as up to 1.3 TeV [17].

6. CONCLUSIONS

Dark Matter that is considered to be electrically neutral, potentially can be formed by stable heavy charged particles bound in neutral atom-like states by Coulomb attraction. Analysis of the cosmological data and atomic composition of the Universe gives the constrains on the particle charge showing that only -2 charged constituents, being trapped by primordial helium in neutral O-helium states, can avoid the problem of overproduction of the anomalous isotopes of chemical elements, which are severely constrained by observations.

Cosmological model of O-helium dark matter can even explain puzzles of direct dark matter searches. This explanation involves minimal number of parameters of new physics, being based on known laws of quantum mechanics and atomic and nuclear physics. However, we have seen that the nontrivial features of OHe-nucleus interaction still leave open the crucial question on the existence and effect of dipole potential barrier in this interaction. Such barrier provides dominance of elastic processes in OHe interaction with matter and existence of shallow potential well in OHe interaction with intermediate mass nuclei. Existence of a 3 keV level in such a well in OHe-Na interaction and annual modulation of energy release due to capture to this level can explain positive result of DAMA/NaI and DAMA/LIBRA experiments, as well as absence of such signal in other detectors.

O-helium hypothesis inevitably leads to existence of anomalous nuclear isotopes, in which single O^{--} is captured, or to exotic states of O-nuclearites with multiple O-particles in nuclei. Search for such anomalous form of nuclear matter extends the set of probes for dark-atom hypothesis.

The crucial problem of OHe scenario is the nuclear physics of OHe. Though it involves only known atomic and nuclear physics the proper quantum mechanical treatment is very complicated in the lack of small parameters in the problem of OHe-nucleus interaction. Such treatment should also take into proper account simultaneous action of Coulomb and nuclear forces on He from the approaching nucleus. There is a hint to solve this problem and the development of the quantitative analysis is under way. As soon as this problem is solved all the richness of the astrophysical features of OHe scenario will find proper physical basis (see e.g., [45]).

OHe hypothesis can also explain observed excess of positron annihilation line in the galactic bulge and high energy positron fraction of cosmic rays. Such explanation implies upper limits on the mass of a double charged constituents within 1 TeV range, challenging their searches at the LHC.

Stable charge -2 states (O^{--}) can be elementary like AC-leptons or technileptons, or look like technibaryons. The latter, composed of techniquarks, reveal their structure at much higher energy scale and should be produced at colliders and accelerators as elementary species. They can also be composite like "heavy quark clusters" $\bar{U}\bar{U}\bar{U}$ formed by anti-U quark in one of the models of fourth generation [12] or $\bar{u}_5\bar{u}_5\bar{u}_5$ of (anti)quarks $\bar{u}_5$ of stable 5th family in the approach [13].

In the context of composite dark matter scenario accelerator search for stable doubly charged leptons acquires the meaning of direct critical test for existence of charged constituents of cosmological dark matter.

The signature for AC leptons and techniparticles is unique and distinctive what allows to separate them from other hypothetical exotic particles. Composite dark matter models can explain observed excess of high energy positrons and gamma radiation in positron annihilation line at the masses of O^{--} in the range of 1 TeV, it makes search for double charged particles in this range direct experimental test for these predictions of composite dark matter models.

Test for composite O^{--} can be only indirect: through the search for heavy hadrons, composed of single U or $\bar{U}$ and light quarks (similar to R-hadrons).

The ATLAS and CMS collaborations at the Large Hadron Collider are searching for the double charged particles

since 2011. The most stringent results achieved so far exclude the existence of such particles up to their mass of 680 GeV. This value was obtained by both ATLAS and CMS collaborations independently. It is expected that if these two collaborations combine their independently gathered statistics of LHC Run 2 (2015–2018), the lower mass limit of double charged particles could reach the level of about 1.3 TeV. It can provide severe test for composite dark matter origin of possible indirect effects of dark matter.

One can conclude that signatures of composite dark matter provide an extensive set of direct and indirect probes challenging their physical and astrophysical test.

AUTHOR CONTRIBUTIONS

The author confirms being the sole contributor of this work and has approved it for publication.

ACKNOWLEDGMENTS

I express my gratitude to K. Belotsky, O. Bulekov, J. R. Cudell, C. Kouvaris, M. Laletin, A. S. Romaniouk, and Yu. S. Smirnov for their collaboration in obtaining original results on which this review is based. The paper involves with proper references the results published by author in Khlopov [1], Bulekov et al. [17], Gani et al. [18], and Khlopov [19]. The work was supported by grant of Russian Science Foundation (project N-18-12-00213).

REFERENCES

1. Khlopov MY. Fundamental particle structure in the cosmological dark matter. *Int J Mod Phys.* (2013) **28**:1330042. doi: 10.1142/S0217751X13300421
2. Stephan CA. Almost-commutative geometries beyond the standard model.
3. Fargion D, Khlopov M, Stephan CA. Cold dark matter by heavy double charged leptons? *Class Quantum Grav.* (2006) **23**:7305. doi: 10.1088/0264-9381/23/24/008
4. Connes A. *Noncommutative Geometry*. London; San Diego, CA: Academic Press (1994).
5. Khlopov MY, Kouvaris, C. Strong interactive massive particles from a strong coupled theory. *Phys Rev D* (2008) **77**:065002. doi: 10.1103/PhysRevD.77.065002
6. Sannino F, Tuominen K. Orientifold theory dynamics and symmetry breaking. *Phys Rev D* (2005) **71**:051901. doi: 10.1103/PhysRevD.71.051901
7. Hong DK, Hsu SD, Sannino F. Composite Higgs from higher representations. *Phys Lett B* (2004) **597**:89. doi: 10.1016/j.physletb.2004.07.007
8. Dietrich DD, Sannino F, Tuominen K. Light composite Higgs from higher representations versus electroweak precision measurements: predictions for LHC. *Phys Rev D* (2005) **72**:055001. doi: 10.1103/PhysRevD.72.055001
9. Dietrich DD , Sannino F, Tuominen K. Light composite Higgs and precision electroweak measurements on the Z resonance: an update. *Phys Rev D* (2006) **73** :037701. doi: 10.1103/PhysRevD.73.037701
10. Gudnason SB, Kouvaris C, Sannino F, Towards working technicolor: effective theories and dark matter. *Phys Rev D* (2006) **73**:115003. doi: 10.1103/PhysRevD.73.115003
11. Gudnason SB, Kouvaris C, Sannino F. Dark matter from new technicolor theories. *Phys Rev D* (2006) **74**:095008. doi: 10.1103/PhysRevD.74.095008
12. Khlopov MY. Composite dark matter from 4th generation. *JETP Lett.* (2006) **83**:1–4. doi: 10.1134/S0021364006010012
13. Mankoc-Borstnik N. Unification of spins and charges in Grassmann space? *Mod Phys Lett A* (1995) **10**:587. doi: 10.1142/S0217732395000624
14. Goertz F. Composite Higgs theory. In: *PoS ALPS2018, 012*. Obergurgl (2018).
15. Khlopov MY, Shibaev RM. Probes for 4th generation constituents of dark atoms in Higgs boson studies at the LHC. *Adv High Ener Phys.* (2014) **2014**:406458. doi: 10.1155/2014/406458
16. Khlopov MY, Kouvaris C. Composite dark matter from a model with composite Higgs boson. *Phys Rev D* (2008) **78**:065040 doi: 10.1103/PhysRevD.78.065040
17. Bulekov OV, Khlopov MY, Romaniouk AS, Smirnov YS. Search for double charged particles as direct test for dark atom constituents. *Bled Works Phys.* (2017) **18**:11.
18. Gani VA, Khlopov MY, Voskresensky DN. Double charged heavy constituents of dark atoms and superheavy nuclear objects. *Phys Rev D* (2019) **99**:015024. doi: 10.1103/PhysRevD.99.015024
19. Khlopov MY. Probes for dark matter physics. *Int J Mod Phys D* (2018) **27**:1841013. doi: 10.1142/S0218271818410134
20. Bernabei R. Belli P, d'Angelo S, Di Marco A, Montecchia F, Cappella F, et al. Dark Matter investigation by DAMA at Gran Sasso. *Int J Mod Phys A* (2013) **28**:1330022. doi: 10.1142/S0217751X13300226
21. Cudell JR, Khlopov MY, Wallemacq Q. The nuclear physics of OHe. *Bled Works Phys.* (2012) **13**:10.
22. Cudell JR, Khlopov MY, Wallemacq Q. Some potential problems of OHe composite dark matter. *Bled Works Phys.*(2014) **15**:66.
23. Wallemacq Q. Milli-interacting dark matter. *Phys Rev D* (2013) **88**:063516. doi: 10.1103/PhysRevD.88.063516
24. Cahn RN, Glashow SL. Chemical signatures for superheavy elementary particles. *Science* (1981) **213**:607. doi: 10.1126/science.213.4508.607
25. Pospelov M. Particle physics catalysis of thermal big bang nucleosynthesis. *Phys Rev Lett.* (2007) **98**:231301. doi: 10.1103/PhysRevLett.98.231301
26. Kohri K, Takayama F. Big bang nucleosynthesis with long-lived charged massive particles. *Phys Rev.* (2007) **D76**:063507. doi: 10.1103/PhysRevD.76.063507
27. de Lavallaz A, Fairbairn M. Neutron stars as dark matter probes. *Phys Rev.* (2010) **D81**:123521.doi: 10.1103/PhysRevD.81.123521
28. Cudell JR, Khlopov MY, Wallemacq Q. Dark atoms and the positron-annihilation-line excess in the galactic bulge. *Adv High Ener Phys.* (2014) **2014**:869425. doi: 10.1155/2014/869425
29. Finkbeiner DP, Weiner N. Exciting dark matter and the INTEGRAL/SPI 511 keV signal. *Phys Rev.* (2007) **D76**:083519. doi: 10.1103/PhysRevD.76.083519
30. Teegarden BJ, Watanabe K, Jean P, Knödlseder J, Lonjou V, Roques JP, et al. INTEGRAL/SPI limits on electron-positron annihilation radiation from the galactic plane. *Astrophys. J.* (2005) **621**:296–300. doi: 10.1086/426859
31. Belotsky K, Khlopov M, Kouvaris C, Laletin M. Decaying Dark Atom constituents and cosmic positron excess. *Adv High Ener Phys.* (2014) **2014**:214258. doi: 10.1155/2014/214258
32. Adriani O, Barbarino GC, Bazilevskaya GA, Bellotti R, Bianco A, Boezio M, et al. Cosmic-Ray Positron Energy Spectrum Measured by PAMELA. *Phys Rev Lett.* (2013) **111**:081102. doi: 10.1103/PhysRevLett.111.081102
33. Aguilar M, Alberti G, Alpat B, Alvino A, Ambrosi G, Andeen K, et al. First result from the alpha magnetic spectrometer on the international space station: precision measurement of the positron fraction in primary cosmic rays of 0.5-350 GeV. *Phys Rev Lett.* (2013) **110**:141102. doi: 10.1103/PhysRevLett.110.141102
34. Aguilar M, Aisa D, Alvino A, Ambrosi G, Andeen K, Arruda L, et al. Electron and positron fluxes in primary cosmic rays measured with the alpha magnetic spectrometer on the international space station. *Phys Rev Lett.* (2014) **113**:121102. doi: 10.1103/PhysRevLett.113.121102
35. Accardo L, Aguilar M, Aisa D, Alpat B, Alvino A, Ambrosi G, et al. High statistics measurement of the positron fraction in primary cosmic rays of 0.5-500 GeV with the alpha magnetic spectrometer

on the international space station. *Phys Rev Lett.* (2014) **113**:121101. doi: 10.1103/PhysRevLett.113.121101
36. Ackermann M, Ajello M, Albert A, Baldini L, Barbiellini G, Bechtol, K, et al. Fermi LAT search for dark matter in gamma-ray lines and the inclusive photon spectrum. *Phys Rev.* (2012) **D86**:022002. doi: 10.1103/PhysRevD.86.022002
37. Belotsky K, Budaev R, Kirillov A, Laletin M. Fermi-LAT kills dark matter interpretations of AMS-02 data. Or not? *J Cosmol Astropart Phys.* (2017) **1701**:021. doi: 10.1088/1475-7516/2017/01/021
38. Kachelriess M, Neronov A, Semikoz DV. Signatures of a two million year old supernova in the spectra of cosmic ray protons, antiprotons and positrons. *Phys Rev Lett.* (2015) **115**:181103. doi: 10.1103/PhysRevLett.115.181103
39. Fairbairn M, Kraan AC, Milstead DA, Sjostrand T, Skands P, Sloan T. Stable massive particles at colliders. *Phys Rep.* (2007) **438**:1. doi: 10.1016/j.physrep.2006.10.002
40. Aad G, Abat E, Abdallah J, Abdelalim AA, Abdesselam A, Abdinov Q, et al. The ATLAS experiment at the CERN large hadron collider. *J Instrumet.* (2008) **3**:S08003. doi: 10.1088/1748-0221/3/08/S08003
41. Aad G, Abajyan T, Abbott B, Abdallah J, Abdel Khalek S, Abdelalim AA, et al. Search for long-lived, multi-charged particles in *pp* collisions at $\sqrt{s} = 7$ TeV using the ATLAS detector. *Phys Lett B* (2013) **722**:305. doi: 10.1016/j.physletb.2013.04.036
42. Aad G, Abbott B, Abdallah J, Abdinov O, Aben R, Abolins M, et al. Search for heavy long-lived multi-charged particles in *pp* collisions at $\sqrt{s} = 8$ TeV using the ATLAS detector. *Eur Phys J C* (2015) **75**:362. doi: 10.1140/epjc/s10052-015-3534-2
43. Chatrchyan S, Hmayakyan G, Khachatryan V, Sirunyan AM, Adam W, Bauer T, et al. The CMS experiment at the CERN LHC. *J Instrument.* (2008) **3**:S08004. doi: 10.1088/1748-0221/3/08/S08004
44. Chatrchyan S, Khachatryan V, Sirunyan AM, Tumasyan A, Adam W, Bauer T, et al. Searches for long-lived charged particles in *pp* collisions at $\sqrt{s} = 7$ and 8 TeV. *J High Energy Phys.* (2013) **1307**:122. doi: 10.1007/JHEP07(2013)122
45. Khlopov MY, Mayorov AG, Soldatov EY. Puzzles of dark matter - more light on dark atoms. *Bled Works Phys.* (2010) **11**:186.

Conflict of Interest Statement: The author declares that the research was conducted in the absence of any commercial or financial relationships that could be construed as a potential conflict of interest.

frontiers in Physics

ORIGINAL RESEARCH
published: 11 March 2019
doi: 10.3389/fphy.2019.00022

Light Scalars in Composite Higgs Models

Giacomo Cacciapaglia[1,2]*, *Gabriele Ferretti*[3], *Thomas Flacke*[4] and *Hugo Serôdio*[5]

[1] Faculté des Sciences, Université de Lyon, Lyon, France, [2] Institut de Physique Nucléaire de Lyon, UMR5822 CNRS/IN2P3, Villeurbanne, France, [3] Department of Physics, Chalmers University of Technology, Göteborg, Sweden, [4] Center for Theoretical Physics of the Universe, Institute for Basic Science, Daejeon, South Korea, [5] Department of Astronomy and Theoretical Physics, Lund University, Lund, Sweden

A composite Higgs boson is likely to be accompanied by additional light states generated by the same dynamics. This expectation is substantiated when realizing the composite Higgs mechanism by an underlying gauge theory. We review the dynamics of such objects, which may well be the first sign of compositeness at colliders. We also update our previous analysis of the bounds from LHC searches to the latest results and discuss the projected reach of the High-Luminosity run.

Keywords: Higgs, composite dynamics, LHC, strong dynamics, collider phenomenology

OPEN ACCESS

Edited by:
António Pestana Morais, University of Aveiro, Portugal

Reviewed by:
Alexander Belyaev, University of Southampton, United Kingdom
Tetsuo Shindou, Kogakuin University, Japan

***Correspondence:**
Giacomo Cacciapaglia
g.cacciapaglia@ipnl.in2p3.fr

Specialty section:
This article was submitted to High-Energy and Astroparticle Physics, a section of the journal Frontiers in Physics

Received: *27 November 2018*
Accepted: *05 February 2019*
Published: *11 March 2019*

Citation:
Cacciapaglia G, Ferretti G, Flacke T and Serôdio H (2019) Light Scalars in Composite Higgs Models. Front. Phys. 7:22. doi: 10.3389/fphy.2019.00022

1. INTRODUCTION

Models of composite Higgs are a valid option for describing new physics beyond the Standard Model (SM). In this approach, the Higgs sector is replaced by confining dynamics, with the merit of solving the problem of hierarchy, as the only mass scale in the sector is dynamically generated, like in quantum chromo-dynamics (QCD). Furthermore, the breaking of the electroweak (EW) symmetry also arises dynamically, in contrast to the SM where it is merely described by a wrong-sign mass term.

The idea of dynamical EW symmetry breaking is as old as the SM itself [1], however in its first form lacked the presence of a light scalar degree of freedom, the Higgs boson. Later, it was proposed that the Higgs may arise as a pseudo-Nambu Goldstone boson (pNGB) of a global symmetry breaking [2]. This latter class of models saw a revival in the 2000's, following the development of holography in warped extra dimensions [3]. A minimal model of composite pNGB Higgs was thus proposed in Agashe et al. [4], and it has since been extensively studied in the literature (see [5–7], and references therein). The Higgs thus arises as a pNGB from the symmetry breaking pattern SO(5)/SO(4), together with the three Goldstones eaten by the W and Z bosons.

A key ingredient is the concept of partial compositeness [8] for the SM fermions, as a means to generate their masses and the SM flavor structures. The generation of a sizeable top-quark mass is particularly challenging and partial compositeness provides a possible solution by mixing the elementary fermions with a composite operator that has a large scaling dimension. This feature, again, follows from the constructions in warped space [9, 10], where the SM fermions mix with bulk ones. We want to stress here that the main motivation behind the introduction of partial compositeness was to address the mass and flavor problems while avoiding the generic appearance of large flavor changing neutral currents among SM fermions. Only later, inspired by the holographic principle [11], did the role of the composite top partners extended to the role of regulators of the loop divergences of the Higgs mass, by assuming the finiteness of the full one loop expression via sum rules [11, 12]. This, in turn, implies the necessity for light and weakly coupled spin-1/2 resonances [12, 13]. Nevertheless, alternatives to regulate the top loops exist, and

the potential generated by such loops can be stabilized by, for instance, the introduction of masses for the underlying fermions [14, 15].

Another approach to composite dynamics, closer in spirit to the origin of the dynamical EW symmetry breaking of Technicolor, consists in defining an underlying theory in terms of gauge and fermion degrees of freedom, that confine at low energies [15]. In this approach, it is not possible to naturally obtain the minimal coset.[1] In turn, once the underlying dynamics is specified, only three kinds of patterns are allowed [19, 20]: SU(N)/Sp(N), SU(N)/SO(N) and SU(N) × SU(N)/SU(N). The minimal model is thus based on SU(4)/Sp(4), which can be obtained with an underlying SU(2) gauge theory [14, 21] and features only 5 pNGBs: the Higgs doublet plus a CP-odd singlet [14, 15]. Other minimal cosets are SU(5)/SO(5) [22] and SU(4) × SU(4)/SU(4) [23].

The inclusion of partial compositeness poses additional constraints in building the model, *in primis* the fact that many additional underlying fermions are needed, therefore loss of asymptotic freedom follows. In Ferretti and Karateev [24], a systematic construction of underling models, with partial compositeness for the top, was done. The main new ingredient was the sequestering of QCD color charges, which need to be carried by the underlying fermions in order to give color to the spin-1/2 resonances, to a new species of fermions, χ, that transforms under a different representation of the confining group than that of the fermions, ψ, giving rise to the composite Higgs. Thus, no dangerous mixing between the EW symmetry breaking and potential color breaking arises. The spin-1/2 bound states, therefore, arise as "chimera baryons" [25] made of $\psi\psi\chi$ or $\psi\chi\chi$, depending on the model. There are few other cases where partial compositeness can be achieved with a single species of fermions: a confining SU(3) gauge symmetry with fermions in the fundamental, *à la* QCD, as proposed in Vecchi [26]; SU(6) with fermions in the two-index anti-symmetric representation and E_6 with the **27**. The QCD colored fermions, in the latter cases, act as "heavy flavors", in order to avoid light QCD colored pNGBs.

Phenomenologically, the most interesting feature of this class of underlying theories is the fact that global symmetries in the effective low-energy model are determined. In particular, one realizes that a symmetry comprising of QCD is unavoidable. Furthermore, there is always a non-anomalous U(1) charge, acting on both species of fermions, which is broken by (at least) the chiral condensate in the EW (Higgs) sector of the theory. This results in one light pNGB singlet under all the SM gauge symmetries. This state may be the lightest of the pNGB spectra, as it typically does not receive any mass contribution from top and gauge loops [27]. The properties of this state have been studied in Cai et al. [28], Belyaev et al. [29], Belyaev et al. [27], DeGrand et al. [30], and Cacciapaglia et al. [31]. At the LHC, it can be copiously produced via gluon fusion with the coupling to gluons being generated by the Wess-Zumino-Witten anomaly term [32, 33] via the presence of the χ-fermions in the pNGB wave function. Couplings to other pNGBs and tops can also be predicted, once the underlying theory is specified. Furthermore, they can be produced via the decays of the top partner resonances [34]. The fact that the properties of this state can be predicted in terms of the underlying theory, and their potential lightness, is the most attractive feature. As a historical note, they were perfect candidates to explain the WW/WZ resonance at 2 TeV Cai et al. [28] and the $\gamma\gamma$ resonance at 750 GeV [29] hinted at by the LHC data, which later appeared to have been statistical fluctuations. Other light states comprise of additional EW-charged pNGBs arising from the Higgs sector, and QCD-colored states coming from the condensation of the χ's.

In this work, we will mainly focus on the singlet pNGB associated to the global U(1) symmetry. If both fermion species condense, it is accompanied by a second pseudo-scalar singlet associated to the anomalous U(1) charges. The latter will receive a mass term from the anomaly, in a similar fashion to the η' in QCD. Nevertheless, it may be relatively light, as expected at large-N_c for instance. We will therefore consider the phenomenology at the LHC to come from the presence of both states. This work follows Belyaev et al. [27] closely, and our main new contribution is the update of the bounds to the latest LHC searches, and the addition of projections at the High-Luminosity-LHC (HL-LHC) run. We will see that the bounds on the compositeness scale derived from the non-discovery of such a state can be much stronger than the typical bounds from electroweak-precision tests. The latter are usually considered the main constraints on models of Composite Higgs. Conversely, they appear to have the best prospects for being discovered at the LHC. The HL-LHC run will be crucial in this case, due to the lightness of such states and the paucity of current searches focusing on the low mass region between 14 and 65 GeV.

Before presenting our results, we should stress that these theories are not full Ultra-Violet (UV) completions of composite Higgs models with partial compositeness. One point is that the number of fermions we can introduce before loosing confinement (asymptotic freedom) is limited, thus one can only have enough to give mass to the top quark in this way. Furthermore, the theory needs to lie outside the conformal Infra-Red (IR) window [35]. It was shown that only 12 models are consistent with these requirements, while having the minimal Higgs cosets [36]. The second point is that the origin of the four-fermion interactions giving rise to the mixing between the SM tops and the composite fermions is not explained. Finally, the consistency of flavor bounds usually requires the theory to enjoy an IR conformal phase right above the condensation scale. This allows to split the scale where the masses of light quarks and leptons are generated from the confinement scale [37, 38], which should not be far from the TeV. In the underlying theory under study, this can be achieved by adding a few additional fermions at a mass close to the condensation scale, such that the theory above this scale is right inside the conformal window. Being just above the lower edge of the conformal window is crucial if one needs the composite fermions to have large anomalous dimensions, as the theory is expected to be strongly interacting around the IR fixed point near the lower edge of the conformal window. A first step

[1] Constructions based on Nambu Jona-Lasinio models with four-fermion interactions [16] or based on Seiberg dualities [17] have been proposed in the literature. See also the attempt in Setford [18].

toward the construction of truly UV complete theories can be found in Cacciapaglia et al. [39], based on the potential presence of a UV safe fixed point, due to large multiplicities of fermions.

As a final introductory word, we should also mention one main benefit of this approach: once an underlying theory is defined, it can be studied on the lattice. Thus, spectra and various properties of the theory in the strong sector can, in principle, be computed. This includes low-energy constants, which are crucial for the generation of the Higgs misalignment potential and the Higgs boson mass [40]. So far, theories based on confining SU(4) [25, 41] and Sp(4) [42–45] are being studied. For SU(4), preliminary results on the spectra [25] show that the chimera baryons tend to be heavy and beyond the reach of the LHC, while first calculations of the relevant form factors Ayyar et al. (Unpublished) show a suppressed mixing to the top. This would disqualify them as "light" top partners that regulate the Higgs mass loop [12, 13], however they would still play a role in generating the top mass and help with the flavor issue. It should be mentioned however that current lattice results do not yet include a realistic multiplicity of fermions, which may be crucial as the realistic models are close to the conformal window. Finally, we mention the possibility that spin-1/2 resonances may arise as a bound state between a fermion and a scalar, both carrying underlying color charges [46] (see also [17]). The price to pay, in this case, is the presence of fundamental scalars in the theory (unless the underlying scalars arise themselves as bound states of a theory that confines at higher energies or are protected by supersymmetry at high scales).

The paper is organized as follows: in section 2 we recap the main properties of the 12 underlying models. In section 3 we summarize the main properties of the pseudo-scalars associated with the two spontaneously broken U(1) global symmetries and present the updated bounds on the singlet pNGBs in section 4. We offer our conclusions in section 5.

2. UNDERLYING MODELS FOR A COMPOSITE HIGGS WITH TOP PARTIAL COMPOSITENESS

In this work we are interested in the underlying models for composite Higgs with top partial compositeness defined in Ferretti and Karateev [24]. These models characterize the underlying dynamics below the condensation scale $\Lambda \approx 4\pi f$, f being the decay constant of the pNGBs. As such, the need to be outside of the conformal window leaves only 12 models [36], listed in **Table 1**. They are defined in terms of a confining gauge interaction, that we call hypercolor (HC), and two species of fermions in two different irreducible representations of the HC. The two species of fermions play different roles: the EW charged ψ's generate the Higgs and the EW symmetry breaks upon condensation, and their multiplicity is chosen to match the minimal cosets; the QCD charged χ's consist of a triplet and an anti-triplet of QCD color, thus always amounting to 6 Weyl spinors. We will also assume that both fermions condense and thus the chiral symmetry in each sector is broken. In principle, the χ's may not condense and the 't Hooft anomaly matching condition may lead to the presence of light composite fermions, that may play the role of top partners [47]. However, assuming the persistent mass condition, it is possible to show that chiral symmetry breaking must occur in both cosets [36]: the argument goes that by giving a common mass to one class of fermions at a time, the chimera baryons that saturate the global 't Hooft anomaly would become massive and thus ineffective. The final answer can only be found on the lattice. The phenomenology of two of the models have been studied in detail, M8 in Barnard et al. [48] and M6 in Ferretti [49]. Lattice studies for the two models are also underway based on $SU(4)_{HC}$ [25] (which also applies to M11), and $Sp(4)_{HC}$ [44, 45] (which also applies to M5). Note that a study based on a Nambu Jona-Lasinio effective model of M8 can be found in Bizot et al. [50]. As shown in **Table 1**, the baryons that enter partial compositeness for the top arise either as $\psi\psi\chi$ or $\psi\chi\chi$ bound states, depending on the representations under HC.

It is expected that the lightest states in these models are the pNGBs, that arise from the breaking of the chiral symmetries in the two sectors, while the fermionic and spin-1 resonances are expected to be heavier. The quantum numbers of the pNGBs in the 12 models are listed in **Table 2**. They can be organized in three classes:

A) The ones arising from the EW coset, i.e., the chiral symmetry breaking in the ψ sector, only carry EW quantum numbers. All cosets contain at least one singlet, thus being non-minimal compared to the holographic SO(5)/SO(4) model. The production rate of these states at the LHC is typically very small, as it is due to EW interactions, and thus are very difficult to observe at the LHC. The neutral components may also couple to two gluons via loops of tops, however still give rise to small production rates. The case of the singlet in the SU(4)/Sp(4) coset has been studied in detail in Galloway et al. [14] and Arbey et al. [51], note however that the same considerations apply to singlets in the other cosets. The SU(5)/SO(5) case can be found in Ferretti [49, 52]. Finally, the $SU(4)^2/SU(4)$ case is special compared to the other two, as it allows for a stable pNGB that may play the role of Dark Matter [53].

B) The ones arising from the chiral breaking in the χ sector, i.e., QCD coset, always carry QCD charges. A ubiquitous member of this class is a neutral color octet [27, 54]. For all those pNGBs, pair production via QCD interactions can be substantial at the LHC [55] for masses below or around 1 TeV. The phenomenology of the color sextet in the context of model M8 has been studied in Cacciapaglia et al. [54]. After Run-I at the LHC, the bound on their masses can be estimated around the 1 TeV scale. This bound is still compatible with the fact that one-loop self-energy diagrams, involving a gluon, put their masses roughly in that range.

C) The U(1) singlets are ubiquitous to all models. Their phenomenology has been studied in detail in Belyaev et al. [27]. They will be the main focus of this work. While they are singlets under the gauge symmetries of the SM, couplings arise via the topological WZW anomalies, which include coupling to gluons. In this, they differ from the EW

TABLE 1 | Model details.

Coset	HC	ψ	χ	$-q_\chi/q_\psi$	Baryon	Name	Lattice
$\frac{SU(5)}{SO(5)} \times \frac{SU(6)}{SO(6)}$	SO(7)	$5 \times \mathbf{F}$	$6 \times \boldsymbol{Sp}$	5/6	$\psi\chi\chi$	M1	
	SO(9)			5/12		M2	
	SO(7)	$5 \times \boldsymbol{Sp}$	$6 \times \mathbf{F}$	5/6	$\psi\psi\chi$	M3	
	SO(9)			5/3		M4	
$\frac{SU(5)}{SO(5)} \times \frac{SU(6)}{Sp(6)}$	Sp(4)	$5 \times \mathbf{A_2}$	$6 \times \mathbf{F}$	5/3	$\psi\chi\chi$	M5	✓
$\frac{SU(5)}{SO(5)} \times \frac{SU(3)^2}{SU(3)}$	SU(4)	$5 \times \mathbf{A_2}$	$3 \times (\mathbf{F}, \bar{\mathbf{F}})$	5/3	$\psi\chi\chi$	M6	✓
	SO(10)	$5 \times \mathbf{F}$	$3 \times (\boldsymbol{Sp}, \overline{\boldsymbol{Sp}})$	5/12		M7	
$\frac{SU(4)}{Sp(4)} \times \frac{SU(6)}{SO(6)}$	Sp(4)	$4 \times \mathbf{F}$	$6 \times \mathbf{A_2}$	1/3	$\psi\psi\chi$	M8	✓
	SO(11)	$4 \times \boldsymbol{Sp}$	$6 \times \mathbf{F}$	8/3		M9	
$\frac{SU(4)^2}{SU(4)} \times \frac{SU(6)}{SO(6)}$	SO(10)	$4 \times (\boldsymbol{Sp}, \overline{\boldsymbol{Sp}})$	$6 \times \mathbf{F}$	8/3	$\psi\psi\chi$	M10	
	SU(4)	$4 \times (\mathbf{F}, \bar{\mathbf{F}})$	$6 \times \mathbf{A_2}$	2/3		M11	✓
$\frac{SU(4)^2}{SU(4)} \times \frac{SU(3)^2}{SU(3)}$	SU(5)	$4 \times (\mathbf{F}, \bar{\mathbf{F}})$	$3 \times (\mathbf{A_2}, \overline{\mathbf{A_2}})$	4/9	$\psi\psi\chi$	M12	

*The first column shows the EW and QCD color cosets, respectively, followed by the representations under the confining hypercolor (HC) gauge group of the EW sector fermions ψ and the QCD colored ones χ. The $-q_\chi/q_\psi$ column indicates the ratio of charges of the fermions under the non-anomalous U(1) combination, while "Baryon" indicate the typical top partner structure. The column "Name" contains the model nomenclature from Belyaev et al. [27], while the last column marks the models that are currently being considered on the lattice. Note that **Sp** indicates the spinorial representation of SO(N), while **F** and $\mathbf{A_2}$ stand for the fundamental and two-index anti-symmetric representations.*

TABLE 2 | Light pNGBs in each of the 12 models.

Model	EW coset					QCD coset					a	η'
	$2_{\pm 1/2}$	3_0	$3_{\pm 1}$	1_0	$1_{\pm 1}$	8_0	$\bar{3}_{2/3}$	$\bar{3}_{4/3}$	$6_{2/3}$	$6_{4/3}$		
M1	1	1	1	1	-	1	-	-	1	-	1	1
M2	1	1	1	1	-	1	-	-	1	-	1	1
M3	1	1	1	1	-	1	-	-	-	1	1	1
M4	1	1	1	1	-	1	-	-	-	1	1	1
M5	1	1	1	1	-	1	1	-	-	-	1	1
M6	1	1	1	1	-	1	-	-	-	-	1	1
M7	1	1	1	1	-	1	-	-	-	-	1	1
M8	1	-	-	1	-	1	-	-	-	1	1	1
M9	1	-	-	1	-	1	-	-	-	1	1	1
M10	2	1	-	2	1	1	-	-	-	1	1	1
M11	2	1	-	2	1	1	-	-	-	1	1	1
M12	2	1	-	2	1	1	-	-	-	-	1	1

For the EW coset ($\psi\psi$ condensate), we list the $SU(2)_L$ multiplets with their hypercharge, for the QCD coset ($\chi\chi$ condensate) the QCD representation and hypercharge. We remark that the only ubiquitous ones are the color octet and the two U(1) singlets, plus one singlet in the EW coset.

cosets, where couplings to gluons can only arise via top loops. We can therefore expect larger production rates for them.

All models in M1-M12 preserve custodial symmetry. Indeed, this requirement is central in their construction and determines the minimum amount of fermionic matter present in each model. For custodial symmetry to be preserved one needs to be able to embed a $SU(2)_L \times SU(2)_R$ group into the unbroken group H of the electroweak cosets G/H. This requirement is satisfied by choosing $H = SO(N_o)$ with $N_o \geq 4$, $H = Sp(2N_p)$ with $N_p \geq 2$ or $H = SU(N_u)$ with $N_u \geq 4$. However, the further requirement that there be a Higgs field in the bi-fundamental of $SU(2)_L \times SU(2)_R$, requires to take $N_o \geq 5$. Thus, $\rho = 1$ at tree level in these constructions, as long as the triplet pNGBs (when present), do not acquire a vacuum expectation value.

3. LIGHT U(1) PSEUDO-SCALARS

In this section we summarize the main properties of the two U(1) pseudo-scalars, one of which associated with non-anomalous global symmetry. Most of the results shown in this section can be

found in Belyaev et al. [27], where a more detailed analysis can be found. We refer to other results in the literature when necessary. This section can be considered a *handbook* for anybody who is interested in studying the phenomenology of such states, as we will provide all the relevant couplings and formulas necessary to compute cross-sections and branching ratios.

Following the notation in Belyaev et al. [27], we call two mass eigenstates $\{a, \eta'\}$, with a being the lighter one, which is also closer to the anomaly-free U(1) boson. The masses, which also determine the mixing angle between the two states, receive three contributions: two from the masses of the underlying fermions ψ and χ, and one from the anomalous U(1) combination. Assuming that $m_\chi \gg m_\psi$, and neglecting the latter, the mixing angle can be determined in terms of the mass eigenvalues. We define the mixing angle α between the mass eigenstates and the pseudo-scalars associated to the $U(1)_\psi$ and $U(1)_\chi$ charges. Thus, in the decoupling limit $M_{\eta'} \gg M_a$, the mixing angle is given by

$$\sin\alpha|_{dec.} = -1/\sqrt{1+\frac{q_\psi^2 N_\psi}{q_\chi^2 N_\chi}\frac{f_\psi^2}{f_\chi^2}}\,, \tag{1}$$

where q_ψ and q_χ are the charges of the anomaly-free U(1) (see **Table 1**), $f_{\psi,\chi}$ are the decay constants in the two sectors, and $N_{\psi,\chi}$ their multiplicity. Note that only the ratio f_ψ/f_χ is not fixed but depends on the strong dynamics (thus calculable on the lattice [25]). However, we can fix it by applying the Maximal Attractive Channel (MAC) hypothesis [56], see Table 3 in **Appendix A**. Once this is fixed, all the couplings of the pseudo-scalars to SM states are fixed in terms of the properties of the underlying dynamics, as we will show below.

The relevant effective Lagrangian for both pseudo-scalars, i.e., $\phi = \{a, \eta'\}$, can be generically parameterized as

$$\begin{aligned}\mathcal{L}_{\rm eff} \supset & \frac{1}{2}(\partial_\mu\phi)(\partial^\mu\phi) - \frac{1}{2}m_\phi^2\phi^2 \\ & + \frac{\phi}{16\pi^2 f_\psi}\big(g_s^2 K_g^\phi G^a_{\mu\nu}\tilde{G}^{a\mu\nu} \\ & + g^2 K_W^\phi W^i_{\mu\nu}\tilde{W}^{i\mu\nu} + g'^2 K_B^\phi B_{\mu\nu}\tilde{B}^{\mu\nu}\big) \\ & - i\sum_f \frac{C_f^\phi m_f}{f_\psi}\phi\bar{\psi}_f\gamma^5\psi_f \\ & + \frac{2v}{f_\psi^2}K_{\phi h}^{\rm eff}\left(\partial_\mu\phi\right)\left(\partial^\mu\phi\right)h + \frac{2m_Z}{f_\psi}K_{hZ}^{\rm eff}\left(\partial_\mu\phi\right)Z^\mu h\end{aligned} \tag{2}$$

with $\tilde{F}^{\mu\nu} = \frac{1}{2}\epsilon^{\mu\nu\rho\sigma}F^{\rho\sigma}$ for $F = \{G^a, W^i, B\}$. Note that we have normalized the couplings with the decay constant in the Higgs sector, f_ψ, which is directly related to the tuning in the misalignment potential as $v = f_\psi \sin\theta$ [27]. We could also have defined a U(1)-singlet decay constant

$$f_a = \sqrt{\frac{q_\psi^2 N_\psi f_\psi^2 + q_\chi^2 N_\chi f_\chi^2}{q_\psi^2 + q_\chi^2}}\,, \tag{3}$$

as in Cacciapaglia et al. [31]. The relation between the two decay constants is given in Table 3.

The Lagrangian in Equation (2) matches with a generic Axion-Like Particle (ALP) Lagrangian [57–59], except that the various coefficients can be computed. The couplings in the last two lines are generated by loops of tops and gauge bosons (dominantly), but differ from the results from a generic ALP Lagrangian [59, 60] due to non-linear couplings of the pNGBs in the composite models [31]. In the following, we shall review how each of the terms in the effective Lagrangian can be calculated. All the numerical coefficients, in the decoupling limit and in the minimal mass splitting limit, are given in Tables 3, 4 in **Appendix A**. The numbers we provide here assume the MAC relation between the decay constants, as used in Cacciapaglia et al. [31], while the values in Belyaev et al. [27] assume $f_\psi = f_\chi$.

The computability of all the coefficients is one of the main appeals of these models, having an underlying gauge theory construction. For each model that has a fixed gauge group and representation for the underlying fermions, once a discrete choice of the representation of the top partners under the global symmetry is done, the phenomenology of the pseudo-scalars is determined in terms of only three independent continuous parameters (the masses m_ϕ with $\phi = a\,, \eta'$ and a common decay constant f_ψ). All the couplings and ratios of the decay constants for the various cosets can be computed as shown in Tables 3, 4 in **Appendix A**. The only assumption we make is that the tops couple dominantly to only one composite operator.

3.1. Couplings to Gauge Bosons

The general couplings of the singlet pseudo-scalars to gauge bosons are almost entirely dictated by the quantum numbers of the underlying dynamics, i.e.,

$$K_V^a = c_5\left(\frac{C_V^\psi}{\sqrt{N_\psi}}\cos\alpha + \frac{f_\psi}{f_\chi}\frac{C_V^\chi}{\sqrt{N_\chi}}\sin\alpha\right)\,, \tag{4}$$

with $K_V^{\eta'}$ obtained from the above expression with the replacement $\alpha \to \alpha + \pi/2$. In the above expression, $c_5 = \sqrt{2}$ for models with $SU(5)/SO(5)$ breaking and 1 otherwise, $C_V^{\psi,\chi}$ are the anomaly coefficients of the singlets associated with $U(1)_{\chi,\psi}$ groups which are fully determined by the SM charges of the underlying fermions[2]. Thus, the only dependence on the mixing angle α remains, which is determined by the masses of the two states. In the Tables in **Appendix A** we give values in the two limiting cases of minimal mass splitting and decoupling.

One can rewrite the WZW interactions in terms of the physical gauge bosons, i.e.,

$$\begin{aligned}\mathcal{L}_{\rm eff} \supset & \frac{\phi}{16\pi^2 f_\psi}\Big(g_s^2 K_{gg}^\phi G^a_{\mu\nu}\tilde{G}^{a\mu\nu} + g^2 K_{WW}^\phi W^+_{\mu\nu}\tilde{W}^{-\mu\nu} \\ & + e^2 K_{\gamma\gamma}^\phi F_{\mu\nu}\tilde{F}^{\mu\nu} + \frac{e^2}{s_W^2 c_W^2}K_{ZZ}^\phi Z_{\mu\nu}\tilde{Z}^{\mu\nu} \\ & + \frac{2e^2}{s_W c_W}K_{Z\gamma}^\phi F_{\mu\nu}\tilde{Z}^{\mu\nu}\Big)\end{aligned} \tag{5}$$

[2]See Table 3 in **Appendix A** of Belyaev et al. [27] for a list of coefficients in all models.

with

$$K^{\phi}_{\gamma\gamma} = K^{\phi}_W + K^{\phi}_B\,, \quad K^{\phi}_{Z\gamma} = c^2_W K^{\phi}_W - s^2_W K^{\phi}_B\,, \\ K^{\phi}_{ZZ} = c^4_W K^{\phi}_W + s^4_W K^{\phi}_B\,. \tag{6}$$

The couplings of a and η' to gauge bosons are thus determined purely from the underlying dynamics with one assumption, i.e., the validity of the MAC hypothesis. The only external dependence arises from the masses via the mixing angle α. Table 3 in **Appendix A** shows the resulting couplings of a and η' for all 12 underlying models. Typically, in a generic mixing angle, the couplings vary between the two limits shown.

The couplings to two-gauge bosons also receive contributions at loop-level, in particular from top-loops, which are particularly relevant at low masses and can affect the production rate via gluon fusion and the decays. These contributions were fully computed in Belyaev et al. [27], and their effect expressed in terms of the Branching Ratio formulas:

$$\Gamma(\phi \to \text{had}) = \frac{\alpha_s^2(m_\phi)\, m_\phi^3}{8\pi^3 f_\psi^2}\left[1 + \frac{83}{4}\alpha_s(m_\phi)\right] \\ \times \left|K^{\phi}_{gg} + C^{\phi}_t\, \mathcal{C}_0\left(0, \tau_{\phi/t}, 0; 1\right)\right|^2 \tag{7a}$$

$$\Gamma(\phi \to \gamma\gamma) = \frac{\alpha^2\, m_\phi^3}{64\pi^3 f_\psi^2}\left|K^{\phi}_{\gamma\gamma} + \frac{8}{3}C^{\phi}_t\, \mathcal{C}_0\, \left(0, \tau_{\phi/t}, 0; 1\right)\right|^2 \tag{7b}$$

$$\Gamma(\phi \to WW) = \frac{\alpha^2\, m_\phi^3\left(1 - 4\tau_{W/\phi}\right)^{3/2}}{32\pi^3 f_\psi^2 s_W^4} \\ \times \left|K^{\phi}_{WW} - \frac{3}{2}C^{\phi}_t\, \mathcal{C}_{1+2}\left(\tau_{W/t}, \tau_{\phi/t}, \tau_{W/t}; \sqrt{\tau_{b/t}}\right)\right|^2 \tag{7c}$$

$$\Gamma(\phi \to Z\gamma) = \frac{\alpha^2\, m_\phi^3\left(1 - \tau_{Z/\phi}\right)^3}{32\pi^3 f_\psi^2 s_W^2 c_W^2} \\ \times \left|K^{\phi}_{Z\gamma} + C^{\phi}_t\left(1 - \frac{8}{3}s_W^2\right)\mathcal{C}_0(\tau_{Z/f}, \tau_{\phi/t}, 0; 1)\right|^2 \tag{7d}$$

$$\Gamma(\phi \to ZZ) = \frac{\alpha^2\, m_\phi^3\left(1 - 4\tau_{Z/\phi}\right)^{3/2}}{64\pi^3 f_\psi^2 s_W^4 c_W^4} \\ \left|K^{\phi}_{ZZ} + C^{\phi}_t\left[s_W^2\left(\frac{8}{3}s_W^2 - 2\right)\mathcal{C}_0\left(\tau_{Z/t}, \tau_{\phi/t}, \tau_{Z/t}; 1\right)\right.\right. \\ \left.\left. -\frac{3}{4}\mathcal{C}_{1+2}\left(\tau_{Z/t}, \tau_{\phi/t}, \tau_{Z/t}; 1\right)\right]\right|^2 \tag{7e}$$

with $\tau_{a/b} = m_a^2/m_b^2$ and $\mathcal{C}_i(\tau_{p_1/t}, \tau_{p_{1+2}/t}, \tau_{p_2/t}; \sqrt{\tau_{f/t}}) \equiv m_t^2 \mathbf{C}_i(p_1^2, (p_1 + p_2)^2, p_2^2; m_f, m_t, m_t)$ the Passarino-Veltman functions with the normalization given in `Package-X` [61]. We have used the short-hand notation $\mathcal{C}_{1+2} \equiv \mathcal{C}_1 + \mathcal{C}_2$ and analytical expression for some of the simplest loop function can be found in Belyaev et al. [27]. C^{ϕ}_t is the coupling to tops, which is discussed in the following subsection.

3.2. Coupling to Tops, Light Quarks, and Leptons

The coupling to tops only depends on the charges under the two U(1)'s of the composite operators that mix to the left-handed and right-handed tops. If we assume that the two top chiralities mix dominantly to one operator, there are only six possible charges that enter the coupling to tops via the top mass operator:

$$(n_\psi, n_\chi) = (\pm 4, 2)\,, \quad (0, \pm 2)\,, \quad (\pm 2, 0)\,, \quad \text{for } \psi\psi\chi\,, \tag{8}$$

$$(n_\psi, n_\chi) = (2, \pm 4)\,, \quad (0, \pm 2)\,, \quad (\pm 2, 0)\,, \quad \text{for } \psi\chi\chi\,, \tag{9}$$

where n_ψ and n_χ are the net numbers of ψ and χ fields, respectively in the two operators coupling to the two top chiralities (see Belyaev et al. [27] for more details). Thus, the C^a_t coefficient reads

$$C^a_t = c_5\left(\frac{n_\psi}{\sqrt{N_\psi}}\cos\alpha + \frac{n_\chi}{\sqrt{N_\chi}}\frac{f_\psi}{f_\chi}\sin\alpha\right). \tag{10}$$

Like above, $C^{\eta'}_t$ is given by $\alpha \to \alpha + \pi/2$.

For the light quarks and leptons, we will assume, for simplicity, that their mass is coming from a direct coupling to a bilinear of ψ's, i.e., via an effective Yukawa coupling. This corresponds to the top case, but with fixed $\{n_\psi, n_\chi\} = \{2, 0\}$.

The coupling to tops above has been computed by writing the effective operators generating the top mass, as in Golterman and Shamir [40] and Golterman and Shamir [62]. However, in Bizot et al. [34] it was noted that computing the coupling of the pseudo-scalars starting from the mixing to the top partners would lead to a different expression, differing by the presence of the mixing angles in the partial compositeness. For the top this has a minor impact on the numerical results, and we therefore chose to remain using the operator case.

3.3. Loop-induced Couplings to the Higgs and to *Zh*

Models with a pseudo-scalar state generically contain a coupling to Zh [60], which is generated at loop level. In our models, the leading contributions to the effective coupling between the singlet pseudo-scalars, Z and Higgs bosons are given by the diagrams in **Figure 1** [31]. Explicit calculation for the coupling $K^{\phi\,\text{eff}}_{hZ}$ defined in Equation (2) gives:

$$K^{\phi\,\text{eff}}_{hZ} = \frac{3m_t^2}{32\pi^2 v m_Z} C^{\phi}_t\left[2(\kappa_t - \kappa_Z)\mathcal{B}_0(\tau_{\phi/t}) - \kappa_t\left(\mathcal{B}_0(\tau_{h/t})\right.\right. \\ - \mathcal{B}_0(\tau_{\phi/t}) + (4 - \tau_{Z/t})\mathcal{C}_0(\tau_{\phi/t}, \tau_{h/t}, \tau_{Z/t}; 1) \\ \left.\left. +(\tau_{\phi/t} + \tau_{h/t} - \tau_{Z/t})\mathcal{C}_1(\tau_{\phi/t}, \tau_{h/t}, \tau_{Z/t}; 1)\right)\right] \tag{11}$$

with $\mathcal{B}_0(\tau_{p/t}) \equiv \mathbf{B}_0(p^2; m_t, m_t)$, see Belyaev et al. [27] for the analytic expression. In the formula, the κ_t and κ_Z are the corrections to the Higgs coupling to tops and Z, respectively, normalized by the SM value. The loop function $\mathbf{B}_0$ is UV-divergent and we have parameterized it in terms of a cutoff, i.e., $1/\epsilon \to -1 + \ln(16\pi^2 f_\psi^2/\mu^2)$. Note that the UV-sensitivity is only present in the term proportional to $(\kappa_t - \kappa_Z)$, which reflects the

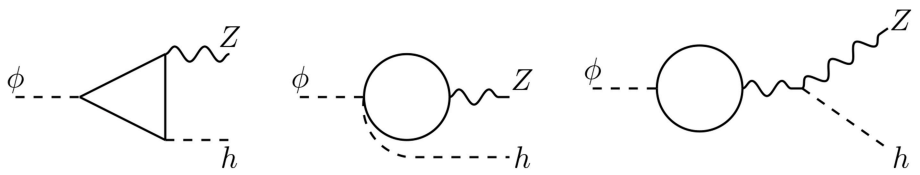

FIGURE 1 | Leading contributions to the decay $\phi \to Zh$.

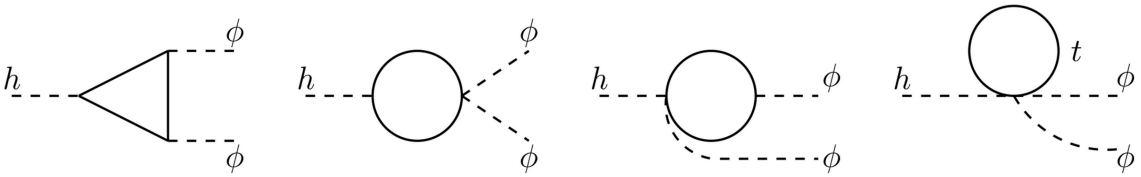

FIGURE 2 | Leading contributions to the decay $h \to \phi\phi$.

non-linearities in the Higgs couplings, a common feature in all composite Higgs models. The partial width for the pseudo-scalar decay gives

$$\Gamma(\phi \to hZ) = \frac{m_\phi^3}{16\pi f_\psi^2} \left| K_{hZ}^{\phi\,\text{eff}} \right|^2 \lambda(1, \tau_{Z/\phi}, \tau_{h/\phi})^{3/2} \tag{12}$$

with $\lambda(x, y, z)$ the Källén function. For very light pseudo-scalars the decay $h \to \phi Z$ is allowed, with a partial width given by the formula above, with the replacement of $m_\phi \leftrightarrow m_h$.

At loop level, a coupling $h\phi^2$ is also generated. This is relevant for $m_\phi < m_h/2$, for which Higgs decays into two pseudo-scalars are open. Explicit calculation of the leading diagrams, shown in **Figure 2**, gives

$$K_{\phi h}^{\text{eff}} = \frac{3\kappa_t}{8\pi^2} \left(\frac{C_t^\phi m_t}{v} \right)^2 \left[\mathcal{B}_0(\tau_{\phi/t}) + 2\,\mathcal{C}_0(\tau_{\phi/t}, \tau_{h/t}, \tau_{\phi/t}; 1) + \frac{1}{1 - 2\tau_{a/h}} \left(\mathcal{B}_0(\tau_{h/t}) - \mathcal{B}_0(\tau_{a/t}) \right) \right]. \tag{13}$$

The Higgs decay to two pseudo-scalars is then given by[3]

$$\Gamma(h \to \phi\phi) = \frac{v^2 m_h^3}{32\pi f_\psi^4} \left| K_{\phi h}^{\text{eff}} \right|^2 \left(1 - 2\tau_{\phi/h}\right)^2 \sqrt{1 - 4\tau_{\phi/h}}\,. \tag{14}$$

4. LHC BOUNDS AND HIGH-LUMINOSITY PROJECTIONS

The presence of the light composite pseudo-scalars can be tested at the LHC via the single production via gluon fusion, which is the dominant production mode, and further decays into a resonant pair of SM states. In this work we include both the effect from the WZW direct coupling to gluons, and the contribution of top and bottom loops. The cross-section calculation is performed at NLO in QCD by use of the `HIGLU` [63] code. For the tops, as shown above, we have six possible top partner assignment choices: following Belyaev et al. [27] and Cacciapaglia et al. [31], in the numerical results we chose the case $\{n_\psi, n_\chi\} = \{2, 0\}$. A discussion of the effect of other choices can be found in **Appendix B**.

The strategy for applying bounds follows Belyaev et al. [27]. We collected all available searches, looking for resonant final states that may come from the pseudo-scalars, and extract a bound from the production cross section times branching ratio, assuming that the efficiencies of the experimental searches are the same on our model. This is a reasonable assumption, as the searches are mainly sensitive to the resonant nature of the signal, and much less on the possible kinematical differences in the production. Furthermore, we do not attempt to do a statistical combination of various searches, as we cannot take into account correlations of the systematic uncertainties in the experiments. Thus, we simply consider the most constraining search or signal region to extract a bound from for each final state. The final result is shown in **Figure 3** for two representative models, M8 and M9. What connects the two is the fact that the global symmetries are the same, thus they can be characterized by the same low energy effective action based on the minimal SU(4)/Sp(4) EW coset and SU(6)/SO(6) QCD coset. However, as shown in the plot, the properties of the two pseudo-scalars are very different, hence leading to very different bounds. Note that we have re-expressed the bound on the cross sections into a bound on the decay constant of the Higgs. This is possible because all the coefficients of the couplings are calculable, as detailed in the previous section.

Before commenting on the numerical results, we will list here all the searches we implemented.

i) The $t\bar{t}$ final state is only relevant for large masses and indicated in orange (Run-II at 13 TeV) and green (Run-I at 8 TeV) on the side-bands of the plots. We implemented a

[3]There is also an additional contribution coming from the diagrams in **Figure 2** that is proportional to p_h^2. This signals the presence of an effective term of the form $\phi^2 \Box h$, however, such contribution is always negligible.

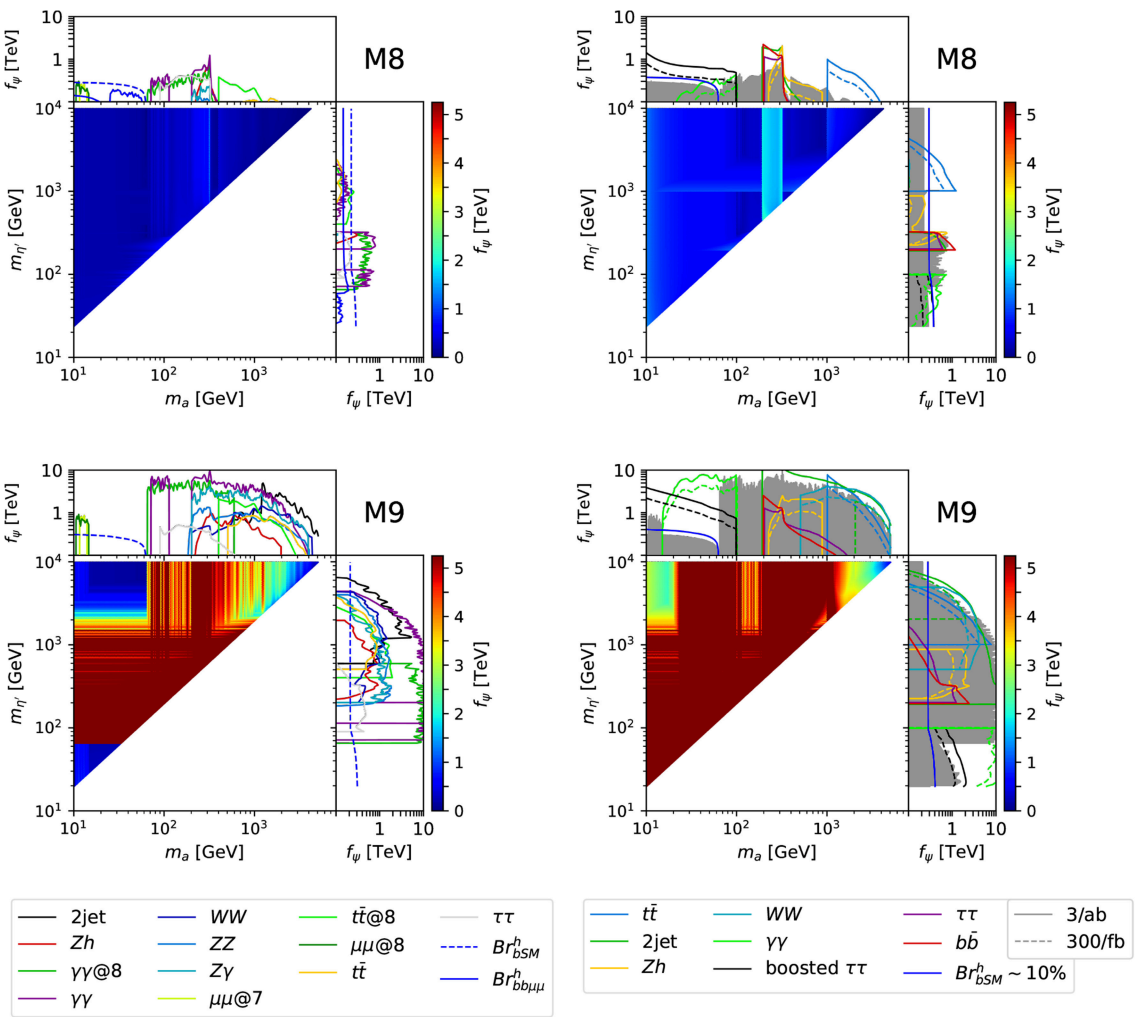

FIGURE 3 | Heat-plots showing the lower bounds on the Higgs decay constant f_ψ in the mass plane of the two pseudo-scalars. The white triangle is not accessible by the masses in each model. The side-bands show the limits from each individual final state. On the left column, we show the current Run-I and Run-II bounds; on the right column, we show the projections at the High-Luminosity LHC run (the solid gray band summarizes the current bounds for comparison). More details in the text. Here we show model M8 (top row) and model M9 (bottom row).

fully hadronic Run-II search by CMS [64], and two Run-I searches by CMS [65] (fully reconstructed tops) and ATLAS [66] (semi-leptonic).

ii) Di-jet searches (black line) can tag the di-gluon decay, however they are only sensitive at relatively large masses because of trigger limitations. We implemented Run-II searches by CMS [67, 68] and ATLAS [69].

iii) Di-boson final states, i.e., WW (dark blue line) and ZZ (light blue line), are mostly relevant above $\approx$ 160 GeV, when resonant decays are kinematically allowed. Many different final states are searched for at the LHC. We include the following Run-II searches by CMS [70–77] and ATLAS [78–81].

iv) Di-photon resonances in this model are as important at low mass as at high mass, because they are generated at the same level as the decays to massive gauge bosons. We show in green the results at Run-I at 8 TeV, and in violet the ones at Run-II at 13 TeV. The implemented searches for ATLAS are at Run-I [82] and at Run-II [83]. For CMS, we use the combined Run-I + Run-II results for high mass [84, 85] and low mass [86, 87] ranges.

v) Similarly, γZ resonant search (cyan line) has an impact at high mass. We implemented the Run-II searches from CMS [88, 89] and ATLAS [90].

vi) A new channel we include in this work, which was previously missed in Belyaev et al. [27], is Zh. The limit, shown by the red line, corresponds to the ATLAS search [91]. This channel is always significantly above he threshold, but usually loses significance at the $t\bar{t}$ threshold.

vii) At the LHC, resonant di-tau searches have been performed for invariant masses above 90 GeV. The limit, shown by the gray line, however, typically plays a limited role because

the branching ratio in taus is small at such mass values. We implemented the following Run-II searches by CMS [92, 93] and ATLAS [94, 95]. They are typically designed to tag supersymmetric heavy Higgses.

viii) At low mass, the di-muon final state becomes relevant. While the branching ratio is very small, suppressed by the muon mass, the cleanness of the final state makes this channel attractive, as long as it can pass the trigger requirements. The only two applicable bounds are a 7 TeV search (lime green light) at low mass done by CMS [96], which tags the mass range between 10 and 15 GeV thanks to a dedicated trigger, and a 8 TeV search (dark green) done by LHCb [97] in the same mass range.

ix) For masses below $m_h/2 \approx 65$ GeV, the decays of the Higgs into two pseudo-scalars starts playing a significant role. We implemented various searches dedicated to this channel, with final states including $b\bar{b}\mu^+\mu^-$ (blue line), 4τ's and 4γ's [98–100], with the two last channels too small to enter in the plots. We also estimated the bound coming from the indirect measurement of undetected decays of the Higgs into new physics, which is currently $\mathrm{BR}_{\mathrm{BSM}} < 30\%$ [101], shown by the dot-dashed blue line. In our specific models, this is stronger than the direct searches, mainly because at the final states the searches focused on have small branching ratios.

x) Finally, we checked that constraints coming from associated production of the pseudo-scalars with $b\bar{b}$ [102, 103] and $t\bar{t}$ [104] are not competitive with production via Z decays [105] ($Z \to a\gamma$).

The plots on the left column of **Figure 3** show the limit on the Higgs decay constant f_ψ in the plane of the two pseudo-scalar masses and for models M8 and M9. For each point in the m_a–$m_{\eta'}$ plane we compute *independently* the bounds on f_ψ coming from the a and η' resonances and then show the most stringent one. In the two side-bands we show the strongest bound coming from a (top band) and η' (right band), split into the various channel we considered. One important observation is that the limit often passes the 1 TeV mark. This is significant as typical electroweak precision bounds on this class of models give a lower limit on f around this scale [106–108]. Cases where the limit can be relaxed have been discussed in Contino and Salvarezza [109], Ghosh et al. [110], and Buarque Franzosi et al. (Unpublished). We note, therefore, that searches for these light pseudo-scalars can be the most constraining probe for these class of models. Also note the presence of a poorly constrained region for the $14 < m_a < 65$ GeV window of the lightest pseudo-scalar (most evident for M9). This is mainly due to the paucity of direct searches that are significant in this low mass window, the strongest bound being on the new physics Higgs decay rate. Note that the latter will not significantly improve at the end of the HL-LHC [111]. It is therefore crucial to close this gap with searches dedicated to this region, which is present for all models. Note also that the constraints on M8 are always rather mild: this is due to the coupling to gluons, which is particularly low in this specific model. The plots, therefore, show how the constraints are particularly sensitive to the details of the underlying models, as the twin models M8 and M9 dramatically show. For comparison, in **Figure 4** we show the bounds for another model, M7, based on the SU(5)/SO(5) coset, which shows an intermediate situation. Similar plots for all the other models are shown in Figures 7–9 in **Appendix C**. They all show a similar pattern of constraints.

A new result we show in this paper is the inclusion of projections for the HL-LHC run. First, we would like to attack the low mass window, which is left open after the Run-II searches, as shown in all plots. In this window, the main decay channels are in two jets (either gluons or b quarks), followed by taus. Di-photon final states are also present, however current searches [83, 86, 87] cannot reach this low mass region due to trigger limitations.

In Cacciapaglia et al. [31] we proposed a new search based on the di-tau final state. To be able to pass the trigger requirements, we proposed to aim at the production of a single a that recoils against a high-p_T jet. This also allows to reduce the background level, while the reduction in the cross section still leaves a large signal rate. We analyzed in detail the case of leptonic decays of the two taus into different flavor leptons. Due to the high boost, the angular separation between the two leptons is typically very small. Thus, imposing an upper cut on the angular separation, $\Delta R_{e\mu} < 1$, allows to efficiently reduce the main background, coming from $t\bar{t}$ and Drell-Yan di-tau production. Fakes in this channel should have a limited impact, thus allowing us to derive reliable estimates for the reach. A key ingredient to improve the reach in the case of a small mass below $30 - 40$ GeV is the reduction of the lower cut on the separation angle between the two leptons. The current minimal separation used at the LHC, see Khachatryan et al. [112] for instance, is $\Delta R_{e\mu} > 0.1 \div 0.2$, as such it would lead to a degradation of the sensitivity for low invariant masses where the boost produces very low angles [31]. It would be necessary, therefore, to relax the isolation criteria and remove the minimal separation in order to optimize the reach. Furthermore, due to the low statistics, it is crucial to reduce at the maximum the systematic errors on the lepton reconstructions. For this reason, we focused on the fully leptonic case. The main systematics in boosted di-tau searches [113] come from hadronic tau decays and from the invariant mass reconstruction, which are not required in our study. We optimistically assume, therefore, that systematic uncertainties below the % level can be achieved. In the right plots of **Figures 3**, **4** and Figures 7–9 in **Appendix C**, we show the projected reach of this proposed search in black. The plots show that in most models it can effectively cover the low mass open window, with enhanced sensitivity to the low mass end. Note also that we only use the opposite-flavor fully leptonic channel. Nevertheless, semi-leptonic decays may also be used, by implementing advanced techniques, like the "mini-isolation" proposed in Rehermann and Tweedie [114], while tests of fully-hadronic di-tau tagging can be found in Katz et al. [115] and Conte et al. [116].

Another method that would allow to cover the low mass window is extracting indirect bounds from the di-photon differential cross section measurements, as proposed in Mariotti et al. [117]. We added a projection of this bound

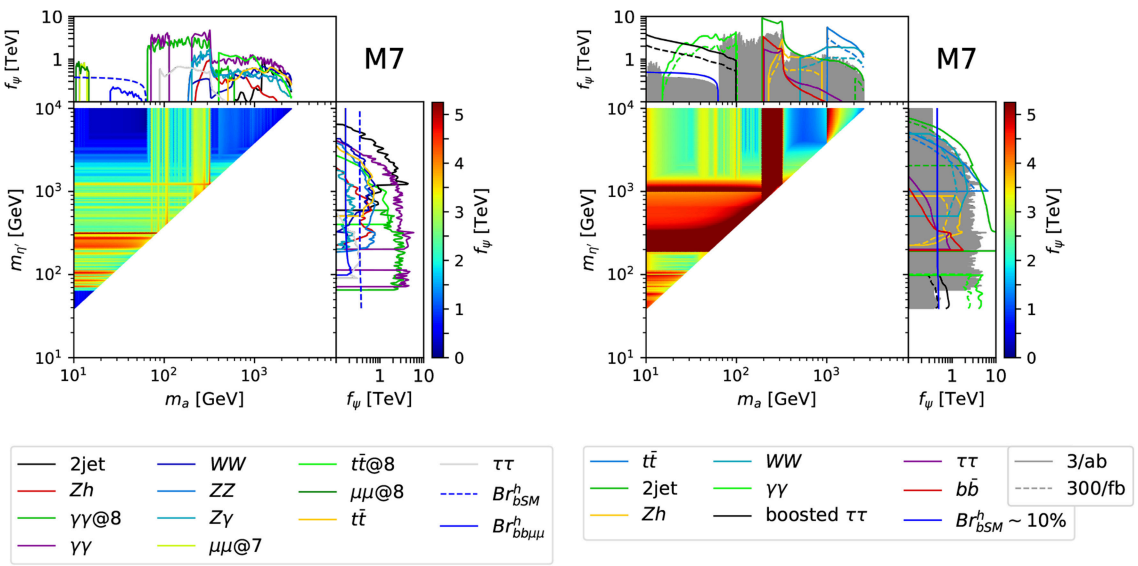

FIGURE 4 | Same as **Figure 3**, for the model M7, based on the EW coset SU(5)/SO(5).

at High-Luminosity in red. **Figure 3** effectively shows the complementarity between the two searches: for M8, the di-tau search gives stronger bounds in the full mass range, while for M9 the di-photon bound is more stringent while di-tau can only compete at the low mass end of the window. In **Figure 4** we show another case, M7, where the complementarity between the two methods at the low and high ends of the open mass window is more evident. To complete the High-Luminosity projections, we also include projections for $t\bar{t}$ [118–120] (in blue), di-jet [119, 121, 122] (in green), Zh [123] (in orange), WW [124] (in cyan), $\tau\tau$ [125] (in violet), and $b\bar{b}$ [119, 122] (in red).

The plots on the right side of the **Figures 3**, **4** and Figures 7–9 in **Appendix C** show that the High-Luminosity run of the LHC will allow to effectively cover the full parameter space of the pseudo-scalar masses for nearly all models, provided that the searches addressing the low mass window are implemented. This is a last chance situation, as the sensitivity of high-energy future colliders to such low masses will be much lower.

Before concluding the section, we would like to comment on another search that can be potentially useful to cover the low-mass open window, i.e., the LHCb search for dark photons in the di-muon final state [126]. The main strength of this search relies on the cancellation of all systematic uncertainties. A recast of this search in the context of a two Higgs doublet model can be found in Haisch et al. [127]. While the systematics associated to the detector effects are reasonably similar between the pseudo-scalar resonance and the dark photon, the production channel (gluon fusion vs. Drell–Yann) remains different, thus a more detailed determination of the acceptances and systematics is needed for a recast in our case. The results of ongoing work will be presented in a separate publication.

5. CONCLUSIONS AND OUTLOOK

We have updated the bounds from various experimental searches on two potentially light pseudo-scalar mesons, which arise in models of composite Higgs with top partial compositeness, with an underlying gauge-fermion description. We have provided a handbook containing all the relevant information necessary to study the phenomenology in any of the variations of the 12 possible basic models. In each model, the couplings of the two states can be computed in terms of the properties of the underlying gauge theory and of the two decay constants in the two sectors, one related to the EW symmetry breaking and the other to QCD carrying states.

We found that, in most models, scanning for masses up to 10 TeV, the non-observation of a resonance allows to set a bound on the compositeness scale, that surpasses the typical bound from electroweak precision tests. This result shows how the observation of these states can be a smoking gun for these class of theories, while also carrying precious information on the details of the underlying models. In all cases, there is a poorly constrained region for masses between 10 and 65 GeV, where the "standard" channels relying on Higgs decays or di-muon searches, give very weak bounds in these models.

We thus reviewed two proposals to cover this window: one based on the search for boosted di-tau systems, and the other on indirect bounds from the di-photon differential cross section measurements. At the High-Luminosity LHC, these two strategies would allow to close the gap. In fact, they are complementary in two aspects: the di-tau is more sensitive to small masses while the photon is more sensitive to larger masses; in models where the photon coupling is suppressed, the tau

channel is most constraining, and vice versa. Finally, we included the projected sensitivity of Zh, WW, $\gamma\gamma$, $t\bar{t}$, $b\bar{b}$, $\tau\tau$ and di-jet searches at High-Luminosity, to push the bounds higher. Our results also show the necessity to keep looking for $t\bar{t}$ resonances down to the mass threshold, as this is the most sensitive channel, in these models, above 350 GeV.

AUTHOR CONTRIBUTIONS

All authors listed have made a substantial, direct and intellectual contribution to the work, and approved it for publication.

ACKNOWLEDGMENTS

We would like to thank Xiabier Cid Vidal, Mike Williams and Martino Borsato for useful feedback on the LHCb dark photon search, and Uli Haisch for discussion on the recast. TF was supported by IBS under the project code IBS-R018-D1. GF is supported in part by a grant from the Wallenberg foundation no. KAW-2017.0100. GC acknowledges partial support from the Institut Franco-Suedois (project Tör), the Labex Lyon Institute of the Origins - LIO (under grant ANR-10-LABX-66 and FRAMA FR3127 Fédération de Recherche André Marie Ampère) and the LIA FKPPL. HS has received funding from the European Research Council (ERC) under the European Union's Horizon 2020 research and innovation program (grant agreement No 668679).

SUPPLEMENTARY MATERIAL

The Supplementary Material for this article can be found online at: https://www.frontiersin.org/articles/10.3389/fphy.2019.00022/full#supplementary-material

REFERENCES

1. Weinberg S. Implications of dynamical symmetry breaking. *Phys Rev.* (1976) **D13**:974–96.
2. Kaplan DB, Georgi H. SU(2) x U(1) breaking by vacuum misalignment. *Phys Lett.* (1984) **136B**:183–6.
3. Contino R, Nomura Y, Pomarol A. Higgs as a holographic pseudoGoldstone boson. *Nucl Phys*. (2003) **B671**:148–74. doi: 10.1016/j.nuclphysb.2003.08.027
4. Agashe K, Contino R, Pomarol A. The minimal composite Higgs model. *Nucl Phys.* (2005) **B719**:165–87. doi: 10.1016/j.nuclphysb.2005.04.035
5. Contino R. The Higgs as a composite nambu-goldstone boson. In: *Physics of the Large and the Small, TASI 09, Proceedings of the Theoretical Advanced Study Institute in Elementary Particle Physics*, 1-26 June 2009 Boulder, CO (2011). p. 235–306.
6. Bellazzini B, Csáki C, Serra J. Composite Higgses. *Eur Phys J.* (2014) **C74**:2766. doi: 10.1140/epjc/s10052-014-2766-x
7. Panico G, Wulzer A. The composite nambu-goldstone Higgs. *Lect Notes Phys.* (2016) **913**:1–316. doi: 10.1007/978-3-319-22617-0
8. Kaplan DB. Flavor at SSC energies: a new mechanism for dynamically generated fermion masses. *Nucl Phys.* (1991) **B365**:259–78.
9. Cacciapaglia G, Csaki C, Galloway J, Marandella G, Terning J, Weiler A. A GIM mechanism from extra dimensions. *JHEP*. (2008) **04**:006. doi: 10.1088/1126-6708/2008/04/006
10. Fitzpatrick AL, Perez G, Randall L. Flavor anarchy in a Randall-Sundrum model with 5D minimal flavor violation and a low Kaluza-Klein scale. *Phys Rev Lett.* (2008) **100**:171604. doi: 10.1103/PhysRevLett.100.171604
11. Marzocca D, Serone M, Shu J. General composite Higgs models. *JHEP*. (2012) 08:013. doi: 10.1007/JHEP08(2012)013
12. Contino R, Da Rold L, Pomarol A. Light custodians in natural composite Higgs models. *Phys Rev.* (2007) **D75**:055014. doi: 10.1103/PhysRevD.75.055014
13. Matsedonskyi O, Panico G, Wulzer A. Light top partners for a light composite Higgs. *JHEP*. (2013) **01**:164. doi: 10.1007/JHEP01(2013)164
14. Galloway J, Evans JA, Luty MA, Tacchi RA. Minimal conformal technicolor and precision electroweak tests. *JHEP*. (2010) **10**:086. doi: 10.1007/JHEP10(2010)086
15. Cacciapaglia G, Sannino F. Fundamental composite (goldstone) Higgs dynamics. *JHEP*. (2014) **04**:111. doi: 10.1007/JHEP04(2014)111
16. von Gersdorff G, Pontón E, Rosenfeld R. The dynamical composite Higgs. *JHEP*. (2015) **06**:119. doi: 10.1007/JHEP06(2015)119
17. Caracciolo F, Parolini A, Serone M. UV completions of composite Higgs models with partial compositeness. *JHEP*. (2013) **02**:066. doi: 10.1007/JHEP02(2013)066
18. Setford J. Composite Higgs models in disguise. *JHEP*. (2018) **01**:092. doi: 10.1007/JHEP01(2018)092
19. Witten E. Current algebra, baryons, and quark confinement. *Nucl Phys*. (1983) **B223**:433–44.
20. Kosower DA. Symmetry breaking patterns in pseudoreal and real gauge theories. *Phys Lett*. (1984) **144B**:215–6.
21. Ryttov TA, Sannino F. Ultra minimal technicolor and its dark matter TIMP. *Phys Rev.* (2008) **D78**:115010. doi: 10.1103/PhysRevD.78.115010
22. Dugan MJ, Georgi H, Kaplan DB. Anatomy of a composite Higgs model. *Nucl Phys*. (1985) **B254**:299–326.
23. Ma T, Cacciapaglia G. Fundamental composite 2HDM: SU(N) with 4 flavours. *JHEP*. (2016) **03**:211. doi: 10.1007/JHEP03(2016)211
24. Ferretti G, Karateev D. Fermionic UV completions of composite Higgs models. *JHEP*. (2014) **03**:077. doi: 10.1007/JHEP03(2014)077
25. Ayyar V, DeGrand T, Golterman M, Hackett DC, Jay WI, Neil ET, et al. Spectroscopy of SU(4) composite Higgs theory with two distinct fermion representations. *Phys Rev D*. (2017) **97**:074505 doi: 10.1103/PhysRevD.97.074505
26. Vecchi L. A dangerous irrelevant UV-completion of the composite Higgs. *JHEP*. (2017) **02**:094. doi: 10.1007/JHEP02(2017)094
27. Belyaev A, Cacciapaglia G, Cai H, Ferretti G, Flacke T, Parolini A, et al. Di-boson signatures as standard candles for partial compositeness. *JHEP*. (2017) **01**:094. doi: 10.1007/JHEP01(2017)094
28. Cai H, Flacke T, Lespinasse M. A composite scalar hint from di-boson resonances? *arXiv:1512.04508* (2015).
29. Belyaev A, Cacciapaglia G, Cai H, Flacke T, Parolini A, Serodio H. Singlets in composite Higgs models in light of the LHC 750 GeV diphoton excess. *Phys Rev*. (2016) **D94**:015004. doi: 10.1103/PhysRevD.94.015004
30. DeGrand T, Golterman M, Neil ET, Shamir Y. One-loop chiral perturbation theory with two fermion representations. *Phys Rev.* (2016) **D94**:025020. doi: 10.1103/PhysRevD.94.025020
31. Cacciapaglia G, Ferretti G, Flacke T, Serodio H. Revealing timid pseudo-scalars with taus at the LHC. *Eur Phys J.* (2018) **C78**:724. doi: 10.1140/epjc/s10052-018-6183-4
32. Wess J, Zumino B. Consequences of anomalous Ward identities. *Phys Lett*. (1971) **37B**:95–97.
33. Witten E. Global aspects of current algebra. *Nucl Phys*. (1983) **B223**:422–32.
34. Bizot N, Cacciapaglia G, Flacke T. Common exotic decays of top partners. *JHEP*. (2018) **06**:065. doi: 10.1007/JHEP06(2018)065
35. Dietrich DD, Sannino F. Conformal window of SU(N) gauge theories with fermions in higher dimensional representations. *Phys Rev*. (2007) **D75**:085018. doi: 10.1103/PhysRevD.75.085018
36. Ferretti G. Gauge theories of partial compositeness: scenarios for Run-II of the LHC. *JHEP*. (2016) **06**:107. doi: 10.1007/JHEP06(2016)107

37. Matsedonskyi O. On Flavour and Naturalness of Composite Higgs Models. *JHEP*. (2015) **02**:154. doi: 10.1007/JHEP02(2015)154
38. Cacciapaglia G, Cai H, Flacke T, Lee SJ, Parolini A, Serodio H. Anarchic Yukawas and top partial compositeness: the flavour of a successful marriage. *JHEP*. (2015) **06**:085. doi: 10.1007/JHEP06(2015)085
39. Cacciapaglia G, Vatani S,Ma T,Wu Y. Towards a fundamental safe theory of composite Higgs and Dark Matter. *arXiv:1812.04005* (2018).
40. Golterman M, Shamir Y. Top quark induced effective potential in a composite Higgs model. *Phys Rev*. (2015) **D91**:094506. doi: 10.1103/PhysRevD.91.094506
41. DeGrand TA, Golterman M, Jay WI, Neil ET, Shamir Y, Svetitsky B. Radiative contribution to the effective potential in composite Higgs models from lattice gauge theory. *Phys Rev*. (2016) **D94**:054501. doi: 10.1103/PhysRevD.94.054501
42. Bennett E, Hong DK, Lee JW, Lin CJD, Lucini B, Piai M, et al. Higgs compositeness in Sp(2N) gauge theories - Resymplecticisation, scale setting and topology. *EPJ Web Conf*. (2018) **175**:08012. doi: 10.1051/epjconf/201817508012
43. Bennett E, Hong DK, Lee JW, Lin CJD, Lucini B, Piai M, et al. Higgs compositeness in Sp(2N) gauge theories - Determining the low-energy constants with lattice calculations. *EPJ Web Conf*. (2018) **175**:08011. doi: 10.1051/epjconf/201817508011
44. Bennett E, Hong DK, Lee JW, Lin CJD, Lucini B, Piai M, et al. Sp(4) gauge theory on the lattice: towards SU(4)/Sp(4) composite Higgs (and beyond). *JHEP*. (2018) **03**:185. doi: 10.1007/JHEP03(2018)185
45. Lee JW, Bennett E, Hong DK, Lin CJD, Lucini B, Piai M, et al. *Progress in the Lattice Simulations of Sp(2N) Gauge Theories*. PoS. (2018) LATTICE2018:192.
46. Sannino F, Strumia A, Tesi A, Vigiani E. Fundamental partial compositeness. *JHEP*. (2016) **11**:029. doi: 10.1007/JHEP11(2016)029
47. Cacciapaglia G, Parolini A. Light 't Hooft top partners. *Phys Rev*. (2016) **D93**:071701. doi: 10.1103/PhysRevD.93.071701
48. Barnard J, Gherghetta T, Ray TS. UV descriptions of composite Higgs models without elementary scalars. *JHEP*. (2014) **02**:002. doi: 10.1007/JHEP02(2014)002
49. Ferretti G. UV Completions of Partial Compositeness: The Case for a SU(4) Gauge Group. *JHEP*. (2014) **06**:142. doi: 10.1007/JHEP06(2014)142
50. Bizot N, Frigerio M, Knecht M, Kneur JL. Nonperturbative analysis of the spectrum of meson resonances in an ultraviolet-complete composite-Higgs model. *Phys Rev*. (2017) **D95**:075006. doi: 10.1103/PhysRevD.95.075006
51. Arbey A, Cacciapaglia G, Cai H, Deandrea A, Le Corre S, Sannino F. Fundamental composite electroweak dynamics: status at the LHC. *Phys Rev*. (2017) **D95**:015028. doi: 10.1103/PhysRevD.95.015028
52. Agugliaro A, Cacciapaglia G, Deandrea A, De Curtis S. Vacuum misalignment and pattern of scalar masses in the SU(5)/SO(5) composite Higgs model. *JHEP*. (2019) 2019:89. doi: 10.1007/JHEP02(2019)089
53. Wu Y, Ma T, Zhang B, Cacciapaglia G. Composite dark matter and Higgs. *JHEP*. (2017) **11**:058. doi: 10.1007/JHEP11(2017)058
54. Cacciapaglia G, Cai H, Deandrea A, Flacke T, Lee SJ, Parolini A. Composite scalars at the LHC: the Higgs, the sextet and the octet. *JHEP*. (2015) **11**:201. doi: 10.1007/JHEP11(2015)201
55. Degrande C, Fuks B, Hirschi V, Proudom J, Shao HS. Automated next-to-leading order predictions for new physics at the LHC: the case of colored scalar pair production. *Phys Rev*. (2015) **D91**:094005. doi: 10.1103/PhysRevD.91.094005
56. Raby S, Dimopoulos S, Susskind L. Tumbling gauge theories. *Nucl Phys*. (1980) **B169**:373–83.
57. Brivio I, Gavela MB, Merlo L, Mimasu K, No JM, del Rey R, et al. ALPs effective field theory and collider signatures. *Eur Phys J*. (2017) 77:572. doi: 10.1140/epjc/s10052-017-5111-3
58. Bellazzini B, Mariotti A, Redigolo D, Sala F, Serra J. R-axion at colliders. *Phys Rev Lett*. (2017) **119**:141804. doi: 10.1103/PhysRevLett.119.141804
59. Bauer M, Neubert M, Thamm A. Collider probes of axion-like particles. *JHEP*. (2017). doi: 10.1007/JHEP12(2017)044
60. Bauer M, Neubert M, Thamm A. Analyzing the CP nature of a new scalar particle via S->Zh decay. *Phys Rev Lett*. (2016) **117**:181801. doi: 10.1103/PhysRevLett.117.181801
61. Patel HH. Package-X: a Mathematica package for the analytic calculation of one-loop integrals. *Comput Phys Commun*. (2015) **197**:276–90. doi: 10.1016/j.cpc.2015.08.017
62. Golterman M, Shamir Y. Effective potential in ultraviolet completions for composite Higgs models. *Phys Rev*. (2018) **D97**:095005. doi: 10.1103/PhysRevD.97.095005
63. Spira M. *HIGLU: A Program for the Calculation of the Total Higgs Production Cross-Section at Hadron Colliders via Gluon Fusion Including QCD Corrections*. (1995) DESY T-95-05.
64. CMS collaboration. Search for $t\bar{t}$ resonances in highly boosted lepton+jets and fully hadronic final states in proton-proton collisions at $\sqrt{s} = 13$ TeV. *JHEP*. (2017) **07**:001. doi: 10.1007/JHEP07(2017)001
65. CMS collaboration. Search for resonant $t\bar{t}$ production in proton-proton collisions at $\sqrt{s} = 8$ TeV. *Phys Rev*. (2016) **D93**:012001. doi: 10.1103/PhysRevD.93.012001
66. ATLAS collaboration. A search for $t\bar{t}$ resonances using lepton-plus-jets events in proton-proton collisions at $\sqrt{s} = 8$ TeV with the ATLAS detector. *JHEP*. (2015) **08**:148. doi: 10.1007/JHEP08(2015)148
67. CMS collaboration. Search for dijet resonances in proton-proton collisions at $\sqrt{s}$ = 13 TeV and constraints on dark matter and other models. *Phys Lett*. (2017) **B769**:520–42. doi: 10.1016/j.physletb.2017.02.012
68. CMS collaboration. *Searches for Dijet Resonances in pp Collisions at* $\sqrt{s} =$ 13 TeV *Using Data Collected in 2016*. Geneva: CERN; 2017. CMS-PAS-EXO-16-056. Available online at: https://cds.cern.ch/record/2256873
69. ATLAS collaboration. Search for new phenomena in dijet events using 37 fb^{-1} of *pp* collision data collected at $\sqrt{s}$ =13 TeV with the ATLAS detector. *Phys Rev*. (2017) **D96**:052004. doi: 10.1103/PhysRevD.96.052004
70. CMS collaboration. Search for massive resonances decaying into *WW*, *WZ*, *ZZ*, *qW*, and *qZ* with dijet final states at $\sqrt{s} = 13$TeV. *Phys Rev*. (2018) **D97**:072006. doi: 10.1103/PhysRevD.97.072006
71. CMS collaboration. Search for massive resonances decaying into WW, WZ or ZZ bosons in proton-proton collisions at $\sqrt{s} = 13$ TeV. *JHEP*. (2017) **03**:162. doi: 10.1007/JHEP03(2017)162
72. CMS collaboration. *Search for Heavy Resonances Decaying to Pairs of Vector Bosons in the* $lv\bar{q}\bar{q}$ *Final State With the CMS Detector in Proton-Proton Collisions at* $\sqrt{s} = 13$ *TeV*. Geneva: CERN; 2017. CMS-PAS-B2G-16-029. Available online at: https://cds.cern.ch/record/2296237.
73. CMS collaboration. *Search for New Resonances Decaying to* WW/WZ $\rightarrow$ lvqq. Geneva: CERN; 2016. CMS-PAS-B2G-16-020. Available online at: https://cds.cern.ch/record/2205880.
74. CMS collaboration. *Search for a New Scalar Resonance Decaying to a Pair of Z Bosons in Proton-Proton Collisions at* $\sqrt{s}$ = *13 TeV*. Geneva: CERN; 2017. CMS-PAS-HIG-17-012. Available online at: https://cds.cern.ch/record/2296714.
75. The CMS Collaboration. Search for ZZ resonances in the 212ν final state in proton-proton collisions at 13 TeV. *J High Energ Phys*. (2018) **2018**:3. doi: 10.1007/JHEP03(2018)003
76. CMS collaboration. *Search for New Diboson Resonances in the Dilepton + Jets Final State at* $\sqrt{s} = 13$ TeV *With 2016 Data*. Geneva: CERN; 2017. CMS-PAS-HIG-16-034. Available online at: https://cds.cern.ch/record/2243295.
77. CMS collaboration. *Search for Heavy Resonances Decaying Into a Z Boson and a Vector Boson in the* $\nu\nu$ $q\bar{q}$ *Final State*. Geneva: CERN; 2017. CMS-PAS-B2G-17-005. Available online at: https://cds.cern.ch/record/2273910
78. ATLAS collaboration. Search for heavy resonances decaying into *WW* in the $ev\mu\nu$ final state in *pp* collisions at $\sqrt{s} = 13$ TeV with the ATLAS detector. *Eur Phys J*. (2018) **C78**:24. doi: 10.1140/epjc/s10052-017-5491-4
79. ATLAS collaboration. Search for WW/WZ resonance production in $lvqq$ final states in *pp* collisions at $\sqrt{s} = 13$ TeV with the ATLAS detector. *JHEP*. (2018) **03**:042. doi: 10.1007/JHEP03(2018)042
80. ATLAS collaboration. Searches for heavy *ZZ* and *ZW* resonances in the *llqq* and $\nu\nu qq$ final states in *pp* collisions at $\sqrt{s} = 13$ TeV with the ATLAS detector. *JHEP*. (2018) **03**:009. doi: 10.1007/JHEP03(2018)009
81. ATLAS collaboration. Search for heavy ZZ resonances in the $l^+l^-l^+l^-$ and $l^+l^-\nu\bar{\nu}$ final states using proton-proton collisions at $\sqrt{s} = 13$ TeV with the ATLAS detector. *Eur Phys J*. (2018) **C78**:293. doi: 10.1140/epjc/s10052-018-5686-3

82. ATLAS collaboration. Search for scalar diphoton resonances in the mass range 65 − 600 GeV with the ATLAS detector in *pp* collision data at $\sqrt{s} = 8$ *TeV*. *Phys Rev Lett*. (2014) **113**:171801. doi: 10.1103/PhysRevLett.113.171801
83. ATLAS collaboration. Search for new phenomena in high-mass diphoton final states using 37 fb^{-1} of proton–proton collisions collected at $\sqrt{s} =$ 13 TeV with the ATLAS detector. *Phys Lett*. (2017) **B775**:105–25. doi: 10.1016/j.physletb.2017.10.039
84. CMS collaboration. Search for high-mass diphoton resonances in proton-proton collisions at 13 TeV and combination with 8 TeV search. *Phys Lett*. (2017) **B767**:147–70. doi: 10.1016/j.physletb.2017.01.027
85. CMS collaboration. Search for resonant production of high-mass photon pairs in proton-proton collisions at $\sqrt{s}$ =8 and 13 TeV. *Phys Rev Lett*. (2016) **117**:051802. doi: 10.1103/PhysRevLett.117.051802
86. CMS collaboration. *Search for New Resonances in the Diphoton Final State in the Mass Range Between 80 and 115 GeV in pp Collisions at* $\sqrt{s} = 8$ *TeV*. Geneva: CERN; 2015. CMS-PAS-HIG-14-037. Available online at: https://cds.cern.ch/record/2063739.
87. CMS collaboration. *Search for New Resonances in the Diphoton Final State in the Mass Range Between 70 and 110 GeV in pp Collisions at* $\sqrt{s} = 8$ *and 13 TeV*. Geneva: CERN; 2017. CMS-PAS-HIG-17-013. Available online at: https://cds.cern.ch/record/2285326.
88. CMS collaboration. Search for $Z\gamma$ resonances using leptonic and hadronic final states in proton-proton collisions at $\sqrt{s} = 13$ TeV. *JHEP*. (2018) **09**:148. doi: 10.1007/JHEP09(2018)148
89. CMS collaboration. Search for high-mass $Z\gamma$ resonances in $e^+e^-\gamma$ and $\mu^+\mu^-\gamma$ final states in proton-proton collisions at $\sqrt{s} = 8$ and 13 TeV. *JHEP*. (2017) **01**:076. doi: 10.1007/JHEP01(2017)076
90. ATLAS collaboration. Searches for the $Z\gamma$ decay mode of the Higgs boson and for new high-mass resonances in *pp* collisions at $\sqrt{s} =$ 13 TeV with the ATLAS detector. *JHEP*. (2017) **10**:112. doi: 10.1007/JHEP10(2017)112
91. ATLAS collaboration. *Search for Heavy Resonances Decaying to a W or Z Boson and a Higgs Boson in Final States With Leptons and b-jets in 36.1 fb*$^{-1}$ *of pp Collision Data at* $\sqrt{s} =$ 13 *TeV with the ATLAS Detector*. Geneva: CERN; 2017. ATLAS-CONF-2017-055. Available online at: https://cds.cern.ch/record/2273871.
92. CMS collaboration. *Search for Additional Neutral MSSM Higgs Bosons in the di-tau Final State in pp Collisions at* $\sqrt{s} =$ 13 *TeV*. Geneva: CERN; 2017. CMS-PAS-HIG-17-020. Available online at: https://cds.cern.ch/record/2296333.
93. CMS collaboration. Search for heavy resonances decaying to tau lepton pairs in proton-proton collisions at $\sqrt{s} =$ 13 TeV. *JHEP*. (2017) **02**:048. doi: 10.1007/JHEP02(2017)048
94. ATLAS collaboration. Search for additional heavy neutral Higgs and gauge bosons in the ditau final state produced in 36 fb^{-1} of pp collisions at $\sqrt{s} =$ 13 TeV with the ATLAS detector. *JHEP*. (2018) **01**:055. doi: 10.1007/JHEP01(2018)055
95. ATLAS collaboration. Search for Minimal Supersymmetric Standard Model Higgs bosons H/A and for a Z' boson in the $\tau\tau$ final state produced in *pp* collisions at $\sqrt{s} =$ 13 TeV with the ATLAS Detector. *Eur Phys J*. (2016) **C76**:585. doi: 10.1140/epjc/s10052-016-4400-6
96. CMS collaboration. Search for a light pseudoscalar Higgs boson in the dimuon decay channel in *pp* collisions at $\sqrt{s} = 7$ TeV. *Phys Rev Lett*. (2012) **109**:121801. doi: 10.1103/PhysRevLett.109.121801
97. LHCb collaboration. Search for a dimuon resonance in the Υ mass region. *JHEP*. (2018) **09**:147. doi: 10.1007/JHEP09(2018)147
98. CMS collaboration. Search for light bosons in decays of the 125 GeV Higgs boson in proton-proton collisions at $\sqrt{s} =$ 8 TeV. *JHEP*. (2017). doi: 10.1007/JHEP10(2017)076
99. ATLAS collaboration. Search for new phenomena in events with at least three photons collected in *pp* collisions at $\sqrt{s} = 8$ TeV with the ATLAS detector. *Eur Phys J*. (2016) **C76**:210. doi: 10.1140/epjc/s10052-016-4034-8
100. ATLAS collaboration. Search for Higgs bosons decaying to *aa* in the $\mu\mu\tau\tau$ final state in *pp* collisions at $\sqrt{s} =$ 8 TeV with the ATLAS experiment. *Phys Rev*. (2015) **D92**:052002. doi: 10.1103/PhysRevD.92.052002
101. ATLAS and CMS collaborations. Measurements of the Higgs boson production and decay rates and constraints on its couplings from a combined ATLAS and CMS analysis of the LHC pp collision data at $\sqrt{s} = 7$ and 8 TeV. *JHEP*. (2016) **08**:045. doi: 10.1007/JHEP08(2016)045
102. CMS collaboration. Search for a low-mass pseudoscalar Higgs boson produced in association with a $b\bar{b}$ pair in pp collisions at $\sqrt{s} = 8$ TeV. *Phys Lett*. (2016) **B758**:296–320. doi: 10.1016/j.physletb.2016.05.003
103. Kozaczuk J, Martin TAW. Extending LHC coverage to light pseudoscalar mediators and coy dark sectors. *JHEP*. (2015) **04**:046. doi: 10.1007/JHEP04(2015)046
104. Casolino M, Farooque T, Juste A, Liu T, Spannowsky M. Probing a light CP-odd scalar in di-top-associated production at the LHC. *Eur Phys J*. (2015) **C75**:498. doi: 10.1140/epjc/s10052-015-3708-y
105. OPAL collaboration. A Measurement of photon radiation in lepton pair events from Z0 decays. *Phys Lett*. (1991) **B273**:338–354.
106. Agashe K, Contino R. The Minimal composite Higgs model and electroweak precision tests. *Nucl Phys*. (2006) **B742**:59–85. doi: 10.1016/j.nuclphysb.2006.02.011
107. Grojean C, Matsedonskyi O, Panico G. Light top partners and precision physics. *JHEP*. (2013) **10**:160. doi: 10.1007/JHEP10(2013)160
108. Contino R, Salvarezza M. Dispersion relations for electroweak observables in composite Higgs models. *Phys Rev*. (2015) **D92**:115010. doi: 10.1103/PhysRevD.92.115010
109. Contino R, Salvarezza M. One-loop effects from spin-1 resonances in Composite Higgs models. *JHEP*. (2015) **07**:065. doi: 10.1007/JHEP07(2015)065
110. Ghosh D, Salvarezza M, Senia F. Extending the analysis of electroweak precision constraints in composite higgs models. *Nucl Phys*. (2017) **B914**:346–87. doi: 10.1016/j.nuclphysb.2016.11.013
111. ATLAS collaboration. *Projections for Measurements of Higgs boson Signal Strengths and Coupling Parameters With the ATLAS Detector at a HL-LHC*. Geneva: CERN; 2014. ATL-PHYS-PUB-2014-016. Available online at: https://cds.cern.ch/record/1956710.
112. CMS collaboration. Search for Narrow High-Mass Resonances in Proton-Proton Collisions at $\sqrt{s} = 8$ TeV Decaying to a Z and a Higgs Boson. *Phys Lett*. (2015) **B748**:255–77. doi: 10.1016/j.physletb.2015.07.011
113. CMS collaboration. *Search for Heavy Resonances Decaying Into Two Higgs Bosons or Into a Higgs and a Vector Boson in Proton-Proton Collisions at 13 TeV*. Geneva: CERN; 2017. CMS-PAS-B2G-17-006. Available online at: http://cds.cern.ch/record/2296716.
114. Rehermann K, Tweedie B. Efficient identification of boosted semileptonic top quarks at the LHC. *JHEP*. (2011) **03**:059. doi: 10.1007/JHEP03(2011)059
115. Katz A, Son M, Tweedie B. Ditau-Jet tagging and boosted higgses from a multi-TeV resonance. *Phys Rev*. (2011) **D83**:114033. doi: 10.1103/PhysRevD.83.114033
116. Conte E, Fuks B, Guo J, Li J, Williams AG. Investigating light NMSSM pseudoscalar states with boosted ditau tagging. *JHEP*. (2016) **05**:100. doi: 10.1007/JHEP05(2016)100
117. Mariotti A, Redigolo D, Sala F, Tobioka K. New LHC bound on low-mass diphoton resonances. *Phys Lett B* 783:13–8 (2017). doi: 10.1016/j.physletb.2018.06.039
118. Azzi P, Cristinziani M. Top quark physics at the high luminosity LHC. In: *Proceedings, 9th International Workshop on Top Quark Physics (TOP 2016)*: September 19-23, 2016 (Olomouc) (2017).
119. Cid Vidal X, D'Onofrio M, Fox PJ, Torre R, Ulmer KA, Aboubrahim A, et al. *Beyond the Standard Model Physics at the HL-LHC and HE-LHC*. CERN-LPCC-2018-05 (2018).
120. CMS collaboration. *Search for Ttbar Resonances at the HL-LHC and HE-LHC with the Phase-2 CMS Detector*. Geneva: CERN; 2018. CMS-PAS-FTR-18-009. Available online at: https://cds.cern.ch/record/2649032.
121. ATLAS collaboration. *Dijet Resonance Searches With the ATLAS Detector at 14 TeV LHC*. Geneva: CERN; 2015. ATL-PHYS-PUB-2015-004. Available online at: https://cds.cern.ch/record/2002136.
122. Chekanov SV, Childers JT, Proudfoot J, Frizzell D, Wang R. Precision searches in dijets at the HL-LHC and HE-LHC. *JINST*. (2018) **13**:P05022. doi: 10.1088/1748-0221/13/05/P05022
123. ATLAS collaboration. *Beyond Standard Model Higgs Boson Searches at a High-Luminosity LHC with ATLAS*. Geneva: CERN; 2013. ATL-PHYS-PUB-2013-016. Available online at: http://cds.cern.ch/record/1611190.
124. ATLAS collaboration. *HL-LHC Prospects for Diboson Resonance Searches and Electroweak Vector Boson Scattering in the* $WW/WZ \to \ell\nu qq$ *final state*.

Geneva: CERN; 2018. ATL-PHYS-PUB-2018-022. Available online at: http://cds.cern.ch/record/2645269.

125. ATLAS collaboration. *Prospects for the Search for Additional Higgs Bosons in the Ditau Final State With the ATLAS Detector at HL-LHC*. Geneva: CERN; 2018. ATL-PHYS-PUB-2018-050. Available online at: http://cds.cern.ch/record/2652284.
126. LHCb collaboration. Search for dark photons produced in 13 TeV *pp* collisions. *Phys Rev Lett*. (2017) **120**:061801. doi: 10.1103/PhysRevLett.120.061801
127. Haisch U, Kamenik JF, Malinauskas A, Spira M. Collider constraints on light pseudoscalars. *JHEP*. (2018) **03**:178. doi: 10.1007/JHEP03(2018)178

Conflict of Interest Statement: The authors declare that the research was conducted in the absence of any commercial or financial relationships that could be construed as a potential conflict of interest.

frontiers in Physics

REVIEW
published: 26 April 2019
doi: 10.3389/fphy.2019.00036

Dark Matter With Stückelberg Axions

Claudio Corianò[1]*, *Paul H. Frampton*[1], *Nikos Irges*[2] and *Alessandro Tatullo*[1]

[1] Dipartimento di Fisica, INFN Sezione di Lecce, Università del Salento, Lecce, Italy, [2] Department of Physics, National Technical University of Athens, Athens, Greece

Here, we review a class of models which generalize the traditional Peccei-Quinn (PQ) axion solution by a Stückelberg pseudoscalar. Such axion models represent a significant variant with respect to earlier scenarios, where axion fields were associated with global anomalies, because of the Stückelberg field, which is essential for the cancellation of gauge anomalies in the presence of extra $U(1)$ symmetries. The extra neutral currents associated to these models have been investigated in the past, in orientifold models with intersecting branes, under the assumption that the Stückelberg scale was in the multi-TeV region. Such constructions, at the field theory level, are quite general and can be interpreted as the four-dimensional field theory realization of the Green-Schwarz mechanism of anomaly cancellation of string theory. We present an overview of models of this type in the TeV/multi TeV range in their original formulation and their recent embeddings into an ordinary GUT theory, presenting an $E_6 \times U(1)_X$ model as an example. In this case the model contains two axions, the first corresponding to a Peccei-Quinn axion, whose misalignment takes place at the QCD phase transition, with a mass in the meV region and which solves the strong CP problem. The second axion is ultralight, in the $10^{-20} - 10^{-22}$ eV region, due to misalignment and decoupling taking place at the GUT scale. The two scales introduced by the PQ solution, the PQ breaking scale and the misalignment scale at the QCD hadron transition, become the Planck and the GUT scales, respectively, with a global anomaly replaced by a gauge anomaly. The periodic potential and the corresponding oscillations are related to a particle whose De Broglie wavelength can reach 10 kpc. Such a sub-galactic scale has been deemed necessary in order to resolve several dark matter issues at the astrophysical level.

Keywords: axion physics, anomalies in gauge field theory, dark matter, Grand Unification theories, string phenomenology and cosmology

OPEN ACCESS

Edited by:
Stefano Moretti,
University of Southampton,
United Kingdom

Reviewed by:
Sayantan Choudhury,
Max-Planck-Institut für Gravitationsphysik, Germany
Bhupal Dev,
Washington University in St. Louis,
United States

***Correspondence:**
Claudio Corianò
claudio.coriano@le.infn.it

Specialty section:
This article was submitted to High-Energy and Astroparticle Physics, a section of the journal Frontiers in Physics

Received: *14 November 2018*
Accepted: *27 February 2019*
Published: *26 April 2019*

Citation:
Corianò C, Frampton PH, Irges N and Tatullo A (2019) Dark Matter With Stückelberg Axions. Front. Phys. 7:36. doi: 10.3389/fphy.2019.00036

1. INTRODUCTION

It is by now well established that astrophysical and cosmological data coming either from measurements of the velocities of stars orbiting galaxies, in their rotation curves, or from the cosmic microwave background, indicate that about $\sim 80\%$ of matter in the universe is in an unknown form, and the expectations for providing an answer to such a pressing question run high. These observational results are justified within the standard ΛCDM dark matter/dark energy model [1] which has been very successful in explaining the data. It predicts a dark energy component about $68 \pm 1\%$ of the total mass/density contributions of our universe in the form of a cosmological constant. The latter accounts for the dark energy dominance in the cosmological expansion at late times and provides the cosmological acceleration measured by Type Ia supernovae [2, 3], with ordinary baryonic dark matter contributing just a few percent of the total mass/energy content

(∼5%) and a smaller neutrino component. Cold dark matter with small density fluctuations, growing gravitationally and a spectral index of the perturbations $n_S \sim 1$ is compatible with an early inflationary stage and accounts for structure formation in most of the early universe eras. By now, data on the CMB, weak lensing and structure formation, covering redshifts from large $z \sim 10^3$ down to $z <\sim O(1)$ where the full nonlinear regime of matter dominance is at work, have been confronted with N-body gravitational simulations for quite some time, with comparisons which are in general agreement with ΛCDM. Such simulations, characterized by perturbations with the above value of the spectral index show the emergence of hierarchical, self-similar structures in the form of halos and sub-halos of singular density ($\rho(r) \sim 1/r$ in terms of the radius r) [4] in the nonlinear regime. However, while the agreement between ΛCDM and the observations is significant at most scales, at a small sub-galactic scale, corresponding to astrophysical distances relevant for the description of the stellar distributions (∼10 kpc), cold dark matter models predict an abundance of low-mass halos in excess of observations [5]. Difficulties in characterizing this sub-galactic region have usually been attributed to inaccurate modeling of its baryonic content, connected with star formation, supernova explosions and black hole activity which take place in that region, causing a redistribution of matter.

There are various possibilities to solve this discrepancy, such as invoking the presence of warm dark matter (WDM), whose free streaming, especially for low mass WDM particles, could erase halos and sub-halos of low mass. At the same time, they could remove the predicted dark matter cusps in $\rho(r)$, present in the simulations for $r \simeq 0$ [4] but are not detected observationally. As observed in Hu et al. [5] and recently re-addressed in Hui et al. [6], these issues define a problem whose resolution may require a cold dark matter component which is ultralight, in the $10^{-20} - 10^{-22}$ eV range. Proposals for such a component of dark matter, find motivations mostly within string theory, where massless moduli in the form of scalar and pseudoscalar fields abound at low energy. They are introduced at the Planck scale and their flat potentials can be lifted by a small amount, giving rise to ultralight particles. However, the characterization of a well-defined gauge structure which may account for the generation Of such ultralight particle(s) and which may eventually connect the speculative scenarios to the electroweak scale, can be pursued in various ways. It has recently been proposed [7] that particles of this kind may emerge from a grand unification in the presence of anomalous abelian symmetries, revisiting previous constructions.

The goal of this review is to summarize the gauge structure of these models which require an anomalous fermion spectrum with gauge invariance restored by a Wess-Zumino interaction, by the inclusion of a Stückelberg axion. Such models can be thought as the field theory realization of the mechanism of anomaly cancellation derived from string theory. The models reviewed here are characterized by some distinctive key features that we discuss, in order to establish their relation to the Peccei-Quinn model, of which they are an extension at a field theory level.

2. ANOMALOUS U(1)'S

The Peccei-Quinn (PQ) mechanism, proposed in the 1970's to solve the strong CP problem [8–10], had originally been realized by assigning an additional abelian chiral charge to the fermion spectrum of the Standard Model (SM). Alternatively, a similar symmetry can be present in a natural way in specific gauge theories based on groups of higher ranks with respect to the SM gauge group. This is the case, for instance of the $U(1)_{PQ}$ symmetry found in the E_6 GUT discussed in Frampton and Kephart [11] (as well as in other realizations), which is naturally present in this theory and which can lead to a solution of the strong CP problem.

As we are going to discuss, the mass of the axion, either in the presence of global or local anomalies is connected to the instanton sector of a non-abelian theory and it is crucial for the mechanism of misalignment to be effective so that the axion couples to the gauge sector of the same theory. In fact, the possibility that more than one axion is part of the spectrum of a certain gauge theory is not excluded, with the mass of each axion controlled by independent mechanism(s) of vacuum misalignment induced at several scales, if distinct gauge couplings for each of such particles with different gauge sectors are present [12, 13]. We will illustrate this point in the extended E_6 theory, in the next sections, where the inclusion of an extra anomalous $U(1)$ gauge symmetry realizes such a scenario. Different mechanisms of vacuum misalignment may be responsible for the generation of axions of different masses, whose sizes may vary considerably.

2.1. Anomaly Cancellation at Field Theory Level With an Axion

In the case of a Stückelberg axion, as already mentioned, the PQ symmetry is generalized from a global to a local gauge symmetry and the Wess-Zumino interactions are needed for the restoration of gauge invariance of the effective action. Such generalizations, originally discussed in the context of low scale orientifold models [14], where anomalous abelian symmetries emerge from stacks of intersecting branes, have in the past been proposed as possible scenarios to be investigated at the LHC [15–20], together with their supersymmetric extensions [13, 21, 22]. While anomalous abelian symmetries are interesting in their own right, especially in the search for extra neutral currents at the LHC [18, 23–25], one of the most significant aspects of such anomalous extensions is in fact the presence of an axion which is needed in order to restore the gauge invariance of the effective action. It was called the "axi-Higgs" in Corianò et al. [14] and Corianò and Irges [15]–for being generated by the mechanism of Higgs-Stückelberg mixing in the CP-odd scalar sector, induced by a PQ-breaking periodic potential, later studied for its implications for dark matter in Corianò et al. [12]. The appearance of such a potential is what allows one component of the Stückelberg field to become physical. A periodic potential can be quickly recognized as being of instanton origin and related to the θ-vacuum of Yang-Mills theory and can be associated with phase transitions in non-abelian theories. Recent developments have considered the possibility that the origin of such a potential of this form can

be set at a very large scale, such as the scale of grand unification (GUT). Its size is related to the value of the gauge coupling at the GUT scale, characterized by a typical instanton suppression, where the mechanism of vacuum misalignment takes place.

2.2. An Ultralight Axion

In the case of a misalignment generated at the GUT scale, the mass of the corresponding axion is strongly suppressed and can reach the far infrared, in the range of $10^{-20} - 10^{-22}$ eV, which is in the optimal range for a possible resolution of several astrophysical issues, such as those mentioned in the introduction [6]. Proposals for a fuzzy component of dark matter require a weakly interacting particle in that mass range. As in the PQ (invisible axion) case. Additionally, in this case two scales are also needed in order to realize a similar scenario. In the PQ case the two scales correspond to f_a, the large PQ breaking scale and the hadronic scale which links the axion mass, f_a, the pion m_π and the light quarks masses m_u, m_d, in an expression that we will summarize below. In the case of Stückelberg axions these fields can be introduced as duals of a 2-form ($B_{\mu\nu}$), defined at the Planck scale (M_P) and coupled to the field strength (F) of an anomalous gauge boson via a $B \wedge F$ interaction [7].

The mechanism of Higgs-axion mixing and the generation of the periodic potential can take place at a typical GUT scale. It is precisely the size of the potential at the GUT scale, which is controlled by the θ-vacuum of the corresponding GUT symmetry, which is responsible for the generation of an ultralight axion in the spectrum. As already mentioned, in the model discussed in Corianò and Frampton [7] a second axion is present, specific to the E_6 part of the $E_6 \times U(1)_X$ symmetry, which is sensitive to the $SU(3)$ color sector of the Standard Model after spontaneous symmetry breaking. This second field takes the role of an ordinary PQ axion and solves the strong CP problem. We will start by recalling the main features of the PQ solution, in particular the emergence of a mass/coupling relation in such a scenario which narrows the window for axion detection down and gets enlarged in the presence of a gauge anomaly in Stückelberg models [20]. We will then turn, in the second part of this review, to a discussion of the Stückelberg extension. We will describe the features of such models in them non-supersymmetric formulation. Their supersymmetric version requires a separate discussion, for predicting both an axion and a neutralino as possible dark matter relics [13, 22].

3. THE INVISIBLE PQ AXION

The theoretical prediction for the mass range in which to locate a PQ axion is currently below the eV region. The PQ solution to the strong CP problem has been formulated according to two main scenarios involving a light pseudoscalar ($a(x)$) which nowadays take the name from the initials of the proponents, the KSVZ axion (or hadronic axion) and the DFSZ [26, 27] axion, the latter introduced in a model which requires, in addition, a scalar sector with two Higgs doublets H_u and H_d, besides the PQ complex scalar Φ.

The small axion mass is attributed to a vacuum misalignment mechanism generated by the structure of the QCD vacuum at the QCD phase transition, which causes a tilt in the otherwise flat PQ potential. The latter undergoes a symmetry breaking at a scale v_{PQ}, in general assumed to lay above the scales of inflation H_I and of reheating (T_R), and hence quite remote from the electroweak/confinement scales. Other possible locations of v_{PQ} with respect to H_I and T_R are also possible.

In both solutions the Peccei-Quinn scalar field Φ, displays an original symmetry which can be broken by gravitational effects, with a physical Goldstone mode $a(x)$ which remains as such from the large v_{PQ} scale down to Λ_{QCD}, when axion oscillations occur. In the DFSZ solution, the axion emerges as a linear combination of the phases of the CP-odd sector and of Φ which are orthogonal to the hypercharge (Y) and are fixed by the normalization of the kinetic term of the axion field a. The solution to the strong CP problem is then achieved by rendering the parameter of the θ-vacuum dynamical, with the angle θ replaced by the axion field ($\theta \to a/f_a$), with f_a being the axion decay constant. The computation of the axion mass m_a is then derived from the vacuum energy of the θ-vacuum $E(\theta)$ once this is re-expressed in terms of the QCD chiral Lagrangian, which in the two quark flavor (u,d) case describes the spontaneous breaking of the $SU(2)_L \times SU(2)_R$ flavor symmetry to a diagonal $SU(2)$ subgroup, with the 3 Goldstone modes $(\pi^\pm, \pi^0)$ being the dynamical field of the low energy dynamics. In this effective chiral description in which the θ parameter is present, the vacuum energy acquires a dependence both on neutral pseudoscalar π^0 and on θ of the form

$$E(\pi^0,\theta) = -m_\pi^2 f_\pi^2 \sqrt{\cos^2\frac{\theta}{2} + \left(\frac{m_d - m_u}{m_d + m_u}\right)^2 \sin^2\frac{\theta}{2}}\cos\left(\pi^0 - \phi(\theta)\right) \quad (1)$$

with

$$\phi(\theta) \equiv \frac{m_d - m_u}{m_d + m_u}\sin\frac{\theta}{2}. \quad (2)$$

At the minimum, when $\pi^0 = f_\pi \phi(\theta)$, the vacuum energy assumes the simpler form

$$E(\theta) = -m_\pi^2 f_\pi^2 \sqrt{1 - \frac{4 m_u m_d}{(m_u + m_d)^2}\sin^2\frac{\theta}{2}} \quad (3)$$

which expanded for small θ gives the well-known relation

$$E(\theta) = -m_\pi^2 f_\pi^2 + \frac{1}{2} m_\pi^2 f_\pi^2 \frac{m_u m_d}{(m_u + m_d)^2}\theta^2 + \ldots \quad (4)$$

and the corresponding axion mass

$$m_a^2 = \frac{m_\pi^2 f_\pi^2}{f_a^2}\frac{m_u m_d}{(m_u + m_d)^2} \quad (5)$$

as $\theta \to a/f_a$. Before getting into a more detailed analysis of the various possible extensions of the traditional PQ scenarios, we briefly review the KSVZ (hadronic) and DFSZ (invisible) axion solutions.

3.1. KSVZ and DFSZ Axions

In both the DFSZ and KSVZ scenarios a global anomalous $U(1)_{PQ}$ symmetry gets broken at some large scale v_{PQ}, with the generation of a Nambu-Goldstone mode from the CP-odd scalar sector. In the KSVZ case the theory includes a heavy quark Q which acquires a large mass by a Yukawa coupling with the scalar Φ. In this case the Lagrangian of Q takes the form

$$\mathscr{L} = |\partial\Phi|^2 + i\bar{Q}\not{D}\ Q + \lambda\Phi\bar{Q}_L Q_R + h.c. - V(\Phi) \tag{6}$$

with a global $U(1)_{PQ}$ chiral symmetry of the form

$$\begin{aligned} \Phi &\to e^{i\alpha}\Phi \\ Q &\to e^{-\frac{i}{2}\alpha\gamma_5} Q \end{aligned} \tag{7}$$

with an $SU(3)_c$ covariant derivative (D) containing the QCD color charge of the heavy fermion Q. The scalar PQ potential can be taken from the usual Mexican-hat form and it is $U(1)_{PQ}$ symmetric. Parameterising the PQ field with respect to its broken vacuum

$$\Phi = \frac{\phi + v_{pq}}{\sqrt{2}} e^{i\frac{a(x)}{v_{PQ}}} + \dots \tag{8}$$

the Yukawa coupling of the heavy quark Q to the CP-odd phase of Φ, $a(x)$, takes the form

$$\lambda\frac{v_{pq}}{\sqrt{2}} e^{i\frac{a(x)}{v_{PQ}}}\bar{Q}_L Q_R. \tag{9}$$

At this stage one assumes that there is a decoupling of the heavy quark from the low energy spectrum by assuming that v_{PQ} is very large. The standard procedure in order to extract the low energy interaction of the axion field is to first redefine the field Q on order to remove the exponential with the axion in the Yukawa coupling

$$e^{i\gamma_5\frac{a(x)}{2v_{PQ}}} Q_{L/R} \equiv Q'_{L/R}. \tag{10}$$

This amounts to a chiral transformation which leaves the fermionic measure non-invariant

$$\mathrm{D}\bar{Q}\mathrm{D}Q \to e^{i\int d^4x \frac{6a(x)}{32\pi^2 v_{PQ}} G(x)\tilde{G}(x)} \mathrm{D}\bar{Q}\mathrm{D}Q \tag{11}$$

and generates a direct coupling of the axion to the anomaly $G\tilde{G}$. Here the factor of 6 is related to the number of L/R components being rotated, which is 6 if Q is assigned to the triplet of $SU(3)_c$.

The kinetic term of Q is not invariant under this field redefinition and generates a derivative coupling of $a(x)$ to the axial vector current of Q. For n_f triplets, for instance, the effective action of the axion, up to dimension-5 takes the form

$$\mathscr{L}_{eff} = \frac{1}{2}\partial_\mu a(x)\partial^\mu a(x) + \frac{6n_f}{32\pi^2 v_{PQ}} a(x) G\tilde{G} + \frac{1}{v_{PQ}}\partial_\mu a\bar{Q}\gamma^\mu\gamma_5 Q + \dots \tag{12}$$

where we have neglected extra higher dimensional contributions, suppressed by v_{PQ}.

In the case of the DFSZ axion, the solution to the strong CP problem is found by introducing a scalar Φ together with two Higgs doublets H_u and H_d. In this case one writes down a general potential, function of these three fields, which is $SU(2) \times U(1)$ invariant and possesses a global symmetry

$$H_u \to e^{i\alpha X_u} H_u, \qquad H_d \to e^{i\alpha X_d} H_d, \qquad \Phi \to e^{i\alpha X_\Phi}\Phi \tag{13}$$

with $X_u + X_d = -2X_\Phi$. It is given by a combination of terms of the form

$$V = V(|H_u|^2, |H_d|^2, |\Phi|^2, |H_u H_d^\dagger|^2, |H_u \cdot H_d|^2, H_u \cdot H_d, \Phi^2) \tag{14}$$

where $H_u \cdot H_d$ denotes the $SU(2)$ invariant scalar product. The identification of the axion field is made by looking for a linear combination of the phases which is not absorbed by a gauge transformation. This can be done, for instance, by going to the unitary gauge and removing all the NG modes of the broken gauge symmetry. The corresponding phase, which is the candidate axion, is the result of a process of mixing the PQ field with the Higgs sector at a scale where the symmetry of the potential is spontaneously broken by the two Higgs fields.

4. TEV SCALE: STÜCKELBERG AXIONS IN ANOMALOUS *U*(1) EXTENSIONS OF THE STANDARD MODEL

Intersecting D-brane models are one of those constructions where generalized axions appear [28–31]. In the case in which several stacks of such branes are introduced, each stack being the domain in which fields with the gauge symmetry $U(N)$ live, several intersecting stacks generate, at their common intersections, fields with the quantum numbers of all the unitary gauge groups of the construction, such as

$$\begin{aligned} U(N_1) \times U(N_2) \times \dots \times U(N_k) = SU(N_1) \times U(1) \times SU(N_2) \\ \times U(1) \times \dots \times SU(N_k) \times U(1). \end{aligned} \tag{15}$$

The phases of the extra $U(1)$'s are rearranged in terms of an anomaly-free generator, corresponding to an (anomaly free) hypercharge $U(1)$ (or $U(1)_Y$), times extra $U(1)$'s which are anomalous, carrying both their own anomalies and the mixed anomalies with all the gauge factors of the Standard Model. This general construction can be made phenomenologically interesting.

Using this approach, the Standard Model can be obtained by taking for example 3 stacks of branes: a first stack of 3 branes, yielding a $U(3)$ gauge symmetry, a second stack of 2 branes, yielding a symmetry $U(2)$ and an extra single $U(1)$ brane, giving a gauge structure of the form $SU(3) \times SU(2) \times U(1) \times U(1) \times U(1)$. Linear combinations of the generators of the three $U(1)$'s allow us to rewrite the entire abelian symmetry in the form $U(1)_Y \times U(1)' \times U(1)''$, with the remaining $U(1)' \times U(1)''$ factors carrying anomalies which need to be canceled by extra operators. The simplest realization of the Standard Models (SM) is obtained by 2 stacks and a single brane at their intersections, giving a symmetry $U(3) \times U(2) \times U(1)$. In this case, in the hypercharge

basis, the gauge structure of the model can be rewritten in the form $SU(3)_c \times SU(2)_w \times U(1)_Y \times U(1)' \times U(1)''$.

We consider the case of a single $U(1)' \equiv U(1)_B$ anomalous gauge symmetry, where the Stückelberg field $b(x)$ couples to the gauge field B_μ by the gauge invariant term

$$\mathscr{L}_{St} = \frac{1}{2}\left(\partial_\mu b - MB_\mu\right)^2 \tag{16}$$

which is the well-known Stückelberg form. M is the Stückelberg mass. The Stückelberg symmetry of the Lagrangian (16) is revealed by acting with gauge transformations of the gauge fields B_μ under which the axion b varies by a local shift

$$\delta_B B_\mu = \partial_\mu \theta_B \qquad\qquad \delta b = M\theta_B \tag{17}$$

parameterized by the local gauge parameters θ_B. Originally, the Stückelberg symmetry was presented as a way to give a mass to an abelian gauge field while still preserving the gauge invariance of the theory. However, it is clear nowadays that its realization is the same one as obtained, for instance, in an abelian-Higgs model when one decouples the radial excitations of the Higgs fields from its phase [20]. The bilinear ∂B mixing present in Equation (16) is an indication that the b field describes a Nambu-Goldstone mode which could, in principle, be removed by a unitary gauge condition. We will come back to this point later in this review. There is a natural way to motivate Equation (16).

If we assume that the $U(1)_B$ gauge symmetry is generated within string theory and realized around the Planck scale, the massive anomalous gauge boson acquires a mass through the presence of an $A \wedge F$ coupling in the bosonic sector of a string-inspired effective action [32]. The starting Lagrangian of the effective theory involves, in this case, an antisymmetric rank-2 tensor $A_{\mu\nu}$ coupled to the field strength $F_{\mu\nu}$ of B_μ

$$L = -\frac{1}{12}H^{\mu\nu\rho}H_{\mu\nu\rho} - \frac{1}{4g^2}F^{\mu\nu}F_{\mu\nu} + \frac{M}{4}\,\epsilon^{\mu\nu\rho\sigma}A_{\mu\nu}\,F_{\rho\sigma}, \tag{18}$$

where

$$H_{\mu\nu\rho} = \partial_\mu A_{\nu\rho} + \partial_\rho A_{\mu\nu} + \partial_\nu A_{\rho\mu}, \qquad F_{\mu\nu} = \partial_\mu B_\nu - \partial_\nu B_\mu \tag{19}$$

is the kinetic term for the 2-form and g is an arbitrary constant. Besides the two kinetic terms for $A_{\mu\nu}$ and B_μ, the third contribution in Equation (18) is the $A \wedge F$ interaction.

The Lagrangian is dualized by using a "first order" formalism, where H is treated independently from the antisymmetric field $A_{\mu\nu}$. This is obtained by introducing a constraint with a Lagrangian multiplier field $b(x)$ in order to enforce the condition $H = dA$ from the equations of motion of b, in the form

$$L_0 = -\frac{1}{12}H^{\mu\nu\rho}H_{\mu\nu\rho} - \frac{1}{4g^2}F^{\mu\nu}\,F_{\mu\nu} - \frac{M}{6}\,\epsilon^{\mu\nu\rho\sigma}H_{\mu\nu\rho}\,B_\sigma + \frac{1}{6}\,b(x)\,\epsilon^{\mu\nu\rho\sigma}\,\partial_\mu H_{\nu\rho\sigma}. \tag{20}$$

The appearance of a scale M in this Lagrangian is crucial for the cosmological implications of such a theory [18], since it defines the energy region where the mechanism of anomaly cancellation comes into play [14]. The last term in (20) is necessary in order to reobtain (18) from (20). If, instead, we integrate by parts the last term of the Lagrangian given in (20) and solve trivially for H we find

$$H^{\mu\nu\rho} = -\epsilon^{\mu\nu\rho\sigma}\left(MB_\sigma - \partial_\sigma b\right), \tag{21}$$

and inserting this result back into (20) we obtain the expression

$$L_A = -\frac{1}{4g^2}\,F^{\mu\nu}\,F_{\mu\nu} - \frac{1}{2}\left(MB_\sigma - \partial_\sigma b\right)^2 \tag{22}$$

which is the Stückelberg form for the mass term of B. This rearrangement of the degrees of freedom is an example of the connection between Lagrangians of antisymmetric tensor fields and their dual formulations which, in this specific case, is an abelian massive Yang-Mills theory in a Stückelberg form.

The axion field, generated by the dualization mechanism, appears as a Nambu-Goldstone mode, which can be removed by a unitary gauge choice. However, as discussed in Corianò et al. [14], the appearance, at a certain scale, of an extra potential which will mix this mode with the scalar sector, will allow to extract a physical component out of b, denoted by χ.

The origin of such a mixing potential is here assumed to be of non-perturbative origin and triggered at a scale below the Stückelberg scale M. It is at this second scale where a physical axion appears in the spectrum of the theory. The local shift invariance of $b(x)$ is broken by the vev of the Higgs sector appearing in the part of the potential that couples the Stückelberg field to the remaining scalars, causing a component of the Stückelberg to become physical. The scale at which this second potential is generated and gets broken is the second scale controlling the mass of the axion, χ. Such a potential is by construction periodic in χ, as we are going to illustrate below, and it is quite similar to the one discussed in Equation (14). Its size is controlled by constants (λ_i) which are strongly suppressed by the exponential factor ($\sim e^{-S_{inst}}$, with S_{inst} the instanton action), determined by the value of the action in the instanton background.

In models with several $U(1)$'s this construction is slightly more involved, but the result of the mixing of the CP odd phases leaves as a remnant, also in this case, only one physical axion [14], whose mass is controlled by the size of the Higgs-axion mixing.

4.1. Stückelberg Models at the TeV Scale With Two-Higgs Doublets

The type of models investigated in the past have been formulated around the TeV scale and discussed in detail in their various sectors [15–20, 33, 34]. We offer a brief description of such realizations, which extend the symmetry of the SM minimally and as such are simpler than in other realizations involving larger gauge symmetries. They have the structure of effective actions where dimension-5 interactions are introduced in order to restore the gauge invariance of the Lagrangian in the presence of an anomalous gauge boson (and corresponding fermion spectrum). Therefore, they are quite different from ordinary anomaly-free versions of the same theories. They include one

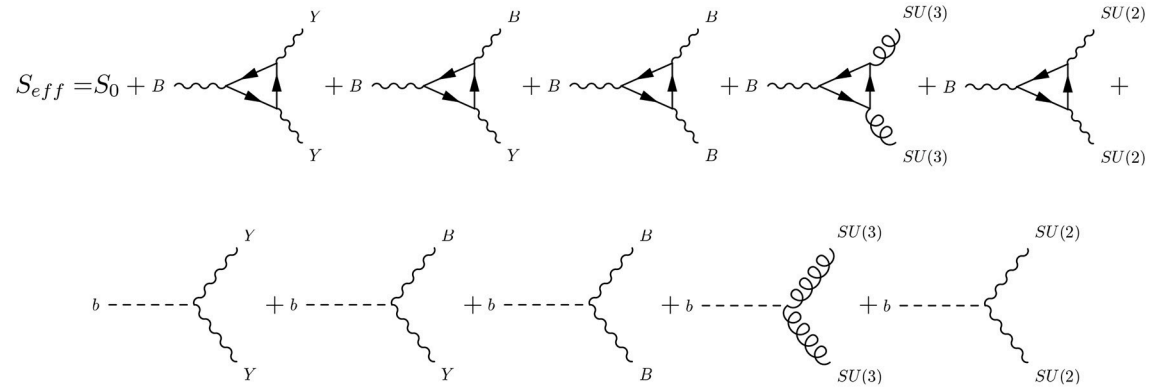

FIGURE 1 | The 1PI effective action for a typical low scale model obtained by adding one extra anomalous $U(1)_B$ to the Standard Model action. Shown are the one-loop trilinear anomalous interactions and the corresponding counterterms, involving the b field.

extra anomalous $U(1)_B$ symmetry, the Stückelberg field and a set of scalars with a sufficiently wide CP odd sector in order to induce a mixing potential between the scalar fields and the Stückelberg. Obviously, such models are of interest at the LHC for predicting anomalous gauge interactions in the form of extra neutral currents [18, 23] with respect to those of the electroweak sector.

The effective action has the structure given by

$$\mathscr{S} = \mathscr{S}_0 + \mathscr{S}_{Yuk} + \mathscr{S}_{an} + \mathscr{S}_{WZ} \tag{23}$$

where $\mathscr{S}_0$ is the classical action. The same structure will characterize also other, more complex, realizations. It contains the usual gauge degrees of freedom of the Standard Model plus the extra anomalous gauge boson B which is already massive before electroweak symmetry breaking, via a Stückelberg mass term, as it is clear from (22). We show the structure of the 1-particle irreducible effective action in **Figure 1**. We consider a 2-Higgs doublet model for definiteness, which will set the ground for more complex extensions that we will address in the next sections. We consider an $SU(3)_c \times SU(2)_w \times U(1)_Y \times U(1)_B$ gauge symmetry model, characterized by an action $\mathscr{S}_0$, corresponding to the first contribution shown in **Figure 1**, plus, one loop corrections which are anomalous and break gauge invariance whenever there is an insertion of the anomalous gauge boson B_μ in the trilinear fermion vertices. In the last line of the same figure are shown the $(b/M)F \wedge F$ Wess-Zumino counterterms needed for restoring gauge invariance, which are suppressed by the Stückelberg scale M. **Table 1** shows the charge assignments of the fermion spectrum of the model, where we have indicated by q the charges for a single generation, having considered the conditions of gauge invariance of the Yukawa couplings. Notice that the two Higgs fields carry different charges under $U(1)_B$, which allow to extend the ordinary scalar potential of the two-Higgs doublet model by a certain extra contribution. This will be periodic in the axi-Higgs χ, after the two Higgses, here denoted as H_u and H_d, acquire a vev. Specifically, q^B_L, q^B_Q denote the charges of the left-handed lepton doublet (L) and of the quark doublet (Q) respectively, while $q^B_{u_r}, q^B_{d_r}, q^B_{e_R}$ are the charges of the right-handed

TABLE 1 | Charges of the fermion and of the scalar fields.

f	Q	u_R	d_R	L	e_R
q^B	q^B_Q	$q^B_{u_R}$	$q^B_{d_R}$	q^B_L	$q^B_{e_R}$

f	$SU(3)_C$	$SU(2)_L$	$U(1)_Y$	$U(1)_B$
Q	3	2	1/6	q^B_Q
u_R	3	1	2/3	$q^B_Q + q^B_u$
d_R	3	1	−1/3	$q^B_Q - q^B_d$
L	1	2	−1/2	q^B_L
e_R	1	1	−1	$q^B_L - q^B_d$
H_u	1	2	1/2	q^B_u
H_d	1	2	1/2	q^B_d

$SU(2)$ singlets (quarks and leptons). We denote by $\Delta q^B = q^B_u - q^B_d$ the difference between the two charges of the up and down Higgses (q^B_u, q^B_d) respectively and from now on we will assume that it is non-zero. The trilinear anomalous gauge interactions induced by the anomalous $U(1)$ and the relative counterterms, which are all parts of the 1-loop effective action, are illustrated in **Figure 1**.

4.2. Fermion/Gauge Field Couplings

The models that we discuss are characterized by one extra neutral current, mediated by a Z' gauge boson. The interaction of the fermions with the gauge fields is defined by the Lagrangian

$$\begin{aligned} L^{quarks}_{int} = &\left(\bar{u}_{Li}\ \bar{d}_{Li}\right)\gamma^\mu\left[-g_s T^a G^a_\mu - g_2\tau^a W^a_\mu - \frac{1}{12}g_Y Y_\mu - \frac{1}{2}g_B q^B_Q B_\mu\right]\begin{pmatrix}u_{Li}\\ d_{Li}\end{pmatrix} + \\ &+ \bar{u}_{Ri}\gamma^\mu\left[-g_s T^a G^a_\mu - g_2\tau^a W^a_\mu - \frac{1}{3}g_Y Y_\mu - \frac{1}{2}g_B q^B_{u_R} B_\mu\right]u_{Ri} \\ &+ \bar{d}_{Ri}\,\gamma^\mu\left[-g_s T^a G^a_\mu - g_2\tau^a W^a_\mu + \frac{1}{6}g_Y Y_\mu - \frac{1}{2}g_B q^B_{d_R} B_\mu\right]d_{Ri}. \end{aligned} \tag{24}$$

while the Higgs sector is characterized by the two Higgs doublets

$$H_u = \begin{pmatrix} H_u^+ \\ H_u^0 \end{pmatrix} \quad H_d = \begin{pmatrix} H_d^+ \\ H_d^0 \end{pmatrix} \tag{25}$$

where H_u^+, H_d^+ and H_u^0, H_d^0 are complex fields with (with some abuse of notation we rescale the fields by a factor of $1/\sqrt{2}$)

$$\begin{aligned} H_u^+ &= \frac{\mathrm{Re}H_u^+ + i\mathrm{Im}H_u^+}{\sqrt{2}}, \quad H_d^- = \frac{\mathrm{Re}H_d^- + i\mathrm{Im}H_d^-}{\sqrt{2}}, \\ H_u^- &= H_u^{+*}, \quad H_d^+ = H_d^{-*}. \end{aligned} \tag{26}$$

Expanding around the vacuum we get for the neutral components

$$H_u^0 = v_u + \frac{\mathrm{Re}H_u^0 + i\mathrm{Im}H_u^0}{\sqrt{2}}, \quad H_d^0 = v_d + \frac{\mathrm{Re}H_d^0 + i\mathrm{Im}H_d^0}{\sqrt{2}}. \tag{27}$$

which will play a key role in determining the mixing of the Stückelberg field in the periodic potential. The electroweak mixing angle is defined by $\cos\theta_W = g_2/g, \sin\theta_W = g_Y/g$, with $g^2 = g_Y^2 + g_2^2$. We also define $\cos\beta = v_d/v$, $\sin\beta = v_u/v$ with $v^2 = v_d^2 + v_u^2$. The matrix rotates the neutral gauge bosons from the interaction to the mass eigenstates after electroweak symmetry breaking and has elements which are $O(1)$, being expressed in terms of ratios of coupling constants, which correspond to mixing angles. It is given by

$$\begin{pmatrix} A_\gamma \\ Z \\ Z' \end{pmatrix} = O^A \begin{pmatrix} W_3 \\ A^Y \\ B \end{pmatrix} \tag{28}$$

which can be approximated to leading order as

$$O^A \simeq \begin{pmatrix} \frac{g_Y}{g} & \frac{g_2}{g} & 0 \\ \frac{g_2}{g} + O(\epsilon_1^2) & -\frac{g_Y}{g} + O(\epsilon_1^2) & \frac{g}{2}\epsilon_1 \\ -\frac{g_2}{2}\epsilon_1 & \frac{g_Y}{2}\epsilon_1 & 1 + O(\epsilon_1^2) \end{pmatrix} \tag{29}$$

where

$$\begin{aligned} \epsilon_1 &= \frac{x_B}{M^2}, \\ x_B &= \left(q_u^B v_u^2 + q_d^B v_d^2\right). \end{aligned} \tag{30}$$

Once the WZ counterterms rotates into the gauge eigenstates and the b field into the physical χ field, there will be a direct coupling of the anomaly to the physical gauge bosons. This will involve both the neutral and the charged sectors. More details can be found in Corianò et al. [17].

4.3. Counterterms

Fixing the values of the counterterms in simple single $U(1)$ models like the one we are reviewing, allows to gain some insight into the possible solutions of the gauge invariance conditions on the Lagrangian. The numerical values of the counterterms appearing in the second line of **Figure 1** are fixed by such conditions, giving

$$\begin{aligned} C_{BYY} &= -\frac{1}{6}q_Q^B + \frac{4}{3}q_{u_R}^B + \frac{1}{3}q_{d_R}^B - \frac{1}{2}q_L^B + q_{e_R}^B, \\ C_{YBB} &= -(q_Q^B)^2 + 2(q_{u_r}^B)^2 - (q_{d_R}^B)^2 + (q_L^B)^2 - (q_{e_R}^B)^2, \\ C_{BBB} &= -6(q_Q^B)^3 + 3(q_{u_R}^B)^3 + 3(q_{d_R}^B)^3 - 2(q_L^B)^3 + (q_{e_R}^B)^3, \end{aligned}$$

$$\begin{aligned} C_{Bgg} &= \frac{1}{2}(-2q_Q^B + q_{d_R}^B + q_{u_R}^B), \\ C_{BWW} &= \frac{1}{2}(-q_L^B - 3q_Q^B). \end{aligned} \tag{31}$$

They are, respectively, the counterterms for the cancellation of the mixed anomaly $U(1)_B U(1)_Y^2$ and $U(1)_Y U(1)_B^2$; the counterterm for the BBB anomaly vertex or $U(1)_B^3$ anomaly, and those of the $U(1)_B SU(3)^2$ and $U(1)_B SU(2)^2$ anomalies. From the Yukawa couplings we get the following constraints on the $U(1)_B$ charges

$$q_Q^B - q_d^B - q_{d_R}^B = 0 \;\; q_Q^B + q_u^B - q_{u_R}^B = 0 \;\; q_L^B - q_d^B - q_{e_R}^B = 0. \tag{32}$$

Using the equations above, we can eliminate some of the charges in the expression of the counterterms, obtaining

$$\begin{aligned} C_{BYY} &= \frac{1}{6}(3q_L^B + 9q_Q^B + 8\Delta q^B), \\ C_{YBB} &= 2\left[q_d^B(q_L^B + 3q_Q^B) + 2\Delta q^B(q_d^B + q_Q^B) + (\Delta q^B)^2\right], \\ C_{BBB} &= (q_L^B - q_d^B)^3 + 3(q_d^B + q_Q^B + \Delta q^B)^3 + 3(q_Q^B - q_d^B)^3 \\ &\quad - 2(q_L^B)^3 - 6(q_Q^B)^3, \\ C_{Bgg} &= \frac{\Delta q^B}{2}, \\ C_{BWW} &= \frac{1}{2}(-q_L^B - 3q_Q^B). \end{aligned} \tag{33}$$

The equations above parametrize, in principle, an infinite class of models whose charge assignments under $U(1)_B$ are arbitrary, with the charges in the last column of **Table 1** taken as their free parameters. The coupling of the axion to the corresponding gauge bosons can be fixed by a complete solution to the anomaly constraints, which may provide us with an insight into the possible mechanisms of misalignment that could take place at both the electroweak and at the QCD phase transitions.

4.4. Choice of the Charges

Due to the presence, in general, of a nonvanishing mixed anomaly of the $U(1)_B$ gauge factor with both $SU(2)$ and $SU(3)$, the Stückelberg axion of the model has interactions with both the strong and the weak sectors, which both support instanton solutions, and therefore could acquire a mass non-perturbatively both at the electroweak and at the QCD phase transitions. In this case we consider the possibility of having sequential misalignments, with the largest contribution to the mass coming from the latter. Obviously, for a choice of charges characterized

by $\Delta q = 0$, in which both doublets of the Higgs sector H_u and H_d carry the same charge under $U(1)_B$, the axion mass will not acquire any instanton correction at the QCD phase transition. In this case the potential responsible for Higgs-axion mixing would vanish. In this scenario a solution to the anomaly equations with a vanishing electroweak interaction of the Stückelberg can be obtained by choosing $q_L^B = -3q_Q^B$.

If instead the charges are chosen in a way to have both non-vanishing weak (C_{BWW}) and strong (C_{Bgg}) counterterms, it is reasonable to expect that the misalignment of the axion potential will be sequential, with a tiny mass generated at the electroweak phase transition, followed by a second misalignment induced at the strong phase transition. The instanton configurations of the weak and strong sectors will be contributing differently to the mass of the physical axion. However, due to the presence of a coupling of this field with the strong sector, its mass will be significantly dominated by the QCD phase transition, as in the Peccei-Quinn case.

4.5. The Scalar Sector

The scalar sector of the anomalous abelian models is characterized, as already mentioned, by the ordinary electroweak potential of the SM involving, in the simplest formulation, two Higgs doublets $V_{PQ}(H_u, H_d)$ plus one extra contribution, denoted as $V_{PQ}(H_u, H_d, b)$ - or V' (PQ breaking) in Corianò et al. [14] - which mixes the Higgs sector with the Stückelberg axion b, needed for the restoration of the gauge invariance of the effective Lagrangian

$$V = V_{PQ}(H_u, H_d) + V_{PQ}(H_u, H_d, b). \tag{34}$$

The appearance of the physical axion in the spectrum of the model takes place after the phase-dependent terms—here assumed to be of non-perturbative origin and generated at a phase transition—find their way in the dynamics of the model and induce a curvature on the scalar potential. The mixing induced in the CP-odd sector determines the presence of a linear combination of the Stückelberg field b and of the Goldstones of the CP-odd sector which acquires a tiny mass. From (34) we have a first term.

$$\begin{aligned} V_{PQ} \;=\; & \mu_u^2 H_u^\dagger H_u + \mu_d^2 H_d^\dagger H_d + \lambda_{uu}(H_u^\dagger H_u)^2 + \lambda_{dd}(H_d^\dagger H_d)^2 \\ & - \; 2\lambda_{ud}(H_u^\dagger H_u)(H_d^\dagger H_d) + 2\lambda'_{ud}|H_u^T \tau_2 H_d|^2 \end{aligned} \tag{35}$$

typical of a two-Higgs doublet model, to which we add a second PQ breaking term

$$\begin{aligned} V_{PQ} \;=\; & \lambda_0(H_u^\dagger H_d e^{-ig_B(q_u-q_d)\frac{b}{2M}}) + \lambda_1(H_u^\dagger H_d e^{-ig_B(q_u-q_d)\frac{b}{2M}})^2 \\ & + \; \lambda_2(H_u^\dagger H_u)(H_u^\dagger H_d e^{-ig_B(q_u-q_d)\frac{b}{2M}}) + \\ & \lambda_3(H_d^\dagger H_d)(H_u^\dagger H_d e^{-ig_B(q_u-q_d)\frac{b}{2M}}) + \text{h.c.} \end{aligned} \tag{36}$$

These terms are allowed by the symmetry of the model and are parameterized by one dimensionful (λ_0) and three dimensionless couplings ($\lambda_1, \lambda_2, \lambda_3$). Their values are weighted by an exponential factor containing as a suppression the instanton action. In the equations below we will rescale λ_0 by the electroweak scale $v = \sqrt{v_u^2 + v_d^2}$ ($\lambda_0 \equiv \bar{\lambda}_0 v$) so as to obtain a homogeneous expression for the mass of χ as a function of the relevant scales of the model which are, besides the electroweak vev v the Stückelberg mass M and the anomalous gauge coupling of the $U(1)_B$, g_B.

The gauging of an anomalous symmetry has some important effects on the properties of this pseudoscalar, first among all the appearance of independent mass and couplings to the gauge fields. This scenario allows then a wider region of parameter space in which one could look for such particles [15, 17, 20], rendering them "axion-like particles" rather than usual axions. We will still refer to them as axions for simplicity. So far only two complete models have been put forward for a consistent analysis of these types of particles, the first one non-supersymmetric [14] and a second one supersymmetric [22].

4.6. The Potential for a Generic Stückelberg Mass

The physical axion χ emerges as a linear combination of the phases of the various complex scalars appearing in combination with the b field. To illustrate the appearance of a physical direction in the phase of the extra potential, we focus our attention on just the CP-odd sector of the total potential, which is the only one that is relevant for our discussion. The expansion of this potential around the electroweak vacuum is given by the parameterization

$$H_u = \begin{pmatrix} H_u^+ \\ v_u + H_u^0 \end{pmatrix} \qquad H_d = \begin{pmatrix} H_d^+ \\ v_d + H_d^0 \end{pmatrix}. \tag{37}$$

where v_u and v_d are the two vevs of the Higgs fields. This potential is characterized by two null eigenvalues corresponding to two neutral Nambu-Goldstone modes (G_0^1, G_0^2) and an eigenvalue corresponding to a massive state with an axion component (χ). In the ($\text{Im}H_d^0, \text{Im}H_u^0, b$) CP-odd basis we obtain the following normalized eigenstates

$$\begin{aligned} G_0^1 \;=\; & \frac{1}{\sqrt{v_u^2 + v_d^2}}(v_d, v_u, 0) \\ G_0^2 \;=\; & \frac{1}{\sqrt{g_B^2(q_d - q_u)^2 v_d^2 v_u^2 + 2M^2\left(v_d^2 + v_u^2\right)}} \\ & \left(-\frac{g_B(q_d - q_u)v_d v_u^2}{\sqrt{v_u^2 + v_d^2}}, \frac{g_B(q_d - q_u)v_d^2 v_u}{\sqrt{v_d^2 + v_u^2}}, \sqrt{2}M\sqrt{v_u^2 + v_d^2}\right) \\ \chi \;=\; & \frac{1}{\sqrt{g_B^2(q_d - q_u)^2 v_u^2 v_d^2 + 2M^2(v_d^2 + v_u^2)}} \\ & \left(\sqrt{2}Mv_u, -\sqrt{2}Mv_d, g_B(q_d - q_u)v_d v_u\right) \end{aligned} \tag{38}$$

and we indicate with O^χ the orthogonal matrix which allows to rotate them to the physical basis

$$\begin{pmatrix} G_0^1 \\ G_0^2 \\ \chi \end{pmatrix} = O^\chi \begin{pmatrix} \mathrm{Im}H_d^0 \\ \mathrm{Im}H_u^0 \\ b \end{pmatrix}, \tag{39}$$

which is given by

$$O^\chi = \begin{pmatrix} \frac{v_d}{v} & \frac{v_u}{v} & 0 \\ -\frac{g_B(q_d-q_u)v_d v_u^2}{v\sqrt{g_B^2(q_d-q_u)^2 v_d^2 v_u^2+2M^2v^2}} & \frac{g_B(q_d-q_u)v_d^2 v_u}{v\sqrt{g_B^2(q_d-q_u)^2 v_d^2 v_u^2+2M^2v^2}} & \frac{\sqrt{2}Mv}{\sqrt{g_B^2(q_d-q_u)^2 v_d^2 v_u^2+2M^2v^2}} \\ \frac{\sqrt{2}Mv_u}{\sqrt{g_B^2(q_d-q_u)^2 v_u^2 v_d^2+2M^2v^2}} & -\frac{\sqrt{2}Mv_d}{\sqrt{g_B^2(q_d-q_u)^2 v_u^2 v_d^2+2M^2v^2}} & \frac{g_B(q_d-q_u)v_d v_u}{\sqrt{g_B^2(q_d-q_u)^2 v_u^2 v_d^2+2M^2v^2}} \end{pmatrix} \tag{40}$$

where $v = \sqrt{v_u^2 + v_d^2}$.

χ inherits WZ interaction since b can be related to the physical axion χ and to the Nambu-Goldstone modes via this matrix as

$$b = O_{13}^\chi G_0^1 + O_{23}^\chi G_0^2 + O_{33}^\chi \chi, \tag{41}$$

or, conversely,

$$\chi = O_{31}^\chi \mathrm{Im}H_d + O_{32}^\chi \mathrm{Im}H_u + O_{33}^\chi b. \tag{42}$$

Notice that the rotation of b into the physical axion χ involves a factor O_{33}^χ which is of order v/M. This implies that χ inherits from b an interaction with the gauge fields which is suppressed by a scale M^2/v. This scale is the product of two contributions: a $1/M$ suppression coming from the original Wess-Zumino counterterm of the Lagrangian ($b/MF\tilde{F}$) and a factor v/M obtained by the projection of b into χ due to O_χ.

The direct coupling of the axion to the physical gauge bosons via the Wess-Zumino counterterms is obtained by the usual rotation to the mass eigenstates which can be obtained from the rotation matrix O^A defined in (29). The final expression of the coupling of the axi-Higgs to the photon $g_{\chi\gamma\gamma}\chi F_\gamma \tilde{F_\gamma}$, is defined by a combination of matrix elements of the rotation matrices O^A and O^χ. Defining $g^2 = g_2^2 + g_Y^2$, the expression of this coefficient can be derived in the form

$$g_{\gamma\gamma}^\chi = \frac{g_B g_Y^2 g_2^2}{32\pi^2 M g^2} O_{33}^\chi \sum_f \left(-q_{f\,L}^B + q_{f\,R}^B \left(q_{f\,R}^Y\right)^2 - q_{f\,L}^B \left(q_{f\,L}^Y\right)^2 \right). \tag{43}$$

Notice that this expression is cubic in the gauge coupling constants, since factors such as g_2/g and g_Y/g are mixing angles while the factor $1/\pi^2$ originates from the anomaly. Therefore, one obtains a general behavior for $g_{\gamma\gamma}^\chi$ of $O(g^3 v/M^2)$, with charges which are, in general, of order unity.

4.7. Periodicity of the Extra Potential

Equivalently, it is possible to reobtain the results above by an analysis of the phases of the extra potential, which shows how this becomes periodic in χ, the axi-Higgs. This approach shows also quite directly the gauge invariance of χ as a physical pseudoscalar. In fact, if we opt for a polar parametrization of the neutral components in the broken phase

$$\begin{aligned} H_u^0 &= \frac{1}{\sqrt{2}} \left(\sqrt{2} v_u + \rho_u^0(x) \right) e^{i\frac{F_u^0(x)}{\sqrt{2}v_u}} \\ H_d^0 &= \frac{1}{\sqrt{2}} \left(\sqrt{2} v_d + \rho_d^0(x) \right) e^{i\frac{F_d^0(x)}{\sqrt{2}v_d}}, \end{aligned} \tag{44}$$

where we have introduced the two phases F_u and F_d of the two neutral Higgs fields, information on the periodicity is obtained by combining all the phases of V'

$$\theta(x) \equiv \frac{g_B(q_d - q_u)}{2M} b(x) - \frac{1}{\sqrt{2}v_u} F_u^0(x) + \frac{1}{\sqrt{2}v_d} F_d^0(x). \tag{45}$$

Using the matrix O^χ to rotate on the physical basis of the CP-odd scalar sector, the phase describing the periodicity of the potential turns out to be proportional to the physical axion χ, modulo a dimensionful constant (σ_χ)

$$\theta(x) \equiv \frac{\chi(x)}{\sigma_\chi}, \tag{46}$$

where we have defined

$$\sigma_\chi \equiv \frac{2 v_u v_d M}{\sqrt{g_B^2 (q_d - q_u)^2 v_d^2 v_u^2 + 2M^2 (v_d^2 + v_u^2)}}. \tag{47}$$

Notice that σ_χ, in our case, takes the role of f_a of the PQ case, where the angle of misalignment is identified by the ratio a/f_a, with a the PQ axion.

As already mentioned, the re-analysis of the V' potential is particularly useful for proving the gauge invariance of χ under a $U(1)_B$ infinitesimal gauge transformation with gauge parameter $\alpha_B(x)$. In this case one gets

$$\begin{aligned} \delta H_u &= -\frac{i}{2} q_u g_B \alpha_B H_u \\ \delta H_d &= -\frac{i}{2} q_d g_B \alpha_B H_d \\ \delta F_0^u &= -\frac{v_u}{\sqrt{2}} q_u g_B \alpha_B \\ \delta F_0^d &= -\frac{v_d}{\sqrt{2}} q_d g_B \alpha_B \\ \delta b &= -M - S\alpha_B \end{aligned} \tag{48}$$

giving for (46) $\delta\theta = 0$. The gauge invariance under $U(1)_Y$ can also be easily proven using the invariance of the Stückelberg field b under the same gauge group, sand the fact that the hypercharges of the two Higgses are equal. Finally, the invariance under $SU(2)$ is obvious since the linear combination of the phases that define $\theta(x)$ are not touched by the transformation.

From the Peccei-Quinn breaking potential we can extract the following periodic potential

$$V' = 4 v_u v_d \left(\lambda_2 v_d^2 + \lambda_3 v_u^2 + \lambda_0 \right) \cos\left(\frac{\chi}{\sigma_\chi} \right) + 2\lambda_1 v_u^2 v_d^2 \cos\left(2\frac{\chi}{\sigma_\chi} \right), \tag{49}$$

with a mass for the physical axion χ given by

$$m_\chi^2 = \frac{2v_u v_d}{\sigma_\chi^2}\left(\bar{\lambda}_0 v^2 + \lambda_2 v_d^2 + \lambda_3 v_u^2 + 4\lambda_1 v_u v_d\right) \approx \lambda v^2. \quad (50)$$

The size of the potential is driven by the combined product of non-perturbative effects, due to the exponentially small parameters $(\bar{\lambda_0}, \lambda_1, \lambda_2, \lambda_3)$, with the electroweak vevs of the two Higgses. Notice also the irrelevance of the Stückelberg scale M in determining the value of $\sigma_\chi \sim O(v)$ and of m_χ near the transition region, due to the large suppression factor λ in Equation (97). One point that needs to be stressed is the fact that at the electroweak epoch the angle of misalignment generated by the extra potential is parameterized by χ/σ_χ, while the interaction of the physical axion with the gauge fields is suppressed by M^2/v. This feature is obviously unusual, since in the PQ case both scales reduce to a single scale, the axion decay constant f_a.

4.8. The Yukawa Couplings and the Axi-Higgs

The Yukawa couplings determine an interaction of the axi-Higgs to the fermions. This interaction is generated by the rotation in the CP-odd sector of the scalars potential, which mixes the CP-odd components, with the inclusion of the Stückelberg b, via the matrix O_χ. The Yukawa couplings of the model are given by

$$\begin{aligned} L_{\rm Yuk}^{unit.} &= -\Gamma^d\,\bar{Q}H_d d_R - \Gamma^d\,\bar{d}_R H_d^\dagger Q - \Gamma^u\,\bar{Q}_L(i\sigma_2 H_u^*)u_R - \Gamma^u\,\bar{u}_R(i\sigma_2 H_u^*)^\dagger Q_L \\ &\quad -\Gamma^e\,\bar{L}H_d e_R - \Gamma^e\,\bar{e}_R H_d^\dagger L \\ &= -\Gamma^d\,\bar{d}H_d^0 P_R d - \Gamma^d\,\bar{d}H_d^{0*} P_L d - \Gamma^u\,\bar{u}H_u^{0*} P_R u - \Gamma^u\,\bar{u}H_u^0 P_L u \\ &\quad -\Gamma^e\,\bar{e}H_d^0 P_R e - \Gamma^e\,\bar{e}H_d^{0*} P_L e, \end{aligned} \quad (51)$$

where the Yukawa coupling constants Γ^d, Γ^u and Γ^e run over the three generations, i.e., $u = \{u, c, t\}$, $d = \{d, s, b\}$ and $e = \{e, \mu, \tau\}$. Rotating the CP-odd and CP-even neutral sectors into the mass eigenstates and expanding around the vacuum one obtains

$$\begin{aligned} H_u^0 =& v_u + \frac{ReH_u^0 + i\,ImH_u^0}{\sqrt{2}} \\ =& v_u + \frac{(h^0\sin\alpha - H^0\cos\alpha) + i\left(O_{11}^\chi G_0^1 + O_{21}^\chi G_0^2 + O_{31}^\chi \chi\right)}{\sqrt{2}} \end{aligned} \quad (52)$$

$$\begin{aligned} H_d^0 =& v_d + \frac{ReH_d^0 + i\,ImH_d^0}{\sqrt{2}} \\ =& v_d + \frac{(h^0\cos\alpha + H^0\sin\alpha) + i\left(O_{12}^\chi G_0^1 + O_{22}^\chi G_0^1 + O_{32}^\chi \chi\right)}{\sqrt{2}} \end{aligned} \quad (53)$$

where the vevs of the two neutral Higgs bosons $v_u = v\sin\beta$ and $v_d = v\cos\beta$ satisfy

$$\tan\beta = \frac{v_u}{v_d}, \qquad v = \sqrt{v_u^2 + v_d^2}. \quad (54)$$

The fermion masses are given by

$$\begin{aligned} m_u &= v_u\Gamma^u, \qquad & m_\nu &= v_u\Gamma^\nu, \\ m_d &= v_d\Gamma^d, \qquad & m_e &= v_d\Gamma^e, \end{aligned} \quad (55)$$

where the generation index has been suppressed. The fermion masses, defined in terms of the two expectation values v_u, v_d of the model, show an enhancement of the down-type Yukawa couplings for large values of $\tan\beta$ while at the same time the up-type Yukawa couplings get a suppression. The couplings of the h^0 boson to fermions are given by

$$\begin{aligned} L_{\rm Yuk}(h^0) =& -\Gamma^d\,\bar{d}_L d_R\left(\frac{\cos\alpha}{\sqrt{2}}h^0\right) - \Gamma^u\,\bar{u}_L u_R\left(\frac{\sin\alpha}{\sqrt{2}}h^0\right) \\ &- \Gamma^e\,\bar{e}_L e_R\left(\frac{\cos\alpha}{\sqrt{2}}h^0\right) + c.c. \end{aligned} \quad (56)$$

The couplings of the H^0 boson to the fermions are

$$\begin{aligned} L_{\rm Yuk}(H^0) =& -\Gamma^d\,\bar{d}_L d_R\left(\frac{\sin\alpha}{\sqrt{2}}H^0\right) - \Gamma^u\,\bar{u}_L u_R\left(-\frac{\cos\alpha}{\sqrt{2}}H^0\right) \\ &- \Gamma^e\,\bar{e}_L e_R\left(\frac{\sin\alpha}{\sqrt{2}}H^0\right) + c.c. \end{aligned} \quad (57)$$

The interaction of χ with the fermions is proportional to the rotation matrix O^χ and to the mass of the fermion. The decay of the axi-Higgs is driven by two contributions, the direct point-like WZ interaction $(\chi/MF\tilde{F})$ and the fermion loop. The amplitude can be separated in the form corresponding to the two contributions from diagrams of **Figures 2A,B**

$$\mathscr{M}^{\mu\nu}(\chi \to \gamma\gamma) = \mathscr{M}_{WZ}^{\mu\nu} + \mathscr{M}_f^{\mu\nu}. \quad (58)$$

The direct coupling related to the anomaly is given by the vertex shown in **Figure 2A**

$$\mathscr{M}_{WZ}^{\mu\nu}(\chi \to \gamma\gamma) = 4g_{\gamma\gamma}^\chi\,\varepsilon[\mu, \nu, k_1, k_2] \quad (59)$$

coming from the WZ counterterm $\chi F_\gamma \tilde{F}_\gamma$ which gives a decay rate of the form

$$\Gamma_{WZ}(\chi \to \gamma\gamma) = \frac{m_\chi^3}{4\pi}(g_{\gamma\gamma}^\chi)^2. \quad (60)$$

We remark that $g_{\gamma\gamma}^\chi$ is of $O(g^3 v/M^2)$, as derived from Equation (43), with charges that have been chosen of $O(1)$. It is

Comparative studies of the decay rate into photons for the axi-Higgs with the ordinary PQ axion have been performed for a Stückelberg scale confined in the TeV range and a mass of χ in the same range expected for the PQ axion. The analysis shows that the total decay rate of χ into photons is of the order $\Gamma_\chi \sim 10^{-50}$ GeV, which is larger than the decay rate of the PQ axion in the same channel (10^{-60}), but small enough to be long-lived, with a lifetime larger than the age of the universe. We show in **Figure 3** the result of this study, where we compare predictions for the decay rate of the axi-Higgs into two photons to that of the ordinary PQ axion.

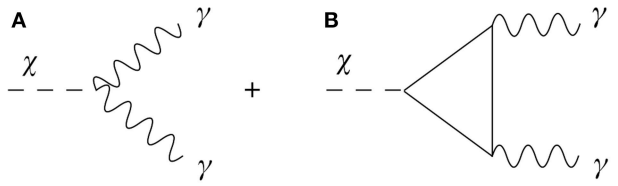

FIGURE 2 | Contributions to the $\chi \to \gamma\gamma$ decay. describing the anomaly contribution **(A)** and the interaction mediated by the Yukava coupling in the fermion loop **(B)**.

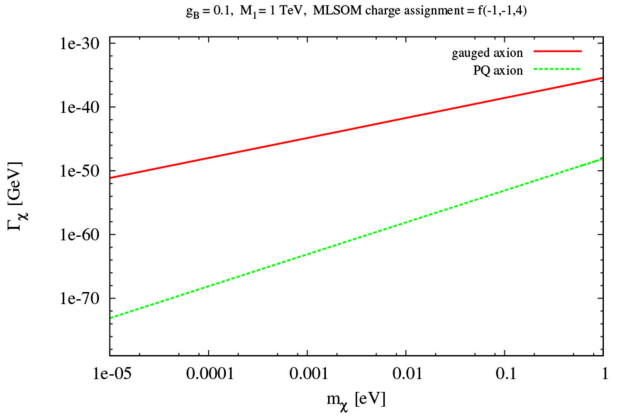

FIGURE 3 | Total decay rate of the axi-Higgs for several mass values. Here, for the PQ axion, we have chosen $f_a = 10^{10}$ GeV.

The charge assignment of the anomalous model has been denoted as $f(-1, 1, 4)$, where we have used the convention

$$f(q^B_{Q_L}, q^B_L, \Delta q^B) \equiv (q^B_{Q_L}, q^B_{u_R}; q^B_{d_R}, q^B_L, q^B_{e_R}, q^B_u, q^B_d). \tag{61}$$

These depend only upon the three free parameters $q^B_{Q_L}$, q^B_L, Δq^B. The parametric solution of the anomaly equations of the model $f(q^B_{Q_L}, q^B_L, \Delta q^B)$, for the particular choice $q^B_{Q_L} = -1, q^B_L = -1$, reproduces the entire charge assignment of a special class of intersecting brane models (see [29, 32] and the discussion in Corianò and Guzzi [20])

$$f(-1, -1, 4) = (-1, 0, 0, -1, 0, +2, -2). \tag{62}$$

We refer to Corianò et al. [12] for further details on these studies.

5. RELIC DENSITY FOR A LOW (∼ 1 TEV) STÜCKELBERG SCALE

The computation of the relic density for the Stückelberg axi-Higgs can be performed as in Corianò et al. [13], adopting a low scale scenario, where the extra V' (49) potential which causes the vacuum misalignment is generated around the electroweak scale.

One starts from the Lagrangian

$$\mathscr{S} = \int d^4x\sqrt{g}\left(\frac{1}{2}\dot{\chi}^2 - \frac{1}{2}m^2_\chi \Gamma_\chi \dot{\chi}\right), \tag{63}$$

where Γ_χ is the decay rate of the axion, where the potential has been expanded around its minimum up to quadratic terms. The same action can be derived from the quadratic approximation to the general expression

$$\mathscr{S} = \int d^4x R^3(t)\left(\frac{1}{2}\sigma^2_\chi\,(\partial_\alpha\theta)^2 - \mu^4\,(1-\cos\theta) - V_0\right) \tag{64}$$

which, as just mentioned, is constructed from the expression of V' given in Equation (49). Here $\mu \sim v$, is the electroweak scale. We also set other contributions to the vacuum potential to zero ($V_0 = 0$). In a Friedmann-Robertson-Walker spacetime metric, with a scaling factor $R(t)$, this action gives the equation of motion

$$\frac{d}{dt}\left[\left(R^3(t)(\dot{\chi} + \Gamma_\chi)\right)\right] + R^3 m^2_\chi(T) = 0. \tag{65}$$

We will neglect the decay rate of the axion in this case and set $\Gamma_\chi \approx 0$. At this point, we are free to set the scale at which the V' potential, which is of non-perturbative origin, is generated. Therefore, it will be zero above the electroweak scale (or temperature T_{ew}), which will give $m_\chi = 0$ for $T \gg T_{ew}$. The general equation of motion derived from Equation (65), introducing a temperature dependent mass, can be written as

$$\ddot{\chi} + 3H\dot{\chi} + m^2_\chi(T)\chi = 0, \tag{66}$$

which allows as a solution a constant value of the misalignment angle $\theta = \theta_i$. The axion energy density is given by

$$\rho = \frac{1}{2}\dot{\chi}^2 + \frac{1}{2}m^2_\chi \chi^2, \tag{67}$$

which after a harmonic averaging, due to the periodic motion, gives

$$\langle\rho\rangle = m^2_\chi \langle\chi^2\rangle. \tag{68}$$

By differentiating Equation (67) and using the equation of motion in (66), followed by the averaging Equation (68) one obtains the relation

$$\langle\dot{\rho}\rangle = \langle\rho\rangle\left(-3H + \frac{\dot{m}}{m}\right), \tag{69}$$

with a mass which is time-dependent through its temperature $T(t)$, while $H(t) = \dot{R}(t)/R(t)$ is the Hubble parameter. One easily finds that the solution of this equation is of the form

$$\langle\rho\rangle = \frac{m_\chi(T)}{R^3(t)} \tag{70}$$

which shows the decay of the energy density with an increasing space volume, valid even for a T-dependent mass. The condition for the oscillations of χ to take place is that the universe has to at least be as old as the period of oscillation. Then the axion field starts oscillating and appears as dark matter, otherwise

θ is misaligned but frozen. This is the physical content of the condition

$$m_\chi(T_i) = 3H(T_i), \tag{71}$$

which allows to identify the initial temperature of the coherent oscillation of the axion field χ, T_i, by equating $m_\chi(T)$ to the Hubble rate, taken as a function of temperature.

In the radiation era, the thermodynamics of all the components of the primordial state is entirely determined by the temperature T, being the system at equilibrium. This is because the contents of the early universe were in approximate thermal equilibrium, being the interaction rates of the constituents were large compared to the interaction rates H.

Pressure and entropy are then just given as a function of the temperature

$$\rho = 3p = \frac{\pi^2}{30} g_{*,T} T^4$$
$$s = \frac{2\pi^2}{45} g_{*,S,T} T^3. \tag{72}$$

Combined with the Friedmann equation they allow to relate the Hubble parameter and the energy density

$$H = \sqrt{\frac{8}{3}\pi G_N \rho}, \tag{73}$$

with $G_N = 1/M_P^2$ being the Newton constant and M_P the Planck mass. The number density of axions n_χ decreases as $1/R^3$ with the expansion, as does the entropy density $s \equiv S/R^3$, where S indicates the comoving entropy density, which remains constant in time, leaving the ratio $Y_a \equiv n_\chi/s$ conserved. An important variable is the abundance of χ at the temperature of oscillations T_i, which is defined as

$$Y_\chi(T_i) = \left.\frac{n_\chi}{s}\right|_{T_i}. \tag{74}$$

At the beginning of the oscillations the total energy density is just the potential one

$$\rho_\chi = n_\chi(T_i) m_\chi(T_i) = 1/2 m_\chi^2(T_i)\chi_i^2, \tag{75}$$

giving for the initial abundance at $T = T_i$

$$Y_\chi(T_i) = \frac{1}{2}\frac{m_\chi(T_i)\chi_i^2}{s} = \frac{45 m_\chi(T_i)\chi_i^2}{4\pi^2 g_{*,S,T} T_i^3} \tag{76}$$

where we have used the expression of the entropy given by Equation (72). At this point, by inserting the expression of ρ given in Equation (72) into the expression of the Hubble rate as a function of density given by Equation (73), the condition for oscillation Equation (71) allows to express the axion mass at $T = T_i$ in terms of the effective massless degrees of freedom evaluated at the same temperature

$$m_\chi(T_i) = \sqrt{\frac{4}{5}\pi^3 g_{*,T_i}}\frac{T_i^2}{M_P}. \tag{77}$$

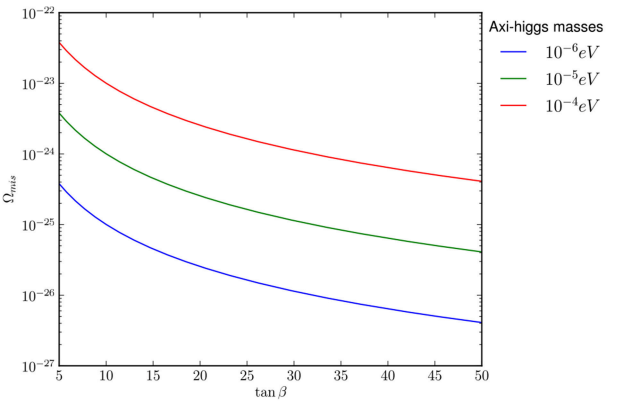

FIGURE 4 | Relic density of the axi-Higgs as a function of $\tan\beta$ for several values of the mass of the axi-Higgs.

This gives for Equation (76) the expression

$$Y_\chi(T_i) = \frac{45\sigma_\chi^2\theta_i^2}{2\sqrt{5\pi g_{*,T_i}} T_i M_P}, \tag{78}$$

where we have expressed χ in terms of the angle of misalignment θ_i at the temperature when oscillations start. Notice that we are assuming that $\theta_i = \langle\theta\rangle$ is the zero mode of the initial misalignment angle after an averaging.

$g_{*,T} = 110.75$ is the number of massless degrees of freedom of the model at the electroweak scale. Using the conservation of the abundance $Y_{a0} = Y_a(T_i)$, the expression of the contribution to the relic density is given by

$$\Omega_\chi^{mis} = \left.\frac{n_\chi}{s}\right|_{T_i} m_\chi \frac{s_0}{\rho_c}. \tag{79}$$

To evaluate (79) we need the values of the critical energy density (ρ_c) and the entropy density today, which are estimated as

$$\rho_c = 5.2 \cdot 10^{-6}\text{GeV/cm}^3 \qquad s_0 = 2970\ \text{cm}^{-3}, \tag{80}$$

with $\theta \simeq 1$. Given these values, the relic density as a function of $\tan\beta = v_u/v_d$, the ratio of the two Higgs vevs, is given in **Figure 4**. In this plot we have varied the oscillation mass and plotted the relic densities as a function of this variable. The variation of v_u has been constrained to give the values of the masses of the electroweak gauge bosons, via an appropriate choice of $\tan\beta$.

For instance, if we assume a temperature of oscillation of $T_i = 100$ GeV, an upper bound for the axi-Higgs mass, which allows the oscillations to take place, is $m_\chi(T_i) \approx 10^{-5}$eV, with $g_{*,T} \approx 100$.

In order to specify σ_χ we have assumed a value of 1 TeV for the Stückelberg mass M_S, with a gauge coupling of the anomalous B_μ, $g_B \approx 1$, and we have taken (q_u, q_d) of order unity, obtaining $\sigma_\chi \simeq 10^2$ GeV. As we lower the oscillation temperature (and hence the mass), the corresponding curves for Ω_χ are down-shifted.

The plot shows that the values of these relic densities at current time are basically vanishing and these small results are to be attributed to the value of σ_χ, which is bound to vary around the electroweak scale. We remind that in the PQ case σ_χ is replaced by the large scale f_a at the QCD phase transition, which determines an enhancement of Ω_χ respect to the current case.

As already mentioned, nonperturbative instanton effects at the electroweak scale are expected to vastly suppress the mass of the axi-Higgs, as derived in (97), in the form

$$m_\chi^2 \sim \Lambda_{ew}^4/v^2, \qquad \text{with} \qquad \Lambda_{ew}^4 \sim \text{Exp}(-2\pi/\alpha_w(v))v^4 \quad (81)$$

$\alpha_W(v)$ being the weak charge at the scale v - which is indeed a rather small value since $\text{Exp}(-2\pi/\alpha_w(v)) \sim e^{-198}$. We will come back to this point in the next section, when discussing the possibility of raising M_S from the TeV range up to the GUT or Planck scales.

For this reason, χ essentially remains a physical but frozen degree of freedom which may undergo a significant (second) misalignment only at the QCD phase transition. The possibility of sequential misalignments has been taken into account both in non-supersymmetric [12] and in supersymmetric models [13]. It is the presence of a coupling of the axion to the gluons, via the color/ $U(1)_B$ mixed anomaly, that χ behaves, in this case, similar to a PQ axion. The misalignment is controlled by the periodic potential generated at the QCD phase transition, being the first misalignment at the electroweak scale irrelevant. In the absence of such mixed anomaly, χ could be classified as a quintessence axion, contributing to the dark energy content of the universe.

We show in **Figure 5** results of a numerical study of $\Omega_{mis}h^2$ as a function of M_S, expressed in units of 10^9 GeV. We show as a darkened area the bound coming from WMAP data [35], given as the average value plus an error band, while the monotonic curve denotes the values of $\Omega_{mis}h^2$ as a function of M_S. It is clear that the relic density of χ can contribute significantly to the dark matter content only if the Stückelberg scale is rather large ($\sim 10^7$ GeV) and negligible otherwise.

In the next section we address another scenario, where we will assume that the Stückelberg scale is around the Planck scale and the breaking of the symmetry which allows a periodic potential for the b field to generate, taken at the GUT scale. This particular choice for the location of the two scales, which is well motivated in a string/brane theory context, opens up the possibility of having an ultra-light axion in the spectrum. The De Broglie wavelength of this hypothetical particle would be around 10 kpc, which is what is required to solve the issues in the modeling of the matter distribution at the sub-galactic scale, that we have discussed in the introduction.

6. STÜCKELBERG MODELS AT THE PLANCK/GUT SCALE AND FUZZY DARK MATTER

By raising the Stückelberg mass near the Planck scale, the Stückelberg construction acquires a fundamental meaning since it can be directly related to the cancellation of a gauge anomaly generated at the same scale [7]. As mentioned above, anomalous

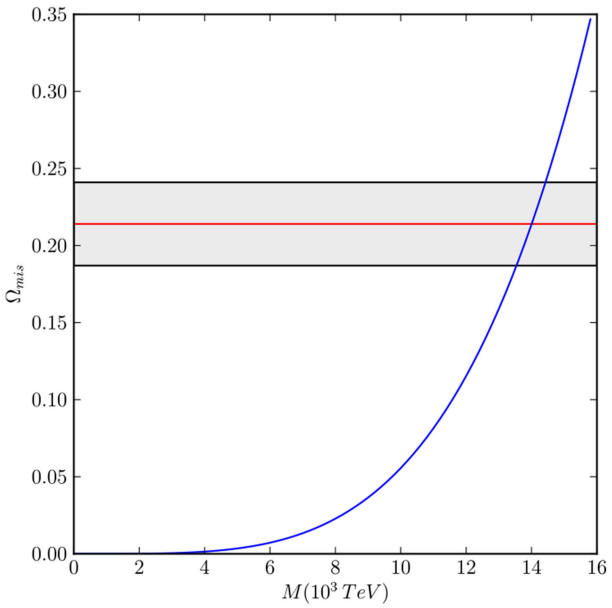

FIGURE 5 | Relic density of the axi-Higgs as a function of M. The gray bar represents the measured value of $\Omega_{DM}h^2 = 0.1123 \pm 0.0035$.

$U(1)$ symmetries are quite generally present in theories of intersecting branes. However, the very same structure emerges also in the low energy limit of heterotic string constructions. At the same time, as shown in Corianò et al. [14], even in the presence of multiple anomalous abelian symmetries, only a single axion is necessary to cancel all anomalies, giving a special status to the Stückelberg field. These considerations define a new context in which to harbor such models. In this context, it is natural to try to identify a consistent formulation within an ordinary gauge theory, by assuming that the axion emerges at the Planck scale M_P, but it acquires a mass at a scale below, which in our case is assumed to be the GUT scale. In this section therefore we are going to consider an extension of the setup discussed in previous sections, under the assumption that their dynamics is now controlled by two scales.

We will consider an E_6 based model, derived from E_8, which appeared in the heterotic string construction of Gross et al. [36] with an $E(8) \times E(8)$ symmetry. After a compactification of six spatial dimensions on a Calabi-Yau manifold [37] the symmetry is reduced to an $E(6)$ GUT gauge theory. Other string theory compactifications predict different GUT gauge structures, such as $SU(5)$ and $SO(10)$. The E_6, however, allows to realize a scenario where two components of dark matter are present, as we are going to elaborate. Fermions are assigned to the **27** representation of $E(6)$, which is anomaly-free. Notice that in $E(6)$ a PQ symmetry is naturally present, as shown in Frampton and Kephart [11], which allows to have an ordinary PQ axion, while at the same time it is a realistic GUT symmetry which can break to the SM. This is the gauge structure to which one may append an anomalous $U(1)_X$ symmetry.

We consider a gauge symmetry of the form $E_6 \times U(1)_X$, where the gauge boson B^μ is in the Stückelberg phase. B_α is the gauge

field of $U(1)_X$ and $B_{\alpha\beta} \equiv \partial_\alpha B_\beta - \partial_\beta B_\alpha$ the corresponding field strength, while g_B its gauge coupling. As already mentioned, the $U(1)_X$ carries an anomalous coupling to the fermion spectrum.

The one-particle irreducible (1PI) effective Lagrangian of the theory at 1-loop level takes the form

$$L = L_{E_6} + L_{St} + L_{anom} + L_{WZ}, \tag{82}$$

in terms of the gauge contribution of E_6 (L_{E_6}), the Stückelberg term L_{St}, the anomalous 3-point functions L_{anom}, generated by the anomalous fermion couplings to the $U(1)_X$ gauge boson, and the Wess-Zumino counterterm (WZ) L_{WZ}. The Stückelberg interaction to the E_6 gauge Lagrangian

$$L_{E_6} = -\frac{1}{4} F^{(E_6)\,\mu\nu} F^{(E_6)}_{\mu\nu}, \tag{83}$$

which enables us to write the Stückelberg part of the Lagrangian as

$$L_{Stueck} = -\frac{1}{4} B_{\alpha\beta} B^{\alpha\beta} - \frac{1}{2}(MB_\alpha - \partial_\alpha b(x))^2. \tag{84}$$

In this final form, M is the mass of the Stückelberg gauge boson associated with $U(1)_X$ which we can be taken from the order of the Planck scale, guaranteeing the decoupling of the axion around M_{GUT}, due to the gravitational suppression of the WZ counterterms. The WZ contribution is the combination of two terms

$$L_{WZ} = c_1 \frac{b}{M} F^{(E_6)\,\mu\nu} F^{(E_6)\,\rho\sigma} \epsilon_{\mu\nu\rho\sigma} + c_2 \frac{b}{M} B_{\mu\nu} B_{\rho\sigma} \epsilon^{\mu\nu\rho\sigma} \tag{85}$$

needed for the cancellation of the $U(1)_X E_6 E_6$ and $U(1)_X^3$ anomalies, for appropriate values of the numerical constants c_1 and c_2, fixed by the charge assignments of the model. The three chiral families will be assigned under $E(6) \times U(1)_X$ respectively to

$$\mathbf{27}_{X_1} \quad \mathbf{27}_{X_2} \quad \mathbf{27}_{X_3}, \tag{86}$$

in which the charges X_i ($i = 1, 2, 3$) are free at the moment, while the cancellation of the $U(1)_X^3$ and $E_6 \times U(1)_X^2$ anomalies implies that

$$\sum_{i=1}^{3} X_i^3 = 0, \qquad \sum_{i=1}^{3} X_i = 0. \tag{87}$$

These need to be violated in order to compensate with a Wess-Zumino term for the restoration of the gauge symmetry of the action.

Concerning the scalar sector, this contains two $\mathbf{351}_{X_i}$ ($i = 1, 2$) irreducible representations, where the $U(1)_X$ charges X_i need to be determined. The **351** is the *antisymmetric* part of the Kronecker product $\mathbf{27} \otimes \mathbf{27}$ where **27** is the defining representation of $E(6)$. The $\mathbf{351}_X$ can be conveniently described by the 2-form $A_{\mu\nu} = -A_{\nu\mu}$ with $\mu, \nu = 1$ to 27. The most general renormalizable potential in L_{E_6} is expressed in terms of $A^{(1)}_{\mu\nu}$ and $A^{(2)}_{\mu\nu}$ of $U(1)_X$ of charges x_1 and x_2 respectively. If we denote the $\mathbf{27}_{X_i}$ of Equation (86) by Ψ_μ with $\mu = 1$ to 27 then the full Lagrangian including the potential V, has an invariance under the global symmetry

$$A^{(1)}_{\mu\nu} \to e^{i\theta} A^{(1)}_{\mu\nu} \quad A^{(2)}_{\mu\nu} \to e^{i\theta} A^{(2)}_{\mu\nu} \quad \Psi_\mu \to e^{-(\frac{1}{2} i\theta)} \Psi_\mu. \tag{88}$$

This is identifiable as a Peccei-Quinn symmetry which is broken at the GUT scale when $E(6)$ is broken to $SU(5)$ [11]. This axionic symmetry can be held responsible for solving the strong CP problem. We couple $A^{(1)}_{\mu\nu}$ to the fermion families $(\mathbf{27})_{X_i}$ $i = 1, 2, 3$. We choose in Equation (86), e.g., $X_1 = X_2 = X_3 = +1$, with the X-charge of $A^{(1)}$ fixed to $X = -2$. The second scalar representation $A^{(2)}$ is decoupled from the fermions, with an $X-$charge for $A^{(2)}$ which is arbitrary and taken for simplicity to be $X = +2$. The potential is expressed in terms of three $E_6 \times U(1)_X$ invariant components,

$$V = V_1 + V_2 + V_p, \tag{89}$$

where

$$V_1 = F(A^{(1)}, A^{(1)}) \qquad V_2 = F(A^{(2)}, A^{(2)}), \tag{90}$$

with V_1 and V_2 denoting the contributions of $(\mathbf{351})_{-2}$ and $(\mathbf{351})_{+2}$, expressed in terms of the function [11]

$$\begin{aligned} F(A^{(i)}, A^{(j)}) \;=\; & M^2_{GUT} A^{(i)}_{\mu\nu} \bar{A^{(j)}}^{\mu\nu} + h_1 \, (A^{(i)}_{\mu\nu} \bar{A^{(j)}}^{\mu\nu})^2 + h_2 \, A^{(i)}_{\mu\nu} \bar{A}^{\nu\sigma} A^{(i)}_{\sigma\tau} \bar{A}^{\tau\mu} \\ & + h_3 \, d^{\mu\nu\lambda} d_{\xi\eta\lambda} A^{(i)}_{\mu\sigma} A^{(i)}_{\nu\tau} \bar{A^{(j)}}^{\xi\sigma} \bar{A^{(j)}}^{\eta\tau} \\ & + h_4 \, d^{\mu\nu\alpha} d^{\sigma\tau\beta} d_{\xi\eta\alpha} d_{\lambda\rho\beta} A^{(i)}_{\mu\sigma} A^{(i)}_{\nu\tau} \bar{A^{(j)}}^{\xi\lambda} \bar{A^{(j)}}^{\eta\rho} \\ & + h_5 \, d^{\mu\nu\alpha} d^{\sigma\beta\gamma} d_{\xi\eta\beta} d_{\lambda\alpha\gamma} A^{(i)}_{\mu\sigma} A^{(i)}_{\nu\tau} \bar{A^{(j)}}^{\xi\lambda} \bar{A^{(j)}}^{\eta\tau} \\ & + h_6 \, d^{\mu\nu\alpha} d^{\sigma\tau\beta} d_{\alpha\beta\gamma} d^{\gamma\zeta\xi} d_{\xi\eta\zeta} d_{\lambda\rho\chi} A^{(i)}_{\mu\sigma} \bar{A^{(j)}}^{\xi\lambda} A^{(i)}_{\nu\tau} \bar{A^{(j)}}^{\eta\rho}, \end{aligned} \tag{91}$$

in which $d_{\alpha\beta\gamma}$ with $\alpha, \beta, \gamma = 1$ to 27 is the $E(6)$ invariant tensor.

As for the two Higgs doublet model discussed in the previous sections, also in this case we are allowed to introduce a periodic potential on the basis of the underlying gauge symmetry, of the form

$$\begin{aligned} V_p \;=\; & M^2_{GUT} A^{(1)}_{\mu\nu} \bar{A^{(2)}}^{\mu\nu} e^{-i4\frac{b}{M_S}} + e^{-i8\frac{b}{M_S}} \Big[(h_1 \, (A^{(1)}_{\mu\nu} \bar{A^{(2)}}^{\mu\nu})^2 + h_2 \, A^{(1)}_{\mu\nu} \bar{A^{(2)}}^{\nu\sigma} \\ & A^{(1)}_{\sigma\tau} \bar{A^{(2)}}^{\tau\mu} + h_3 \, d^{\mu\nu\lambda} d_{\xi\eta\lambda} A^{(1)}_{\mu\sigma} A^{(1)}_{\nu\tau} \bar{A^{(2)}}^{\xi\sigma} \bar{A^{(2)}}^{\eta\tau} \\ & + h_4 \, d^{\mu\nu\alpha} d^{\sigma\tau\beta} d_{\xi\eta\alpha} d_{\lambda\rho\beta} A^{(1)}_{\mu\sigma} A^{(1)}_{\nu\tau} \bar{A^{(2)}}^{\xi\lambda} \bar{A^{(2)}}^{\eta\rho} \\ & + h_5 \, d^{\mu\nu\alpha} d^{\sigma\beta\gamma} d_{\xi\eta\beta} d_{\lambda\alpha\gamma} A^{(1)}_{\mu\sigma} A^{(1)}_{\nu\tau} \bar{A^{(2)}}^{\xi\lambda} \bar{A^{(2)}}^{\eta\tau} \\ & + h_6 \, d^{\mu\nu\alpha} d^{\sigma\tau\beta} d_{\alpha\beta\gamma} d^{\gamma\zeta\xi} d_{\xi\eta\zeta} d_{\lambda\rho\chi} A^{(1)}_{\mu\sigma} \bar{A^{(2)}}^{\xi\lambda} A^{(1)}_{\nu\tau} \bar{A^{(2)}}^{\eta\rho} \Big] + h.c. \end{aligned} \tag{92}$$

and which become periodic at the GUT scale after symmetry breaking, similar to the case considered in Corianò et al. [12] and Corianò et al. [13]. This potential is expected to be of nonperturbative origin and generated at the scale of the GUT

phase transition. Additionally, in this case the size of the contributions in V_p, generated by instanton effects at the GUT scale, are expected to be exponentially suppressed, however, the size of the suppression is related to the value of the gauge coupling at the corresponding scale.

6.1. The Periodic Potential

The breaking of the $E_6 \times U(1)_X$ symmetry at M_{GUT} can follow different routes such as $E(6) \supset SU(3)_C \times SU(3)_L \times SU(3)_H$ where

$$\begin{aligned}(\mathbf{351}) &= (1,3^*,3) + (1,3^*,6^*) + (1,6,3) + (3,3,1) + (3,6^*,1) \\ &+ (3,3,8) + (3^*,1,3^*) + (3^*,1,6) + (3^*,8,3^*) + (6^*,3,1) \\ &+ (6,1,3^*) + (8,3^*,3) \end{aligned} \tag{93}$$

of which the color singlets are only the 45 states for each of the two $(\mathbf{351})_{X_i}$

$$(1,3^*,3)_{X_i} \qquad (1,3^*,6^*)_{X_i} \qquad (1,6,3)_{X_I} \quad i=1,2. \tag{94}$$

One easily realizes that there are exactly nine color-singlet $SU(2)_L$-doublets in the $(\mathbf{351}^{'})_{-2}$ and 9 in the $(\mathbf{351}^{'})_{+2}$, that we may denote as $H_j^{(1)}$, $H_j^{(2)}$, with $j = 1, 2 \ldots 9$, which appear in the periodic potential in the form

$$\begin{aligned}V_p \sim & \sum_{j=1}^{12} \lambda_0 M_{\rm GUT}^2 (H_j^{(1)\dagger} H_j^{(2)} e^{-4ig_B \frac{b}{M_S}}) + \sum_{j,k=1}^{12} \\ & \Big[\lambda_1 (H_j^{(1)\dagger} H_j^{(2)} e^{-i4g_B \frac{b}{M_S}})^2 + \lambda_2 (H_i^{(1)\dagger} H_i)(H_i^{(1)\dagger} H_j^{(2)} e^{-i4g_B \frac{b}{M_S}}) \\ & + \lambda_3 (H_k^{(2)\dagger} H_k^{(2)})(H_j^{(1)\dagger} H_k^{(2)} e^{-i4g_B \frac{b}{M_S}}) \Big] + \text{h.c.}, \end{aligned} \tag{95}$$

where we neglect all the other terms generated from the decomposition (93) which will not contribute to the breaking. The assumption that such a potential is instanton generated at the GUT scale, with parameters λ_i's induces a specific value of the instanton suppression which is drastically different from the case of a Stückelberg scale located at TeV/multi TeV range.

For simplicity we will consider only a typical term in the expression above, involving two neutral components, generically denoted as $H^{(1)\,0}$ and $H^{(2)\,0}$, all remaining contributions being similar. In this simplified case the axi-Higgs χ is generated by the mixing of the CP odd components of two neutral Higgses. The analysis follows the approach discussed before rather closely, in the simplest two-Higgs doublet model, which defines the template for such constructions. Therefore, generalizing this procedure, the structure of V_p after the breaking of the $E_6 \times U(1)_X$ symmetry can be summarized in the form

$$V_p \sim v_1 v_2 \left(\lambda_2 v_2^2 + \lambda_3 v_1^2 + \overline{\lambda_0} M_{GUT}^2\right) \cos\left(\frac{\chi}{\sigma_\chi}\right) + \lambda_1 v_1^2 v_2^2 \cos\left(2\frac{\chi}{\sigma_\chi}\right), \tag{96}$$

with a mass for the physical axion χ given by

$$m_\chi^2 \sim \frac{2v_1 v_2}{\sigma_\chi^2} \left(\bar{\lambda}_0 v_1^2 + \lambda_2 v_2^2 + \lambda_3 v_1^2 + 4\lambda_1 v_1 v_2\right) \approx \lambda v^2 \tag{97}$$

with $v_1 \sim v_2 \sim v \sim M_{GUT}$. Assuming that M_S, the Stückelberg mass, is of the order of $M_{\rm Planck}$ and that the breaking of the $E_6 \times U(1)_X$ symmetry takes place at the GUT scale $M_{GUT} \sim 10^{15}$ GeV, (e.g., $v_1 \sim v_2 \sim M_{GUT}$) then

$$\sigma_\chi \sim M_{\rm GUT} + O(M_{\rm GUT}^2/M_{\rm Planck}^2), \qquad m_\chi^2 \sim \lambda_0 M_{\rm GUT}^2, \tag{98}$$

where all the λ_i's in V_p are of the same order. The potential V_p is generated by the instanton sector and the size of the numerical coefficients appearing in its expression, are constrained to specific values. One obtains $\lambda_0 \sim e^{-2\pi/\alpha(M_{\rm GUT})}$, with the value of the coupling $4\pi g_B^2 = \alpha_{\rm GUT}$ fixed at the GUT scale. If we assume that $1/33 \leq \alpha_{GUT} \leq 1/32$, then $e^{-201} \sim 10^{-91} \leq \lambda_0 \leq e^{-205} \sim 10^{-88}$, and the mass of the axion χ takes the approximate value

$$10^{-22}\ \text{eV} < m_\chi < 10^{-20}\ \text{eV}, \tag{99}$$

which contains the allowed mass range for an ultralight axion, as discussed in a recent analysis of the astrophysical constraints on this type of dark matter [6].

6.2. Detecting Ultralight Axions

One of the interesting issues on which future research has to concentrate, concerns the possibility of suggesting new ways to detect such a specific class of particles. Several proposals for the detection of generic ultralight bosons [38–40] in the astrophysical context have recently been presented. For instance, it has been observed that light boson fields around spinning black holes can trigger superradiant instabilities, which can be strong enough to imprint gravitational wave detection. This could be used to set constraints on their masses and couplings. Other proposals [41] have suggested to use the precise astronomical ephemeris as a way to detect such a light dark matter, as celestial solar system bodies feel the dark matter wind which acts as a resistant force opposing their motions. The bodies feel the dark matter wind because our solar system moves with respect to the rest frame of the dark matter halo, so that the scattering off the dark matter acts as a resistant force opposing their motions.

At the moment, from our perspective, how to distinguish between the various proposals that have been put forward in the recent literature, remains an open issue. The models that we have presented are, however, very specific, since they are accompanied by a well-defined gauge structure and are, as such, susceptible of in-depth analysis. We should also mention that another specific property of such models is their interplay with the flavor sector, especially the neutrino sector, together with their impact on leptogenesis and $SO(10)$ grand unification. This would allow for the establishment of a possible link between the neutrino mass spectrum and the axion mass and would be an intermediate step to cover, prior to a discussion of the general astrophysical suggestions for their detections, mentioned above. An in-depth analysis of some of these issues is underway.

7. CONCLUSIONS

The invisible axion owes its origin to a global $U(1)_{PQ}$ (Peccei-Quinn, PQ) symmetry which was spontaneously broken in the

early universe and explicitly broken to a discrete Z_N symmetry by instanton effects at the QCD phase transition [42]. The breaking occurred at a temperature T_{PQ} below which the symmetry can nonlinearly realize. Two distinctive features of an axion solution– as derived from the original Peccei-Quinn (PQ) proposal [8] and its extensions [26, 27, 43, 44]- such as (a) the appearance of a single scale f_a ($f_a \sim 10^{10} - 10^{12}$ GeV) which controls both their mass and their coupling to the gauge fields, via an $a(x)F\tilde{F}$ operator, where $a(x)$ is the axion field and (b) their non-thermal decoupling at the hadron phase transition, attributed to a mechanism of vacuum misalignment. The latter causes axions to be a component of cold rather than hot dark matter, even for small values of their mass, currently expected to be in the μeV-meV range. The gauging of an abelian anomalous symmetry brings in a generalization of the PQ scenario. As extensively discussed in Corianò and Irges [15], Corianò et al. [16], Corianò et al. [17], Armillis et al. [18], Corianò et al. [19], and Corianò and Guzzi [20] it enlarges the parameter space for the corresponding axion. This construction allows to bypass the mass/coupling relation for ordinary PQ axions, which has often been softened in various analyses of "axion-like particles" [45].

Original analyses of Stückelberg models, motivated within the theory of intersecting branes, where anomalous $U(1)$'s are present, have resulted in the identification of a special pseudoscalar field, the Stückelberg field b. Its mixing with the CP-odd scalar sector allows the extraction of a one-gauge invariant component, called the axi-Higgs χ, whose mass and couplings to the gauge fields are model dependent. If string theory via its numerous possible geometric (and otherwise) compactifications [6] provides a natural arena where axion type of fields are ubiquitously present, then the possibility that an ultralight axion of this type is a component of dark matter is quite feasible. As we have discussed, its ultralight nature is a natural consequence of the implementation of the construction reflecting the low energy structure of the heterotic string theory by involving two scales, the Planck and the GUT scale. Given the mass of such axion, it is obvious that its search has to be inferred indirectly by astrophysical observations.

In short, we have seen that Stückelberg models with an axion provide a new perspective on an old problem and allow to open up new directions in the search for the constituents of dark matter of our universe.

AUTHOR CONTRIBUTIONS

All authors listed have made a substantial, direct and intellectual contribution to the work, and approved it for publication.

FUNDING

This is a contributed paper to the volume Phenomena Beyond the Standard Model: What do we expect for New Physics to look like?

REFERENCES

1. Ade PAR, Aghanim N, Arnaud M, Ashdown M, Aumont J, Baccigalupi C. et al. Planck 2015 results. XIII. Cosmological parameters. *Astron Astrophys.* (2016) **594**:A13. doi: 10.1051/0004-6361/201525830
2. Riess AG, Filippenko AV, Challis P, Clocchiattia A, Diercks A, Garnavich PM, et al. Observational evidence from supernovae for an accelerating universe and a cosmological constant. *Astron J.* (1998) **116**:1009–38.
3. Perlmutter S, Aldering G, Goldhaber G, Knop RA, Nugent P, Castro PG. et al. Measurements of Omega and Lambda from 42 high redshift supernovae. *Astrophys J.* (1999) **517**:565–86.
4. Navarro JF, Frenk CS, White SDM. A Universal density profile from hierarchical clustering. *Astrophys J.* (1997) **490**:493–508.
5. Hu W, Barkana R, Gruzinov A. Cold and fuzzy dark matter. *Phys Rev Lett.* (2000) **85**:1158–61. doi: 10.1103/PhysRevLett.85.1158
6. Hui L, Ostriker JP, Tremaine S, Witten E. Ultralight scalars as cosmological dark matter. *Phys Rev.* (2017) **D95**:043541. doi: 10.1103/PhysRevD.95.043541
7. Corianò C, Frampton PH. Dark matter as ultralight axion-like particle in $E_6 \times U(1)_X$ GUT with QCD axion. *Phys Lett.* (2018) **B782**:380–6. doi: 10.1016/j.physletb.2018.05.067
8. Peccei RD, Quinn HR. Constraints imposed by CP conservation in the presence of instantons. *Phys Rev.* (1977) **D16**:1791–7.
9. Sikivie P. Axion cosmology. *Lect Notes Phys.* (2008) **741**:19–50. doi: 10.1016/j.physrep.2016.06.005
10. Kim JE, Carosi G. Axions and the strong CP problem. *Rev Mod Phys.* (2010) **82**:557–602. doi: 10.1103/RevModPhys.82.557
11. Frampton PH, Kephart TW. Exceptionally simple E(6) theory. *Phys Rev.* (1982) **D25**:1459.
12. Corianò C, Guzzi M, Lazarides G, Mariano A. Cosmological properties of a gauged axion. *Phys Rev.* (2010) **D82**:065013. doi: 10.1103/PhysRevD.82.065013
13. Corianò C, Guzzi M, Mariano A. Relic densities of dark matter in the U(1)-extended NMSSM and the gauged axion supermultiplet. *Phys Rev.* (2012) **D85**:095008. doi: 10.1103/PhysRevD.85.095008
14. Corianò C, Irges N, Kiritsis E. On the effective theory of low scale orientifold string vacua. *Nucl Phys.* (2006) **B746**:77–135. doi: 10.1016/j.nuclphysb.2006.04.009
15. Corianò C, Irges N. Windows over a new low energy axion. *Phys Lett.* (2007) **B651**:298–305.
16. Corianò C, Irges N, Morelli S. Stuckelberg axions and the effective action of anomalous Abelian models. 1. A Unitarity analysis of the Higgs-axion mixing. *JHEP.* (2007) **0707**:008. doi: 10.1088/1126-6708/2007/07/008
17. Corianò C, Irges N, Morelli S. Stueckelberg axions and the effective action of anomalous Abelian models. II: a SU(3)C × SU(2)W × U(1)Y × U(1)B model and its signature at the LHC. *Nucl Phys.* (2008) **B789**:133–74. doi: 10.1016/j.nuclphysb.2007.07.027
18. Armillis R, Corianò C, Guzzi M, Morelli S. An anomalous extra Z prime from intersecting branes with drell-yan and direct photons at the LHC. *Nucl Phys.* (2009) **B814**:156. doi: 10.1016/j.nuclphysb.2009.01.016
19. Corianò C, Guzzi M, Morelli S. Unitarity bounds for gauged axionic interactions and the green-schwarz mechanism. *Eur Phys J.* (2008) **C55**:629–52. doi: 10.1140/epjc/s10052-008-0616-4
20. Corianò C, Guzzi M. Axions from intersecting branes and decoupled chiral fermions at the large hadron collider. *Nucl Phys.* (2010) **B826**:87–147. doi: 10.1016/j.nuclphysb.2009.09.031
21. Corianò C, Guzzi M, Irges N, Mariano A. Axion and neutralinos from supersymmetric extensions of the standard model with anomalous U(1)'s. *Phys Lett.* (2009) **B671**:87–90. doi: 10.1016/j.physletb.2008.12.003
22. Corianò C, Guzzi M, Mariano A, Morelli S. A light supersymmetric axion in an anomalous abelian extension of the standard model. *Phys Rev.* (2009) **D80**:035006. doi: 10.1103/PhysRevD.80.035006

23. Armillis R, Corianò C, Guzzi M. Trilinear anomalous gauge interactions from intersecting branes and the neutral currents sector. *JHEP*. (2008) **05**:015. doi: 10.1088/1126-6708/2008/05/015
24. Coriano C, Faraggi AE, Guzzi M. Searching for extra Z-prime from strings and other models at the LHC with leptoproduction. *Phys Rev*. (2008) **D78**:015012. doi: 10.1103/PHYSREVD.78.015012
25. Anastasopoulos P, Fucito F, Lionetto A, Pradisi G, Racioppi A, Stanev YS. Minimal anomalous U(1)-prime extension of the MSSM. *Phys Rev*. (2008) **D78**:085014. doi: 10.1103/PhysRevD.78.085014
26. Dine M, Fischler W, Srednicki M. A simple solution to the strong CP problem with a harmless axion. *Phys Lett*. (1981) **B104**:199.
27. Zhitnitsky AR. On possible suppression of the axion hadron interactions. (In Russian). *Sov J Nucl Phys*. (1980) **31**:260.
28. Kiritsis E. D-branes in standard model building, gravity and cosmology. *Phys. Rept*. (2005) **421**:105–90. doi: 10.1016/j.physrep.2005.09.001
29. Ibanez LE, Marchesano F, Rabadan R. Getting just the standard model at intersecting branes. *JHEP*. (2001) **11**:002. doi: 10.1088/1126-6708/2001/11/002
30. Antoniadis I, Kiritsis E, Rizos J, Tomaras TN. D-branes and the standard model. *Nucl Phys*. (2003) **B660**:81–115. doi: 10.1016/S0550-3213(03)00256-6
31. Blumenhagen R, Kors B, Lust D, Stieberger S. Four-dimensional string compactifications with D-Branes, orientifolds and fluxes. *Phys Rept*. (2007) **445**:1–193. doi: 10.1016/j.physrep.2007.04.003
32. Ghilencea DM, Ibanez LE, Irges N, Quevedo F, TeV-scale Z' bosons from D-branes. *JHEP*. (2002) **08**:016. doi: 10.1088/1126-6708/2002/08/016
33. Armillis R, Corianò C, Guzzi M, Morelli S. Axions and anomaly-mediated interactions: the green- schwarz and wess-zumino vertices at higher orders and g-2 of the muon. *JHEP*. (2008) **10**:034. doi: 10.1088/1126-6708/2008/10/034
34. Frampton PH, Kong OCW. Horizontal symmetry for quark and squark masses in supersymmetric SU(5). *Phys Rev Lett*. (1996) 77:1699–702.
35. Jarosik N, Bennett CL, Dunkley J, Gold B, Greason MR, Halpern M. et al. Seven-year wilkinson microwave anisotropy probe (WMAP) observations: sky maps, systematic errors, and basic results. *Astrophys J Suppl*. (2011) **192**:14. doi: 10.1088/0067-0049/192/2/14
36. Gross DJ, Harvey JA, Martinec EJ, Rohm R. The heterotic string. *Phys Rev Lett*. (1985) **54**:502–5.
37. Candelas P, Horowitz GT, Strominger A, Witten E. Vacuum configurations for superstrings. *Nucl Phys*. (1985) **B258**:46–74.
38. Dev PSB, Lindner M, Ohmer S. Gravitational waves as a new probe of bose—Einstein condensate dark matter. *Phys Lett*. (2017) **B773**:219–24. doi: 10.1016/j.physletb.2017.08.043
39. Brito R, Ghosh S, Barausse E, Berti E, Cardoso V, Dvorkin I, et al. Gravitational wave searches for ultralight bosons with LIGO and LISA. *Phys Rev*. (2017) **D96**:064050. doi: 10.1103/PhysRevD.96.064050
40. Baumann D, Chia HS, Porto RA. Probing ultralight bosons with binary black holes. *Phys Rev*. (2019) **D99**:044001. doi: 10.1103/PhysRevD.99.044001
41. Fukuda H, Matsumoto S, Yanagida TT. Direct detection of ultralight dark matter via astronomical ephemeris. *Phys Lett*. (2019) **B789**:220–27. doi: 10.1016/j.physletb.2018.12.038
42. Sikivie P. Of axions, domain walls and the early universe. *Phys Rev Lett*. (1982) **48**:1156–9.
43. Kim JE. Weak interaction singlet and strong CP invariance. *Phys Rev Lett*. (1979) **43**:103.
44. Shifman MA, Vainshtein AI, Zakharov VI. Can confinement ensure natural CP invariance of strong interactions? *Nucl Phys*. (1980) **B166**:493.
45. Roncadelli M, Galanti G, De Angelis A. "Axion-like particles and e-ASTROGAM," in *Proceedings of the 1st e-ASTROGAM Scientific Workshop*, De Angelis A, Tatischeff V, Giusti M, editors. 2017, Feb 28-Mar 2, Padova (2017). p. 532.

Conflict of Interest Statement: The authors declare that the research was conducted in the absence of any commercial or financial relationships that could be construed as a potential conflict of interest.

frontiers in Physics

REVIEW
published: 15 May 2019
doi: 10.3389/fphy.2019.00073

New Physics Suggested by Atomki Anomaly

Luigi Delle Rose[1,2], *Shaaban Khalil*[3*], *Simon J. D. King*[2,4] *and Stefano Moretti*[2,5]

[1] INFN, Sezione di Firenze, Department of Physics and Astronomy, University of Florence, Florence, Italy, [2] School of Physics and Astronomy, University of Southampton, Southampton, United Kingdom, [3] Center for Fundamental Physics, Zewail City of Science and Technology, Giza, Egypt, [4] INFN, Sezione di Padova, Dipartimento di Fisica ed Astronomia G. Galilei, Università di Padova, Padua, Italy, [5] Rutherford Appleton Laboratory, Particle Physics Department, Didcot, United Kingdom

We consider several extensions of the Standard Model (SM) which can explain the anomalies observed by the Atomki collaboration in the decay of excited states of Beryllium via a new boson with a mass around 17 MeV yielding e^+e^- pairs. We show how both spin-0 and 1 solutions are possible and describe the Beyond the SM (BSM) scenarios that can accommodate these. They include BSM frameworks with either an enlarged Higgs, or gauge sector, or both.

Keywords: Atomki anomaly, 2HDM, U(1), Z′, low scale

OPEN ACCESS

Edited by:
Frank Franz Deppisch, University College London, United Kingdom

Reviewed by:
Daisuke Nomura, High Energy Accelerator Research Organization, Japan
Michael Andreas Schmidt, University of New South Wales, Australia

***Correspondence:**
Shaaban Khalil
skhalil@zewailcity.edu.eg

Specialty section:
This article was submitted to High-Energy and Astroparticle Physics, a section of the journal Frontiers in Physics

Received: *25 February 2019*
Accepted: *23 April 2019*
Published: *15 May 2019*

Citation:
Delle Rose L, Khalil S, King SJD and Moretti S (2019) New Physics Suggested by Atomki Anomaly. Front. Phys. 7:73. doi: 10.3389/fphy.2019.00073

1. INTRODUCTION

The quest for New Physics (NP) above and Beyond the Standard Model (BSM) has always seen a 2-fold approach. On the one hand, the high energy frontier has been pursued, typically through multi-purpose experiments at hadron accelerators, like the $Sp\bar{p}S$, Tevatron, and LHC. On the other hand, the high precision frontier has been exploited, typically at lepton collider experiments, like LEP and SLC. Alongside this time honored two-prong pursuit, over the years, a transversal dimension, covering both hadron and lepton colliders, centered on flavor physics, has also developed. So that, presently, the attention of the particle physics community in unveiling some NP has mainly been concentrated upon these three research strands. However, surprises may arise in other contexts, notably from (much) lower energy experiments. In this respect, results from $(g-2)$ of the muon are prototypical. Another interesting result which has recently been reported is the one in Krasznahorkay et al. [1] (see also [2–5]), by the Atomki experiment [6]. The latter is a pair spectrometer for measuring multi-polarities of nuclear transitions, specifically, using a multi-detector array designed and constructed for the simultaneous measurement of energy and angular correlations of electron-positron pairs, in turn emerging via internal pair creation from a variety of nuclear transitions in various isotopes, such as ^{16}O, ^{12}C, and ^{8}Be. The intriguing result reported in Krasznahorkay et al. [1] concerns e^+e^- correlations measured for the isovector magnetic dipole 17.64 MeV state (with spin-parity and isospin, $J^P = 1^+$, $T = 1$, respectively), and the isoscalar magnetic dipole 18.15 MeV state ($J^P = 1^+$, $T = 0$) in their transitions to the ground state ($J^P = 0^+$, $T = 0$) for the Beryllium case. Significant deviations from the internal pair creation rate were observed at large angles in the angular correlation for the isoscalar transition with a confidence level of more than 5σ. This observation may indicate that, in an intermediate step, a (light) neutral boson with a mass of $16.70 \pm 0.35\,(\text{stat}) \pm 0.5\,(\text{sys})$ MeV has been created. In fact, also the 17.64 MeV transition eventually appeared to present a similar anomaly, albeit less significant, with a boson mass broadly compatible with the above one, i.e., $17.0 \pm 0.5\,(\text{stat}) \pm 0.5\,(\text{sys})$ MeV[1].

[1]It should however be mentioned that this second anomaly was never documented in a published paper, only in proceedings contributions.

The purpose of this review is to discuss possible solutions to these results, assuming that the neutral boson could be either a spin-1 or spin-0 object, belonging to a variety of BSM scenarios. The plan is as follows. In the next section we consider the characteristics of the results reported by the Atomki experiment. Then we describe possible candidate particles for such a light bosonic state. Finally, we illustrate the embedding of such solutions in possible theoretical models, in presence of a variety of experimental constraints emerging from both low and high energy experiments. We finally conclude.

2. THE ATOMKI EXPERIMENT AND 17 MEV BERYLLIUM ANOMALY

The Atomki pair spectrometer experiment [6] was set up for searching e^+e^- internal pair creation in the decay of excited ^{8}Be nuclei (henceforth, ^{8}Be*), the latter being produced with the help of a beam of protons directed on a ^{7}Li target. The proton beam was tuned in such a way that the different ^{8}Be excitations could be separated in energy with high accuracy.

In the data collection stage, a clear anomaly was observed in the decay of ^{8}Be* with $J^P = 1^+$ into the ground state ^{8}Be with spin-parity 0^+ (both with $T = 0$), where ^{8}Be* had an excitation energy of 18.15 MeV [1]. Upon analysis of the electron-positron properties, the spectra of both their opening angle θ and invariant mass M presented the characteristics of an excess consistent with an intermediate boson (henceforth, X) being produced on-shell in the decay of the ^{8}Be* state, with the X object subsequently decaying into e^+e^- pairs. As mentioned, the best fit to the mass M_X of X was given as $M_X = 16.7 \pm 0.35\,(\text{stat}) \pm 0.5\,(\text{sys})$ MeV, [1] in correspondence of a ratio of Branching Ratios (BRs) obtained as

$$\mathcal{B} \equiv \frac{\text{BR}(^8\text{Be}^* \to X + {}^8\text{Be})}{\text{BR}(^8\text{Be}^* \to \gamma + {}^8\text{Be})} \times \text{BR}(X \to e^+e^-) = 5.8 \times 10^{-6}. \quad (1)$$

The signal appeared as a bump over the monotonically decreasing background from pure Quantum Electro-Dynamics (QED) interactions, i.e., internal pair creation via $\gamma^* \to e^+e^-$ splittings. This excess appeared only for symmetric energies of e^+e^-, as expected from an on-shell non-relativistic particle. In addition, the opening angle of electron-positron pair and their invariant mass distributions presented the characteristics of an excess consistent with an intermediate boson. The measurements yielded the mentioned value M_X from the invariant mass $m_{e^+e^-}$, in correspondence of an angular excess around $\sim 135^\circ$, as shown in **Figure 1**. The best fit to data was obtained for a new particle interpretation, in which case the statistical significance of the excess is 6.8 sigma. The aforementioned result from the 17.64 MeV transition yielded $M_X = 17.0 \pm 0.5\,(\text{stat}) \pm 0.5\,(\text{sys})$ as best fit, in correspondence of an angular peak around 155° with $\mathcal{B} = 4.0 \times 10^{-6}$. The corresponding significance is nowhere near discovery though.

3. CANDIDATES FOR THE NEW BOSON

An explanation of the nature of the intermediate particle, X, decaying to electron-positron pairs, was attempted by considering it as boson either with spin zero (scalar or pseudoscalar) or with spin one (vector or axial-vector). We introduce all possible combinations in turn.

3.1. Scalar Particle

If the intermediate particle X is a scalar, ϕ ($J^P = 0^+$), then the decay $^8\text{Be}^*(1^+) \to {}^8\text{Be}(0^+) + \phi$ implies, due to angular momentum conservation, that ϕ should have $L = 1$. Also, from parity conservation, it must have a parity equal to $(-1)^L$, which is -1 and this contradicts the assumption that ϕ is scalar with even parity. Therefore, one can conclude that a scalar intermediate particle is ruled out.

3.2. Pseudoscalar Particle

The situation is different if the intermediate particle is a pseudoscalar, A ($J^P = 0^-$) [8]. In this case, given the quantum numbers of the ^{8}Be* and ^{8}Be states, the intermediate boson can indeed be a $J^P = 0^-$ pseudoscalar particle if it was emitted with $L = 1$ orbital momentum. It was in fact shown in Ellwanger and Moretti [8] that A can account for the Atomki results if its Yukawa couplings with the SM fermions are of order of the Yukawa couplings of the SM Higgs.

3.3. Vector Particle

A neutral vector boson is the most common example considered for explaining this signal [7, 9–18]. It was emphasized that it can be a valid candidate if its coupling is constrained as $g' \sim 10^{-3}$.

3.4. Axial-Vector Particle

The pure axial-vector boson is also considered and it was shown that it can be a candidate if its coupling satisfies $g' \sim 10^{-4}$, as done in Kozaczuk et al. [19], Feng et al. [7], and Kahn et al. [20]. The case of general spin-one boson, with no definite parity, i.e., it is a mix of vector and axial-vector, could be a possible candidate after taking care of stringent constraints from atomic parity violation.

The couplings of these new light bosons with the SM particles remain an open question and subject to severe constraints from several experiments.

4. EXPERIMENTAL CONSTRAINTS ON THE PSEUDOSCALAR EXPLANATION

The reduced couplings ξ_q of a pseudoscalar A to quarks is defined as

$$\mathcal{L}_{Aqq} = \xi_q \frac{m_q}{v} A \bar{q} i \gamma_5 q, \quad (2)$$

with $v \sim 246$ GeV. Assuming such fundamental interactions and adopting the nuclear shell model wave functions with definite isospin $T = 0$ of Ellwanger and Moretti [8], one finds that

$$\xi_u + \xi_d \approx 0.6 \quad (3)$$

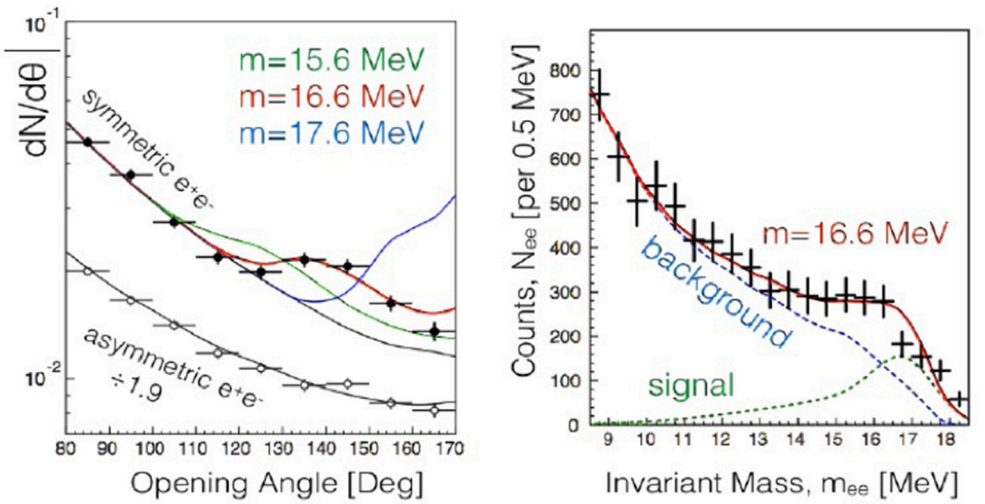

FIGURE 1 | Angular and invariant mass distributions of the internal conversion electron-positron pairs measured by the Atomki spectrometer (from Feng et al. [7]).

or, for $\xi_u = \xi_d \equiv \xi$, $\xi \approx 0.3$. Furthemore, if A has Yukawa couplings to quarks and leptons which are proportional to the Yukawa couplings of the SM Higgs boson rescaled by generation independent factors $\xi_d \approx \xi_u \approx \xi_e$ (or $\xi_u \ll \xi_d$), and the Yukawa couplings to BSM fermions are not much larger than the electric charge e, A has a BR of about 99% into e^+e^- and only about 1% into $\gamma\gamma$. Its total width is then dominated by $A \to e^+e^-$ and given by

$$\Gamma(A) = \xi_e^2 \frac{m_e^2}{8\pi v^2} M_A = \xi_e^2 \cdot 2.9 \times 10^{-15}\ \text{GeV} \tag{4}$$

for $M_A = 17$ MeV. Its decay length is

$$l_A = \frac{p_A}{M_A \Gamma(A)}\ . \tag{5}$$

For the decay $^8\text{Be}^* \to {}^8\text{Be} + A$ with $M(^8\text{Be}^*) - M(^8\text{Be}) = 18.15$ MeV we obtain

$$l_A \sim \frac{1}{\xi_e^2} \cdot 2.5\ \text{cm}. \tag{6}$$

(For $M_A = 17.9$ MeV, $2\,\sigma$ above the central value in M_X from the 18.15 MeV transition, we obtain $l_A \sim \frac{1}{\xi_e^2} \times 1.1$ cm.) In order to explain the observed anomaly in the Atomki pair spectrometer experiment [1], l_A should then not be much larger than 1 cm leading to

$$\xi_e \gtrsim 1\ , \tag{7}$$

depending somewhat on the precise value of M_A.

Light pseudoscalars are subject to constraints from searches for axions or axion-like particles. For recent summaries of constraints relevant for light pseudoscalars decaying dominantly into e^+e^-, see [21–25]. However, since we allow for different Yukawa type couplings rescaled by ξ_u, ξ_d, and ξ_e with respect to SM Higgs couplings, at least some experimental constraints studied therein have to be reconsidered. Constraints from $\pi^0 \to \gamma + X$ from the NA48/2 experiment, which play a major role for the Z' scenario [7, 9], do not apply here since the decay $\pi^0 \to \gamma + A$ would violate parity.

Constraints also originate from flavor violating meson decays, analyzed recently in Dolan et al. [21], and are mainly due to the following decays: $K^+ \to \pi^+ + A$ [constrained by the $K_{\mu 2}$ experiment [26]], $K^+ \to \pi^+ + \textit{invisible}$ (measured by the experiments E787 [27] and BNL-E949 [28]), $B_s \to \mu^+\mu^-$ [measured by the LHCb collaboration [29] and the CMS collaboration [30], see [31] for a LHCb/CMS combination] and $B^0 \to K_S^0 + \textit{invisible}$ [measured by CLEO [32]]. It turns out that the most stringent Flavor Changing Neutral Current (FCNC) constraint is due to $K^+ \to \pi^+ + A$ from the $K_{\mu 2}$ experiment [26]. This process depends on a loop-induced *Asd* vertex (with W bosons and up-type quarks in the loop) which depends, in turn, on the couplings of A to d- and u-type quarks. Constraints from Yamazaki et al. [26] can lead to

$$\xi_d \lesssim 2 \times 10^{-2}. \tag{8}$$

A similar constraint can be obtained from the process $B \to K + A$.

Constraints from searches for $K^+ \to \pi^+ + \textit{invisible}$ from E787 and BNL-E949 [27, 28] apply only if A decays outside the detectors, i.e., if ξ_e is small enough. According to Andreas et al. [22], identifying now C_{Aff} in Andreas et al. [22] with ξ_e, this is not the case for $\xi_e \gtrsim 0.3$.

According to Dolan et al. [21], the constraints from $B_s \to \mu^+\mu^-$ (through an off-shell A) rule out any $\xi \gtrsim 0.7$ which is weaker than the constraint (8) from $K^+ \to \pi^+ + A$. Again, the loop contributions to the *Asb* vertex considered in Dolan et al. [21] are incomplete within an Ultra-Violet (UV) complete extension of the Higgs sector, and could again be canceled by additional BSM contributions as in the case of the *Asd* vertex.

The constraints from $B^0 \to K_S^0 + invisible$ measured by CLEO [32] apply only if the pseudoscalar A produced in $B^0 \to K_S^0 + A$ decays outside the detector. Accordingly these constraints depend both on the BR($B^0 \to K_S^0 + A$), hence on the *Asb* vertex or on ξ_u, ξ_d, and on the A decay length which depends on ξ_e. These quantities are identified in Dolan et al. [21] where a limit $\xi \gtrsim 3.5$ on all flavors satisfies the constraints, since then the A decay length becomes short enough despite the large production rate. Using this constraint only for ξ_e is conservative, if $\xi_u, \xi_d < \xi_e$ is assumed.

Finally, $\xi_e \gtrsim 3.5$ satisfies also bounds on A production in radiative Υ decays $\Upsilon \to \gamma + invisible$ interpreted as $\Upsilon \to \gamma + A$ from CLEO [33] and BaBar [34], which apply only if A decays outside the detectors. For $M_A \sim 17$ MeV, following [22], this is not the case for $\xi_e \gtrsim 1.5$.

Other important constraints on light pseudoscalars originate from beam dump experiments. From the Orsay experiment of Davier and Nguyen Ngoc [35], lifetimes τ_A in the range 5×10^{-12} s $\lesssim \tau_A \lesssim 2 \times 10^{-9}$ s are ruled out for $M_A \sim 17 - 18$ MeV. This has already been translated into constraints on a reduced pseudoscalar-fermion Yukawa coupling C_{Aff} in Andreas et al. [22], where $C_{Aff} = \xi_e$ in our notation. Following Andreas et al. [22], $0.4 \lesssim C_{Aff} \lesssim 4$ is ruled out by this constraint. Since $\xi_e < 0.4$ is incompatible with (7), one is left with

$$\xi_e \gtrsim 4\,. \tag{9}$$

This constraint leads automatically to the satisfaction of the lower bound $\xi_e \gtrsim 3.5$ from $B^0 \to K_S^0 + invisible$, as well as to a short enough decay length (7) for the Atomki pair spectrometer experiment. It is also compatible with the exclusion from the NA64 experiment [36] provided that $\xi_e \lesssim 15$.

Another potentially relevant experiment is the proton beam dump on copper CHARM experiment [37]. In Bergsma et al. [37] constraints were derived assuming that the production cross section and decay length of light pseudoscalars correspond to those of axions, which is not the case here. Relevant is the analysis in Dolan et al. [21] which uses the production of light pseudoscalars in $K \to \pi + A$ and $B \to X + A$ decays. For universally rescaled Yukawa couplings the region $\xi \gtrsim 1$ satisfies the constraints, since then the decay length of A is too short to reach the decay region of the CHARM experiment. This constraint does not supersede the one in Equation (9).

5. EXPLANATION OF THE BERYLLIUM ANOMALY WITH A PSEUDOSCALAR

One of the less well-studied solutions is that of the pseudoscalar, but this has been done in Ellwanger and Moretti [8]. It was initially dismissed by Feng et al. [7, 9] and subsequent authors by the argument that for such axion-like pseudoscalars A, fermion loops generate couplings of the form $g_{A\gamma\gamma} A F^{\mu\nu}(\gamma)\tilde{F}_{\mu\nu}(\gamma)$ which are strongly constrained by axion searches. However, light pseudoscalars in this mass range with tree level Yukawa couplings to electrons decay dominantly into electron-positron pairs, unless Yukawa couplings to other charged fermions f with mass m_f are much larger than m_f/m_e compensating $g_{A\gamma\gamma} \approx 1/(8\pi m_f)$. For solutions to the Atomki anomaly, we require such couplings to electrons and hence one should dismiss the pseudoscalar solution.

To summarize the previous section investigating the constraints, couplings of the form $\xi_u + \xi_d \sim 0.6$ and $\xi_e > 4$ should satisfy all aforementioned constraints and provide an explanation to the Atomki anomaly, with the caveat that FCNCs must be suppressed by loop contributions at the level of at least 10%.

Ultimately, it will be the Atomki experiment itself which will be in a position to either confirm or disprove the light pseudoscalar hypothesis. In fact, the experiment is currently planning to study the $\gamma\gamma$ decays of the 17 MeV particle, also in $4He \to \gamma\gamma$ [3], in order to distinguish between a vector boson and pseudoscalar boson scenario. According to the Landau-Yang theorem, the (on-shell) decay of a vector boson by double γ-emission is forbidden, however, the decay of a pseudoscalar one is allowed [38]. The angular correlation of the γ-rays will be measured by using 15 large (3" × 3") $LaBr_3$ detectors. If the A boson with a mass of 17 MeV is created in the decay of the $J^P = 0^-$ state and in turn decays into two γ-rays, their angular correlation θ should peak at

$$\cos\theta = 1 - \frac{M_A^2}{2E_\gamma E_{\gamma'}}, \tag{10}$$

where M_A is the mass of the A boson (17 MeV) and $E_{\gamma,\gamma'}$ are the energies of the two photons. However, it should be kept in mind that a light pseudoscalar with tree level coupling to electrons would have a loop-induced BR to di-photons of only one percent or so, hence hardly visible with current Atomki data sets. At any rate, results in this respect, are eagerly awaited.

6. EXPERIMENTAL CONSTRAINTS ON THE SPIN-1 EXPLANATION

Let us assume that the generic coupling of a new vector boson, Z', to the SM fermions is given by the following interaction Lagrangian

$$-\mathcal{L}_{\text{int}} = Z'_\mu \sum_f \bar{\psi}_f \gamma^\mu \left(C_{f,V} + \gamma_5 C_{f,A}\right) \psi_f. \tag{11}$$

Experimental Constraints on the Lepton Couplings

We have not seen a Z' in the electron beam dump experiment SLAC E141. Therefore, a Z' has not been produced, hence

$$C_{e,V}^2 + C_{e,A}^2 < 10^{-17} \tag{12}$$

or, else, a Z' has been caught in the dump, hence

$$\frac{C_{e,V}^2 + C_{e,A}^2}{\text{BR}(Z' \to e^+e^-)} \gtrsim 3.7 \times 10^{-9}. \tag{13}$$

We have not seen a Z' either in the electron beam dump experiment NA64 [36]. If a Z' has been caught in the dump, this places the (stronger than E141) condition

$$\frac{C_{e,V}^2 + C_{e,A}^2}{\mathrm{BR}(Z' \to e^+e^-)} \gtrsim 1.6 \times 10^{-8}\,. \tag{14}$$

The parity-violating Møller scattering measured at the SLAC E158 experiment [39] imposes a constraint on the product $C_{e,V}C_{e,A}$ of the Z', namely

$$|C_{e,V}C_{e,A}| \lesssim 10^{-8}, \tag{15}$$

for $M_{Z'} \simeq 17$ MeV [20].

Furthermore, there could be contributions of a Z' to the magnetic moments of electron and muon. The one-loop ones δa_l, mediated by a Z', lead to

$$\delta a_l = \frac{r_{m_l}}{4\pi^2}\left[C_{l,V}^2\, g_V(r_{m_l}) - C_{l,A}^2\, g_A(r_{m_l})\right], \tag{16}$$

where $r_{m_l} \equiv (m_l/M_{Z'})^2$ and g_V, g_A are given by

$$\begin{aligned} g_V(r) &= \int_0^1 dz \frac{z^2(1-z)}{1-z+rz^2}, \\ g_A(r) &= \int_0^1 dz \frac{(z-z^2)(4-z)+2rz^3}{1-z+rz^2}\,. \end{aligned} \tag{17}$$

The light boson contribution to the anomalous magnetic moment of the electron is required to be within the 2σ uncertainty of the departure of the SM prediction from the experimental result [40]. Concerning the muon anomalous magnetic moment [41], which has been measured at Brookhaven National Laboratory (BNL) to a precision of 0.54 parts per million, the current average of the experimental results is given by Bennett et al. [42], Blum et al.[43], and Lindner et al. [44]

$$a_\mu^{\mathrm{exp}} = 11659208.9(6.3) \times 10^{-10}, \tag{18}$$

which is different from the SM prediction by 3.3 to 3.6σ: $\Delta a_\mu = a_\mu^{\mathrm{exp}} - a_\mu^{\mathrm{SM}} = (28.3 \pm 8.7 \text{ to } 28.7 \pm 8.0) \times 10^{-10}$. We require again that the contribution of a Z' to $(g-2)_\mu$, which is mainly due to its axial-vector component, is less than the 2σ uncertainty of the discrepancy between the SM result and the experimental measure. For $M_{Z'} \simeq 17$ MeV, one then finds

$$\begin{aligned} \delta a_e &= 7.6 \times 10^{-6} C_{e,V}^2 - 3.8 \times 10^{-5} C_{e,A}^2 \simeq -10.5(8.1) \\ &\quad \times 10^{-13}, \end{aligned} \tag{19}$$

$$\delta a_\mu = 0.009 C_{\mu,V}^2 - C_{\mu,A}^2 \leq 2.9(90) \times 10^{-9}. \tag{20}$$

Electron-positron colliders (like KLOE2) would be sensitive to a new spin-1 gauge boson via the channel $e^+e^- \to \gamma, Z, Z' \to e^+e^-$. From this process one finds

$$(C_{e,V}^2 + C_{e,A}^2)\mathrm{BR}(Z' \to e^+e^-) \lesssim 3.7 \times 10^{-7}. \tag{21}$$

Similarly, Z' contributions to neutrino-electron scattering implies a bound on the product of the electron and neutrino couplings to the Z' [45, 46].

Experimental Constraints on the Quark Couplings

The couplings of a light Z' state with quarks are, in general, strongly constrained from $\pi^0 \to Z' + \gamma$ searches at the NA48/2 experiment [47]. The process is proportional to the anomaly factor $N_\pi = \frac{1}{2}(2C_{u,V} + C_{d,V})^2$. Therefore, one gets the following limit:

$$|2C_{u,V} + C_{d,V}| \lesssim \frac{3.6 \times 10^{-4}}{\sqrt{\mathrm{BR}(Z' \to e^+e^-)}} \tag{22}$$

for $M_{Z'} \simeq 17$ MeV. The contribution of the axial components is induced by chiral symmetry breaking effects and is, therefore, suppressed by the light quark masses.

Furthermore, atomic parity violation in Cesium (Cs) must be considered. In fact, very strong constraints on a light Z' can be extracted from the measurement of the effective weak charge of the Cs atom [48, 49]:

$$\begin{aligned} \Delta Q_w &= \frac{-2\sqrt{2}}{G_F} C_{e,A}\left[C_{u,V}(2Z+N) + C_{d,V}(Z+2N)\right] \\ &\quad \left(\frac{0.8}{(17\ \mathrm{MeV})^2}\right) \lesssim 0.71 \end{aligned} \tag{23}$$

at 2σ [50].

7. A $U(1)'$ EXTENSION OF THE SM WITH A LIGHT AND WEAKLY INTERACTING Z'

We consider a generic extension to the SM described by a new Abelian group $U(1)'$ [51–57]. Due to the presence of two such Abelian symmetries, $U(1)_Y \times U(1)'$, the most general kinetic Lagrangian of the corresponding fields, $\hat{B}_\mu$ and $\hat{B}'_\mu$, allows for a gauge invariant operator mixing the two field strengths. In particular, the quadratic Lagrangian for the two gauge fields is given by

$$\mathcal{L}_{\mathrm{kin}} = -\frac{1}{4}\hat{F}_{\mu\nu}\hat{F}^{\mu\nu} - \frac{1}{4}\hat{F}'_{\mu\nu}\hat{F}'^{\mu\nu} - \frac{\kappa}{2}\hat{F}'_{\mu\nu}\hat{F}^{\mu\nu}, \tag{24}$$

with κ being the kinetic mixing parameter. Since the parameterizations above may be inconvenient for practical computations, it is often useful to recast the kinetic Lagrangian into a diagonal form by removing the mixing operator through a rotation and rescaling of the Abelian fields. This transformation, while diagonalizing Equation (24), introduces a non-diagonal term in the interactions such that the covariant derivative may be written as

$$\mathcal{D}_\mu = \partial_\mu + \ldots + i g_1 Y B_\mu + i(\tilde{g}Y + g' z)B'_\mu, \tag{25}$$

where Y and z are, respectively, the hypercharge and the $U(1)'$ charge, and B_μ, B'_μ are the rotated fields. The parameter $\tilde{g}$ replaces κ and describes the mixing between the two Abelian groups while g' is the usual gauge coupling associated to the extra Abelian symmetry $U(1)'$.

Due to the mixing term in the gauge covariant derivative, after spontaneous symmetry breaking, the EW Vacuum Expectation Value (VEV) contributes to the $U(1)'$ breaking even if the Higgs sector is neutral under the new Abelian symmetry. For instance, in a scenario with only one Higgs doublet, the neutral gauge boson mass matrix can be extracted from the Higgs Lagrangian and reads as

$$-\mathcal{L}_{\rm Higgs} = \frac{v^2}{8}(g_2 W_\mu^3 - g_1 B_\mu - g_\Phi B'_\mu)^2 + \frac{m_{B'}^2}{2} B'^2_\mu + \ldots, \quad (26)$$

where $g_\Phi = \tilde{g} + 2 z_\Phi g'$ with z_Φ being the $U(1)'$ charge of the SM Higgs or a combination of charges in multi-Higgs doublet scenarios. As stated above, a non-vanishing g_Φ can be achieved either by the non-zero $U(1)'$ charges of the Higgs sector, $z_\Phi \neq 0$, or by the presence of the kinetic mixing $\tilde{g} \neq 0$. Both of them contribute to a $Z-Z'$ mass mixing. The mass term $m_{B'}^2$ represents a possible source for the Z' mass from a SM neutral sector. This can be realized, for instance, by the VEV v' of a SM-singlet complex scalar χ, with a z_χ charge under $U(1)'$. In this case $m_{B'} = g' z_\chi v'$. We remark here that, for our purposes, it is not necessary to specify the origin of the B' mass term and other mechanisms, beside Spontaneous Symmetry Breaking (SSB) with a complex scalar, can be also envisaged. Moreover, the mixing in the neutral gauge sector is only triggered by the g_Φ parameter and, as such, is unaffected by the details of the scalar sector in which the B' mass term is generated.

The diagonalization of the mass matrix provides the relation between the interaction and the mass eigenstates and is described by the rotation matrix

$$\begin{pmatrix} B^\mu \\ W_3^\mu \\ B'^\mu \end{pmatrix} = \begin{pmatrix} \cos\theta_w & -\sin\theta_w \cos\theta' & \sin\theta_w \sin\theta' \\ \sin\theta_w & \cos\theta_w \cos\theta' & -\cos\theta_w \sin\theta' \\ 0 & \sin\theta' & \cos\theta' \end{pmatrix} \begin{pmatrix} A^\mu \\ Z^\mu \\ Z'^\mu \end{pmatrix} \quad (27)$$

where θ_w is the usual weak mixing angle and θ' is a new mixing angle, with $-\pi/4 \leq \theta' \leq \pi/4$, defined as Accomando et al. [58]

$$\tan 2\theta' = \frac{2 g_\Phi g_Z}{g_{\Phi^2} + 4 m_{B'}^2/v^2 - g_Z^2}, \quad (28)$$

where $g_Z = \sqrt{g_1^2 + g_2^2}$ is the EW coupling, $g_\Phi = \tilde{g} + 2 z_\Phi g'$ and $g_{\Phi^2} = g_\Phi^2$. The masses of the Z and Z' gauge bosons are then given by

$$M_{Z,Z'} = g_Z \frac{v}{2} \left[\frac{1}{2} \left(\frac{g_{\Phi^2} + 4 m_{B'}^2/v^2}{g_Z^2} + 1 \right) \mp \frac{g_\Phi}{\sin 2\theta' \, g_Z} \right]^{\frac{1}{2}}. \quad (29)$$

For a light and weakly interacting Z', namely $g', \tilde{g} \ll g_Z$ and $m_{B'}^2 \ll v^2$, the mixing angle and the masses can be expanded at leading order as

$$M_Z^2 \simeq \frac{1}{4} g_Z^2 v^2, \qquad M_{Z'}^2 \simeq m_{B'}^2, \qquad \tan 2\theta' \simeq -2 \frac{g_\Phi}{g_Z}. \quad (30)$$

While the SM Z mass is correctly reproduced by the EW VEV, the mass of the Z' is controlled by the $m_{B'}$ parameter or, equivalently, by the VEV v' of the SM-singlet χ which is then given by $v' = M_{Z'}/(g' z_\chi)$. The Z' massless limit for $m_{B'} = 0$ is naively expected since if SSB is turned off in the scalar sector, no scalar degrees of freedom can provide the longitudinal component of a massive Z'. For a 17 MeV Z' with $g' \sim 10^{-3}$ the VEV of χ is $v' \sim 10$ GeV.

The expansions in Equation (30) are applicable if the Higgs sector is populated by only one $SU(2)$ doublet, as in the SM. This assumption can be obviously relaxed and more Higgs doublets can be implemented. We show, indeed, in the following sections that this possibility leads to an interesting phenomenology in the Z' sector and provides alternative solutions to the ^{8}Be anomaly.

For instance, in a scenario with two $SU(2)$ doublet scalars, Φ_1 and Φ_2 with the same hypercharge $Y = 1/2$ and two different charges z_{Φ_1} and z_{Φ_2} under the extra $U(1)'$, the diagonalization of the neutral gauge mass matrix is obtained through the mixing angle θ' in Equation (28) with

$$\begin{aligned} g_\Phi &= (\tilde{g} + 2 g' z_{\Phi_1}) \cos^2\beta + (\tilde{g} + 2 g' z_{\Phi_2}) \sin^2\beta, \\ g_{\Phi^2} &= (\tilde{g} + 2 g' z_{\Phi_1})^2 \cos^2\beta + (\tilde{g} + 2 g' z_{\Phi_2})^2 \sin^2\beta. \end{aligned} \quad (31)$$

The angle β is defined as usual as $\tan\beta = v_2/v_1$ with $v^2 = v_1^2 + v_2^2$. In the small coupling limit the Z' mass is given by

$$M_{Z'}^2 \simeq m_{B'}^2 + \frac{v^2}{4} g'^2 \left(z_{\Phi_1} - z_{\Phi_2} \right)^2 \sin^2(2\beta), \quad (32)$$

which, differently from the previous case, is non-vanishing even when $m_{B'} \simeq 0$ due to mismatch between z_{Φ_1} and z_{Φ_2}. In the limit in which there is no contribution from the dark scalar sector, one finds for $M_{Z'} \simeq 17$ MeV and $v \simeq 246$ GeV, $\tilde{g} \sim g' \sim 10^{-4}$. Interestingly, as we will show below, the same order of magnitude of the gauge couplings is required to explain the ^{8}Be anomaly with a Z' gauge boson characterized by axial-vector couplings.

In summary, for the case of one Higgs doublet, we showed that the limit $m_{B'} \ll v$ leads to $M_{Z'} \simeq m_{B'}$ with the SM Higgs sector playing no role in the generation of the Z' mass. In contrast, in a multi-Higgs scenario, like in a 2-Higgs Doublet Model (2HDM), if $z_{\Phi_1} \neq z_{\Phi_2}$, the symmetry breaking of the $U(1)'$ can actually be realized without any contribution from the dark scalar sector, namely with $v' = 0$. In fact, the longitudinal degree of freedom of the Z' is provided by the typical CP-odd state of the 2HDM spectrum which, differently from standard constructions, is characterized by a missing pseudoscalar field among the physical states. Before moving to this 2HDM realization, though, we ought to discuss the Z' interactions with the SM fermions emerging from the present construct.

7.1. The Z' Interactions With the SM Fermions

The interactions between the SM fermions and the Z' gauge boson are described by the Lagrangian $\mathcal{L}_{\rm int} = -J^\mu_{Z'} Z'_\mu$ where the gauge current is given by

$$J^\mu_{Z'} = \sum_f \bar{\psi}_f \gamma^\mu \left(C_{f,L} P_L + C_{f,R} P_R \right) \psi_f \quad (33)$$

with coefficients

$$C_{f,L} = -g_Z s' \left(T_f^3 - s_w^2 Q_f\right) + (\tilde{g} Y_{f,L} + g' z_{f,L})\, c' ,$$
$$C_{f,R} = g_Z s_w^2 s' Q_f + (\tilde{g} Y_{f,R} + g' z_{f,R})\, c' . \quad (34)$$

In the previous equations we have adopted the shorthand notation $s_w \equiv \sin\theta_w$, $c_w \equiv \cos\theta_w$, $s' \equiv \sin\theta'$ and $c' \equiv \cos\theta'$ and introduced Y_f the hypercharge, z_f the $U(1)'$ charge, T_f^3 the third component of the weak isospin and Q_f the electric charge. Analogously, the vector and axial-vector components of the Z' interactions are [57]

$$C_{f,V} = \frac{C_{f,R} + C_{f,L}}{2} = \frac{1}{2}\Big[-g_Z s'(T_f^3 - 2s_w^2 Q_f) + c'\tilde{g}(2Q_f - T_f^3) + c' g'(z_{f,L} + z_{f,R})\Big] ,$$
$$C_{f,A} = \frac{C_{f,R} - C_{f,L}}{2} = \frac{1}{2}\Big[(g_Z s' + \tilde{g} c') T_f^3 - c' g'(z_{f,L} - z_{f,R})\Big] \quad (35)$$

The vector and axial-vector coefficients simplify considerably in the limit $g', \tilde{g} \ll g_Z$. By noticing that $s' \simeq -g_\Phi / g_Z$, we get

$$C_{f,V} \simeq \tilde{g} c_w^2 Q_f + g' \Big[z_\Phi (T_f^3 - 2s_w^2 Q_f) + z_{f,V}\Big] ,$$
$$C_{f,A} \simeq g' \Big[-z_\Phi T_f^3 + z_{f,A}\Big] , \quad (36)$$

where we have introduced the vector and axial-vector $U(1)'$ charges $z_{f,V/A} = 1/2(z_{f,R} \pm z_{f,L})$ and z_Φ can be either the $U(1)'$ charge of the Higgs or $z_{\Phi_1} \cos^2\beta + z_{\Phi_2} \sin^2\beta$ in a 2HDM scenario.

The Z' couplings are characterized by the sum of three different contributions. The kinetic mixing $\tilde{g}$ induces a vector-like term proportional to the Electro-Magnetic (EM) current which is the only source of interactions when all the SM fields are neutral under $U(1)'$. In this case the Z' is commonly dubbed *dark photon*. The second term is induced by the z_Φ, the $U(1)'$ charge in the Higgs sector, and leads to a *dark Z*, namely a gauge boson mixing with the SM Z boson. Finally there is the standard gauge interaction proportional to the fermionic $U(1)'$ charges $z_{f,V/A}$.

We can delineate different scenarios depending on the structure of the axial-vector couplings of the Z' boson. In particular, the $C_{f,A}$ coefficients can be suppressed with respect to the vector-like counterparts (see also [20]). This is realized, for instance, when only one $SU(2)$ doublet is considered and the gauge invariance of the Yukawa Lagrangian under the new Abelian symmetry is enforced. Indeed, the latter requires the $U(1)'$ charge of the Higgs field to satisfy the conditions

$$z_\Phi = z_Q - z_d = -z_Q + z_u = z_L - z_e . \quad (37)$$

Inserting the previous relations into Equation (36), we find $C_{f,A} \simeq 0$ which describes a Z' with only vector interactions with charged leptons and quarks. We stress again that the suppression of the axial-vector coupling is only due to the structure of the scalar sector, which envisions only one $SU(2)$ doublet, and the gauge invariance of the Yukawa Lagrangian. This feature is completely unrelated to the $U(1)'$ charge assignment of the fermions, the requirement of anomaly cancelation and the matter content potentially needed to account for it.

In contrast, in the scenario characterized by two Higgs doublets, the axial-vector couplings of the Z' are, in general, of the same order of magnitude of the vector ones and the cancelation between the two terms of $C_{f,A}$ in Equation (36) is not achieved regardless of the details of the Yukawa Lagrangian (such as which type 2HDM). The same result can be achieved if a single Higgs doublet is considered but the conditions in Equation (37) are not satisfied as in scenarios in which the fermion masses are generated radiatively or through horizontal symmetries.

To summarize, we can identify three different situations that can provide a light Z' with interactions potentially explaining the Beryllium anomaly. In all of them, the SM is extended by an additional Abelian gauge group.

1. The SM scalar sector is unchanged, being characterized by only one Higgs doublet. In this case the mass of the Z' is entirely generated in the dark sector. The Yukawa Lagrangian preserves the SM structure and its gauge invariance under the $U(1)'$ necessary implies that the Z' has only vector interactions with the SM fermions at leading order in the couplings $\tilde{g}, g'$.
2. The SM scalar sector is extended by an additional Higgs doublet. Even though the Yukawa Lagrangian is invariant under the local $U(1)'$ symmetry, the cancelation between the two terms in $C_{f,A}$ in Equation (36) does not occur and both the vector and axial-vector couplings of the Z' are non-vanishing. The mass of the Z' acquires contribution from both the dark and the EW sectors.
3. The SM scalar sector is characterized by a single Higgs doublet but the constraints in Equation (37) are avoided by relying on more complicated Yukawa structures. As such, the cancelation providing $C_{f,A} \simeq 0$ is not realized and the vector and axial-vector interactions of the Z' are of the same order of magnitude.

We will discuss the three scenarios in the following sections focusing on their implications in the interpretation of the ^{8}Be anomaly.

Before concluding this section we briefly go through the conditions required by the cancelation of gauge and gravitational anomalies which strongly constrain the charge assignment of the SM spectrum under the extra $U(1)'$ gauge symmetry. These conditions can be eventually combined with the requirement of gauge invariance of the Lagrangian responsible for the generation of the fermion masses which may also involve non-renormalisable operators. We will also allow for extra

TABLE 1 | Family universal charge assignment in the $U(1)'$ extension of the SM.

	$SU(3)$	$SU(2)$	$U(1)_Y$	$U(1)'$
Q_L	3	2	1/6	z_Q
u_R	3	1	2/3	z_u
d_R	3	1	−1/3	$2z_Q - z_u$
L	1	2	−1/2	$-3z_Q$
e_R	1	1	−1	$-2z_Q - z_u$
ν_R	1	1	0	$-4z_Q + z_u$

SM-singlet fermions which can be easily interpreted as right-handed neutrinos. We assign the charges z_Q and z_L for the $SU(2)$ quark and lepton doublets, z_u, z_d, z_e for the corresponding right-handed components and z_ν for the n_R right-handed neutrinos. We obtain the following gauge and gravitational anomaly cancelation conditions:

$$\begin{aligned}
U(1)'SU(3)SU(3): &\quad \sum_i^3 (2z_{Q_i} - z_{u_i} - z_{d_i}) = 0\,,\\
U(1)'SU(3)SU(3): &\quad \sum_i^3 (3z_{Q_i} + z_{L_i}) = 0\,,\\
U(1)'U(1)_Y U(1)_Y: &\quad \sum_i^3 \left(\frac{z_{Q_i}}{6} - \frac{4}{3}z_{u_i} - \frac{z_{d_i}}{3} + \frac{z_{L_i}}{2} - z_{e_i}\right) = 0\,,\\
U(1)'U(1)'U(1)_Y: &\quad \sum_i^3 \left(z_{Q_i}^2 - 2z_{u_i}^2 + z_{d_i}^2 - z_{L_i}^2 + z_{e_i}^2\right) = 0\,,\\
U(1)'U(1)'U(1)': &\quad \sum_i^3 \left(6z_{Q_i}^3 - 3z_{u_i}^3 - 3z_{d_i}^3 + 2z_{L_i}^3 - z_{e_i}^3\right) + \sum_i^{n_R} z_{\nu_i} = 0\,,\\
U(1)'GG: &\quad \sum_i^3 \left(6z_{Q_i} - 3z_{u_i} - 3z_{d_i} + 2z_{L_i} - z_{e_i}\right) + \sum_i^{n_R} z_{\nu_i} = 0.
\end{aligned} \tag{38}$$

A simple solution is found for instance in the family universal case with $n_R = 3$ and $z_{\nu_i} = z_\nu$ and it is defined in terms of only two $U(1)'$ charges, z_Q and z_u as shown in **Table 1**. As an example, the $U(1)_{B-L}$ is reproduced by $z_Q = z_u = 1/3$ while the sequential $U(1)'$ is obtained for $z_Q = 1/6$ and $z_u = 2/3$.

7.2. Z' With Vector Couplings

The simplest $U(1)'$ extension of the SM, which may account for an extra neutral light gauge boson potentially explaining the ^{8}Be anomaly, is characterized by a single Higgs doublet. As already explained above, the gauge invariance of the Yukawa interactions fixes the $U(1)'$ charge of the Higgs to satisfy the restrictions in Equation (37) thus leading to a suppression of the Z' axial-vector couplings to the quarks and charged leptons with respect to the vector ones.

In this scenario, the anomalous internal pair creation transition of the excited stated of the Beryllium described by the normalized BR is given by

$$\frac{\mathrm{BR}(^8\mathrm{Be}^* \to X + {}^8\mathrm{Be})}{\mathrm{BR}(^8\mathrm{Be}^* \to \gamma + {}^8\mathrm{Be})} = \frac{1}{e^2}(C_{p,V} + C_{n,V})^2 \frac{|\vec{k}_{Z'}|^3}{|\vec{k}_\gamma|^3} \tag{39}$$

in which any dependence from the nuclear matrix elements factors out in the ratio of BRs. Moreover, the partial decay width of the Z' into SM fermions is

$$\Gamma(Z' \to f\bar{f}) = \frac{M_{Z'}}{12\pi}\sqrt{1 - \frac{4m_f^2}{M_{Z'}^2}}\left[C_{f,V}^2 + C_{f,A}^2 + 2(C_{f,V}^2 - 2C_{f,A}^2)\frac{m_f^2}{M_{Z'}^2}\right] \tag{40}$$

Since $M_{Z'} \simeq 17$ MeV, the light Z' can only decay into electrons and active neutrinos (assuming heavier right-handed neutrinos, if any).

While $C_{f,A} \simeq 0$, the explicit expressions of the vector couplings of the Z' are

$$\begin{aligned}
C_{p,V} &= \tilde{g}c_w^2 - 2g'z_H s_w^2 + g'(z_H + 3z_Q)\,,\\
C_{n,V} &= -g'\left(z_H - 3z_Q\right)\,,\\
C_{e,V} &= -\tilde{g}c_w^2 + 2g'z_H s_w^2 - g'(z_H - z_L)\,,\\
C_{\nu,V} &= -C_{\nu,A} = \frac{g'}{2}(z_H + z_L)\,,
\end{aligned} \tag{41}$$

where we have introduced the proton and neutron couplings $C_{p,V} = 2C_{u,V} + C_{d,V}$, $C_{n,V} = C_{u,V} + 2C_{d,V}$ and we have exploited the gauge invariance of the Yukawa Lagrangian. Moreover, the cancelation of the anomaly in the $U(1)'SU(2)SU(2)$ triangle diagram given in Equation (38) leads to $3z_Q + z_L = 0$, namely $C_{\nu,V} = -2C_{n,V}$.

The acceptable range of couplings is Feng et al. [7, 9]

$$\begin{aligned}
|C_{p,V}| &\lesssim 1.2 \times 10^{-3}\, e\,,\\
|C_{n,V}| &= (2 - 10) \times 10^{-3}\, e\,,\\
|C_{e,V}| &= (0.2 - 1.4) \times 10^{-3}\, e\,,\\
\sqrt{|C_{\nu,V}C_{e,V}|} &\lesssim 3 \times 10^{-4} e\,,
\end{aligned} \tag{42}$$

where $\mathrm{BR}(Z' \to e^+e^-) = 1$ has been assumed. The first two conditions ensure that the Atomki anomaly is correctly reproduced while avoiding, at the same time, the strong constraint from the $\pi^0 \to Z'\gamma$ decay. As the coupling to proton is smaller than the corresponding one to neutron, the Z' realizing this particular configuration has been dubbed *protophobic*. The bound on the electron coupling is mainly obtained from KLOE2, $(g-2)_e$ and beam dump experiments, while the neutrino coupling is constrained by neutrino scattering off electrons at the Taiwan EXperiment On Neutrinos (TEXONO) [45]. Reinterpreting the bounds obtained in Bilmis et al. [46], where a $B - L$ scenario

without mixing has been considered, for a general vector-like Z', one can show that the C_ν coupling must be much smaller than the typical value of $C_{n,V}$ required to explain the ^{8}Be anomaly, thus invalidating the $C_{\nu,V} = -2C_{n,V}$ condition required by the consistency of this simple model.

A possible way to suppress the neutrino coupling, without affecting the neutron one, could be to invoke the presence of additional neutral fermionic degrees of freedom, charged under the $U(1)'$ symmetry and mixed to the left-handed neutrinos, so that the effective coupling of the Z' to the physical neutrino mass eigenstate would be significantly reduced. This mixing is commonly realized in the seesaw mechanism, which is naturally envisaged in the Abelian extension considered here since right-handed neutrinos are required to cancel the gauge anomalies, but it can hardly account for the bounds determined by the neutrino-electron scattering experiments. Such a strategy has been discussed in Feng et al. [7], however, here we show two alternative solutions based on the exploitation of the Z' axial-vector interactions.

8. EXPLANATION OF THE BERYLLIUM ANOMALY WITH A FAMILY UNIVERSAL *U*(1)′

In this section we investigate the explanation of the Atomki anomaly in a scenario characterized by an extra $U(1)'$ model and two Higgs doublets.

One possibility studied as a solution to the Atomki anomaly is a well-known realization of the scalar potential and Yukawa interactions with two scalar doublets is the so-called type-II in which the up-type quarks couple to one Higgs (conventionally chosen to be Φ_2) while the down-type quarks couple to the other (Φ_1). The constraint from anomaly cancelation arising from the $U(1)'SU(3)SU(3)$ triangle diagram together with the gauge invariance of the Yukawa Lagrangian require $2z_Q - z_d - z_u = z_{\Phi_1} - z_{\Phi_2} = 0$, in the type-II scenario. In order to satisfy this condition with $z_{\Phi_1} \neq z_{\Phi_2}$, extra colored states are necessarily required which will bring additional terms into the anomaly cancelation conditions and so the equation above will be modified and no longer require equal Higgs charges under the new gauge group. These states must be vector-like under the SM gauge group and chiral under the extra $U(1)'$. This option has been explored in detail in Kahn et al. [20]. In this work, the constraints on new vector bosons with axial vector couplings in a family-universal scenario which includes extra colored states to cancel anomaly conditions is considered. In this review focus on a different, more minimal scenario than this, which does not require additional states, but modifies the scalar theory to affect the condition of anomaly cancelation.

The gauge invariance condition above is modified when the scalar sector reproduces the structure of the type-I 2HDM in which only one (Φ_2) of the two Higgs doublets participates in the Yukawa interactions. In this theory, the corresponding Lagrangian is the same as the SM one and its gauge invariance simply requires $z_{\Phi_2} = -z_Q + z_u = z_Q - z_d = z_L - z_e$, without constraining the $U(1)'$ charge of Φ_1, in the type-I scenario. In this way, we allow for gauge invariance even when $z_{\Phi_1} \neq z_{\Phi_2}$. Differently from the type-II scenario in which extra colored states are required to build an anomaly-free model, in the type-I case the UV consistency of the theory can be easily satisfied introducing only SM-singlet fermions as demanded by the anomaly cancelation conditions of the $U(1)'U(1)'U(1)'$ and $U(1)'GG$ correlators. Nevertheless, the mismatch between z_Φ and $z_{f,A} = \pm z_{\Phi_2}/2$ (for up-type and down-type quarks, respectively) prevents $C_{f,A}$ to be suppressed and the Z' interactions are given by Delle Rose et al. [57],

$$
\begin{aligned}
C_{u,V} &= \frac{2}{3}\tilde{g}c_w^2 + g'\left[z_\Phi\left(\frac{1}{2} - \frac{4}{3}s_w^2\right) + z_{u,V}\right],\\
C_{u,A} &= -\frac{g'}{2}\cos^2\beta(z_{\Phi_1} - z_{\Phi_2}),\\
C_{d,V} &= -\frac{1}{3}\tilde{g}c_w^2 + g'\left[z_\Phi\left(-\frac{1}{2} + \frac{2}{3}s_w^2\right) + z_{d,V}\right],\\
C_{d,A} &= \frac{g'}{2}\cos^2\beta(z_{\Phi_1} - z_{\Phi_2}),\\
C_{e,V} &= -\tilde{g}c_w^2 + g'\left[z_\Phi\left(-\frac{1}{2} + 2s_w^2\right) + z_{e,V}\right],\\
C_{e,A} &= \frac{g'}{2}\cos^2\beta(z_{\Phi_1} - z_{\Phi_2}),\\
C_{\nu,V} &= -C_{\nu,A} = \frac{g'}{2}(z_\Phi + z_L).
\end{aligned}
\tag{43}
$$

As pointed out in Feng et al. [7], the contribution of the axial-vector couplings to the $^8\text{Be}^* \to {}^8\text{Be}\,Z'$ decay is proportional to $|\vec{k}_{Z'}|/M_{Z'} \ll 1$, where $\vec{k}_{Z'}$ is the momentum of the Z', while the vector component is suppressed by $|\vec{k}_{Z'}|^3/M_{Z'}^3$. Therefore, in our case, being $C_{f,V} \sim C_{f,A}$, we can neglect the effects of the vector couplings of the Z' and their interference with the axial counterparts. For a Z' with only axial-vector couplings to quarks, the transition $^8\text{Be}^* \to {}^8\text{Be}\,Z'$ is described by the partial width [19]

$$
\Gamma = \frac{k}{18\pi}\left(2 + \frac{E_k^2}{M_{Z'}^2}\right)\left|a_n\langle 0||\sigma^n||1\rangle + a_p\langle 0||\sigma^p||1\rangle\right|^2, \tag{44}
$$

where the neutron and proton coefficients $a_n = (a_0 - a_1)/2$ and $a_p = (a_0 + a_1)/2$ are defined in terms of

$$
\begin{aligned}
a_0 &= \left(C_{u,A} + C_{d,A}\right)\left(\Delta u^{(p)} + \Delta d^{(p)}\right) + 2\,C_{s,A}\Delta s^{(p)},\\
a_1 &= \left(C_{u,A} - C_{d,A}\right)\left(\Delta u^{(p)} - \Delta d^{(p)}\right),
\end{aligned}
\tag{45}
$$

with $\Delta u^{(p)} = 0.897(27)$, $\Delta d^{(p)} = -0.367(27)$ and $\Delta s^{(p)} = -0.026(4)$ [59]. The reduced nuclear matrix elements of the spin operators have been computed in Kozaczuk et al. [19] and are given by $\langle 0||\sigma^n||1\rangle = -0.132 \pm 0.033$, $\langle 0||\sigma^p||1\rangle = -0.047 \pm 0.029$ for the isoscalar $^8\text{Be}^* \to {}^8\text{Be}$ transition and $\langle 0||\sigma^n||1\rangle = -0.073 \pm 0.029$, $\langle 0||\sigma^p||1\rangle = 0.102 \pm 0.028$ for the isovector $^8\text{Be}^{*'} \to {}^8\text{Be}$ transition.

Notice that the axial couplings of the quarks and, therefore, the width of the $^8\text{Be}^* \to {}^8\text{Be}\,Z'$ decay are solely controlled by

the product $g' \cos^2\beta$ while the kinetic mixing $\tilde{g}$ only affects the BR($Z' \to e^+e^-$) since the $Z' \to \nu\nu$ decay modes are allowed (we assume that the $Z' \to \nu_R\nu_R$ decays are kinematically closed). For definiteness, we consider a $U(1)_{\text{B-L}}$ charge assignment with $z_{Q_L} = z_{u_R} = 1/3$, with other charges defined using **Table 1**, and $z_{\Phi_2} = 0$, $z_{\Phi_1} = 1$ and $\tan\beta = 1$. Analog results may be obtained for different $U(1)'$ charge assignments and values of $\tan\beta$. We show in **Figure 2** the parameter space explaining the Atomki anomaly together with the most constraining experimental results.

The orange region, where the Z' gauge couplings comply with the best-fit of the ^{8}Be* decay rate in the mass range $M_{Z'} = 16.7\,\text{MeV} - 17.6\,\text{MeV}$ [1, 7], encompasses the uncertainties on the computation of the nuclear matrix elements [19]. The region above it is excluded by the non-observation of the same transition in the isovector excitation $^8\text{Be}^{*'}$ [1]. The horizontal gray band selects the values of g' accounting for the Z' mass in the negligible $m_{B'}$ case in which the $U(1)'$ symmetry breaking is driven by the two Higgs doublets. Furthermore, among all other experimental constraints involving a light Z' that may be relevant for this analysis we have shown the most restrictive ones.

The strongest bound comes from the atomic parity violation in Cs and it represents a constraint on the product of $C_{e,A}$ and a combination of $C_{u,V}$ and $C_{d,V}$. This bound can be avoided if the Z' has either only vector or axial-vector couplings but in the general scenario considered here, it imposes severe constraints on the gauge couplings $g', \tilde{g}$ thus introducing a fine-tuning in the two gauge parameters.

We finally comment on the constraints imposed by neutrino-electron scattering processes [45, 60, 61], the strongest one being from $\bar{\nu}_e e$ scattering at the TEXONO experiment [45], which affect a combination of $C_{e,V/A}$ and $C_{\nu,V}$. As discussed above, in the protophobic scenario, in which the Z' has only vector interactions, the constrained ν coupling to the Z' boson is in high tension with the measured ^{8}Be* decay rate since $C_{\nu,V} = -2C_{n,V}$ and a mechanism to suppress the neutrino coupling must be envisaged [7]. This bound is, in general, alleviated if one attempts to explain the Atomki anomaly with a Z' boson with axial-vector interactions since the required gauge couplings $g', \tilde{g}$ are smaller than the ones needed in the protophobic case. Neutrino couplings are also constrained by meson decays, like, for instance $K^\pm \to \pi^\pm\nu\nu$ which has been studied in Davoudiasl et al. [62] and where it has been shown that the corresponding constraint is relaxed by a destructive interference effect induced by the charged Higgs. As the results presented in Davoudiasl et al. [62] relies on the Goldstone boson equivalence approximation, we have computed the full one-loop corrections to the $K^\pm \to \pi^\pm Z'$ process in the $U(1)'$-2HDM scenario. The results are in agreement with the estimates in Davoudiasl et al. [62]. In our setup, for $g' \sim 10^{-4}$ and $\tan\beta = 1$, $M_{H^\pm} \sim 600$ GeV can account for the destructive interference quoted above between the $W^\pm$ and $H^\pm$ loops. For instance, we find $\text{BR}(K^\pm \to \pi^\pm Z' \to \pi^\pm\nu\nu) \simeq 0.1\,\text{BR}(K^\pm \to \pi^\pm\nu\nu)_{\text{exp}}$ for $M_{H^\pm} \sim 615$ GeV with $\text{BR}(Z' \to \nu\nu) \simeq 30\%$ which is the maximum value for the invisible Z' decay rate in the allowed region (orange and gray shaded area) shown in **Figure 2**. A similar constraint arises from the B meson decay to invisible but is less severe than the one discussed above [63]. The $B^\pm \to K^\pm Z'$ process is characterized by the same loop corrections appearing in $K^\pm \to \pi^\pm Z'$, with the main difference being the dependence on the Cabibbo-Kobayashi-Maskawa (CKM) matrix elements. Therefore, the suppression effect induced by the charge Higgs mass affects both processes in the same region of the parameter space, thus ensuring that the bound from the invisible B decays is satisfied once the constraint from the analogous K meson decay is taken into account.

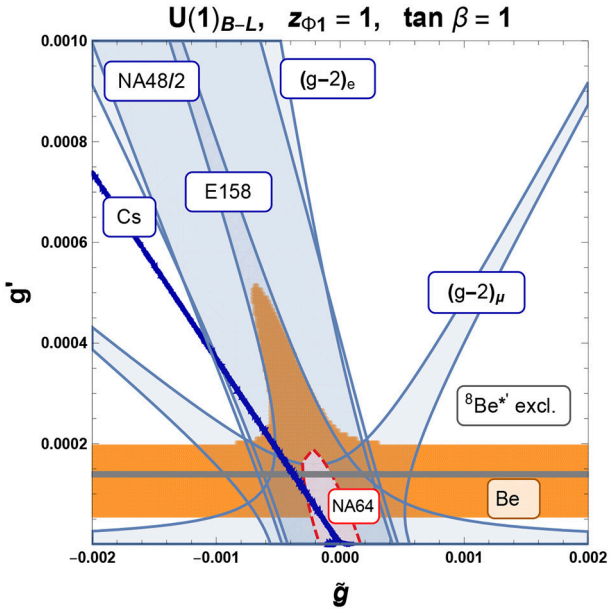

FIGURE 2 | Allowed parameter space (orange region) explaining the anomalous ^{8}Be* decay. The white region above is excluded by the non-observation of the same anomaly in the $^8\text{Be}^{*'}$ transition. Also shown (shaded regions) is the allowed parameter space by the $g-2$ of electrons and muons and the Møller scattering at SLAC E158 and pion decay from NA48/2. The beam dump experiment NA64 allows parameter space outside the red shaded region with dashed line. Finally, the blue line selects values of g' and $\tilde{g}$ compatible with the weak nuclear charge measurement of Cesium. The horizontal gray band delineates values of g' for which the Z' mass is solely generated by the SM vev.

9. EXPLANATION OF THE BERYLLIUM ANOMALY WITH A FAMILY NON-UNIVERSAL *U*(1)′

The final alternative is to consider a single Higgs doublet, as with the SM, but non-standard Yukawa interactions, to allow axial couplings through the violation of Equation (37), as done in Delle Rose et al. [64]. This is done for the first two generations of fermions and the third has SM-like gauge-invariance, motivated by $\mathcal{O}(1)$ couplings. We begin by modifying the Yukawa couplings for the first two generations as follows,

$$-\mathcal{L}_{Yuk} = \Gamma^u \frac{\chi^{n_{ij}}}{M^{n_{ij}}} \overline{Q}_{L,i} \tilde{H} u_{R,j} + \Gamma^d \frac{\chi^{l_{ij}}}{M^{l_{ij}}} \overline{Q}_{L,i} H d_{R,j}$$

$$+ \Gamma^e \frac{\chi^{m_{ij}}}{M^{m_{ij}}} \bar{L}_i H e_{R,j} + h.c., \tag{46}$$

where the exponent, n_{ij}, of the non-renormalisable scale, M, is defined by the $U(1)'$ charges of the fields, such that these new Yukawa terms are gauge invariant. Subsequently, one may obtain fermion masses either at tree-level or radiatively by the method of Ref. Froggatt and Nielsen [65][2]. There are several models which motivate radiative mass generation for the lighter generations, as done in Demir et al. [66], alternatively, there exist mass generation dynamics by horizontal symmetries, as in Froggatt and Nielsen [65]. We do not specify these dynamics, and simply leave an effective approach. We finally enforce that the first two generations are flavor universal, differing from the third, $z_{i_1} = z_{i_2}$ for $i = \{Q, u_R, d_R, L, e_R\}$, where the condition (37) is not applied to $z_{i_{1,2}}$. We now consider further constraints on the charge assignment. We also enforce the chiral anomaly cancelation conditions in Equation (38), which will be satisfied by solely the fermionic content of the SM, supplemented by two right-handed neutrinos.

Our remaining constraints on the charge assignment are motivated by the non-observation of BSM physics. As discussed above, there are strong constraints on coupling to neutrinos, which would enhance processes such as $K^{\pm} \to \pi^{\pm}\nu\nu$ [62], as well as electron-neutrino interactions, measured by the TEXONO experiment [7, 45, 46, 67]. To avoid these stringent constraints, we therefore impose no couplings to the neutrinos, i.e., $C_{V,\nu} = C_{A,\nu} = 0$. This subsequently yields a relation between the neutrino and Higgs charges,

$$z_{L_1} = z_{L_2} = z_{L_3} = -z_H. \tag{47}$$

Another constraint is to require that one indeed does have axial couplings for the up/down quarks to the Z', as required to explain the anomaly,

$$-z_{Q_{1,2}} - z_H + z_{u_{1,2}} \neq 0, \tag{48}$$
$$-z_{Q_{1,2}} + z_H + z_{d_{1,2}} \neq 0. \tag{49}$$

Our final constraint is from the atomic parity violation in Cs. As can be seen from other solutions, this provides a stringent bound on models with axial couplings for electrons. We thus also forbid interactions of this kind, and due to requiring universality for the first two generations, this will also forbid axial couplings for the muon,

$$C_{e,A} = C_{\mu,A} = 0. \tag{50}$$

Preventing the appearance of these axial couplings will also help to avoid bounds from both $(g-2)_e$ and avoid worsening the discrepancy in $(g-2)_\mu$.

Combining all these constraints yields a single, unique charge assignment. We have a normalization choice, and choose to set $z_H = 1$. This unique choice is shown in **Table 2**.

[2]Lagrangians of this form have been used to motivate solutions to the flavor problem, so it may be of interest to investigate whether this $U(1)'$ may explain the allowed masses and mixings, but we perform no such careful investigation here.

TABLE 2 | Charge assignment of the SM particles under the family-dependent (non-universal) $U(1)'$.

	$SU(3)$	$SU(2)$	$U(1)_Y$	$U(1)'$
Q_1	3	2	1/6	1/3
Q_2	3	2	1/6	1/3
Q_3	3	2	1/6	1/3
u_{R_1}	3	1	2/3	−2/3
u_{R_2}	3	1	2/3	−2/3
u_{R_3}	3	1	2/3	4/3
d_{R_1}	3	1	−1/3	4/3
d_{R_2}	3	1	−1/3	4/3
d_{R_3}	3	1	−1/3	−2/3
L_1	1	2	−1/2	−1
L_2	1	2	−1/2	−1
L_3	1	2	−1/2	−1
e_{R_1}	1	1	−1	0
e_{R_2}	1	1	−1	0
e_{R_3}	1	1	−1	−2
H	1	2	1/2	1

This numerical charge assignment satisfies the discussed anomaly cancelation conditions, enforces a gauge invariant Yukawa sector of the third generation and family universality in the first two fermion generations as well as no coupling of the Z' to the all neutrino generations.

Now, we consider constraints on the new gauge coupling, and gauge-kinetic mixing parameters $(g', \tilde{g})$, given this charge selection. Unlike the previous scenarios considered, since this is family non-universal, one finds tree level FCNCs, which should be analyzed. In diagonalizing the quarks into the mass basis, off-diagonal couplings are generated, due to different coupling strengths between the first two and third quark generations. We now discuss the consequences of this on experimental observables. We begin with $K \to \pi e^+ e^-$ through a tree-level exchange of an on-shell Z'. There are no contributions to the $\mu^+\mu^-$ decay as $M_{Z'} \sim 17\,\text{MeV} < 2m_\mu$. There are stringent limits from LHCb [68], though these are inapplicable in our case due to the small invariant mass of the e^+e^- pair. There is only sensitivity to energies above 20 MeV, due to photon conversion in the detector, and so energy resolution strongly degrades around these invariant masses. It is possible that future upgrades will lower this threshold and thus act as a discovery tool, or to disprove this scenario.

Another flavor observable is from meson mixing measurements. We begin with $B^0 - \bar{B}^0$, following the procedure as done in Bečirević et al. [69], but now assuming a much lighter propagator than their scenario, $P \equiv (m_B^2 - M_{Z'}^2)^{-1} \simeq m_B^{-2}$, as opposed to their $P \simeq M_{Z'}^{-2}$. One subsequently finds the requirement

$$|g_{sb}^{L(R)}| \lesssim 10^{-6}, \tag{51}$$

where (assuming Minimal Flavor Violation (MFV) in the quark sector and using CKM matrix elements),

$$g_{sb}^L = g' \left(V_{\text{CKM}}^T \, \text{Diag}(z_{Q_1}, z_{Q_1}, z_{Q_3}) \, V_{\text{CKM}} \right)_{23}, \tag{52}$$

$$g^R_{sb} = g'\left(V^T_{\rm CKM}\ {\rm Diag}(z_{u_{R_1}}, z_{u_{R_1}}, z_{u_{R_3}})\ V_{\rm CKM}\right)_{23}, \qquad (53)$$

Since our charge assignment is family universal for LH quarks, $g^L_{sb} = 0$, see **Table 2**, only the right-handed sector will contribute to the FCNC. This is suppressed by CKM factors, $g^R_{sb} \propto V_{tb}V_{ts}$, and so one finds a condition on the couplings, $g', \tilde{g} \lesssim 10^{-4}$.

Proceeding in a similar faction but for $K - \bar{K}$ oscillations will yield a weaker constraint on the couplings. Although the propagator suppression is less severe, $P \simeq m_K^{-2} > m_B^{-2}$, the CKM suppression is much stronger, $g^R_{sd} \propto V_{td}V_{ts}$, and one finds the constraint $g', \tilde{g} \lesssim 10^{-3}$. In this review, we do not perform a full flavor analysis, but require these approximate constraints.

Finally, we present the allowed parameter space in **Figure 3** for this scenario with one Higgs doublet extended by a $U(1)'$, with a charge assignment shown in **Table 2**. The red, purple and green bands show regions which can explain the Atomki anomaly for 16.7, 17.3 and 17.6 MeV Z' masses, respectively. These overlap in places and are independent of $\tilde{g}$ as the axial coupling depends solely on g' and ${\rm BR}(Z' \to e^+e^-) = 1$ everywhere. These bands have upper bounds due to the non-observation of the $^8{\rm Be}^{*'}$ anomaly. Also shown on the plot are the bounds from $(g-2)_\mu$, where the allowed region is inside the dashed line and $(g-2)_e$, where the allowed region is shaded in blue inside the dotted lines. In addition, the allowed region from NA64 is also shown, where one should be outside the red shaded region. The overall allowed region is therefore between the NA64 and $(g-2)_e$ lines, in the overlap shaded in blue. The other experimental constraints (electron positron collider (KLOE2), Moller scattering (E158), pion decay (NA48/2), E141, and atomic parity violation of Cs), similar to $(g-2)_\mu$, do not limit the allowed parameter space in blue, and are not shown on the plot.

Figure 4 shows the quantity $\mathcal{B}$, as defined in Equation (1), over a range of Z' masses. For each fixed mass value, a scan is performed over $(g', \tilde{g})$, in a range compatible with other experimental constraints, and the Atomki anomaly (i.e., over the dark blue and colored regions in **Figure 3**). For each scanned point in $\{M_{Z'},\ g'.\ \tilde{g}\}$, there is a range of branching ratios, due to uncertainties in the Nuclear Matrix Elements (NMEs). This lower limit for all points is lower than the Atomki branching ratios, so only the upper $\mathcal{B}$ is of importance, and this is plotted. Also drawn, in orange, is the required branching ratio, as published by the Atomki collaboration, see **Table 3**. A given point is then allowed if the upper $\mathcal{B}$ limit lies above the orange dots. For larger $M_{Z'}$ values, the largest $\mathcal{B}$ decreases, and a larger number of the scanned points lie above the Atomki points. This suggests that at higher masses, there is slightly more parameter space available for the 17.6 MeV solution, in comparison to the 16.7 MeV one. This is reflected in the slightly different widths shown in **Figure 3**.

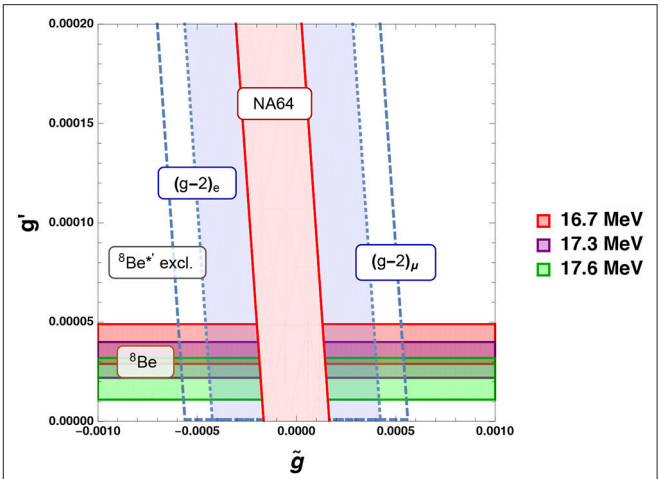

FIGURE 3 | Allowed parameter space mapped on the $(g', \tilde{g})$ plane explaining the anomalous ^{8}Be* decay for Z' solutions with mass 16.7 (red), 17.3 (purple), and 17.6 (green) MeV. The white regions are excluded by the non-observation of the same anomaly in the $^8{\rm Be}^{*'}$ transition. Also shown are the constraints from $(g-2)_\mu$, to be within the two dashed lines; $(g-2)_e$, to be inside the two dotted lines (shaded in blue) and the electron beam dump experiment, NA64, to be outside the shaded red region, which lies between the two solid lines. The surviving parameter space lies at small positive and negative $\tilde{g}$ (though not at $\tilde{g} = 0$), inside the shaded blue region which overlaps the Atomki anomaly solutions.

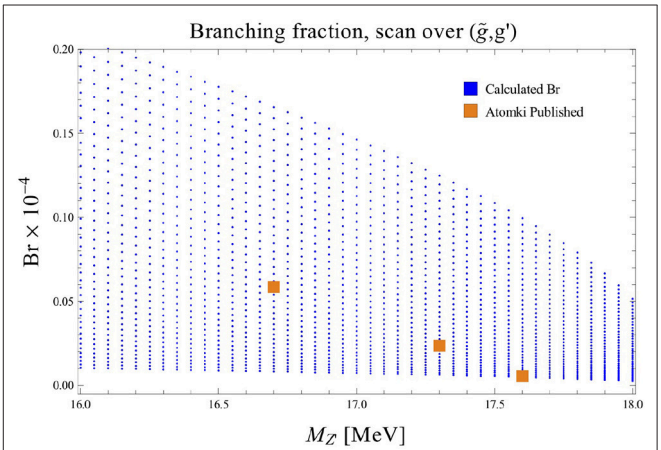

FIGURE 4 | Values of the upper limit $\mathcal{B}$ (lower limits are smaller than the scale of the plot), as defined in Equation (1), vs. the mass of the Z' obtained scanning over the allowed parameter space in $(g', \tilde{g})$, obtained from **Figure 3** for each mass step taken (in blue). The Atomki collaboration solutions are also shown (in orange).

10. CONCLUSIONS

While there remains the possibility that the Atomki anomaly can be explained as a statistical fluctuation combined with yet unknown nuclear physics properties and/or unforeseen experimental conditions, the fact that presently such an effect has been determined with a 6.8σ significance, including a near-perfect fit of both the mass and angular excesses to the possibility of a new particle with a mass of about 17 MeV been produced, calls for a thorough investigation of plausible theoretical explanations.

With this in mind, in this review, we have presented particle physics scenarios that extend the SM to include the presence of either a spin-0 (pseudoscalar, A) boson or a spin-1 (axial-vector, Z') boson, both of which can be made compliant with a variety of

TABLE 3 | Solutions to the Atomki anomaly, with best fit mass value (16.7 MeV) from Krasznahorkay et al. [1] and subsequent alternative masses (17.3 and 17.6 MeV) from Feng et al. [7] along with the corresponding ratio of BRs, $\mathcal{B}$, as defined in Equation (1).

$M_{Z'}$ (MeV)	$\mathcal{B}$
16.7	5.8×10^{-6}
17.3	2.3×10^{-6}
17.6	5.0×10^{-7}

experimental data. Assuming the standard Lagrangian structures describing A and Z' interactions with SM fermionic currents in both the lepton and quark sectors, we have determined the required couplings of such bosons to explain the Beryllium data.

As for the theoretically embeddings of these solutions, we can conclude the following. A light pseudoscalar state can appear in models with extended Higgs sectors in which an approximate ungauged global symmetry is spontaneously broken, examples of which include (type-II) 2HDMs with a SM-singlet near the Peccei-Quinn or R-symmetric limit, although in this case isospin breaking effects and non-universality in the Yukawa couplings of the new state to electrons and d-quarks must be allowed for. As for light gauge bosons with significant axial-vector couplings, two possible theoretical frameworks have been proven to be viable. Both require an additional $U(1)'$ group mixing with the SM one, $U(1)_Y$. In one case, which retains the SM Higgs sector, a family non-universal set of Z' couplings to the known fermions must be invoked. In the other case, Z' couplings to quarks and fermions of the SM can be retained in their universal form, yet this requires an enlarged Higgs sector, which we have identified as possibly being a type-I 2HDM. Needless to say, these two theoretical frameworks were constructed in presence of gauge invariance and anomaly cancelations plus they do not require isospin breaking.

While the above list of possible theoretical setups is clearly not exhaustive, it at least provides somewhat minimal frameworks (only containing enlarged Higgs and gauge sectors, possibly including heavy neutrinos but no exotic particles) within which further data upcoming from the Atomki experiment can be interpreted to pave the way for more dedicated phenomenological studies, which may in turn lead to refinements on the theoretical side.

AUTHOR CONTRIBUTIONS

All authors worked on all parts of the manuscript. Listed below are which sections were first drafted by the different authors, but subsequently all authors contributed to all parts. LDR: Experimental constraints on the quark couplings and A $U(1)'$ extension of the SM with a light and weakly interacting Z′. SK: The Atomki experiment and 17 MeV beryllium anomaly, Candidates for the new boson, and Explanation of the beryllium anomaly with a pseudoscalar. SJDK: Experimental constraints on the spin-1 explanation, Experimental constraints on the lepton couplings, and Explanation of the beryllium anomaly with a family universal $U(1)'$. SM: Introduction, Experimental constraints on the pseudoscalar explanation, Explanation of the beryllium anomaly with a family non-universal $U(1)'$.

ACKNOWLEDGMENTS

The work of LD and SM is supported in part by the NExT Institute. SM also acknowledges partial financial contributions from the STFC Consolidated Grant ST/L000296/1. Furthermore, the work of LD has been supported by the STFC/COFUND Rutherford International Fellowship Programme (RIFP). SJDK and SK have received support under the H2020-MSCA grant agreements InvisiblesPlus (RISE) No. 690575 and Elusives (ITN) No. 674896. In addition SK was partially supported by the STDF project 13858. All authors acknowledge support under the H2020-MSCA grant agreement NonMinimalHiggs (RISE) No. 645722.

REFERENCES

1. Krasznahorkay AJ, Csatlós M, Csige L, Gácsi Z, Gulyás J, Hunyadi M, et al. Observation of anomalous internal pair creation in Be8 : a possible indication of a light, Neutral Boson. *Phys Rev Lett*. (2016) **116**:042501. doi: 10.1103/PhysRevLett.116.042501
2. Krasznahorkay AJ, Csatlós M, Csige L, Gácsi Z, Ketel TJ, Krasznahorkay A, et al. On the creation of the 17 MeV X boson in the 17.6 MeV M1 transition of ^{8}*Be*. *EPJ Web Conf*. (2017) **142**:01019. doi: 10.1051/epjconf/201714201019
3. Krasznahorkay AJ, Csatlós M, Csige L, Gulyás J, Hunyadi M, Ketel TJ, et al. New results on the Be-8 anomaly. In: *55th International Winter Meeting on Nuclear Physics*. Bormio (2017).
4. Krasznahorkay AJ, Csatlós M, Csige L, Gulyás J, Hunyadi M, Ketel TJ, et al. New experimental results for the 17 MeV particle created in ^{8}*Be*. *EPJ Web Conf*. (2017) **137**:08010. doi: 10.1051/epjconf/201713708010.
5. Krasznahorkay AJ, Csatlós M, Csige L, Gácsi Z, Gulyás J, Nagy Á, et al. New results on the ^{8}Be anomaly. *J Phys Conf Ser*. (2018) **1056**:012028. doi: 10.1088/1742-6596/1056/1/012028
6. Gulyás J, Ketel TJ, Krasznahorkay AJ, Csatlós M, Csige L, Gácsi Z, et al. A pair spectrometer for measuring multipolarities of energetic nuclear transitions. *Nucl Instrum Methods*. (2016) **A808**:21–8. doi: 10.1016/j.nima.2015.11.009.
7. Feng JL, Fornal B, Galon I, Gardner S, Smolinsky J, Tait TMP, et al. Particle physics models for the 17 MeV anomaly in beryllium nuclear decays. *Phys Rev*. (2017) **D95**:035017. doi: 10.1103/PhysRevD.95.035017
8. Ellwanger U, Moretti S. Possible explanation of the electron positron anomaly at 17 MeV in ^{8}*Be* transitions through a light pseudoscalar. *J High Energy Phys*. (2016) **11**:039. doi: 10.1007/JHEP11(2016)039
9. Feng JL, Fornal B, Galon I, Gardner S, Smolinsky J, Tait TMP, et al. Protophobic fifth-force interpretation of the observed anomaly in ^{8}Be nuclear transitions. *Phys Rev Lett*. (2016) **117**:071803. doi: 10.1103/PhysRevLett.117.071803
10. Gu PH, He XG. Realistic model for a fifth force explaining anomaly in $^8Be^* \rightarrow {}^8Be\ e^+e^-$ Decay. *Nucl Phys*. (2017) **B919**:209–17. doi: 10.1016/j.nuclphysb.2017.03.023
11. Chen LB, Liang Y, Qiao CF. X(16.7) production in electron-position collision. *arXiv:1607.03970*. (2016).
12. Liang Y, Chen LB, Qiao CF. X(16.7) as the solution of the NuTeV anomaly. *Chin Phys*. (2017) **C41**:063105. doi: 10.1088/1674-1137/41/6/063105

13. Jia LB, Li XQ. The new interaction suggested by the anomalous ^{8}Be transition sets a rigorous constraint on the mass range of dark matter. *Eur Phys J.* (2016) **C76**:706. doi: 10.1140/epjc/s10052-016-4561-3
14. Kitahara T, Yamamoto Y. Protophobic light vector boson as a mediator to the dark sector. *Phys Rev.* (2017) **D95**:015008. doi: 10.1103/PhysRevD.95.015008
15. Chen CS, Lin GL, Lin YH, Xu F. The 17 MeV anomaly in beryllium decays and $U(1)$ portal to dark matter. *Int J Mod Phys.* (2017) **A32**:1750178. doi: 10.1142/S0217751X17501780
16. Seto O, Shimomura T. Atomki anomaly and dark matter in a radiative seesaw model with gauged $B - L$ symmetry. *Phys Rev.* (2017) **D95**:095032. doi: 10.1103/PhysRevD.95.095032
17. Neves MJ, Helayël-Neto JA. A unified hidden-sector-electroweak model, paraphotons and the X-Boson. *arXiv:1611.07974.* (2016).
18. Chiang CW, Tseng PY. Probing a dark photon using rare leptonic kaon and pion decays. *Phys Lett.* (2017) **B767**:289–94. doi: 10.1016/j.physletb.2017.02.022
19. Kozaczuk J, Morrissey DE, Stroberg SR. Light axial vector bosons, nuclear transitions, and the ^{8}Be anomaly. *Phys Rev.* (2017) **D95**:115024. doi: 10.1103/PhysRevD.95.115024
20. Kahn Y, Krnjaic G, Mishra-Sharma S, Tait TMP. Light weakly coupled axial forces: models, constraints, and projections. *J High Energy Phys.* (2017) **05**:002. doi: 10.1007/JHEP05(2017)002
21. Dolan MJ, Kahlhoefer F, McCabe C, Schmidt-Hoberg K. A taste of dark matter: flavour constraints on pseudoscalar mediators. *J High Energy Phys.* (2015) **03**:171. doi: 10.1007/JHEP07(2015)103,10.1007/JHEP03(2015)171
22. Andreas S, Lebedev O, Ramos-Sanchez S, Ringwald A. Constraints on a very light CP-odd Higgs of the NMSSM and other axion-like particles. *J High Energy Phys.* (2010) 08:003. doi: 10.1007/JHEP08(2010)003
23. Essig R, Harnik R, Kaplan J, Toro N. Discovering new light states at neutrino experiments. *Phys Rev.* (2010) D82:113008. doi: 10.1103/PhysRevD.82.113008
24. *Fundamental Physics at the Intensity Frontier* (2012). Available online at: http://lss.fnal.gov/archive/preprint/fermilab-conf-12-879-ppd.shtml.
25. Döbrich B, Jaeckel J, Kahlhoefer F, Ringwald A, Schmidt-Hoberg K. ALPtraum: ALP production in proton beam dump experiments. *J High Energy Phys.* (2016) 02:018. doi: 10.1007/JHEP02(2016)018
26. Yamazaki T, Ishikawa T, Taniguchi T, Yamanaka T, Tanimori T, Enomoto R, et al. Search for a neutral boson in a two-body decay of K+ —> PI+ X0. *Phys Rev Lett.* (1984) 52:1089–91.
27. Adler S, Aoki M, Ardebili M, Atiya MS, Bazarko AO, Bergbusch PC. Further search for the decay K+ —> $\pi^+ \nu\bar{\nu}$ anti-nu in the momentum region $P <$ 195-MeV/c. *Phys Rev.* (2004) **D70**:037102. doi: 10.1103/PhysRevD.70.037102
28. Artamonov AV, Bassalleck B, Bhuyan B, Blackmore EW, Bryman DA, Chen S. Study of the decay $K^+ \to \pi^+ \nu\bar{\nu}$ in the momentum region $140 < P_\pi < 199$ MeV/c. *Phys Rev.* (2009) **D79**:092004. doi: 10.1103/PhysRevD.79.092004
29. Aaij R, Adeva B,Adinolfi M, Ajaltouni Z, Akar S, Albrecht J, et al. Measurement of the $B_s^0 \to \mu^+\mu^-$ branching fraction and search for $B^0 \to \mu^+\mu^-$ decays at the LHCb experiment. *Phys Rev Lett.* (2013) **111**:101805. doi: 10.1103/PhysRevLett.111.101805
30. Chatrchyan S, Khachatryan V, Sirunyan AM, Tumasyan A, Adam W, Bergauer T. Measurement of the $B_s^0 \to \mu^+\mu^-$ Branching Fraction and Search for $B^0 \to \mu^+\mu^-$ with the CMS Experiment. *Phys Rev Lett.* (2013) **111**:101804. doi: 10.1103/PhysRevLett.111.101804
31. Khachatryan V, Sirunyan AM, Tumasyan A, Adam W, Bergauer T, Dragicevic M, et al. Observation of the rare $B_s^0 \to \mu^+\mu^-$ decay from the combined analysis of CMS and LHCb data. *Nature.* (2015) **522**:68–72. doi: 10.1038/nature14474
32. Ammar R, Bean A, Besson D, Zhao X, Anderson S, Frolov VV, et al. Search for the familon via B+- —> pi+- X0, B+- —> K+- X0, and B0 —> K0(S)X0 decays. *Phys Rev Lett.* (2001) **87**:271801. doi: 10.1103/PhysRevLett.87.271801
33. Balest R, , Cho K, Ford T, Johnson DR, Lingel K, Lohner M, et al. Upsilon (1s) —> gamma + noninteracting particles. *Phys Rev.* (1995) **D51**:2053–60.
34. Aubert B, Bona M, Karyotakis Y, Lees JP, Poireau V, Prencipe E. Search for Invisible Decays of a Light Scalar in Radiative Transitions $\upsilon_{3S} \to \gamma$ A0. In: *Proceedings, 34th International Conference on High Energy Physics (ICHEP 2008)*. Philadelphia, PA (2008). Available online at: http://www-public.slac.stanford.edu/sciDoc/docMeta.aspx?slacPubNumber=slac-pub-13328.
35. Davier M, Nguyen Ngoc H. An unambiguous search for a light higgs boson. *Phys Lett.* (1989) **B229**:150–5.
36. Banerjee D, Burtsev VE, Chumakov AG, Cooke D, Crivelli P, Depero E, et al. Search for a hypothetical 16.7 MeV gauge Boson and dark photons in the NA64 experiment at CERN. *Phys Rev Lett.* (2018) **120**:231802. doi: 10.1103/PhysRevLett.120.231802
37. Bergsma F, Dorenbosch J, Allaby JV, Amaldi U, Barbiellini G, Berger C. Search for axion like particle production in 400-GeV proton - copper interactions. *Phys Lett.* (1985) **157B**:458–62. doi: 10.1016/0370-2693(85)90400-9
38. Moretti S. Variations on a Higgs theme. *Phys Rev.* (2015) **D91**:014012. doi: 10.1103/PhysRevD.91.014012
39. Anthony PL, Arnold RG, Arroyo C, Bega K, Biesiada J, Bosted PE, et al. Precision measurement of the weak mixing angle in Moller scattering. *Phys Rev Lett.* (2005) **95**:081601. doi: 10.1103/PhysRevLett.95.081601
40. Giudice GF, Paradisi P, Passera M. Testing new physics with the electron g-2. *J High Energy Phys.* (2012) **11**:113. doi: 10.1007/JHEP11(2012)113
41. Altmannshofer W, Chen CY, Bhupal Dev PS, Soni A. Lepton flavor violating Z' explanation of the muon anomalous magnetic moment. *Phys Lett.* (2016) **B762**:389–98. doi: 10.1016/j.physletb.2016.09.046
42. Bennett GW, Bousquet B, Brown HN, Bunce G, Carey RM, Cushman P. Final report of the muon E821 anomalous magnetic moment measurement at BNL. *Phys Rev.* (2006) **D73**:072003. doi: 10.1103/PhysRevD.73.072003
43. Blum T, Denig A, Logashenko I, de Rafael E, Roberts BL, Teubner T, et al. The Muon (g-2) theory value: present and future. *arXiv:1311.2198.* (2013).
44. Lindner M, Platscher M, Queiroz FS. A call for new physics : the Muon anomalous magnetic moment and lepton flavor violation. *Phys Rept.* (2018) **731**:1–82. doi: 10.1016/j.physrep.2017.12.001
45. Deniz M, Lin ST, Singh V, Li J, Wong HT, Bilmis S. Measurement of $\bar{\nu}_e$-electron scattering cross-section with a CsI(Tl) scintillating crystal array at the Kuo-Sheng nuclear power reactor. *Phys Rev.* (2010) D81:072001. doi: 10.1103/PhysRevD.81.072001
46. Bilmis S, Turan I, Aliev TM, Deniz M, Singh L, Wong HT. Constraints on dark photon from neutrino-electron scattering experiments. *Phys Rev.* (2015) **D92**:033009. doi: 10.1103/PhysRevD.92.033009
47. Raggi M. NA48/2 studies of rare decays. *Nuovo Cim.* (2016) **C38**:132. doi: 10.1393/ncc/i2015-15132-0
48. Davoudiasl H, Lee HS, Marciano WJ. 'Dark' Z implications for parity violation, rare meson decays, and higgs physics. *Phys Rev.* (2012) **D85**:115019. doi: 10.1103/PhysRevD.85.115019
49. Bouchiat C, Fayet P. Constraints on the parity-violating couplings of a new gauge boson. *Phys Lett.* (2005) **B608**:87–94. doi: 10.1016/j.physletb.2004.12.065
50. Porsev SG, Beloy K, Derevianko A. Precision determination of electroweak coupling from atomic parity violation and implications for particle physics. *Phys Rev Lett.* (2009) **102**:181601. doi: 10.1103/PhysRevLett.102.181601
51. Fayet P. On the search for a new Spin 1 Boson. *Nucl Phys.* (1981) **B187**:184–204.
52. Fayet P. Effects of the Spin 1 partner of the Goldstino (Gravitino) on neutral current phenomenology. *Phys Lett.* (1980) **95B**:285–9.
53. Fayet P. Extra U(1)'s and new forces. *Nucl Phys.* (1990) **B347**:743–68.
54. Fayet P. U-boson production in e+ e- annihilations, psi and Upsilon decays, and Light Dark Matter. *Phys Rev.* (2007) **D75**:115017. doi: 10.1103/PhysRevD.75.115017
55. Fayet P. U(1)(A) Symmetry in two-doublet models, U bosons or light pseudoscalars, and psi and Upsilon decays. *Phys Lett.* (2009) **B675**:267–71. doi: 10.1016/j.physletb.2009.03.078
56. Fayet P. The light U boson as the mediator of a new force, coupled to a combination of Q, B, L and dark matter. *Eur Phys J.* (2017) **C77**:53. doi: 10.1140/epjc/s10052-016-4568-9
57. Delle Rose L, Khalil S, Moretti S. Explanation of the 17 MeV Atomki anomaly in a U(1)' -extended two Higgs doublet model. *Phys Rev.* (2017) **D96**:115024. doi: 10.1103/PhysRevD.96.115024
58. Accomando E, Coriano C, Delle Rose L, Fiaschi J, Marzo C, Moretti S. Z', Higgses and heavy neutrinos in U(1)' models: from the LHC to the GUT scale. *J High Energy Phys.* (2016) **07**:086. doi: 10.1007/JHEP07(2016)086
59. Bishara F, Brod J, Grinstein B, Zupan J. Chiral effective theory of dark matter direct detection. *JCAP.* (2017) **1702**:009. doi: 10.1088/1475-7516/2017/02/009
60. Vilain P, Wilquet G, Beyer R,Flegel W, Grote H,Mouthuy T, et al. Precision measurement of electroweak parameters from the scattering

of muon-neutrinos on electrons. *Phys Lett*. (1994) **B335**:246–52. doi: 10.1016/0370-2693(94)91421-4.
61. Bellini G, Benziger J, Bick D, Bonetti S, Bonfini G, Buizza Avanzini M. Precision measurement of the ^{7}Be solar neutrino interaction rate in Borexino. *Phys Rev Lett*. (2011) **107**:141302. doi: 10.1103/PhysRevLett.107.141302
62. Davoudiasl H, Lee HS, Marciano WJ. Muon $g-2$, rare kaon decays, and parity violation from dark bosons. *Phys Rev*. (2014) **D89**:095006. doi: 10.1103/PhysRevD.89.095006
63. Patrignani C, Agashe K, Aielli G, Amsler C, Antonelli M, Asner DM. Review of particle physics. *Chin Phys*. (2016) **C40**:100001. doi: 10.1088/1674-1137/40/10/100001
64. Delle Rose L, Khalil S, King SJD, Moretti S, Thabt AM. Atomki anomaly in family-dependent $U(1)'$ extension of the standard model. *Phys Rev*. (2019) **D99**:055022. doi: 10.1103/PhysRevD.99.055022
65. Froggatt CD, Nielsen HB. Hierarchy of Quark Masses, Cabibbo Angles and CP Violation. *Nucl Phys*. (1979) **B147**:277–98. doi: 10.1016/0550-3213(79)90316-X
66. Demir DA, Kane GL, Wang TT. The Minimal U(1)' extension of the MSSM. *Phys Rev*. (2005) **D72**:015012. doi: 10.1103/PhysRevD.72.015012
67. Khan AN. Global analysis of the source and detector nonstandard interactions using the short baseline $\nu-e$ and $\bar{\nu}-e$ scattering data. *Phys Rev*. (2016) **D93**:093019. doi: 10.1103/PhysRevD.93.093019
68. Aaij R, et al. Angular analysis of the $B^0 \to K^{*0}e^+e^-$ decay in the low-q^2 region. *J High Energy Phys*. (2015) **04**:064. doi: 10.1007/JHEP04(2015)064
69. Bečirevíá D, Sumensari O, Zukanovich Funchal R. Lepton flavor violation in exclusive $b \to s$ decays. *Eur Phys J*. (2016) **C76**:134. doi: 10.1140/epjc/s10052-016-3985-0

Conflict of Interest Statement: The authors declare that the research was conducted in the absence of any commercial or financial relationships that could be construed as a potential conflict of interest.

frontiers in Physics

ORIGINAL RESEARCH
published: 31 May 2019
doi: 10.3389/fphy.2019.00080

Mini Review on Vector-Like Leptonic Dark Matter, Neutrino Mass, and Collider Signatures

Subhaditya Bhattacharya[1], *Purusottam Ghosh*[1], *Nirakar Sahoo*[2,3] *and Narendra Sahu*[4]*

[1] Department of Physics, Indian Institute of Technology Guwahati, North Guwahati, India, [2] Institute of Physics, Bhubaneswar, India, [3] Homi Bhabha National Institute, Training School Complex, Mumbai, India, [4] Department of Physics, Indian Institute of Technology, Hyderabad, India

We review a class of models in which the Standard Model (SM) is augmented by vector-like leptons: one doublet and a singlet, which are odd under an unbroken discrete Z_2 symmetry. As a result, the neutral component of these additional vector-like leptons are stable and behave as dark matter. We study the phenomenological constraints on the model parameters and elucidate the parameter space for relic density, direct detection and collider signatures of dark matter. In such models, we further add a scalar triplet of hypercharge two and study the consequences. In particular, after electro weak symmetry breaking (EWSB), the triplet scalar gets an induced vacuum expectation value (vev), which yield Majorana masses not only to the light neutrinos but also to vector-like leptonic doublet DM. Due to the Majorana mass of DM, the Z mediated elastic scattering with nucleon is forbidden and hence allowing the model to survive from stringent direct search bound. The DM without scalar triplet lives in a small singlet-doublet leptonic mixing region ($\sin\theta \leq 0.1$) due to large contribution from singlet component and have small mass difference ($\Delta m \sim 10$ GeV) with charged companion, the NLSP (next to lightest stable particle), to aid co-annihilation for yielding correct relic density. Both these observations change to certain extent in presence of scalar triplet to aid observability of hadronically quiet leptonic final states at LHC, while one may also confirm/rule-out the model through displaced vertex signal of NLSP, a characteristic signature of the model in relic density and direct search allowed parameter space.

Keywords: physics beyond the SM, neutrino mass, dark matter, collider signature, dark matter direct detection

OPEN ACCESS

Edited by:
Roman Pasechnik, Faculty of Science, Lund University, Sweden

Reviewed by:
Oscar Zapata, University of Antioquia, Colombia
Chandan Hati, UMR6533 Laboratoire de Physique de Clermont (LPC), France

***Correspondence:**
Narendra Sahu
nsahu@iith.ac.in

Specialty section:
This article was submitted to High-Energy and Astroparticle Physics, a section of the journal Frontiers in Physics

Received: *22 January 2019*
Accepted: *06 May 2019*
Published: *31 May 2019*

Citation:
Bhattacharya S, Ghosh P, Sahoo N and Sahu N (2019) Mini Review on Vector-Like Leptonic Dark Matter, Neutrino Mass, and Collider Signatures. Front. Phys. 7:80. doi: 10.3389/fphy.2019.00080

1. INTRODUCTION

The existence of dark matter (DM) in a large scale (> a few kpc) has been proven irrefutably by various astrophysical observations. The prime among them are galaxy rotation curves [1, 2], gravitational lensing [3], and large scale structure of the Universe. See for a review [4, 5]. In the recent years the satellite borne experiments like Wilkinson Microwave Anisotropy Probe (WMAP) [6] and PLANCK [7, 8] precisely determined the relic abundance of DM by measuring the temperature fluctuation in the cosmic microwave background radiation (CMBR). All the above said evidences of DM emerge via gravitational interaction in astrophysical environments, which make a challenge to probe the existence of DM in a terrestrial laboratory where density of DM is feeble.

Alternatively one can explore other elementary properties of DM which can be probed at an earth based laboratory. In fact, one can assign a weak interaction property to DM through which it can be thermalized in the early Universe at a temperature above its mass scale. As the temperature falls due to adiabatic expansion of the Universe, the DM gets decoupled from the thermal bath below its mass scale. As a result the ratio: $n_{\rm DM}/s$, where s is the entropy density, remains constant and is precisely measured by PLANCK in terms of $\Omega_{\rm DM}h^2 = 0.1186 \pm 0.0020$ [7, 8].

The particle nature of DM, apart from relic abundance, is completely unknown. In particular, the mass, spin, and interaction apart from gravity, etc. This leads to huge uncertainty in search of DM. Despite this, many experiments are currently operational, that uses direct, indirect and collider search methods. Xenon-100 [9], LUX [10], Xenon-1T [11, 12], PANDA [13] are some of the direct DM search experiments which are looking for signature of DM via nuclear scattering, while PAMELA [14, 15], AMS-2 [16], Fermi gamma ray space telescope [17], IceCube [18, 19], etc., are some of the indirect DM search experiments which are looking for signature of DM in the sky. The search of DM is also going on at collider experiments like large Hadron Collider (LHC) [20–22]. Except some excess in the antiparticle flux in the indirect search data, direct and collider searches for DM has produced null observation so far. This in turn put a strong bound on the DM mass and coupling with which it can interact to the visible sector of the universe.

After the Higgs discovery in 2012 at CERN LHC, the standard model (SM) seems to be complete. However, it is found that none of the particles in SM can be a candidate of DM, which is required to be stable on cosmological time scale. While neutrinos in SM are stable, but their relic density is far less than the required DM abundance and is also disfavored from the structure formation. Moreover, neutrinos are massless within the SM. A tiny but non-zero neutrino mass generation requires the SM to be extended. This opens up the possibility of exploring new models of DM, while explaining non-zero masses for neutrinos in the same framework and thus predict a measurable alternation to DM phenomenology, which can be examined in some of the above said experiments.

In this review we explore the possibility of leptonic DM and non-zero neutrino masses [23] in a framework beyond the SM. The simplest leptonic DM can arise by augmenting the SM with an additional singlet fermion [24–42] χ, stabilized by a $\mathcal{Z}_2$ symmetry. However, unless we assume the presence of an additional scalar singlet, which acquires vacuum expectation value (vev) and thus mixes with SM Higgs, the lepton singlet DM cannot possess renormalizable interaction with visible sector. The next possibility is to introduce a vector-like leptonic doublet: $N = (N^0 \;\; N^-)^T$, which is also odd under the $\mathcal{Z}_2$ symmetry. The annihilation cross-section of such fermions are large due to Z mediation and correct relic density can only be achieved at a very high DM mass. However, the combination of singlet χ with the doublet vector-like lepton N provides a good candidate of DM [43–52], which has been discussed in details here. We discuss the phenomenological constraints on model parameters and then elucidate the allowed parameter space of such models from relic density and direct detection constraints. We also indicate collider search strategies for such DM. It turns out that the displaced vertex of the charged fermion: $N^\pm$ [also called next to lightest stable particle (NLSP)] is a natural signature of such DM model.

In an attempt to address neutrino mass generation in the same framework, we further add a scalar triplet Δ of hypercharge 2 and study the consequences [53]. In particular, after electro weak symmetry breaking (EWSB), the triplet scalar acquires an induced vacuum expectation value (vev) which give rise sub-eV Majorana masses to light neutrinos through the Type II Seesaw mechanism [54–60]. The scalar triplet also generates a Majorana mass for the neutral component of the vector-like lepton doublet: N^0, which constitutes a minor component of the DM. Due to Majorana mass of DM, the Z mediated elastic scattering with nucleon is forbidden [61–65]. As a result, the model survives from the stringent direct search bound. In absence of scalar triplet, the singlet-doublet DM is allowed to have only a tiny fraction of doublet component ($\sin\theta \leq 0.1$) to evade direct search bound. In this limit, due to large contribution from the singlet component, the annihilation cross section of the DM becomes smaller than what it requires to achieve correct relic density. To make it up for correct relic density, the DM additionally requires to co-annihilate with its charged and heavy neutral companions and therefore requires small mass difference ($\Delta m \sim 10$ GeV) with charged companion or NLSP. However, in presence of the scalar triplet, we show that both the singlet-doublet mixing ($\sin\theta$) and the mass difference with NLSP (Δm) can be relaxed and larger parameter space is available for correct relic density and being compatible with the latest direct detection bounds. Moreover, the scalar triplet aid observability of hadronically quiet leptonic final states at LHC while one may also confirm/rule-out the model through displaced vertex of NLSP, a characteristic signature of the model in relic density and direct search allowed parameter space.

The paper is arranged as follows. In section 2, we briefly discuss about a vector-like singlet leptonic DM. In section 3, we discuss the viable parameter space of a vector-like inert doublet lepton DM. It is shown that an inert lepton doublet DM alone is ruled out due to large Z-mediated elastic scattering with the nucleus. However, in presence of a scalar triplet of hyper charge-2, the inert lepton doublet DM can be reinstated in a limited parameter space, which we discuss in section 4. Moreover in section 4, we discuss how the scalar triplet can give rise non-zero masses to active neutrinos via type-II seesaw [54–60]. In section 5 we discuss how an appropriate combination of singlet and doublet vector like leptons can give rise a nice possibility of DM in a wide range of parameter space. A triplet extension of singlet-doublet leptonic DM is further discussed in section 6. We discuss collider signature of singlet-doublet leptonic DM in presence of a scalar triplet in section 7 and conclude in section 8. We provide some vertices of inert lepton doublet (ILD) DM in presence of scalar triplet in **Appendix A**.

2. VECTOR-LIKE LEPTONIC SINGLET DARK MATTER

A simplest possibility to explain DM content of the present Universe is to augment the SM by adding a vector-like singlet lepton χ. The stability of χ can be ensured by imposing an

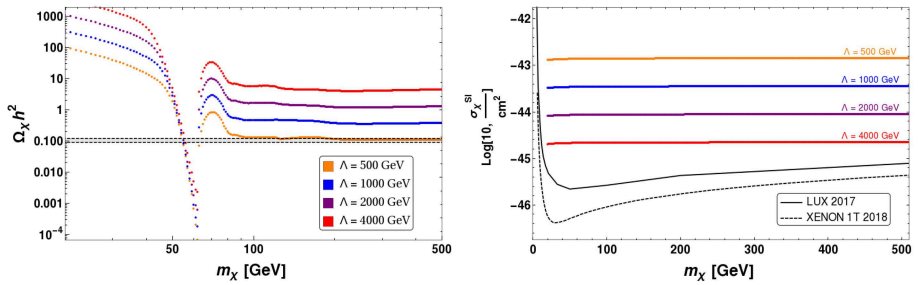

FIGURE 1 | (Left) Relic density as a function of singlet DM mass, m_χ for different values of Λ mentioned in the figure inset. **(Right)** SI DD cross-section vs. DM mass, m_χ for different values of Λ.

additional discrete Z_2 symmetry, under which χ is odd while all other particles are even. In fact, a singlet DM has been discussed extensively in the literature [24–42]. Here we briefly recapitulate the main features to show the allowed parameter space by observed relic density and latest constraint from direct detection experiments.

The Lagrangian describing the singlet leptonic DM χ can be given as:

$$\mathcal{L} = \overline{\chi}\,(i\gamma^\mu\partial_\mu - m_\chi)\,\chi - \frac{1}{\Lambda}\Big(H^\dagger H - \frac{v^2}{2}\Big)\overline{\chi}\,\chi. \qquad (1)$$

Notice that the Lagrangian introduces two new parameters: DM mass, m_χ and the new physics scale Λ connecting DM to the SM through effective dimension five operator, on which the DM phenomenology depends. In the early Universe, χ freezes out via the interaction $\overline{\chi}\chi \rightarrow$ SM particles to give rise a net relic density that we observe today. We use **micrOmegas** [66] to calculate the relic density as well as spin independent elastic cross-section with nucleon of χ. In **Figure 1**, we show relic abundance (left-panel) and spin independent direct detection (SIDD) cross section (right panel) as a function of DM mass (m_χ) for different values $\Lambda \sim \{500 - 4000\}$ GeV [1]. We observe that the constraint on SIDD cross section favors large values of Λ, while large Λ values yield over abundance of DM. We also note in the right panel **Figure 1**, that the SIDD cross section is very less sensitive to DM mass. This is because the direct search cross-section is proportional to the effective DM-nucleon reduced mass square ($\mu_r = \frac{m_N m_\chi}{m_N + m_\chi}$) (see Equations 58, 59), where $m_N < m_\chi$ yields a mild dependence on DM mass. This feature is observed in rest of the analysis as well.

Therefore, a singlet leptonic DM alone is almost ruled out. However, the dark sector of the Universe may not be simple as in the case of singlet leptonic DM. In the following we discuss a few more models with larger number of parameters, yet predictive. We end this section by noting that one can think of a pseudoscalar propagator to yield an effective DM-SM interaction of the form $(\bar{\chi}\gamma_5\chi)(H^\dagger H)/\Lambda$. In this case, the relic density and direct search cross-sections become velocity dependent (see for example in Ghorbani [67]). Please also see section 5 below Equation (35) for more details.

[1]The scale Λ is a priori unknown and should be validated from experimental constraints. In effective theory consideration, we ensure that $m_\chi < \Lambda$.

3. INERT LEPTON DOUBLET DARK MATTER

Let us assume that the dark sector is composed of a vector-like lepton doublet: $N = (N^0\ N^-)^T$, which is odd under an extended $\mathcal{Z}_2$ symmetry [hence called inert lepton doublet (ILD)], while all the Standard Model (SM) fields are even. As a result the neutral component of the ILD N is stable. The quantum numbers of dark sector fields and that of SM Higgs under the SM gauge group, augmented by a $\mathcal{Z}_2$ symmetry, are given in **Table 1**. We will check if N^0 can be a viable candidate of DM with correct relic abundance while satisfying the direct detection constraints from the null observation at various terrestrial laboratories.

The Lagrangian of the model is given as:

$$\mathcal{L}^{IL} = \overline{N}\,[i\gamma^\mu(\partial_\mu - ig\frac{\sigma^a}{2}W_\mu^a - ig'\frac{Y}{2}B_\mu) - m_N]\,N. \qquad (2)$$

Thus the only new parameter introduced in the above Lagrangian is the mass of N, i.e., m_N. Expanding the covariant derivative of the above Lagrangian $\mathcal{L}^{IL}$, we get the interaction terms of N^0 and $N^\pm$ with the SM gauge bosons as:

$$\begin{aligned}\mathcal{L}_{int}^{IL} &= \overline{N}i\gamma^\mu(-ig\frac{\sigma^a}{2}W_\mu^a + i\frac{g'}{2}B_\mu)N \\ &= \Big(\frac{e_0}{2\sin\theta_W\cos\theta_W}\Big)\overline{N^0}\gamma^\mu Z_\mu N^0 + \frac{e_0}{\sqrt{2}\sin\theta_W}\overline{N^0}\gamma^\mu W_\mu^+ N^- \\ &\quad + \frac{e_0}{\sqrt{2}\sin\theta_W}N^+\gamma^\mu W_\mu^- N^0 - e_0 N^+\gamma^\mu A_\mu N^- \\ &\quad - \Big(\frac{e_0}{2\sin\theta_W\cos\theta_W}\Big)\cos 2\theta_W N^+\gamma^\mu Z_\mu N^-. \qquad (3)\end{aligned}$$

where $g = e_0/\sin\theta_W$ and $g' = e_0/\cos\theta_W$ with e_0 being the electromagnetic coupling constant and θ_W being the Weinberg angle.

Since N is a doublet under $SU(2)_L$, it can contribute to invisible Z-decay width if its mass is <45 GeV which is strongly constrained. Therefore, in our analysis we will assume $m_N >$ 45 GeV.

3.1. Relic Abundance of ILD Dark Matter

The number changing annihilation and co-annihilation processes which control freeze-out and hence relic density of DM N^0 are shown in **Figures 2–4**.

To estimate the relic density of DM in this framework one needs to solve the relevant Boltzmann equation:

$$\frac{dn_{N^0}}{dt} + 3Hn_{N^0} = -\langle\sigma v\rangle_{N^0\overline{N^0}\to SMSM}\left(n_{N^0}^2 - n_{N^0}^{eq\,2}\right) - \langle\sigma v\rangle_{N^0N^\pm\to SMSM}\left(n_{N^0}n_{N^\pm} - n_{N^0}^{eq}n_{N^\pm}^{eq}\right). \quad (4)$$

TABLE 1 | Quantum numbers of additional dark sector fermion and SM Higgs under $\mathcal{G} \equiv SU(3)_C \times SU(2)_L \times U(1)_Y \times \mathcal{Z}_2$.

Fields	$SU(3)_C$	×	$SU(2)_L$	×	$U(1)_Y$	×	$\mathcal{Z}_2$
$N = \begin{pmatrix} N^0 \\ N^- \end{pmatrix}$	1		2		−1		−
$H = \begin{pmatrix} H^+ \\ H^0 \end{pmatrix}$	1		2		1		+

To find the relic density of ILD DM, here we adopted **micrOmegas** [66] and implemented the model in it. Notice that the relic density of DM is mainly controlled by DM mass, m_N and SM gauged couplings. Since SM gauge couplings are fixed, the only relevant parameter which controls the relic density is the DM mass, m_N. The behavior of relic density with DM mass shown in **Figure 5** along with correct relic density bound which is shown in gray patch. Note here that a sharp drop around DM mass $m_N \sim m_h/2$ due to Higgs resonance. From **Figure 5** we can see that the DM mass around $m_N \sim 1$ TeV only satisfy current relic density bound. For heavier mass of N^0 we get over abundance of DM (due to small cross section), while for lighter mass of N^0 we get under abundance of DM (due to large cross-section).

3.2. Direct Search Constraint on ILD Dark Matter

In a direct detection experiment, the DM N^0 scatters with the nucleon through t-channel Z mediated diagram, as shown

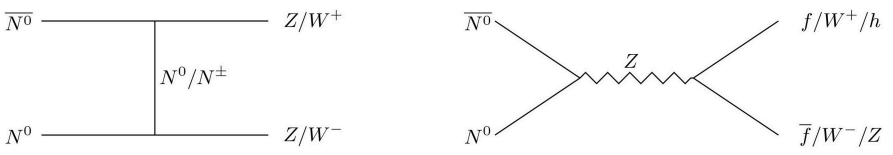

FIGURE 2 | Annihilation of ILD DM to SM particles.

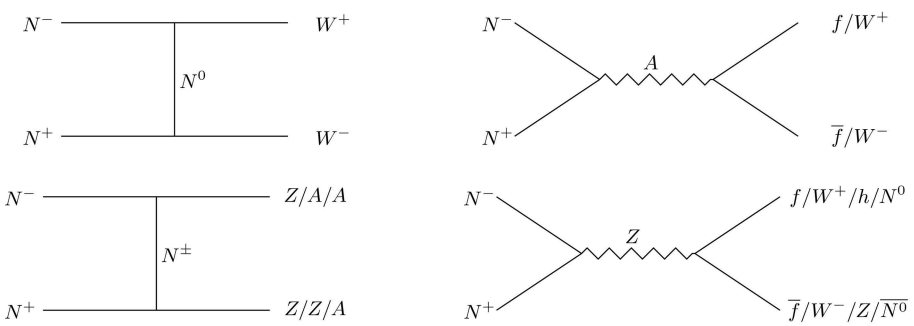

FIGURE 3 | Annihilation of charged partner of ILD DM to SM particles which contributes as co-annihilation with ILD DM.

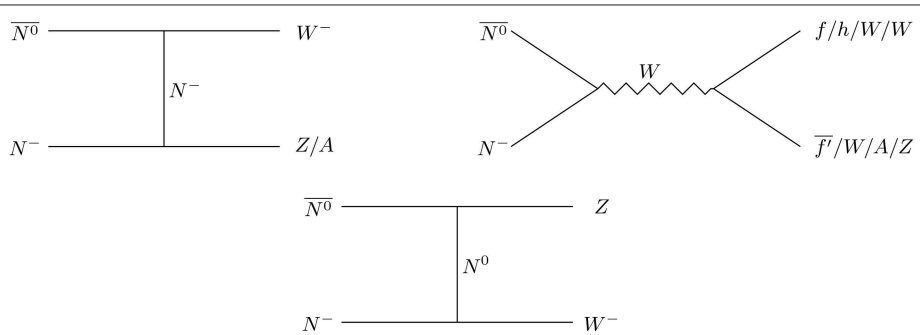

FIGURE 4 | Co-annihilation processes of DM N^0 with its charged partner $N^\pm$ to SM particles.

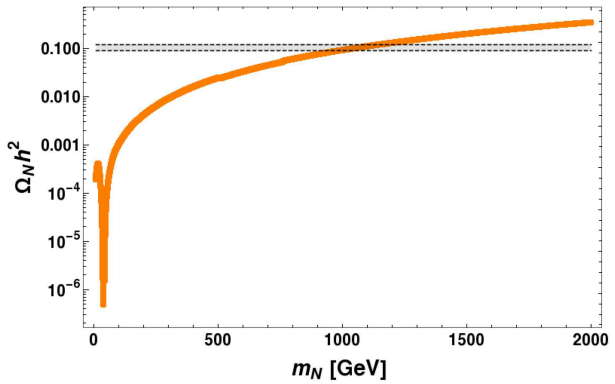

FIGURE 5 | Variation of relic density of DM N^0 with mass m_N. The gray patch corresponds to relic density allowed limit from PLANCK: $0.1166 \leq \Omega h^2 \leq 0.1206$.

schematically in the left panel of **Figure 6**. Like relic density we obtain the DM-nucleon cross-section using **micrOmegas** [66]. Since $\overline{N^0}N^0Z$ interaction is coming from SM gauge coupling and which is large, so the outcome of spin independent direct detection (SIDD) cross section becomes large. The SIDD cross-section in this case is plotted with DM mass, m_N, which is shown in orange colored patch in right panel of **Figure 6**. The green patch in this **Figure 6** indicates relic density allowed mass range in the same plane. LUX 2017 [10] and XENON 1T [11, 12] direct detection limits are also plotted in the same figure (right panel of **Figure 6**). Thus we see that an ILD DM is completely ruled out by direct detection bound. However, as we discuss in section 4 the ILD DM can be resurrected in presence of a scalar triplet of hyper charge 2. Moreover, the scalar triplet will generate sub-eV masses of active neutrinos through type-II seesaw.

4. TRIPLET EXTENSION OF THE ILD DARK MATTER

We now extend the ILD dark matter model with a scalar triplet, Δ ($Y_\Delta = 2$) which is even under the discrete $\mathcal{Z}_2$ symmetry. The Lagrangian of this extended sector is given as:

$$\mathcal{L}^{II} = \mathrm{Tr}[(D_\mu \Delta)^\dagger (D^\mu \Delta)] - V(H, \Delta) + \mathcal{L}^{II}_{\mathrm{Yuk}}, \tag{5}$$

where the covariant derivative is defined as

$$D_\mu \Delta = \partial_\mu \Delta - ig\Big[\frac{\sigma^a}{2} W^a_\mu, \Delta\Big] - ig' \frac{Y_\Delta}{2} B_\mu \Delta$$

and in the adjoint representation the triplet Δ can be expressed in a 2×2 matrix form: $\Delta = \begin{pmatrix} \frac{H^+}{\sqrt{2}} & H^{++} \\ \delta^0 & -\frac{H^+}{\sqrt{2}} \end{pmatrix}$.

Similarly the scalar doublet H can be written in component form as:

$$H = \begin{pmatrix} \phi^+ \\ \phi^0 \end{pmatrix}. \tag{6}$$

The modified scalar potential including Δ and H can be given as:

$$\begin{aligned} V(H, \Delta) \;=\; & -\mu_H^2 (H^\dagger H) + \frac{\lambda_H}{4} \big(H^\dagger H\big)^2 + M_\Delta^2 \,\mathrm{Tr}[\Delta^\dagger \Delta] \\ & + \lambda_1 (H^\dagger H) \mathrm{Tr}[\Delta^\dagger \Delta] + \lambda_2 \big(\mathrm{Tr}[\Delta^\dagger \Delta]\big)^2 \\ & + \lambda_3 \mathrm{Tr}[(\Delta^\dagger \Delta)^2] + \lambda_4 H^\dagger \Delta \Delta^\dagger H \\ & + \big[\mu \big(H^T i\sigma^2 \Delta^\dagger H\big) + \mathrm{h.c.}\big], \end{aligned} \tag{7}$$

where we assume that M_Δ^2 is positive. So the scalar triplet Δ does not acquire any vev. However, it acquires an induced vev after EW phase transition. The vevs of the scalar fields are given by:

$$\langle \Delta \rangle = \begin{pmatrix} 0 & 0 \\ v_t/\sqrt{2} & 0 \end{pmatrix} \quad \text{and} \quad \langle H \rangle = \begin{pmatrix} 0 \\ v/\sqrt{2} \end{pmatrix}. \tag{8}$$

Since the addition of a scalar triplet can modify the ρ parameter, whose observed value: $\rho = 1.00037 \pm 0.00023$ [68], does not differ much from SM prediction: $\rho = 1$, so we have a constraint on the vev v_t as:

$$v_t \leq 3.64\mathrm{GeV}\,. \tag{9}$$

On the other hand electroweak symmetry breaking gives $\sqrt{v^2 + 2v_t^2} = 246\mathrm{GeV}$. This implies that $v_t << v$.

Now minimizing the scalar potential, $V(H, \Delta)$ (in Equation 7) we get:

$$\begin{aligned} M_\Delta^2 \;&=\; \frac{2\mu v^2 - \sqrt{2}(\lambda_1 + \lambda_4) v^2 v_t - 2\sqrt{2}(\lambda_2 + \lambda_3) v_t^3}{2\sqrt{2} v_t}, \\ \mu_H^2 \;&=\; \frac{\lambda_H v^2}{4} + \frac{(\lambda_1 + \lambda_4) v_t^2}{2} - \sqrt{2}\mu v_t\,. \end{aligned} \tag{10}$$

In the limit $v_t << v$, from Equation (10) we get the vevs,

$$v_t = \frac{\mu v^2}{M_\Delta^2 + (\lambda_1 + \lambda_4) v^2/2} \quad \text{and} \quad v \approx \frac{2\mu_H}{\sqrt{\lambda_H}}. \tag{11}$$

In presence of the scalar triplet Δ, the Yukawa interactions in Equation (5) are given by:

$$\mathcal{L}^{II}_{Yuk} = \frac{1}{\sqrt{2}} \big[(f_L)_{\alpha\beta} \overline{L^c_\alpha} i\sigma^2 \Delta L_\beta + f_N \overline{N^c} i\sigma^2 \Delta N + h.c.\big], \tag{12}$$

where L is the SM lepton doublet and α, β denote family indices. The Yukawa interactions importantly inherit the source of neutrino masses (first term in square bracket) and DM-SM interactions (second term in square bracket).

4.1. Scalar Doublet-Triplet Mixing

The quantum fluctuations around the minimum of scalar potential, $V(H, \Delta)$ can be given as:

$$\Delta = \begin{pmatrix} \frac{H^+}{\sqrt{2}} & H^{++} \\ \frac{v_t + h_t + iA^0}{\sqrt{2}} & -\frac{H^+}{\sqrt{2}} \end{pmatrix} \quad \text{and} \quad H = \begin{pmatrix} 0 \\ \frac{v+h}{\sqrt{2}} \end{pmatrix}. \tag{13}$$

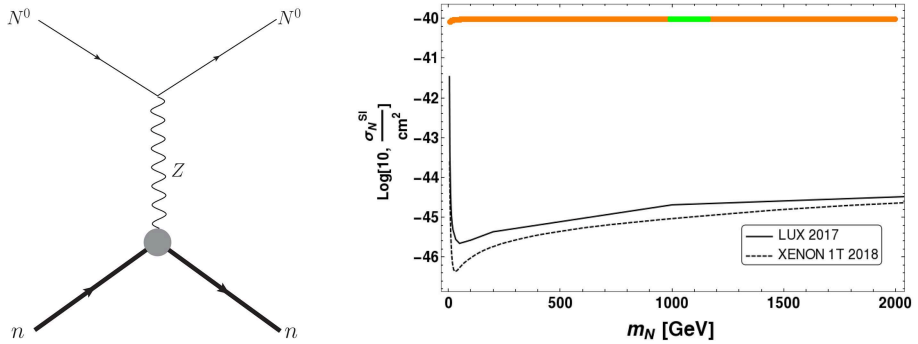

FIGURE 6 | Left: Feynman diagram for direct detection (DD) of DM, N^0. **Right**: Spin independent(SI) DM-nucleon cross-section is plotted in $m_N - \sigma_N^{SI}$ plane. Relic density allowed DM mass region is indicated here by green patch.

Thus the scalar sector constitute two CP-even Higgses: h and h_t, one CP-odd Higgs: A^0, one singly charged scalar: $H^{\pm}$ and one doubly charged scalar: $H^{\pm\pm}$. In the limit $v_t << v$, the mass matrix of the CP-even Higgses: h and h_t, is given by:

$$\mathcal{M}^2 = \begin{pmatrix} m_h^2 & -\sqrt{2}\mu v \\ -\sqrt{2}\mu v & m_T^2 \end{pmatrix}, \tag{14}$$

where $m_h^2 \approx \lambda_H v^2/2$ and $m_T^2 = \mu v^2/\sqrt{2}v_t$. Diagonalizing the above mass matrix we get two neutral physical Higgses: H_1 and H_2:

$$H_1 = \cos\alpha\, h + \sin\alpha\, h_t, \quad H_2 = -\sin\alpha\, h + \cos\alpha\, h_t\,, \tag{15}$$

where H_1 is the standard model like Higgs and H_2 is the triplet like scalar. The corresponding mass eigenvalues are m_{H_1} (SM like Higgs) and m_{H_2} (triplet like scalar) are given by:

$$\begin{aligned} m_{H_1}^2 &\approx m_h^2 - \frac{(\mu v/\sqrt{2})^2}{m_T^2 - m_h^2}, \\ m_{H_2}^2 &\approx m_T^2 + \frac{(\mu v/\sqrt{2})^2}{m_T^2 - m_h^2}\,. \end{aligned} \tag{16}$$

The mixing angle is given by

$$\tan 2\alpha = \frac{-\sqrt{2}\mu v}{(m_T^2 - m_h^2)}\,. \tag{17}$$

From Equations (9, 11, 17) we see that there exist an upper bound on the mixing angle

$$\sin\alpha < 0.02 \left(\frac{174\text{ GeV}}{v}\right)\left(\frac{1}{1 - 0.39\frac{(m_h/125\text{ GeV})^2}{(m_T/200\text{ GeV})^2}}\right). \tag{18}$$

We also get a constraint on $\sin\alpha$ from SM Higgs phenomenology, since the mixing can change the strength of the Higgs coupling to different SM particles. See for example [69, 70], in which the global fit yields a constraint on mixing angle $\sin\alpha \lesssim 0.5$, which is much larger than the above constraint obtained using ρ parameter.

From Equation (7), all the couplings $\lambda_H, \lambda_1, \lambda_2, \lambda_3, \lambda_4$ and μ can be expressed in terms of physical scalar masses: m_{H_1}, m_{H_2}, $m_{H^{\pm}}$, $m_{H^{\pm\pm}}$, m_{A^0} and the vevs v and v_t as Arhrib et al. [71] :

$$\begin{aligned} \lambda_H &= \frac{2}{v^2}\left(m_{H_1}^2\cos^2\alpha + m_{H_2}^2\sin^2\alpha\right), \\ \lambda_1 &= \frac{4m_{H^{\pm}}^2}{v^2+4v_t^2} - \frac{2m_{A^0}^2}{v^2+4v_t^2} + \frac{\sin 2\alpha}{2v_t v}\left(m_{H_1}^2 - m_{H_2}^2\right), \\ \lambda_2 &= \frac{1}{v_t^2}\Big[\frac{1}{2}\left(m_{H_1}^2\sin^2\alpha + m_{H_2}^2\cos^2\alpha\right) + \frac{v^2}{2(v^2+4v_t^2)}m_{A^0}^2 \\ &\quad - \frac{2v^2}{v^2+4v_t^2}m_{H^{\pm}}^2 + m_{H^{\pm\pm}}^2\Big], \\ \lambda_3 &= \frac{1}{v_t^2}\Big[\frac{2v^2}{v^2+2v_t^2}m_{H^{\pm}}^2 - \frac{v^2}{v^2+4v_t^2}m_{A^0}^2 - m_{H^{\pm\pm}}^2\Big], \\ \lambda_4 &= \frac{4m_{A^0}^2}{v^2+4v_t^2} - \frac{4m_{H^{\pm}}^2}{v^2+2v_t^2}, \\ \mu &= \frac{\sqrt{2}v_t}{v^2+4v_t^2}m_{A^0}^2. \end{aligned} \tag{19}$$

where m_{A^0} is the mass of pseudo scalar. It is important to note that the quartic couplings λ_2 and λ_3 are inversely proportional to the triplet vev v_t which has important consequences for dark matter relic abundance that we discuss in section 4.4.

4.2. Non-zero Neutrino Masses

The coupling of scalar triplet Δ to SM lepton and Higgs doublet combinely break the lepton number by two units as given in Equation (12). As a result the $\Delta L_\alpha L_\beta$ coupling yields Majorana masses to three flavors of active neutrinos as Magg and Wetterich [54], Lazarides et al. [55], Mohapatra and Senjanovic [56], Ma and Sarkar [57], Konetschny and Kummer [58], Schechter and Valle [59], Cheng and Li [60]:

$$(M_\nu)_{\alpha\beta} = \sqrt{2}(f_L)_{\alpha\beta}\langle\Delta\rangle \approx (f_L)_{\alpha\beta}\frac{-\mu v^2}{\sqrt{2}M_\Delta^2}\,. \tag{20}$$

Assuming $\mu \simeq M_\Delta \simeq \mathcal{O}(10^{13})$ GeV, we can explain neutrino masses of order 1eV with a coupling strength $f_L \simeq 1$. However, the scale of M_Δ can be brought down to $\sim$ TeV by taking the coupling to be much smaller $f_L \simeq 10^{-11}$, and indeed represents a bit of fine tuning in the neutrino sector.

To get the neutrino mass eigen values, the above mass matrix can be diagonalized by the usual U_{PMNS} matrix as :

$$M_\nu = U_{\rm PMNS}\, M_\nu^{diag}\, U_{\rm PMNS}^T\,, \tag{21}$$

where U_{PMNS} is given by

$$U_{\rm PMNS} = \begin{pmatrix} c_{12}c_{13} & s_{12}c_{13} & s_{13}e^{-i\delta_{13}} \\ -s_{12}c_{23} - c_{12}s_{23}s_{13}e^{i\delta_{13}} & c_{12}c_{23} - s_{12}s_{23}s_{13}e^{i\delta_{13}} & s_{23}c_{13} \\ s_{12}s_{23} - c_{12}c_{23}s_{13}e^{i\delta_{13}} & -c_{12}s_{23} - s_{12}c_{23}s_{13}e^{i\delta_{13}} & c_{23}c_{13} \end{pmatrix}.U_{ph}\,, \tag{22}$$

with c_{ij}, s_{ij} stand for $\cos\theta_{ij}$ and $\sin\theta_{ij}$ respectively and U_{ph} is given by

$$U_{ph} = \text{Diag}\left(e^{-i\gamma_1}, e^{-i\gamma_2}, 1\right)\,. \tag{23}$$

Where γ_1, γ_2 are two Majorana phases. The diagonal matrix M_ν^{diag} = Diag (m_1, m_2, m_3) with diagonal entries are the mass eigen values for the neutrinos. The current neutrino oscillation data at 3σ confidence level give the constraint on mixing angles [68] :

$$0.259 < \sin^2\theta_{12} < 0.359,\ 0.374 < \sin^2\theta_{23} < 0.628,\ 0.0176 < \sin^2\theta_{13} < 0.0295\,. \tag{24}$$

However little information is available about the CP violating Dirac phase δ as well as the Majorana phases. Although the absolute mass of neutrinos is not measured yet, the mass square differences have already been measured to a good degree of accuracy :

$$\begin{aligned} \Delta m_0^2 \equiv m_2^2 - m_1^2 &= (6.99 - 8.18) \times 10^{-5}\text{eV}^2 \\ |\Delta m_{\rm atm}^2| \equiv |m_3^2 - m_1^2| &= (2.23 - 2.61) \times 10^{-3}\text{eV}^2\,. \end{aligned} \tag{25}$$

One of the main issues of neutrino physics lies in the sign of the atmospheric mass square difference $|\Delta m_{\rm atm}^2| \equiv |m_3^2 - m_1^2|$, which is still unknown. This yields two possibilities: normal hierarchy (NH) ($m_1 < m_2 < m_3$) or inverted hierarchy (IH) ($m_3 < m_1 < m_2$). Another possibility, yet allowed, is to have a degenerate (DG) neutrino mass spectrum ($m_1 \sim m_2 \sim m_3$). Assuming that the neutrinos are Majorana, the mass matrix can be written as:

$$M_\nu = \begin{pmatrix} a & b & c \\ b & d & e \\ c & e & f \end{pmatrix}. \tag{26}$$

Using equations (21), (22), (24) and (25), we can estimate the unknown parameters in neutrino mass matrix of Equation (26). To estimate the parameters in NH, we use the best fit values of the oscillation parameters. For a typical value of the lightest neutrino mass of $m_1 = 0.0001$ eV, we get the mass parameters (in eV) as :

$$a = 0.003833,\ b = 0.00759,\ c = 0.002691,$$
$$d = 0.023865,\ e = 0.02083,\ f = 0.03038. \tag{27}$$

Similarly for IH case, choosing the lightest neutrino mass $m_3 = 0.001$ eV, we get the mass parameters (in eV) as :

$$\begin{aligned} a = 0.0484,\ b = -0.00459,\ c = -0.00573, \\ d = 0.02893,\ e = -0.02366,\ f = 0.02303. \end{aligned} \tag{28}$$

In both the cases, we put the Dirac and Majorana phases to be zero for simplicity.

The analysis of neutrino mass is more indicative here than being exhaustive. This is essentially to build the connection between the dark sector and neutrino sector advocated in the model set up. One can easily perform a scan over the mass matrix parameters to obtain correct ranges of the neutrino observables, and that of course lies in the vicinity of the aforementioned values. But, we do not aim to elaborate that in this draft. We have not also adhered to a specific lepton mixing matrix pattern (say tri-bi-maximal mixing) coming from a defined underlying flavor symmetry (say A_4), which will be able to correlate different parameters of the mass matrix.

The mass of the scalar triplet can also be brought down to TeV scale by choosing appropriate Yukawa coupling as explained before. If the triplet mass is order of a few hundreds of GeV, then it can give interesting dilepton signals in the collider. See for example, [72–78] for a detailed discussion regarding the dilepton signatures of the scalar triplet at collider.

4.3. Pseudo-Dirac Nature of ILD Dark Matter

From Equation (12) we see that the vev of Δ induces a Majorana mass to N^0 which is given by:

$$m = \sqrt{2} f_N \langle\Delta\rangle \approx f_N \frac{-\mu v^2}{\sqrt{2} M_\Delta^2}\,. \tag{29}$$

Thus the N^0 has a large Dirac mass M_N (as in Equation 2) and a small Majorana mass m as shown in the above Equation (29). Therefore, we get a mass matrix in the basis $\{N_L^0, (N_R^0)^c\}$ as:

$$\mathcal{M} = \begin{pmatrix} m & M_N \\ M_N & m \end{pmatrix}. \tag{30}$$

Thus the Majorana mass m splits the Dirac spinor N^0 into two pseudo-Dirac states $N_{1,2}^0$ with mass eigenvalues $M_N \pm m$. The mass splitting between the two pseudo-Dirac states $N_{1,2}^0$ is given by

$$\delta m = 2m = 2\sqrt{2} f_N \langle\Delta\rangle\,. \tag{31}$$

Note that $\delta m << M_N$ from the estimate of induced vev of the triplet and hence does not play any role in the relic abundance calculation. However, the sub-GeV order mass splitting plays a crucial role in direct detection by forbidding the Z-boson mediated DM-nucleon elastic scattering. Now from Equations (20, 29) we see that the ratio:

$$R = \frac{(M_\nu)}{m} = \frac{f_L}{f_N} \lesssim 10^{-5}\,, \tag{32}$$

where we assume $M_\nu \sim 1$ eV and $m \sim 100$ keV. Here the mass splitting between the two states N_1^0 and N_2^0 is chosen to be $\mathcal{O}(100)$ keV in order to forbid the Z-mediated inelastic scattering with the nucleons in direct detection. Thus, we see that the ratio $R \lesssim 10^{-5}$ is heavily fine tuned. In other words, the scalar triplet strongly decay to ILD dark matter, while its decay to SM leptons is suppressed.

4.4. Effect of Scalar Triplet on Relic Abundance of ILD Dark Matter

In presence of a scalar triplet, when the DM mass is larger than the triplet mass, a few additional annihilation and co-annihilation channels open up as shown in **Figures 7–10** in addition to the previously mentioned Feynman diagrams given in **Figures 2–4**. These additional channels also play a key role in number changing processes of DM, N^0 to yield a modified freeze-out abundance. We numerically calculate relic density of N^0 DM once again by implementing the model in the code **micrOmegas** [66]. The parameter space, in comparison to the ILD dark matter alone, is enhanced due to the additional coupling of N^0 with Δ. In particular, the new parameters are: triplet scalar masses $m_{H_2}, m_{A^0}, m_{H^\pm}, m_{H^{\pm\pm}}$, vev of scalar triplet v_t, coupling of scalar triplet with ILD dark matter N^0, i.e., f_N, scalar doublet-triplet mixing $\sin\alpha$.

To understand the effect of the triplet scalar on relic density of ILD DM, we show in **Figure 11** the variation of relic density as a function of DM mass (m_N) with different choices of triplet vev (v_t) while keeping a fixed f_N and $\sin\alpha$. In the left panel of **Figure 11** we choose the scalar doublet-triplet mixing to be $\sin\alpha = 0.001$ while in the right-panel of **Figure 11** we choose $\sin\alpha = 0.1$. In both cases we set the physical CP even, CP odd and charged triplet scalar masses respectively at $m_{H_2} = 280$, $m_{A^0} = 280, m_{H^\pm} = 300$ and $m_{H^{\pm\pm}} = 310$ GeV and $f_N = 0.1$. We note that there is a resonance drop near $m_N \sim m_Z/2$ as usual for Z mediated s-channel diagrams. Additionally we find that near $m_N \sim 280$ GeV (which is the mass of H_2), relic density drops suddenly because of new annihilation processes $NN \to \Delta\Delta$ start to contribute (see diagrams in **Figures 7–10**). With larger triplet vev $v_t \sim$ GeV, the effect of annihilation to scalar triplet becomes subdued. This can be understood as follows. First of all, we see that the quartic couplings involving the triplet, as given in Equation (19), are inversely proportional to the triplet vev (v_t). In a typical annihilation process: $N^-\overline{N^{-c}} \to H^-H^-$, mediated by H^{--}, the vertex $H^{--}H^-H^-$ is proportional to $\sqrt{2}v_t\lambda_3 \sim 1/v_t$, which diminishes with larger v_t. On the other hand, let us consider the process: $N^0\overline{N^{0c}} \to H^{++}H^{--}$, which has a significant contribution to the total relic density. This process is mediated by H_1 and H_2. In small $\sin\alpha$ limit, the H_1 mediated diagram is vanishingly small as the $N^0\bar{N}^0H_1 \sim \sin\alpha$. So, H_2 mediation dominates here. However, the vertex involving $H_2H^{++}H^{--}$ is proportional to $(2\cos\alpha\lambda_2 v_t - \sin\alpha\lambda_1 v_d)$. One can see that for small v_t, the first term is negligible, while for a larger v_t, the first term becomes comparable to that of the second one and has a cancelation. This cancelation therefore decreases the annihilation cross-section to the chosen final state. Such a phenomena is also present for co-annihilation processes like $N^-\overline{N^{-c}} \to H^{--}H_2$ etc., where the vertices involve a combination of λ_1, and λ_2. On the other hand, for smaller values of triplet vev ($v_t \sim 0.01$ GeV), there is a larger drop in relic density due to the additional annihilation channels (to the triplet scalars as mentioned). Therefore, the DM N^0 achieves correct relic density for larger DM mass m_N (as compared to that of the case in absence of triplet). Moreover, we set $f_N = 0.1$ in both cases. It is straightforward to see that annihilation to the triplet final states are proportional to f_N. Therefore, with larger f_N, the drop in relic density in the vicinity of triplet scalar mass decreases even further. In summary, the presence of scalar triplet shifts the relic density of ILD DM to a higher DM mass region which crucially depends on the choice of the triplet vev as well as ΔNN coupling f_N.

An important conclusion about ILD dark matter is that the mass of DM (m_N) is around 1 TeV which satisfies the observed relic abundance. This implies the mass of N^-, the charged partner of N^0, is about 1 TeV as well. However, the electroweak correction induces a small mass splitting between N^0 and N^- to be around 162 MeV. Therefore, N^- can give rise a displaced vertex signature through the 3-body decay $N^- \to N^0\ell^-\bar{\nu}_\ell$ [79]. But the main drawback is that the production cross-section of $N^\pm$ of mass $\sim$ TeV is highly suppressed at LHC as this can only be possible through Drell-Yan. Therefore, in section 5 we discuss a more predictive model by enlarging the dark sector with an additional singlet fermion χ.

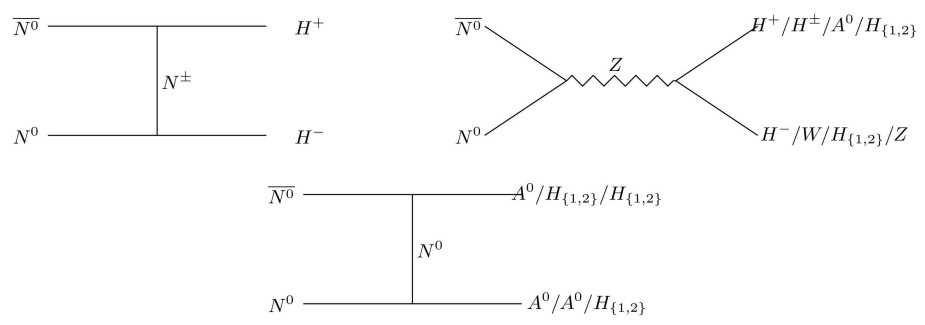

FIGURE 7 | Additional annihilation $N^0\overline{N^0}$, in presence of scalar triplet.

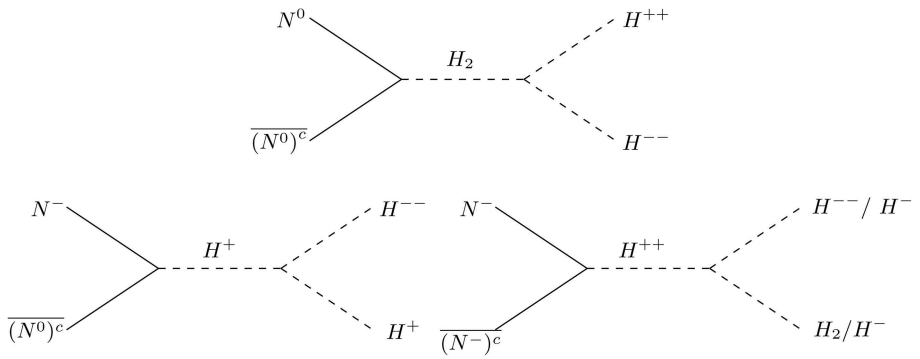

FIGURE 8 | Dominant annihilation ($N^0\overline{(N^0)^c}$) and co-annihilation ($N^-\overline{(N^0)^c}$, $N^-\overline{(N^-)^c}$) processes of ILD DM (N^0) to scalar triplet in final states.

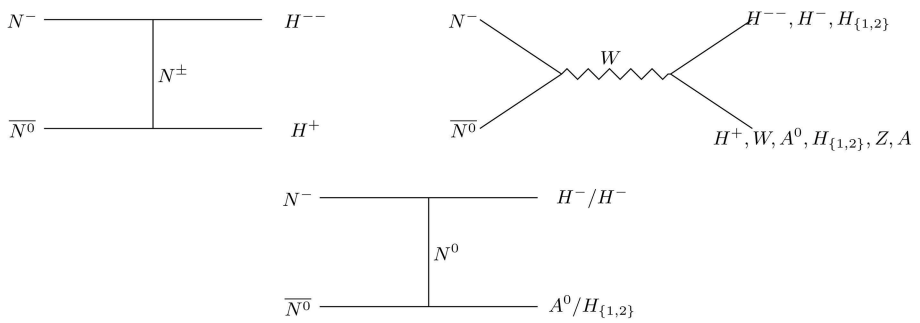

FIGURE 9 | Co-annihilation channels of ILD DM (N^0), with charged fermions N^- in presence of scalar triplet.

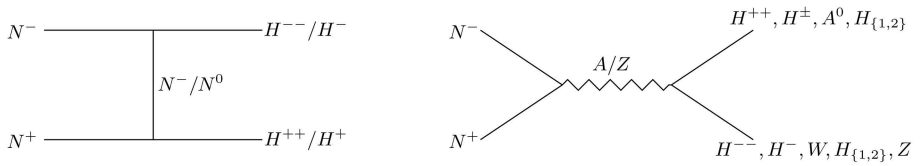

FIGURE 10 | Co-annihilation processes involving only charged partner of ILD DM, $N^\pm$ in presence of scalar triplet.

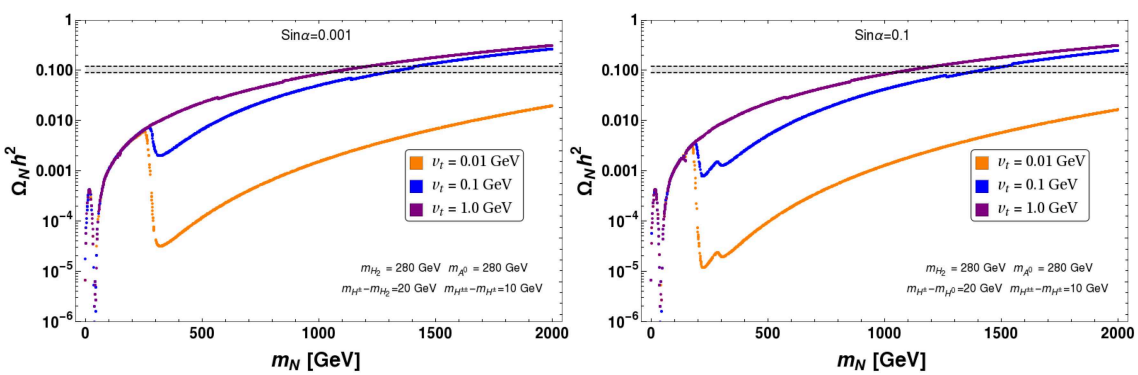

FIGURE 11 | Relic density vs. m_N plot for different choices triplet vev, v_t, keeping $\sin\alpha = 0.001$ **(left)** and $\sin\alpha = 0.1$ **(right)**. Others parameters are mentioned in the figure. The gray patch indicates relic density bounds. In both cases we set $f_N = 0.1$.

4.5. Effect of Salar Triplet on Direct Detection of ILD Dark Matter

As discussed in section 3.2, the ILD dark matter alone is ruled out due to large Z-mediated elastic scattering with nucleus. However, it can be reinstated in presence of the scalar triplet, which not only forbids the Z-mediated elastic scattering [61–65] but also provides a new portal for the detection of ILD dark matter via the doublet-triplet mixing as we discuss below.

The interaction of DM with the Z boson with the kinetic term is given as

$$\mathcal{L}_{Z-DM} \supset i\bar{N^0}\left(\gamma^\mu \partial_\mu - ig_Z \gamma^\mu Z_\mu\right) N^0\,, \tag{33}$$

where $ig_Z = \frac{g}{2\cos\theta_W}$. After the symmetry breaking the scalar triplet Δ gets an induced vev and hence gives Majorana mass to the ILD dark matter N_0 as shown in Equation (29). The presence of such Majorana mass term splits the Dirac DM state into two real Majorana states N_1^0 and N_2^0 with a mass splitting of δm as discussed in section 4.3. Now we rewrite the Lagrangian involving DM-Z interaction in terms of the new Majorana states as:

$$\mathcal{L}_{\mathrm{Z-DM}} \supset \overline{N_1^0} i\gamma^\mu \partial_\mu N_1^0 + \overline{N_2^0} i\gamma^\mu \partial_\mu N_2^0 - ig_z \overline{N_1^0}\gamma^\mu N_2^0 Z_\mu\,. \tag{34}$$

We can see that the dominant gauge interaction becomes off-diagonal. The absence of diagonal interaction term for the DM-Z vertex leads to the vanishing contribution to elastic scattering of the DM with the nucleus. However, there could be an inelastic scattering through Z mediation, which is suppressed if the mass splitting between two states is of the order $\mathcal{O}(100)$ keV or less. But the Yukawa term involving DM and Δ is still diagonal in the new basis and hence can lead to elastic scattering through a mixing between the doublet-triplet Higgs. Assuming N_1^0 to be the lightest among the two Majorana states, hence being the DM, the relevant diagram for the elastic scattering is shown in **Figure 12**.

The direct detection cross-section mainly depends on m_{H_2}, f_N and $\sin\alpha$. We have plotted the spin independent direct detection cross-section as a function of the DM mass $m_{N_1^0}$ in **Figure 13**. Keeping $m_{H_2} = 280$ GeV (Solid) and $m_{H_2} = 600$ GeV (Dashed) fixed, we have shown the cross-section for three different values $\{f_N = 0.01, 0.1, 1\}$ in Red, Blue, and Green color, respectively. Since there is a relative negative sign between the two amplitudes, the destructive interference is more for m_{H_2} comparable to SM Higgs. Hence cross section for $m_{H_2} = 280$ GeV turns out to be smaller than $m_{H_2} = 600$ GeV. But if we increase the mass of m_{H_2} to TeV scale then H_2 mediated process will be suppressed due to the large mass in the propagator and only H_1 mediated process will contribute. The direct search cross-section increases with larger Yukawa coupling f_N from 0.01 to 1 and can be is easily seen from the **Figure 13**. Since the DM couples dominantly to the triplet scalar, the more the mixing angle ($\sin\alpha$), the more is the cross-section which can be clearly seen from the left and right panel of **Figure 13**. But all these cross-sections are well below the present experimental bound of LUX and Xenon-1T. Note that the relic density allowed parameter space of ILD DM in presence of a scalar triplet live in a very high DM mass region $\sim$ *TeV* with moderate f_N and Higgs data unambiguously indicates that the mixing angle ($\sin\alpha$) should be kept small, as we have shown in **Figure 13**. Therefore, the ILD becomes a viable DM candidate in the presence of a triplet scalar allowed by both relic density and direct search constraints.

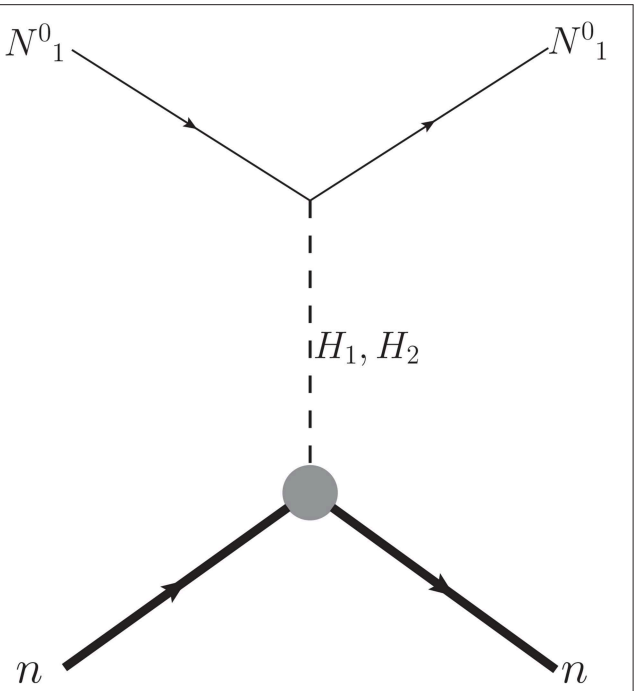

FIGURE 12 | Elastic scattering of the ILD DM(N^0) with the nucleon through scalar mediation due to doublet triplet mixing.

5. SINGLET-DOUBLET LEPTONIC DARK MATTER

Now let us assume that the dark sector is composed of two vector like leptons : a doublet, $N = (N^0 \;\; N^-)^T$ and a singlet χ, which are odd under an extended $\mathcal{Z}_2$ symmetry while all the Standard Model (SM) fields are even. As a result the lightest odd particle in the dark sector is stable and behave as a candidate of DM. The quantum numbers of dark sector fields and that of SM Higgs under the SM gauge group, augmented by a $\mathcal{Z}_2$ symmetry, are given in **Table 2**.

The Lagrangian of the model can be given as follows:

$$\begin{aligned}\mathcal{L}^{VF} &= \overline{N}\left[i\gamma^\mu(\partial_\mu - ig\frac{\sigma^a}{2}W_\mu^a - ig'\frac{Y}{2}B_\mu) - m_N\right]N \\ &\quad + \overline{\chi}\left(i\gamma^\mu\partial_\mu - m_\chi\right)\chi - (Y_1\overline{N}\widetilde{H}\chi + h.c).\end{aligned} \tag{35}$$

Note that here we have assumed to have a CP conserving interaction between the additional vector like fermion to the SM Higgs. One may also think of a coupling $-(Y_1\overline{N}\gamma_5\widetilde{H}\chi + h.c)$ that will violate CP. Now, it is a bit intriguing to think of such interactions before the debate on the SM Higgs to be a scalar or a pseudoscalar is settled. The outcome of such an interaction will alter the subsequent phenomenology significantly. For example, it is known that advocating a pseudoscalar (S) interaction to a vector like DM (ψ), for example,

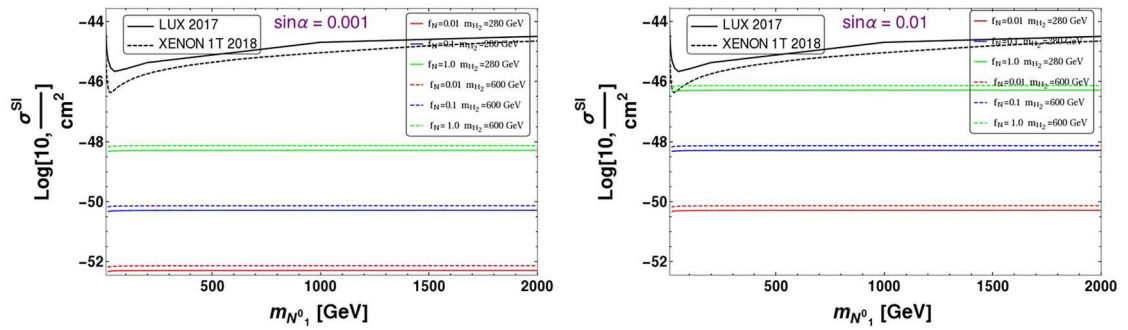

FIGURE 13 | SI direct detection cross-section σ^{SI} as a function of DM mass $m_{N_1^0}$ for $\sin\alpha = 0.001$ **(Left)** and $\sin\alpha = 0.01$ **(Right)**. Different choices of the coupling $\{f_N = 0.01, 0.1, 1\}$ are shown in Red, Blue, and Green color, respectively. Dashed and solid lines corresponds to different values of the heavy Higgs $m_{H_2} = 600, 280$ GeVs, respectively. The bound from LUX 2017 and XENON1T 2018 are shown.

TABLE 2 | Quantum numbers of additional dark sector fermions and that of Higgs under $\mathcal{G} \equiv SU(3)_C \times SU(2)_L \times U(1)_Y \times \mathcal{Z}_2$.

Fields	$SU(3)_C$ ×	$SU(2)_L$ ×	$U(1)_Y$ ×	$\mathcal{Z}_2$
$N = \begin{pmatrix} N^0 \\ N^- \end{pmatrix}$	1	2	−1	−
χ	1	1	0	−
$H = \begin{pmatrix} H^+ \\ H^0 \end{pmatrix}$	1	2	1	+

with a term like $-yS\bar{\psi}\gamma_5\psi$ indicates that DM-nucleon scattering becomes velocity dependent and therefore reduces the direct search constraint significantly to allow the model live in a larger allowed parameter space. However, the Yukawa interaction term itself ($-yS\bar{\psi}\gamma_5\psi$) do not violate parity as S is assumed to be pseudoscalar by itself (see for example in Ghorbani [67]).

After Electroweak symmetry breaking (EWSB) the SM Higgs acquires a vacuum expectation value v. The quantum field around the vacuum can be given as: $H = \begin{pmatrix} 0 & \frac{1}{\sqrt{2}}(v+h) \end{pmatrix}^T$ where $v = 246$ GeV. The presence of the Yukawa term: $Y_1\overline{N}\widetilde{H}\chi$ term in the Lagrangian (Equation 35), arises an admixture between N^0 and χ. The bare mass terms of the vector like fermions in $\mathcal{L}^{VF}$ then take the following form:

$$\begin{aligned} -\mathcal{L}^{VF}_{mass} &= m_N\overline{N^0}N^0 + m_N N^+N^- + m_\chi\overline{\chi}\chi + \frac{Y_1 v}{\sqrt{2}}\overline{N^0}\chi \\ &\quad + \frac{Y_1 v}{\sqrt{2}}\overline{\chi}N^0 \\ &= \overline{\begin{pmatrix} \chi & N^0 \end{pmatrix}}\begin{pmatrix} m_\chi & \frac{Y_1 v}{\sqrt{2}} \\ \frac{Y_1 v}{\sqrt{2}} & m_N \end{pmatrix}\begin{pmatrix} \chi \\ N^0 \end{pmatrix} + m_N N^+N^-. \end{aligned} \tag{36}$$

The unphysical basis, $\begin{pmatrix} \chi & N^0 \end{pmatrix}^T$ is related to physical basis, $\begin{pmatrix} N_1 & N_2 \end{pmatrix}^T$ through the following unitary transformation:

$$\begin{pmatrix} \chi \\ N^0 \end{pmatrix} = \mathcal{U}\begin{pmatrix} N_1 \\ N_2 \end{pmatrix} = \begin{pmatrix} \cos\theta & -\sin\theta \\ \sin\theta & \cos\theta \end{pmatrix}\begin{pmatrix} N_1 \\ N_2 \end{pmatrix}, \tag{37}$$

where the mixing angle

$$\tan 2\theta = -\frac{\sqrt{2}Y_1 v}{m_N - m_\chi}. \tag{38}$$

The mass eigenvalues of the physical states N_1 and N_2 are respectively given by:

$$\begin{aligned} m_{N_1} &= m_\chi \cos^2\theta + m_N \sin^2\theta + \frac{Y_1 v}{\sqrt{2}}\sin 2\theta \\ m_{N_2} &= m_\chi \sin^2\theta + m_N \cos^2\theta - \frac{Y_1 v}{\sqrt{2}}\sin 2\theta \end{aligned} \tag{39}$$

For small $\sin\theta$ ($\sin\theta \to 0$) limit, m_{N_1} and m_{N_2} can be further expressed as:

$$\begin{aligned} m_{N_1} &\simeq m_\chi + \frac{Y_1 v}{\sqrt{2}}\sin 2\theta \equiv m_\chi - \frac{(Y_1 v)^2}{(m_N - m_\chi)}, \\ m_{N_2} &\simeq m_N - \frac{Y_1 v}{\sqrt{2}}\sin 2\theta \equiv m_N + \frac{(Y_1 v)^2}{(m_N - m_\chi)}. \end{aligned} \tag{40}$$

Here we have considered $Y_1 v/\sqrt{2} \ll m_\chi < m_N$. Hence $m_{N_1} < m_{N_2}$. Therefore, N_1 becomes the stable DM candidate. From Equations (38, 39), one can write :

$$\begin{aligned} Y_1 &= -\frac{\Delta m \sin 2\theta}{\sqrt{2}v}, \\ m_N &= m_{N_1}\sin^2\theta + m_{N_2}\cos^2\theta. \end{aligned} \tag{41}$$

where $\Delta m = m_{N_2} - m_{N_1}$[2] is the mass difference between the two mass eigenstates and m_N is the mass of electrically charged component of vector like fermion doublet N^-.

[2]We would like to remind the readers that N_1 and N_2 are not same as N_1^0 and N_2^0. $N_{1,2}$ are the physical eigenstates arising out of the singlet (χ) doublet (N) admixture. Here, N_1 is the DM while N_2 is the NLSP. Where as, N_1^0 and N_2^0 are the two pseudo Dirac states that emerge from the neutral component (N^0) of the vector-like lepton doublet (N) due to the majorana mass term acquired by N^0 in presence of the scalar triplet Δ.

Therefore, one can express interaction terms of $\mathcal{L}^{VF}$ in mass basis of N_1 and N_2 as

$$\begin{aligned}\mathcal{L}^{VF}_{int} &= \Big(\frac{e_0}{2\sin\theta_W\cos\theta_W}\Big)\Big[\sin^2\theta\overline{N_1}\gamma^\mu Z_\mu N_1 + \cos^2\theta\overline{N_2}\gamma^\mu Z_\mu N_2 \\ &\quad + \sin\theta\cos\theta(\overline{N_1}\gamma^\mu Z_\mu N_2 + \overline{N_2}\gamma^\mu Z_\mu N_1)\Big] \\ &+ \frac{e_0}{\sqrt{2}\sin\theta_W}\sin\theta\overline{N_1}\gamma^\mu W^+_\mu N^- + \frac{e_0}{\sqrt{2}\sin\theta_W}\cos\theta\overline{N_2}\gamma^\mu W^+_\mu N^- \\ &+ \frac{e_0}{\sqrt{2}\sin\theta_W}\sin\theta N^+\gamma^\mu W^-_\mu N_1 + \frac{e_0}{\sqrt{2}\sin\theta_W}\cos\theta N^+\gamma^\mu W^-_\mu N_2 \\ &- \Big(\frac{e_0}{2\sin\theta_W\cos\theta_W}\Big)\cos 2\theta_W N^+\gamma^\mu Z_\mu N^- - e_0 N^+\gamma^\mu A_\mu N^- \\ &- \frac{Y_1}{\sqrt{2}}h\Big[\sin 2\theta(\overline{N_1}N_1 - \overline{N_2}N_2) + \cos 2\theta(\overline{N_1}N_2 + \overline{N_2}N_1)\Big] \qquad (42)\end{aligned}$$

The relevant DM phenomenology of the model then mainly depend on following three independent parameters :

$$\{\, m_{N_1},\ \Delta m,\ \sin\theta\} \qquad (43)$$

5.1. Constraints on the Model Parameters

The model parameters are not totally free from theoretical and experimental bounds. Here we would like to discuss briefly the constraints coming from Perturbativity, invisible decay widths of Z and H, and corrections to electroweak parameters.

- **Perturbativity**: The upper limit of perturbativity bound on quartic and Yukawa couplings of the model are given by,

$$|Y_1| < \sqrt{4\pi}\,. \qquad (44)$$

- **Invisible decay width of Higgs:** If the mass of DM is below $m_h/2$, then Higgs can decay to two invisible particles in final state and will yield invisible decay width. Recent Large Hadron Collider (LHC) data put strong constraint on the invisible branching fraction of Higgs to be $Br(h \to inv) \leq 0.24$ [80–82], which can be expressed as:

$$\frac{\Gamma(h \to inv.)}{\Gamma(h \to SM) + \Gamma(h \to inv.)} \leq 0.24\,, \qquad (45)$$

where $\Gamma(h \to SM) = 4.2$ MeV for Higgs mass $m_h = 125.09$ GeV, obtained from recent measured LHC data [68]. Therefore, the invisible Higgs decay width is given by

$$\Gamma(h \to inv.) \leq 1.32\ \text{MeV}, \qquad (46)$$

where

$$\begin{aligned}\Gamma(h \to inv.) &= \Gamma(h \to \overline{N_1}N_1). \qquad (47)\\ &= \frac{1}{16\pi}\Big(Y_1\sin 2\theta\Big)^2 m_h\ \Big(1 - \frac{4m^2_{N_1}}{m^2_h}\Big)^{\frac{3}{2}}\ \Theta(m_h - 2m_{N_1})\,,\end{aligned}$$

where the step function $\Theta(m_h - 2m_{N_1}) = 1$ if $m_{N_1} \leq m_h/2$ and is 0 if $m_{N_1} > m_h/2$. The decay width of Higgs to DM is proportional to $Y_1 = -\frac{\Delta m \sin 2\theta}{\sqrt{2}v}$. Therefore, it depends on the mass splitting with NLSP (Δm) as well as on the doublet singlet mixing ($\sin\theta$). The invisible Higgs decay constraint on the model for $m_{N_1} < m_h/2$ is shown in **Figure 14**, where we have shown the exclusion in $M_{N_1} - \sin\theta$ plane for different choices of Δm ranging from 10 GeV to 500 GeV. The inner side of the contour is excluded. This essentially shows that with large $\Delta m \sim 500$ GeV, essentially all of $m_{N_1} \leq m_h/2$ is excluded, while for a small $\Delta m \sim 10$ GeV, the constraint is milder due to less Higgs decay width and excludes only regions for DM masses $M_{N_1} \leq 30$ GeV within $\sin\theta \sim \{0.6 - 0.8\}$. Therefore, even in $m_{N_1} \leq m_h/2$ region, if Δm and $\sin\theta$ are small, which turns out to be the case for satisfying relic density and direct search as we demonstrate later, then are allowed by the Higgs invisible decay constraint.

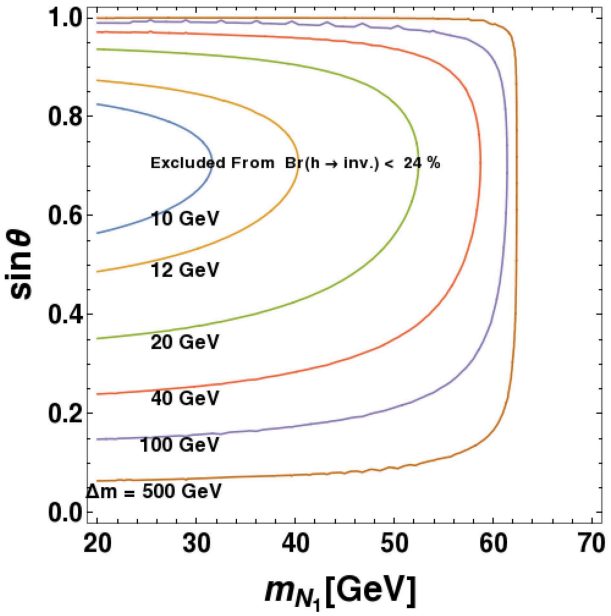

FIGURE 14 | Constraints from Higgs invisible decay width is shown in $m_{N_1} - \sin\theta$ plane. Here each contour line correspond to different value of Δm depicted in the figure. Inner region of each contour line excluded from Higgs invisible decay width, $\Gamma(h \to inv.) \leq 1.32$ MeV for a particular value of Δm.

- **Invisible decay width of Z:** If the masses of dark sector particles are below $m_Z/2$, then Z can decay to dark sector particles leading to an increase of Z-decay width. However, from current observation, invisible decay width of Z boson is strongly bounded. The upper limit on invisible Z-decay width is given by Patrignani et al. [68]:

$$\Gamma(Z \to inv.) = 499.0 \pm 1.5\ \ \text{MeV}\,, \qquad (48)$$

where the decay of Z to N_1 DM is given as:

$$\begin{aligned}\Gamma(Z \to \overline{N_1}N_1) &= \frac{1}{48\pi}\Big(\frac{g\,\sin^2\theta}{\cos\theta_W}\Big)^2 m_Z\ \Big(1 + \frac{2m^2_{N_1}}{m^2_Z}\Big) \\ &\quad \sqrt{1 - \frac{4m^2_{N_1}}{m^2_Z}}\ \Theta(m_Z - 2m_{N_1})\,. \qquad (49)\end{aligned}$$

TABLE 3 | Global fit for the electroweak precision parameters taken from reference [87].

	$10^3\hat{S}$	$10^3\hat{T}$	10^3W	10^3Y
Light Higgs	0.0 ± 1.3	0.1 ± 0.9	0.1 ± 1.2	-0.4 ± 0.8

The $Z-$ invisible decay does not play a crucial role in small $\sin\theta$ regions, which are required for the DM to achieve correct relic density, thus allowing almost all of the $M_{N_1} \leq m_Z/2$ parameter space of the model.

5.2. Corrections to the Electroweak Precision Parameters

Addition of a vector like fermion doublet to the SM gives correction to the electroweak precision test parameters S, T and U[83–86]. The values of these parameters are tightly constrained by experiments. The new observed parameters are infect four in number $\hat{S}$, $\hat{T}$, W and Y [87], where the $\hat{S}$, $\hat{T}$ are related to Peskin-Takeuchi parameters S, T as $\hat{S} = \alpha S/4\sin^2\theta_w$, $\hat{T} = \alpha T$, while W and Y are two new set of parameters. The measured values of these parameters at LEP-I and LEP-II put a lower bound on the mass scale of vector like fermions. The result of a global fit of the parameters is presented in the **Table 3** for a light Higgs [87][3].

In the present scenario, we have a vector like doublet and a singlet fermion field are added to the SM. But the physical states are a charged fermion N^-, and two singlet doublet mixed neutral fermions N_1 (dominant singlet component) and N_2 (dominant doublet component). Therefore, the contribution to the precision parameters also depends on the mixing angle $\sin\theta$. The expression for $\hat{S}$ in terms m_{N_1}, m_{N_2}, m_N and $\sin\theta$ of is given as Cynolter and Lendvai [88]:

$$\begin{aligned}\hat{S} = \frac{g^2}{16\pi^2}\Bigg[\frac{1}{3}\Bigg\{&\ln\left(\frac{\mu_{ew}^2}{m_N^2}\right) - \cos^4\theta\ln\left(\frac{\mu_{ew}^2}{m_{N_2}^2}\right) \\ &- \sin^4\theta\ln\left(\frac{\mu_{ew}^2}{m_{N_1}^2}\right)\Bigg\} - 2\sin^2\theta\cos^2\theta\Bigg\{\ln\left(\frac{\mu_{ew}^2}{m_{N_1}m_{N_2}}\right) \\ &+ \frac{m_{N_1}^4 - 8m_{N_1}^2m_{N_2}^2 + m_{N_2}^4}{9(m_{N_1}^2 - m_{N_2}^2)^2} \\ &+ \frac{(m_{N_1}^2 + m_{N_2}^2)(m_{N_1}^4 - 4m_{N_1}^2m_{N_2}^2 + m_{N_2}^4)}{6(m_{N_1}^2 - m_{N_2}^2)^3}\ln\left(\frac{m_{N_2}^2}{m_{N_1}^2}\right) \\ &+ \frac{m_{N_1}m_{N_2}(m_{N_1}^2 + m_{N_2}^2)}{2(m_{N_1}^2 - m_{N_2}^2)^2} + \frac{m_{N_1}^3m_{N_2}^3}{(m_{N_1}^2 - m_{N_2}^2)^3}\ln\left(\frac{m_{N_2}^2}{m_{N_1}^2}\right)\Bigg\}\Bigg]\end{aligned} \tag{50}$$

where μ_{ew} is at the EW scale.

In the left panel of **Figure 15**, we have plotted $\hat{S}$ as a function of m_{N_2} keeping $m_{N_1} = 200$ GeV for different values of the mixing angle. In the right panel, we have shown the allowed values of $\hat{S}$ in the plane of $m_{N_2} - m_N$ vs. m_{N_2} for $\sin\theta = 0.05$ (Green Color), $\sin\theta = 0.1$ (Red color) and $\sin\theta = 0.2$ (Maroon color). We observed that $\hat{S}$ does not put strong constraints on m_{N_1} and m_{N_2}. Moreover, small values of $\sin\theta$ allows a small mass splitting between N_2 and N^- which relaxes the constraint on $\hat{T}$ parameter as we discuss below. The expression for $\hat{T}$ is given as Cynolter and Lendvai [88]:

$$\begin{aligned}\hat{T} = \frac{g^2}{16\pi^2M_W^2}\Big[&2\sin^2\theta\cos^2\theta\,\Pi(m_{N_1}, m_{N_2}, 0) \\ &-2\cos^2\theta\,\Pi(m_N, m_{N_2}, 0) - 2\sin^2\theta\,\Pi(m_N, m_{N_1}, 0)\Big]\end{aligned} \tag{51}$$

where $\Pi(a, b, 0)$ is given by:

$$\begin{aligned}\Pi(a,b,0) = &-\frac{1}{2}(M_a^2 + M_b^2)\left(\text{Div} + \ln\left(\frac{\mu_{ew}^2}{M_aM_b}\right)\right) \\ &-\frac{1}{4}(M_a^2 + M_b^2) - \frac{(M_a^4 + M_b^4)}{4(M_a^2 - M_b^2)}\ln\frac{M_b^2}{M_a^2} \\ &+M_aM_b\left\{\text{Div} + \ln\left(\frac{\mu_{ew}^2}{M_aM_b}\right) + 1\right. \\ &\left.+\frac{(M_a^2 + M_b^2)}{2(M_a^2 - M_b^2)}\ln\frac{M_b^2}{M_a^2}\right\}\end{aligned} \tag{52}$$

with $\text{Div} = \frac{1}{\epsilon} + \ln 4\pi - \gamma_\epsilon$ contains the divergent term in dimensional regularization method. From the left panel of **Figure 16** we see that for $\sin\theta < 0.05$ we don't get strong constraints on m_{N_2} and m_{N_1}. Moreover, small values of $\sin\theta$ restricts the value of $m_{N_2} - m_N$ to be less than a GeV. As a result large m_{N_2} values are also allowed. Near $m_{N_2} \approx m_N$, $\hat{T}$ vanishes as expected. The value of Y and W are usually suppressed by the masses of new fermions. Since the allowed masses of N_1, N_2 and $N^\pm$ are above 100 GeV by the relic density constraint (to be discussed later), so Y and W are naturally suppressed.

5.3. Relic Density of Singlet-Doublet Leptonic Dark Matter

As stated earlier, the lightest stable physical state N_1 is the DM, which is an admixture of a singlet vector-like fermion (χ) and the neutral component of a vector-like fermionic doublet (N). Due to presence of mass hierarchy between dark sector particles N_1, N_2 and N^-, the lightest component N_1 not only annihilate with itself but also co-annihilate with N_2 and N^- to yield a net a relic density. The relevant diagrams are shown in **Figures 17–19**.

We assume all the heavier particles: N_2 and N^- in the dark sector ultimately decay to lightest stable particle N_1. So in this scenario one can write the Boltzmann equation in terms of total number density $n = n_{N_1} + n_{N_2} + n_{N^\pm}$ as

$$\frac{dn}{dt} + 3Hn = -\langle\sigma v\rangle_{eff}\left(n^2 - n_{eq}^2\right), \tag{53}$$

where

$$\langle\sigma v\rangle_{eff} = \frac{g_1^2}{g_{eff}^2}\langle\sigma v\rangle_{\overline{N_1}N_1} + \frac{2g_1g_2}{g_{eff}^2}\langle\sigma v\rangle_{\overline{N_1}N_2}\left(1 + \frac{\Delta m}{m_{N_1}}\right)^{\frac{3}{2}}e^{-x\frac{\Delta m}{m_{N_1}}}$$

[3]The value $\hat{S}$, $\hat{T}$, W and Y are obtained using a Higgs mass $m_h = 115$ GeV. However, we now know that the SM Higgs mass is 125 GeV. Therefore, the value of $\hat{S}$, $\hat{T}$, W and Y are expected to change. But this effect is nullified by the small values of $\sin\theta$.

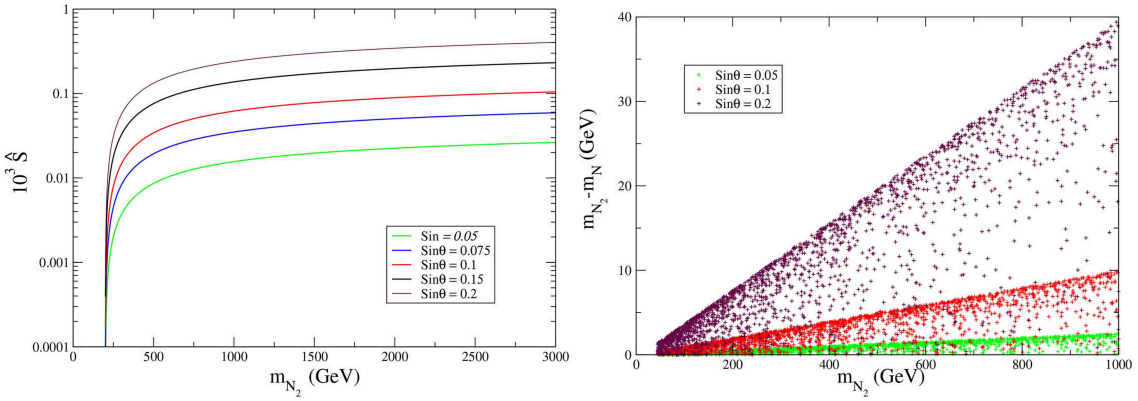

FIGURE 15 | In the left panel, $\hat{S}$ is shown as a function of m_{N_2} for $m_{N_1} = 200$ GeV and sin$\theta = 0.05$ (Green color), sin$\theta = 0.075$ (Blue color), sin$\theta = 0.1$ (Red color), sin$\theta = 0.15$ (Black color), and sin$\theta = 0.2$ (Maroon color). In the right panel, allowed values of $\hat{S}$ is plotted in $m_{N_2} - m_N$ vs. m_{N_2} plane for $\sin\theta = 0.05$ (Green Color), sin$\theta = 0.1$ (Red color), and sin$\theta = 0.2$ (Maroon color).

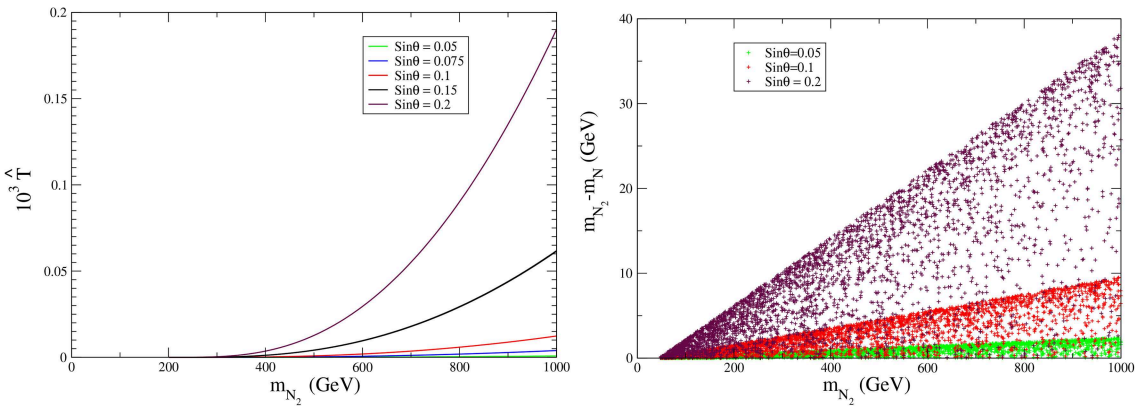

FIGURE 16 | In the left panel, $\hat{T}$ is shown as a function of m_{N_2} for $m_{N_1} = 200$ GeV and sin$\theta = 0.05$ (Green color), sin$\theta = 0.075$ (Blue color), sin$\theta = 0.1$ (Red color), sin$\theta = 0.15$ (Black color), and sin$\theta = 0.2$ (Maroon color). In the right panel, allowed values of $\hat{T}$ is plotted in $m_{N_2} - m_N$ vs. m_{N_2} plane for $\sin\theta = 0.05$ (Green color), $\sin\theta = 0.1$ (Red color), and sin$\theta = 0.2$ (Maroon color).

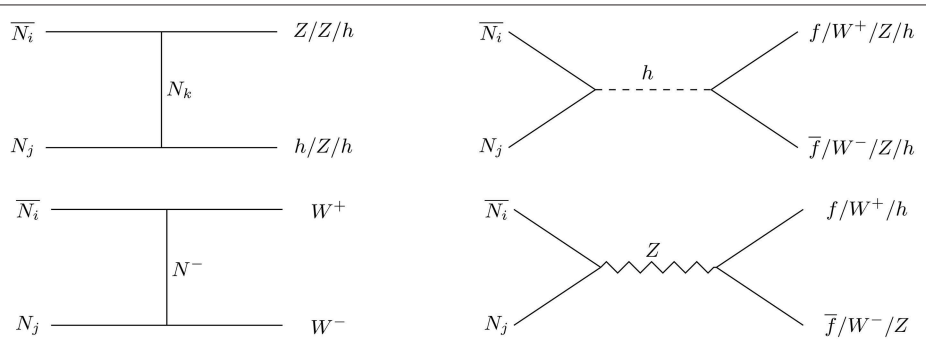

FIGURE 17 | Annihilation ($i = j$) and co-annihilation ($i \neq j$) of vector-like fermion DM. Here ($i, j = 1, 2$).

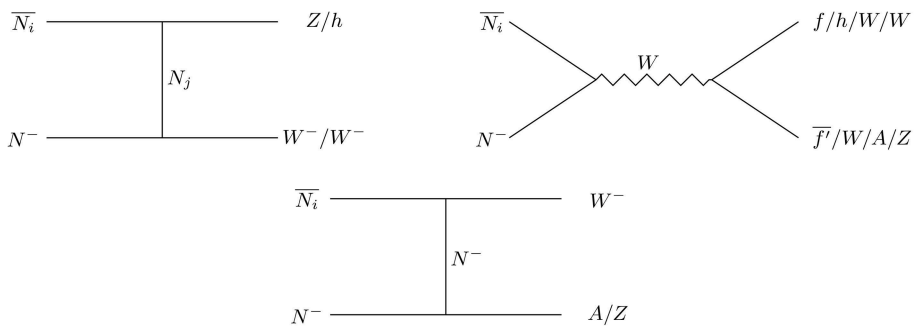

FIGURE 18 | Co-annihilation process of N_i ($i = 1, 2$) with the charge component N^- to SM particles.

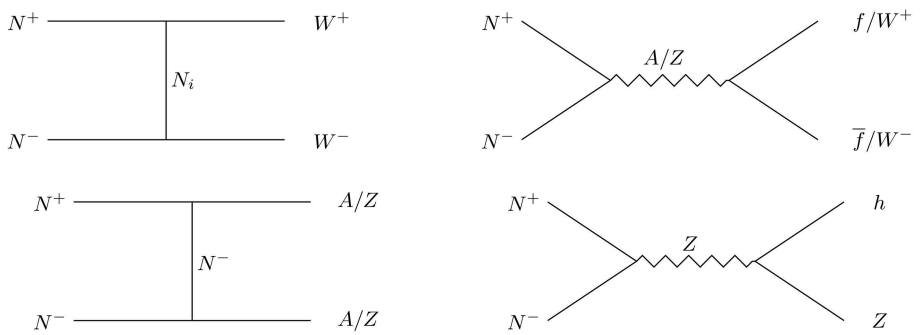

FIGURE 19 | Co-annihilation process of charged fermions $N^{\pm}$ to SM particles in final states.

$$
\begin{aligned}
&+\frac{2g_1g_3}{g_{eff}^2}\langle\sigma v\rangle_{\overline{N_1}N^-}\left(1+\frac{\Delta m}{m_{N_1}}\right)^{\frac{3}{2}}e^{-x\frac{\Delta m}{m_{N_1}}}\\
&+\frac{2g_2g_3}{g_{eff}^2}\langle\sigma v\rangle_{\overline{N_2}N^-}\left(1+\frac{\Delta m}{m_{N_1}}\right)^{3}e^{-2x\frac{\Delta m}{m_{N_1}}}\\
&+\frac{g_2^2}{g_{eff}^2}\langle\sigma v\rangle_{\overline{N_2}N_2}\left(1+\frac{\Delta m}{m_{N_1}}\right)^{3}e^{-2x\frac{\Delta m}{m_{N_1}}}\\
&+\frac{g_3^2}{g_{eff}^2}\langle\sigma v\rangle_{N^+N^-}\left(1+\frac{\Delta m}{m_{N_1}}\right)^{3}e^{-2x\frac{\Delta m}{m_{N_1}}}. \qquad (54)
\end{aligned}
$$

In above equation, g_{eff}, defined as effective degrees of freedom, which is given by

$$
g_{eff} = g_1 + g_2\left(1+\frac{\Delta m}{m_{N_1}}\right)^{\frac{3}{2}}e^{-x\frac{\Delta m}{m_{N_1}}} + g_3\left(1+\frac{\Delta m}{m_{N_1}}\right)^{\frac{3}{2}}e^{-x\frac{\Delta m}{m_{N_1}}}, \qquad (55)
$$

where g_1, g_2 and g_3 are the degrees of freedom of N_1, N_2 and N^-, respectively and $x = x_f = \frac{m_{N_1}}{T_f}$, where T_f is the freeze out temperature. Then the relic density of the N_1 DM can be given by Griest and Seckel [89], Chatterjee and Sahu [90], and Patra et al. [91]

$$
\Omega_{N_1}h^2 = \frac{1.09\times10^9\text{GeV}^{-1}}{g_\star^{1/2}M_{PL}}\frac{1}{J(x_f)}, \qquad (56)
$$

where $J(x_f)$ is given by

$$
J(x_f) = \int_{x_f}^{\infty}\frac{\langle\sigma|v|\rangle_{eff}}{x^2}\,dx. \qquad (57)
$$

We note here that the freeze-out abundance of N_1 DM is controlled by the annihilation and co-annihilation channels as shown in **Figures 17–19**. Therefore, the important parameters which decide the relic abundance of N_1 are mass of DM (m_{N_1}), the mass splitting (Δm) between the DM and the next-to-lightest stable particle (NLSP) and the singlet-doublet mixing angle $\sin\theta$. Here we use MicrOmega [66] to calculate the relic density of N_1 DM.

Variation of relic density of N_1 DM is shown in **Figure 20** as a function of its mass, for a fixed $\Delta m = 10 - 100$ GeV (in left and right panels of **Figure 20**, respectively) and different choices of mixing angle $\sin\theta$. We note that the annihilation cross-section increases with $\sin\theta$, due to larger $SU(2)$ component, resulting in smaller relic density. The resonance drop at $m_Z/2$ and at $m_h/2$ is observed due to s-channel Z and H mediated contributions to relic abundance. Another important feature of **Figure 20** is that when Δm is small, relic density is smaller due to large co-annihilation contribution (less Boltzmann suppression followed from Equation 54). This feature can also be corroborated from **Figure 21**, where we have shown relic density as a function of DM mass by keeping a fixed range of $\sin\theta$ and chosen different possible Δm. Alternatively in **Figure 21**, we have shown relic

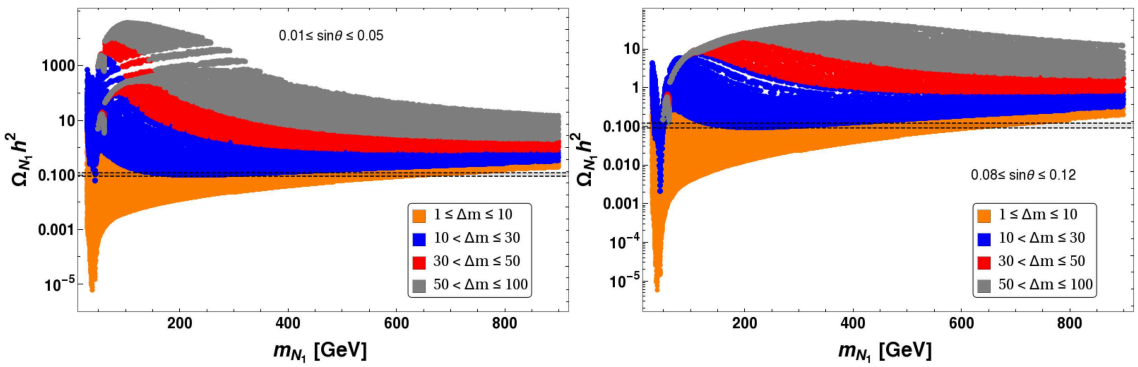

FIGURE 20 | Variation of relic density with DM mass m_{N_1} keeping fixed range of $\sin\theta$: $0.01 \leq \sin\theta \leq 0.05$ (left panel) and $0.08 \leq \sin\theta \leq 0.12$ (right panel). The different color patches corresponds to different Δm region : $1 \leq \Delta m(\text{inGeV}) \leq 10$ (Orange), $10 < \Delta m(\text{inGeV}) \leq 30$ (Blue), $30 < \Delta m(\text{inGeV}) \leq 50$ (Red) and $50 < \Delta m(\text{inGeV}) \leq 100$ (Gray). Correct relic density, $0.1166 \leq \Omega h^2 \leq 0.1206$ is shown by black dashed line. All the masses are in GeVs.

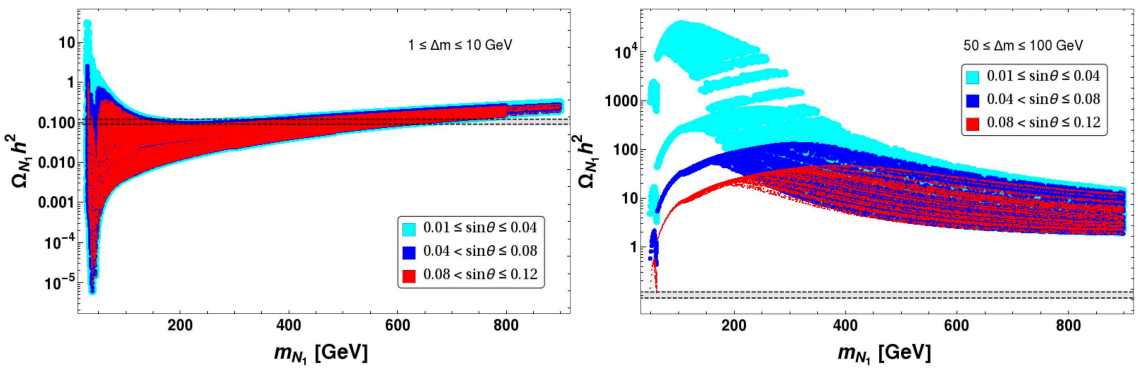

FIGURE 21 | Variation of relic density with DM mass m_{N_1} keeping fixed region of Δm: $1 \leq \Delta m \leq 10$ GeV (left panel) and $50 \leq \Delta m \leq 100$ GeV (right panel). The different color patches are corresponding to different $\sin\theta$ region : $0.01 \leq \sin\theta \leq 0.04$ (Cyan), $0.04 < \sin\theta \leq 0.08$ (Blue), $0.08 < \sin\theta \leq 0.12$ (Red). Correct relic density, $0.1166 \leq \Omega h^2 \leq 0.1206$ is shown by black dashed line. All the masses are in GeVs.

density as a function of DM mass by keeping a fixed range of Δm, while varying $\sin\theta$. We see from the left panel of **Figure 21** that for small Δm co-annihilation dominates and hence the effect of $\sin\theta$ on relic abundance is quite negligible. On the other hand, from the right panel of **Figure 21**, we see that for large Δm, where co-annihilation is suppressed, the effect of $\sin\theta$ on relic abundance is clearly visible. For small $\sin\theta$, the effective annihilation cross-section is small which leads to large relic abundance, while for large $\sin\theta$ the relic abundance is small provided that the Δm is big enough to avoid co-annihilation contributions.

From **Figure 22**, we see that for a wide range of singlet-doublet mixing ($\sin\theta$), we can get correct relic abundance in the plane of m_{N_1} vs. Δm. Different ranges of $\sin\theta$ are indicted by different color codes. To understand our result, we divide the plane of m_{N_1} vs. Δm into two regions: (i) the bottom portion with small Δm, where Δm decreases with larger mass of N_1, (ii) the top portion with larger mass splitting Δm, where Δm increases slowly with larger DM mass m_{N_1}. In the former case, for a given range of $\sin\theta$, the annihilation cross-section decreases for large mass of N_1. Therefore, we need more co-annihilation contribution to compensate, which requires Δm to decrease. This also imply that the region below to each colored zone is under abundant (small Δm implying large co-annihilation for a given mass of N_1), while the region above is over abundant (large Δm implying small co-annihilation for a given mass of N_1). To understand the allowed parameter space in region (ii), we first note that co-annihilation contribution is much smaller here due to large Δm, so the annihilation processes effectively contribute to relic density. Now, let us recall that the Yukawa coupling $Y \propto \Delta m \sin\theta$. Therefore, for a given $\sin\theta$, larger Δm can lead to larger Y and therefore larger annihilation cross-section to yield under abundance, which can only be tamed down to correct relic density by having a larger DM mass. Hence in case-(ii), the region above to each colored zone (allowed region of correct relic density) is under abundant, while the region below to each colored zone is over abundant. Thus, the over and under abundant regions of both cases (i) and (ii) are consistent with each other.

5.4. Constraints on Parameters From Direct Search of Singlet-Doublet Leptonic Dark Matter

Let us now turn to constraints on parameters from direct search of N_1 DM in terrestrial laboratories. Due to singlet-doublet mixing, the N_1 DM in direct search experiments can scatter

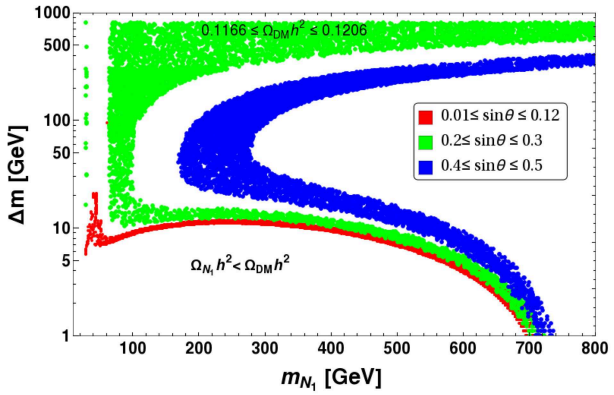

FIGURE 22 | Relic density allowed region are shown in $m_{N_1} - \Delta m$ plane for different range of range of $\sin\theta$: {0.01 − 0.12} (Red), {0.2 − 0.03} (Green), and {0.4 − 0.5} (Blue).

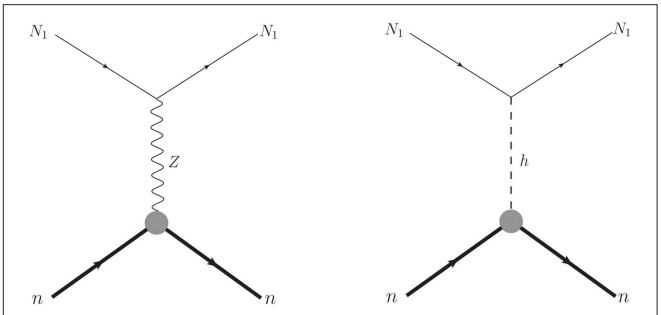

FIGURE 23 | Feynman diagrams of SI direct detection of singlet-doublet N_1 DM.

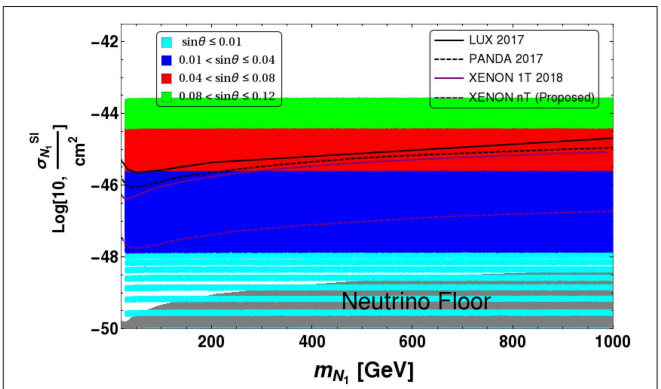

FIGURE 24 | Spin independent direct detection cross-section σ^{SI} as a function of DM mass m_{N_1} for different range of $\sin\theta$: {0.001 − 0.01} (Cyan),{0.01 − 0.04} (Blue), {0.04 − 0.08} (red), and {0.08 − 0.12} (Green). The direct search limits from LUX, PANDA, XENON1T are shown while that of the future sensitivity of XENONnT is also indicated.

off the target nucleus via Z and Higgs mediated processes as shown by the Feynman graphs in **Figure 23**. The cross-section per nucleon for Z-boson mediation is given by Goodman and Witten [92] and Essig [93]

$$\sigma_{\rm SI}^{Z} = \frac{1}{\pi A^2}\mu_r^2|\mathcal{M}|^2 \tag{58}$$

where A is the mass number of the target nucleus, $\mu_r = M_1 m_n/(M_1 + m_n) \approx m_n$ is the reduced mass, m_n is the mass of nucleon (proton or neutron) and $\mathcal{M}$ is the amplitude for Z-boson mediated DM-nucleon cross-section given by

$$\mathcal{M} = \sqrt{2}G_F[\tilde{Z}(f_p/f_n) + (A - \tilde{Z})]f_n \sin^2\theta\,, \tag{59}$$

where f_p and f_n are the interaction strengths (including hadronic uncertainties) of DM with proton and neutron, respectively and $\tilde{Z}$ is the atomic number of the target nucleus. On the other hand, the spin-independent DM-nucleon cross-section per nucleon mediated via the exchange of SM Higgs is given by:

$$\sigma_{\rm SI}^{h} = \frac{1}{\pi A^2}\mu_r^2\left[Zf_p + (A - Z)f_n\right]^2 \tag{60}$$

where the effective interaction strengths of DM with proton and neutron are given by:

$$f_{p,n} = \sum_{q=u,d,s} f_{Tq}^{(p.n)}\alpha_q\frac{m_{(p,n)}}{m_q} + \frac{2}{27}f_{TG}^{(p,n)}\sum_{q=c,t,b}\alpha_q\frac{m_{p.n}}{m_q} \tag{61}$$

with

$$\alpha_q = \frac{Y\sin 2\theta}{M_h^2}\left(\frac{m_q}{v}\right). \tag{62}$$

In Equation (61), the different coupling strengths between DM and light quarks are given by Bertone et al. [4] $f_{Tu}^{(p)} = 0.020 \pm 0.004, f_{Td}^{(p)} = 0.026 \pm 0.005, f_{Ts}^{(p)} = 0.118 \pm 0.062, f_{Tu}^{(n)} = 0.014 \pm 0.004, f_{Td}^{(n)} = 0.036 \pm 0.008, f_{Ts}^{(n)} = 0.118 \pm 0.062$. The coupling of DM with the gluons in target nuclei is parameterized by

$$f_{TG}^{(p,n)} = 1 - \sum_{q=u,,d,s} f_{Tq}^{(p,n)}. \tag{63}$$

Thus from Equations (60–63) the spin-independent DM-nucleon cross-section is given to be:

$$\sigma_{\rm SI}^{h} = \frac{4}{\pi A^2}\mu_r^2\frac{Y^2\sin^2 2\theta}{M_h^4}\left[\frac{m_p}{v}\left(f_{Tu}^{p} + f_{Td}^{p} + f_{Ts}^{p} + \frac{2}{9}f_{TG}^{p}\right) + \frac{m_n}{v}\left(f_{Tu}^{n} + f_{Td}^{n} + f_{Ts}^{n} + \frac{2}{9}f_{TG}^{n}\right)\right]^2. \tag{64}$$

In the above equation the only unknown quantity is Y or $\sin 2\theta$ which can be constrained by requiring that $\sigma_{\rm SI}^{h}$ is less than the current DM-nucleon cross-sections.

Now we make a combined analysis by taking both Z and H mediated diagrams taken into account together. In **Figure 24**, we show the spin-independent cross-section for N_1 DM within its mass range $m_{N_1}: 1 - 1000$ GeV. The plot is obtained by varying $\sin\theta$ within $\{0.001 - 0.12\}$ with $\sin\theta = \{0.001 - 0.01\}$

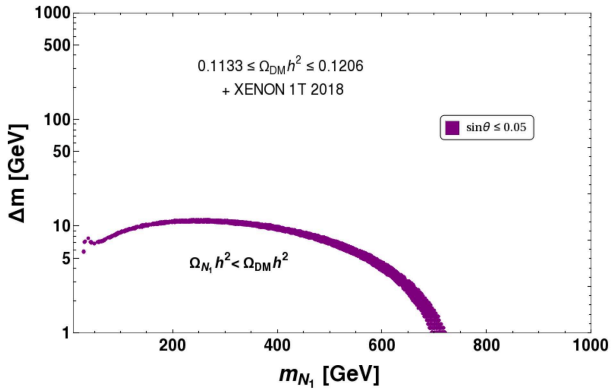

FIGURE 25 | Relic density and direct detection (XENON 1T 2018) allowed parameter space plotted in $m_{N_1} - \Delta m$ plane.

(Cyan), $\sin\theta = \{0.01 - 0.04\}$ (Blue), $\sin\theta = \{0.04 - 0.08\}$ (Red), $\sin\theta = \{0.08 - 0.12\}$ (Green). It clearly shows that the larger is $\sin\theta$, the stronger is the interaction strength (through larger contribution from Z mediation) and hence the larger is the DM-nucleon cross-section. Hence, it turns out that direct search experiments constraints $\sin\theta$ to a large extent. For example, we see that $\sin\theta \leq 0.04$, for the DM mass $m_{N_1} > 300$ GeV. The effect of Δm on DM-nucleon cross-section is less. However, we note that Δm plays a dominant role in the relic abundance of DM. Approximately, $\sin\theta \leq 0.05$ (Blue points) are allowed for most of the parameter space except for smaller DM masses. Cyan points indicate $\sin\theta < 0.01$. The discrete bands correspond to specific values of $\sin\theta$ chosen for the scan and essentially one can consider the whole region together to fall into this category which evidently have sensitivity close to neutrino floor. Note here, the scanned points in **Figure 24**, do not satisfy relic abundance.

Now let us turn to the parameter space, simultaneously allowed by observed relic density and latest constraints from direct DM search experiments, such as Xenon-1T. In **Figure 25**, we have shown the allowed parameter space again in $m_{N_1} - \Delta m$ plane. We see that null observation from direct search crucially tames down the relic density allowed parameter space to $\sin\theta < 0.05$ (Purple). **Figure 25** also shows that large singlet-doublet mixing, i.e., $\sin\theta \gtrsim 0.05$, allowed by correct relic density, is no more allowed by direct search limit in accordance with **Figure 24**.

We finally summarize the DM analysis of singlet doublet case here. The model offers an interesting phenomenology to exploit singlet-doublet mixing ($\sin\theta$) in accordance with DM mass (m_{N_1}) and the splitting with charged fermion content (Δm) to yield a large available parameter space for correct relic density. However, due to Z-mediated process contributing to direct detection of singlet-doublet leptonic dark matter, a stringent constraint on $\sin\theta \leq 0.05$ arises. This leads the DM to be allowed only in small Δm region (as in **Figure 25**) to achieve correct relic density through co-annihilation processes. However, this constraint can be relaxed in presence of a scalar triplet as we discuss below. Moreover, the triplet can also give rise Majorana masses to light neutrinos (see section 4.2) through type-II seesaw to address DM and neutrinos in the same framework.

6. TRIPLET EXTENSION OF SINGLET-DOUBLET LEPTONIC DARK MATTER

6.1. Pseudo-Dirac Nature of Singlet-Doublet Leptonic Dark Matter

As discussed in section 5, the DM is assumed to be $N_1 = \cos\theta\chi + \sin\theta N^0$ with a Dirac mass m_{N_1}. However, from Equation (12) we see that the vev of Δ induces a Majorana mass to N_1 due to singlet-doublet mixing and is given by:

$$m_1 = \sqrt{2} f_N \sin^2\theta \langle\Delta\rangle \approx f_N \sin^2\theta \frac{-\mu v^2}{\sqrt{2} M_\Delta^2}\,. \tag{65}$$

Thus the N^0 has a large Dirac mass m_{N_1} and a small Majorana mass m as shown in the above Equation (65). Therefore, we get a mass matrix in the basis $\{N_{1L}, (N_{1R})^c\}$ as:

$$\mathcal{M} = \begin{pmatrix} m_1 & m_{N_1} \\ m_{N_1} & m_1 \end{pmatrix}. \tag{66}$$

Thus the Majorana mass m splits the Dirac spinor N_1 into two pseudo-Dirac states $\psi_{1,2}$ with mass eigenvalues $m_{N_1} \pm m$. The mass splitting between the two pseudo-Dirac states $\psi_{1,2}$ is given by

$$\delta m_1 = 2m_1 = 2\sqrt{2} f_N \sin^2\theta \langle\Delta\rangle\,. \tag{67}$$

Note that $\delta m_1 << m_{N_1}$ from the estimate of induced vev of the triplet and hence does not play any role in the relic abundance calculation. However, the sub-GeV order mass splitting plays a crucial role in direct detection by forbidding the Z-boson mediated DM-nucleon elastic scattering. Now from Equations (20, 65) we see that the ratio:

$$R = \frac{M_\nu}{m_1} = \frac{f_L}{f_N \sin^2\theta}\,. \tag{68}$$

Thus we see that for $R \sim 10^{-5}$ the ratio, $f_L/f_N \sim 10^{-3}$ if we assume $\sin\theta = 0.1$, which is much larger than the singlet-doublet mixing being used in section 5.4.

6.2. Effect of Scalar Triplet on Relic Abundance and Direct Search of Singlet-Doublet Dark Matter

We already have noted the diagrams that are present due to the addition of a scalar triplet for the ILD DM to freeze-out (see section 4.4). The main features of having an additional scalar triplet in the singlet-doublet DM model is very similar to what we have discussed before in case of ILD DM. The additional freedom that we have in case of singlet-doublet leptonic DM is to play with the mixing parameter $\sin\theta$ and Δm.

Let us first study relic density as a function of DM mass in presence of scalar triplet. This is shown in **Figure 26**, where we

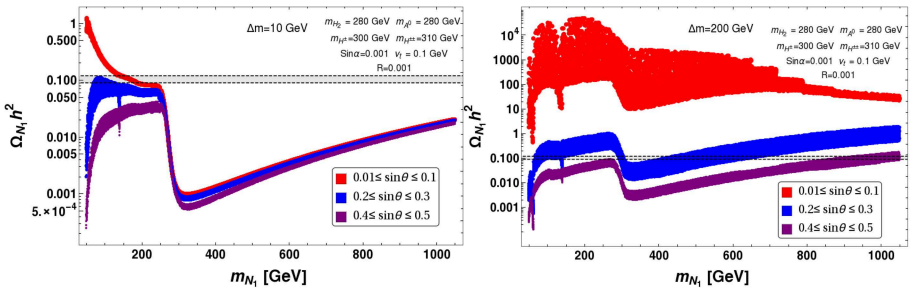

FIGURE 26 | Variation of relic density with DM mass m_{N_1} keeping fixed region of Δm: $\Delta m = 10$ GeV (left panel) and $\Delta m = 200$ GeV (right panel) in presence of scalar triplet. Different color patches correspond to different $\sin\theta$ region : $0.01 \leq \sin\theta \leq 0.1$ (Red), $0.2 < \sin\theta \leq 0.3$ (Blue), $0.4 < \sin\theta \leq 0.5$ (Purple). Correct relic density, $0.1166 \leq \Omega h^2 \leq 0.1206$ is shown by black dashed line. All the masses are in GeVs.

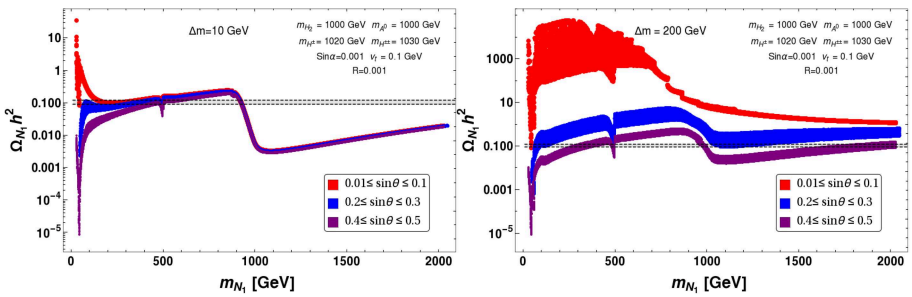

FIGURE 27 | Variation of relic density with DM mass m_{N_1} keeping fixed region of Δm: $\Delta m = 10$ GeV (left panel) and $\Delta m = 200$ GeV (right panel) for heavy scalar triplet mass, $m_{H_2} = 1000$ GeV. Different color patches correspond to different $\sin\theta$ region : $0.01 \leq \sin\theta \leq 0.1$ (Red), $0.2 < \sin\theta \leq 0.3$ (Blue), $0.4 < \sin\theta \leq 0.5$ (Purple). Correct relic density, $0.1166 \leq \Omega h^2 \leq 0.1206$ is shown by black dashed line. All the masses are in GeVs.

choose two fixed values of $\Delta m = 10, 200$ GeV in left and right panel, respectively for a scalar triplet mass around 280 GeV. Different possible ranges of $\sin\theta$ are shown by different color codes. The main feature is again to see a drop in relic density near the value of the triplet mass, where the additional annihilation channel to the scalar triplet reduces relic density significantly. For small Δm, co-annihilation channels play an important part and therefore different mixing angles do not affect relic density significantly (compare left and right panel figures). Also due to large co-annihilation for small Δm as in the left panel, the relic density turns out to be much smaller than the right panel figure where Δm is large and do not offer the co-annihilation channels to be operative. An additional resonance drop at half of the triplet scalar mass is observed here (~ 140 GeV) due to s-channel triplet mediated processes.

A similar plot is shown in **Figure 27** with larger value of the scalar triplet mass $\sim$ 1000 GeV. Obviously the features from **Figure 26**, is mostly retained where the drop in relic density is observed around $\sim$ 1000 GeV and the drop is also smaller than what we had for smaller triplet mass.

Relic density allowed parameter space of the model in $m_{N_1} - \Delta m$ plane is shown in left panel of **Figure 28**. The bottom part of the allowed parameter space is again due to co-annihilation. For small $\sin\theta \sim 0.1$ (red points), this is the only allowed parameter space except the resonance at the extreme left hand side. For larger $\sin\theta$, the resonance drops of doublet and triplet scalars also yield correct relic density. There is an under-abundant region when the triplet channel opens up, which is then reduced with larger DM mass. Therefore, it ends up with two different patches (both for blue and purple points) to be allowed below and above the scalar triplet mass. The direct search constraint in presence of scalar triplet thankfully omits the Z mediated diagram due to the pseudo-Dirac splitting and allows a larger $\sin\theta \sim 0.3$. However, in addition to the Yukawa coupling (Y) initiated SM Higgs mediation, there is an added contribution from the heavy Higgs due to the doublet triplet mixing. We have already seen before that the effect of the additional contribution to direct search cross-section is small in the small $\sin\alpha$ limit with a moderate choice of f_N. Therefore, we have omitted such contributions in generating the direct search allowed parameter space of the model as shown in the right panel of **Figure 28**. This again depicts that the model in presence of scalar triplet earns more freedom in relaxing Δm and $\sin\theta$ to some extent.

7. COLLIDER SIGNATURES

Finally, we discuss the collider signature of the model, which can be subdivided into two categories: (i) Displaced vertex signature and (ii) Excess in leptonic final states.

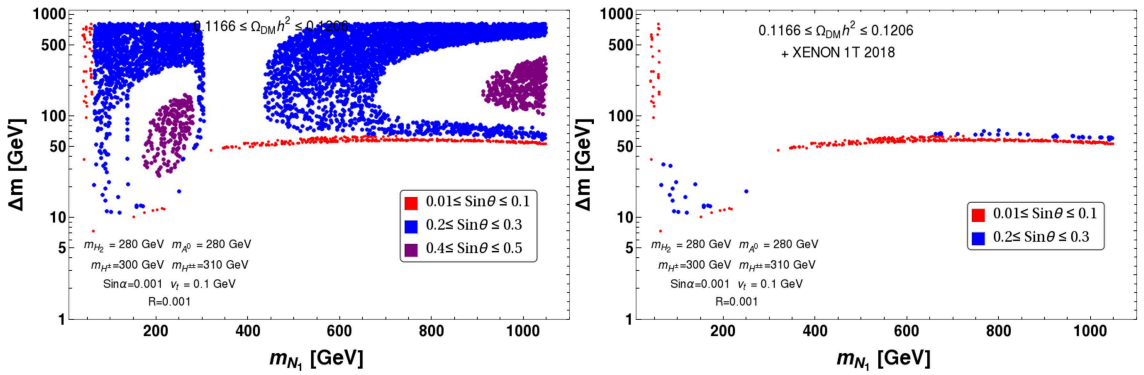

FIGURE 28 | Relic density (left panel) and both relic density and direct search (XENON 1T 2018) (right panel) allowed parameter space plotted in $m_{N_1} - \Delta m$ plane with different range of $\sin\theta$: $0.01 \leq \sin\theta \leq 0.1$ (Red), $0.2 < \sin\theta \leq 0.3$ (Blue), $0.4 < \sin\theta \leq 0.5$ (Purple).

7.1. Displaced Vertex Signature

In the small $\sin\theta$ limit, the charged inert fermion can show a displaced vertex signature. If the mass difference between the N^- and N_1 is greater than W^- mass then N^- can decay via a two body process. But if the mass difference is smaller than M_W, then N^- can decay via three body process say $N^- \to N_1 l^- \bar{\nu}_l$. The three body decay width is given as Bhattacharya et al. [53]:

$$\Gamma = \frac{G_F^2 sin^2\theta}{24\pi^3} m_N^5 I \tag{69}$$

where G_F is the Fermi coupling constant and I is given as:

$$I = \frac{1}{4}\lambda^{1/2}(1,a^2,b^2)F_1(a,b) + 6F_2(a,b)\ln\left(\frac{2a}{1+a^2-b^2-\lambda^{1/2}(1,a^2,b^2)}\right). \tag{70}$$

In the above Equation $F_1(a,b)$ and $F_2(a,b)$ are two polynomials of $a = m_{N_1}/m_N$ and $b = m_\ell/m_N$, where m_ℓ is the charged lepton mass. Up to $\mathcal{O}(b^2)$, these two polynomials are given by

$$\begin{aligned} F_1(a,b) &= \left(a^6 - 2a^5 - 7a^4(1+b^2) + 10a^3(b^2-2) \right. \\ &\quad \left. + a^2(12b^2-7) + (3b^2-1)\right) \\ F_2(a,b) &= \left(a^5 + a^4 + a^3(1-2b^2)\right). \end{aligned} \tag{71}$$

In Equation (70), $\lambda^{1/2} = \sqrt{1+a^4+b^4-2a^2-2b^2-2a^2b^2}$ defines the phase space. In the limit $b = m_\ell/m_N \to 1 - a = \delta M/m_N$, $\lambda^{1/2}$ goes to zero and hence $I \to 0$. The life time of N^- is then given by $\tau \equiv \Gamma^{-1}$. We take the freeze out temperature of DM to be $T_f = m_{N_1}/20$. Since the DM freezes out during radiation dominated era, the corresponding time of DM freeze-out is given by :

$$t_f = 0.301 g_\star^{-1/2} \frac{m_{\rm pl}}{T_f^2}, \tag{72}$$

where $g_\star$ is the effective massless degrees of freedom at a temperature T_f and $m_{\rm pl}$ is the Planck mass. Demanding that N^- should decay before the DM freezes out (i.e., $\tau \lesssim t_f$) we get

$$\sin\theta \gtrsim 1.1789 \times 10^{-5} \left(\frac{1.375\times10^{-5}}{I}\right)^{1/2} \left(\frac{200\text{GeV}}{m_N}\right)^{5/2} \left(\frac{g_\star}{106.75}\right)^{1/4} \left(\frac{m_{N_1}}{180\text{GeV}}\right). \tag{73}$$

The lower bound on the mixing angle depends on the mass of N^- and N_1. For a typical value of $m_N = 200$ GeV, $m_{N_1} = 180$ GeV, we get $\sin\theta \gtrsim 1.17 \times 10^{-5}$. Since τ is inversely proportional to m_N^5, larger the mass, smaller will be the lower bound on the mixing angle.

To explore more whether we can get the relic abundance and displaced vertex simultaneously, we have shown in **Figure 29** relic abundance as a function of DM mass keeping the mass splitting $\Delta M \leq 50$ GeV and $\sin\theta = 10^{-4}$. In this small mixing angle limit there are coannihilation channels (see **Figure 19**) which are independent of $\sin\theta$ contributes to relic density. We choose the set of points which are giving us the correct relic density and tried to find the displaced vertex value. We have plotted in the right panel of **Figure 29** displaced vertex (Γ^{-1}) as a function of m_N. We can see that in the large mass of m_N, the displaced vertex is very small as expected as Γ^{-1} decreases with increase in mass. For larger mixing angles displaced vertex is suppressed. Again $\sin\theta$ cannot be arbitrarily small as shown in Equation (73), so Γ^{-1} will not be very large.

7.2. Hadronically Quiet Dilepton Signature

Since our proposed scenario have one vector like leptonic doublet, there is a possibility of producing charge partner pair of the doublet (N^+ N^-) at proton collider (LHC). The decay of $N^\pm$ further produce leptonic final states through on-shell/off-shell $W^\pm$ mediator to yield opposite sign dilepton plus missing energy as is shown in **Figure 30**. Obviously, W can decay to jets as well, to yield single lepton plus two jets and missing energy signature or that of four jets plus missing energy signature. But, LHC being a QCD machine, the jet rich final states are prone to

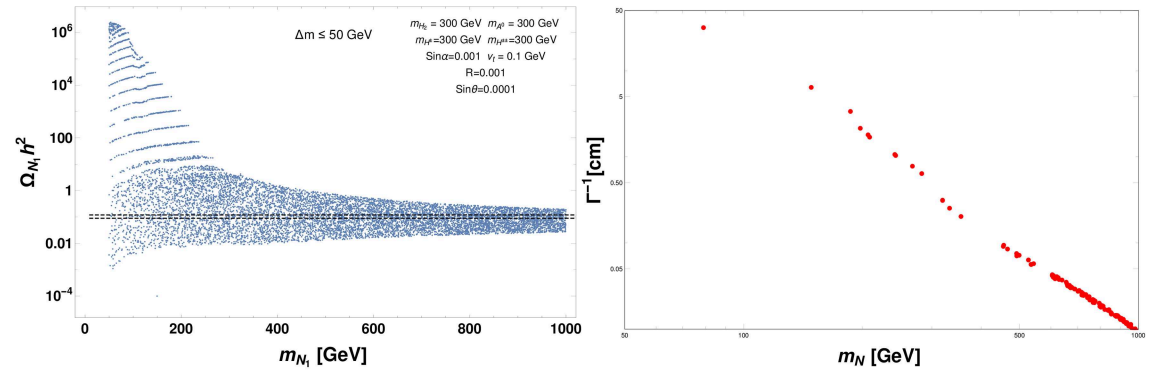

FIGURE 29 | Variation of relic density with DM mass m_{N_1} keeping fixed $\Delta m \leq 50$ GeV (left panel). Black dashed lines correspond to measured value of relic density by PLANCK. Displaced vertex (Γ^{-1}) is plotted as a function of m_N (right panel). For the displaced vertex we choose the set of parameters satisfying relic density from the left panel figure.

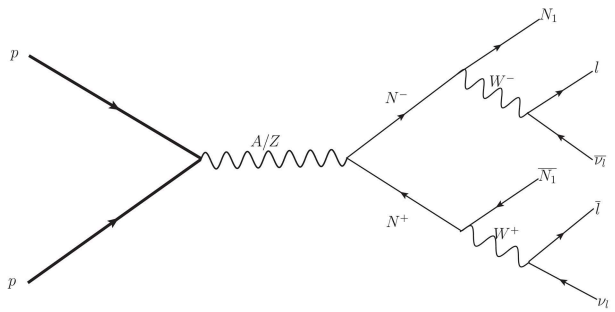

FIGURE 30 | Feynman diagram for producing hadronically quiet opposite sign dilepton plus missing energy ($\ell^+\ell^- + (\not{E}_T)$) signal events at LHC.

very heavy SM background and cannot be segregated from that of the signal. We therefore refrain from calculating the other two possibilities here. A detailed analysis of collider signature of this model will be addressed in Barman et al. [94].

Doublet-singlet fermion DM in absence or in presence of scalar triplet do not distinguish to yield a different final state from that of $\ell^+\ell^- + (\not{E}_T)$ shown in **Figure 30**. However, there is an important distinction that we discuss briefly here. N^+ N^- production cross-section depends on the charge lepton masses and nothing else, leptonic decay branching fraction is also fixed. However, the splitting between DM (N^0) and its charged partner ($N^\pm$) ($\Delta m = m_{N^\pm} - m_{N^0}$) is seen in the missing energy distribution. The signal can only be segregated from that of the SM background when the splitting is large and it falls within the heaps of SM background when Δm is small. This feature can distinguish between the two cases of singlet doublet DM in presence and in absence of scalar triplet. To illustrate, we choose two benchmark points from two scenarios: *i*) doublet singlet leptonic DM (BP1) in absence of scalar triplet and *ii*) doublet singlet leptonic DM in presence of triplet (BP2), shown in **Table 4**. For BP1, we see that $\Delta m = 10$ GeV, has to be very small because relic density and direct search (XENON 1T 2018) put strong constraint on Δm ($\leq$ 12 GeV). On the other hand, presence of triplet in this scenario can relax the situation to some

TABLE 4 | DM mass, $\sin\theta$, $\Delta m = m_{N^\pm} - m_{N_1}$, relic density, and SI direct search cross-sections of two benchmark points are mentioned for collider study.

BPs	{ m_{N_1}, $\sin\theta$ }	Δm	$\Omega_{N_1}h^2$	$\sigma^{SI}_{N_1}$ (in cm^2)	DM models
BP1	{ 141, 0.03 }	10	0.1201	7.6×10^{-47}	Doublet singlet DM
BP2	{ 50, 0.102 }	147	0.1165	1.2×10^{-47}	Doublet singlet DM + Triplet scalar

BP1 correspond to singlet doublet fermion DM scenario. BP2 depicts the case of singlet doublet DM model with an additional triplet in the picture. Note here that others parameters for BP2 remains same mentioned inset of the ***Figure 28****.*

extent, and one may choose large $\Delta m \sim 150$ GeV for low DM mass ($\sim$ 50 GeV) and obey both relic density and direct search constraint, as indicated in BP2. Again, we note here, that such a low DM mass is still allowed by the Invisible Higgs data due to small $\sin\theta$ that we have taken here.

To study the collider signature of the model, we first implemented the model in **FeynRule** [95]. To generate events files, we used **Madgraph** [96] and further passed to **Pythia** [97] for analysis. We have imposed further selection cuts on leptons ($\ell = e, \mu$) and jets as follows to mimic the actual collider environment:

- Lepton isolation: Leptons are the main constituent of the signal. We impose transverse momentum cut of $p_T > 20$ GeV, pseudorapidity of $|\eta| < 2.5$ and separation cut $\Delta R \geq 0.2$ for separating from other leptons. Additionally, $\Delta R \geq 0.4$ is required to separate the leptons from jets. The definition of separation in azimuthal-pseudorapidity plane is $\Delta R = \sqrt{(\Delta\eta)^2 + (\Delta\phi)^2}$.
- Jet formation and identification is performed in Pythia. We use cone-algorithm and impose that the jet initiator parton must have $p_T \geq 20$ GeV and forms a jet within a cone of $\Delta R \leq 0.4$. Jets are required to be defined for our events as to have zero jets.

Using above basic cuts, we have studied hadronically quite opposite signed dilepton final states :

$$\text{Signal}:: \ \ell^+\ell^- + (\not{E}_T): \quad \text{p p} \to \text{N}^+ \ \text{N}^-, (\text{N}^- \to \ \ell^- \ \overline{\nu_\ell} \ \text{N}_1),$$

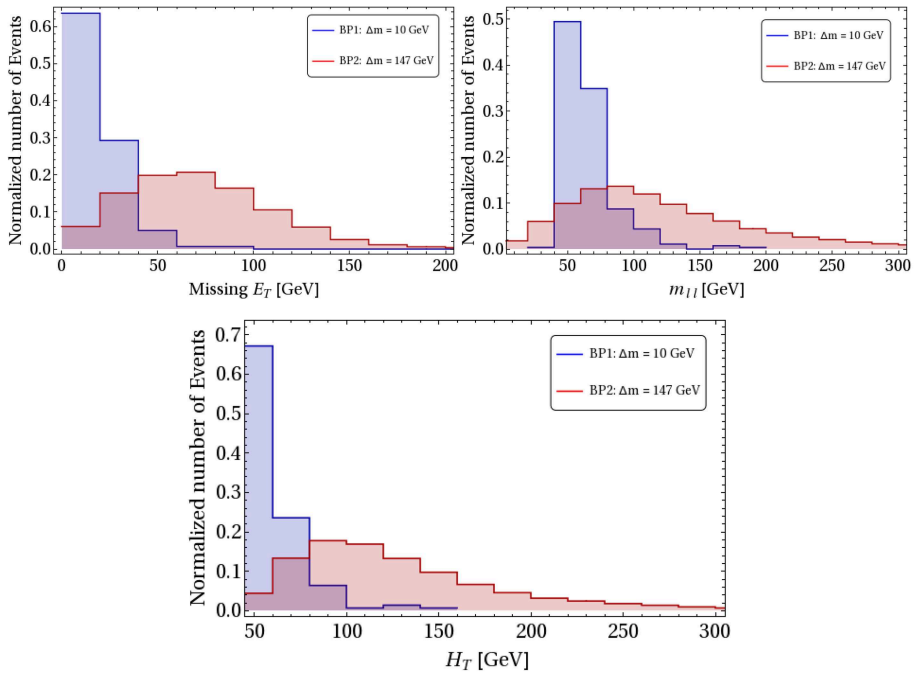

FIGURE 31 | Missing energy ($\not{E}_T$), invariant mass of dilepton ($m_{\ell\ell}$), and transverse mass (H_T) distributions of the hadronically quite dilepton signal events ($\ell^+\ell^- + \not{E}_T$) for C.O.M. energy, $\sqrt{s} = 14$ TeV at LHC.

$$(N^+ \to \ell^+ \nu_\ell \overline{N_1}), \text{ where } \ell = e, \mu \ .$$

The distribution of signal events with respect to missing Energy ($\not{E}_T$), invariant mass of OSD ($m_{\ell\ell}$) and effective momentum (H_T) is shown in **Figure 31**, respectively top left, top right and bottom panel. We see that each of the distribution becomes flatter and the peak is shifted to higher energy value with larger Δm. As we have already mentioned that SM background yields a very similar distribution to that of BP1 and therefore cannot be segregated from small Δm cases. For details of background estimate and distribution, see for example, [98]. Without further selection cuts, the signals constitute a very tiny fraction of hadronically quiet dilepton channel at LHC. To reduce SM background, further selection cuts must be employed:

- $m_{\ell\ell} < |m_z - 15|$ and $m_{\ell\ell} > |m_z + 15|$,
- $H_T > 100,\ 200$ GeV,
- $\not{E}_T > 100,\ 200$ GeV.

We see that the signal events for BP1, after such a cut is reduced significantly, while for BP2, we are still left with moderately large number of events as shown in **Table 5**.

To summarize, we point out that singlet-doublet fermion DM can possibly yield a displaced vertex signature out of the charged fermion decay, thanks to small mass splitting and small $\sin\theta$, while due to the same reason, seeing an excess in leptonic final state will be difficult. On the other hand, the model where singlet-doublet fermion DM is extended with a scalar triplet satisfy relic density and direct search with a larger mass splitting between the DM and charged companion which allows such a case to yield a lepton excess to be probed at LHC, but the displaced vertex signature may get subdued due to this. The complementarity of the two cases will be elaborated in Barman et al. [94]. We also note that scalar triplet extension do not allow the fermion DM to have any mass to also accommodate large Δm. This is only possible in the vicinity of Higgs resonance. We can however, earn a freedom on choosing a large Δm at any fermion mass value in the presence of a second DM component and see a lepton signal excess as has been pointed out in Barman et al. [94].

TABLE 5 | Signal events for above mentioned benchmark points with $\sqrt{s} = 14$ TeV at the LHC for the luminosity $\mathcal{L} = 100\ fb^{-1}$ after $\not{E}_T$, H_T and $m_{\ell\ell}$ cuts.

BPs	Δm (GeV)	$\sigma_{pp\to N^+N^-}$ (fb)	$\not{E}_T$ (GeV)	H_T (GeV)	σ^{OSD}(fb)	$N^{\text{OSD}}_{\text{eff}} = \sigma^{\text{OSD}} \times \mathcal{L}$
BP1	10	12.01	>100	>100	< 0.0003	< 1
			>100	>100	0.711	71
				>200	0.250	25
BP2	147	33.11	>200	> 100	0.040	4
				>200	0.039	4

8. CONCLUSIONS AND FUTURE DIRECTIONS

Vector like leptons stabilized by a symmetry, provide a simple solution to DM problem of the universe. The relic density allowed parameter space provide a wide class of phenomenological implications to be explored in DM direct search experiments and in collider searches through signal excess or displaced vertex. In this article, we have provided a thorough analysis of different possible models in such a category. The results have been illustrated with parameter space scans, taking into account

the constraints coming from non-observation of DM in present direct search data, constraints from electroweak precision tests, vacuum stability, invisible decay widths of Higgs and Z etc., to see the allowed region where the model(s) can be probed in upcoming experiments.

We first reviewed the possibility of vector-like leptonic singlet χ, doublet N and their combination $\chi - N$ as viable candidates of DM. First we discussed about a vector-like singlet leptonic DM χ. In this case, the DM can only couple to visible sector through non-renormalizable dimension-5 operator $\overline{\chi}\chi H^{\dagger}H/\Lambda$, where Λ denotes a new physics (NP) scale. We find relic density allowed parameter space of the model requires Λ to be 500 GeV or less for DM mass ranging between 100 GeV to 500 GeV. However, the direct search cross-section for such Λ is much larger than the constraints obtained from XENON1T data. Therefore, a singlet lepton is almost ruled out being a viable candidate of DM.

We then discussed the possibility of neutral component of a vector-like inert lepton doublet (ILD) N^0 to be a viable DM candidate. Since the doublet has only gauge interaction, the correct relic abundance can be obtained only at heavy DM mass around $\sim$ TeV. Again, the doublet DM suffers a stringent constraint from Z-mediated elastic scattering at direct search experiments. The relic density allowed parameter space therefore lies way above than the XENON1T bound of not observing a DM in direct search experiment. Therefore, an ILD DM alone is already ruled out. However, we showed that in presence of a scalar triplet, an ILD DM can be reinstated by forbidding the Z-mediated elastic scattering with the nucleons thanks to pseudo Dirac splitting. Due to additional interaction of ILD in presence of a scalar triplet, the mass of ILD DM is pushed to a higher side to achieve correct relic density. Moreover, the scalar triplet mixes with the SM doublet Higgs and paves a path for detecting the ILD DM at terrestrial laboratories. The presence of scalar triplet also yield a non-zero neutrino mass to three flavors of active neutrinos which are required by oscillation data. However, we noticed that the parameter space of an ILD DM is very limited to a very high mass due to its gauge coupling.

We then searched for a combination of singlet χ and neutral component of doublet $N = (N^-, N^0)$ being a viable candidate of DM. This is possible if both of the fermion fields possess same Z_2 symmetry. They mix after electroweak symmetry breaking. In fact, we found that the appropriate combination of a singlet-doublet can be a viable DM candidate in a large parameter space spanning DM mass between Z resonance to $\sim$ 700 GeV. The singlet-doublet mixing plays a key role in deciding the relic abundance of DM as well as detecting it in terrestrial laboratories. In fact, we found that a large singlet component admixture with a small doublet component is an appropriate combination to be a viable candidate for DM, particularly to meet direct search bounds ($\sin\theta \leq 0.05$). However, it is difficult for a DM with large singlet component to yield correct relic density due to small annihilation cross-section. Therefore, it has to depend heavily on co-annihilation to make up the small annihilation cross section, which in turn requires a small mass difference between the DM N_1 and its partners $N^{\pm}, N_2$. In particular, if the mixing angle is very small (around $\sin\theta \sim 10^{-4}$), the decay of NLSP ($N^- \rightarrow N_1 + l^- + \bar{\nu}_l$) gives a measurable displaced vertex signature at LHC, aided by a small mass difference of N^- with the DM (N_1). However, this typical feature makes it difficult to identify any signal excess from production of the NLSP at LHC.

The situation becomes more interesting in presence of a scalar triplet. The latter, not only enhances the allowed parameter space of singlet-doublet mixed DM (by allowing a larger mixing $\sin\theta \lesssim 0.2$ and also a larger mass splitting between NLSP and DM), but also generates masses to three flavors active neutrinos via type-II seesaw. Presence of scalar triplet may also pave the path to discover this model through hadronically quiet dilepton channel at LHC. We would also like to add here that if the DM (singlet-doublet admixture) including the SM particles are charged under an additional flavor symmetry, say A_4, then non-zero value of θ_{13} can be obtained from the flavor charge of DM, which has been elaborated in Bhattacharya et al. [99, 100].

AUTHOR CONTRIBUTIONS

All authors listed have made a substantial, direct and intellectual contribution to the work, and approved it for publication.

ACKNOWLEDGMENTS

We thank Basabendu Barman for helpful discussions. SB would like to acknowledge the support from DST-INSPIRE faculty grant IFA-13-PH-57 at IIT Guwahati. PG also like to thank MHRD, Government of India for research fellowship.

REFERENCES

1. Zwicky F. Die Rotverschiebung von extragalaktischen Nebeln. *Helv Phys Acta.* (1933) **6**:110–27. [*Gen Rel Grav.* (2009) **41**:207].
2. Rubin VC, Ford Jr WK. Rotation of the Andromeda Nebula from a spectroscopic survey of emission regions. *Astrophys J.* (1970) **159**:379.
3. Clowe D, Bradac M, Gonzalez AH, Markevitch M, Randall SW, Jones C, et al. A direct empirical proof of the existence of dark matter. *Astrophys J.* (2006) **648**:L109–13. doi: 10.1086/508162
4. Bertone G, Hooper D, Silk J. Particle dark matter: evidence, candidates and constraints. *Phys Rept.* (2005) **405**:279–390. doi: 10.1016/j.physrep.2004.08.031
5. Jungman G, Kamionkowski M, Griest K. Supersymmetric dark matter. *Phys Rept.* (1996) **267**:195–373.
6. Hinshaw G, Larson D, Komatsu E, Spergel DN, Bennett CL, Dunkley J, et al. WMAP Collaboration. Nine-year Wilkinson Microwave Anisotropy Probe (WMAP) observations: cosmological parameter results. *Astrophys J Suppl.* (2013) **208**:19. doi: 10.1088/0067-0049/208/2/19
7. Ade PAR, Aghanim N, Armitage-Caplan C, Arnaud M, Ashdown M, Atrio-Barandela F, et al. Planck Collaboration. Planck 2013 results. XVI. Cosmological parameters. *Astron Astrophys.* (2014) **571**:A16. doi: 10.1051/0004-6361/201321591
8. Aghanim N, Akrami Y, Ashdown M, Aumont J, Baccigalupi C, Ballardini M, et al. Planck collaboration. Planck 2013 results. VI. Cosmological parameters. *arXiv*: 1807.06209 (2018).
9. Aprile E, Alfonsi M, Arisaka K, Arneodo F, Balan C, Baudis L, et al. XENON100 Collaboration. Dark matter results From 225

live days of XENON100 data. *Phys Rev Lett.* (2012) **109**:181301. doi: 10.1103/PhysRevLett.109.181301
10. Akerib DS, Alsum S, Arajo HM, Bai X, Bailey AJ, Balajthy J, et al. LUX Collaboration. Limits on spin-dependent WIMP-nucleon cross section obtained from the complete LUX exposure. *Phys Rev Lett.* (2017) **118**:251302. doi: 10.1103/PhysRevLett.118.251302
11. Aprile E, Aalbers J, Agostini F, Alfonsi M, Althueser L, Amaro FD, et al. XENON Collaboration. Physics reach of the XENON1T dark matter experiment. *JCAP.* (2016) **1604**:027. doi: 10.1088/1475-7516/2016/04/027
12. Aprile E, Aalbers J, Agostini F, Alfonsi M, Althueser L, Amaro FD, et al. XENON Collaboration. Dark matter search results from a one ton-year exposure of XENON1T. *Phys Rev Lett.* (2018) **121**:111302. doi: 10.1103/PhysRevLett.121.111302
13. Cui X, Abdukerim A, Chen W, Chen X, Chen Y, Dong B, et al. PandaX-II Collaboration. Dark matter results from 54-ton-day exposure of PandaX-II experiment. *Phys Rev Lett.* (2017) **119**:181302. doi: 10.1103/PhysRevLett.119.181302
14. Adriani O, Barbarino GC, Bazilevskaya GA, Bellotti R, Bianco A, Boezio M, et al. PAMELA Collaboration. Cosmic-ray positron energy spectrum measured by PAMELA. *Phys Rev Lett.* (2013) **111**:081102. doi: 10.1103/PhysRevLett.111.081102
15. Adriani O, Barbarino GC, Bazilevskaya GA, Bellotti R, Bianco A, Boezio M, et al. PAMELA Collaboration. The cosmic-ray electron flux measured by the PAMELA experiment between 1 and 625 GeV. *Phys Rev Lett.* (2011) **106**:201101. doi: 10.1103/PhysRevLett.106.201101
16. Corti C, AMS Collaboration. The cosmic ray electron and positron spectra measured by AMS-02. *arXiv*:1402.0437 (2014).
17. Atwood WB, Abdo AA, Ackermann M, Althouse W, Anderson B, Axelsson M, et al. Fermi-LAT Collaboration. The large area telescope on the Fermi gamma-ray space telescope mission. *Astrophys J.* (2009) **697**:1071. doi: 10.1088/0004-637X/697/2/1071
18. Aartsen MG, Ackermann M, Adams J, Aguilar JA, Ahlers M, Ahrens M, et al. IceCube Collaboration. Search for neutrinos from dark matter self-annihilations in the center of the milky way with 3 years of IceCube/DeepCore. *Eur Phys J C.* (2017) **77**:627. doi: 10.1140/epjc/s10052-017-5213-y
19. Aartsen MG, Ackermann M, Adams J, Aguilar JA, Ahlers M, Ahrens M, et al. IceCube Collaboration. Search for neutrinos from decaying dark matter with IceCube. *Eur Phys J C.* (2018) **78**:831. doi: 10.1140/epjc/s10052-018-6273-3
20. Aaboud M, ATLAS Collaboration. Search for dark matter at $\sqrt{s} = 13$ TeV in final states containing an energetic photon and large missing transverse momentum with the ATLAS detector. *Eur Phys J C.* (2017) **77**:393. doi: 10.1140/epjc/s10052-017-4965-8
21. Burns DR. *A Collider Search for Dark Matter Produced in Association With a Higgs Boson With the CMS Detector at the 13 TeV LHC*. CERN-THESIS-2017-048. Davis, CA: University of California.
22. Kopecky AC. *A Search for Dark Matter in the Monophoton Final State at CMS*. CERN-THESIS-2012-265.
23. Fukuda S, Fukuda Y, Ishitsuka M, Itow Y, Kajita T, Kameda J, et al. Super-Kamiokande Collaboration. Constraints on neutrino oscillations using 1258 days of Super-Kamiokande solar neutrino data. *Phys Rev Lett.* (2001) **86**:5656–60. doi: 10.1103/PhysRevLett.86.5656
24. Kim YG, Lee KY. The minimal model of fermionic dark matter. *Phys Rev D.* (2007) **75**:115012. doi: 10.1103/PhysRevD.75.115012
25. Kim YG, Lee KY, Shin S. Singlet fermionic dark matter. *JHEP.* (2008) **0805**:100. doi: 10.1088/1126-6708/2008/05/100
26. Pospelov M, Ritz A, Voloshin MB. Secluded WIMP dark matter. *Phys Lett B.* (2008) **662**:53. doi: 10.1016/j.physletb.2008.02.052
27. Kim YG, Shin S. Singlet fermionic dark matter explains DAMA signal. *JHEP.* (2009) **0905**:036. doi: 10.1088/1126-6708/2009/05/036
28. Heo JH. Minimal dirac fermionic dark matter with nonzero magnetic dipole moment. *Phys Lett B* (2010) **693**:255. doi: 10.1016/j.physletb.2010.08.035
29. Cao QH, Chen CR, Li CS, Zhang H. Effective dark matter model: relic density, CDMS II, Fermi LAT and LHC. *JHEP.* (2011) **1108**:018. doi: 10.1007/JHEP08(2011)018
30. Lopez-Honorez L, Schwetz T, Zupan J. Higgs portal, fermionic dark matter, and a Standard Model like Higgs at 125 GeV. *Phys Lett B.* (2012) **716**:179. doi: 10.1016/j.physletb.2012.07.017
31. Ettefaghi MM, Moazzemi R. Annihilation of singlet fermionic dark matter into two photons. *JCAP.* (2013) **1302**:048. doi: 10.1088/1475-7516/2013/02/048
32. Fairbairn M, Hogan R. Singlet fermionic dark matter and the electroweak phase transition. *JHEP.* (2013) **1309**:022. doi: 10.1007/JHEP09(2013)022
33. Esch S, Klasen M, Yaguna CE. Detection prospects of singlet fermionic dark matter. *Phys Rev D* (2013) **88**:075017. doi: 10.1103/PhysRevD.88.075017
34. Dutta Banik A, Majumdar D. Extension of minimal fermionic dark matter model: a study with Two Higgs doublet model. *Eur Phys J C.* (2015) **75**:364. doi: 10.1140/epjc/s10052-015-3589-0
35. Fedderke MA, Chen JY, Kolb EW, Wang LT. The fermionic dark matter Higgs portal: an effective field theory approach. *JHEP.* (2014) **1408**:122. doi: 10.1007/JHEP08(2014)122
36. Bagherian Z, Ettefaghi MM, Haghgouyan Z, Moazzemi R. A new parameter space study of the fermionic cold dark matter model. *JCAP.* (2014) **1410**:033. doi: 10.1088/1475-7516/2014/10/033
37. Kim YG, Lee KY, Park CB, Shin S. Secluded singlet fermionic dark matter driven by the Fermi gamma-ray excess. *Phys Rev D.* (2016) **93**:075023. doi: 10.1103/PhysRevD.93.075023
38. Ettefaghi M, Moazzemi R. Analyzing of singlet fermionic dark matter via the updated direct detection data. *Eur Phys J C.* (2017) **77**:343. doi: 10.1140/epjc/s10052-017-4894-6
39. Kim YG, Lee KY, Nam SH. Singlet fermionic dark matter with Veltman conditions. *Phys Lett B.* (2018) **782**:316. doi: 10.1016/j.physletb.2018.05.044
40. McDonald J, Sahu N. Z(2)-Singlino dark matter in a portal-like extension of the minimal supersymmetric standard model. *JCAP.* (2008) **0806**:026. doi: 10.1088/1475-7516/2008/06/026
41. McDonald J, Sahu N. KeV warm dark matter via the supersymmetric Higgs portal. *Phys Rev D.* (2009) **79**:103523. doi: 10.1103/PhysRevD.79.103523
42. Sahu N, Sarkar U. Extended Zee model for neutrino mass, leptogenesis and sterile neutrino like dark matter. *Phys Rev D.* (2008) **78**:115013. doi: 10.1103/PhysRevD.78.115013
43. Arkani-Hamed N, Dimopoulos S, Kachru S. *Predictive Landscapes and New Physics at a TeV*. *arXiv*:hep-th/0501082 (2005).
44. Mahbubani R, Senatore L. The minimal model for dark matter and unification. *Phys Rev D.* (2006) **73**:043510. doi: 10.1103/PhysRevD.73.043510
45. Eramo FD. Dark matter and Higgs boson physics. *Phys Rev D.* (2007) **76**:083522. doi: 10.1103/PhysRevD.76.083522
46. Enberg R, Fox PJ, Hall LJ, Papaioannou AY, Papucci M. LHC and dark matter signals of improved naturalness. *JHEP.* (2007) **0711**:014. doi: 10.1088/1126-6708/2007/11/014
47. Cohen T, Kearney J, Pierce A, Tucker-Smith D. Singlet-doublet dark matter. *Phys Rev D.* (2012) **85**:075003. doi: 10.1103/PhysRevD.85.075003
48. Cheung C, Sanford D. Simplified models of mixed dark matter. *JCAP.* (2014) **1402**:011. doi: 10.1088/1475-7516/2014/02/011
49. Restrepo D, Rivera A, Sánchez-Peláez M, Zapata O, Tangarife W. Radiative neutrino masses in the singlet-doublet fermion dark matter model with scalar singlets. *Phys Rev D.* (2015) **92**:013005. doi: 10.1103/PhysRevD.92.013005
50. Calibbi L, Mariotti A, Tziveloglou P. Singlet-doublet model: dark matter searches and LHC constraints. *arXiv*:1505.03867 (2015).
51. Cynolter G, Kovacs J, Lendvai E. Doublet-singlet model and unitarity. *Mod Phys Lett A.* (2015) **31**:1650013. doi: 10.1142/S0217732316500139
52. Bhattacharya S, Sahoo N, Sahu N.Minimal vectorlike leptonic dark matter and signatures at the LHC. *Phys Rev D.* (2016) **93**:115040. doi: 10.1103/PhysRevD.93.115040
53. Bhattacharya S, Sahoo N, Sahu N. Singlet-doublet fermionic dark matter, neutrino mass and collider signatures. *Phys Rev D.* (2017) **96**:035010. doi: 10.1103/PhysRevD.96.035010
54. Magg M, Wetterich C. Neutrino mass problem and gauge hierarchy. *Phys Lett.* (1980) **94B**:61. doi: 10.1016/0370-2693(80)90825-4
55. Lazarides G, Shafi Q, Wetterich C. Proton lifetime and fermion masses in an SO(10) model. *Nucl Phys B.* (1981) **181**:287. doi: 10.1016/0550-3213(81)90354-0
56. Mohapatra RN, Senjanovic G. Neutrino masses and mixings in gauge models with spontaneous parity violation. *Phys Rev D.* (1981) **23**:165. doi: 10.1103/PhysRevD.23.165

57. Ma E, Sarkar U. Neutrino masses and leptogenesis with heavy Higgs triplets. *Phys Rev Lett.* (1998) **80**:5716. doi: 10.1103/PhysRevLett.80.5716
58. Konetschny W, Kummer W. Nonconservation of total lepton number with scalar bosons. *Phys Lett.* (1977) **70B**:433. doi: 10.1016/0370-2693(77)90407-5;
59. Schechter J, Valle JWF. Neutrino masses in SU(2) x U(1) theories. *Phys Rev D.* (1980) **22**:2227. doi: 10.1103/PhysRevD.22.2227
60. Cheng TP, Li LF. Neutrino masses, mixings and oscillations in SU(2) x U(1) models of electroweak interactions. *Phys Rev D.* (1980) **22**:2860. doi: 10.1103/PhysRevD.22.2860
61. Tucker-Smith D, Weiner N. Inelastic dark matter. *Phys Rev D.* (2001) **64**:043502. doi: 10.1103/PhysRevD.64.043502
62. Cui Y, Morrissey DE, Poland D, Randall L. Candidates for inelastic dark matter. *JHEP.* (2009) **0905**:076. doi: 10.1088/1126-6708/2009/05/076
63. Arina C, Sahu N. Asymmetric inelastic inert doublet dark matter from triplet scalar leptogenesis. *Nucl Phys B.* (2012) **854**:666. doi: 10.1016/j.nuclphysb.2011.09.014
64. Arina C, Gong JO, Sahu N. Unifying darko-lepto-genesis with scalar triplet inflation. *Nucl Phys B.* (2012) **865**:430. doi: 10.1016/j.nuclphysb.2012.07.029
65. Arina C, Mohapatra RN, Sahu N. Co-genesis of matter and dark matter with vector-like fourth generation leptons. *Phys Lett B.* (2013) **720**:130. doi: 10.1016/j.physletb.2013.01.059
66. Belanger G, Boudjema F, Pukhov A, Semenov A. Dark matter direct detection rate in a generic model with micrOMEGAs 2.2. *Comput Phys Commun.* (2009) **180**:747. doi: 10.1016/j.cpc.2008.11.019
67. Ghorbani K. Fermionic dark matter with pseudo-scalar Yukawa interaction. *JCAP.* (2015) **1501**:015. doi: 10.1088/1475-7516/2015/01/015
68. Patrignani C, Agashe K, Aielli G, Amsler C, Antonelli M, Asner DM, et al. Particle Data Group. Review of particle physics. *Chin Phys C.* (2016) **40**:100001. doi: 10.1088/1674-1137/40/10/100001
69. Cheung K, Ko P, Lee JS, Tseng PY. Bounds on Higgs-Portal models from the LHC Higgs data. *JHEP.* (2015) **1510**:057. doi: 10.1007/JHEP10(2015)057
70. Hartling K, Kumar K, Logan HE. Indirect constraints on the Georgi-Machacek model and implications for Higgs boson couplings. *Phys Rev D.* (2015) **91**:015013. doi: 10.1103/PhysRevD.91.015013
71. Arhrib A, Benbrik R, Chabab M, Moultaka G, Peyranere MC, Rahili L, et al. The Higgs potential in the type II seesaw model. *Phys Rev D.* (2011) **84**:095005. doi: 10.1103/PhysRevD.84.095005
72. Akeroyd AG, Aoki M, Sugiyama H. Probing majorana phases and neutrino mass spectrum in the Higgs triplet model at the CERN LHC. *Phys Rev D.* (2008) **77**:075010. doi: 10.1103/PhysRevD.77.075010
73. Garayoa J, Schwetz T. Neutrino mass hierarchy and Majorana CP phases within the Higgs triplet model at the LHC. *JHEP.* (2008) **0803**:009. doi: 10.1088/1126-6708/2008/03/009
74. Chun EJ, Lee KY, Park SC. Testing Higgs triplet model and neutrino mass patterns. *Phys Lett B.* (2003) **566**:142. doi: 10.1016/S0370-2693(03)00770-6
75. Kadastik M, Raidal M, Rebane L. Direct determination of neutrino mass parameters at future colliders. *Phys Rev D.* (2008) **77**:115023. doi: 10.1103/PhysRevD.77.115023
76. Fileviez Perez P, Han T, Huang GY, Li T, Wang K. Neutrino masses and the CERN LHC: testing type II seesaw. *Phys Rev D.* (2008) **78**:015018. doi: 10.1103/PhysRevD.78.015018
77. Majee SK, Sahu N. Dilepton signal of a type-II seesaw at CERN LHC: reveals a TeV scale B-L symmetry. *Phys Rev D.* (2010) **82**:053007. doi: 10.1103/PhysRevD.82.053007
78. McDonald J, Sahu N, Sarkar U. Type-II seesaw at collider, lepton asymmetry and singlet scalar dark matter. *JCAP.* (2008) **0804**:037. doi: 10.1088/1475-7516/2008/04/03
79. Thomas SD, Wells JD. Phenomenology of massive vectorlike doublet leptons. *Phys Rev Lett.* (1998) **81**:34. doi: 10.1103/PhysRevLett.81.34
80. Aad G, ATLAS Collaboration. Search for invisible decays of a Higgs boson using vector-boson fusion in pp collisions at $\sqrt{s} = 8$ TeV with the ATLAS detector. *JHEP.* (2016) **1601**:172. doi: 10.1007/JHEP01(2016)172
81. Baek S, Ko P, Park WI. Invisible Higgs decay width vs. dark matter direct detection cross section in Higgs portal dark matter models. *Phys Rev D.* (2014) **90**:055014. doi: 10.1103/PhysRevD.90.055014
82. Djouadi A, Lebedev O, Mambrini Y, Quevillon J. Implications of LHC searches for Higgs–portal dark matter. *Phys Lett B.* (2012) **709**:65. doi: 10.1016/j.physletb.2012.01.062;
83. Peskin ME, Takeuchi T. Estimation of oblique electroweak corrections. *Phys Rev D.* (1992) **46**:381–409.
84. Lavoura L, Silva JP. The oblique corrections from vector–like singlet and doublet quarks. *Phys Rev D.* (1993) **47**:2046–57.
85. del Aguila F, de Blas J, Perez-Victoria M. Effects of new leptons in electroweak precision data. *Phys Rev D.* (2008) **78**:013010. doi: 10.1103/PhysRevD.78.013010
86. Erler J, Langacker P. Precision constraints on extra fermion generations. *Phys Rev Lett.* (2010) **105**:031801. doi: 10.1103/PhysRevLett.105.031801
87. Barbieri R, Pomarol A, Rattazzi R, Strumia A. Electroweak symmetry breaking after LEP-1 and LEP-2. *Nucl Phys B.* (2004) **703**:127. doi: 10.1016/j.nuclphysb.2004.10.014
88. Cynolter G, Lendvai E. Electroweak precision constraints on vector-like fermions. *Eur Phys J C.* (2008) **58**:463. doi: 10.1140/epjc/s10052-008-0771-7
89. Griest K, Seckel D. Three exceptions in the calculation of relic abundances. *Phys Rev D.* (1991) **43**:3191.
90. Chatterjee A, Sahu N. Resurrecting L-type sneutrino dark matter in light of neutrino masses and LUX data. *Phys Rev D.* (2014) **90**:095021. doi: 10.1103/PhysRevD.90.095021
91. Patra S, Sahoo N, Sahu N. Dipolar dark matter in light of the 3.5 keV x-ray line, neutrino mass, and LUX data. *Phys Rev D.* (2015) **91**:115013. doi: 10.1103/PhysRevD.91.115013
92. Goodman MW, Witten E. Detectability of certain dark matter candidates. *Phys Rev D.* (1985) **31**:3059.
93. Essig R. Direct detection of non-chiral dark matter. *Phys Rev D.* (2008) **78**:015004. doi: 10.1103/PhysRevD.78.015004
94. Barman B, Bhattacharya S, Ghosh P, Kadam S, Sahu N. Fermion dark matter with scalar triplet at direct and collider searches. *arXiv*:1902.01217 (2019).
95. Alloul A, Christensen ND, Degrande C, Duhr C, Fuks B. FeynRules 2.0—a complete toolbox for tree-level phenomenology. *Comput Phys Commun.* (2014) **185**:2250. doi: 10.1016/j.cpc.2014.04.012
96. Alwall J, Herquet M, Maltoni F, Mattelaer O, Stelzer T. MadGraph 5: going beyond. *JHEP.* (2011) **1106**:128. doi: 10.1007/JHEP06(2011)128
97. Sjostrand T, Mrenna S, Skands PZ. PYTHIA 6.4 physics and manual. *JHEP.* (2006) **0605**:026. doi: 10.1088/1126-6708/2006/05/026
98. Bhattacharya S, Ghosh P, Sahu N. Multipartite dark matter with scalars, fermions and signatures at LHC. *JHEP.* (2019) **1902**:059. doi: 10.1007/JHEP02(2019)059
99. Bhattacharya S, Karmakar B, Sahu N, Sil A. Flavor origin of dark matter and its relation with leptonic nonzero θ_{13} and Dirac CP phase δ. *JHEP.* (2017) **1705**:068. doi: 10.1007/JHEP05(2017)068
100. Bhattacharya S, Karmakar B, Sahu N, Sil A. Unifying the flavor origin of dark matter with leptonic nonzero θ_{13}. *Phys Rev D.* (2016) **93**:115041. doi: 10.1103/PhysRevD.93.115041

Conflict of Interest Statement: The authors declare that the research was conducted in the absence of any commercial or financial relationships that could be construed as a potential conflict of interest.

APPENDIX A: COUPLINGS OF ILD DARK MATTER WITH SCALAR TRIPLETS AND SM PARTICLES

Trilinear vertices involving ILD and triplet Scalar:

$$\begin{aligned}
\overline{(N^-)^c} N^- H^{++} &: \sqrt{2} f_N \\
\overline{(N^-)^c} N^0 H^+ &: f_N \\
\overline{(N^0)^c} N^0 H_1 &: -\sin\alpha\, f_N \\
\overline{(N^0)^c} N^0 H_2 &: -\cos\alpha\, f_N \\
\overline{(N^0)^c} N^0 A^0 &: -i f_N
\end{aligned} \tag{A1}$$

Trilinear vertices involving triplet scalars:

$$\begin{aligned}
H^{++} H^- H^- &: \sqrt{2} v_t \lambda_3 \quad \propto \quad 1/v_t \\
H^{++} H^{--} H_2 &: -\left(2\cos\alpha\ v_t \lambda_2 - \sin\alpha\ v\ \lambda_1\right) \\
&\xrightarrow{\sin\alpha \to 0} \quad -2 v_t \lambda_2 \quad \propto \quad 1/v_t \\
H^{++} H^{--} H_1 &: -\left(\cos\alpha\ v\lambda_1 + 2\sin\alpha\ v_t\ \lambda_2\right)
\end{aligned} \tag{A2}$$

Trilinear vertices involving ILD and SM particles:

$$\begin{aligned}
\overline{N^0} N^- W^+ &: \frac{e_0}{\sqrt{2}\sin\theta_W}\gamma^\mu \\
N^- N^+ Z &: -\frac{e_0}{\sin 2\theta_W}\cos 2\theta_W \gamma^\mu \\
N^- N^+ A &: -e_0\gamma^\mu \\
\overline{N^0} N^0 Z &: \frac{e_0}{\sin 2\theta_W}\gamma^\mu
\end{aligned} \tag{A3}$$

frontiers in Physics

REVIEW
published: 04 June 2019
doi: 10.3389/fphy.2019.00076

GUT Physics in the Era of the LHC

Djuna Croon[1], *Tomás E. Gonzalo*[2,3]*, *Lukas Graf*[4,5], *Nejc Košnik*[6,7] *and Graham White*[1]

[1] TRIUMF Theory Group, Vancouver, BC, Canada, [2] Department of Physics, University of Oslo, Oslo, Norway, [3] ARC Centre of Excellence for Particle Physics at the Tera-Scale, School of Physics and Astronomy, Monash University, Melbourne, VIC, Australia, [4] Department of Physics and Astronomy, University College London, London, United Kingdom, [5] Max-Planck-Institut für Kernphysik, Heidelberg, Germany, [6] Department of Physics, University of Ljubljana, Ljubljana, Slovenia, [7] Jožef Stefan Institute, Ljubljana, Slovenia

Grand Unified Theories (GUTs) are one of the most interesting high-energy completions of the Standard Model, because they provide a rich, powerful and elegant group-theoretical framework able to resolve a variety of problems remaining in our current understanding of particle physics. They usually act as motivators for many low energy BSM theories, such as left-right symmetric or supersymmetric models, and they serve to fill the gap between the experimentally reachable low energies and the physics in the ultraviolet. In recent years, however, they have fallen slightly from the spotlight, in favor of "simplified" models with more specific phenomenological predictions. The aim of this review is to summarize the state of the art on GUTs and argue for their importance in modern physics. Recent advances in experiments permit to test the predictions of GUTs at different energy scales. First, as GUTs can play a role in the inflationary dynamics of the early Universe, their imprints could be found in the CMB observations by the Planck satellite. Remarkably enough, GUTs could manifest themselves also in terrestrial tests; several planned experiments aim to probe the proton stability and to establish order of magnitude higher bounds on its lifetime. Moreover, the predictions of specific GUT models could be tested even at the LHC thanks to its high energy reach, via searches for exotic states or additional contributions to flavor anomalies.

Keywords: grand unified theories, supersymmetry, colliders, neutrinos, cosmology, gravitational waves, flavour, leptoquarks

OPEN ACCESS

Edited by:
António Pestana Morais, University of Aveiro, Portugal

Reviewed by:
Zhenbin Wu, University of Illinois at Chicago, United States
Joel Wesley Walker, Sam Houston State University, United States

***Correspondence:**
Tomás E. Gonzalo
tomas.gonzalo@monash.edu

Specialty section:
This article was submitted to High-Energy and Astroparticle Physics, a section of the journal Frontiers in Physics

Received: *15 December 2018*
Accepted: *02 May 2019*
Published: *04 June 2019*

Citation:
Croon D, Gonzalo TE, Graf L, Košnik N and White G (2019) GUT Physics in the Era of the LHC. Front. Phys. 7:76. doi: 10.3389/fphy.2019.00076

1. INTRODUCTION

The Standard Model (SM) [1–3] of particle physics is an incredible successful theory of subatomic physics. It describes the electroweak and strong interactions of fundamental particles with surprising accuracy up to the energy scales of modern day experiments. Further supported by the discovery of the Higgs boson [4, 5], it stands as one of the best evidences that symmetries and the mechanism of spontaneous symmetry breaking play a critical role on the Universe at the smallest scales [6–8].

In spite of its success at explaining with astonishing precision most of the observed phenomena, the SM cannot be the ultimate theory of particle physics. The Higgs quartic coupling in the SM becomes negative at scales $\gtrsim 10^{10}$ GeV, rendering the vacuum state of the theory unstable at high energies [9]. New physics must then surface below or around that scale to stabilize the vacuum. Furthermore, there is a continuously increasing amount of observations that are in tension with the predictions of the SM. From the discovery of neutrino oscillations [10, 11] to the recent anomalies in the flavor sector [12–14], these phenomena cannot be explained with the SM alone and contributions from beyond the SM (BSM) physics may be required to accommodate them.

Grand Unified Theories (GUTs) [15–19] are well motivated extensions of the SM that can address several of its outstanding issues. As the SM does for electromagnetism and weak nuclear decays, GUTs exploit the power of symmetries and group theory to unify the electroweak and strong interactions into a single force. As can be noticed in **Figure 1**, the flow of the SM gauge couplings already hints at a possible unification at a high scale, thereby providing further motivation for GUTs as appealing BSM models.

The predicted unification of forces provides an explanation for the *ad hoc* nature of the SM charge assignments and their accidental anomaly cancellation [20, 21]. Through the introduction of new fields and symmetries, GUTs can resolve many of the issues of the SM: they can provide an explanation for the lightness of neutrino masses, as well as introducing additional contributions that can accommodate some of the observed flavor anomalies. In addition, GUTs can also live alongside other BSM models, such as Supersymmetry (SUSY), with both theories complementing each other and on the whole becoming a better candidate for a successful BSM theory [22].

Naturally living at high energies, it is expected that GUTs have some observable consequences for the cosmological evolution of the Universe, as they can play a role during the inflationary epoch and their phase transitions may be the source for matter-antimatter asymmetry or gravitational waves [23]. With or without SUSY, GUTs also make predictions that can be tested at low energy experiments such as particle colliders, which can search for new exotic states or deviations on flavor observables. Some of its high energy repercussions can also be probed with precision experiments, with nucleon decay measurements at the forefront. In short, Grand Unified Theories have observable effects in many fronts and can be probed by current and upcoming experiments in the near future.

Therefore, throughout this review we will focus on the description of GUT models and their observable consequences. We will introduce the basic concepts and summarize some of the modern research in GUTs. Out of all the possible observable probes of GUTs, we will focus on a subset of them. In the cosmological front we will outline the advances on inflationary GUTs, detail their observable gravitational wave signatures, from cosmic strings and phase transitions, and their relation with mechanisms for baryo and leptogenesis. The low energy front will cover collider searches for supersymmetry, leptoquarks and exotic states. Lastly, a number of precision tests of unification will be detailed, including nucleon decay, flavor observables and neutrinoless double beta decay.

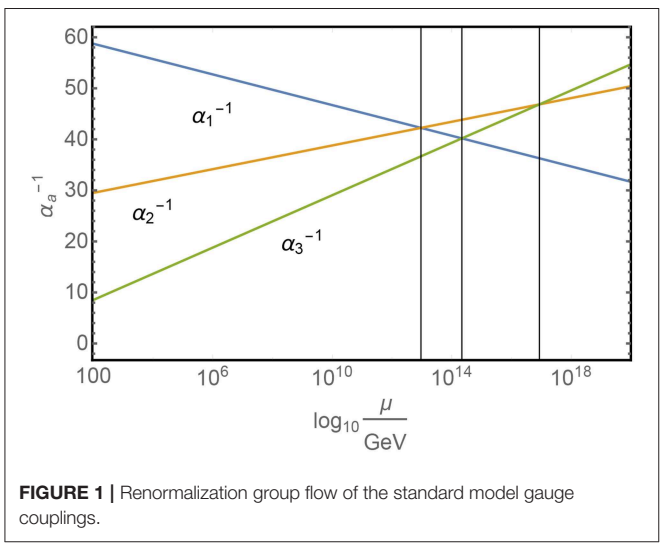

FIGURE 1 | Renormalization group flow of the standard model gauge couplings.

As ultraviolet (UV) completions of the Standard Model that live at very high energies, GUTs are often closely related to theories of gravity, such as string theory. In fact, many unified theories arise as four-dimensional compactifications in some realization of superstring theory [24, 25]. However, throughout this review we will not concern ourselves with these string theory realizations. For a review on embedding GUTs in the heterotic string and outcomes of string compactification for unified theories see Raby [22].

2. BASICS ON GUT MODELS

Grand Unified Theories are extensions of the SM with larger symmetry groups. Strictly speaking, GUTs require that the unified group be a simple group, e.g., $SU(5)$, $SO(10)$, or E_6. However, here we use the term GUT more loosely, referring to any extension of the SM symmetries including product groups such as $SU(5) \times U(1)$ and $SU(4) \times SU(2) \times SU(2)$. Candidate groups for a realistic GUT model must satisfy two conditions: they must contain the SM group as a subgroup and they must have complex representations that reproduce the chiral structure of the SM. Although groups with pseudoreal representations have been studied as candidates for unified theories, E_7 [26], we will not consider them here.

2.1. *SU*(5)

The first appearance of a GUT in the literature dates back to 1974 when H. Georgi and S. Glashow proposed the unification of the SM gauge group into a simple group, $SU(5)$ [15]. In their proposal all the left-handed fermions of a single generation fell into two representations of the group, $\bar{\mathbf{5}}$ and **10**, in the following way

$$\bar{\mathbf{5}} \leftrightarrow \begin{pmatrix} d_1^c \\ d_2^c \\ d_3^c \\ e \\ -\nu \end{pmatrix}, \quad \mathbf{10} \leftrightarrow \begin{pmatrix} 0 & u_3^c & -u_2^c & u_1 & d_1 \\ -u_3^c & 0 & u_1^c & u_2 & d_2 \\ u_2^c & -u_1^c & 0 & u_3 & d_3 \\ -u_1 & -u_2 & -u_3 & 0 & e^c \\ -d_1 & -d_2 & -d_3 & -e^c & 0 \end{pmatrix}. \quad (1)$$

and the gauge and Higgs sector of the theory were embedded into the **24** and **5** representations, respectively. In addition to the SM Higgs boson present in the representation **5**, often a scalar $\bar{\mathbf{5}}$ representation is also present, which contains a second $SU(2)_L$ doublet, necessary for UV completions of two-Higgs doublet models (2HDM) [27].

The Georgi-Glashow (GG) model was the first attempt of a fully-unified model for particle physics, and it provided a neat explanation for the hypercharge quantization in the SM. The

traceless hypercharge generator can be written as [21]

$$Y = \alpha \, \mathrm{diag}(-\tfrac{1}{3}, -\tfrac{1}{3}, -\tfrac{1}{3}, \tfrac{1}{2}, \tfrac{1}{2}) \tag{2}$$

which when acting upon the representations of $SU(5)$ results in the specific hypercharge assignments of the SM fields, i.e., for $\alpha = 1$, $Y(Q) = 1/6$, $Y(L) = -1/2$, $Y(u^c) = -2/3$, $Y(d^c) = 1/3$ and $Y(e^c) = 1$. In unified theories one often uses the "GUT normalization" of the hypercharge, which corresponds simply to a rescaling of the charges and gauge couplings as $Y_{GUT} = \sqrt{3/5}\, Y$ and $g_1 = \sqrt{5/3}\, g'$ [28].

Spontaneous symmetry breaking of $SU(5)$ happens when a scalar field in a non-trivial representation of the group acquires a vacuum expectation value (vev). The minimal representation of $SU(5)$ that can achieve this goal while keeping the SM phase unbroken is the **24** [15, 29]. This vev provides a mass to the off-diagonal $SU(5)$ gauge bosons while the SM gauge bosons remain massless.

By virtue of the unification into a single gauge group, the GG model requires strict unification of the SM gauge couplings, which is hinted at but not really achieved in the SM [28, 29], as can be seen in **Figure 1**, as well as that of Yukawa couplings for each of the two representations, a difficult task in its minimal version [30, 31].

The minimal $SU(5)$ version suffers from other afflictions beyond the failed gauge and Yukawa unification mentioned above. One of these is the introduction of an artificial hierarchy, known as doublet-triplet splitting [32, 33], in the components to the Higgs representation **5**. The colored components must be quite heavy to avoid rapid proton decay whereas the uncolored components must be relatively light, for they correspond to the SM Higgs doublet, now know to have a mass of $m_h = 125.18$ GeV [34]. Solutions to this problem in several $SU(5)$ models have been proposed, such as the "missing partner mechanism" [33, 35] or the "double missing partner mechanism" [36, 37].

Another case where the minimal $SU(5)$ falls short is the lack of a mechanism for the generation of neutrino masses. Extended scalar sectors can generate neutrino masses in the type-I [38] and type-III [39] seesaw mechanisms[1], but the resulting theories are often non-renormalisable. Renormalisable $SU(5)$ models can also be constructed where the neutrino masses are generated via a mixture of type-I and type-III seesaw [40] or the Zee mechanism [41, 42].

Worst of all, however, is the fact that the vanilla $SU(5)$ model predicts rapid proton decay. The lifetime of the proton can be naively estimated as [30]

$$\tau_p \sim \frac{M_X^4}{m_p^5}, \tag{3}$$

with m_p the mass of the proton and M_X the mass of the mediator field at the scale of unification. The apparent unification of gauge couplings happens at an energy scale $\mu \sim 10^{15}$ GeV, which gives a half life for the proton of the order of 10^{31} years, far below the experimental bound from the Super-Kamiokande experiment of 1.6×10^{34} years [43]. Particular choices of the Higgs sector of the $SU(5)$ model, however, avoid this issue, rendering non-minimal $SU(5)$ models viable candidates [44–46]. Furthermore, $SU(5)$ models with vector-like fermions can be consistent with current limits and even predict an upper bound on the lifetime of proton decay [47].

One of the fundamental issues with GUT models, which remains as a concern today, is the gauge hierarchy problem. The large hierarchy between the mass scale of unification and the electroweak scale poses a problem since it causes large loop corrections to the Higgs mass [48]. Supersymmetry (SUSY) was proposed as a solution to this issue [49] and even acted as a motivation for unified theories since some of its minimal realizations, such as the MSSM, predicted the unification of gauge couplings, as can be seen in **Figure 2**.

Supersymmetric GUTs are in fact rather popular and have in some cases been proven to be more successful at representing nature than regular GUTs [50]. In SUSY $SU(5)$ theories the scale of unification is typically larger than in non-supersymmetric models[2], around $\mu \sim 2 \times 10^{16}$ GeV as can be seen in **Figure 2**. This has two advantageous consequences for these models: the larger mass scale for the gauge mediators imposes a further suppression on nucleon decay processes, consistent with experimental measurements [50]; and pushes the unification scale beyond the scale of inflation, which helps to dilute the magnetic monopoles naturally present in the theory [52]. Another issue in vanilla $SU(5)$ models that can be addressed in its supersymmetric version is the doublet-triplet splitting, where the Higgs doublets are made light via cancellations of the superpotential parameters [32, 33, 53, 54].

2.2. Flipped *SU*(5)

An alternative solution to the issues of $SU(5)$ models, without supersymmetry, is what is now known as *flipped* $SU(5)$ [55, 56]. The flipped version differs from regular $SU(5)$ in its gauge group, extended to $SU(5) \times U(1)$, and the manner in which the SM particle fields are embedded into representations of the group. In contrast to Equation (1), the matter representations in the flipped $SU(5)$ model are

$$\overline{\mathbf{5}} \leftrightarrow \begin{pmatrix} u_1^c \\ u_2^c \\ u_3^c \\ e \\ -\nu \end{pmatrix}, \quad \mathbf{10} \leftrightarrow \begin{pmatrix} 0 & d_3^c & -d_2^c & u_1 & d_1 \\ -d_3^c & 0 & d_1^c & u_2 & d_2 \\ d_2^c & -d_1^c & 0 & u_3 & d_3 \\ -u_1 & -u_2 & -u_3 & 0 & \nu^c \\ -d_1 & -d_2 & -d_3 & -\nu^c & 0 \end{pmatrix}, \quad \mathbf{1} \leftrightarrow \left(e^c\right), \tag{4}$$

where ν^c labels the right-handed neutrino field, whose presence provides a mechanism for neutrino mass generation, which was absent in vanilla $SU(5)$.

With these different embeddings of the SM fields, the hypercharge operator is no longer contained in $SU(5)$, as in Equation (2), but it is rather a combination of diagonal generators of both $SU(5)$ and $U(1)$. With standard normalization the

[1] See section 3.2 for details on neutrino mass generation through the seesaw mechanism.

[2] A detailed description of unification in SUSY $SU(5)$ can be found in Dorsner et al. [51].

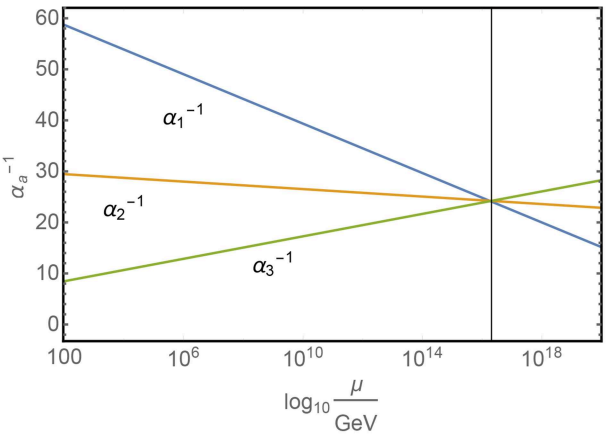

FIGURE 2 | Renormalization Group flow of the MSSM gauge couplings.

hypercharge operator can be written as [57]

$$Y = -\frac{1}{5}T_{24} + \frac{1}{5}X, \tag{5}$$

where T_{24} is a diagonal generator of $SU(5)$ and X the $U(1)$ charge.

Due to the extended gauge sector and modified unified conditions of flipped $SU(5)$, proton decay does not become an issue [57]. In addition, in flipped $SU(5)$ magnetic monopoles cannot be created since the supergroup containing the charge operator is not a simple group [52, 57].

As was the case with regular $SU(5)$ models, flipped $SU(5)$ can be extended with the help of supersymmetry. The combination of solutions to the issues of the $SU(5)$ model that both SUSY and flipped $SU(5)$ offer makes SUSY flipped $SU(5)$ one of the most popular GUTs in the literature [58, 59], in spite of not realizing a full unification of gauge couplings.

Flipped $SU(5)$ models are also well motivated from their UV completions, since they can easily be derived naturally from weakly-coupled string theory. As opposed to vanilla $SU(5)$, which undergoes symmetry breaking via a **24**-dimensional representation, the flipped $SU(5)$ model does not require large dimensional representations, as it breaks via a $\mathbf{10}_1$, and it is therefore easier to obtain from a manifold compactification of string theory [60, 61].

2.3. Pati-Salam and the Left-Right Symmetry

Around the same time that the $SU(5)$ model was proposed, R. Pati and A. Salam suggested another extension of the SM [16]. They proposed a rearrangement of the SM fields into a different group configuration, $SU(4)_c \times SU(2)_L \times SU(2)_R$. Though not really a fully unified theory, it provided a partial unification of leptons and quarks into a single color group, $SU(4)_c$, while at the same time introducing another copy of $SU(2)$ for the right-handed sector of the theory. This model automatically contains a right-handed neutrino, embedded into a $SU(2)_R$ doublet with the right-handed charged lepton. Thus, the SM fields fall into two representations of the group in the following way

$$\{\mathbf{4},\mathbf{2},\mathbf{1}\} \leftrightarrow \begin{pmatrix} u_1 & u_2 & u_3 & \nu \\ d_1 & d_2 & d_3 & e \end{pmatrix},$$
$$\{\bar{\mathbf{4}},\mathbf{1},\mathbf{2}^*\} \leftrightarrow \begin{pmatrix} d_1^c & d_2^c & d_3^c & e^c \\ -u_1^c & -u_2^c & -u_3^c & -\nu^c \end{pmatrix}. \tag{6}$$

One of the major successes of the Pati-Salam (PS) model was being the first appearance of a left-right symmetric model, with a right-handed sector $SU(2)_R$ and a heavy right-handed gauge boson W_R [62]. It was also the original proposal for the idea of quark-lepton complementarity. As an amalgamation of the two ideas, the PS group maximally contains the left-right symmetry group, $SU(3)_c \times SU(2)_L \times SU(2)_R \times U(1)_{B-L}$ [17, 63], as well as the quark-lepton unified group, $SU(4)_c \times SU(2)_L \times U(1)_R$ [64, 65].

Left-right symmetric models, *à la* Pati-Salam or of the type $SU(3)_c \times SU(2)_L \times SU(2)_R \times U(1)_{B-L}$, are fairly popular because they naturally include a right-handed neutrino and can generate light neutrino masses via some type of seesaw mechanism [66, 67]. Similar to PS, left-right symmetric (LR) models are not fully unified theories, yet they can be an intermediate step on the breaking chain of a PS model [68] or some other unified theory [69].

Symmetry breaking in the PS model can happen through a number of different paths, depending on the vev of the scalar fields in the theory. The most compelling paths preserve either the LR symmetry, with the LR group $SU(3)_c \times SU(2)_L \times SU(2)_R \times U(1)_{B-L}$ as an intermediate step, or quark-lepton unification, with $SU(4)_c \times SU(2)_L \times U(1)_R$ as a subgroup [70]. Further symmetry breaking from the LR symmetry model happens when either a pair of $SU(2)$ doublets (one left-handed and one right-handed) [62, 71], or a pair of $SU(2)$ triplets (left and right-handed) [68] acquire a vev. In both PS and LR theories, the hypercharge operator is written as a linear combination of the diagonal $SU(2)_R$ generator and the $B - L$ charge [$U(1)_{B-L}$ generator embedded in $SU(4)_c$ in PS] as

$$Y = T_R^3 + \frac{1}{2}(B - L). \tag{7}$$

As opposed to the case of $SU(5)$ the proton is often stable in PS and LR models. This occurs because the gauge sector of the theory preserves B and L number independently and the only scalar fields that can mediate the transition are in antisymmetric representations, rarely seen in PS or LR models [68].

The addition of supersymmetry to PS and left-right symmetric models [72] is not as straightforward as with other GUT models. The simplest scenario with both SUSY and LR symmetry was shown to fail to achieve spontaneous symmetry breaking [73]. In order to circumvent this issue one must either add extra fields, such as a parity-odd singlet[3] [74] or an extra Higgs field [75], or alternatively supplement the Lagrangian with non-renormalizable operators [76]. One of the main advantages of

[3]Although successful in achieving spontaneous symmetry breaking (SSB) in this SUSY LR model, the resulting vacuum state does not preserve the electromagnetic charge.

SUSY LR models, and the reason why so much effort is put on resolving the SSB issue, is that they naturally preserve R-parity, since $B - L$ is a gauge symmetry of the theory, which forbids the dangerous baryon and lepton number violating operators that appear in the MSSM, thereby making the lightest SUSY particle stable [77].

2.4. $SO(10)$

Although the GG and PS models seem quite distinct in their approach to unification, they have a common ancestor. Both $SU(5) \times U(1)$ and $SU(4) \times SU(2) \times SU(2)$ are maximal subgroups of another Lie group of larger dimension, $SO(10)$. This was first realized by Fritzsch and Minkowski [18], and independently by Georgi [19], who proposed a model of unification with several intermediate steps. $SO(10)$ has since been the most popular choice as a unification group, since it provides a vast display of options for field configurations and symmetry breaking patterns.

One of the many key features of $SO(10)$ models is that they fully unify a generation of SM fermions into a single representation of the group. Thus, the 16 Weyl fermions, including right-handed neutrinos, can be embedded into the fundamental **16** representation of $SO(10)$ as

$$\mathbf{16} = \{u_1^c, d_1^c, d_1, u_1, \nu^c, e^c, d_2, u_2, u_2^c, d_2^c, d_3, u_3, u_3^c, d_3^c, e, \nu\}_L. \quad (8)$$

Due to the transformation properties of the $SO(10)$ group, the spinor representation **16** is a complex representation, thereby satisfying chirality as observed in the Standard Model. Additionally $SO(10)$ is a "safe algebra" [78], it does not suffer from anomalies as, for example, the $SU(5)$ case above, which makes model building in $SO(10)$ easier for it does not rely on some specific field configurations to cancel the gauge anomalies [79].

Despite the large amount of $SO(10)$ models in the literature, a common feature is that the gauge fields are embedded in the adjoint representation of the group, that is **45**,

$$\begin{aligned}\mathbf{45} \to\ & \{\mathbf{8}, \mathbf{1},\ 0\} \oplus \{\mathbf{1}, \mathbf{3},\ 0\} \oplus \{\mathbf{1}, \mathbf{1},\ 0\} && \leftarrow \text{SM gauge bosons}\\ & \left.\begin{aligned}&\oplus \{\mathbf{3}, \mathbf{2},\ \tfrac{1}{6}\} \oplus \{\overline{\mathbf{3}}, \mathbf{2}, -\tfrac{1}{6}\} \oplus \{\mathbf{3}, \mathbf{2},\ \tfrac{1}{6}\}\\ &\oplus \{\overline{\mathbf{3}}, \mathbf{2}, -\tfrac{1}{6}\} \oplus \{\overline{\mathbf{3}}, \mathbf{1}, -\tfrac{2}{3}\} \oplus \{\mathbf{3}, \mathbf{1},\ \tfrac{2}{3}\}\\ &\oplus \{\mathbf{1}, \mathbf{1},\ 1\} \oplus \{\mathbf{1}, \mathbf{1}, -1\} \oplus \{\mathbf{1}, \mathbf{1},\ 0\}.\end{aligned}\right\} && \leftarrow \text{leptoquarks},\end{aligned}$$

which contains the SM gauge bosons as well as off-diagonal components which, as happened in $SU(5)$, can mediate quark-lepton transitions, known as leptoquarks. The Yukawa sector in $SO(10)$ models is often also quite recurrent because, at the renormalizable level, it can only be of the form [80]

$$\begin{aligned}\mathcal{L}_{Yuk} = \mathsf{Y} \cdot \mathbf{16}^T C_L C_{10} (\Gamma_i \Phi^i + \Gamma_{[i}\Gamma_j\Gamma_{k]}\Phi^{ijk} +\\ \Gamma_{[i}\Gamma_j\Gamma_k\Gamma_l\Gamma_{m]}\Phi^{ijklm})\mathbf{16}, \quad (9)\end{aligned}$$

where Y is the matrix of Yukawa couplings, C_L and C_{10} the charge conjugation matrices in the Poincaré and $SO(10)$ groups, Γ_i the generators of $SO(10)$ in the spinor representation and Φ^i, Φ^{ijk}, and Φ^{ijklm} are scalar fields in the **10**, **120**, and $\overline{\mathbf{126}}$ representations, respectively. The SM Higgs field is, therefore, some linear combination of these fields and hence the SM fermion masses directly follow from the Yukawa matrix $\mathbf{Y}$ and the vacuum expectation values of the scalar fields. The particular choice of the scalar sector is typically guided by the principle of minimality. While the minimal regular (non-SUSY) $SO(10)$ model with SSB driven by the **45** and **126** Higgs representations has been revived and still represents a phenomenologically viable scenario [81–85], this is not the case of the minimal SUSY $SO(10)$ model [86, 87].

Symmetry breaking in $SO(10)$ models can occur through one of many different paths. Since both $SU(5) \times U(1)$ and $SU(4) \times SU(2) \times SU(2)$ are subgroups of $SO(10)$, they can be an intermediate step on the symmetry breaking path toward the Standard Model, as can be any of their respective subgroup [70, 88, 89]. Alternatively $SO(10)$ can be broken directly to the SM group, without intermediate steps [90]. All the possible breaking paths from $SO(10)$ can be seen in **Figure 3**. The particular symmetry breaking scenario that is realized in a $SO(10)$ model depends exclusively on the scalar sector of the theory and the configuration of the vacuum, and it constitutes one of the major differences among $SO(10)$ models in the literature.

Regular $SO(10)$ models may suffer from some of the same issues as regular $SU(5)$, namely rapid proton decay can occur with a low unification scale. The main solution to this problem, as it was with $SU(5)$, is the addition of supersymmetry. SUSY $SO(10)$ [90, 91] theories are rather popular and given the large number of degrees of freedom they possess, such as symmetry breaking pattern, field content, etc., they can easily avoid many of the traditional issues in unified theories.

Alike to the $SU(5)$ model, it is possible to construct alternative embeddings of the SM fermions into representations of the group via the addition of an Abelian group. In the *flipped* $SO(10) \times U(1)$ model [92] the SM fermion content is not fully embedded into the **16** representation of the group, but rather into the direct product $\mathbf{16}_1 \oplus \mathbf{10}_{-2} \oplus \mathbf{1}_4$. This model loses its unified nature in favor of more degrees of freedom for the Yukawa and symmetry breaking sectors of the theory, which are no longer constrained by the statements above [80].

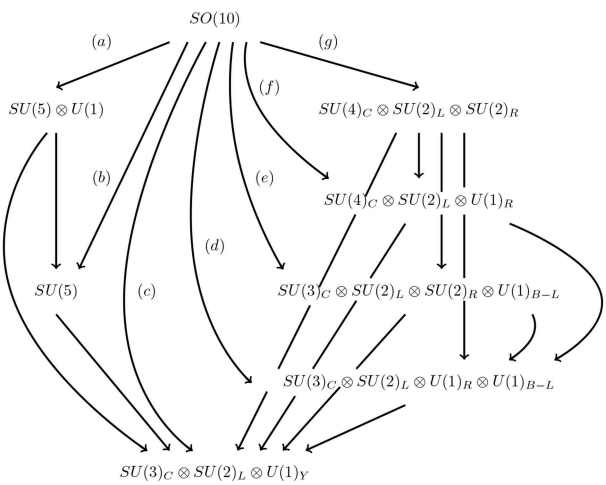

FIGURE 3 | Patterns of symmetry breaking from $SO(10)$ to the SM group [21].

2.5. E_6

The GUT models described so far have unification groups that are part of the infinite series $SU(n)$ or $SO(2n)$, which means that for each successful model with particular n there is an infinite number of alternatives with order larger than n. For instance, the $SO(18)$ group has been studied as a candidate for gauge and family unification [93]. The exceptional algebras, however, are unique so they are more aesthetically appealing candidates as theories of unification [20, 94]. Among all exceptional algebras, only E_6 is large enough to contain the SM as a subgroup and admits complex representations.

The fermionic content in the E_6 theory is embedded in the fundamental **27**-dimensional representation of the group, which contains the SM fermions plus exotic fields. The particular allocations of SM fermions into the **27** representation depends on the subgroup of E_6 that breaks into after SSB, which is typically either the trinification group, $SU(3)_c \times SU(3)_L \times SU(3)_R$ [95–97] or $SO(10) \times U(1)$ [98, 99]. The decomposition of the fundamental **27** into these subgroups is

$$\begin{aligned} \mathbf{27} &\rightarrow \{\mathbf{1},\mathbf{3},\mathbf{3}\} + \{\mathbf{3},\mathbf{3},\mathbf{1}\} + \{\bar{\mathbf{3}},\mathbf{1},\bar{\mathbf{3}}\}, && [SU(3)_c \times SU(3)_L \times SU(3)_R] \\ \mathbf{27} &\rightarrow \mathbf{16}_1 + \mathbf{10}_{-2} + \mathbf{1}_4, && [SO(10) \times U(1)] \end{aligned} \tag{10}$$

The field content in E_6 models is quite vast. There are 78 gauge bosons, of which only 45 survive at lower scales if $SO(10)$ is the breaking path, or even fewer in the case of $SU(3) \times SU(3) \times SU(3)$, just 24. The minimal scalar content needs at least a scalar field in the combination $\overline{\mathbf{27}} + \overline{\mathbf{351}} + \overline{\mathbf{351}'}$, which contains the SM Higgs, and a scalar responsible for SSB of E_6, which is dependent upon the pattern of symmetry breaking, e.g., a **78** for breaking to $SO(10) \times U(1)$.

One of the main motivations for E_6 as a unification group comes from superstring theory, where it was shown to emerge as a four-dimensional compactification of the heterotic $E_8 \times E_8$ superstring theory [24, 25]. In fact, the presence of compactified extra dimensions near the scale of E_6 breaking can trigger symmetry breaking of the E_6 group via the Hosotani mechanism [100] straight into $SU(3) \times SU(2) \times U(1) \times U(1) \times U(1)$.

Most of the research in E_6 theories has been typically considered only within the scope of supersymmetry, which ties in with their motivation as low-energy limits of superstring theory where spacetime supersymmetry emerges naturally after compactification. Being a simple Lie group, E_6 benefits from the prediction of gauge coupling unification in supersymmetry, as did $SU(5)$ and $SO(10)$, which strengthens the motivation. In addition to the rich phenomenology of the MSSM, the E_6 model adds quite a few phenomenological predictions on its own, from exotic fermion states to new heavy gauge bosons [101, 102].

3. SELECTED TOPICS IN GUTS

Model building in unified theories involves more than the selection of the group theory properties as introduced in section 2. There are a few outstanding issues that need to be addressed in order to construct a realistic model. Gauge coupling unification is typically one of the most pressing issues, which can often be resolved by intermediate steps in the breaking chain or by the addition of supersymmetry to the theory. In this section we describe the interplay between SUSY and GUTs, as well as other topics such as the generation of light neutrino masses and the unification of the Yukawa couplings.

3.1. Supersymmetry and GUTs

Supersymmetry is a very appealing theory on its own right. It is one of the most aesthetically pleasing extensions of the Standard Model and it has an extremely rich phenomenology that can be readily tested at colliders and other experiments. SUSY GUTs [22] are a conglomerate of the numerous advantages of unified theories and the predicting power of supersymmetry. One of the most attractive features of SUSY is that it can stabilize the electroweak scale against quantum corrections, the so called *hierarchy problem* [103, 104] and provides a mechanism for dynamic electroweak symmetry breaking [105, 106].

In addition, if R-parity is conserved [107] the lightest supersymmetric particle (LSP) is stable. Therefore, SUSY automatically predicts the existence of a Dark Matter candidate and can easily produce scenarios with the correct relic abundance [108, 109].

As previously mentioned, one of the major motivations for SUSY GUTs is that the minimal MSSM model predicts gauge coupling unification at some high scale $\sim 10^{16}$ [110]. As was seen in **Figure 2**, just taking the one-loop RGE flow of the gauge couplings, the unification at the GUT scale is fairly successful. The RGEs for the gauge couplings at one-loop have an analytic solution of the form [111]

$$\alpha_i^{-1}(\mu) = \alpha_{GUT}^{-1} + \frac{b_i}{2\pi} \log\left(\frac{M_{GUT}}{\mu}\right) \tag{11}$$

where $i = 1, 2, 3$ labels the coupling of the $U(1)$, $SU(2)$, and $SU(3)$ subgroups of the SM gauge group, and b_i are parameters that depend on the field content. For the MSSM these are $b_i = (33/5, 1, -3)$. With a degenerate sparticle spectrum at 100 GeV, these one-loop RGEs unify at $M_{GUT} \sim 2.5 \times 10^{16}$ GeV with $\alpha_{GUT} \sim 0.0388$.

This picture, however, relies on a light and almost degenerate supersymmetric spectrum. For heavier or split spectra the situation changes drastically, often spoiling gauge unification altogether. A unification measure can be defined to assess how the unification of gauge couplings changes with the masses of the supersymmetric particles as

$$\Delta\mu = \frac{\min(\mu_{12}, \mu_{23})}{\max(\mu_{12}, \mu_{23})}, \tag{12}$$

where μ_{ij} is the energy scale at which α_i^{-1} and α_j^{-1} unify. **Figure 4** shows how the unification measure varies with respect to the SUSY scale for an MSSM model with degenerate SUSY masses (blue). One can distinctly see that for larger sparticle masses, the unification of gauge couplings significantly worsens, from a 70% unification for $M_{SUSY} \sim 100$ GeV to <30% at $M_{SUSY} \sim 1$ TeV.

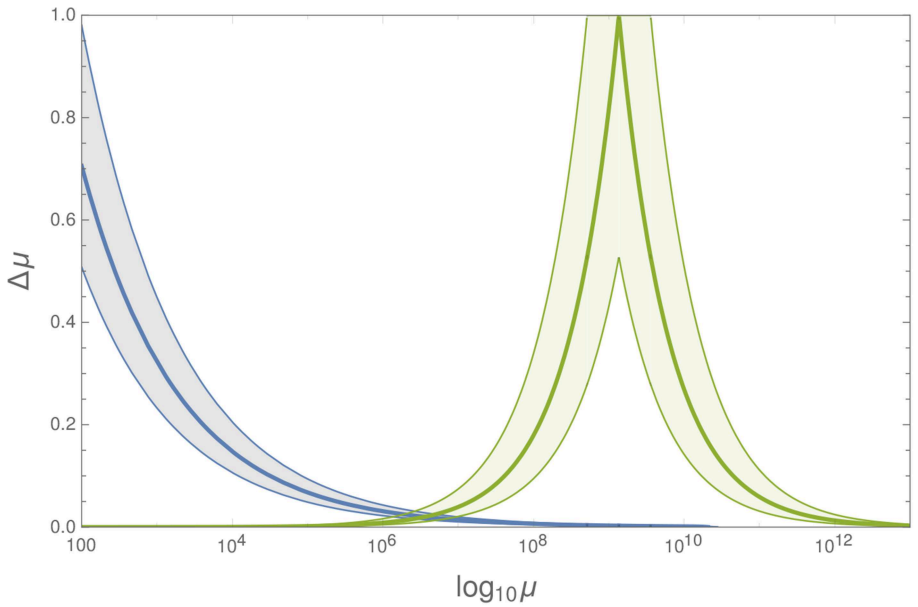

FIGURE 4 | Evolution of the unification measure with the SUSY scale for the MSSM with almost degenerate masses (blue) and scenario with lighter electroweakinos (green), calculated at one-loop. Shaded regions include threshold corrections over the solid lines.

Consequently, in addition to solving the little hierarchy problem without too much fine tuning, a light sparticle spectrum is clearly preferred to achieve gauge coupling unification.

In spite of the appeal of SUSY GUTs, the combined effort of several collider experiments has not found any clear evidences of SUSY particles[4]. Hence, minimal and light versions of the MSSM are in tension with experimental evidence and that makes achieving gauge coupling unification much harder. This tension relaxes slightly once the mass degeneracy condition is forgone. If the sparticle masses vary considerably across the spectrum, it is possible to evade experimental bounds for those masses more strongly constrained (e.g., gluinos, squarks, etc.) while keeping part of the spectrum light. Mass splittings across the supersymmetric spectrum can be taken into account by the contribution of threshold corrections at the SUSY scale, which are of the type [112, 113]

$$\lambda_i(M_{SUSY}) = \frac{1}{12\pi}\left(\sum_{\phi} S_i(\phi)\log\frac{m_\phi}{M_{SUSY}} + 8\sum_{\psi} S_i(\psi)\log\frac{m_\psi}{M_{SUSY}}\right), \tag{13}$$

with ϕ the scalar fields in the MSSM (sfermions), m_ϕ their masses and $S(\phi)$ their Dynkin indices; and ψ the fermions in the MSSM (gauginos and Higgsinos), m_ψ and $S(\psi)$ their masses and Dynkin indices. The shaded blue region in **Figure 4** corresponds to MSSM models with slightly non-degenerate masses. Although these models exhibit the same trend as before, decreasing the unification measure as M_{SUSY} increases, some of these achieve a better gauge coupling unification than the degenerate case, with up to 60% unification for $M_{SUSY} \sim 1$ TeV.

Supersymmetric models with large splittings in the particle spectrum can modify this picture significantly. A special case, known as Split Supersymmetry [114, 115], has all the sfermions decoupled at the GUT scale and only gauginos and Higgsinos remain light, protected by chiral symmetry. This model is very well motivated within the context of unified theory, because the decoupled fields form full multiplets of $SU(5)$, so the unification of the gauge couplings is not affected [114]. Hence, the behavior of the unification measure for these models is identical to the semi-degenerate MSSM case from above (blue line and shaded region in **Figure 4**), but has the advantage of allowing a lighter spectrum since some of the strongest experimental constraints are on the squark masses, which are decoupled from the spectrum. These Split-SUSY models, however, predict the existence of a light gluino, which is unfortunately strongly constrained by experiments. Alternative versions of this model with light electroweakinos ($\sim$ 100 GeV) and heavy gluinos ($\sim$ 5 TeV) have been studied [116], but these fail to provide successful gauge coupling unification for a light spectrum, slowly improving at larger scales, as can be noticed from the green solid line and shaded region (threshold corrections) in **Figure 4**. Split-SUSY and the light electroweakino model are just two extreme cases, the former requiring very light spectrum for successful unification and the latter a heavy spectrum. A number of models can be constructed with different spectra that have intermediate predictions for gauge coupling unification. In fact, with a precise analyses of threshold corrections, a number of supersymmetric models with large mass splittings have been shown to achieve exact unification, with a relatively light spectrum [117].

[4]See section 6.1 for more details on searches for Supersymmetry.

3.2. Neutrino Masses

The observed oscillations of neutrino flavors [10, 118] require any successful extension of the SM to incorporate non-zero masses for at least two neutrino species. Effectively, these masses are generated by the 5-dimensional Weinberg operator

$$\mathcal{O}_W = \frac{c_W}{\Lambda} LLHH, \tag{14}$$

where c_W is the Wilson coefficient, Λ denotes the operator's cut-off scale and L and H are the lepton and Higgs doublets, respectively. A typical UV-completion of this effective operator is some kind of seesaw mechanism [66, 119], which allows to satisfy elegantly the requirement of tiny neutrino mass size. Generally, these neutrino mass schemes assume a presence of new, heavy degrees of freedom, which are ideally motivated by other BSM physics. As has been shown, a number of different seesaw set-ups can be very naturally incorporated within the GUT framework. Provided that only a single type of new particle is added to the SM field content, there are three basic tree-level seesaw types [120].

3.2.1. Seesaw Type I

In the original and simplest seesaw mechanism of type I the right-handed neutrino singlets must be added to the model [66, 121–123]. As the current experimental data require only two neutrinos to be massive, the minimal scenario must include two right-handed neutrino states. This extension then allows to write both Dirac and Majorana neutrino mass terms

$$\mathcal{L}_N = -y^\nu \overline{L}^\ell \tilde{H} N^I - \frac{1}{2}[M_M]_{IJ} {N^I}^T C N^J + \text{h.c.}, \tag{15}$$

where y^ν is the matrix of neutrino Yukawa couplings and M_M denotes the Majorana mass matrix. Hence, taking $m_D = y^\nu v$, with v being the SM Higgs vev, the neutrino mass matrix can be written in the usual form

$$\mathsf{M} = \begin{pmatrix} 0 & m_D \\ m_D^T & M_M \end{pmatrix}. \tag{16}$$

The block-diagonalisation of this matrix leads to the light mass of the oscillating neutrinos

$$M_\nu^I = -m_D M_M^{-1} m_D^T, \tag{17}$$

as the Majorana mass parameter can be chosen to be arbitrarily large. Considering the neutrino Yukawa couplings of order one and the Majorana mass around 10^{14} GeV, the desired neutrino mass sizes of order $m_\nu \approx 0.1$ eV are obtained. The type-I seesaw mechanism can be implemented in the GUT framework. Particularly, it arises very naturally in $SO(10)$ GUT, where the right-handed neutrino singlet can be accommodated together with all the other fermions in a single $\mathbf{16}_F$ spinor representation.

3.2.2. Seesaw Type II

The second possibility to construct a seesaw mechanism is to assume a heavy scalar $SU(2)_L$-triplet Δ_L,

$$\{\mathbf{1},\mathbf{3},2\} \equiv \Delta_L = \mathbf{\Delta}_L \cdot \boldsymbol{\tau} = \begin{pmatrix} \frac{1}{\sqrt{2}}\Delta^+ & \Delta^{++} \\ \Delta^0 & -\frac{1}{\sqrt{2}}\Delta^+ \end{pmatrix}, \tag{18}$$

which allows to write the following Lagrangian terms

$$\mathcal{L}_\Delta = \left[y^\Delta_{\ell\ell'} {L^\ell}^T C(i\tau^2)\Delta_L L^{\ell'} + \mu H^T (i\tau^2)\Delta_L^* H + \text{h.c.} \right] + M_\Delta^2 Tr[\Delta\Delta^\dagger]. \tag{19}$$

Diagonalisation of the type-II seesaw mass matrix [67, 124, 125] then generates neutrino mass

$$M_\nu^{II} = \frac{\mu v^2}{M_\Delta^2} y^\Delta \tag{20}$$

and for $M_\Delta \gg v$ the required suppression is obtained.

Also this seesaw can be responsible for neutrino mass generation in GUTs. For instance, in $SO(10)$ unification the left-handed scalar triplet is contained by the **126** Higgs field, which is usually considered to be present in the scalar sector of the theory. It has been shown that type-II seesaw can be the dominant neutrino mass scheme within both SUSY [126] and non-SUSY [127] $SO(10)$ GUTs.

3.2.3. Seesaw Type III

The third option for a UV-completion of the Weinberg operator in Equation (14) is to introduce new fermionic $SU(2)_L$ triplets $\mathbf{T}_F^I$ [128][5]. Their interaction with the SM content is analogous to the type I seesaw, namely,

$$\mathcal{L}_{T_F} = y^{T_F}_{\ell J} {L^\ell}^T C(i\tau^2)(\mathbf{T}_F^J \cdot \boldsymbol{\tau})H + M_{IJ}^{T_F} (\mathbf{T}_F^I)^T C \mathbf{T}_F^J + \text{h.c.}. \tag{21}$$

The neutrino mass matrix for type III seesaw then reads

$$M_\nu^{III} = (y^{T_F})^T v^2 [M^{T_F}]^{-1} y^{T_F} \tag{22}$$

and for $M^{T_F} \gg y^{T_F} v$ the smallness of neutrino masses is ensured.

The incorporation of the type-III seesaw mechanism into GUTs has been studied in literature [39, 120, 129]. When implemented within $SU(5)$ models, type-III seesaw comes automatically in hand with the type-I seesaw, as both fields responsible for these mechanisms share the same adjoint representation $\mathbf{24}_F$.

3.2.4. Inverse Seesaw

At low energies the light neutrino masses can be generated at tree level via the so called inverse seesaw mechanism. This string theory motivated [25] scheme can be constructed when a non-minimal lepton content of a given theory is assumed. Namely, extra singlet leptons must be added to the model, which is in general allowed for any gauge theory [119]. The minimalistic extension of the SM particle content leading to inverse seesaw requires a pair of left-handed two-component lepton singlets N^c and S [98]. Taking three generations of these new singlet fields, one can write the 9×9 mass matrix of the neutral leptons in the basis $\{\nu_L^\ell, N^{I^c}, S^A\}$ (with $A = a, b, c$) as

$$\mathsf{M}^{\text{IS}} = \begin{pmatrix} 0 & m_D & 0 \\ m_D^T & 0 & M \\ 0 & M^T & \mu \end{pmatrix}, \tag{23}$$

[5] Similarly to the right-handed neutrino singlets, only two triplets are necessary, although three (one per flavor) are considered here.

where M and μ are the mass matrices corresponding to the $SU(2)_L$ singlets, while m_D is the Dirac neutrino mass matrix as usual. As predicted by some string models, the Majorana mass entries corresponding to ν_L and N are zero. Thus, the only Majorana mass parameter is the matrix μ, which corresponds to the extra singlet S. This entry is then responsible for lepton number violation. If μ is set to be zero, the $B-L$ symmetry is restored, the matrix $\mathsf{M}^{\rm IS}$ degenerates and the three oscillating neutrinos become massless.

On the other hand, for non-vanishing μ such that $\mu \ll m_D \ll M$ the resulting mass matrix of the light neutrino eigenstates reads

$$M_\nu^{\rm IS} = m_D M^{-1} \mu [M^T]^{-1} m_D^T. \tag{24}$$

The main difference from the standard seesaw scenarios is that in the present case neutrinos become light for $\mu \to 0$, not for large values of Majorana mass parameter. This is also the reason why one talks about "inverse" seesaw. As vanishing μ enhances the symmetry of the theory, the assumption of its small value can be considered to be natural [130, 131].

3.2.5. Linear Seesaw

A particularly interesting realization of the inverse seesaw mechanism can be constructed within the $SO(10)$ GUTs framework with broken D-parity [132]. The so called linear seesaw mechanism consists in extending the minimal fermionic content of the $SO(10)$ model, contained by three copies of the $\mathbf{16}_F$ representation, by three gauge singlets S^A. The original version of this scheme was designed within the supersymmetric $SO(10)$ framework; however, it can be constructed also in non-supersymmetric scenarios. The mass matrix for the neutral fermions in the basis $\{\nu_L^\ell, N^{I^c}, S^A\}$ has the following form

$$\mathsf{M}^{\rm LS} = \begin{pmatrix} 0 & \mathrm{m}_D & \mathrm{m}_L \\ \mathrm{m}_D^T & 0 & \mathrm{M} \\ \mathrm{m}_L^T & \mathrm{M}^T & 0 \end{pmatrix}. \tag{25}$$

Here, m_D denotes the Dirac neutrino mass, M is the heaviest Dirac neutrino mass term mixing N-S and m_L stands for the small term mixing ν-S, which breaks the $(B-L)$ symmetry. The light neutrino masses are then given by the expression

$$\mathrm{M}_\nu^{\rm LS} \simeq \mathrm{m}_D^T \mathrm{M}^{-1} \mathrm{m}_L + (\mathrm{M}^{-1}\mathrm{m}_L)^T \mathrm{m}_D, \tag{26}$$

which depends linearly on m_D (and therefore also on corresponding Yukawa couplings). In the present scenario it is the large parameter M given by the unification scale what ensures the smallness of neutrino masses. Hence, the lightness of neutrinos is independent of the $(B-L)$ symmetry breaking scale, which can consequently lie at low, experimentally accessible energies without spoiling the desired size of neutrino masses or the unification.

3.2.6. Other Neutrino Mass Models

Despite the success of seesaw mechanisms, one can think of a number of alternative neutrino mass generation schemes. From the phenomenological point of view, these can be even more interesting, as they often predict (unlike the three usual seesaws) a low-energy origin of neutrino masses. The light neutrino masses are obtained using a small lepton-number-violating parameter (similarly as in the inverse seesaw), or they can be suppressed by loops and small Yukawa couplings. While the former option can be realized e.g., within supersymmetric models with R-parity breaking [133], the latter possibility refers to the models of neutrino mass generation via calculable radiative corrections (i.e., the Zee mechanism) [41, 134]. A two-loop mechanism generating neutrino masses within a minimal $SO(10)$ GUT was identified by Witten [135] and the same scheme can be constructed also in the flipped $SU(5)$ context [136–138].

3.3. Yukawa Coupling Unification and Fermion Masses

In fully unified theories, such as $SU(5)$ and $SO(10)$, the gauge couplings must unify at some high energy scale. This is typically achieved automatically in SUSY GUTs, as mentioned above, due to the RGE flow of the MSSM gauge couplings (c.f. **Figure 2**), but it can also be achieved through the addition of new scalar representations [139] or with a multi-step symmetry breaking pattern [91].

Along gauge coupling unification, $SU(5)$ and $SO(10)$ models also require the unification of the Yukawa couplings. The largest hierarchy on the fermion masses happens in the third generation where $m_t/m_b \sim 40$ and $m_b/m_\tau \sim 2.3$, hence Yukawa unification in GUTs is always studied within the third generation only. In $SU(5)$ the charged leptons live in the same representation as the down-type quarks, $\overline{\mathbf{5}}$, and as such it is expected that at the GUT scale $y_b = y_\tau$, whereas in $SO(10)$ all SM fermions are embedded into the same 16-dimensional representation, so the unification condition becomes $y_t = y_b = y_\tau$.

Although a natural prediction of GUTs, Yukawa unification is not easily achieved in the vanilla $SU(5)$ and $SO(10)$ models [29–31]. As can be seen in the left-side plot of **Figure 5**, the Yukawa couplings in the SM are far from unification. In spite of this, a few successful attempts to solve the unification of y_b and y_τ in $SU(5)$ inspired models have been performed, either by including large scalar $SU(5)$ representations to the field content [31, 139, 140] or by adding Planck scale suppressed interaction of the Higgs field to the SM fermions [141].

In SUSY GUTs, however, Yukawa unification can often be achieved in some regions of the full supersymmetric parameter space. As can be seen in the right-side picture in **Figure 5**, the Yukawa couplings in the MSSM tend to run toward convergence at high scales, and they can be seen to almost unify for large values of $\tan\beta$ [142–145]. This occurs because the third generation fermion masses depend on $\tan\beta$ in the following way [146]

$$m_t = \frac{v}{\sqrt{2}} y_t \sin\beta, \quad m_b = \frac{v}{\sqrt{2}} y_b \cos\beta, \quad m_\tau = \frac{v}{\sqrt{2}} y_\tau \cos\beta, \tag{27}$$

which can realize the hierarchy $m_t \gg m_b, m_\tau$ even in $SO(10)$ or E_6 models where one expects $y_t \sim y_b \sim y_\tau$. These solutions with large $\tan\beta$ can spoil radiative EW symmetry breaking in unified models, since $B\mu \simeq \frac{M_A^2}{\tan\beta} \simeq 0$ implies that $m_{H_d}^2 - m_{H_u}^2 > m_Z^2$ [147], contrary to the unified picture where $m_{H_u}^2 = m_{H_d}^2$. This issue can often be resolved either by *ad hoc* splittings of the Higgs

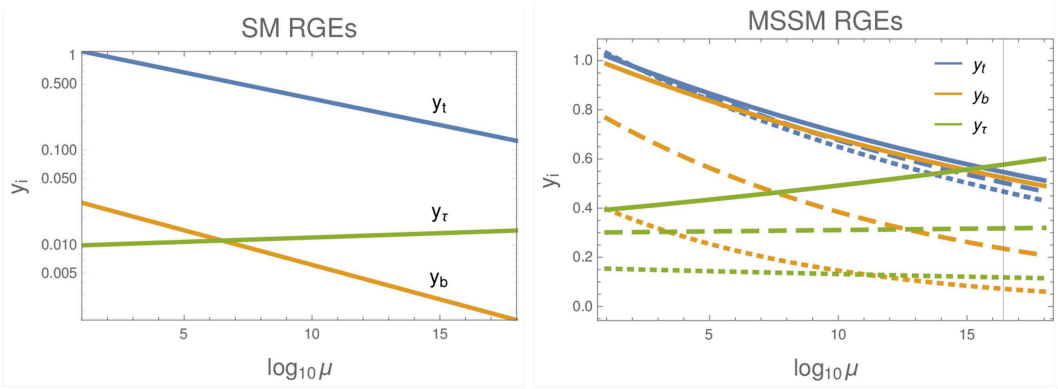

FIGURE 5 | One loop renormalisation group flow of the SM **(left)** and MSSM **(right)** Yukawa couplings, with $m_0 = 2$ TeV, $m_{1/2} = 3$ TeV, $A_0 = 0$ and $\tan\beta = 40$ (solid), $\tan\beta = 30$ (dashed) and $\tan\beta = 15$ (dotted).

soft masses at the GUT scale, or by considering the effect of D-terms in the boundary conditions at the GUT scale [148], which naturally imposes a splitting of $m^2_{H_d} - m^2_{H_u} = 4m^2_D$.

In addition to satisfying $m_t \gg m_b, m_\tau$ for unified Yukawa couplings, one can lift the hierarchy between m_b and m_τ with the inclusion of radiative corrections on the b mass. At one loop the b quark couples to H_u via a gluino or Higgsino loop [146], as can be seen in **Figure 6**, which adds a correction to m_b of the type [149]

$$\delta m_b \simeq \frac{v}{\sqrt{2}} y_b \frac{\sin\beta}{16\pi^2}\left(\frac{8}{3}g_3^2\frac{\mu m_{\tilde{g}}}{m_{\tilde{b}^2}} + y_t^2\frac{\mu A_t}{m_{\tilde{t}^2}}\right). \tag{28}$$

Though similar corrections appear for m_t and m_τ, they are negligible compared to δm_b. The correction on m_t is not proportional to $\tan\beta$, which is required to be large to satisfy $t-b-\tau$ unification. Further, δm_τ does not have a gluino loop and the Higgsino contribution is inversely proportional to $m_{\tilde{\nu}_t}$ which is typically much larger than $m_{\tilde{t}}$, and therefore the contribution is small. These radiative corrections on m_b are proportional to $\tan\beta$ and therefore can be significant, up to 50% [148], which can spoil the hierarchy $m_t \gg m_b$. There are regions of the SUSY parameter space, however, where it is possible to reduce δm_b while keeping $\tan\beta$ large [148–150], thereby successfully predicting $t - b - \tau$ unification, even factoring in LHC searches [151].

In SUSY $SU(5)$ models the more straightforward boundary condition $y_b = y_\tau$ is imposed. It was found that, in addition to the large $\tan\beta$ scenarios from above, $b-\tau$ unification can also be achieved in a region of parameter space with low $\tan\beta$ [152, 153]. However, a sufficiently low $\tan\beta$ might struggle to lift sufficiently the tree level Higgs mass to the observed value, and hence there remains some tension between unified $b - \tau$ models of low $\tan\beta$ and the observed Higgs mass [154].

A number of other mechanisms have been proposed to satisfy the Yukawa unification conditions. Intermediate breaking steps, such as the Pati-Salam group, can modify the Yukawas RGEs in a favorable manner achieving quasi-unification [155, 156]. Non-canonical seesaw mechanisms in neutrino models require $b - \tau$ unification to match the observed neutrino mixings [157]. Or the inclusion of certain higher dimensional operators can successfully yield Yukawa unification [158].

Beyond the unification of the Yukawa couplings for each of the families of SM fermions, the mass hierarchies among the different families remains an open question. Although GUTs by themselves do not make predictions on the nature of this hierarchy, they often include a fair amount of parameters and mixing matrices that are unconstrained and can fit the fermion masses. Additionally GUTs are often extended with family symmetries, continuous or discrete, which can, with a smaller set of parameters, accurately predict the fermion mass hierarchies, as well as their mixings and CP phases encoded in the CKM and UPMNS matrices [159–163]. We will not discuss family symmetries any further since they fall beyond the scope of this work.

4. MODERN DAY GUTS

Since their first appearance in the late 70s, a large number of GUT models have been proposed. These vary according to the symmetry group employed, the symmetry breaking mechanism and field content among others. Some of them were driven by the experimental results of the time and other by new theoretical insights. In this section we attempt to outline a small, non-exhaustive, subset of GUT models, aiming to explore those with strong phenomenological consequences and some that have been in the spotlight in recent years. We thus focus on left-right symmetric models, SUSY $SO(10)$, trinification models and E_6SSM.

4.1. Left-Right Symmetric Models

One of the minimal extensions of the SM is the earlier mentioned left-right symmetric model [16, 17, 62, 63, 67]. Despite not being real GUTs, LR models can very conveniently play the role of an intermediate symmetry restored between the electroweak scale and the GUT scale [69, 164, 165]. The LR framework has attracted a lot of attention particularly in connection with the LHC [166–178], as it typically predicts new physics at energies that can be probed by the collider searches.

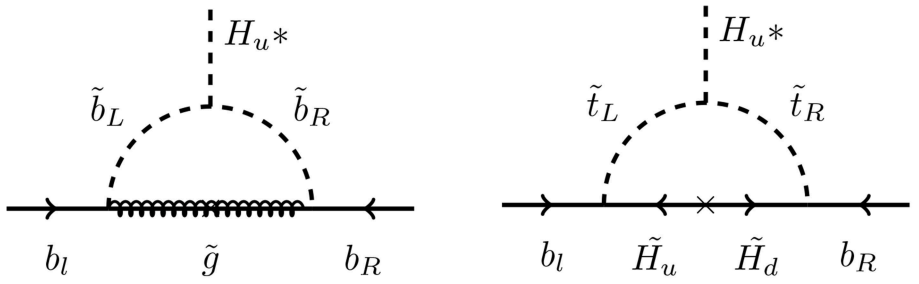

FIGURE 6 | One-loop radiative corrections to m_b.

The fermionic particle content of LR models is given by a straightforward LR symmetric extension of the SM content, i.e., the right-handed doublets are introduced

$$L_R^\ell = \begin{pmatrix} N^\ell \\ \ell_R \end{pmatrix} \leftrightarrow \begin{pmatrix} \nu_L^\ell \\ \ell_L \end{pmatrix} = L^\ell, \tag{29}$$

$$Q_R^i = \begin{pmatrix} u_R^i \\ d_R^i \end{pmatrix} \leftrightarrow \begin{pmatrix} u_L^i \\ d_L^i \end{pmatrix} = Q^i. \tag{30}$$

As a result, right-handed neutrinos are naturally included making the left-handed neutrinos acquire mass in the LR models, which is a highly desirable feature of a BSM model. The presence of the right-handed neutrino partners is also essential for cancellation of the $B - L$ gauge anomaly.

The Higgs sector of LR symmetric theories can vary. The minimal scenarios mostly include a scalar bi-doublet[6]

$$\Phi \equiv \{\mathbf{1}, \mathbf{2}, \mathbf{2}, 0\} = \begin{pmatrix} \phi_1^0 & \phi_2^+ \\ \phi_1^- & \phi_2^0 \end{pmatrix}, \tag{31}$$

containing the SM Higgs, which subsequently gives masses to quarks and leptons. The corresponding vev reads

$$\langle \Phi \rangle = \begin{pmatrix} v_{\Phi 1} & 0 \\ 0 & v_{\Phi 2} \end{pmatrix}, \tag{32}$$

where $v \equiv \sqrt{v_1^2 + v_2^2}$ and it mixes the left-handed and right-handed gauge bosons as described below.

Besides the bi-doublet, typically a pair of scalar triplets

$$\Delta_L \equiv \{\mathbf{1}, \mathbf{3}, \mathbf{1}, -2\}, \quad \Delta_R \equiv \{\mathbf{1}, \mathbf{1}, \mathbf{3}, -2\}, \tag{33}$$

or doublets

$$\chi_L \equiv \{\mathbf{1}, \mathbf{2}, \mathbf{1}, -1\}, \quad \chi_R \equiv \{\mathbf{1}, \mathbf{1}, \mathbf{2}, -1\}, \tag{34}$$

must be added to the Higgs sector in order to break the LR gauge group to the SM. In fact, the right-handed scalar is enough to do so, but inclusion of the left-handed triplet (or doublet) preserves the LR symmetry (so called "manifest LR symmetry"), i.e., the $SU(2)_L$ and $SU(2)_R$ gauge couplings are equal: $g_L = g_R$.

If no additional fermions besides the SM fermionic content are considered, at least two bi-doublets must be present in the scalar sector to account for the correct SM flavor physics [164]. In a model with a single bi-doublet the Yukawa Lagrangian implies that the up-quark mass matrix is proportional to the down-quark mass matrix (independently of the vev structure); thus, the CKM matrix becomes trivial $V_{\rm CKM} = 1$.

Consequently, the LR symmetry breaking takes place in two steps. At first, the neutral component of right-handed scalar triplet (or doublet) gets the vev v_R and breaks the LR gauge group to the SM gauge group. Subsequently, the bi-doublet acquiring its vev breaks the SM gauge group to $SU(3)_C \otimes U(1)_Q$. Based on the observations it can be assumed that $v_R \gg v_{\Phi 1}, v_{\Phi 2}$.

Depending on the scalar content of a particular LR model, different ways of light neutrino mass generation can be employed. Having right-handed neutrino singlets means that type-I seesaw is always the option. In general, the neutrino mass matrix can take the form

$$\mathrm{M}_\nu = \begin{pmatrix} \mathrm{M}_{M,L} & \mathrm{m}_D \\ \mathrm{m}_D^T & \mathrm{M}_{M,R} \end{pmatrix}, \tag{35}$$

where m_D denotes the Dirac mass matrix, while $\mathrm{M}_{M,L}$ and $\mathrm{M}_{M,R}$ are the Majorana mass matrices corresponding to the left-handed and right-handed neutrinos, respectively.

The Yukawa couplings in LR models include the scalar bi-doublet,

$$\mathcal{L}_{\rm Yukawa}^{\Phi} = \mathrm{y}_{\ell\ell'}^{\Phi} L^{\ell\,T} C \Phi L_R^{\ell'} + \tilde{\mathrm{y}}_{\ell\ell'}^{\Phi} L^{\ell\,T} C \tilde{\Phi} L_R^{\ell'} + \text{h.c.}, \tag{36}$$

where $\tilde{\Phi} = \sigma^2 \Phi^* \sigma^2$. Then the Dirac neutrino mass matrix and the mass matrix of charged leptons are in the broken phase given by

$$\mathrm{m}_D = \mathrm{y}^{\Phi} v_{\Phi 1} + \tilde{\mathrm{y}}^{\Phi} v_{\Phi 2}, \tag{37}$$

$$\mathrm{m}_\ell = \mathrm{y}^{\Phi} v_{\Phi 2} + \tilde{\mathrm{y}}^{\Phi} v_{\Phi 1}. \tag{38}$$

In case that the right-handed scalar triplet Δ_R is responsible for the LR symmetry breaking, one can write also the Yukawa couplings for the right-handed lepton doublet in the form

$$\mathcal{L}_{\rm Yukawa}^{\Delta_R} = \frac{1}{2} \mathrm{y}_{\ell\ell'}^{\Delta_R} (L_R^\ell)^T C (i\tau^2) \Delta_R L_R^{\ell'} + \text{h.c.}, \tag{39}$$

[6]Here, the representations are labeled the usual way in the order $\{SU(3)_C, SU(2)_L, SU(2)_R, U(1)_{B-L}\}$.

where $\Delta_R = \boldsymbol{\Delta}_R \cdot \boldsymbol{\tau}$. After the triplet acquires its vev

$$\langle \Delta_R \rangle = \begin{pmatrix} 0 & 0 \\ v_R & 0 \end{pmatrix}, \tag{40}$$

the LR symmetry is broken and the right-handed neutrino receives Majorana mass $\mathrm{M}_{M,R} = \mathrm{y}^{\Delta_R} v_R \gg v$, which allows for type-I seesaw mechanism.

When the Higgs sector contains also the left-handed scalar triplet Δ_L with vev

$$\langle \Delta_L \rangle = \begin{pmatrix} 0 & 0 \\ v_L & 0 \end{pmatrix}, \tag{41}$$

it generates the left-handed Majorana mass matrix $\mathrm{M}_{M,L} = \mathrm{y}^{\Delta_L} v_L$ switching on type-II seesaw mechanism.

In principle, the type-I and type-II seesaws can be combined giving the "full" seesaw matrix (35). The resulting light neutrino mass matrix reads

$$\mathrm{M}_\nu^{\mathrm{I+II}} = \mathrm{M}_{M,L} - \mathrm{m}_D [\mathrm{M}_{M,R}]^{-1} \mathrm{m}_D^T. \tag{42}$$

Specifically, if $v_{\Phi 2} = 0$ is assumed for simplicity, then the formula (42) can be rewritten in terms of the parameters of the LR models as

$$\mathrm{M}_\nu^{\mathrm{LR}} = \mathrm{y}^{\Delta_L} v_L - \frac{v_{\Phi 1}^2}{v_R} \mathrm{y}^{\Phi} [\mathrm{y}^{\Delta_R}]^{-1} \mathrm{y}^{\Phi T}. \tag{43}$$

Hence, if the hierarchy $v_R \gg v_{\Phi 1} \gg v_L$ is satisfied, the neutrino masses become small.

In models with the LR symmetry breaking driven by the right-handed doublet χ_R instead of the triplet Δ_R the light neutrino masses can be obtained employing the inverse [98, 179–181] and/or linear [175, 182, 183] seesaw mechanisms, provided that a singlet fermion $\{\mathbf{1}, \mathbf{1}, \mathbf{1}, 0\}$ is added to the model particle content. Alternatively, it is also possible to construct the type-III seesaw mechanism, if a left-handed or right-handed fermionic triplet is present within the LR model [184, 185]. Lastly, neutrino mass generation in LR models via the Zee mechanism can be achieved with the addition of a charged scalar boson $\{\mathbf{1}, \mathbf{1}, \mathbf{1}, 2\}$ [186].

4.2. SUSY *SO*(10) Models

Supersymmetric $SO(10)$ models are rather appealing GUTs, for they combine together the advantages of SUSY, Pati-Salam and $SU(5)$ models. As briefly outlined in section 2.4, $SO(10)$ models unify all fermions of a generation in the SM into a single representation, of dimension **16**. This decomposes into the maximal subgroups as

$$\begin{aligned} \mathbf{16} &\to \{\mathbf{4}, \mathbf{2}, \mathbf{1}\} + \{\bar{\mathbf{4}}, \mathbf{1}, \mathbf{2}\}, \quad [SU(4)_c \times SU(2)_L \times SU(2)_R], \\ \mathbf{16} &\to \mathbf{10}_{-1} + \bar{\mathbf{5}}_3 + \mathbf{1}_{-5}, \quad [SU(5) \times U(1)]. \end{aligned} \tag{44}$$

As mentioned before, at the renormalizable level the Yukawa sector of $SO(10)$ includes the Higgs representations **10**, **120**, and $\overline{\mathbf{126}}$, which are promoted to superfields in SUSY $SO(10)$. Hence, the superpotential of the Yukawa sector is

$$W_Y = \mathbf{16}^T \left(\mathrm{Y}_{10} \mathbf{10} + \mathrm{Y}_{120} \mathbf{120} + \mathrm{Y}_{126} \overline{\mathbf{126}} \right) \mathbf{16}. \tag{45}$$

where Y_i are matrices of Yukawa couplings in family space. One of the most remarkable features of SUSY $SO(10)$ is that, starting from a Yukawa unified scenario, Y_{10} and Y_{126} are sufficient to reproduce the full mass spectrum of SM fermions, along with the measured values of mixings in the quark and neutrino sector [187–197]. The mass matrices of SM fermions M_i can be written as [86]

$$\begin{aligned} \mathrm{M}_d &= v_{10}^d \mathrm{Y}_{10} + v_{126}^d \mathrm{Y}_{126} \\ \mathrm{M}_u &= v_{10}^u \mathrm{Y}_{10} + v_{126}^u \mathrm{Y}_{126} \\ \mathrm{M}_l &= v_{10}^d \mathrm{Y}_{10} - 3 v_{126}^d \mathrm{Y}_{126} \\ \mathrm{M}_D &= v_{10}^u \mathrm{Y}_{10} - 3 v_{126}^u \mathrm{Y}_{126} \\ \mathrm{M}_L &= v_L \mathrm{Y}_{126} \\ \mathrm{M}_R &= v_R \mathrm{Y}_{126} \end{aligned} \tag{46}$$

where M_D, M_L, and M_R are the Dirac and Majorana masses in types I and II seesaw (c.f. section 3.2), and the v's are the various vacuum expectation values of **10**, $\overline{\mathbf{126}}$ and the left and right-handed $SU(2)$ triplets.

The minimal SUSY $SO(10)$ model therefore contains the Higgs superfields **10** and $\overline{\mathbf{126}}$, responsible for fermion masses, and a pair of representations **126** and **210** which trigger the symmetry breaking of $SO(10)$ [198–200]. Although quite appealing due to its minimal set of model parameters, this model does not achieve the right level of gauge coupling unification and suffers from rapid proton decay [87, 201].

Many solutions have been implemented to resurrect minimal $SO(10)$ models. The spectrum of soft masses in the low energy MSSM strongly affects the outcome of gauge coupling unification, as was seen in section 3.1, hence modifications on the hierarchy of soft masses can help toward solving the issues with SUSY $SO(10)$ models [202–206]. Additionally, extended scalar sectors, either containing a **120** [207, 208] or a **54** [209] representation, can increase the unification scale through strong threshold effects, thereby alleviating the constraint of nucleon decay. Recently it has been shown that a combination of new Higgs representations with a modified spectrum of soft masses can accommodate gauge coupling unification and nucleon decay constraints, while still being able to predict a suitable spectrum of fermion masses [210].

As with many GUT models, SUSY $SO(10)$ makes predictions that can be tested in a number of different fronts. Collider searches at the LHC [211, 212] as well as dark matter searches [213] can discover the predicted light, TeV-scale, states. Precision tests such as nucleon decays [214, 215], lepton flavor violation [216] and flavor observables [217] can probe the validity of the models at high scales. For more details on probing SUSY $SO(10)$ and GUTs in general see sections 5–7.

4.3. Trinification

As a maximal subgroup of E_6, the trinification gauge group $SU(3)_c \times SU(3)_L \times SU(3)_R$ is an alternative approach to SUSY $SO(10)$ on the road to E_6 unification. The matter content of

trinification models per generation typically looks like [218]

$$\{\mathbf{1},\mathbf{3},\overline{\mathbf{3}}\} = \begin{pmatrix} h_{11} & h_{22} & e \\ h_{21} & h_{22} & \nu \\ e^c & \nu^c & \phi \end{pmatrix}, \quad \{\mathbf{3},\overline{\mathbf{3}},\mathbf{1}\} = \begin{pmatrix} u & d & D \end{pmatrix}, \quad \{\overline{\mathbf{3}},\mathbf{3},\mathbf{1}\} = \begin{pmatrix} u^c & d^c & D^c \end{pmatrix} \tag{47}$$

where h_{ij} are the components of two Higgs doublets, ϕ a SM singlet field and D and D^c color-triplets. An additional Z_3 symmetry is often considered to make the gauge couplings unify at the GUT scale, $g_c = g_L = g_R$.

Given the presence of exotic fields in the matter multiplets, trinification models struggle to trigger spontaneous symmetry breaking without making the matter content impossibly heavy. Additional Higgs multiplets [219–222] and/or non-renormalizable operators [223–226] are usually introduced to alleviate this issue. Unfortunately these models tend to produce tension with current limits on proton decay [227] and collider searches [228, 229].

The fundamental challenge behind the issues of trinification is the complicated vacuum structures and the large number of parameters they depend on. Solutions to this problem involve the addition of family symmetries which reduce the number of parameters and facilitate the study of the symmetry breaking vacuum [230], further simplified by embedding the theory into larger dimensional groups such as E_8 [231, 232].

4.4. E_6SSM

The Exceptional Supersymmetric Standard Model (ESSM or E_6SSM) [233, 234] is an extension of the MSSM motivated as a low energy effective theory from a E_6 unified GUT model at high scales. At low scales it has the gauge group $SU(3)_c \times SU(2)_L \times U(1)_Y \times U(1)_N$, where the additional $U(1)_N$ factor is leftover from the symmetry breaking of E_6. All the superfields in the theory are contained in three copies of the **27** representation of E_6, which decompose under the $SU(5) \times U(1)_N$ subgroup as [235]

$$\mathbf{27}^i \to \mathbf{10}^i_1 + \overline{\mathbf{5}}^i_2 + \overline{\mathbf{5}}^i_{-3} + \mathbf{5}^i_{-2} + \mathbf{1}^i_5 + \mathbf{1}^i_0, \tag{48}$$

where $\mathbf{10}^i_1$ and $\overline{\mathbf{5}}^i_2$ are the matter multiplets for all three generations, with the standard embeddings of matter fields in $SU(5)$ (c.f. section 2.1). The superfields $\overline{\mathbf{5}}^i_{-3}$ and $\mathbf{5}^i_{-2}$ contain the two Higgs doublets of the MSSM, H_u and H_d, plus two copies of pairs of exotic doublets, $H_u^{1,2}$ and $H_d^{1,2}$ and three copies of exotic triplets D_i and $\overline{D}_i$. Lastly, the singlets $\mathbf{1}^i_5$ and $\mathbf{1}^i_0$ correspond to exotic singlet fields S_i, responsible for $U(1)_N$ breaking at low scales, and right-handed neutrino fields N_i, respectively.

Anomaly cancellation of the $U(1)_N$ factor in the E_6SSM model is guaranteed so long as the only decoupled state is the singlet neutrino field. N_i can be as large as necessary to provide light neutrino masses through type I seesaw mechanism and generate the baryon assymmetry of the Universe via leptogenesis [236, 237]. The remaning fields of the $\mathbf{27}^i$ multiplets charged under $U(1)_N$ remain at energies below the breaking of $U(1)_N$ and hence anomalies cancel. Light colored states have dangerous consequences, however, for they can mediate baryon and lepton number violating interactions leading to rapid proton decay. In order to avoid that, the original E_6SSM model postulates the existence of an approximate Z_2 symmetry that forbids those interactions. An exact Z_2 symmetry can also be considered [238, 239], but in such a case additional exotic states must be introduced to ensure that the exotic quarks are not stable.

Gauge coupling unification in the E_6SSM model requires the addition of incomplete multiplets of E_6 at low scales, since full multiplets do not modify the unification properties of the RGE flow. A pair of fields H and $\overline{H}$ in conjugate representations are added, to ensure no anomalies are reintroduced. Alternatively, a Pati-Salam intermediate step has been postulated that achieves gauge coupling unification without the need of additional superfields. This "minimal" E_6SSM model, however, predicts unification at the Planck scale so quantum gravity corrections may play a role and affect the outcome of unification [240].

The E_6SSM has a rather rich phenomenology since most of the predicted exotic states live at low energies. The constrained E_6SSM (cE_6SSM) is a version of the full E_6SSM that exploits the properties of unification of E_6 and assumes universal scalar and gaugino soft masses at the GUT scale [241, 242]. Predictions of the cE_6SSM include contributions to the Higgs mass and rare decays [243, 244] together with light exotic states, such as the Z'_N associated with the $U(1)_N$ broken symmetry, and the color triplet fermions D and $\overline{D}$, all of which can be probed at the LHC [245]. Lastly, as in the MSSM the lightest supersymmetric particle is stable, so it is a valid candidate for dark matter. In contrast with the regular neutralino dark matter in the MSSM, the dark matter candidate in the E_6SSM is a mixture of binos, winos and higgsinos, as well as the inert singlinos and higgsinos in $H^i_{u,d}$ and S_i [246–250].

5. COSMOLOGY AND THE EARLY UNIVERSE

5.1. Inflation and GUTs

Cosmic inflation plays an important role in theories of Grand Unification, as it is needed to dilute relics such as magnetic monopoles, which are produced ubiquitously in GUT models[7]. The requirement to dilute these relics therefore determines the scale of inflation in specific models [251]. Moreover, since generic inflation models are associated with a scale $\Lambda_{\text{inflation}} \sim 10^{16}$ GeV, it becomes attractive to associate the inflaton with a GUT scalar.

To agree with observations, inflation models need to predict a large number of observable e-folds ($N = \int_{t_0}^{t_e} H dt \gtrsim 60$), as well as small spectrum density of fluctuations $\delta\rho/\rho \sim 10^{-5}$. For an effectively single field model, this can be illustrated by the tension between the Lyth bound (a measure of the field excursion necessary to solve the problems inflation was invented to solve) given in terms of the number of e-foldings N [252],

$$\Delta\phi \sim \left(\frac{r}{0.002}\right)^{1/2} \left(\frac{N}{60}\right) M_p \tag{49}$$

[7]However, there are exceptions, most notably the flipped $SU(5)$ SUSY GUT theories.

and the amplitude of the Cosmic Microwave Background (CMB) anisotropies, which implies [253, 254],

$$\Lambda_{inf}^4 = \left(2.2 \times 10^{16}\ \text{GeV}\right)^4 \left(\frac{r}{0.2}\right). \tag{50}$$

It is clear, then, that inflation requires a very flat scalar potential. Hence, it is attractive to consider inflation models in which the potential is dynamically generated [255–258].

A successful example of such a model was realized as early as 1983 [259]. This paper considered a potential of a Coleman-Weinberg form [255],

$$V(\phi) = A\phi^4 \left(\log \frac{\phi^2}{v_\phi^2} - \frac{1}{4}\right) + C \tag{51}$$

Such a potential can only be made compatible with CMB constraints if A is very small (presently, $A \lesssim 10^{-14}$ [260]). Therefore, the potential in Equation (51) cannot be due to loops of $SU(5)$ gauge bosons. Instead, [259] considered a model in which the inflaton transformed as a singlet of $SU(5)$, couples weakly to the adjoint and fundamental Higgs fields, and therefore obtains a vacuum expectation value when $SU(5)$ breaks into the SM. The original CW-GUT inflation model [259] predicts primordial gravitational waves with tensor-to-scalar index $0.02 \leq r \leq 0.1$ [261]. Although this is currently not in tension with the CMB-constraints [253, 254], several modifications have been proposed which predict smaller r [260, 262–264].

An alternative class of GUT inflation models are based on no-scale supergravity. It was realized in 2013 [265] that particular realizations of no-scale supergravity (SUGRA) models of inflation can be equivalent to the Starobinsky model [266], in which inflation is realized from a non-minimal Einstein-Hilbert action $S = \frac{1}{2}\int dx\sqrt{-g}(R + R^2/6M^2)$. The correspondence can be seen by a conformal transformation, such that the model is equivalent to canonical gravity plus a scalar field [265, 267]. The scalar potential then becomes

$$V(\phi) = \frac{3}{4}M^2\left(1 - e^{-\sqrt{2/3}\phi}\right)^2. \tag{52}$$

Starobinsky-like models are attractive candidates for inflation models, as they make viable predictions for inflationary observables without the need to introduce a large set of finely tuned parameters. Examples of no-scale SUGRA inflation models include sneutrino inflation, which can be consistently implemented in flipped $SU(5)$ SUSY GUTs [268–272]. Other no-scale GUT inflation models identify the inflaton with the Higgs boson, and circumvent the problems associated with conventional Higgs inflation [273, 274].

A phenomenological approach was taken by Hertzberg and Wilczek [275]. Here it was assumed that inflation is driven by the vacuum energy associated with unification. It was shown that several examples of large-field ($\Delta\phi \sim M_p$) models of inflation give predictions consistent with the CMB-constraints [253, 254].

GUT-inflation has also been studied in combination with other cosmological scenarios, most importantly with non-thermal leptogenesis and the seesaw mechanism for neutrino masses [276–278][8]. Models of sneutrino inflation are well suited for this purpose [268–272].

5.2. Cosmological Constraints on Cosmic Strings

Cosmic strings are generic cosmological predictions of many GUT theories [279–281]. Field theories with broken gauge symmetries may have a vacuum state that is not unique, such that different points in physical space may have distinct (but degenerate) vacuum configurations. By continuity of the field, the interpolating field values must be taken on in between these points, which gives rise to an energetic object called a topological defect, or (in the one-dimensional case) a string.

The simplest description of cosmic strings after their formation approximates the fundamental *Nambu-Goto* strings. Nambu-Goto strings are characterized by the dimensionless string tension $G\mu$, where μ is the mass per unit length and G is Newton's constant. Strings produced at the GUT scale typically have a mass per unit length of the order of $\mu \sim 10^{21}\,\text{kg}\,\text{m}^{-1}$ and a thickness of 10^{-24} m, such that the tension is $G\mu \sim 10^{-6}$ [282]. For comparison, strings formed around the electroweak scale are expected to have much smaller tensions, $G\mu \sim 10^{-34}$. As the expansion of the Universe stretches strings, while the string tension stays constant and in the absence of a decay mechanism, ρ_{strings} would grow with the scale factor and eventually dominate the energy density of the Universe. Cosmic strings can decay into gravitational or scalar radiation, however. In the presence of such a decay channel an attractor scaling solution is reached, in which the strings maintain a constant fraction of the energy budget.

Cosmic strings could be detected through gravitational lensing and anisotropies in the CMB [283, 284]. Cosmic strings imprint on the CMB as line-like discontinuities, caused by a boost of photons toward the observer as a string moves across the line of sight [285, 286]. Planck data constrains the Nambu-Goto string tension $G\mu < 1.8 \times 10^{-7}$ [287], the non-local string tension $G\mu < 10.6 \times 10^{-7}$ [287] and the Abelian Higgs string model $G\mu < 2.0 \times 10^{-7}$ [288].

If the strings decay gravitationally, such radiation can be observed in Gravitational Wave (GW) experiments [289–293]. Strong gravitational radiation bursts may be produced by cusps [294–298]: the LIGO/VIRGO collaboration reported an experimental upper limit of $G\mu < 10^{-8}$ in some regions of the parameter space, in which gravitational backreaction determines the size of the loops [299]. Pulsar Timing Arrays (PTAs) potentially give more stringent bounds, as they can already probe the stochastic GW background; depending on the model, $G\mu < \mathcal{O}(10^{-12} - 10^{-11})$ [300–302]. However, the relative importance of the gravitational decay channel has been the source of some disagreement in the literature. Simulations of Nambu-Goto strings [303–308] and full field-theoretic simulations of the Abelian Higgs model [309–311] differ in the typical scale on which the strings form loops. Loops of the order of the string width r_s can radiate heavy particles (as the natural mass of coupled particles is $m \sim r_s^{-1}$); loops of the typical inter-string spacing ξ are expected to decay gravitationally [312].

[8] We expand more on the topic of the baryon assymmetry in subsection 5.4.

Recent field-theory simulations [311] suggest a mechanism to transport energy from large to small scales, which is not currently understood. Numerical results [313–315] also indicate that the simplest analytical models are due an update, when non-Abelian gauge groups are considered. Furthermore, different groups simulating Nambu-Goto strings differ in the distribution of the loop size. Simulations in which the gravitational radiation back-reacts on the string have smoother features, which hinders the formation of smaller loops [303–305]. In these simulations, the PTA constraints on the stochastic background and LIGO/VIRGO constraints on burst are stronger [301].

The shape of the fractional energy density $\Omega_{GW} \equiv f/\rho_c(d\rho_{\rm GW}/df)$ power spectrum from cosmic strings is expected to be nearly scale-invariant, with an amplitude defined by the characteristic string tension $G\mu$, such that if it has a large enough amplitude, the signal would be seen in frequency windows of different experiments [316]. This distinguishes the power spectrum from other sources. In particular, an observation of GW at pulsar timing arrays, if coming from cosmic strings, will draw attention to interferometer searches for this source.

5.3. Gravitational Waves From Phase Transitions

Grand unification models can accommodate a rich scalar sector, which can result in a complicated cosmological history involving exotic phase transitions. Some GUT inspired possibilities are: a color breaking phase transition where color is broken and restored when leptoquarks acquire a vacuum expectation value in an intermediate transition, which can catalyse baryogenesis [317, 318], $B-L$ and L violating phase transitions [319–322], hidden sector phase transitions [323–326], and a Pati-Salam transition [327]. If any such phase transition occurs through bubble nucleation, an observable relic gravitational wave spectrum can be seen today, for a review see Mazumdar and White [328], Caprini and Figueroa [329], and Weir [330]. Furthermore, GUT models often require the existence of extra singlets. For example, the E_6SSM model studied in Athron et al. [241] had 3 generations of singlets and such singlets can, in principle, catalyse the electroweak phase transition to be strongly first order as well [331–333].

The gravitational wave spectrum generated from a cosmic phase transition has three contributions: a contribution from the collision of scalar shells, and potentially long-lasting contributions from sound waves and turbulence in the plasma. The total spectrum can thus be written as,

$$\Omega(f)h^2 = \Omega_{\rm coll}(f)h^2 + \Omega_{\rm sw}(f)h^2 + \Omega_{\rm turb}(f)h^2\,. \qquad (53)$$

Although much uncertainty remains about the precise form of these spectra, all three are controlled by four thermal parameters, which can be computed by first principles [328, 334]: the latent heat released during the transition (conventionally normalized by the radiation energy density), denoted α, the nucleation rate (conventionally normalized to the Hubble parameter) β/H, the temperature at which the transition occurs T_* and the velocity of the bubble wall v_w. The collision term is expected to be sub-dominant for transitions associated with a broken gauge group [335]. The sound wave contribution to the power spectrum is [334] and [336]

$$h^2\Omega_{\rm sw} = 8.5\times10^{-6}\left(\frac{100}{g_*}\right)^{-1/3}\Gamma^2\overline{U}_f^4\left(\frac{\beta}{H}\right)^{-1}v_w S_{\rm sw}(f), \quad (54)$$

where $\overline{U}_f^2 \sim (3/4)\kappa_f\alpha_T$ is the rms fluid velocity, $\Gamma \sim 4/3$ is the adiabatic index, κ_f is the efficiency of converting the latent heat into gravitational waves and g_* the number of relativistic degrees of freedom. The frequency dependence is captured by the spectral state

$$S_{\rm sw} = \left(\frac{f}{f_{\rm sw}}\right)^3\left(\frac{7}{4+3\left(\frac{f}{f_{\rm sw}}\right)^2}\right)^{7/2},$$
$$f_{\rm sw} = 8.9\times10^{-7}{\rm Hz}\frac{1}{v_w}\left(\frac{\beta}{H}\right)\left(\frac{T_*}{\rm Gev}\right)\left(\frac{g_*}{100}\right)^{1/6}.$$

The other notable, albeit sub-dominant, contribution is the contribution from magneto-hydrodynamic turbulence in the plasma. The power spectrum from this contribution is given by [337],

$$h^2\Omega_{\rm turb} = 3.354\times10^{-4}\left(\frac{\beta}{H}\right)^{-1}\left(\frac{\kappa\epsilon\alpha}{(1+\alpha}\right)^{3/2}\left(\frac{100}{g^*}\right)^{1/3}v_w S_{\rm turb}(f), \qquad (55)$$

where ϵ is the fraction of the energy that contributes to turbulence, typically taken to be in the range $(0.05, 0.1)$ [334]. In this case the spectral form is a function of two time scales,

$$S_{turb} = \frac{(f/f_{\rm turb})^3}{[1+(f/f_{\rm turb})]^{11/3}(1+\frac{8\pi f}{h_*})},$$
$$f_{\rm turb} = 27\mu{\rm Hz}\frac{1}{v_w}\left(\frac{T_N}{100{\rm GeV}}\right)\frac{\beta}{H}\left(\frac{g^*}{100}\right)^{1/6},$$

where h^* is the Hubble rate at the transition temperature[9].

For a single scalar field transition, without a tree-level barrier between the true and the false vacuum, β/H tends to be $O(10^3)$ or greater [232]. The transition temperature is the same order of magnitude as the mass of the scalar. Therefore, transitions with scalar masses $O(10^5)$ GeV can be probed by ground-based interferometers such as the Einstein Telescope [338], Kagra [339] and cosmic explorer [340], whereas space-based LISA will probe transitions at the electroweak scale [334]. The former can be more directly related to studies of GUTs-we show benchmark examples for a Pati-Salam phase transition are shown in **Figure 7**. The visibility of the spectrum tends to grow with the ratio v/m, the gauge coupling constant g, the rank of the (sub) group being broken and the number of other particles acquiring a mass during

[9]Note that the existence of two time scales in the spectral form means that the peak amplitude for the turbulence contribution cannot be found simply be setting the frequency to either h_* or $f_{\rm turb}$ in Equation 55.

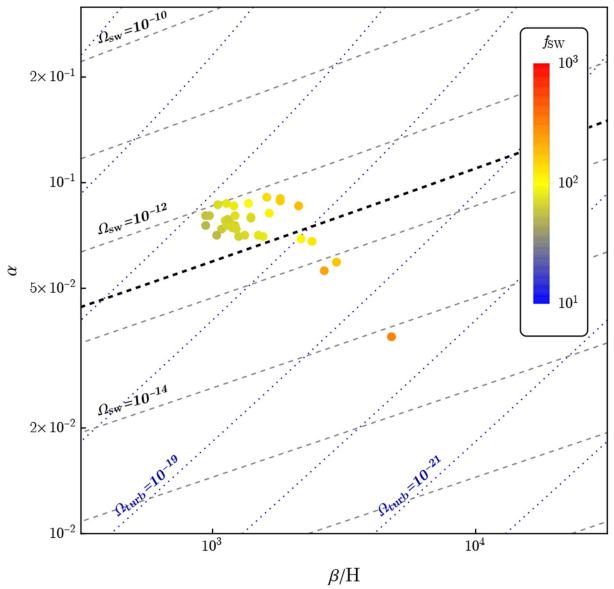

FIGURE 7 | Plane of thermal parameters with contours of constant sound wave (in black) and turbulence (in blue) peak amplitude. The thicker line shows the peak sensitivity of the Einstein telescope [338]. Points denote thermal parameters produced by a Pati-Salam phase transition with a Pati-Salam scale of $M_{PS} = 10^5$ GeV. The peak frequency for the sound wave spectrum is indicated by the color scaling. Figure taken from Croon et al. [327].

the transition [323]. Furthermore, it was found in Croon et al. [323] that some non-trivial model discrimination is possible if one observes a primordial power spectra due to the increase in visibility as well as moderate correlations between thermal parameters, shown in **Figure 8** for $SU(N)/SU(N-1)$ cosets.

If multiple scalar fields are involved in a transition the barrier between the true and false vacuum can persist at zero temperature due to triscalar or non renormalizable operators [333, 343]. In such a case significantly more supercooling is possible and the transition temperature is no longer confined to be the same order of magnitude as the scalar mass. This implies that β/H can be quite small and the latent heat can be large, increasing the visibility of the gravitational wave and reducing the peak frequency. A caveat to this is that recent work found that phase transitions that involve a large amount of supercooling may fail to complete due to the onset of inflation [344]. Regardless, the thermal parameter space in the case of multifield phase transitions is broader, which minimizes model discrimination somewhat, though not completely [323].

5.4. Baryo-/Leptogenesis

The existence of a baryon asymmetry in the Universe (BAU) is one of the central problems of modern cosmology [345, 346]. At the same time, the concordance between different measurements of the primordial baryon asymmetry is a triumph of modern cosmology with BBN and CMB limits giving [347, 348]

$$\eta_B = \begin{cases} (6.2 \pm 0.4) \times 10^{-10} & \text{BBN} \\ (6.14 \pm 0.03) \times 10^{-10} & \text{CMB} \end{cases} \quad (56)$$

respectively. Any explanation for the baryon asymmetry must satisfy the three Sakharov conditions [349]

- Baryon number B violation
- C and CP violation
- A departure from thermal equilibrium.

Early attempts at generating the BAU focused on B violating decays (for a review see [350]). Such decays typically violate $B + L$ while conserving $B - L$ (for an exception see [351]). For example, $SU(5)$ GUTs are invariant under changes to a global phase conjugate to $B - L$ number, whereas $SO(10)$ has a local $U(1)_{B-L}$ symmetry. However, any primordial $B+L$ asymmetry is washed out by $B+L$ violating electroweak sphalerons. Therefore, only a primordial $B - L$ asymmetry will be preserved unless sphalerons are quenched.

Leptogenesis allows for a $B - L$ violating operator, $m\overline{\nu}_R^c \nu_R$, that is also responsible for a light neutrino mass via type-I seesaw mechanism (see section 3.2). CP violating decays of such sterile neutrinos ensure a net $B - L$ asymmetry which electroweak sphalerons convert to a baryon asymmetry. Electroweak baryogenesis by contrast uses the sphalerons themselves to generate a net $B + L$ asymmetry which cannot be washed out before the sphalerons are quenched [345, 346]. More specifically, if the electroweak phase transition is strongly first order, bubbles of electroweak broken phase populate a medium of symmetric phase with sphalerons quenched only inside such bubbles. Particles can have CP violating interactions with the bubble wall which biases the sphalerons to produce a net $B + L$ asymmetry. Some of this asymmetry is swept up in the expanding bubble wall where it is preserved.

GUTs are only relevant to electroweak baryogenesis if the GUT model motivates some light BSM states. Recent work on electroweak baryogenesis in the E_6-SSM utilized three generations of singlet superfields to motivate a CPV source involving singlino-Higgsino interactions with the bubble wall [331].

A feature of leptogenesis during GUTs is the possibility of new CP violating decay channels due to the presence of leptoquarks [352, 353]. This allows a lower minimum mass for the lightest sterile neutrino than in the minimal scenario [236][10]. Much of the recent focus on baryogenesis within GUTs involves leptogenesis with some intriguing concordance achieved in the case of $SU(5)$ [355] and $SO(10)$ GUTs [271, 278, 356–360]. A generic feature of $SO(10)$ GUTs is normal ordering of neutrino masses and a negative Dirac phase [361], both of which are favored by current observational limits [360]. Furthermore, many GUTs, including $SO(10)$, predict a Dirac neutrino mass matrix that is not too different from the up quark mass matrix and $SO(10)$ leptogenesis also achieves agreement in the currently observed atmospheric mixing angle in the first octant. Realistic models with two right-handed neutrinos can emerge in $\Delta(27) \times SO(10)$ models and $A4 \times SU(5)$ supersymmetric models [362, 363]. The third right-handed neutrino can either decouple because it is very heavy or because its Yukawa coupling is very small. The

[10]This limit of course is for the non resonant regime. In case of resonant leptogenesis the masses of the sterile neutrinos can be very low [354].

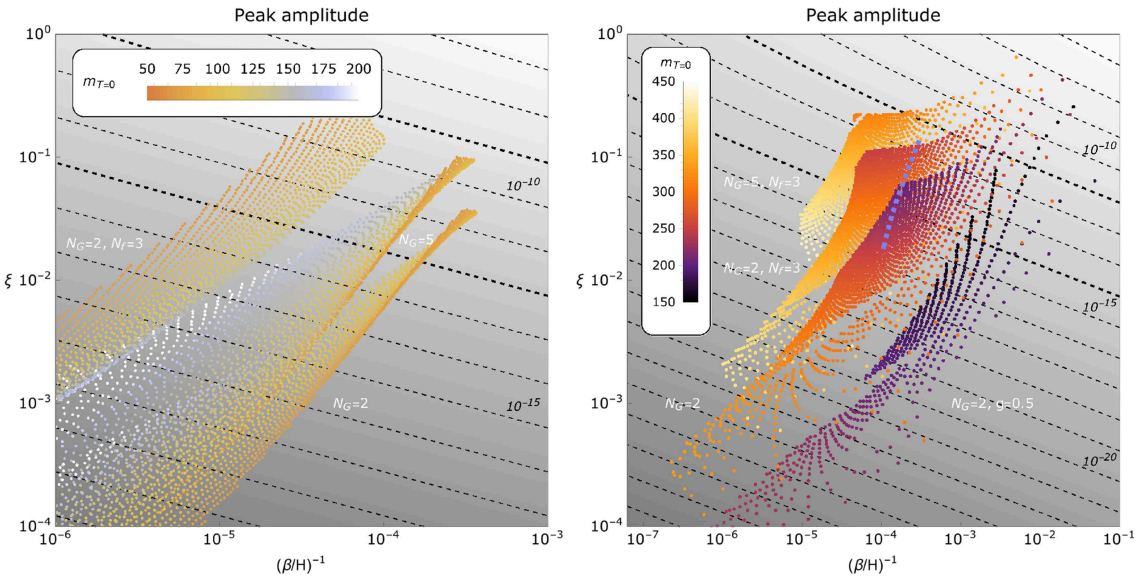

FIGURE 8 | Thermal parameters from a renormalizable potential for a scalar field in the fundamental representation of $SU(N_G)$ which gets broken to $SU(N_G - 1)$ **(left)**. **Right** panel is the same aside from the inclusion of a non-renormalizable sextet term in the potential and the gauge coupling constant is fixed to unity. In the above N_G denotes the order of the group, N_f is the number of fermions in the fundamental representation that are strongly coupled to the scalar field, in direct analogy with the SM save that the Yukawa couplings are set to unity. Note that ξ is the ratio of latent heat to radiation energy density more commonly denoted α. Contours of constant peak amplitude for the sound wave spectrum are shown with the darker line corresponding to LISA sensitivity range for a power law spectrum that has been integrated over frequency [341]. Note in the above $v_w = 0.5$ for the left plot and $v_w = 1$ for the right plot using the efficiency terms in Espinosa et al. [342]. Figure taken from Croon et al. [323].

latter case implies a stable particle that can play the role of dark matter [364].

6. DIRECT COLLIDER SEARCHES FOR GUTS

6.1. Searches for Supersymmetry

As we have seen in section 3.1 supersymmetry plays a rather important role on many unified theories and motivates the unification of gauge couplings at large scales. However, both its solution to the hierarchy problem and gauge coupling unification often rely on a light sparticle spectrum, around or below the TeV scale. Thus, searches for supersymmetric particles has been part of the research programme in collider physics for the last few decades, from searches at LEP and the Tevatron, to the recent results of the LHC, and it is still part of the proposed physics programme for future colliders, e.g., CLIC, ILC, or VLHC [365–368].

In R-parity conserving SUSY the lightest supersymmetric particle (LSP) is stable. This has strong consequences for SUSY searches, for the LSP will escape the collider in the form of missing transverse energy (MET)[11] [369]. In addition, R-parity requires that sparticles are pair-produced in colliders, hence the different searches for supersymmetry are classified according to the particle that is produced in pairs. The production cross sections of the different sparticle species are rather different and often determine the exclusion or detection power of a particular channel. For instance, the strongest exclusion limits at the LHC across the sparticle spectrum are on first and second generation squarks and gluinos which, as can be seen in **Figure 9**, have the largest production cross sections [370, 371].

Squarks and gluinos are produced in pairs at the LHC in the combinations $\tilde{g}\tilde{g}$, $\tilde{q}\tilde{q}$ and $\tilde{q}\tilde{g}$ and their main decay channels are $\tilde{q} \rightarrow q\tilde{\chi}_1^0$ and $\tilde{g} \rightarrow q\bar{q}\tilde{\chi}_1^0$, with the neutralino LSP escaping the collider. Hence the typical signature for these processes has multiple jets and large missing energy. The decay topologies for these signatures are depicted in **Figure 10**. Other decay modes for squark and gluinos involve the production of charginos or heavier neutralinos, $\tilde{q} \rightarrow q\tilde{\chi}_2^0$, $\tilde{q} \rightarrow q'\tilde{\chi}_1^{\pm}$, $\tilde{g} \rightarrow q\bar{q}\tilde{\chi}_2^0$ and $\tilde{g} \rightarrow q\bar{q}\tilde{\chi}_1^{\pm}$, which then decay to W and Z bosons and $\tilde{\chi}_1^0$. The final state signatures depend on the decay modes of the gauge bosons, and can have (0–4) leptons, jets and MET. ATLAS and CMS have reported results from the last run of the LHC at 13 TeV and 36 fb^{-1} for searches with jets and MET final states [372–374], with one lepton, jets and MET [375–377], same and opposite-sign dilepton pairs, jets and MET [378, 379], two or three leptons, jets and MET [380, 381], 3rd generation squarks (with and without Higgs reconstruction) and MET [382–384] and hadronic τ decays, jets and MET [385], among others. These searches set a lower limit for a range of simplified models on the mass of the gluino of $m_{\tilde{g}} \gtrsim 2.1$ TeV and the mass of the first and second generation squarks of $m_{\tilde{q}} \gtrsim 1.5$ TeV.

[11] In cases where a charged next-to-lightest SUSY particle (NSLP) is stable at detector timescales, no clear MET signal is produced, since the NLSP will decay to the LSP outside the detector.

The next strongest production cross section is that of stop and sbottom pairs. The main decay channel for stops and sbottoms is $\tilde{t} \to t\tilde{\chi}_1^0$ and $\tilde{b} \to b\tilde{\chi}_1^0$, respectively. This topology is similar to the decay of first and second generation squarks, with the added complexity that neither t or b produce a clean jet, but rather have many decay channels that can result in numerous jets, leptons and, of course, MET. Secondary decay channels for $\tilde{t}$ and $\tilde{b}$ involve decays to a chargino, $\tilde{t} \to b\tilde{\chi}_1^\pm$ and $\tilde{b} \to t\tilde{\chi}_1^\pm$, with subsequent decays involving W bosons, or decays into a heavy neutralino, $\tilde{t} \to t\tilde{\chi}_2^0$ and $\tilde{b} \to b\tilde{\chi}_2^0$, which in turn decays into a Z or a Higgs boson and $\tilde{\chi}_1^0$. The latest searches of the LHC experiments for pair-produced stops and sbottoms target final states with jets and MET [374, 386, 387], b-jets and MET [388, 389], one lepton, jets and MET [390, 391], two and three leptons, jets and MET [379–381, 392, 393] and final states with a h or a Z boson and MET [394], among others. These searches exclude masses of stops and sbottoms up to $m_{\tilde{t}} \sim 1$ TeV and $m_{\tilde{b}} \sim 900$ GeV for some simplified models.

In the cases where the colored sector of a supersymmetric model has large masses, the direct production of chargino, neutralino and slepton pairs dominate. A pair of directly produced sleptons decay typically like $\tilde{l} \to l\tilde{\chi}_1^0$. Neutralinos and charginos are produced in pairs in a number of different combinations, the most commonly studied of which are $\tilde{\chi}_2^0\tilde{\chi}_1^\pm$ and $\tilde{\chi}_1^\pm\tilde{\chi}_1^\pm$. The decays of heavy neutralinos and charginos produce W, Z or Higgs bosons and the lightest neutralino. Further decay of W and Z sets the final states targeted by ATLAS and CMS searches, such as the final state with two leptons and MET [395–397], many leptons and MET [397–400], leptons, jets and MET [393], taus and MET [401, 402], and b-jets plus MET [403], among others. Due to their low production cross sections, the exclusion limits on slepton masses from direct production are quite weak and they only reach up to around $m_{\tilde{l}} \sim$ 500 GeV. Stronger limits on slepton masses can be inferred from neutralino/chargino production with sleptons in the cascade, reaching up to $\sim$ 850 GeV. The limits on electroweakinos (neutralinos and charginos) are very sensitive to the parameter choices for the simplified model analyses performed by the experiments, hence the exclusion limits on $\tilde{\chi}_2^0$ and $\tilde{\chi}_1^\pm$ vary from search to search and from signal region to signal region, roughly in the range $m_{\tilde{\chi}_2^0}, m_{\tilde{\chi}_1^\pm} \in (500\text{ GeV}, 1.1\text{ TeV})$. Similarly the limits on the lightest neutralino varies in the range $m_{\tilde{\chi}_1^0} \in (200, 700)$ GeV. In addition, there is a hint of an excess in one of the two and three lepton final state analyses by the ATLAS collaboration in the low $m_{\tilde{\chi}_1^0}$ region, with a reported significance of 2 and 3σ in the $2l$ and $3l$ channels, respectively [399].

In addition to sparticle searches, SUSY can also be probed through searches for heavy and charged Higgs bosons. The MSSM predicts the existence of two CP-even scalars, h and H, one CP-odd pseudoscalar, A, and a charged scalar $H^\pm$. The lightest CP-even scalar, h, is said to be "SM-like," as its mass and couplings are aligned with the Higgs boson discovered at the LHC [4, 5], the so called *alignment limit*. Neutral heavy Higgses can be produced at the LHC in the same manner as the SM Higgs, that is by gluon fusion, vector boson fusion (VBF) and associated production, with a t and/or b quark. Thus, the same mechanisms that lead to the discovery of the SM Higgs are employed to set exclusion limits on heavier neutral (pseudo)scalars, including signatures where H is produced in resonance and decays into two light Higgs bosons $pp \to H \to hh$. The final states targeted by these exotic Higgs searches consist of 2–4 leptons, jets and MET from on- and off-shell W and Z bosons [404, 405], two leptons and MET [406, 407], final states with four b-jets [408, 409] or two b-jets and WW [410], $\gamma\gamma$ [411, 412], $\tau\tau$ [413, 414], $\mu\mu$ [415], or $t\bar{t}$ [416]

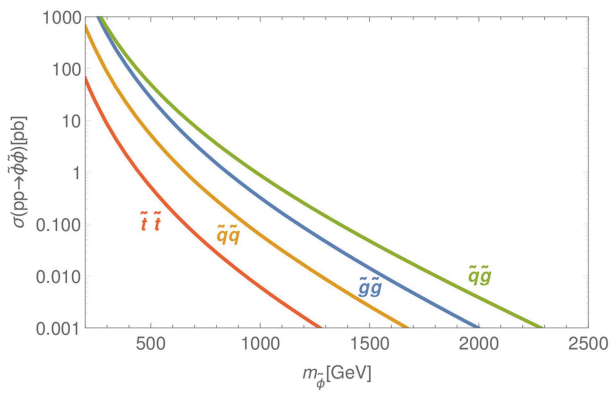

FIGURE 9 | Pair production cross sections as a function of the mass of sparticle $\tilde{\phi}$ at center of mass energy $\sqrt{s} = 13$ TeV.

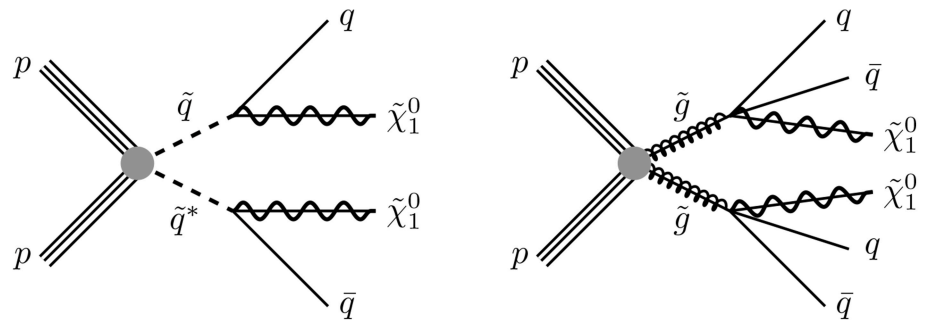

FIGURE 10 | Most simple topologies for the production of squarks and gluinos at the LHC with decays to jets + MET.

decays, ditau final states [417, 418] and diphotons, with and without associated W bosons [419–421]. Charged Higgs bosons, $H^{\pm}$ can typically be produced with associated resonant and non-resonant top-quark production. Their main decay channels are $H^{\pm} \to W^{\pm}Z$ [422, 423], $H^{\pm} \to t(c)b$ [416, 424] and $H^{\pm} \to \tau^{\pm}\nu$ [416, 425]. Since no excess has been found for either heavy H or $H^{\pm}$, the experiments set upper limits that strongly depend on the production cross section and, in turn, on $\tan\beta$. For H the limits range from $m_H < 400$ GeV for $\tan\beta = 2$ and production cross sections limits of 0.1 pb for larger masses. For $H^{\pm}$ with $m_{H^{\pm}} < 160$ GeV excluded for all values of $\tan\beta$ and $m_{H^{\pm}} < 1.1$ TeV excluded for $\tan\beta = 60$.

Many unified theories automatically preserve R-parity, such as left-right symmetric or Pati-Salam models, as well as supergroups of them, $SO(10)$ or E_6. This is because they contain a gauged $U(1)_{B-L}$ subgroup which effectively makes the LSP stable [76]. Other models, such as $SU(5)$, may have R-parity violating (RPV) interactions, though in general they will be suppresed since they can lead to rapid proton decay. Since the LSP is no longer stable, collider signatures of RPV typically contain multiple leptons [400], multiple jets [426–429] or both [430, 431] in the final state. These searches often impose strong upper limits on sparticle masses that range from 150 GeV to a few TeV for $\tilde{t}$, depending on the channel, and from 1 to 2 TeV, for $\tilde{g}$.

If the LSP is metastable or the lightest chargino and neutralino are almost degenerate, they can live long enough to leave a displaced vertex or a disappearing track on the detector. Detailed searches have been performed by ATLAS [432–436] and CMS [437–439] to search for these long-lived particles, and they have reached exclusion limits comparable to those of the detailed searches above.

Most of the searches described above assumed a neutralino LSP, which is typically the case in gravity mediated SUSY breaking. In gauge mediated SUSY breaking (GSMB) and general gauge mediation (GGM) the LSP is actually a nearly massless gravitino. In these cases new decay channels are open with photons [440–443], Z's [400, 403], Higgses [400, 403, 444], and τs [385, 445] in the final state (see **Figure 11**).

Although the LHC results are the most recent and, for the most part, they supersede the results of previous collider experiments, such as those at the Tevatron, some experimental limits from LEP still remain relevant today. In particular for models with a significant production of neutralino/chargino or slepton pairs, the limits from ALEPH [446, 447], OPAL [448, 449], L3 [450, 451], and DELPHI [452] on sleptons and electroweakino masses are rather pertinent, as they are largely model independent.

Many of the SUSY searches above are performed using simplified models, e.g., ATLAS jets and MET search assumes a 50–50 split between the decay modes of gluinos [372]. Therefore, the mass and cross section limits obtained are weakened in more complicated models. In order to assess the relevance of many of these exclusion limits on several popular SUSY models, a full global fit of the parameter space of the model is required. Several of these fits have been performed for the CMSSM, NUMH1 and NUMH2 [453–459], phenomenological MSSM models [460–462], SUSY GUT models [463] and electroweak-sector MSSM models [116], by the Zfitter [464][12], SuperBayes [465, 466][13], Fittino [467][14], MasterCode [468][15], and GAMBIT [469–476][16] collaborations.

6.2. Collider Searches for Leptoquarks

Leptoquarks (LQs) are associated either with the vector (spin 1) particles that correspond to the gauge bosons of the unified gauge group or they can be scalars (spin 0) and belong to a Higgs sector of a unified theory. Vector LQ mass is typically of the order of the unification scale and can only be accessible directly at colliders if the unification scale is low enough (e.g., Pati-Salam models). Scalar representations can also contain light fields, most notably the SM Higgs, but come at the cost of severe fine tuning, as discussed in the section 2 on the example of doublet-triplet splitting problem in 5-dim. representation of $SU(5)$. In non-supersymmetric unified models the presence of light colored scalars tends to aid unification (see e.g., [477]). Another important difference is that the scalar LQ interactions can be analyzed without specifying the concrete GUT completion in the ultraviolet. On the other hand, vector (gauge) LQs are sensitive to the mass generation mechanism that is specified in the ultraviolet. Therefore, effective vector LQ models are not renormalizable [478]. Furthermore, even the couplings of vector LQs to the SM gauge sector are not completely fixed by the gauge quantum numbers [479, 480].

Altogether there are six scalar and six vector leptoquarks, listed in **Table 1**, that couple to the SM matter at the renormalizable level [480–482]. The fermionic number $F \equiv 3B + L$ of leptoquarks that do not couple to diquarks (ϕqq) and are potentially B and L conserving, must be $F = 0$, whereas LQs with $|F| = 2$ in general destabilize the proton via $B - L$ conserving decays.

The most important phenomenological characteristic of light LQs (of mass of the order few TeV) is their color triplet nature allowing them to be produced in pairs via strong interactions in a largely model independent manner. In this section we will focus on the on-shell production of LQs at pp colliders, since the current mass constraints are dominated by LHC searches. For specific signatures of LQ production in colliders with alternative initial states (see [480]). Pair production of leptoquarks is model independent for the $gg \to \mathrm{LQ}\overline{\mathrm{LQ}}$ partonic process, while the parton level process $q\bar{q} \to \mathrm{LQ}\overline{\mathrm{LQ}}$ is affected also by the t-channel lepton exchange diagram (bottom right diagram in **Figure 12**) that introduces some model dependence when the leptoquark flavor couplings are non-negligible. The partonic cross sections for pair production at leading order

[12] zfitter.desy.de/
[13] www.ft.uam.es/personal/rruiz/superbayes
[14] flcwiki.desy.de/Fittino
[15] cern.ch/mastercode/
[16] gambit.hepforge.org

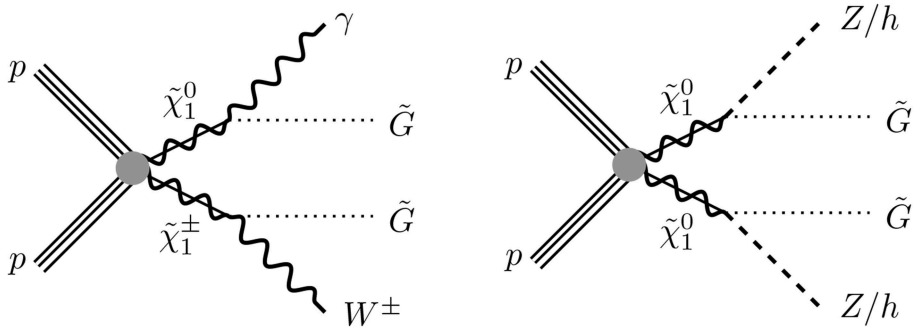

FIGURE 11 | Topologies for SUSY searches with gravitino LSP and γ and h/Z final states.

TABLE 1 | List of scalar and vector LQs.

LQ symbol	$[SU(3), SU(2), U(1)]$	Spin	F
S_3	$(\bar{\mathbf{3}}, \mathbf{3}, 1/3)$	0	-2
$\tilde{S}_1$	$(\bar{\mathbf{3}}, \mathbf{1}, 4/3)$	0	-2
S_1	$(\bar{\mathbf{3}}, \mathbf{1}, 1/3)$	0	-2
$\overline{S}_1$	$(\bar{\mathbf{3}}, \mathbf{1}, -2/3)$	0	-2
R_2	$(\mathbf{3}, \mathbf{2}, 7/6)$	0	0
$\tilde{R}_2$	$(\mathbf{3}, \mathbf{2}, 1/6)$	0	0
U_3	$(\mathbf{3}, \mathbf{3}, 2/3)$	1	0
$\tilde{U}_1$	$(\mathbf{3}, \mathbf{1}, 5/3)$	1	0
U_1	$(\mathbf{3}, \mathbf{1}, 2/3)$	1	0
$\overline{U}_1$	$(\mathbf{3}, \mathbf{1}, -1/3)$	1	0
V_2	$(\bar{\mathbf{3}}, \mathbf{2}, 5/6)$	1	-2
$\tilde{V}_2$	$(\bar{\mathbf{3}}, \mathbf{2}, -1/6)$	1	-2

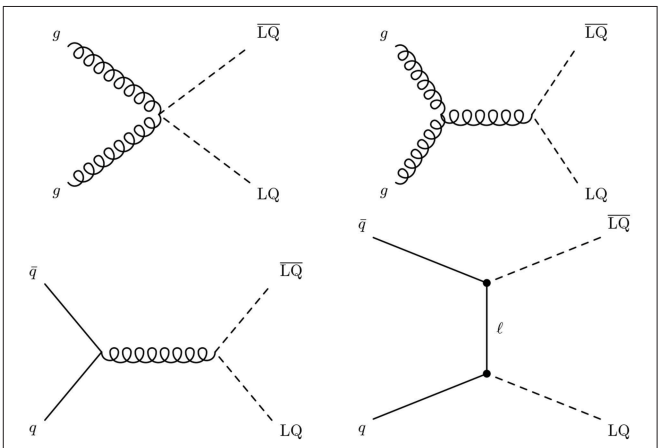

FIGURE 12 | Representative diagrams for leptoquark pair production at pp colliders. Dots denote the LQ-q-ℓ coupling.

are [483–488]:

$$\hat{\sigma}(gg \to \phi\bar{\phi}) = \frac{\alpha_3^2\pi}{96\hat{s}}\left[\beta(41-31\beta^2)+(18\beta^2-\beta^4-17)\log\frac{1+\beta}{1-\beta}\right], \quad (57)$$

$$\hat{\sigma}(q\bar{q} \to \phi\bar{\phi}) = \frac{2\alpha_3^2\pi}{27\hat{s}}\beta^3, \quad (58)$$

where $\hat{s}$ is the partonic center-of-mass energy squared, α_3 is the strong coupling constant, and $\beta = \sqrt{1-4m_\phi^2/\hat{s}}$. A model independent study of weak doublet scalar LQs at the LHC and the interplay with low energy flavor processes was performed in [489], where it was also shown that searches for single LQ production could be more sensitive in the regime of large Yukawas and/or LQ masses. An analysis of pair and single production, along with the corresponding UFO model files `LQ_NLO`, both for scalar and a vector leptoquark has been presented in Doršner and Greljo [490].

On the other hand, single leptoquark production at pp colliders is always model dependent (**Figure 13**). Single leptoquark searches are more effective at larger LQ masses [489].

On the decay side of the process, experimental searches for pair and single LQ production are targeting a resonance in the $j\ell$ channel. The decay width of a scalar leptoquark into a lepton-quark final state is given by [490] and [491]:

$$\Gamma(\phi \to q\ell) = \frac{|y_{q\ell}|^2 m_\phi^2}{16\pi}\left[1+\frac{\alpha_s}{\pi}\left(\frac{9}{2}-\frac{4\pi^2}{9}\right)\right]. \quad (59)$$

Current bounds from dedicated leptoquark pair production have been commonly extracted in the framework that assumed LQ coupling only to a single generation of SM fermions, whereas realistic LQ scenarios could posses richer flavor structure [480, 492]. The experimental upper bounds are given for the product of cross section and the LQ branching fraction probability β^2, where β is the probability for LQs to decay to a final state with charged leptons. There have been numerous analyses performed at the LHC for leptoquarks being either of 1st [493], 2nd [494], or 3rd [495–499] generation. More recent studies, motivated by the observed lepton universality violation in B-meson decays, allow also for cross-generational couplings, e.g., [500]. Finally, also single LQ production

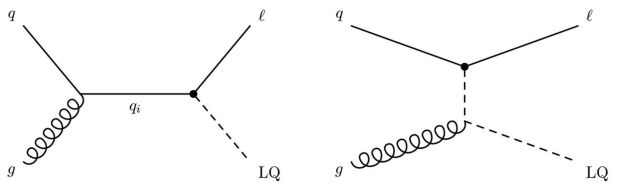

FIGURE 13 | Representative diagrams for single leptoquark production at *pp* colliders. Dots denote the LQ-q-ℓ coupling.

channels are being studied [501]. To conclude, the current lower bounds on leptoquark masses from direct searches at the LHC range from several 100 GeV to above the TeV scale, where the exact bound depends on the size of the flavor couplings.

6.3. Other Exotic Searches

Many unified theories include heavy sterile neutrinos that contribute to the mass of the light neutrinos via type-I seesaw mechanism (see section 3.2). These are often associated with the symmetry breaking of a left-right sector of the theory, and thus they are expected to be heavier than the EW scale. Direct searches for heavy neutrinos at colliders often target a decay channel where final state has two same-sign leptons, via s or t-channel production of a gauge boson that can be left or right handed [502]. **Figure 14** shows the Feynman diagram for the golden channel for heavy neutrino searches, $pp \to W \to Nl \to Wll \to lljj$. The ATLAS and CMS experiments at the LHC have performed searches for heavy neutrinos in LR models with masses $M_N \approx (20, 1,600)$ GeV and have imposed strong limits on the couplings between active and sterile neutrinos [503–505].

Other searches for sterile neutrinos are performed in beam dump experiments [506], where the neutrinos are produced in semileptonic decays of mesons, with masses below 2 GeV [507–510]. For intermediate masses below the Z resonance, the strongest limits come from the decay Z bosons by the LEP experiments DELPHI and L3 [511, 512].

In addition to singlet fermions and colored leptoquarks, the LHC looks for heavy colorless vector bosons as part of their exotic searches programme. Charged W' and neutral Z' vector bosons are predicted in a number of GUT frameworks and they can often live at low scales, which positions them within the reach of colliders. Clear examples of this are the left-right symmetric models described in section 4.1, that predict light W_R and Z_R bosons, or the light Z_N appearing in E_6SSM models .

These states are produced at pp colliders through Drell-Yan processes $pp \to W'/Z'$ and subsequently decay into leptons or jets. One of the most targeted processes for W' involve the decay into heavy neutrinos, as in **Figure 14**, with two same or opposite sign leptons (depending on the Majorana or Dirac nature of the heavy neutrinos) and jets [503, 504]. These searches often use a simplified model where $g_R = g_L$ and $M_N = M'_W/2$ resulting in high exclusion limits with $M_{W'} \gtrsim 4.5$ TeV, but it has been shown that these limits weaken somewhat in more general models [173–175]. CMS also reported a search for W' where the vector boson decays to $\tau\bar{\nu}_\tau$, the τ decaying hadronically [513], with slightly weaker limits.

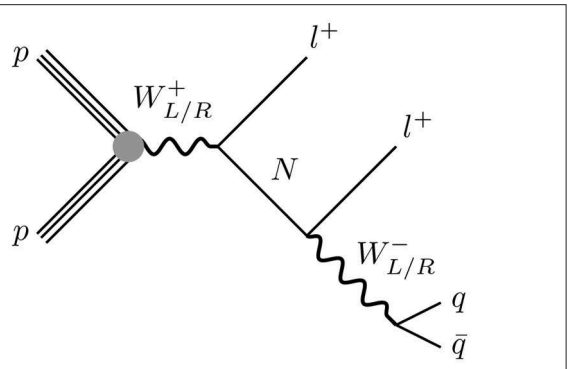

FIGURE 14 | Diagram for direct searches of neutrinos via $W_{L/R}$ production.

Narrow resonance searches for Z' have been performed by ATLAS and CMS, targeting final states with two opposite-sign leptons. These searches have yielded model-dependent exclusion limits on $M_{Z'}$. For E_6-inspired Z', the limits vary around $M_{Z'} \gtrsim (3, 3.5)$ TeV, whereas for LR models they are moderately stronger $M_{Z'} \gtrsim 4$ TeV [514, 515].

Lastly, GUTs predict a plethora of different scalar states that can be observed at the LHC if they are light enough, e.g., $\Delta_{L,R}$ in LR symmetric models. Searches for neutral and singly charged scalar bosons are identical to the searches for supersymmetric Higgs bosons in section 6.1, so we will not repeat them here. Doubly-charged scalars, such as the $\delta_L^{\pm\pm} \in \Delta_L$ in LR models, have been studied by ATLAS and CMS in multilepton final states [516, 517], diboson final states [518] and in long-lived particle studies [519] with model-dependent limits below 1 TeV.

7. PRECISION TESTS OF UNIFICATION

7.1. Proton Decay

Unified theories may contain gauge or scalar bosons that mediate transitions between leptons and quarks. These transitions violate baryon B and lepton L number separately and hence can cause the rapid decay of nucleons [520–529].

In the language of Effective Field Theory, nucleon decay transitions are generated by higher dimensional operators suppressed by the mass of the heavy mediator. The most relevant contribution to nucleon decay comes from dimension-6 operators of the form $qqql$, mediated either by a gauge or scalar boson. In SUSY GUTs, however, dimension 4 and 5 operators can appear, involving R-parity violating interactions and mixing among sfermions, respectively. Assuming the conservation of R parity and minimal flavor violation (MFV) in the sfermion sector, however, dimension 4 and 5 contributions can be made negligible [530–532]. Therefore, dimension 6 operators dominate the contributions

to nucleon decay. These are, in general, model dependent, so calculating the decay width requires knowledge of the flavor structure at the GUT scale and varies among the different decay channels [533, 534]. However, with some simplifying assumptions one can approximate the decay width of the proton as [535]

$$\Gamma_p \approx \alpha_{GUT}^2 \frac{m_p^5}{M_{GUT}^4}. \tag{60}$$

There are several decay channels for the proton and neutron, each with a different experimental bound. The most stringent of them, known as the *gold channel* for proton decay is $p \to e^+\pi^0$, whose parton-level diagrams can be seen in **Figure 15**, and with a lower limit on the half-life, set by the Super-Kamiokande, of $\tau > 1.6 \times 10^{34}$ years [43]. Other processes with slighly lower bounds are $\tau(p \to \mu^+\pi^0) > 7.7 \times 10^{33}$ years [43], $\tau(p \to \nu K^+) > 5.9 \times 10^{33}$ years [536] and $\tau(nn \to e^\pm\mu^\mp) > 4.4 \times 10^{33}$ years [537].

The next generation of experiments for nucleon decay has already been proposed. Hyper Kamiokande will take the place of Super-K and has a projected sensitivity in the golden channel $p \to e^+\pi^0$ of $\sim 10^{35}$ years [538]. The Deep Underground Neutrino Experiment (DUNE) [539] expects to improve the limit on $p \to \nu K^+$ to $\sim 3 \times 10^{34}$ years. These increased limits will probe unified teories at the highest scales and could be the smoking gun for them. In case of a positive signal from either of these experiments, precision calculations of proton decay processes with controlled uncertainties will become invaluable [84, 540].

7.2. Flavor Phenomenology of Light Leptoquarks

Several flavor couplings of scalar leptoquarks to leptons and quarks, which are in general connected to the GUT contractions of scalar and fermionic representations, allow their virtual effects to be tested in low-energy flavor observables. Such are the decays of hadrons or leptons, precision observables at LEP, and static properties of particles such as dipole moments. On the high-p_T front, the LHC is also becoming competitive as a flavor probe for virtual effects of particles that are too massive to be produced on-shell.

The correlations between lepton-quark-LQ couplings are determined at low scales by the weak isospin and hypercharge. As an example, consider the weak doublet leptoquark $R_2(3, 2, 7/6)$ (see **Table 1**), which can couple to two-types of lepton-quark bilinears:

$$\begin{aligned}\mathcal{L} &= Y_R^{ij}\overline{Q}_i'\ell_{Rj}'R_2 + Y_L^{ij}\overline{u}_{Ri}'\widetilde{R}_2^\dagger L_j' \\ &= (VY_R)^{ij}\overline{u}_{Li}\ell_{Rj}R_2^{\frac{5}{3}} + Y_R^{ij}\overline{d}_{Li}\ell_{Rj}R_2^{\frac{2}{3}} \\ &\quad + Y_L^{ij}\overline{u}_{Ri}\nu_{Lj}R_2^{\frac{2}{3}} - Y_L^{ij}\overline{u}_{Ri}\ell_{Lj}R_2^{\frac{5}{3}}.\end{aligned} \tag{61}$$

Here i, j are the flavor indices, primed fields are written in the interaction basis, unprimed fields are in the mass basis, except for the neutrinos which are aligned with charged leptons. There are three important features in the above Lagrangian. First, since R_2 is a weak doublet it must couple to left-handed quark doublets, which implies that CKM matrix V relates the couplings of up-type and down-type quarks. Second, R_2 couples to both chiralities of quarks and leptons, which leads to scalar and/or tensor effective interactions and could lead to enhanced effects in meson mixing amplitudes, dipole moments, and radiative decays [480]. Third, as $F = 0$ for R_2 we cannot construct interaction term with diquark coupling, implying that proton cannot decay via $\Delta(B - L) = 0$ process. Generalizing to other LQ states, weak triplets only talk to the left-handed fermions ($2 \otimes 2$), leading to strictly chiral interaction, whereas singlet LQs can talk to $2 \otimes 2$ and $1 \otimes 1$ fermion bilinears.

Among the flavor constraints, leptoquarks naturally (at tree-level) contribute to semileptonic effective operators at low scales, therefore the most relevant observables are (semi-)leptonic decays of mesons, baryons, or τ leptons. The most notable charged-current and flavor changing neutral current (FCNC) constraints, and the general framework to address them in leptoquark models, have been spelled out in Leurer [541], Davidson et al. [482], and Doršner et al. [480]. The most constraining are the FCNC observables, where the tree-level LQ contribution can easily stand out of the SM signal, which is 1-loop suppressed in the case of quark FCNC and absent in the case of lepton FCNC. Effective dimension-6 interactions for 4 lepton or 4 quark operators, which drive the $\ell \to \ell'\ell'\ell''$ (see section 7.4) and meson mixing processes, occur at one-loop [480]. Therefore, meson mixing is in general not among the strictest constraints on LQs (for B_s mixing see e.g., [542]).

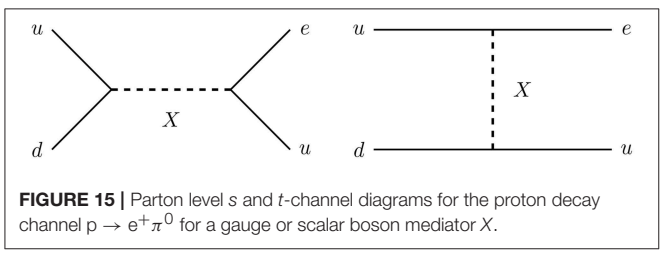

FIGURE 15 | Parton level *s* and *t*-channel diagrams for the proton decay channel $p \to e^+\pi^0$ for a gauge or scalar boson mediator *X*.

7.3. Lepton Flavor Universality

Lepton flavor universality (LFU) ratios, defined as ratios between rates for processes that differ only in lepton flavor, are very well suited to test the validity of the SM. The main advantage is that in the Standard Model LFU is respected by all gauge interactions, the only breaking comes from mass splitting among leptons, which leads to efficient cancellation of hadronic and parametric uncertainties in LFU ratios. Recently, two LFU ratios in *B*-meson decays have been observed

$$R_{D^{(*)}} = \frac{\mathcal{B}(B \to D^{(*)}\tau\overline{\nu}_\tau)}{\mathcal{B}(B \to D^{(*)}l\overline{\nu}_l)}, \quad R_{K^{(*)}} = \frac{\mathcal{B}(B \to K^{(*)}\mu\mu)}{\mathcal{B}(B \to K^{(*)}ee)}, \tag{62}$$

where $l = e, \mu$. Several experiments found that the ratios $R_{D^{(*)}}$ are larger than $R^{\rm SM}_{D^{(*)}}$. The measurements of R_D [13, 543, 544] differ by $\sim 2\,\sigma$ with respect to the SM prediction [545] and by $\sim 3\,\sigma$ in the case of R_{D^*} [546–548]. Combined significance reaches 4σ deviation from the SM [549]. The LHCb experiment has also measured $R_{K^{(*)}}$ LFU ratios, related to the neutral-current process $b \to sll$, and found them to be lower than expected in the SM. While R_K was measured in a single kinematical region, $q^2 \in [1.1, 6]\,\text{GeV}^2$ [12], R_{K^*} was measured also in the ultra-low region $q^2 \in [0.045, 1.1]\,\text{GeV}^2$ [550]. Each of the $R_{K^{(*)}}$ measurements is $\sim 2.5\,\sigma$ below the SM prediction level [551, 552], and furthermore, there are discrepancies in $b \to s\ell\ell$ driven decays that are coherent with the deviation in $R_K^{(*)}$ if there is $\sim$ 20% reduction in the vector Wilson coefficient C_9 [553, 554].

Light leptoquarks are prime candidates to explain one or both of those puzzles. For the $R_{D^{(*)}}$ the effective Lagrangian contains four relevant operators:

$$\begin{aligned}\mathcal{L}^{b\to c\tau\bar{\nu}_\tau}_{\rm eff} = -\frac{4\,G_F}{\sqrt{2}} V_{cb}\big[&(1+g_{V_L})(\bar{c}_L\gamma_\mu b_L)(\bar{\tau}_L\gamma^\mu \nu_{\tau L}) \\ &+ g_{S_L}(\mu)\,(\bar{c}_R b_L)(\bar{\tau}_R \nu_{\tau L}) + g_{S_R}(\mu)\,(\bar{c}_L b_R)(\bar{\tau}_R \nu_{\tau L}) \\ &+ g_T(\mu)\,(\bar{c}_R \sigma_{\mu\nu} b_L)(\bar{\tau}_R \sigma^{\mu\nu} \nu_{\tau L})\big].\end{aligned} \tag{63}$$

Model independently it has been shown that $R_{D^{(*)}}$ can be explained either by rescaling the SM semileptonic operator (g_{V_L}), by turning on g_T, or by particular combinations of scalar and tensor operators, $g_{S_L} = \pm 4 g_T$ operators, that arise in presence of a non-chiral LQ [555–558]. In order to address $R_{K^{(*)}}$ one has to modify the vector Wilson coefficient C_9 whereas the axial Wilson coefficient C_{10} may also be present in the effective Lagrangian:

$$\mathcal{H}^{b\to s\mu\mu}_{\rm eff} = -\frac{\alpha G_F V_{tb} V^*_{ts}}{\sqrt{2}\pi}\,(\bar{s}_L\gamma_\mu b_L)(\bar{\mu}\gamma^\mu(C_9 + C_{10}\gamma^5)\mu. \tag{64}$$

Also purely left-handed scenarios with $C_9 = -C_{10} \approx -0.6$, which are characteristic of LQ weak-singlet or triplet exchange, are in good agreement with $R_{K^{(*)}}$ and the global fit of $b \to s\ell\ell$. Such left-handed leptoquark solutions have been put forward: triplet scalar S_3, singlet vector U_1, triplet vector U_3 [557, 558]. For loop-level explanation of $R_{K^{(*)}}$ one can also invoke singlet S_1 [559] or doublet R_2 [560], but at the price of large couplings. There are several proposals with scalar leptoquarks that address $R_{K^{(*)}}$ and/or $R_{D^{(*)}}$ [559, 561–566], some in the context of unified theories such as $SU(5)$ [567–569], left-right symmetry [570], Pati-Salam [571, 572], $SO(10)$ [573] and others [574]. Recently it was realized that a singlet vector leptoquark $U_1^\mu(3,1,2/3)$ generates left-handed interactions and partially resolves both LFU puzzles, in many UV frameworks [575–577], including three-flavor extensions of the Pati-Salam model [578–584].

Finally, moderately large leptoquark couplings dictated by the above LFU anomalies can be also observed in processes with virtual LQ exchange, typically in the t-channel, resulting in a final state with at least one charged lepton. Inspired by the abovementioned LFU anomalies, processes with final state leptons have been studied, which can probe LQ scenarios for LFU violation observed in B meson decays [585–588]. In this case, LQ cannot be produced on-shell and the sensitivity does not deteriorate abruptly with rising LQ mass. Instead there is a smooth transition to the effective theory picture, where heavy LQ is integrated out. Thus, among the LQ induced processes the t-channel has the best mass reach for LQs and it is thus complementary to pair and single production [489, 490]. Another recent set of observables at the LHC, targeting the LQ scenarios that are well suited to explain the LFU anomalies $R_{D^{(*)}}$, are the searches with a single τ lepton in the final state [589][17]. Third generation leptoquarks could also be probed in $t\bar{t}$ final states [591].

7.4. Lepton Flavor Violation and Dipole Moments

In the SM with massive neutrinos, lepton flavor violation (LFV) can occur via the mixing in the neutrino sector. It is, however, heavily suppressed due to the GIM mechanism [592], as the rate depends on the neutrino masses resulting in an unobservable prediction of order 10^{-55} [593]. Extensions of the SM modify this prediction by introducing additional sources of lepton flavor violation [594–596]. New physics can then be probed by testing the deviations of certain lepton flavor violating processes with respect to the experimental limits.

Charged lepton flavor violating processes are typically of three types: $l^-_\alpha \to l^-_\beta\gamma$, $l^-_\alpha \to l^-_\beta l^-_\gamma l^+_\delta$ (with $\alpha \neq \beta$) and $\mu - e$ conversion in nuclei [597]. One-loop contributions to the first two processes can occur through a dipole and box diagrams as depicted in **Figure 16**, with a scalar or vector mediator(s) $X(X')$ and a SM or exotic fermion(s) $f(f')$ running in the loop. Contributions to $\mu - e$ conversion follows from the penguin (center) and box (right) diagrams with $l_\alpha = \mu$, $l_\beta = e$ and $l_{\gamma,\delta} = q$.

Unified theories often contain a number of exotic states capable of fulfilling the role of X and f in **Figure 16**, violating lepton flavor either by interactions between the leptons and mediators or by mixing in the leptonic sector. The latter case is realized in GUT models with heavy neutrinos (c.f. left-right models in section 4.1), where the mixing between active and sterile neutrinos enhances the LFV contribution [598–600]. The contribution to the branching ratios of the most constraining LFV processes, $\mu \to e\gamma$, $\mu \to eee$ and $\mu - e$ conversion, in these models, with heavy neutrinos of mass M_{N_I}, active-sterile mixing $\Theta_{\alpha I}$, a right-handed gauge boson W_R and left and right-handed scalar triplets δ_L and δ_R, can be written as [601], [602], and [174]

[17] See also [590] for constraints on couplings to light quarks.

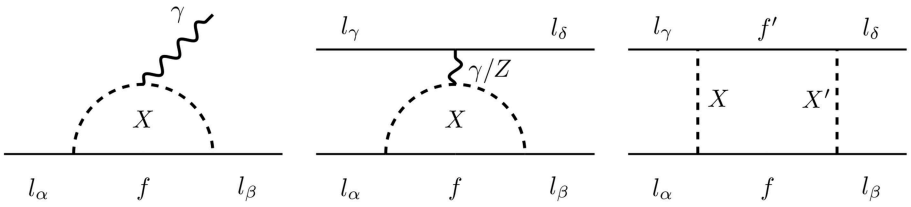

FIGURE 16 | Diagrams contributing to LFV processes, $l_\alpha^- \to l_\beta^- \gamma$ (left) and $l_\alpha^- \to l_\beta^- l_\gamma^- l_\delta^+$ (center and right) with X and X' scalar or vector mediators and f and f' fermions.

$$
\begin{aligned}
BR(\mu \to e\gamma) &\sim 1.5 \times 10^{-7} |\Theta^*_{eI}\Theta_{\mu I}|^2 \left(\frac{g_R}{g_L}\right)^4 \left(\frac{m_{N_I}}{m_{W_R}}\right)^4 \left(\frac{1\,\text{TeV}}{M_{W_R}}\right)^4, \\
BR(\mu \to eee) &\sim \frac{1}{2} |\Theta^*_{eI}\Theta_{\mu I}|^2 |\Theta_{eI}|^4 \left(\frac{g_R}{g_L}\right)^4 \left(\frac{m_{N_I}}{m_{W_R}}\right)^4 \left(\frac{M^4_{W_R}}{M^4_{\delta_R}} + \frac{M^4_{W_R}}{M^4_{\delta_L}}\right), \\
R^N(\mu - e) &\sim 0.73 \times 10^{-9} X_N |\Theta^*_{eI}\Theta_{\mu I}|^2 \left(\frac{g_R}{g_L}\right)^4 \left(\frac{m_{N_I}}{m_{W_R}}\right)^4 \left(\frac{1\,\text{TeV}}{M_{\delta_R}}\right)^4 \left(\log \frac{m^2_{\delta_R}}{m^2_\mu}\right)^2.
\end{aligned}
\tag{65}
$$

In supersymmetric GUTs there are many possible sources of lepton flavor violation, parametrised by the mixing in the slepton sector of the MSSM, which has contributions to LFV processes of the type [603]

$$
BR(l_\alpha \to l_\beta \gamma) \approx \frac{48\pi^3 \alpha_{\text{em}}}{G_F^2} \frac{|(m^2_{\tilde{L}})_{ij}|^2 + |(m^2_{\tilde{e}})_{ij}|^2}{M^8_{SUSY}} BR(l_\alpha \to l_\beta \nu_\alpha \overline{\nu}_\beta). \tag{66}
$$

Off-diagonal entries in the slepton mass matrices can be the result of non-minimal flavor violating interactions or non-canonical Yukawa textures at the GUT scale, where the soft masses are supposed to unify [604, 605]. In addition, slepton mixing can be induced in minimal flavor violating (MFV) SUSY via seesaw mechanisms [606–612] or, for Yukawa-unified theories (see section 3.3), it can depend on the CKM matrix at the GUT scale [596]. LFV contributions can also arise in SUSY models where R-parity is violated, explicitly or spontaneously, with interaction terms of the type $l_i l_j \tilde{\nu}_k$ that induce tree-level contributions to $l \to lll$ decays and $\mu \to e$ conversion, as well as new dipole contributions to $l \to l\gamma$ [613–617].

The anomalous electric, d_i, and magnetic, a_i, dipole moments of quarks and leptons follow from processes identical to the diagram on the left in **Figure 16**, where l_α and l_β have the same flavor. Hence contributions from heavy states running in the loops can have a strong effect that can be tested experimentally. As with LFV, the SM contribution to electric dipole moments (EDMs) is tiny, as it is proportional to the CP-violation phase in the CKM matrix [618, 619]. EDMs have not been observed experimentally, so deviations from the SM prediction due to CP-violation in other sectors is strongly constrained [620]. Other sources of CP violation can appear in neutrino mixing [619], phases in fermion-sfermion couplings [621] or extended Higgs sectors [622]. Anomalous magnetic moments (AMM), on the other hand, have been measured with extreme accuracy. In fact, the precision of both the experimental measurement and theoretical prediction for a_μ has shown a discrepancy of more than 3 standard deviations [34]. New physics contributions have been shown to resolve that tension, particularly in the context of supersymmetry [623].

In the presence of light leptoquarks anomalous dipole moments of leptons or quarks are one-loop processes [480]. A special feature of non-chiral leptoquarks, such as R_2 with couplings (61), is that both l_{ij} and r_{ij} are non-zero in the interaction Lagrangian $\overline{q}^i \left[l_{ij} P_R + r_{ij} P_L\right] \ell^j \phi$ which then leads to the anomalous moment of the muon:

$$
a_\mu = -\frac{3m_\mu^2}{8\pi^2 m_\phi^2} \sum_q \Bigg[\left(|l_{q\mu}|^2 + |r_{q\mu}|^2\right) \left(Q_\phi/4 - 1/6\right) - \frac{m_q}{m_\mu} \log \frac{m_q^2}{m_\phi^2} \text{Re}(r^*_{q\mu} l_{q\mu}) \left(Q_\phi - 1\right) \Bigg],
$$

where m_ϕ and Q_ϕ are the charge and mass of the leptoquark and q is the flavor of the quark in the loop (see the leftmost diagram in **Figure 16**). Shown is the leading order contribution in m_q. The first term increases a_μ only when $Q_\phi > 2/3$ and it is present for all scalar LQ states that couple to a muon. The second term is relevant for non-chiral LQs and it is chirally enhanced by m_q/m_ℓ, possibly leading to large effects with moderate couplings to b or t quark. Furthermore, the sign of the non-chiral term is adjustable. On the other hand, the same mechanism also enhances dipole LFV transitions, e.g., $\mu \to e\gamma$, $\tau \to \mu\gamma$ [560]. Non-chiral LQs may also generate quark or lepton electric dipole moments at 1-loop [624, 625].

Whichever the mechanism, it is clear that LFV and anomalous dipole moments are predicted by many GUT models, with varying strengths for different processes. The full list of processes and their current experimental upper bounds and measurements can be seen in **Table 2**, where the experiments that have studied the processes are detailed. Furthermore, new experiments are

TABLE 2 | Upper bounds at 90% C.L on LFV processes and EDMs, and measurements of AMMs, along with the experiments that provided them.

Process	Branch. Frac.	Reference
$\mu^- \to e^-\gamma$	4.2×10^{-13}	MEG [626]
$\tau^- \to e^-\gamma$	5.4×10^{-8}	BaBar [627], Belle [628]
$\tau^- \to \mu^-\gamma$	5.0×10^{-8}	BaBar [627], Belle [628]
$\mu^- \to e^-e^-e^+$	1.0×10^{-12}	SINDRUM [629]
$\tau^- \to e^-e^-e^+$	1.4×10^{-8}	BaBar [630], Belle [631]
$\tau^- \to \mu^-\mu^-\mu^+$	1.2×10^{-8}	ATLAS [632], BaBar [630], Belle [631], LHCb [633]
$\tau^- \to \mu^-e^-e^+$	1.1×10^{-8}	BaBar [630], Belle [631]
$\tau^- \to e^-e^-\mu^+$	0.84×10^{-8}	BaBar [630], Belle [631]
$\tau^- \to e^-\mu^-\mu^+$	1.6×10^{-8}	BaBar [630], Belle [631]
$\tau^- \to \mu^-\mu^-e^+$	0.98×10^{-8}	BaBar [630], Belle [631]
$\mu - e$ (Ti)	1.7×10^{-12}	SINDRUM II [634]
$\mu - e$ (Pb)	4.6×10^{-11}	SINDRUM II [635]
$\mu - e$ (Au)	8.0×10^{-13}	SINDRUM II [636]
d_e	1.1×10^{-29} *e cm*	ACME II [637]
d_μ	1.9×10^{-19} *e cm*	Muon g-2 [638]
d_τ	4.5×10^{-17} *e cm*	Belle [639]
$a_e(10^{-13})$	11596521809.1 ± 2.6	[640]
$a_\mu(10^{-10})$	11659208.9 ± 8.7	Muon g-2 [641]

The HFLAV average is quoted for limits by different experiments [549].

TABLE 3 | An overview of both current and future major $0\nu\beta\beta$ decay searches.

Experiment	Isotope	Status	M [kg]	$T^{0\nu\beta\beta}_{1/2}$ limit [y]
CUORE	^{130}Te	running	200	(3.5×10^{26})
EXO-200	^{136}Xe	running	110	1.1×10^{25}
nEXO	^{136}Xe	R&D	5000	$(10^{27}$-$10^{28})$
GERDA	^{76}Ge	running	21.6	5.3×10^{25}
		in progress	40	$(\sim 10^{26})$
KamLAND-Zen	^{136}Xe	running	383	1.1×10^{26}
		in progress	600	(2×10^{26})
LEGEND	^{76}Ge	R&D	200	$(\sim 10^{27})$
		R&D	1000	$(\sim 10^{28})$
Majorana Dem.	^{76s}Ge	running	44.1	1.9×10^{25}
NEXT	^{136}Xe	in progress (demo)	100	(5.9×10^{25})
SNO+	^{130}Te	in progress	1300	(2×10^{26})
SuperNEMO	^{82}Se (^{150}Nd)	in progress (demo)	100	$(\sim 10^{26})$

For each experiment the following information is shown: used isotope, operational status, the deployed mass M of the isotope in question and the measured or expected (for experiment in preparation these values are shown in parentheses) sensitivity $T^{0\nu\beta\beta}_{1/2}$. For some experiments (GERDA, KamLAND-Zen, LEGEND) characteristics of more stages of development are given. In case of SuperNEMO, the primary isotope to be tested is ^{82}Se and in the future the measurement will be repeated with a ^{150}Nd source.

being developed at this moment that will attempt to improve the limits on processes like $\mu \to eee$ (Mu3e [642]) and $\mu - e$ conversion (COMET [643], Mu2e [644]), with projected limits up to four orders of magnitude stronger than previous studies. Additionally, a new measurement of a_μ has been performed by the Muon g-2 experiment and it is expected to be released soon [645], which may confirm the deviation observed before, and thus further motivate the need of new physics.

7.5. Neutrinoless Double Beta Decay

This rare nuclear process corresponding to a simultaneous conversion of two neutrons to two protons and two electrons within the nucleus [646] is of great interest for particle physics, as it clearly does not conserve lepton number, and thus violates the corresponding accidental Abelian global symmetry of the SM. Consequently, a strong experimental effort is being made to observe this unique process. Unfortunately, its observation will be very difficult, as $0\nu\beta\beta$ decay is expected to be extremely rare. There is a number of experiments, some in operation, other being constructed or planned, attempting to measure the decay. An overview of the major collaborations is shown in **Table 3**. The current experimental lower limits on its half-life are around 10^{26} years [647, 648] and the future searches should reach sensitivities by one or two orders of magnitude higher.

As can be shown, the existence of $0\nu\beta\beta$ decay implies the Majorana nature of neutrinos (and vice versa) [649–651] and as such it represents one of the best probes of this BSM hypothesis. Therefore, in GUT models allowing for Majorana neutrino mass generation $0\nu\beta\beta$ decay can be in principle always triggered. This, however, does not say anything about the underlying mechanism and the resulting $0\nu\beta\beta$ decay rate. The prominent *standard (mass) mechanism* of $0\nu\beta\beta$ decay assumes a light Majorana neutrino exchange between the two beta-decaying neutrons. In the SM with light massive neutrinos this process can be depicted as shown in **Figure 17**, left. Besides the standard scenario a number of *non-standard mechanisms* triggering $0\nu\beta\beta$ decay can be constructed. The effective treatment of these exotic mechanisms can be conveniently employed (see e.g., [652–656]).

As for the UV-complete $0\nu\beta\beta$ decay mechanisms, a variety of interesting ones can be constructed within GUTs. For instance, in the left-right symmetric models (where, of course, the standard light neutrino exchange is available) one can think of several exotic mechanisms involving exchange of heavy neutrino as well as light and heavy W vector bosons [657]. In the simplest exotic case the light neutrino exchange is substituted by a heavy right-handed neutrino exchange, which means that the involved vector currents and emitted electrons must be also right-handed. Due to the large mass of the propagating neutrino, the interaction can be considered to be contact and we refer to this contribution as to short-range mechanism. Since the right-handed currents are present in left-right symmetric models, it is also possible to draw $0\nu\beta\beta$ decay mechanisms, in which the neutrino exchange does not violate chirality. This means that the contribution is not proportional to the neutrino mass and the two outgoing electrons are of opposite chiralities. A possible mechanism of this type is depicted in **Figure 17**, right. As apparent, the diagram involves one right-handed and one left-handed vector current and since the light neutrino propagator is present, one refers to this contribution as to a long-range $0\nu\beta\beta$ decay mechanism.

Leptoquarks, particles appearing prominently in GUTs, can also trigger non-standard $0\nu\beta\beta$ decay contributions. It has been described that this is the case, when different leptoquark multiplets mix via a possible leptoquark-Higgs coupling violating lepton number [658, 659]. Diagrams of this type of contributions to $0\nu\beta\beta$ decay are shown in **Figure 18**. The specific helicity structure of the effective four-fermion interaction leads to the fact that this contribution can dominate over the standard

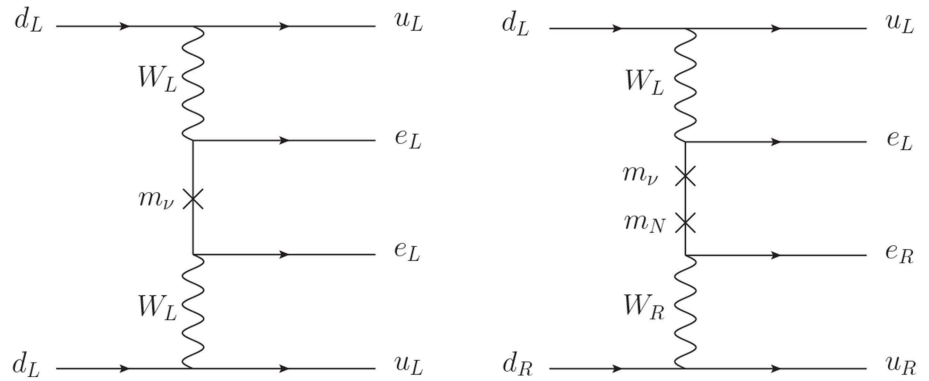

FIGURE 17 | The standard mass mechanism of $0\nu\beta\beta$ decay **(left)** and a non-standard contribution that can be constructed in the left-right symmetric models using vector currents of opposite chiralities **(right)**.

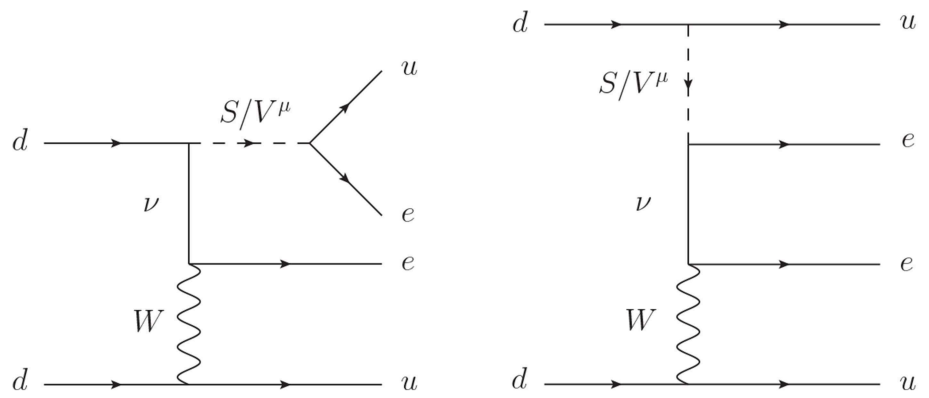

FIGURE 18 | The exotic $0\nu\beta\beta$ decay mechanisms involving scalar or vector leptoquarks S, V^μ.

mass mechanism. The current lower limits on $0\nu\beta\beta$ decay half-life then allow to derive the bounds on corresponding leptoquark parameters.

Neutrinoless double beta decay can be triggered also in supersymmetric theories aspiring for grand unification. In the simplest case, if the MSSM with broken R parity is considered, $0\nu\beta\beta$ decay diagrams involving R-parity-violating couplings and supersymmetric mediators can be drawn [660–664]. An example of a supersymmetric $0\nu\beta\beta$ decay mechanism is depicted in **Figure 19**. Again, from non-observation of $0\nu\beta\beta$ decay it is possible to derive limits on the unknown model parameters.

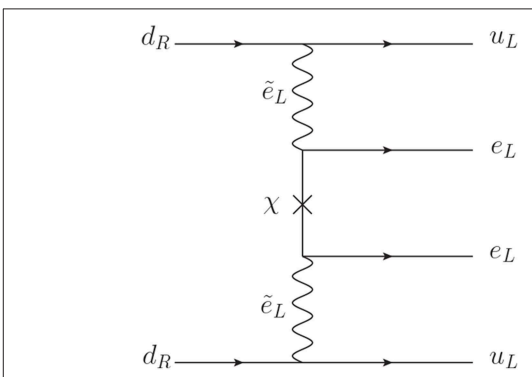

FIGURE 19 | An example of a $0\nu\beta\beta$ decay mechanism that can be triggered in R-parity-violating MSSM.

8. OUTLOOK AND FUTURE PROSPECTS FOR GUTS

Among the vast landscape of theories beyond the Standard Model, Grand Unified Theories stand out as appealing candidates. As we have seen, GUTs are a collection of ideas from group theory, supersymmetry, neutrino physics, flavor physics and more, which positions them as some of the most complete and attractive theories in the literature. Indeed they are among the few BSM theories capable of simultaneously affecting the highest energy scales, influencing the cosmology of the early Universe, and the low energies, within reach of colliders and terrestrial experiments.

Throughout this review article we have provided a rough sketch of the status of GUTs and some of the associated research

in the field. We have described the basic principles behind them and their first appearance in the world of particle physics in the late 70s. A lot of effort was spent in the years after and many of the greatest models were designed at that time. Research in GUTs has continued since, focusing either on specific topics within and alongside them, or on particular models that compiled a few advances in the field. We have thus summarized a non-exhaustive selection of topics and models that are at the forefront of research in unified theories, aiming to provide an overview of the current state of the art.

We are fortunate enough to live in a time where experimental searches are abundant and they cover a rather vast range of fronts. The most cutting-edge technologies have been and are being developed to push the boundaries of our current understanding of particle physics and cosmology. Grand unified theories are and will be put under the microscope by many of these experimental advances, which will confirm, constrain or outright exclude some of the existing models.

The recent observation of gravitational wave signatures opens a new window into the history of the Universe, where events and phenomena that ocurred in the early Universe can be observed with gravitational wave detectors. Cosmic phase transitions associated with patterns of symmetry breaking in unified theories are such events, as they can be the source of stochastic gravitational waves that can be observed today. Transition temperatures above the EW scale, typically associated with the breaking of some intermediate step in a GUT model, can be studied by future gravitational wave experiments such as a LISA, the Einstein telescope, Kagra, the Cosmic Explorer, BBO and DEIGO. Also in the cosmological frontier, GUTs can have a serious impact on the inflationary epoch of the Universe, testable in measurements of the CMB, and can contribute to the baryon asymmetry of the Universe, via baryo and leptogenesis.

At the time of writing we have reached the end of the second run of the LHC, with an outstanding recorded integrated luminosity of about 150 fb^{-1}. Analyses of the accumulated data, however, are still under way and they will probably spill well into the start run 3 in 2021. Many of the analyses already published have strong consequences for the predictions of unified theories, as are direct searches for supersymmetry, leptoquarks or other exotics at ATLAS and CMS. Upcoming results from ongoing and future analyses of the results from the LHC experiments may strengthen the bounds on light states as predicted by SUSY GUTs and other models, or they might show hints of the existence of new particles, whose relevance for GUTs would need to be determined. Upgraded versions of the LHC (HL-LHC, VLHC or FCC) or other future colliders (ILC, CLIC) will certainly boost this programme with increased accuracy and higher energies, which will further probe the low-hanging states predicted by GUTs.

Where colliders search for the low scale predictions of GUTs, precision experiments can explore the intermediate and high scales associated with unification. Nucleon decay limits are often among the strongest probes of fully unified theories and future experiments such as Hyper-Kamiokande and DUNE may set even stronger exclusion limits or perhaps measure signs of proton decay, which would be a smoking gun for GUTs. Furthermore, GUTs can provide contributions to a number of flavor and precision observables, such as LFU, LFV, EDM, AMM, or $0\nu\beta\beta$, some of which are in tension with the SM. Confirmation of these flavor anomalies with more collected data by LHCb and other experiments would be undeniable evidence of the need for new physics models and GUTs are very well suited for that purpose.

To conclude, Grand Unified Theories are still at the vanguard of research in BSM models. They can explain many of the issues of the SM and can accommodate the recent results from the cosmological, precision and collider frontiers with relative ease. Contrary to "simplified" models, GUTs are complete theories that can simultaneously make a large number of testable predictions on the different fronts. Fortunately, these predictions can be explored by upcoming analyses and future experiments, which can set strong exclusion limits in a subset of GUT models. On a more optimistic note, any observation in, for instance, SUSY searches at colliders, gravitational waves signatures or proton decay will stack the odds in favor of some GUT models and will significantly shape the future of the research in particle physics.

AUTHOR CONTRIBUTIONS

TG has lead the development of this review. All other authors have contributed equally.

ACKNOWLEDGMENTS

The authors would like to thank P. Athron, F. Deppisch, A. Kvellestad, and Y. Zhang for helpful discussions. TG was partly funded by the Research Council of Norway under FRIPRO project number 230546/F20 and partly supported by the ARC Centre of Excellence for Particle Physics at the Tera-scale, grant CE110001004. NK was supported by the Slovenian Research Agency under the research core funding grant P1-0035 and No. J1-8137. TRIUMF receives federal funding via a contribution agreement with the National Research Council of Canada and the Natural Science and Engineering Research Council of Canada.

REFERENCES

1. Glashow S. Partial symmetries of weak interactions. *Nucl.Phys.* (1961) **22**:579–88. doi: 10.1016/0029-5582(61)90469-2
2. Weinberg S. A model of leptons. *Phys Rev Lett.* (1967) **19**:1264.
3. Salam A. Weak and electromagnetic interactions. *Conf Proc C.* (1968) **680519**:367–77.
4. Aad G, Abajyan T, Abbott B, Abdallah J, Khalek SA, Abdelalim AA, et al. Observation of a new particle in the search for the Standard Model Higgs boson with the ATLAS detector at the LHC. *Phys Lett.* (2012) **B716**:1–29.
5. Chatrchyan S, Khachatryan V, Sirunyan AM, Tumasyan A, Adam W, Aguilo E, et al. Observation of a new boson at a mass of 125 GeV with the CMS experiment at the LHC. *Phys Lett.* (2012) **B716**:30–61. doi: 10.1016/j.physletb.2012.08.021
6. Higgs PW. Broken symmetries and the masses of gauge bosons. *Phys Rev Lett.* (1964) **13**:508–9.

7. Englert F, Brout R. Broken symmetry and the mass of gauge vector mesons. *Phys Rev Lett.* (1964) **13**:321–3.
8. Guralnik GS, Hagen CR, Kibble TWB. Global conservation laws and massless particles. *Phys Rev Lett.* (1964) **13**:585–7.
9. Degrassi G, Di Vita S, Elias-Miro J, Espinosa JR, Giudice GF, Isidori G, et al. Higgs mass and vacuum stability in the Standard Model at NNLO. *J High Energy Phys.* (2012) **08**:098.
10. Fukuda Y, Hayakawa T, Ichihara E, Inoue K, Ishihara K, Ishino H, et al. Evidence for oscillation of atmospheric neutrinos. *Phys Rev Lett.* (1998) **81**:1562–7.
11. Ahmad QR, Allen RC, Andersen TC, Anglin JD, Buhler G, Barton JC, et al. Measurement of the rate of $\nu_e + d \rightarrow p + p + e^-$ interactions produced by ^8B solar neutrinos at the Sudbury Neutrino Observatory. *Phys Rev Lett.* (2001) **87**:071301. doi: 10.1103/PhysRevLett.87.071301
12. Aaij R, Adeva B, Adinolfi M, Affolder A, Ajaltouni Z, Akar S, et al. Test of lepton universality using $B^+ \rightarrow K^+\ell^+\ell^-$ decays. *Phys Rev Lett.* (2014) **113**:151601. doi: 10.1103/PhysRevLett.113.151601
13. Aaij R, Adeva B, Adinolfi M, Affolder A, Ajaltouni Z, Akar S, et al. Measurement of the ratio of branching fractions $\mathcal{B}(\overline{B}^0 \rightarrow D^{*+}\tau^-\overline{\nu}_\tau)/\mathcal{B}(\overline{B}^0 \rightarrow D^{*+}\mu^-\overline{\nu}_\mu)$. *Phys Rev Lett.* (2015) **115**:111803. doi: 10.1103/PhysRevLett.115.111803
14. Aaij R, Adeva B, Adinolfi M, Ajaltouni Z, Akar S, Albrecht J, et al. Measurement of the $B_s^0 \rightarrow \mu^+\mu^-$ branching fraction and effective lifetime and search for $B^0 \rightarrow \mu^+\mu^-$ decays. *Phys Rev Lett.* (2017) **118**:191801. doi: 10.1103/PhysRevLett.118.191801
15. Georgi H, Glashow SL. Unity of all elementary-particle forces. *Phys Rev Lett.* (1974) **32**:438–41.
16. Pati JC, Salam A. Lepton number as the fourth color. *Phys Rev.* (1974) **D10**:275–89.
17. Mohapatra RN, Pati JC. Left-right gauge symmetry and an isoconjugate model of CP violation. *Phys Rev.* (1975) **D11**:566–71.
18. Fritzsch H, Minkowski P. Unified interaction of leptons and hadrons. *Ann Phys.* (1975) **93**:193–266.
19. Georgi H. The state of the art-gauge theories. *AIP Conf Proc.* (1975) **23**:575–82.
20. Langacker P. Grand unified theories and proton decay. *Phys Rept.* (1981) **72**:185.
21. Gonzalo Velasco T. *Model Building and Phenomenology in Grand Unified Theories*. University Coll. London (2015). Available online at: http://discovery.ucl.ac.uk/id/eprint/1471160
22. Raby S. Supersymmetric grand unified theories. *Lect Notes Phys.* (2017) **939**:1–308. doi: 10.1007/978-3-319-55255-2
23. Nath P. High energy physics and cosmology at the unification frontier: opportunities and challenges in the coming years. *Int J Mod Phys.* (2018) **A33**:1830017. doi: 10.1142/S0217751X1830017X
24. Candelas P, Horowitz GT, Strominger A, Witten E. Vacuum configurations for superstrings. *Nucl Phys.* (1985) **B258**:46–74.
25. Witten E. Symmetry breaking patterns in superstring models. *Nucl Phys.* (1985) **B258**:75. doi: 10.1016/0550-3213(85)90603-0
26. Gursey F, Sikivie P. E(7) as a universal gauge group. *Phys Rev Lett.* (1976) **36**:775.
27. Branco GC, Ferreira PM, Lavoura L, Rebelo MN, Sher M, Silva JP. Theory and phenomenology of two-Higgs-doublet models. *Phys Rept.* (2012) **516**:1–102.
28. Georgi H, Quinn HR, Weinberg S. Hierarchy of interactions in unified gauge theories. *Phys Rev Lett.* (1974) **33**:451–4.
29. Buras AJ, Ellis JR, Gaillard MK, Nanopoulos DV. Aspects of the grand unification of strong, weak and electromagnetic interactions. *Nucl Phys.* (1978) **B135**:66–92.
30. Chanowitz MS, Ellis JR, Gaillard MK. The price of natural flavor conservation in neutral weak interactions. *Nucl Phys.* (1977) **B128**:506–36.
31. Georgi H, Jarlskog C. A new lepton-quark mass relation in a unified theory. *Phys Lett.* (1979) **86B**:297–300.
32. Dimopoulos S, Georgi H. Softly broken supersymmetry and SU(5). *Nucl Phys.* (1981) **B193**:150–62.
33. Masiero A, Nanopoulos DV, Tamvakis K, Yanagida T. Naturally massless higgs doublets in supersymmetric SU(5). *Phys Lett.* (1982) **115B**:380–4.
34. Tanabashi M, Hagiwara K, Hikasa K, Nakamura K, Sumino Y, Takahashi F, et al. Review of particle physics. *Phys Rev.* (2018) **D98**:030001. doi: 10.1088/1674-1137/40/10/100001
35. Grinstein B. A supersymmetric SU(5) gauge theory with no gauge hierarchy problem. *Nucl Phys.* (1982) **B206**:387.
36. Hisano J, Moroi T, Tobe K, Yanagida T. Suppression of proton decay in the missing partner model for supersymmetric SU(5) GUT. *Phys Lett.* (1995) **B342**:138–44.
37. Antusch S, de Medeiros Varzielas I, Maurer V, Sluka C, Spinrath M. Towards predictive flavour models in SUSY SU(5) GUTs with doublet-triplet splitting. *J High Energy Phys.* (2014) **09**:141. doi: 10.1007/JHEP09(2014)141
38. Dorsner I, Fileviez Perez P, Gonzalez Felipe R. Phenomenological and cosmological aspects of a minimal GUT scenario. *Nucl Phys.* (2006) **B747**:312–27. doi: 10.1016/j.nuclphysb.2006.05.006
39. Bajc B, Senjanovic G. Seesaw at LHC. *J High Energy Phys.* (2007) **08**:014. doi: 10.1088/1126-6708/2007/08/014
40. Fileviez Perez P. Renormalizable adjoint SU(5). *Phys Lett.* (2007) **B654**:189–93. doi: 10.1016/j.physletb.2007.07.075
41. Zee A. A theory of lepton number violation, neutrino majorana mass, and oscillation. *Phys Lett.* (1980) **93B**:389.
42. Fileviez Perez P, Murgui C. Renormalizable SU(5) unification. *Phys Rev. D.* (2016) **94**:075014. doi: 10.1103/PhysRevD.94.075014
43. Abe K, Haga Y, Hayato Y, M Ikeda KI, Kameda J, et al. Search for proton decay via $p \rightarrow e^+\pi^0$ and $p \rightarrow \mu^+\pi^0$ in 0.31 megaton years exposure of the super-kamiokande water cherenkov detector. *Phys Rev D.* (2017) **95**:012004. doi: 10.1103/PhysRevD.95.012004
44. Dorsner I, Fileviez Perez P. Unification without supersymmetry: neutrino mass, proton decay and light leptoquarks. *Nucl Phys.* (2005) **B723**:53–76. doi: 10.1016/j.nuclphysb.2005.06.016
45. Dorsner I, Fileviez Perez P. Unification versus proton decay in SU(5). *Phys Lett.* (2006) **B642**:248–52. doi: 10.1016/j.nuclphysb.2005.06.016
46. Fornal B, Grinstein B. Grand unified theory with a stable proton. (2018) *Int J Mod Phys.* **A33**:1844013. doi: 10.1142/S0217751X1844013X
47. Fileviez Pérez P, Gross A, Murgui C. Seesaw scale, unification, and proton decay. *Phys Rev D.* (2018) **98**:035032. doi: 10.1103/PhysRevD.98.035032
48. Weinberg S. Implications of dynamical symmetry breaking. *Phys Rev* . (1976) **D13**:974–96. doi: 10.1103/PhysRevD.13.974
49. Martin SP. A supersymmetry primer. (1997) **18**:1–98. doi: 10.1142/9789812839657_0001
50. Nanopoulos DV, Tamvakis K. SUSY GUTS: 4 - GUTS: 3. *Phys Lett.* (1982) **113B**:151–8. doi: 10.1016/0370-2693(82)90413-0
51. Dorsner I, Fileviez Perez P, Rodrigo G. On unification and nucleon decay in supersymmetric grand unified theories based on SU(5). *Phys Lett.* (2007) **B649**:197–205. doi: 10.1016/j.physletb.2007.03.062
52. 't Hooft G. Magnetic monopoles in unified gauge theories. *Nucl Phys.* (1974) **B79**:276–84. doi: 10.1016/0550-3213(74)90486-6
53. Witten E. Mass hierarchies in supersymmetric theories. *Phys Lett.* (1981) **105B**:267. doi: 10.1016/0370-2693(81)90885-6
54. Dimopoulos S, Georgi H. Solution of the Gauge Hierarchy Problem. *Phys Lett.* (1982) **117B**:287–90. doi: 10.1016/0370-2693(82)90720-1
55. De Rujula A, Georgi H, Glashow SL. FLAVOR GONIOMETRY BY PROTON DECAY. *Phys Rev Lett.* (1980) **45**:413. doi: 10.1103/PhysRevLett.45.413
56. Barr SM. A new symmetry breaking pattern for SO(10) and proton decay. *Phys Lett.* (1982) **B112**:219. doi: 10.1016/0370-2693(82)90966-2
57. Derendinger JP, Kim JE, Nanopoulos DV. Anti-SU(5). *Phys Lett.* (1984) **B139**:170. doi: 10.1016/0370-2693(84)91238-3
58. Antoniadis I, Ellis JR, Hagelin JS, Nanopoulos DV. Supersymmetric flipped SU(5) revitalized. *Phys Lett.* (1987) **B194**:231. doi: 10.1016/0370-2693(87)90533-8
59. Ellis JR, Hagelin JS, Kelley S, Nanopoulos DV. Aspects of the flipped unification of strong, weak and electromagnetic interactions. *Nucl Phys.* (1988) **B311**:1. doi: 10.1016/0550-3213(88)90141-1
60. Campbell BA, Ellis JR, Hagelin JS, Nanopoulos DV, Ticciati R. Flipped SU(5) from manifold compactification of the ten-dimensional heterotic string. *Phys Lett.* (1987) **B198**:200–4. doi: 10.1016/0370-2693(87)91496-1

61. Antoniadis I, Ellis JR, Hagelin JS, Nanopoulos DV. GUT model building with fermionic four-dimensional strings. *Phys Lett*. (1988) **B205**:459–65. doi: 10.1016/0370-2693(88)90978-1
62. Senjanovic G, Mohapatra RN. Exact left-right symmetry and spontaneous violation of parity. *Phys Rev*. (1975) **D12**:1502. doi: 10.1103/PhysRevD.12.1502
63. Mohapatra RN, Pati JC. A natural left-right symmetry. *Phys Rev*. (1975) **D11**:2558. doi: 10.1103/PhysRevD.11.2558
64. Smirnov AD. The minimal quark-lepton symmetry model and the limit on Z-prime mass. *Phys Lett*. (1995) **B346**:297–302. doi: 10.1016/0370-2693(95)00015-D
65. Fileviez Perez P, Wise MB. Low scale quark-lepton unification. *Phys Rev D*. (2013) **88**:057703. doi: 10.1103/PhysRevD.88.057703
66. Mohapatra RN, Senjanovic G. Neutrino mass and spontaneous parity violation. *Phys Rev Lett*. (1980) **44**:912. doi: 10.1103/PhysRevLett.44.912
67. Mohapatra RN, Senjanovic G. Neutrino masses and mixings in gauge models with spontaneous parity violation. *Phys Rev*. (1981) **D23**:165. doi: 10.1103/PhysRevD.23.165
68. Mohapatra RN, Marshak RE. Local B-L symmetry of electroweak interactions, majorana neutrinos and neutron oscillations. *Phys Rev Lett*. (1980) **44**:1316–9. doi: 10.1103/PhysRevLett.44.1316
69. Lindner M, Weiser M. Gauge coupling unification in left-right symmetric models. *Phys Lett*. (1996) **B383**:405–14. doi: 10.1016/0370-2693(96)00775-7
70. Aulakh CS, Bajc B, Melfo A, Rasin A, Senjanovic G. SO(10) theory of R-parity and neutrino mass. *Nucl Phys*. (2001) **B597**:89–109. doi: 10.1016/S0550-3213(00)00721-5
71. Senjanovic G. Spontaneous breakdown of parity in a class of gauge theories. *Nucl Phys*. (1979) **B153**:334–64. doi: 10.1016/0550-3213(79)90604-7
72. Antoniadis I, Leontaris GK. A SUPERSYMMETRIC SU(4) x O(4) MODEL. *Phys Lett*. (1989) **B216**:333–5. doi: 10.1016/0370-2693(89)91125-8
73. Kuchimanchi R, Mohapatra RN. No parity violation without R-parity violation. *Phys Rev*. (1993) **D48**:4352–60. doi: 10.1103/PhysRevD.48.4352
74. Cvetic M. Effects of the parity-odd singlet on the $N = 1$ supergravity theory within the left-right symmetric model. *Phys Lett*. (1985) **164B**:55–60. doi: 10.1016/0370-2693(85)90030-9
75. Aulakh CS, Benakli K, Senjanovic G. Reconciling supersymmetry and left-right symmetry. *Phys Rev Lett*. (1997) **79**:2188–91. doi: 10.1103/PhysRevLett.79.2188
76. Aulakh CS, Melfo A, Senjanovic G. Minimal supersymmetric left-right model. *Phys Rev*. (1998) **D57**:4174–8. doi: 10.1103/PhysRevD.57.4174
77. Aulakh CS, Melfo A, Rasin A, Senjanovic G. Supersymmetry and large scale left-right symmetry. *Phys Rev*. (1998) **D58**:115007. doi: 10.1103/PhysRevD.58.115007
78. Georgi H, Glashow SL. Gauge theories without anomalies. *Phys Rev*. (1972) **D6**:429. doi: 10.1103/PhysRevD.6.429
79. Adler SL. Axial vector vertex in spinor electrodynamics. *Phys Rev*. (1969) **177**:2426–38. doi: 10.1103/PhysRev.177.2426
80. Mohapatra RN, Sakita B. SO(2n) grand unification in an SU(N) basis. *Phys Rev*. (1980) **D21**:1062. doi: 10.1103/PhysRevD.21.1062
81. Bertolini S, Di Luzio L, Malinsky M. The quantum vacuum of the minimal SO(10) GUT. *J Phys Conf Ser*. (2010) **259**:012098. doi: 10.1088/1742-6596/259/1/012098
82. Bertolini S, Di Luzio L, Malinsky M. Seesaw scale in the minimal renormalizable SO(10) grand unification. *Phys Rev*. (2012) **D85**:095014. doi: 10.1103/PhysRevD.85.095014
83. Bertolini S, Di Luzio L, Malinsky M. Light color octet scalars in the minimal SO(10) grand unification. *Phys Rev*. (2013) **D87**:085020. doi: 10.1103/PhysRevD.87.085020
84. Kolesova H, Malinsky M. Proton lifetime in the minimal SO(10) GUT and its implications for the LHC. *Phys Rev*. (2014) **D90**:115001. doi: 10.1103/PhysRevD.90.115001
85. Graf L, Malinsky M, Mede T, Susic V. One-loop pseudo-Goldstone masses in the minimal *SO*(10) Higgs model. *Phys Rev D*. (2017) **95**:075007. doi: 10.1103/PhysRevD.95.075007
86. Bertolini S, Schwetz T, Malinsky M. Fermion masses and mixings in SO(10) models and the neutrino challenge to SUSY GUTs. *Phys Rev*. (2006) **D73**:115012. doi: 10.1103/PhysRevD.73.115012
87. Aulakh CS, Garg SK. MSGUT : From bloom to doom. *Nucl Phys*. (2006) **B757**:47–78. doi: 10.1016/j.nuclphysb.2006.07.030
88. Aulakh CS, Girdhar A. SO(10) a la Pati-Salam. *Int J Mod Phys*. (2005) **A20**:865–94. doi: 10.1142/S0217751X0502001X
89. Anastaze G, Derendinger JP, Buccella F. INTERMEDIATE SYMMETRIES IN THE SO(10) MODEL WITH (16+16) + 45 HIGGSES. *Z Phys*. (1983) **C20**:269–73. doi: 10.1007/BF01574861
90. Clark TE, Kuo TK, Nakagawa N. A SO(10) SUPERSYMMETRIC GRAND UNIFIED THEORY. *Phys Lett*. (1982) **115B**:26–8. doi: 10.1016/0370-2693(82)90507-X
91. Aulakh CS, Mohapatra RN. Implications of supersymmetric SO(10) grand unification. *Phys Rev*. (1983) **D28**:217. doi: 10.1103/PhysRevD.28.217
92. Tamvakis K. FLIPPED SO(10). *Phys Lett*. (1988) **B201**:95–100. doi: 10.1016/0370-2693(88)90087-1
93. Reig M, Valle JWF, Vaquera-Araujo CA, Wilczek F. A Model of Comprehensive Unification. *Phys Lett*. (2017) **B774**:667–70. doi: 10.1016/j.physletb.2017.10.038
94. Langacker P, Wang J. U(1)-prime symmetry breaking in supersymmetric E(6) models. *Phys Rev*. (1998) **D58**:115010. doi: 10.1103/PhysRevD.58.115010
95. Gursey F, Ramond P, Sikivie P. A universal gauge theory model based on E6. *Phys Lett*. (1976) **60B**:177–80. doi: 10.1016/0370-2693(76)90417-2
96. Achiman Y, Stech B. Quark lepton symmetry and mass scales in an E6 unified gauge model. *Phys Lett*. (1978) **77B**:389–93. doi: 10.1016/0370-2693(78)90584-1
97. Shafi Q. E(6) as a unifying gauge symmetry. *Phys Lett*. (1978) **79B**:301–3. doi: 10.1016/0370-2693(78)90248-4
98. Mohapatra RN, Valle JWF. Neutrino mass and baryon number nonconservation in superstring models. *Phys Rev*. (1986) **D34**:1642. doi: 10.1103/PhysRevD.34.1642
99. Buccella F, Miele G. SO(10) from supersymmetric *E*(6). *Phys Lett*. (1987) **B189**:115–7. doi: 10.1016/0370-2693(87)91280-9
100. Hosotani Y. Dynamical mass generation by compact extra dimensions. *Phys Lett*. (1983) **126B**:309–13. doi: 10.1016/0370-2693(83)90170-3
101. Hewett JL, Rizzo TG. Low-energy phenomenology of superstring inspired E(6) models. *Phys Rept*. (1989) **183**:193. doi: 10.1016/0370-1573(89)90071-9
102. London D, Rosner JL. Extra gauge bosons in E(6). *Phys Rev*. (1986) **D34**:1530. doi: 10.1103/PhysRevD.34.1530
103. Dimopoulos S, Raby S, Wilczek F. Supersymmetry and the scale of unification. *Phys Rev*. (1981) **D24**:1681–3. doi: 10.1103/PhysRevD.24.1681
104. Witten E. Dynamical breaking of supersymmetry. *Nucl Phys*. (1981) **B188**:513. doi: 10.1016/0550-3213(81)90006-7
105. Ibanez LE, Ross GG. SU(2)-L x U(1) symmetry breaking as a radiative effect of supersymmetry breaking in guts. *Phys Lett*. (1982) **110B**:215–20. doi: 10.1016/0370-2693(82)91239-4
106. Ellis JR, Nanopoulos DV, Tamvakis K. Grand unification in simple supergravity. *Phys Lett*. (1983) **121B**:123–9. doi: 10.1016/0370-2693(83)90900-0
107. Farrar GR, Fayet P. Phenomenology of the production, decay, and detection of new hadronic states associated with supersymmetry. *Phys Lett*. (1978) **76B**:575–9. doi: 10.1016/0370-2693(78)90858-4
108. Ellis JR, Hagelin JS, Nanopoulos DV, Olive KA, Srednicki M. Supersymmetric relics from the big bang. *Nucl Phys*. (1984) **B238**:453–76. doi: 10.1016/0550-3213(84)90461-9
109. Jungman G, Kamionkowski M, Griest K. Supersymmetric dark matter. *Phys Rept*. (1996) **267**:195–373. doi: 10.1016/0370-1573(95)00058-5
110. Ellis JR, Kelley S, Nanopoulos DV. Probing the desert using gauge coupling unification. *Phys Lett*. (1991) **B260**:131–7. doi: 10.1016/0370-2693(91)90980-5
111. Martin SP, Vaughn MT. Two loop renormalization group equations for soft supersymmetry breaking couplings. *Phys Rev*. (1994) **D50**:2282. doi: 10.1103/PhysRevD.50.2282
112. Hall LJ. Grand unification of effective gauge theories. *Nucl Phys*. (1981) **B178**:75–124. doi: 10.1016/0550-3213(81)90498-3
113. Weinberg S. Effective gauge theories. *Phys Lett*. (1980) **91B**:51–5. doi: 10.1016/0370-2693(80)90660-7

114. Giudice GF, Romanino A. Split supersymmetry. *Nucl Phys*. (2004) **B699**:65–89. doi: 10.1016/j.nuclphysb.2004.08.001
115. Arkani-Hamed N, Dimopoulos S. Supersymmetric unification without low energy supersymmetry and signatures for fine-tuning at the LHC. *J High Energy Phys*. (2005) **06**:073. doi: 10.1088/1126-6708/2005/06/073
116. Athron P, Balázs C, Buckley A, Cornell JM, Danninger M, Farmer B, et al. Combined collider constraints on neutralinos and charginos. (2018). doi: 10.1140/epjc/s10052-019-6837-x
117. Ellis SAR, Wells JD. Visualizing gauge unification with high-scale thresholds. *Phys Rev*. (2015) **D91**:075016. doi: 10.1103/PhysRevD.91.075016
118. Pontecorvo B. Neutrino experiments and the problem of conservation of leptonic charge. *Sov Phys JETP*. (1968) **26**:984–8. doi: 10.1016/B978-0-12-395657-6.50020-3
119. Schechter J, Valle JWF. Neutrino masses in SU(2) x U(1) theories. *Phys Rev*. (1980) **D22**:2227. doi: 10.1103/PhysRevD.22.2227
120. Ma E. Pathways to naturally small neutrino masses. *Phys Rev Lett*. (1998) **81**:1171–4. doi: 10.1103/PhysRevLett.81.1171
121. Minkowski P. $\mu \to e\gamma$ at a rate of one out of 10^9 muon decays? *Phys Lett*. (1977) **67B**:421–8. doi: 10.1016/0370-2693(77)90435-X
122. Yanagida T. HORIZONTAL SYMMETRY AND MASSES OF NEUTRINOS. *Conf Proc*. (1979) **C7902131**:95–9.
123. Gell-Mann M, Ramond P, Slansky R. Complex spinors and unified theories. *Conf Proc*. (1979) **C790927**:315–21.
124. Magg M, Wetterich C. Neutrino mass problem and gauge hierarchy. *Phys Lett*. (1980) **94B**:61–4. doi: 10.1016/0370-2693(80)90825-4
125. Lazarides G, Shafi Q, Wetterich C. Proton lifetime and fermion masses in an SO(10) model. *Nucl Phys*. (1981) **B181**:287–300. doi: 10.1016/0550-3213(81)90354-0
126. Goh HS, Mohapatra RN, Nasri S. SO(10) symmetry breaking and type II seesaw. *Phys Rev*. (2004) **D70**:075022. doi: 10.1103/PhysRevD.70.075022
127. Mohapatra RN, Parida MK. Type II seesaw dominance in non-supersymmetric and split susy SO(10) and proton life time. *Phys Rev*. (2011) **D84**:095021. doi: 10.1103/PhysRevD.84.095021
128. Foot R, Lew H, He XG, Joshi GC. Seesaw neutrino masses induced by a triplet of leptons. *Z Phys*. (1989) **C44**:441. doi: 10.1007/BF01415558
129. Fileviez Perez P. Supersymmetric adjoint SU(5). *Phys Rev*. (2007) **D76**:071701. doi: 10.1103/PhysRevD.76.071701
130. Gonzalez-Garcia MC, Valle JWF. Fast decaying neutrinos and observable flavor violation in a new class of majoron models. *Phys Lett*. (1989) **B216**:360–6. doi: 10.1016/0370-2693(89)91131-3
131. 't Hooft G. Naturalness, chiral symmetry, and spontaneous chiral symmetry breaking. *NATO Sci Ser B*. (1980) **59**:135–57. doi: 10.1007/978-1-4684-7571-5_9
132. Malinsky M, Romao JC, Valle JWF. Novel supersymmetric SO(10) seesaw mechanism. *Phys Rev Lett*. (2005) **95**:161801. doi: 10.1103/PhysRevLett.95.161801
133. Hirsch M, Valle JWF. Supersymmetric origin of neutrino mass. New *J Phys*. (2004) **6**:76. doi: 10.1088/1367-2630/6/1/076
134. Babu KS. Model of 'Calculable' majorana neutrino masses. *Phys Lett*. (1988) **B203**:132–6. doi: 10.1016/0370-2693(88)91584-5
135. Witten E. Neutrino masses in the minimal O(10) theory. *Phys Lett*. (1980) **91B**:81–4. doi: 10.1016/0370-2693(80)90666-8
136. Leontaris GK, Vergados JD. The Seesaw mechanism in string models. *Phys Lett*. (1991) **B258**:111–7. doi: 10.1016/0370-2693(91)91217-J
137. Arbeláez Rodríguez C, Kolešová H, Malinský M. Witten's mechanism in the flipped SU(5) unification. *Phys Rev D*. (2014) **89**:055003. doi: 10.1103/PhysRevD.89.055003
138. Harries D, Malinský M, Zdráhal M. Witten's loop in the minimal flipped *SU*(5) unification revisited. *Phys Rev D*. (2018) **98**:095015. doi: 10.1103/PhysRevD.98.095015
139. Giveon A, Hall LJ, Sarid U. SU(5) unification revisited. *Phys Lett*. (1991) **B271**:138–44. doi: 10.1016/0370-2693(91)91289-8
140. Antusch S, King SF, Spinrath M. GUT predictions for quark-lepton Yukawa coupling ratios with messenger masses from non-singlets. *Phys Rev D*. (2014) **89**:055027. doi: 10.1103/PhysRevD.89.055027
141. Ellis JR, Gaillard MK. Fermion masses and higgs representations in SU(5). *Phys Lett*. (1979) **88B**:315–9. doi: 10.1016/0370-2693(79)90476-3
142. Kelley S, Lopez JL, Nanopoulos DV. Yukawa unification. *Phys Lett*. (1992) **B274**:387–92. doi: 10.1016/0370-2693(92)92003-Y
143. Ananthanarayan B, Lazarides G, Shafi Q. Top mass prediction from supersymmetric guts. *Phys Rev*. (1991) **D44**:1613–5. doi: 10.1103/PhysRevD.44.1613
144. Antusch S, Spinrath M. Quark and lepton masses at the GUT scale including SUSY threshold corrections. *Phys Rev*. (2008) **D78**:075020. doi: 10.1103/PhysRevD.78.075020
145. Antusch S, Spinrath M. New GUT predictions for quark and lepton mass ratios confronted with phenomenology. *Phys Rev*. (2009) **D79**:095004. doi: 10.1103/PhysRevD.79.095004
146. Babu KS, Kolda CF. Signatures of supersymmetry and Yukawa unification in Higgs decays. *Phys Lett*. (1999) **B451**:77–85. doi: 10.1016/S0370-2693(99)00204-X
147. Olechowski M, Pokorski S. Electroweak symmetry breaking with nonuniversal scalar soft terms and large tan beta solutions. *Phys Lett*. (1995) **B344**:201–10. doi: 10.1016/0370-2693(94)01571-S
148. Blazek T, Dermisek R, Raby S. Yukawa unification in SO(10). *Phys Rev*. (2002) **D65**:115004. doi: 10.1103/PhysRevD.65.115004
149. Hall LJ, Rattazzi R, Sarid U. The Top quark mass in supersymmetric SO(10) unification. *Phys Rev*. (1994) **D50**:7048–65. doi: 10.1103/PhysRevD.50.7048
150. King SF, Oliveira M. Yukawa unification as a window into the soft supersymmetry breaking Lagrangian. *Phys Rev*. (2001) **D63**:015010. doi: 10.1103/PhysRevD.63.015010
151. Baer H, Raza S, Shafi Q. A heavier gluino from t-b-t Yukawa-unified SUSY. *Phys Lett*. (2012) **B712**:250–4. doi: 10.1016/j.physletb.2012.04.075
152. Langacker P, Polonsky N. The Bottom mass prediction in supersymmetric grand unification: Uncertainties and constraints. *Phys Rev*. (1994) **D49**:1454–67. doi: 10.1103/PhysRevD.49.1454
153. Langacker P, Polonsky N. Implications of Yukawa unification for the Higgs sector in supersymmetric grand unified models. *Phys Rev*. (1994) **D50**:2199–217. doi: 10.1103/PhysRevD.50.2199
154. Baer H, Gogoladze I, Mustafayev A, Raza S, Shafi Q. Sparticle mass spectra from SU(5) SUSY GUT models with $b - \tau$ Yukawa coupling unification. *J High Energy Phys*. (2012) **03**:047. doi: 10.1007/JHEP03(2012)047
155. Gomez ME, Lazarides G, Pallis C. Yukawa quasi-unification. *Nucl Phys*. (2002) **B638**:165–85. doi: 10.1016/S0550-3213(02)00483-2
156. Gogoladze I, Khalid R, Raza S, Shafi Q. $t - b - \tau$ Yukawa unification for $\mu < 0$ with a sub-TeV sparticle spectrum. *J High Energy Phys*. (2010) **12**:055. doi: 10.1007/JHEP12(2010)055
157. Bajc B, Senjanovic G, Vissani F. b - tau unification and large atmospheric mixing: a Case for noncanonical seesaw. *Phys Rev Lett*. (2003) **90**:051802. doi: 10.1103/PhysRevLett.90.051802
158. Anderson G, Raby S, Dimopoulos S, Hall LJ, Starkman GD. A Systematic SO(10) operator analysis for fermion masses. *Phys Rev*. (1994) **D49**:3660–90. doi: 10.1103/PhysRevD.49.3660
159. Altarelli G, Feruglio F. Discrete flavor symmetries and models of neutrino mixing. *Rev Mod Phys*. (2010) **82**:2701–29. doi: 10.1103/RevModPhys.82.2701
160. Ishimori H, Kobayashi T, Ohki H, Shimizu Y, Okada H, Tanimoto M. Non-abelian discrete symmetries in particle physics. *Prog Theor Phys Suppl*. (2010) **183**:1–163. doi: 10.1143/PTPS.183.1
161. Grimus W, Ludl PO. Finite flavour groups of fermions. *J Phys*. (2012) **A45**:233001. doi: 10.1088/1751-8113/45/23/233001
162. King SF, Luhn C, Stuart AJ. A grand Delta(96) x SU(5) flavour model. *Nucl Phys*. (2013) **B867**:203–35. doi: 10.1016/j.nuclphysb.2012.09.021
163. de Anda FJ, King SF. $SU(3) \times SO(10)$ in 6d. *J High Energy Phys*. (2018) **10**:128. doi: 10.1007/JHEP10(2018)128
164. Arbeláez C, Hirsch M, Malinský M, Romão JC. LHC-scale left-right symmetry and unification. *Phys Rev*. (2014) **D89**:035002. doi: 10.1103/PhysRevD.89.035002
165. Deppisch FF, Gonzalo TE, Graf L. Surveying the SO(10) model landscape: the left-right symmetric case. *Phys Rev*. (2017) **D96**:055003. doi: 10.1103/PhysRevD.96.055003
166. Senjanovic G. Seesaw at LHC through left-right symmetry. *Int J Mod Phys*. (2011) **A26**:1469–91. doi: 10.1142/S0217751X1105302X

167. Nemevsek M, Nesti F, Senjanovic G, Zhang Y. First limits on left-right symmetry scale from LHC data. *Phys Rev*. (2011) **D83**:115014. doi: 10.1103/PhysRevD.83.115014
168. Han T, Lewis I, Ruiz R, Si Zg. Lepton number violation and W' chiral couplings at the LHC. *Phys Rev*. (2013) **D87**:035011. doi: 10.1103/PhysRevD.87.039906
169. Das SP, Deppisch FF, Kittel O, Valle JWF. Heavy neutrinos and lepton flavour violation in left-right symmetric models at the LHC. *Phys Rev*. (2012) **D86**:055006. doi: 10.1103/PhysRevD.86.055006
170. Bambhaniya G, Chakrabortty J, Gluza J, Kordiaczynska M, Szafron R. Left-right symmetry and the charged higgs bosons at the LHC. *J High Energy Phys*. (2014) **05**:033. doi: 10.1007/JHEP05(2014)033
171. Chen CY, Dev PSB, Mohapatra RN. Probing heavy-light neutrino mixing in left-right seesaw models at the LHC. *Phys Rev D*. (2013) **88**:033014. doi: 10.1103/PhysRevD.88.033014
172. Lee CH, Bhupal Dev PS, Mohapatra RN. Natural TeV-scale left-right seesaw mechanism for neutrinos and experimental tests. *Phys Rev D*. (2013) **88**:093010. doi: 10.1103/PhysRevD.88.093010
173. Deppisch FF, Gonzalo TE, Patra S, Sahu N, Sarkar U. Signal of right-handed charged gauge bosons at the LHC? *Phys Rev D*. (2014) **90**:053014. doi: 10.1103/PhysRevD.90.053014
174. Deppisch FF, Gonzalo TE, Patra S, Sahu N, Sarkar U. Double beta decay, lepton flavor violation, and collider signatures of left-right symmetric models with spontaneous D-parity breaking. *Phys Rev D*. (2015) **91**:015018. doi: 10.1103/PhysRevD.91.015018
175. Deppisch FF, Graf L, Kulkarni S, Patra S, Rodejohann W, Sahu N, et al. Reconciling the 2 TeV excesses at the LHC in a linear seesaw left-right model. *Phys Rev D*. (2016) **93**:013011. doi: 10.1103/PhysRevD.93.013011
176. Bhupal Dev PS, Mohapatra RN. Unified explanation of the *eejj*, diboson and dijet resonances at the LHC. *Phys Rev Lett*. (2015) **115**:181803. doi: 10.1103/PhysRevLett.115.181803
177. Mitra M, Ruiz R, Scott DJ, Spannowsky M. Neutrino jets from high-mass W_R gauge bosons in TeV-Scale left-right symmetric models. *Phys Rev D*. (2016) **94**:095016. doi: 10.1103/PhysRevD.94.095016
178. Helo JC, Li H, Neill NA, Ramsey-Musolf M, Vasquez JC. Probing neutrino Dirac Mass in Left-Right Symmetric Models at the LHC and Next Generation Colliders. *Phys Rev D*. (2018) **99**:055042. doi: 10.1103/PhysRevD.99.055042
179. Mohapatra RN. Mechanism for understanding small neutrino mass in superstring theories. *Phys Rev Lett*. (1986) **56**:561–3. doi: 10.1103/PhysRevLett.56.561
180. Dev PSB, Mohapatra RN. TeV scale inverse seesaw in SO(10) and leptonic non-unitarity effects. *Phys Rev*. (2010) **D81**:013001. doi: 10.1103/PhysRevD.81.013001
181. Brdar V, Smirnov AY. Low scale left-right symmetry and naturally small neutrino mass. *J High Energy Phys*. (2018) **1902**:045. doi: 10.1007/JHEP02(2019)045
182. Akhmedov EK, Lindner M, Schnapka E, Valle JWF. Left-right symmetry breaking in NJL approach. *Phys Lett*. (1996) **B368**:270–80. doi: 10.1016/0370-2693(95)01504-3
183. Akhmedov EK, Lindner M, Schnapka E, Valle JWF. Dynamical left-right symmetry breaking. *Phys Rev*. (1996) **D53**:2752–80. doi: 10.1103/PhysRevD.53.2752
184. Fileviez Perez P. Type III Seesaw and Left-Right Symmetry. *J High Energy Phys*. (2009) **03**:142. doi: 10.1088/1126-6708/2009/03/142
185. Duerr M, Fileviez Perez P, Lindner M. Left-right symmetric theory with light sterile neutrinos. *Phys Rev D*. (2013) **88**:051701. doi: 10.1103/PhysRevD.88.051701
186. Fileviez Perez P, Murgui C, Ohmer S. Simple left-right theory: lepton number violation at the LHC. *Phys Rev D*. (2016) **94**:051701. doi: 10.1103/PhysRevD.94.051701
187. Babu KS, Mohapatra RN. Predictive neutrino spectrum in minimal SO(10) grand unification. *Phys Rev Lett*. (1993) **70**:2845–8. doi: 10.1103/PhysRevLett.70.2845
188. Albright CH, Barr SM. Construction of a minimal Higgs SO(10) SUSY GUT model. *Phys Rev*. (2000) **D62**:093008. doi: 10.1103/PhysRevD.62.093008
189. Fukuyama T, Okada N. Neutrino oscillation data versus minimal supersymmetric SO(10) model. *J High Energy Phys*. (2002) **11**:011. doi: 10.1088/1126-6708/2002/11/011
190. Goh HS, Mohapatra RN, Ng SP. Minimal SUSY SO(10) model and predictions for neutrino mixings and leptonic CP violation. *Phys Rev*. (2003) **D68**:115008. doi: 10.1103/PhysRevD.68.115008
191. Goh HS, Mohapatra RN, Ng SP. Minimal SUSY SO(10), b tau unification and large neutrino mixings. *Phys Lett*. (2003) **B570**:215–21. doi: 10.1016/j.physletb.2003.08.011
192. Bertolini S, Frigerio M, Malinsky M. Fermion masses in SUSY SO(10) with type II seesaw: a Non-minimal predictive scenario. *Phys Rev*. (2004) **D70**:095002. doi: 10.1103/PhysRevD.70.095002
193. Matsuda K, Koide Y, Fukuyama T. Can the SO(10) model with two Higgs doublets reproduce the observed fermion masses? *Phys Rev*. (2001) **D64**:053015. doi: 10.1103/PhysRevD.64.053015
194. Matsuda K, Koide Y, Fukuyama T, Nishiura H. How far can the SO(10) two Higgs model describe the observed neutrino masses and mixings? *Phys Rev*. (2002) **D65**:033008. doi: 10.1103/PhysRevD.65.033008
195. Babu KS, Macesanu C. Neutrino masses and mixings in a minimal SO(10) model. *Phys Rev*. (2005) **D72**:115003. doi: 10.1103/PhysRevD.72.115003
196. Dueck A, Rodejohann W. Fits to SO(10) Grand Unified Models. *J High Energy Phys*. (2013) **09**:024. doi: 10.1007/JHEP09(2013)024
197. Deppisch T, Schacht S, Spinrath M. Confronting SUSY SO(10) with updated lattice and neutrino data. *J High Energy Phys*. (2019) **01**:005. doi: 10.1007/JHEP01(2019)005
198. Aulakh CS, Bajc B, Melfo A, Senjanovic G, Vissani F. The Minimal supersymmetric grand unified theory. *Phys Lett*. (2004) **B588**:196–202. doi: 10.1016/j.physletb.2004.03.031
199. Aulakh CS, Girdhar A. SO(10) MSGUT: Spectra, couplings and threshold effects. *Nucl Phys*. (2005) **B711**:275–313. doi: 10.1016/j.nuclphysb.2005.01.008
200. Bajc B, Melfo A, Senjanovic G, Vissani F. The Minimal supersymmetric grand unified theory. 1. Symmetry breaking and the particle spectrum. *Phys Rev*. (2004) **D70**:035007. doi: 10.1103/PhysRevD.70.035007
201. Bajc B, Melfo A, Senjanovic G, Vissani F. Fermion mass relations in a supersymmetric SO(10) theory. *Phys Lett*. (2006) **B634**:272–7. doi: 10.1063/1.2149692
202. Bajc B, Dorsner I, Nemevsek M. Minimal SO(10) splits supersymmetry. *J High Energy Phys*. (2008) **11**:007. doi: 10.1088/1126-6708/2008/11/007
203. De Romeri V, Hirsch M, Malinsky M. Soft masses in SUSY SO(10) GUTs with low intermediate scales. *Phys Rev*. (2011) **D84**:053012. doi: 10.1103/PhysRevD.84.053012
204. Deppisch FF, Desai N, Gonzalo TE. Compressed and Split Spectra in Minimal SUSY SO(10). *Frontin Phys*. (2014) **2**:27. doi: 10.3389/fphy.2014.00027
205. Poh Z, Raby S. Yukawa Unification in an SO(10) SUSY GUT: SUSY on the Edge. *Phys Rev D*. (2015) **92**:015017. doi: 10.1103/PhysRevD.92.015017
206. Ellis SAR, Gherghetta T, Kaneta K, Olive KA. New Weak-Scale Physics from SO(10) with High-Scale Supersymmetry. *Phys Rev D*. (2018) **98**:055009. doi: 10.1103/PhysRevD.98.055009
207. Dutta B, Mimura Y, Mohapatra RN. Suppressing proton decay in the minimal SO(10) model. *Phys Rev Lett*. (2005) **94**:091804. doi: 10.1103/PhysRevLett.94.091804
208. Aulakh CS, Garg SK. The new minimal supersymmetric GUT: spectra, RG analysis and fermion fits. *Nucl Phys*. (2012) **B857**:101–42. doi: 10.1016/j.nuclphysb.2011.12.003
209. Fukuyama T, Ilakovac A, Kikuchi T, Meljanac S, Okada N. SO(10) group theory for the unified model building. *J Math Phys*. (2005) **46**:033505. doi: 10.1063/1.1847709
210. Babu KS, Bajc B, Saad S. Resurrecting minimal yukawa sector of SUSY SO(10). *J High Energy Phys*. (2018) **10**:135. doi: 10.1007/JHEP10(2018)135
211. Bhupal Dev PS, Mohapatra RN. Electroweak symmetry breaking and proton decay in SO(10) SUSY-GUT with TeV W(R). *Phys Rev D*. (2010) **82**:035014. doi: 10.1103/PhysRevD.82.035014
212. Anandakrishnan A, Bryant BC, Raby S, Wingerter A. LHC phenomenology of SO(10) models with Yukawa Unification. *Phys Rev D*. (2013) **88**:075002. doi: 10.1103/PhysRevD.88.075002

213. Baer H, Kraml S, Sekmen S, Summy H. Dark matter allowed scenarios for Yukawa-unified SO(10) SUSY GUTs. *J High Energy Phys*. (2008) **03**:056. doi: 10.1088/1126-6708/2008/03/056
214. Goh HS, Mohapatra RN, Nasri S, Ng SP. Proton decay in a minimal SUSY SO(10) model for neutrino mixings. *Phys Lett*. (2004) **B587**:105–16. doi: 10.1016/j.physletb.2004.02.063
215. Mohapatra RN, Severson M. Leptonic *CP* violation and proton decay in SUSY SO(10). *J High Energy Phys*. (2018) **09**:119. doi: 10.1007/JHEP09(2018)119
216. Masiero A, Vempati SK, Vives O. Seesaw and lepton flavor violation in SUSY SO(10). *Nucl Phys*. (2003) **B649**:189–204. doi: 10.1016/S0550-3213(02)01031-3
217. Dermisek R, Raby S, Roszkowski L, Ruiz de Austri R. Dark matter and B(s) —> mu+ mu- with minimal SO(10) soft SUSY breaking II. *J High Energy Phys*. (2005) **09**:029. doi: 10.1088/1126-6708/2005/09/029
218. Babu KS, He XG, Pakvasa S. Neutrino masses and proton decay modes in SU(3) X SU(3) X SU(3) trinification. *Phys Rev*. (1986) **D33**:763. doi: 10.1103/PhysRevD.33.763
219. Sayre J, Wiesenfeldt S, Willenbrock S. Minimal trinification. *Phys Rev*. (2006) **D73**:035013. doi: 10.1103/PhysRevD.73.035013
220. Stech B. The mass of the Higgs boson in the trinification subgroup of E6. *Phys Rev*. (2012) **D86**:055003. doi: 10.1103/PhysRevD.86.055003
221. Willenbrock S. Triplicated trinification. *Phys Lett*. (2003) **B561**:130–4. doi: 10.1016/S0370-2693(03)00419-2
222. Wang MY, Carlson ED. The Breaking of the SU(3)**3 gauge group. *arXiv:hep-ph/9302215* (1992).
223. Cauet C, Pas H, Wiesenfeldt S. Trinification, the hierarchy problem and inverse seesaw neutrino masses. *Phys Rev*. (2011) **D83**:093008. doi: 10.1103/PhysRevD.83.093008
224. Dvali GR, Shafi Q. Gauge hierarchy in SU(3)(C) x SU(3)(L) x SU(3)-R and low-energy implications. *Phys Lett*. (1994) **B326**:258–63. doi: 10.1016/0370-2693(94)91319-6
225. Carone CD. Tri-N-ification. *Phys Rev*. (2005) **D71**:075013. doi: 10.1103/PhysRevD.71.075013
226. Nath P, Arnowitt RL. Symmetry breaking in three generation calabi-yau manifolds. *Phys Rev*. (1989) **D39**:2006.
227. Maekawa N, Shafi Q. Supersymmetric $SU^{(3)}3$ unification with anomalous U(1)(a) gauge symmetry. *Prog Theor Phys*. (2003) **109**:279–93. doi: 10.1143/PTP.109.279
228. Hetzel J, Stech B. Low-energy phenomenology of trinification: an effective left-right-symmetric model. *Phys Rev*. (2015) **D91**:055026. doi: 10.1103/PhysRevD.91.055026
229. Stech B. Trinification Phenomenology and the structure of Higgs Bosons. *J High Energy Phys*. (2014) **08**:139. doi: 10.1007/JHEP08(2014)139
230. Camargo-Molina JE, Morais AP, Pasechnik R, Wessén J. On a radiative origin of the Standard Model from Trinification. *J High Energy Phys*. (2016) **09**:129. doi: 10.1007/JHEP09(2016)129
231. Camargo-Molina JE, Morais AP, Ordell A, Pasechnik R, Sampaio MOP, Wessén J. Reviving trinification models through an E6 - extended supersymmetric GUT. *Phys Rev*. (2017) **D95**:075031. doi: 10.1103/PhysRevD.95.075031
232. Camargo-Molina JE, Morais AP, Ordell A, Pasechnik R, Wessén J. Scale hierarchies, symmetry breaking and particle spectra in SU(3)-family extended SUSY trinification. *Phys Rev*. (2019) **D99**:035041. doi: 10.1103/PhysRevD.99.035041
233. King SF, Moretti S, Nevzorov R. Theory and phenomenology of an exceptional supersymmetric standard model. *Phys Rev*. (2006) **D73**:035009. doi: 10.1103/PhysRevD.73.035009
234. King SF, Moretti S, Nevzorov R. Exceptional supersymmetric standard model. *Phys Lett*. (2006) **B634**:278–84. doi: 10.1016/j.physletb.2005.12.070
235. Athron P, Hall JP, Howl R, King SF, Miller DJ, Moretti S, et al. Aspects of the exceptional supersymmetric standard model. *Nucl Phys Proc Suppl*. (2010) **200-202**:120–9. doi: 10.1016/j.nuclphysbps.2010.02.074
236. King SF, Luo R, Miller DJ, Nevzorov R. Leptogenesis in the exceptional supersymmetric standard model: flavour dependent lepton asymmetries. *J High Energy Phys*. (2008) **12**:042. doi: 10.1088/1126-6708/2008/12/042
237. Nevzorov R. Leptogenesis as an origin of hot dark matter and baryon asymmetry in the E_6 inspired SUSY models. *Phys Lett*. (2018) **B779**:223–9. doi: 10.1016/j.physletb.2018.02.020
238. Nevzorov R. E_6 inspired supersymmetric models with exact custodial symmetry. *Phys Rev*. (2013) **D87**:015029. doi: 10.1103/PhysRevD.87.015029
239. Nevzorov R. Quasifixed point scenarios and the Higgs mass in the E6 inspired supersymmetric models. *Phys Rev*. (2014) **D89**:055010. doi: 10.1103/PhysRevD.89.055010
240. Howl R, King SF. Planck scale unification in a supersymmetric standard model. *Phys Lett*. (2007) **B652**:331–7. doi: 10.1016/j.physletb.2007.07.035
241. Athron P, King SF, Miller DJ, Moretti S, Nevzorov R. The constrained exceptional supersymmetric standard model. *Phys Rev*. (2009) **D80**:035009. doi: 10.1103/PhysRevD.80.035009
242. Athron P, King SF, Miller DJ, Moretti S, Nevzorov R. Predictions of the constrained exceptional supersymmetric standard model. *Phys Lett*. (2009) **B681**:448–56. doi: 10.1016/j.physletb.2009.10.051
243. Athron P, King SF, Miller DJ, Moretti S, Nevzorov R. Constrained Exceptional Supersymmetric Standard Model with a Higgs Near 125 GeV. *Phys Rev*. (2012) **D86**:095003. doi: 10.1103/PhysRevD.86.095003
244. Athron P, Mühlleitner M, Nevzorov R, Williams AG. Non-Standard Higgs Decays in U(1) Extensions of the MSSM. *J High Energy Phys*. (2015) **01**:153. doi: 10.1007/JHEP01(2015)153
245. Athron P, King SF, Miller DJ, Moretti S, Nevzorov R. LHC signatures of the constrained exceptional supersymmetric standard model. *Phys Rev*. (2011) **D84**:055006. doi: 10.1103/PhysRevD.84.055006
246. Hall JP, King SF. Neutralino dark matter with inert higgsinos and singlinos. *J High Energy Phys*. (2009) **08**:088. doi: 10.1088/1126-6708/2009/08/088
247. Hall JP, King SF. Bino dark matter and big bang nucleosynthesis in the constrained E_6SSM with massless inert singlinos. *J High Energy Phys*. (2011) **06**:006. doi: 10.1007/JHEP06(2011)006
248. Hall JP, King SF, Nevzorov R, Pakvasa S, Sher M, Nevzorov R, et al. Novel Higgs Decays and Dark Matter in the E(6)SSM. *Phys Rev*. (2011) **D83**:075013. doi: 10.1103/PhysRevD.83.075013
249. Athron P, Harries D, Nevzorov R, Williams AG. E_6 Inspired SUSY benchmarks, dark matter relic density and a 125 GeV Higgs. *Phys Lett*. (2016) **B760**:19–25. doi: 10.1016/j.physletb.2016.06.040
250. Athron P, Harries D, Nevzorov R, Williams AG. Dark matter in a constrained E_6 inspired SUSY model. *J High Energy Phys*. (2016) **12**:128. doi: 10.1007/JHEP12(2016)128
251. Rocher J, Sakellariadou M. Supersymmetric grand unified theories and cosmology. *J Cosmol Astropart Phys*. (2005) **0503**:004. doi: 10.1088/1475-7516/2005/03/004
252. Lyth DH. What would we learn by detecting a gravitational wave signal in the cosmic microwave background anisotropy? *Phys Rev Lett*. (1997) **78**:1861–3. doi: 10.1103/PhysRevLett.78.1861
253. Ade PAR, Aghanim N, Arnaud M, Arroja F, Ashdown M, Aumont J, et al. Planck 2015 results. XX. Constraints on inflation. *Astron Astrophys*. (2016) **594**:A20. doi: 10.1051/0004-6361/201525898
254. Akrami Y, Arroja F, Ashdown M, Aumont J, Baccigalupi C, Ballardini M, et al. Planck 2018 results. X. Constraints on inflation. *arXiv:1807.06211* (2018).
255. Coleman SR, Weinberg EJ. Radiative corrections as the origin of spontaneous symmetry breaking. *Phys Rev*. (1973) **D7**:1888–910. doi: 10.1103/PhysRevD.7.1888
256. Croon D, Sanz V. Saving natural inflation. *J Cosmol Astropart Phys*. (2015) **1502**:008. doi: 10.1088/1475-7516/2015/02/008
257. Croon D, Sanz V, Setford J. Goldstone inflation. *J High Energy Phys*. (2015) **10**:020. doi: 10.1007/JHEP10(2015)020
258. Croon D, Sanz V, Tarrant ERM. Reheating with a composite Higgs boson. *Phys Rev*. (2016) **D94**:045010. doi: 10.1103/PhysRevD.94.045010
259. Shafi Q, Vilenkin A. Inflation with SU(5). *Phys Rev Lett*. (1984) **52**:691–4. doi: 10.1103/PhysRevLett.52.691
260. Barenboim G, Chun EJ, Lee HM. Coleman-Weinberg Inflation in light of Planck. *Phys Lett*. (2014) **B730**:81–88. doi: 10.1016/j.physletb.2014.01.039

261. Okada N, Senoguz VN, Shafi Q. The observational status of simple inflationary models: an update. Turk *J Phys*. (2016) **40**:150–62. doi: 10.3906/fiz-1505-7
262. Cerioni A, Finelli F, Tronconi A, Venturi G. Inflation and reheating in induced gravity. *Phys Lett*. (2009) **B681**:383–6. doi: 10.1016/j.physletb.2009.10.066
263. Panotopoulos G. Nonminimal GUT inflation after Planck results. *Phys Rev*. (2014) **D89**:047301. doi: 10.1103/PhysRevD.89.047301
264. Karam A, Pappas T, Tamvakis K. Nonminimal coleman–weinberg inflation with an R^2 term. *J Cosmol Astropar Phys*. (2018) **2019**:006. doi: 10.1088/1475-7516/2019/02/006
265. Ellis J, Nanopoulos DV, Olive KA. No-Scale supergravity realization of the starobinsky model of inflation. *Phys Rev Lett*. (2013) **111**:111301. doi: 10.1103/PhysRevLett.111.129902
266. Starobinsky AA. A new type of isotropic cosmological models without singularity. *Phys Lett*. (1980) **B91**:99–102. doi: 10.1016/0370-2693(80)90670-X
267. Whitt B. Fourth order gravity as general relativity plus matter. *Phys Lett*. (1984) **145B**:176–8. doi: 10.1016/0370-2693(84)90332-0
268. Croon D, Ellis J, Mavromatos NE. Wess-zumino inflation in light of planck. *Phys Lett*. (2013) **B724**:165–9. doi: 10.1016/j.physletb.2013.06.016
269. Ellis J, Nanopoulos DV, Olive KA. A no-scale supergravity framework for sub-Planckian physics. *Phys Rev*. (2014) **D89**:043502. doi: 10.1103/PhysRevD.89.043502
270. Ellis J, Gonzalo TE, Harz J, Huang WC. Flipped GUT Inflation. *J Cosmol Astropart Phys*. (2015) **1503**:039. doi: 10.1088/1475-7516/2015/03/039
271. Ellis J, Garcia MAG, Nagata N, Nanopoulos DV, Olive KA. Starobinsky-like inflation and neutrino masses in a No-Scale SO(10) model. *J Cosmol Astropart Phys*. (2016) **1611**:018. doi: 10.1088/1475-7516/2016/11/018
272. Gonzalo TE, Heurtier L, Moursy A. Sneutrino driven GUT inflation in supergravity. *J High Energy Phys*. (2017) **06**:109. doi: 10.1007/JHEP06(2017)109
273. Ellis J, He HJ, Xianyu ZZ. New higgs inflation in a No-Scale supersymmetric SU(5) GUT. *Phys Rev*. (2015) **D91**:021302. doi: 10.1103/PhysRevD.91.021302
274. Ellis J, He HJ, Xianyu ZZ. Higgs inflation, reheating and gravitino production in No-Scale supersymmetric GUTs. *J Cosmol Astropart Phys*. (2016) **1608**:068. doi: 10.1088/1475-7516/2016/08/068
275. Hertzberg MP, Wilczek F. Inflation driven by unification energy. *Phys Rev*. (2017) **D95**:063516. doi: 10.1103/PhysRevD.95.063516
276. Rehman MU, Shafi Q, Wickman JR. GUT inflation and proton decay after WMAP5. *Phys Rev*. (2008) **D78**:123516. doi: 10.1103/PhysRevD.78.123516
277. Boucenna SM, Morisi S, Shafi Q, Valle JWF. Inflation and majoron dark matter in the seesaw mechanism. *Phys Rev*. (2014) **D90**:055023. doi: 10.1103/PhysRevD.90.055023
278. Sravan Kumar K, Vargas Moniz P. Conformal GUT inflation, proton lifetime and non-thermal leptogenesis. *arXiv:1806.09032* (2018).
279. Kibble TWB. Topology of cosmic domains and strings. *J Phys*. (1976) **A9**:1387–98. doi: 10.1088/0305-4470/9/8/029
280. Kibble TWB. Some implications of a cosmological phase transition. *Phys Rept*. (1980) **67**:183. doi: 10.1016/0370-1573(80)90091-5
281. Jeannerot R, Rocher J, Sakellariadou M. How generic is cosmic string formation in SUSY GUTs. *Phys Rev*. (2003) **D68**:103514. doi: 10.1103/PhysRevD.68.103514
282. Achucarro A, Martins CJAP. Cosmic strings. In: Meyers, RA editor. *Encyclopedia of Complexity and Systems Science*. New York, NY: Springer (2009). doi: 10.1007/978-0-387-30440-3_107
283. Vilenkin A. Cosmological density fluctuations produced by vacuum strings. *Phys Rev Lett*. (1981) **46**:1169–72. doi: 10.1103/PhysRevLett.46.1169
284. Brandenberger RH, Turok N. Fluctuations from cosmic strings and the microwave background. *Phys Rev*. (1986) **D33**:2182. doi: 10.1103/PhysRevD.33.2182
285. Gott JR III. Gravitational lensing effects of vacuum strings: exact solutions. *Astrophys J*. (1985) **288**:422–7. doi: 10.1086/162808
286. Kaiser N, Stebbins A. Microwave anisotropy due to cosmic strings. *Nature*. (1984) **310**:391–3. doi: 10.1038/310391a0
287. Ade PAR, Aghanim N, Arnaud M, Ashdown M, Aumont J, Baccigalupi C, et al. Planck 2015 results. XIII. Cosmological parameters. *Astron Astrophys*. (2016) **594**:A13. doi: 10.1051/0004-6361/201525830
288. Lizarraga J, Urrestilla J, Daverio D, Hindmarsh M, Kunz M. New CMB constraints for Abelian Higgs cosmic strings. *J Cosmol Astropart Phys*. (2016) **1610**:042. doi: 10.1088/1475-7516/2016/10/042
289. Vilenkin A. Gravitational radiation from cosmic strings. *Phys Lett*. (1981) **107B**:47–50. doi: 10.1016/0370-2693(81)91144-8
290. Vachaspati T, Vilenkin A. Gravitational radiation from cosmic strings. *Phys Rev*. (1985) **D31**:3052. doi: 10.1103/PhysRevD.31.3052
291. Caldwell RR, Allen B. Cosmological constraints on cosmic string gravitational radiation. *Phys Rev*. (1992) **D45**:3447–68. doi: 10.1103/PhysRevD.45.3447
292. Siemens X, Mandic V, Creighton J. Gravitational wave stochastic background from cosmic (super)strings. *Phys Rev Lett*. (2007) **98**:111101. doi: 10.1103/PhysRevLett.98.111101
293. Sanidas SA, Battye RA, Stappers BW. Projected constraints on the cosmic (super)string tension with future gravitational wave detection experiments. *Astrophys J*. (2013) **764**:108. doi: 10.1088/0004-637X/764/1/108
294. Damour T, Vilenkin A. Gravitational wave bursts from cosmic strings. *Phys Rev Lett*. (2000) **85**:3761–4. doi: 10.1103/PhysRevLett.85.3761
295. Damour T, Vilenkin A. Gravitational wave bursts from cusps and kinks on cosmic strings. *Phys Rev*. (2001) **D64**:064008. doi: 10.1103/PhysRevD.64.064008
296. Damour T, Vilenkin A. Gravitational radiation from cosmic (super)strings: bursts, stochastic background, and observational windows. *Phys Rev*. (2005) **D71**:063510. doi: 10.1103/PhysRevD.71.063510
297. Siemens X, Creighton J, Maor I, Ray Majumder S, Cannon K, Read J. Gravitational wave bursts from cosmic (super)strings: quantitative analysis and constraints. *Phys Rev*. (2006) **D73**:105001. doi: 10.1103/PhysRevD.73.105001
298. Olum KD, Blanco-Pillado JJ. Field theory simulation of Abelian Higgs cosmic string cusps. *Phys Rev*. (1999) **D60**:023503. doi: 10.1103/PhysRevD.60.023503
299. Aasi J, Abadie J, Abbott BP, Abbott R, Abbott T, Abernathy MR, et al. Constraints on cosmic strings from the LIGO-Virgo gravitational-wave detectors. *Phys Rev Lett*. (2014) **112**:131101. doi: 10.1103/PhysRevLett.112.131101
300. Sanidas SA, Battye RA, Stappers BW. Constraints on cosmic string tension imposed by the limit on the stochastic gravitational wave background from the European Pulsar Timing Array. *Phys Rev*. (2012) **D85**:122003. doi: 10.1103/PhysRevD.85.122003
301. Abbott BP, Abbott R, Abbott TD, Acernese F, Ackley K, Adams C, et al. Constraints on cosmic strings using data from the first Advanced LIGO observing run. *Phys Rev*. (2018) **D97**:102002. doi: 10.1103/PhysRevD.97.102002
302. Blanco-Pillado JJ, Olum KD, Siemens X. New limits on cosmic strings from gravitational wave observation. *Phys Lett*. (2018) **B778**:392–6. doi: 10.1016/j.physletb.2018.01.050
303. Lorenz L, Ringeval C, Sakellariadou M. Cosmic string loop distribution on all length scales and at any redshift. *J Cosmol Astropart Phys*. (2010) **1010**:003. doi: 10.1088/1475-7516/2010/10/003
304. Ringeval C, Sakellariadou M, Bouchet F. Cosmological evolution of cosmic string loops. *J Cosmol Astropart Phys*. (2007) **0702**:023. doi: 10.1088/1475-7516/2007/02/023
305. Ringeval C, Suyama T. Stochastic gravitational waves from cosmic string loops in scaling. *J Cosmol Astropart Phys*. (2017) **1712**:027. doi: 10.1088/1475-7516/2017/12/027
306. Blanco-Pillado JJ, Olum KD, Shlaer B. The number of cosmic string loops. *Phys Rev*. (2014) **D89**:023512. doi: 10.1103/PhysRevD.89.023512
307. Blanco-Pillado JJ, Olum KD. Stochastic gravitational wave background from smoothed cosmic string loops. *Phys Rev*. (2017) **D96**:104046. doi: 10.1103/PhysRevD.96.104046
308. Martins CJAP, Shellard EPS. Fractal properties and small-scale structure of cosmic string networks. *Phys Rev*. (2006) **D73**:043515. doi: 10.1103/PhysRevD.73.043515

309. Hindmarsh M, Stuckey S, Bevis N. Abelian higgs cosmic strings: small scale structure and loops. *Phys Rev*. (2009) **D79**:123504. doi: 10.1103/PhysRevD.79.123504
310. Hindmarsh M, Rummukainen K, Tenkanen TVI, Weir DJ. Improving cosmic string network simulations. *Phys Rev*. (2014) **D90**:043539. doi: 10.1103/PhysRevD.90.043539
311. Hindmarsh M, Lizarraga J, Urrestilla J, Daverio D, Kunz M. Scaling from gauge and scalar radiation in Abelian Higgs string networks. *Phys Rev*. (2017) **D96**:023525. doi: 10.1103/PhysRevD.96.023525
312. Brandenberger RH. On the decay of cosmic string loops. *Nucl Phys*. (1987) **B293**:812–28. doi: 10.1016/0550-3213(87)90092-7
313. Hindmarsh M, Rummukainen K, Weir DJ. Numerical simulations of necklaces in SU(2) gauge-Higgs field theory. *Phys Rev*. (2017) **D95**:063520. doi: 10.1103/PhysRevD.95.063520
314. Hindmarsh M, Rummukainen K, Weir DJ. New solutions for non-Abelian cosmic strings. *Phys Rev Lett*. (2016) **117**:251601. doi: 10.1103/PhysRevLett.117.251601
315. Lopez-Eiguren A, Urrestilla J, Achúcarro A, Avgoustidis A, Martins CJAP. Evolution of Semilocal String Networks: II. Velocity estimators. *Phys Rev*. (2017) **D96**:023526. doi: 10.1103/PhysRevD.96.023526
316. Figueroa DG, Hindmarsh M, Urrestilla J. Exact scale-invariant background of gravitational waves from cosmic defects. *Phys Rev Lett*. (2013) **110**:101302. doi: 10.1103/PhysRevLett.110.101302
317. Patel HH, Ramsey-Musolf MJ, Wise MB. Color Breaking in the early universe. *Phys Rev*. (2013) **D88**:015003. doi: 10.1103/PhysRevD.88.015003
318. Ramsey-Musolf MJ, Winslow P, White G. Color breaking baryogenesis. *Phys Rev*. (2018) **D97**:123509. doi: 10.1103/PhysRevD.97.123509
319. Long AJ, Tesi A, Wang LT. Baryogenesis at a lepton-number-breaking phase transition. *J High Energy Phys*. (2017) **10**:095. doi: 10.1007/JHEP10(2017)095
320. Schmitz K. *The B-L Phase Transition: Implications for Cosmology and Neutrinos*. Hamburg U. (2012). Available online at: http://www-library.desy.de/cgi-bin/showprep.pl?thesis12-039
321. Buchmuller W, Domcke V, Schmitz K. Spontaneous B-L breaking as the origin of the hot early universe. *Nucl Phys*. (2012) **B862**:587–632. doi: 10.1016/j.nuclphysb.2012.05.001
322. Buchmüller W, Domcke V, Kamada K, Schmitz K. The gravitational wave spectrum from cosmological $B-L$ breaking. *J Cosmol Astropart Phys*. (2013) **1310**:003. doi: 10.1088/1475-7516/2013/10/003
323. Croon D, Sanz V, White G. Model discrimination in gravitational wave spectra from dark phase transitions. *J High Energy Phys*. (2018) **08**:203. doi: 10.1007/JHEP08(2018)203
324. Schwaller P. Gravitational waves from a dark phase transition. *Phys Rev Lett*. (2015) **115**:181101. doi: 10.1103/PhysRevLett.115.181101
325. Breitbach M, Kopp J, Madge E, Opferkuch T, Schwaller P. Dark, cold, and noisy: constraining secluded hidden sectors with gravitational waves. *arXiv:1811.11175* (2018).
326. Baldes I, Garcia-Cely C. Strong gravitational radiation from a simple dark matter model. *arXiv:1809.01198* (2018).
327. Croon D, Gonzalo TE, White G. Gravitational waves from a pati-salam phase transition. *J High Energy Phys*. (2019) **02**:083. doi: 10.1007/JHEP02(2019)083
328. Mazumdar A, White G. Cosmic phase transitions: their applications and experimental signatures. *J High Energy Phys*. (2018) doi: 10.1088/1361-6633/ab1f55. [Epub ahead of print].
329. Caprini C, Figueroa DG. Cosmological backgrounds of gravitational waves. *Class Quant Grav*. (2018) **35**:163001. doi: 10.1088/1361-6382/aac608
330. Weir DJ. Gravitational waves from a first order electroweak phase transition: a brief review. *Phil Trans Roy Soc Lond*. (2018) **A376**:20170126. doi: 10.1098/rsta.2017.0126
331. Chao W. Electroweak baryogenesis in the exceptional supersymmetric standard model. *J Cosmol Astropart Phys*. (2015) **1508**:055. doi: 10.1088/1475-7516/2015/08/055
332. Chiang CW, Ramsey-Musolf MJ, Senaha E. Standard model with a complex scalar singlet: cosmological implications and theoretical considerations. *Phys Rev*. (2018) **D97**:015005. doi: 10.1103/PhysRevD.97.015005
333. Profumo S, Ramsey-Musolf MJ, Wainwright CL, Winslow P. Singlet-catalyzed electroweak phase transitions and precision Higgs boson studies. *Phys Rev*. (2015) **D91**:035018. doi: 10.1103/PhysRevD.91.035018
334. Caprini C, Hindmarsh M, Huber S, Konstandin T, Kozaczuk J, Nardini G, et al. Science with the space-based interferometer eLISA. II: gravitational waves from cosmological phase transitions. *J Cosmol Astropart Phys*. (2016) **1604**:001. doi: 10.1088/1475-7516/2016/04/001
335. Bodeker D, Moore GD. Electroweak bubble wall speed limit. *J Cosmol Astropart Phys*. (2017) **1705**:025. doi: 10.1088/1475-7516/2017/05/025
336. Hindmarsh M, Huber SJ, Rummukainen K, Weir DJ. Shape of the acoustic gravitational wave power spectrum from a first order phase transition. *Phys Rev*. (2017) **D96**:103520. doi: 10.1103/PhysRevD.96.103520
337. Caprini C, Durrer R, Servant G. The stochastic gravitational wave background from turbulence and magnetic fields generated by a first-order phase transition. *J Cosmol Astropart Phys*. (2009) **0912**:024. doi: 10.1088/1475-7516/2009/12/024
338. Punturo M, Abernathy M, Acernese F, Allen B, Andersson N, Arun K, et al. The einstein telescope: a third-generation gravitational wave observatory. *Class Quant Grav*. (2010) **27**:194002. doi: 10.1088/0264-9381/27/19/194002
339. Akutsu T, Ando M, Arai K, Arai Y, Araki S, Araya A, et al. KAGRA: 2.5 Generation interferometric gravitational wave detector. *Nat Astron*. (2018) **3**:35–40. doi: 10.1038/s41550-018-0658-y
340. Abbott BP, Abbott R, Abbott TD, Abernathy MR, Ackley K, Adams C, et al. Exploring the Sensitivity of Next Generation Gravitational Wave Detectors. *Class Quant Grav*. (2017) **34**:044001. doi: 10.1088/1361-6382/aa51f4
341. Thrane E, Romano JD. Sensitivity curves for searches for gravitational-wave backgrounds. *Phys Rev*. (2013) **D88**:124032. doi: 10.1103/PhysRevD.88.124032
342. Espinosa JR, Konstandin T, No JM, Servant G. Energy budget of cosmological first-order phase transitions. *J Cosmol Astropart Phys*. (2010) **1006**:028. doi: 10.1088/1475-7516/2010/06/028
343. Grojean C, Servant G, Wells JD. First-order electroweak phase transition in the standard model with a low cutoff. *Phys Rev*. (2005) **D71**:036001. doi: 10.1103/PhysRevD.71.036001
344. Ellis J, Lewicki M, No JM. On the maximal strength of a first-order electroweak phase transition and its gravitational wave signal. *J Cosmol Astropart Phys*. (2018) **04**:003. doi: 10.1088/1475-7516/2019/04/003
345. White GA. *A Pedagogical Introduction to Electroweak Baryogenesis*. IOP Concise Physics. Morgan & Claypool (2016). doi: 10.1088/978-1-6817-4457-5ch1
346. Morrissey DE, Ramsey-Musolf MJ. Electroweak baryogenesis. New *J Phys*. (2012) **14**:125003. doi: 10.1088/1367-2630/14/12/125003
347. Aghanim N, Akrami Y, Ashdown M, Aumont J, Baccigalupi C, Ballardini M, et al. Planck 2018 results. VI. Cosmological parameters. (2018) .
348. Riemer-Sørensen S, Jenssen ES. Nucleosynthesis predictions and high-precision deuterium measurements. *Universe*. (2017) **3**:44. doi: 10.3390/universe3020044
349. Sakharov AD. Violation of CP Invariance, C asymmetry, and baryon asymmetry of the universe. *Pisma Zh Eksp Teor Fiz*. (1967) **5**:32–5.
350. Riotto A. Theories of baryogenesis. In: *Proceedings, Summer School in High-energy physics and cosmology: Trieste, Italy, June 29-July 17, 1998* Trieste (1998). p. 326–436.
351. Gu PH, Sarkar U. SO(10) GUT baryogenesis. *Phys Lett*. (2008) **B663**:80–2. doi: 10.1016/j.physletb.2008.04.001
352. Gehrlein J, Petcov ST, Spinrath M, Zhang X. Leptogenesis in an SU(5) $\times$ A_5 golden ratio flavour model. *Nucl Phys*. (2015) **B896**:311–29. doi: 10.1016/j.nuclphysb.2015.08.019
353. Falcone D, Tramontano F. Leptogenesis with SU(5) inspired mass matrices. *Phys Lett*. (2001) **B506**:1–6. doi: 10.1016/S0370-2693(01)00403-8
354. Pilaftsis A, Underwood TEJ. Resonant leptogenesis. *Nucl Phys*. (2004) **B692**:303–45. doi: 10.1016/j.nuclphysb.2004.05.029
355. Blanchet S, Fileviez Perez P. Baryogenesis via leptogenesis in adjoint SU(5). *J Cosmol Astropart Phys*. (2008) **0808**:037. doi: 10.1088/1475-7516/2008/08/037
356. Chianese M, Di Bari P. Strong thermal *SO*(10)-inspired leptogenesis in the light of recent results from long-baseline neutrino experiments. *J High Energy Phys*. (2018) **05**:073. doi: 10.1007/JHEP05(2018)073

357. Di Bari P, Re Fiorentin M. A full analytic solution of $SO(10)$-inspired leptogenesis. *J High Energy Phys*. (2017) **10**:029. doi: 10.1007/JHEP10(2017)029
358. Di Bari P, Re Fiorentin M. Supersymmetric $SO(10)$-inspired leptogenesis and a new N_2-dominated scenario. *J Cosmol Astropart Phys*. (2016) **1603**:039. doi: 10.1088/1475-7516/2016/03/039
359. Di Bari P, Marzola L, Re Fiorentin M. Decrypting $SO(10)$-inspired leptogenesis. *Nucl Phys*. (2015) **B893**:122–57. doi: 10.1016/j.nuclphysb.2015.02.005
360. Di Bari P, Marzola L. SO(10)-inspired solution to the problem of the initial conditions in leptogenesis. *Nucl Phys*. (2013) **B877**:719–51. doi: 10.1016/j.nuclphysb.2013.10.027
361. Esteban I, Gonzalez-Garcia MC, Hernandez-Cabezudo A, Maltoni M, Schwetz T. Global analysis of three-flavour neutrino oscillations: synergies and tensions in the determination of $\theta_2 3$, $\delta_C P$, and the mass ordering. *J High Energy Phys*. (2018) **01**:106. doi: 10.1007/JHEP01(2019)106
362. Björkeroth F, de Anda FJ, de Medeiros Varzielas I, King SF. Leptogenesis in a $\Delta(27) \times SO(10)$ SUSY GUT. *J High Energy Phys*. (2017) **01**:077. doi: 10.1007/JHEP01(2017)077
363. Björkeroth F, de Anda FJ, de Medeiros Varzielas I, King SF. Towards a complete $A_4\times$ SU(5) SUSY GUT. *J High Energy Phys*. (2015) **06**:141. doi: 10.1007/JHEP06(2015)141
364. Anisimov A, Di Bari P. Cold dark matter from heavy right-handed neutrino mixing. *Phys Rev*. (2009) **D80**:073017. doi: 10.1103/PhysRevD.80.073017
365. De Roeck A, Ellis J, Grojean C, Heinemeyer S, Jakobs K, Weiglein G, et al. From the LHC to Future Colliders. *Eur Phys J*. (2010) **C66**:525–83. doi: 10.1140/epjc/s10052-010-1244-3
366. Aarons G, Djouadi A, Lykken J, Moenig K, Okada Y, Oreglia M, et al. *International Linear Collider*. Reference Design Report. Vol. 2. physics at the ILC. *arXiv:0709.1893* (2007).
367. Baer H, Barklow T, Fujii K, Gao Y, Hoang A, Kanemura S, et al. The *International Linear Collider*. Technical Design Report. Vol. 2. Physics. (2013). doi: 10.2172/1095028
368. Linssen L, Miyamoto A, Stanitzki M, Weerts H. Physics and Detectors at CLIC: CLIC Conceptual Design Report. *arXiv:1202.5940* (2012).
369. Haber HE, Kane GL. The search for supersymmetry: probing physics beyond the standard model. *Phys Rept*. (1985) **117**:75–263. doi: 10.1016/0370-1573(85)90051-1
370. Borschensky C, Krämer M, Kulesza A, Mangano M, Padhi S, Plehn T, et al. Squark and gluino production cross sections in pp collisions at $\sqrt{s}$ = 13, 14, 33 and 100 TeV. *Eur Phys J*. (2014) **C74**:3174. doi: 10.1140/epjc/s10052-014-3174-y
371. Beenakker W, Borschensky C, Krämer M, Kulesza A, Laenen E. NNLL-fast: predictions for coloured supersymmetric particle production at the LHC with threshold and Coulomb resummation. *J High Energy Phys*. (2016) **12**:133. doi: 10.1007/JHEP12(2016)133
372. Aaboud M, Abbott B, Abdinov O, Abeloos B, Abidi SH, AbouZeid O, et al. Search for squarks and gluinos in final states with jets and missing transverse momentum using 36 fb^{-1} of $\sqrt{s} = 13$ TeV pp collision data with the ATLAS detector. *Phys Rev*. (2018) **D97**:112001. doi: 10.1103/PhysRevD.97.112001
373. Sirunyan AM, Tumasyan A, Adam W, Ambrogi F, Asilar E, Bergauer T, et al. Search for natural and split supersymmetry in proton-proton collisions at $\sqrt{s}$ = 13 TeV in final states with jets and missing transverse momentum. *J High Energy Phys*. (2018) **05**:025. doi: 10.1007/JHEP05(2018)025
374. Sirunyan AM, Tumasyan A, Adam W, Ambrogi F, Asilar E, Bergauer T, et al. Search for supersymmetry in multijet events with missing transverse momentum in proton-proton collisions at 13 TeV. *Phys Rev*. (2017) **D96**:032003. doi: 10.1103/PhysRevD.96.032003
375. Aaboud M, Aad G, Abbott B, Abdinov O, Abeloos B, Abidi SH, et al. Search for squarks and gluinos in events with an isolated lepton, jets, and missing transverse momentum at $\sqrt{s} = 13$ TeV with the ATLAS detector. *Phys Rev*. (2017) **D96**:112010. doi: 10.1103/PhysRevD.96.112010
376. Sirunyan AM, Tumasyan A, Adam W, Ambrogi F, Asilar E, Bergauer T, et al. Search for supersymmetry in events with one lepton and multiple jets exploiting the angular correlation between the lepton and the missing transverse momentum in proton-proton collisions at $\sqrt{s}$ = 13 TeV. *Phys Lett*. (2018) **B780**:384–409. doi: 10.1016/j.physletb.2018.03.028
377. Sirunyan AM, Tumasyan A, Adam W, Ambrogi F, Asilar E, Bergauer T, et al. Search for Supersymmetry in *pp* Collisions at $\sqrt{s} = 13$ TeV in the Single-Lepton Final State Using the Sum of Masses of Large-Radius Jets. *Phys Rev Lett*. (2017) **119**:151802. doi: 10.1103/PhysRevLett.119.151802
378. Aaboud M, Georges Aad (Marseille C, Abdinov O, Abeloos B, Abidi SH, et al. Search for new phenomena using the invariant mass distribution of same-flavour opposite-sign dilepton pairs in events with missing transverse momentum in $\sqrt{s} = 13$ TeV pp collisions with the ATLAS detector. *Eur Phys J*. (2018) **C78**:625. doi: 10.1140/epjc/s10052-018-6081-9
379. Sirunyan AM, Tumasyan A, Adam W, Ambrogi F, Asilar E, Bergauer T, et al. Search for top squarks and dark matter particles in opposite-charge dilepton final states at $\sqrt{s}$ = 13 TeV. *Phys Rev*. (2018) **D97**:032009. doi: 10.1103/PhysRevD.97.032009
380. Aaboud M, Aad G, Abbott B, Abdinov O, Abeloos B, Abidi SH, et al. Search for supersymmetry in final states with two same-sign or three leptons and jets using 36 fb^{-1} of $\sqrt{s}$ = 13 TeV *pp* collision data with the ATLAS detector. *J High Energy Phys*. (2017) **09**:084. doi: 10.1007/JHEP09(2017)084
381. Sirunyan AM, Tumasyan A, Adam W, Ambrogi F, Asilar E, Bergauer T, et al. Search for supersymmetry in events with at least three electrons or muons, jets, and missing transverse momentum in proton-proton collisions at $\sqrt{s}$ = 13 TeV. *J High Energy Phys*. (2018) **02**:067. doi: 10.1007/jhep02(2018)067
382. Aaboud M, Aad G, Abbott B, Abdinov O, Abeloos B, Abidi SH, et al. Search for supersymmetry in final states with missing transverse momentum and multiple *b*-jets in proton-proton collisions at $\sqrt{s}$ = 13 TeV with the ATLAS detector. *J High Energy Phys*. (2018) **06**:107. doi: 10.1007/JHEP06(2018)107
383. Sirunyan AM, Tumasyan A, Adam W, Ambrogi F, Asilar E, Bergauer T, et al. Search for physics beyond the standard model in events with high-momentum higgs bosons and missing transverse momentum in proton-proton collisions at 13 TeV. *Phys Rev Lett*. (2018) **120**:241801. doi: 10.1103/PhysRevLett.120.241801
384. Sirunyan AM, Tumasyan A, Adam W, Ambrogi F, Asilar E, Bergauer T, et al. Search for supersymmetry in proton-proton collisions at 13 TeV using identified top quarks. *Phys Rev*. (2018) **D97**:012007. doi: 10.1103/PhysRevD.97.012007
385. Aaboud M, Aad G, Abbott B, Abdinov O, Abeloos B, Abhayasinghe DK, et al. Search for squarks and gluinos in final states with hadronically decaying τ-leptons, jets, and missing transverse momentum using *pp* collisions at $\sqrt{s}$ = 13 TeV with the ATLAS detector. *Phys Rev*. (2018) **99**:012009. doi: 10.1103/PhysRevD.99.012009
386. Aaboud M, Aad G, Abbott B, Abdinov O, Abeloos B, Abidi SH, et al. Search for a scalar partner of the top quark in the jets plus missing transverse momentum final state at $\sqrt{s}$=13 TeV with the ATLAS detector. *J High Energy Phys*. (2017) **12**:085. doi: 10.1007/JHEP12(2017)085
387. Sirunyan AM, Tumasyan A, Adam W, Ambrogi F, Asilar E, Bergauer T, et al. Search for top squark pair production in pp collisions at $\sqrt{s}$ = 13 TeV using single lepton events. *J High Energy Phys*. (2017) **10**:019. doi: 10.1007/JHEP10(2017)019
388. Aaboud M, Aad G, Abbott B, Abdinov O, Abeloos B, Abidi SH, et al. Search for supersymmetry in events with *b*-tagged jets and missing transverse momentum in *pp* collisions at $\sqrt{s} = 13$ TeV with the ATLAS detector. *J High Energy Phys*. (2017) **11**:195. doi: 10.1007/JHEP11(2017)195
389. Sirunyan AM, Tumasyan A, Adam W, Ambrogi F, Asilar E, Bergauer T, et al. Search for the pair production of third-generation squarks with two-body decays to a bottom or charm quark and a neutralino in proton-proton collisions at $\sqrt{s}$ = 13 TeV. *Phys Lett*. (2018) **B778**:263–91. doi: 10.1016/j.physletb.2018.01.012
390. Aaboud M, Aad G, Abbott B, Abdinov O, Abeloos B, Abidi SH, et al. Search for top-squark pair production in final states with one lepton, jets, and missing transverse momentum using 36 fb^{-1} of $\sqrt{s}$ = 13 TeV pp collision data with the ATLAS detector. *J High Energy Phys*. (2018) **06**:108. doi: 10.1007/JHEP09(2018)050
391. Sirunyan AM, Tumasyan A, Adam W, Ambrogi F, Asilar E, Bergauer T, et al. Search for top squarks decaying via four-body or chargino-mediated modes in single-lepton final states in proton-proton collisions at $\sqrt{s} = 13$ TeV. *J High Energy Phys*. (2018) **09**:065. doi: 10.1007/JHEP09(2018)065

392. Aaboud M, Aad G, Abbott B, Abdinov O, Abeloos B, Abidi SH, et al. Search for direct top squark pair production in final states with two leptons in $\sqrt{s} = 13$ TeV pp collisions with the ATLAS detector. *Eur Phys J.* (2017) **C77**:898.
393. Sirunyan AM, Tumasyan A, Adam W, Ambrogi F, Asilar E, Bergauer T, et al. Searches for pair production of charginos and top squarks in final states with two oppositely charged leptons in proton-proton collisions at $\sqrt{s} = 13$ TeV. *J High Energy Phys*. (2018) **11**:079. doi: 10.1007/JHEP11(2018)079
394. Aaboud M, Aad G, Abbott B, Abdinov O, Abeloos B, Abidi SH, et al. Search for direct top squark pair production in events with a Higgs or Z boson, and missing transverse momentum in $\sqrt{s} = 13$ TeV pp collisions with the ATLAS detector. *J High Energy Phys*. (2017) **08**:006. doi: 10.1007/JHEP11(2017)195
395. Aaboud M, Aad G, Abbott B, Abdinov O, Abeloos B, Abidi SH, et al. Search for electroweak production of supersymmetric states in scenarios with compressed mass spectra at $\sqrt{s} = 13$ TeV with the ATLAS detector. *Phys Rev*. (2018) **D97**:052010. doi: 10.1103/PhysRevD.97.052010
396. Sirunyan AM, Tumasyan A, Adam W, Ambrogi F, Asilar E, Bergauer T, et al. Search for supersymmetric partners of electrons and muons in proton-proton collisions at $\sqrt{s} = 13$ TeV. *Phys Lett*. (2018) **B790**:140–166. doi: 10.1016/j.physletb.2019.01.005
397. Sirunyan AM, Tumasyan A, Adam W, Ambrogi F, Asilar E, Bergauer T, et al. Combined search for electroweak production of charginos and neutralinos in proton-proton collisions at $\sqrt{s} = 13$ TeV. *J High Energy Phys*. (2018) **03**:160. doi: 10.1007/JHEP03(2018)160
398. Aaboud M, Aad G, Abbott B, Abdinov O, Abeloos B, Abidi SH, et al. Search for electroweak production of supersymmetric particles in final states with two or three leptons at $\sqrt{s} = 13$ TeV with the ATLAS detector. (2018) **C78**:995. doi: 10.1140/epjc/s10052-018-6423-7
399. Aaboud M, Aad G, Abbott B, Abdinov O, Abeloos B, Abhayasinghe DK, et al. Search for chargino-neutralino production using recursive jigsaw reconstruction in final states with two or three charged leptons in proton-proton collisions at $\sqrt{s} = 13$ TeV with the ATLAS detector. *Phys Rev*. (2018) **D98**:092012. doi: 10.1103/PhysRevD.98.092012
400. Aaboud M, Aad G, Abbott B, Abdinov O, Abeloos B, Abidi SH, et al. Search for supersymmetry in events with four or more leptons in $\sqrt{s} = 13$ TeV pp collisions with ATLAS. *Phys Rev*. (2018) **D98**:032009. doi: 10.1103/PhysRevD.98.032009
401. Aaboud M, Aad G, Abbott B, Abdinov O, Abeloos B, Abidi SH, et al. Search for the direct production of charginos and neutralinos in final states with tau leptons in $\sqrt{s} = 13$ TeV pp collisions with the ATLAS detector. *Eur Phys J*. (2018) **C78**:154. doi: 10.1140/epjc/s10052-018-5583-9
402. Sirunyan AM, Tumasyan A, Adam W, Ambrogi F, Asilar E, Bergauer T, et al. Search for supersymmetry in events with a τ lepton pair and missing transverse momentum in proton-proton collisions at $\sqrt{s} = 13$ TeV. *J High Energy Phys*. (2018) **11**:151. doi: 10.1007/JHEP11(2018)151
403. Aaboud M, Aad G, Abbott B, Abdinov O, Abeloos B, Abidi SH, et al. Search for pair production of higgsinos in final states with at least three b-tagged jets in $\sqrt{s} = 13$ TeV pp collisions using the ATLAS detector. *Phys Rev*. (2018) **D98**:092002. doi: 10.1140/epjc/s10052-018-6457-x
404. Aaboud M, Aad G, Abbott B, Abdinov O, Abeloos B, Abhayasinghe DK, et al. Search for Higgs boson pair production in the $WW^{(*)}WW^{(*)}$ decay channel using ATLAS data recorded at $\sqrt{s} = 13$ TeV. *arXiv:1811.11028* (2018).
405. Aaboud M, Aad G, Abbott B, Abdinov O, Abeloos B, Abidi SH, et al. Search for heavy ZZ resonances in the $\ell^+\ell^-\ell^+\ell^-$ and $\ell^+\ell^-\nu\bar{\nu}$ final states using proton-proton collisions at $\sqrt{s} = 13$ TeV with the ATLAS detector. *Eur Phys J*. (2018) **C78**:293. doi: 10.1140/epjc/s10052-018-5686-3
406. Aaboud M, Aad G, Abbott B, Abdinov O, Abeloos B, Abidi SH, et al. Search for heavy resonances decaying into WW in the $e\nu\mu\nu$ final state in pp collisions at $\sqrt{s} = 13$ TeV with the ATLAS detector. *Eur Phys J*. (2018) **C78**:24. doi: 10.1140/epjc/s10052-017-5491-4
407. Sirunyan AM, Tumasyan A, Adam W, Ambrogi F, Asilar E, Bergauer T, et al. A search for pair production of new light bosons decaying into muons in proton-proton collisions at 13 TeV. *arXiv:1812.00380* (2018).
408. Aaboud M, Aad G, Abbott B, Abdinov O, Abeloos B, Abidi SH, et al. Search for pair production of Higgs bosons in the $b\bar{b}b\bar{b}$ final state using proton-proton collisions at $\sqrt{s} = 13$ TeV with the ATLAS detector. *J High Energy Phys*. (2018) **01**:030. doi: 10.1007/JHEP01(2019)030
409. Sirunyan AM, Tumasyan A, Adam W, Ambrogi F, Asilar E, Bergauer T, et al. Search for beyond the standard model Higgs bosons decaying into a $b\bar{b}$ pair in pp collisions at $\sqrt{s} = 13$ TeV. *J High Energy Phys*. (2018) **08**:113. doi: 10.1007/JHEP08(2018)113
410. Aaboud M, Aad G, Abbott B, Abdinov O, Abeloos B, Abhayasinghe DK, et al. Search for Higgs boson pair production in the $b\bar{b}WW^*$ decay mode at $\sqrt{s} = 13$ TeV with the ATLAS detector. *J High Energy Phys*. (2018) **04**:092 . doi: 10.1007/JHEP04(2019)092
411. Aaboud M, Aad G, Abbott B, Abdinov O, Abeloos B, Abhayasinghe DK, et al. Search for Higgs boson pair production in the $\gamma\gamma b\bar{b}$ final state with 13 TeV pp collision data collected by the ATLAS experiment. *J High Energy Phys*. (2018) **11**:040. doi: 10.1007/JHEP11(2018)040
412. Sirunyan AM, Tumasyan A, Adam W, Ambrogi F, Asilar E, Bergauer T, et al. Search for a standard model-like Higgs boson in the mass range between 70 and 110 GeV in the diphoton final state in proton-proton collisions at $\sqrt{s} = 8$ and 13 TeV. *Phys Lett*. (2018) **B793**:320–47. doi: 10.1016/j.physletb.2019.03.064
413. Aaboud M, Aad G, Abbott B, Abdinov O, Abeloos B, Abhayasinghe DK, et al. Search for Resonant and Nonresonant Higgs Boson Pair Production in the $b\bar{b}\tau^+\tau^-$ Decay Channel in pp Collisions at $\sqrt{s} =$ 13TeV with the ATLAS Detector. *Phys Rev Lett*. (2018) **121**:191801. doi: 10.1103/PhysRevLett.121.191801
414. Khachatryan V, Sirunyan AM, Tumasyan A, Wolfgang Adam EA, Bergauer T, et al. Search for light bosons in decays of the 125 GeV Higgs boson in proton-proton collisions at $\sqrt{s} = 8$ TeV. *J High Energy Phys*. (2017) **10**:076. doi: 10.1007/JHEP10(2017)076
415. Sirunyan AM, Tumasyan A, Adam W, Ambrogi F, Asilar E, Bergauer T, et al. Search for a light pseudoscalar Higgs boson produced in association with bottom quarks in pp collisions at $\sqrt{s} = 8$ TeV. *J High Energy Phys*. (2017) **11**:010. doi: 10.1007/JHEP11(2017)010
416. Aaboud M, Aad G, Abbott B, Abdinov O, Abeloos B, Abhayasinghe DK, et al. Search for charged Higgs bosons decaying into top and bottom quarks at $\sqrt{s} = 13$ TeV with the ATLAS detector. *J High Energy Phys*. (2018) **11**:085. doi: 10.1007/JHEP11(2018)085
417. Aaboud M, Aad G, Abbott B, Abdinov O, Abeloos B, Abidi SH, et al. Search for additional heavy neutral Higgs and gauge bosons in the ditau final state produced in 36 fb^{-1} of pp collisions at $\sqrt{s} = 13$ TeV with the ATLAS detector. *J High Energy Phys*. (2018) **01**:055. doi: 10.1007/JHEP11(2018)051
418. Sirunyan AM, Tumasyan A, Adam W, Ambrogi F, Asilar E, Bergauer T, et al. Search for additional neutral MSSM Higgs bosons in the $\tau\tau$ final state in proton-proton collisions at $\sqrt{s} = 13$ TeV. *J High Energy Phys*. (2018) **09**:007. doi: 10.1007/JHEP09(2018)007
419. Aaboud M, Aad G, Abbott B, Abdinov O, Abeloos B, Abidi SH, et al. Search for new phenomena in high-mass diphoton final states using 37 fb^{-1} of proton–proton collisions collected at $\sqrt{s} = 13$ TeV with the ATLAS detector. *Phys Lett*. (2017) **B775**:105–25. doi: 10.1016/j.physletb.2017.10.039
420. Aaboud M, Aad G, Abbott B, Abdinov O, Abeloos B, Abhayasinghe DK, et al. Search for Higgs boson pair production in the $\gamma\gamma WW^*$ channel using pp collision data recorded at $\sqrt{s} = 13$ TeV with the ATLAS detector. *Eur Phys J*. (2018) **C78**:1007. doi: 10.1103/PhysRevD.98.092002
421. Aaboud M, Aad G, Abbott B, Abdinov O, Abeloos B, Abhayasinghe DK, et al. A search for pairs of highly collimated photon-jets in pp collisions at $\sqrt{s} = 13$ TeV with the ATLAS detector. *Phys Rev*. (2018) **D99**:012008. doi: 10.1103/PhysRevD.99.012008
422. Aad G, Abbott B, Abdallah J, Abdinov O, Aben R, Abolins M, et al. Search for a charged higgs boson produced in the vector-boson fusion mode with decay $H^\pm \to W^\pm Z$ Using pp collisions at $\sqrt{s} = 8$ TeV with the ATLAS experiment. *Phys Rev Lett*. (2015) **114**:231801. doi: 10.1103/PhysRevLett.114.231801
423. Sirunyan AM, Tumasyan A, Adam W, Ambrogi F, Asilar E, Bergauer T, et al. Search for Charged Higgs Bosons Produced via Vector Boson Fusion and Decaying into a Pair of W and Z Bosons Using pp Collisions at $\sqrt{s} =$ 13 TeV. *Phys Rev Lett*. (2017) **119**:141802. doi: 10.1103/PhysRevLett.119.141802
424. Sirunyan AM, Tumasyan A, Adam W, Ambrogi F, Asilar E, Bergauer T, et al. Search for a charged Higgs boson decaying to charm and bottom quarks in proton-proton collisions at $\sqrt{s} = 8$ TeV. *J High Energy Phys*. (2018) **11**:115. doi: 10.1007/JHEP11(2018)115

425. Aaboud M, Aad G, Abbott B, Abdallah J, Abdinov O, Abeloos B, et al. Search for charged Higgs bosons produced in association with a top quark and decaying via $H^{\pm} \to \tau\nu$ using *pp* collision data recorded at $\sqrt{s} = 13$ TeV by the ATLAS detector. *Phys Lett*. (2016) **B759**:555–74. doi: 10.1016/j.physletb.2016.06.017
426. Aaboud M, Aad G, Abbott B, Abdinov O, Abeloos B, Abidi SH, et al. Search for R-parity-violating supersymmetric particles in multi-jet final states produced in *p-p* collisions at $\sqrt{s} = 13$ TeV using the ATLAS detector at the LHC. *Phys Lett*. (2018) **B785**:136–58. doi: 10.1016/j.physletb.2018.08.021
427. Aaboud M, Aad G, Abbott B, Abdinov O, Abeloos B, Abidi SH, et al. Search for new phenomena in a lepton plus high jet multiplicity final state with the ATLAS experiment using $\sqrt{s} = 13$ TeV proton-proton collision data. *J High Energy Phys*. (2017) **09**:088. doi: 10.1007/JHEP09(2017)088
428. Aaboud M, Aad G, Abbott B, Abdinov O, Abeloos B, Abidi SH, et al. A search for pair-produced resonances in four-jet final states at $\sqrt{s} = 13$ TeV with the ATLAS detector. *Eur Phys J*. (2018) **C78**:250. doi: 10.1140/epjc/s10052-018-5693-4
429. Sirunyan AM, Tumasyan A, Adam W, Ambrogi F, Asilar E, Bergauer T, et al. Search for *R*-parity violating supersymmetry in pp collisions at $\sqrt{s} = 13$ TeV using b jets in a final state with a single lepton, many jets, and high sum of large-radius jet masses. *Phys Lett*. (2018) **B783**:114–39. doi: 10.1016/j.physletb.2018.06.028
430. Aaboud M, Aad G, Abbott B, Abdinov O, Abeloos B, Abidi SH, et al. Search for B-L R -parity-violating top squarks in $\sqrt{s}$ =13TeV pp collisions with the ATLAS experiment. *Phys Rev*. (2018) **D97**:032003. doi: 10.1103/PhysRevD.97.032003
431. Sirunyan AM, Tumasyan A, Adam W, Ambrogi F, Asilar E, Bergauer T, et al. Search for resonant production of second-generation sleptons with same-sign dimuon events in proton-proton collisions at $\sqrt{s} = 13$ TeV. *Eur Phys J*. (2018) **C79**:305. doi: 10.1140/epjc/s10052-019-6800-x
432. Aaboud M, Aad G, Abbott B, Abdinov O, Abeloos B, Abhayasinghe DK, et al. Search for long-lived particles produced in *pp* collisions at $\sqrt{s} = 13$ TeV that decay into displaced hadronic jets in the ATLAS muon spectrometer. *Phys Rev*. (2018) **D99**:052005. doi: 10.1103/PhysRevD.99.052005
433. Aaboud M, Aad G, Abbott B, Abdinov O, Abeloos B, Abhayasinghe DK, et al. Search for heavy charged long-lived particles in proton-proton collisions at $\sqrt{s} = 13$ TeV using an ionisation measurement with the ATLAS detector. *Phys Lett*. (2019) **B788**:96–116. doi: 10.1016/j.physletb.2018.10.055
434. Aaboud M, Aad G, Abbott B, Abdinov O, Abeloos B, Abidi SH, et al. Search for long-lived, massive particles in events with displaced vertices and missing transverse momentum in $\sqrt{s}$ = 13 TeV *pp* collisions with the ATLAS detector. *Phys Rev*. (2018) **D97**:052012. doi: 10.1103/PhysRevD.97.052012
435. Aaboud M, Aad G, Abbott B, Abdinov O, Abeloos B, Abidi SH, et al. Search for long-lived charginos based on a disappearing-track signature in pp collisions at $\sqrt{s} = 13$ TeV with the ATLAS detector. *J High Energy Phys*. (2018) **06**:022. doi: 10.1007/JHEP06(2018)022
436. Aaboud M, Aad G, Abbott B, Abdinov O, Abeloos B, Abhayasinghe DK, et al. Search for long-lived particles in final states with displaced dimuon vertices in *pp* collisions at $\sqrt{s} = 13$ TeV with the ATLAS detector. *Phys Rev D*. (2018) **99**:012001. doi: 10.1103/PhysRevD.99.012001
437. Sirunyan AM, Tumasyan A, Adam W, Ambrogi F, Asilar E, Bergauer T, et al. Search for new long-lived particles at $\sqrt{s} = 13$ TeV. *Phys Lett*. (2018) **B780**:432–54. doi: 10.1016/j.physletb.2018.03.019
438. Sirunyan AM, Tumasyan A, Adam W, Ambrogi F, Asilar E, Bergauer T, et al. Search for long-lived particles decaying into displaced jets in proton-proton collisions at $\sqrt{s} = 13$ TeV. *Phys Rev*. (2018) **D99**:032011. doi: 10.1103/PhysRevD.99.032011
439. Sirunyan AM, Tumasyan A, Adam W, Ambrogi F, Asilar E, Bergauer T, et al. Search for long-lived particles with displaced vertices in multijet events in proton-proton collisions at $\sqrt{s}$ =13 TeV. *Phys Rev*. (2018) **D98**:092011. doi: 10.1103/PhysRevD.98.092011
440. Sirunyan AM, Tumasyan A, Adam W, Ambrogi F, Asilar E, Bergauer T, et al. Search for gauge-mediated supersymmetry in events with at least one photon and missing transverse momentum in pp collisions at $\sqrt{s} = 13$ TeV. *Phys Lett*. (2018) **B780**:118–43. doi: 10.1016/j.physletb.2018.02.045
441. Sirunyan AM, Tumasyan A, Adam W, Ambrogi F, Asilar E, Bergauer T, et al. Search for supersymmetry in events with at least one photon, missing transverse momentum, and large transverse event activity in proton-proton collisions at $\sqrt{s} = 13$ TeV. *J High Energy Phys*. (2017) **12**:142. doi: 10.1007/JHEP12(2017)142
442. Aaboud M, Aad G, Abbott B, Abdallah J, Abdinov O, Abeloos B, et al. Search for supersymmetry in a final state containing two photons and missing transverse momentum in $\sqrt{s}$ = 13 TeV *pp* collisions at the LHC using the ATLAS detector. *Eur Phys J*. (2016) **C76**:517. doi: 10.1140/epjc/s10052-016-4344-x
443. Aaboud M, Aad G, Abbott B, Abdinov O, Abeloos B, Abidi SH, et al. Search for photonic signatures of gauge-mediated supersymmetry in 13 TeV *pp* collisions with the ATLAS detector. *Phys Rev*. (2018) **D97**:092006. doi: 10.1103/PhysRevD.97.092006
444. Sirunyan AM, Tumasyan A, Adam W, Ambrogi F, Asilar E, Bergauer T, et al. Search for Higgsino pair production in *pp* collisions at $\sqrt{s}$ = 13TeV in final states with large missing transverse momentum and two Higgs bosons decaying via $H \to b\bar{b}$. *Phys Rev*. (2018) **D97**:032007. doi: 10.1103/PhysRevD.97.032007
445. Aaboud M, Aad G, Abbott B, Abdinov O, Abeloos B, Abidi SH, et al. Search for top squarks decaying to tau sleptons in *pp* collisions at $\sqrt{s} = 13$ TeV with the ATLAS detector. *Phys Rev*. (2018) **D98**:032008. doi: 10.1103/PhysRevD.98.032008
446. Heister A, Schael S, Barate R, Bruneliere R, Bonis ID, Decamp D, et al. Search for charginos nearly mass degenerate with the lightest neutralino in e+ e- collisions at center-of-mass energies up to 209-GeV. *Phys Lett*. (2002) **B533**:223–36. doi: 10.1016/S0370-2693(02)01584-8
447. Heister A, Schael S, Barate R, Bruneliere R, Bonis ID, Decamp D, et al. Absolute lower limits on the masses of selectrons and sneutrinos in the MSSM. *Phys Lett*. (2002) **B544**:73–88. doi: 10.1016/S0370-2693(02)02471-1
448. Abbiendi G, Ainsley C, Akesson PF, Alexander G, Allison J, Amaral P, et al. Search for chargino and neutralino production at $s^{(1/2)}$ = 192-GeV to 209 GeV at LEP. *Eur Phys J*. (2004) **C35**:1–20. doi: 10.1140/epjc/s2004-01758-8
449. Abbiendi G, Ainsley C, Akesson PF, Alexander G, Allison J, Amaral P, et al. Search for anomalous production of dilepton events with missing transverse momentum in e+ e- collisions at $s^{(1/2)}$ = 183-Gev to 209-GeV. *Eur Phys J*. (2004) **C32**:453–73. doi: 10.1140/epjc/s2003-01466-y
450. Acciarri M, Achard P, Adriani O, Aguilar-Benitez M, Alcaraz J, Alemanni G, et al. Search for charginos and neutralinos in e^+e^- collisions at $\sqrt{S}$ = 189-GeV. *Phys Lett*. (2000) **B472**:420–33. doi: 10.1016/S0370-2693(99)01388-X
451. Achard P, Adriani O, Aguilar-Benitez M, Alcaraz J, Alemanni G, Allaby J, et al. Search for scalar leptons and scalar quarks at LEP. *Phys Lett*. (2004) **B580**:37–49. doi: 10.1016/j.physletb.2003.10.010
452. Abdallah J, Abreu P, Adam W, Adzic P, Albrecht T, Alderweireld T, et al. Searches for supersymmetric particles in e+ e- collisions up to 208-GeV and interpretation of the results within the MSSM. *Eur Phys J*. (2003) **C31**:421–79. doi: 10.1140/epjc/s2003-01355-5
453. Roszkowski L, Ruiz de Austri R, Trotta R, Tsai YLS, Varley TA. Global fits of the Non-Universal Higgs Model. *Phys Rev*. (2011) **D83**:015014. doi: 10.1103/PhysRevD.83.015014
454. Bertone G, Cerdeno DG, Fornasa M, Ruiz de Austri R, Strege C, Trotta R. Global fits of the cMSSM including the first LHC and XENON100 data. *J Cosmol Astropart Phys*. (2012) **1201**:015. doi: 10.1088/1475-7516/2012/01/015
455. Bechtle P, Bringmann T, Desch K, Dreiner H, Hamer M, Hensel C, et al. Constrained Supersymmetry after two years of LHC data: a global view with Fittino. *J High Energy Phys*. (2012) **06**:098. doi: 10.1007/JHEP06(2012)098
456. Buchmueller O, Cavanaugh R, Roeck AD, Dolan MJ, Ellis JR, Flacher H, et al. The CMSSM and NUHM1 after LHC Run 1. *Eur Phys J*. (2014) **C74**:2922. doi: 10.1140/epjc/s10052-014-2922-3
457. Buchmueller O, Cavanaugh R, Citron M, Roeck AD, Dolan MJ, Ellis JR, et al. The NUHM2 after LHC Run 1. *Eur Phys J*. (2014) **C74**:3212. doi: 10.1140/epjc/s10052-014-3212-9
458. Han C, Hikasa Ki, Wu L, Yang JM, Zhang Y. Status of CMSSM in light of current LHC Run-2 and LUX data. *Phys Lett*. (2017) **B769**:470–76. doi: 10.1016/j.physletb.2017.04.026
459. Athron P, Balázs C, Bringmann T, Buckley A, Chrząszcz M, Conrad J, et al. Global fits of GUT-scale SUSY models with GAMBIT. *Eur Phys J*. (2017) **C77**:824. doi: 10.1140/epjc/s10052-017-5167-0

460. Bagnaschi E, Sakurai K, Borsato M, Buchmueller O, Citron M, Costa JC, et al. Likelihood Analysis of the pMSSM11 in Light of LHC 13-TeV Data. *Eur Phys J*. (2018) **C78**:256. doi: 10.1140/epjc/s10052-018-5697-0
461. Athron P, Balázs C, Bringmann T, Buckley A, Chrząszcz M, Conrad J, et al. A global fit of the MSSM with GAMBIT. *Eur Phys J*. (2017) **C77**:879. doi: 10.1140/epjc/s10052-017-5196-8
462. Bertone G, Calore F, Caron S, Ruiz R, Kim JS, Trotta R, et al. Global analysis of the pMSSM in light of the Fermi GeV excess: prospects for the LHC Run-II and astroparticle experiments. *J Cosmol Astropart Phys*. (2016) **1604**:037. doi: 10.1088/1475-7516/2016/04/037
463. Bagnaschi E, Costa JC, Sakurai K, Borsato M, Buchmueller O, Cavanaugh R, et al. Likelihood Analysis of Supersymmetric SU(5) GUTs. *Eur Phys J*. (2017) **C77**:104. doi: 10.1140/epjc/s10052-017-4639-6
464. Arbuzov AB, Awramik M, Czakon M, Freitas A, Grunewald MW, Monig K, et al. ZFITTER: A Semi-analytical program for fermion pair production in e+ e- annihilation, from version 6.21 to version 6.42. *Comput Phys Commun*. (2006) **174**:728–58. doi: 10.1016/j.cpc.2005.12.009
465. Ruiz de Austri R, Trotta R, Roszkowski L. A markov chain monte carlo analysis of the CMSSM. *J High Energy Phys*. (2006) **05**:002. doi: 10.1088/1126-6708/2006/05/002
466. Trotta R, Feroz F, Hobson MP, Roszkowski L, Ruiz de Austri R. The Impact of priors and observables on parameter inferences in the Constrained MSSM. *J High Energy Phys*. (2008) **12**:024. doi: 10.1088/1126-6708/2008/12/024
467. Bechtle P, Desch K, Wienemann P. Fittino, a program for determining MSSM parameters from collider observables using an iterative method. *Comput Phys Commun*. (2006) **174**:47–70. doi: 10.1016/j.cpc.2005.09.002
468. Buchmueller O, Cavanaugh R, De Roeck A, Ellis JR, Flacher H, Heinemeyer S, et al. Likelihood Functions for Supersymmetric Observables in Frequentist Analyses of the CMSSM and NUHM1. *Eur Phys J*. (2009) **C64**:391–415. doi: 10.1140/epjc/s10052-009-1159-z
469. Athron P, Balazs C, Bringmann T, Buckley A, Chrząszcz M, et al. GAMBIT: The Global and Modular Beyond-the-Standard-Model Inference Tool. *Eur Phys J*. (2017) **C77**:784. doi: 10.1140/epjc/s10052-017-5321-8
470. Athron P, Balázs C, Dal LA, Edsjö J, Farmer B, Gonzalo TE, et al. SpecBit, DecayBit and PrecisionBit: GAMBIT modules for computing mass spectra, particle decay rates and precision observables. *Eur Phys J*. (2018) **C78**:22. doi: 10.1140/epjc/s10052-017-5390-8
471. Bringmann T, Conrad J, Cornell JM, Dal LA, Edsjö J, Farmer B, et al. DarkBit: a GAMBIT module for computing dark matter observables and likelihoods. *Eur Phys J*. (2017) **C77**:831. doi: 10.1140/epjc/s10052-017-5155-4
472. Martinez GD, McKay J, Farmer B, Scott P, Roebber E, Putze A, et al. Comparison of statistical sampling methods with ScannerBit, the GAMBIT scanning module. *Eur Phys J*. (2017) **C77**:761. doi: 10.1140/epjc/s10052-017-5274-y
473. Balázs C, Buckley A, Dal LA, Farmer B, Jackson P, Krislock A, et al. ColliderBit: a GAMBIT module for the calculation of high-energy collider observables and likelihoods. *Eur Phys J*. (2017) **C77**:795. doi: 10.1140/epjc/s10052-017-5285-8
474. Bernlochner FU, Chrzaszcz M, Dal LA, Farmer B, Jackson P, Kvellestad A, et al. FlavBit: A GAMBIT module for computing flavour observables and likelihoods. *Eur Phys J*. (2017) **C77**:786. doi: 10.1140/epjc/s10052-017-5157-2
475. Athron P, Balázs C, Bringmann T, Buckley A, Chrząszcz M, Conrad J, et al. Status of the scalar singlet dark matter model. *Eur Phys J*. (2017) **C77**:568. doi: 10.1140/epjc/s10052-017-5113-1
476. Athron P, Balázs C, Beniwal A, Bloor S, Camargo-Molina JE, Cornell JM, et al. Global analyses of Higgs portal singlet dark matter models using GAMBIT. *Eur Phys J*. (2019) **C79**:38. doi: 10.1140/epjc/s10052-018-6513-6
477. Murayama H, Yanagida T. A viable SU(5) GUT with light leptoquark bosons. Mod *Phys Lett*. (1992) **A7**:147–52. doi: 10.1142/S0217732392000070
478. Biggio C, Bordone M, Di Luzio L, Ridolfi G. Massive vectors and loop observables: the $g-2$ case. *J High Energy Phys*. (2016) **10**:002. doi: 10.1007/JHEP10(2016)002
479. Gabrielli E, Marzola L, Raidal M, Veermäe H. Dark matter and spin-1 milli-charged particles. *J High Energy Phys*. (2015) **08**:150. doi: 10.1007/JHEP08(2015)150
480. Doršner I, Fajfer S, Greljo A, Kamenik JF, Košnik N. Physics of leptoquarks in precision experiments and at particle colliders. *Phys Rept*. (2016) **641**:1–68. doi: 10.1016/j.physrep.2016.06.001
481. Buchmuller W, Ruckl R, Wyler D. Leptoquarks in Lepton-Quark Collisions. *Phys Lett*. (1987) **B191**:442–8. doi: 10.1016/0370-2693(87)90637-X
482. Davidson S, Bailey DC, Campbell BA. Model independent constraints on leptoquarks from rare processes. *Z Phys*. (1994) **C61**:613–44. doi: 10.1007/BF01552629
483. Grifols JA, Mendez A. Pair Production of Colored Hypermesons at Very High-energy. *Phys Rev*. (1982) **D26**:324. doi: 10.1103/PhysRevD.26.324
484. Antoniadis I, Baulieu L, Delduc F. Supersymmetric enhancement factor for the one jet cross-section in $p\bar{p}$ Reactions. *Z Phys*. (1984) **C23**:119. doi: 10.1007/BF01557587
485. Eichten E, Hinchliffe I, Lane KD, Quigg C. Super Collider Physics. *Rev Mod Phys*. (1984) **56**:579–707. doi: 10.1103/RevModPhys.56.579
486. Altarelli G, Ruckl R. Searching for a Scalar Top at the CERN $p\bar{p}$ Collider. *Phys Lett*. (1984) **144B**:126–32. doi: 10.1016/0370-2693(84)90190-4
487. Dawson S, Eichten E, Quigg C. Search for supersymmetric particles in hadron-hadron collisions. *Phys Rev*. (1985) **D31**:1581. doi: 10.1103/PhysRevD.31.1581
488. Blumlein J, Boos E, Kryukov A. Leptoquark pair production in hadronic interactions. *Z Phys*. (1997) **C76**:137–53. doi: 10.1007/s002880050538
489. Dorsner I, Fajfer S, Greljo A. Cornering Scalar Leptoquarks at LHC. *J High Energy Phys*. (2014) **10**:154. doi: 10.1007/JHEP10(2014)154
490. Doršner I, Greljo A. Leptoquark toolbox for precision collider studies. *J High Energy Phys*. (2018) **05**:126. doi: 10.1007/JHEP05(2018)126
491. Plehn T, Spiesberger H, Spira M, Zerwas PM. Formation and decay of scalar leptoquarks / squarks in e p collisions. *Z Phys*. (1997) **C74**:611–4. doi: 10.1007/s002880050426
492. Diaz B, Schmaltz M, Zhong YM. The leptoquark Hunter's guide: Pair production. *J High Energy Phys*. (2017) **10**:097. doi: 10.1007/JHEP10(2017)097
493. Sirunyan AM, Tumasyan A, Adam W, Ambrogi F, Asilar E, Bergauer T, et al. Search for pair production of first-generation scalar leptoquarks at $\sqrt{s} = 13$ TeV. *Phys Rev*. (2018) **D99**:052002. doi: 10.1103/PhysRevD.99.052002
494. Aaboud M, Aad G, Abbott B, Abdallah J, Abdinov O, Abeloos B, et al. Search for scalar leptoquarks in pp collisions at $\sqrt{s} = 13$ TeV with the ATLAS experiment. New *J Phys*. (2016) **18**:093016. doi: 10.1088/1367-2630/18/9/093016
495. Aad G, Abbott B, Abdallah J, Abdinov O, Aben R, Abolins M, et al. Searches for scalar leptoquarks in pp collisions at $\sqrt{s} = 8$ TeV with the ATLAS detector. *Eur Phys J*. (2016) **C76**:5. doi: 10.1140/epjc/s10052-015-3823-9
496. Khachatryan V, Sirunyan AM, Tumasyan A, Adam W, Asilar E, Bergauer T, et al. Search for heavy neutrinos or third-generation leptoquarks in final states with two hadronically decaying τ leptons and two jets in proton-proton collisions at $\sqrt{s} = 13$ TeV. *J High Energy Phys*. (2017) **03**:077. doi: 10.1007/JHEP03(2017)077
497. Sirunyan AM, Tumasyan A, Adam W, Asilar E, Bergauer T, Brandstetter J, et al. Search for third-generation scalar leptoquarks and heavy right-handed neutrinos in final states with two tau leptons and two jets in proton-proton collisions at $\sqrt{s} = 13$ TeV. *J High Energy Phys*. (2017) **07**:121. doi: 10.1007/JHEP07(2017)121
498. Sirunyan AM, Tumasyan A, Adam W, Ambrogi F, Asilar E, Bergauer T, et al. Constraints on models of scalar and vector leptoquarks decaying to a quark and a neutrino at $\sqrt{s} = 13$ TeV. *Phys Rev*. (2018) **D98**:032005. doi: 10.1103/PhysRevD.98.032005
499. Sirunyan AM, Tumasyan A, Adam W, Ambrogi F, Asilar E, Bergauer T, et al. Search for third-generation scalar leptoquarks decaying to a top quark and a τ lepton at $\sqrt{s} = 13$ TeV. *Eur Phys J*. (2018) **C78**:707. doi: 10.1140/epjc/s10052-018-6143-z
500. Sirunyan AM, Tumasyan A, Adam W, Ambrogi F, Asilar E, Bergauer T, et al. Search for leptoquarks coupled to third-generation quarks in proton-proton collisions at $\sqrt{s} = 13$ TeV. *Phys Rev Lett*. (2018) **121**:241802. doi: 10.1103/PhysRevLett.121.241802

501. Khachatryan V, Sirunyan AM, Tumasyan A, Adam W, Asilar E, Bergauer T, et al. Search for single production of scalar leptoquarks in proton-proton collisions at $\sqrt{s} = 8$ *TeV*. *Phys Rev*. (2016) **D93**:032005. doi: 10.1103/PhysRevD.93.032005
502. Deppisch FF, Bhupal Dev PS, Pilaftsis A. Neutrinos and Collider Physics. New *J Phys*. (2015) **17**:075019. doi: 10.1088/1367-2630/17/7/075019
503. Aaboud M, Aad G, Abbott B, Abdinov O, Abeloos B, Abhayasinghe DK, et al. Search for heavy Majorana or Dirac neutrinos and right-handed *W* gauge bosons in final states with two charged leptons and two jets at $\sqrt{s}$ = 13 TeV with the ATLAS detector. *J High Energy Phys*. (2018) **01**:016. doi: 10.1007/JHEP01(2019)016
504. Sirunyan AM, Tumasyan A, Adam W, Ambrogi F, Asilar E, Bergauer T, et al. Search for a heavy right-handed W boson and a heavy neutrino in events with two same-flavor leptons and two jets at $\sqrt{s} = 13$ TeV. *J High Energy Phys*. (2018) **05**:148. doi: 10.1007/JHEP05(2018)148
505. Sirunyan AM, Tumasyan A, Adam W, Ambrogi F, Asilar E, Bergauer T, et al. Search for heavy neutral leptons in events with three charged leptons in proton-proton collisions at $\sqrt{s} = 13$ TeV. *Phys Rev Lett*. (2018) **120**:221801. doi: 10.1103/PhysRevLett.120.221801
506. Drewes M, Garbrecht B. Combining experimental and cosmological constraints on heavy neutrinos. *Nucl Phys*. (2017) **B921**:250–315. doi: 10.1016/j.nuclphysb.2017.05.001
507. Bergsma F, Dorenbosch J, Allaby JV, Amaldi U, Barbiellini G, Berger C, et al. A Search for Decays of Heavy Neutrinos in the Mass Range 0.5-GeV to 2.8-GeV. *Phys Lett*. (1986) **166B**:473–8. doi: 10.1016/0370-2693(86)91601-1
508. Bernardi G, Carugno G, Chauveau J, Dicarlo F, Dris M, Dumarchez J, et al. FURTHER LIMITS ON HEAVY NEUTRINO COUPLINGS. *Phys Lett*. (1988) **B203**:332–34. doi: 10.1016/0370-2693(88)90563-1
509. Vilain P, Wilquet G, Petrak S, Beyer R, Flegel W, Grote H, et al. Search for heavy isosinglet neutrinos. *Phys Lett*. (1995) **B343**:453–58. doi: 10.1016/0370-2693(94)01422-9
510. Vaitaitis A, Drucker RB, Formaggio J, Adams T, Alton A, Avvakumov S, et al. Search for neutral heavy leptons in a high-energy neutrino beam. *Phys Rev Lett*. (1999) **83**:4943–6. doi: 10.1103/PhysRevLett.83.4943
511. Adriani O, Aguilar-Benitez M, Ahlen S, Alcaraz J, Aloisio A, Alverson G, et al. Search for isosinglet neutral heavy leptons in Z0 decays. *Phys Lett*. (1992) **B295**:371–82.
512. Abreu P, Adam W, Adye T, Azhinenko I, Alekseev GD, Alemany R, et al. Search for neutral heavy leptons produced in Z decays. *Z Phys*. (1997) **C74**:57–71. doi: 10.1007/s002880050370
513. Sirunyan AM, Tumasyan A, Adam W, Ambrogi F, Asilar E, Bergauer T, et al. Search for a W' boson decaying to a τ lepton and a neutrino in proton-proton collisions at $\sqrt{s} = 13$ TeV. *Phys Lett*. (2018) **B792**:107. doi: 10.1016/j.physletb.2019.01.069
514. Aaboud M, Aad G, Abbott B, Abdinov O, Abeloos B, Abidi SH, et al. Search for new high-mass phenomena in the dilepton final state using 36 fb^{-1} of proton-proton collision data at $\sqrt{s} = 13$ TeV with the ATLAS detector. *J High Energy Phys*. (2017) **10**:182. doi: 10.1007/JHEP10(2017)182
515. Collaboration C. Search for a high-mass resonance decaying into a dilepton final state in 13 fb^{-1} of pp collisions at $\sqrt{s} = 13$ TeV. (2016). Available online at: http://cds.cern.ch/record/2205764
516. Aaboud M, Aad G, Abbott B, Abdinov O, Abeloos B, Abidi SH, et al. Search for doubly charged Higgs boson production in multi-lepton final states with the ATLAS detector using proton-proton collisions at $\sqrt{s} = 13$ TeV. *Eur Phys J*. (2018) **C78**:199. doi: 10.1140/EPJC/S10052-018-5661-Z
517. Collaboration C. A search for doubly-charged Higgs boson production in three and four lepton final states at $\sqrt{s} = 13$ TeV. (2017).
518. Aaboud M, Aad G, Abbott B, Abdinov O, Abeloos B, Abhayasinghe DK, et al. Search for doubly charged scalar bosons decaying into same-sign *W* boson pairs with the ATLAS detector. Submitted to: *Eur Phys J*. (2018) **79**:58. doi: 10.1140/epjc/s10052-018-6500-y
519. Aaboud M, Aad G, Abbott B, Abbott DC, Abdinov O, Abeloos B, et al. Search for heavy long-lived multi-charged particles in proton-proton collisions at $\sqrt{s}$ = 13 TeV using the ATLAS detector. (2018) *Phys Rev D*. **99**:052003. doi: 10.1103/PhysRevD.99.052003
520. Abbott LF, Wise MB. The effective hamiltonian for nucleon decay. *Phys Rev*. (1980) **D22**:2208. doi: 10.1103/PhysRevD.22.2208
521. Marciano WJ, Senjanovic G. Predictions of supersymmetric grand unified theories. *Phys Rev*. (1982) **D25**:3092. doi: 10.1103/PhysRevD.25.3092
522. Dimopoulos S, Raby S, Wilczek F. Proton decay in supersymmetric models. *Phys Lett*. (1982) **112B**:133. doi: 10.1016/0370-2693(82)90313-6
523. Nath P, Chamseddine AH, Arnowitt RL. Nucleon Decay in Supergravity Unified Theories. *Phys Rev*. (1985) **D32**:2348–58. doi: 10.1103/PhysRevD.32.2348
524. Arnowitt RL, Chamseddine AH, Nath P. NUCLEON DECAY BRANCHING RATIOS IN SUPERGRAVITY SU(5) GUTS. *Phys Lett*. (1985) **156B**:215–9. doi: 10.1016/0370-2693(85)91512-6
525. Hisano J, Murayama H, Yanagida T. Nucleon decay in the minimal supersymmetric SU(5) grand unification. *Nucl Phys*. (1993) **B402**:46–84. doi: 10.1016/0550-3213(93)90636-4
526. Lucas V, Raby S. Nucleon decay in a realistic SO(10) SUSY GUT. *Phys Rev*. (1997) **D55**:6986–7009. doi: 10.1103/PhysRevD.55.6986
527. Goto T, Nihei T. Effect of RRRR dimension five operator on the proton decay in the minimal SU(5) SUGRA GUT model. *Phys Rev*. (1999) **D59**:115009. doi: 10.1103/PhysRevD.59.115009
528. Murayama H, Pierce A. Not even decoupling can save minimal supersymmetric SU(5). *Phys Rev*. (2002) **D65**:055009. doi: 10.1103/PhysRevD.65.055009
529. Dermisek R, Mafi A, Raby S. SUSY GUTs under siege: proton decay. *Phys Rev*. (2001) **D63**:035001. doi: 10.1103/PhysRevD.63.035001
530. Bajc B, Fileviez Perez P, Senjanovic G. Proton decay in minimal supersymmetric SU(5). *Phys Rev*. (2002) **D66**:075005. doi: 10.1103/PhysRevD.66.075005
531. Bajc B, Fileviez Perez P, Senjanovic G. Minimal supersymmetric SU(5) theory and proton decay: where do we stand? In: *Beyond the Desert: Accelerator, Non-accelerator and Space Approaches Into the Next Millennium. Proceedings, 3rd International Conference on particle physics beyond the standard model, Oulu, Finland, June 2-7, 2002*), Oulu (2002). p. 131–9.
532. Emmanuel-Costa D, Wiesenfeldt S. Proton decay in a consistent supersymmetric SU(5) GUT model. *Nucl Phys*. (2003) **B661**:62–82. doi: 10.1016/S0550-3213(03)00301-8
533. Dorsner I, Fileviez Perez P. How long could we live? *Phys Lett*. (2005) **B625**:88–95. doi: 10.1016/j.physletb.2005.08.039
534. Fileviez Perez P. Fermion mixings versus d = 6 proton decay. *Phys Lett*. (2004) **B595**:476–83. doi: 10.1016/j.physletb.2004.06.061
535. Nath P, Fileviez Perez P. Proton stability in grand unified theories, in strings and in branes. *Phys Rept*. (2007) **441**:191–317. doi: 10.1016/j.physrep.2007.02.010
536. Abe K, Hayato Y, Iyogi K, Kameda J, Miura M, Moriyama S, et al. Search for proton decay via $p \to \nu\nu K^+$ using 260 kiloton year data of Super-Kamiokande. *Phys Rev*. (2014) **D90**:072005. doi: 10.1103/PhysRevD.90.072005
537. Sussman S, Abe K, Bronner C, Hayato Y, Ikeda M, Iyogi K, et al. Dinucleon and nucleon decay to two-body final states with no hadrons in super-kamiokande. *arXiv:1811.12430* (2018).
538. Abe K, Abe K, Aihara H, Aimi A, Akutsu R, Andreopoulos C, et al. Hyper-kamiokande design report. *arXiv:1805.04163* (2018).
539. Acciarri R, Acero MA, Adamowski M, Adams C, Adamson P, Adhikari S, et al. Long-baseline neutrino facility (LBNF) and deep underground neutrino experiment (DUNE). *arXiv:1512.06148* (2015).
540. Kolešová H, Malinský M. Flavour structure of GUTs and uncertainties in proton lifetime estimates. (2016) *Phys Rev*. **D99**:035005. doi: 10.1103/PhysRevD.99.035005
541. Leurer M. A Comprehensive study of leptoquark bounds. *Phys Rev*. (1994) **D49**:333–42. doi: 10.1103/PhysRevD.49.333
542. Di Luzio L, Kirk M, Lenz A. Updated B_s-mixing constraints on new physics models for $b \to s\ell^+\ell^-$ anomalies. *Phys Rev*. (2018) **D97**:095035. doi: 10.1103/PhysRevD.97.095035
543. Lees JP, Poireau V, Tisserand V, Wu SL, Grauges E, Palano A, et al. Measurement of an excess of $\overline{B} \to D^{(*)}\tau^-\overline{\nu}_\tau$ decays and implications for charged higgs bosons. *Phys Rev*. (2013) **D88**:072012. doi: 10.1103/PhysRevD.88.072012

544. Hirose S, Iijima T, Adachi I, Adamczyk K, Aihara H, Said SA, et al. Measurement of the τ lepton polarization and $R(D^*)$ in the decay $\overline{B} \to D^*\tau^-\overline{\nu}_\tau$. *Phys Rev Lett*. (2017) **118**:211801. doi: 10.1103/PhysRevLett.118.211801
545. Bailey JA, Bazavov A, Bernard C, Bouchard CM, DeTar C, Du D, et al. B→Dℓv form factors at nonzero recoil and $|V_{cb}|$ from 2+1-flavor lattice QCD. *Phys Rev*. (2015) **D92**:034506. doi: 10.1103/PhysRevD.92.034506
546. Fajfer S, Kamenik JF, Nisandzic I. On the $B \to D^*\tau\overline{\nu}_\tau$ Sensitivity to New Physics. *Phys Rev*. (2012) **D85**:094025. doi: 10.1103/PhysRevD.85.094025
547. Bernlochner FU, Ligeti Z, Papucci M, Robinson DJ. Combined analysis of semileptonic B decays to D and D^*: $R(D^{(*)})$, $|V_{cb}|$, and new physics. *Phys Rev*. (2017) **D95**:115008. doi: 10.1103/PhysRevD.95.115008
548. Bigi D, Gambino P, Schacht S. A fresh look at the determination of $|V_{cb}|$ from $B \to D^*\ell\nu$. *Phys Lett*. (2017) **B769**:441–5. doi: 10.1016/j.physletb.2017.04.022
549. Amhis Y, Banerjee S, Ben-Haim E, Bernlochner F, Bozek A, Bozzi C, et al. Averages of b-hadron, c-hadron, and τ-lepton properties as of summer 2016. *Eur Phys J*. (2016) **C77**:895. doi: 10.1140/epjc/s10052-017-5058-4
550. Aaij R, Adeva B, Adinolfi M, Ajaltouni Z, Akar S, Albrecht J, et al. Test of lepton universality with $B^0 \to K^{*0}\ell^+\ell^-$ decays. *J High Energy Phys*. (2017) **08**:055. doi: 10.1007/JHEP08(2017)055
551. Hiller G, Kruger F. More model-independent analysis of $b \to s$ processes. *Phys Rev*. (2004) **D69**:074020. doi: 10.1103/PhysRevD.69.074020
552. Bordone M, Isidori G, Pattori A. On the Standard Model predictions for R_K and R_{K^*}. *Eur Phys J*. (2016) **C76**:440. doi: 10.1140/epjc/s10052-016-4274-7
553. D'Amico G, Nardecchia M, Panci P, Sannino F, Strumia A, Torre R, et al. Flavour anomalies after the R_{K^*} measurement. *J High Energy Phys*. (2017) **09**:010. doi: 10.1007/JHEP09(2017)010
554. Capdevila B, Crivellin A, Descotes-Genon S, Matias J, Virto J. Patterns of New Physics in $b \to s\ell^+\ell^-$ transitions in the light of recent data. *J High Energy Phys*. (2018) **01**:093. doi: 10.1007/JHEP01(2018)093
555. Bhattacharya B, Datta A, London D, Shivashankara S. Simultaneous Explanation of the R_K and $R(D^{(*)})$ Puzzles. *Phys Lett*. 2015) **B742**:370–4. doi: 10.1016/j.physletb.2015.02.011
556. Freytsis M, Ligeti Z, Ruderman JT. Flavor models for $\overline{B} \to D^{(*)}\tau\overline{\nu}$. *Phys Rev*. (2015) **D92**:054018. doi: 10.1103/PhysRevD.92.054018
557. Buttazzo D, Greljo A, Isidori G, Marzocca D. B-physics anomalies: a guide to combined explanations. *J High Energy Phys*. (2017) **11**:044. doi: 10.1007/JHEP11(2017)044
558. Angelescu A, Becirevic D, Faroughy DA, Sumensari O. Closing the window on single leptoquark solutions to the B-physics anomalies. *J High Energy Phys*. (2018) **10**:183. doi: 10.1007/JHEP10(2018)183
559. Bauer M, Neubert M. Minimal Leptoquark Explanation for the $R_{D^{(*)}}$, R_K, and $(g-2)_g$ Anomalies. *Phys Rev Lett*. (2016) **116**:141802. doi: 10.1103/PhysRevLett.116.141802
560. Becirevic D, Sumensari O. A leptoquark model to accommodate $R_K^{\rm exp} < R_K^{\rm SM}$ and $R_{K^*}^{\rm exp} < R_{K^*}^{\rm SM}$. *J High Energy Phys*. (2017) **08**:104. doi: 10.1007/JHEP08(2017)104
561. Becirevic D, Fajfer S, Košnik N, Sumensari O. Leptoquark model to explain the B-physics anomalies, R_K and R_D. *Phys Rev*. (2016) **D94**:115021. doi: 10.1103/PhysRevD.94.115021
562. Becirevic D, Košnik N, Sumensari O, Zukanovich Funchal R. Palatable Leptoquark Scenarios for Lepton Flavor Violation in Exclusive $b \to s\ell_1\ell_2$ modes. *J High Energy Phys*. (2016) **11**:035. doi: 10.1007/JHEP11(2016)035
563. Chen CH, Nomura T, Okada H. Excesses of muon $g-2$, $R_{D^{(*)}}$, and R_K in a leptoquark model. *Phys Lett*. (2017) **B774**:456–64. doi: 10.1016/j.physletb.2017.10.005
564. de Medeiros Varzielas I, King SF. $R_{K^{(*)}}$ with leptoquarks and the origin of Yukawa couplings. *J High Energy Phys*. (2018) **11**:100. doi: 10.1007/JHEP11(2018)100
565. Camargo-Molina JE, Celis A, Faroughy DA. Anomalies in Bottom from new physics in Top. *Phys Lett*. (2018) **B784**:284–93. doi: 10.1016/j.physletb.2018.07.051
566. Crivellin A, Müller D, Ota T. Simultaneous explanation of $R(D^{(*)})$ and $b\to s\mu^+\mu^-$: the last scalar leptoquarks standing. *J High Energy Phys*. (2017) **09**:040. doi: 10.1007/JHEP09(2017)040
567. Cox P, Kusenko A, Sumensari O, Yanagida TT. SU(5) Unification with TeV-scale Leptoquarks. *J High Energy Phys*. (2017) **03**:035. doi: 10.1007/JHEP03(2017)035
568. Doršner I, Fajfer S, Faroughy DA, Košnik N. The role of the S_3 GUT leptoquark in flavor universality and collider searches. *J High Energy Phys*. (2017) **10**:188. doi: 10.1007/JHEP10(2017)188
569. Becirevic D, Doršner I, Fajfer S, Košnik N, Faroughy DA, Sumensari O. Scalar leptoquarks from grand unified theories to accommodate the B-physics anomalies. *Phys Rev*. (2018) **D98**:055003. doi: 10.1103/PhysRevD.98.055003
570. Das D, Hati C, Kumar G, Mahajan N. Towards a unified explanation of $R_{D^{(*)}}$, R_K and $(g-2)_\mu$ anomalies in a left-right model with leptoquarks. *Phys Rev*. (2016) **D94**:055034. doi: 10.1103/PhysRevD.94.055034
571. Heeck J, Teresi D. Pati-Salam explanations of the B-meson anomalies. (2018). doi: 10.1007/JHEP12(2018)103
572. Aydemir U, Minic D, Sun C, Takeuchi T. B-decay anomalies and scalar leptoquarks in unified Pati-Salam models from noncommutative geometry. *J High Energy Phys*. (2018) **09**:117. doi: 10.1007/JHEP09(2018)117
573. Aydemir U, Mandal T, Mitra S. A single TeV-scale scalar leptoquark in **SO**(**10**) grand unification and **B**-decay anomalies. (2019).
574. Faber T, Hudec M, Malinský M, Meinzinger P, Porod W, Staub F. A unified leptoquark model confronted with lepton non-universality in B-meson decays. *Phys Lett*. (2018) **B787**:159–66. doi: 10.1016/j.physletb.2018.10.051
575. Sahoo S, Mohanta R, Giri AK. Explaining the R_K and $R_{D^{(*)}}$ anomalies with vector leptoquarks. *Phys Rev*. (2017) **D95**:035027. doi: 10.1103/PhysRevD.95.035027
576. Crivellin A, Greub C, Saturnino F, Müller D. Importance of loop effects in explaining the accumulated evidence for New Physics in B Decays with a Vector Leptoquark. *Phys Rev Lett*. (2018) **122**:011805. doi: 10.1103/PhysRevLett.122.011805
577. Sahoo S, Mohanta R. Impact of vector leptoquark on $\overline{B} \to \overline{K}^* l^+ l^-$ anomalies. *J Phys*. (2018) **G45**:085003. doi: 10.1088/1361-6471/aaca12
578. Assad N, Fornal B, Grinstein B. Baryon number and lepton universality violation in leptoquark and diquark models. *Phys Lett*. (2018) **B777**:324–31. doi: 10.1016/j.physletb.2017.12.042
579. Calibbi L, Crivellin A, Li T. Model of vector leptoquarks in view of the B-physics anomalies. *Phys Rev*. (2018) **D98**:115002. doi: 10.1103/PhysRevD.98.115002
580. Di Luzio L, Greljo A, Nardecchia M. Gauge leptoquark as the origin of B-physics anomalies. *Phys Rev*. (2017) **D96**:115011. doi: 10.1103/PhysRevD.96.115011
581. Di Luzio L, Fuentes-Martin J, Greljo A, Nardecchia M, Renner S. Maximal Flavour Violation: a Cabibbo mechanism for leptoquarks. *J High Energy Phys*. (2018) **11**:081. doi: 10.1007/JHEP11(2018)081
582. Greljo A, Stefanek BA. Third family quark-lepton unification at the TeV scale. *Phys Lett*. (2018) **B782**:131–8. doi: 10.1016/j.physletb.2018.05.033
583. Bordone M, Cornella C, Fuentes-Martín J, Isidori G. Low-energy signatures of the PS^3 model: from B-physics anomalies to LFV. *J High Energy Phys*. (2018) **10**:148. doi: 10.1007/JHEP10(2018)148
584. Bordone M, Cornella C, Fuentes-Martin J, Isidori G. A three-site gauge model for flavor hierarchies and flavor anomalies. *Phys Lett*. (2018) **B779**:317–23. doi: 10.1016/j.physletb.2018.02.011
585. Faroughy DA, Greljo A, Kamenik JF. Confronting lepton flavor universality violation in B decays with high-p_T tau lepton searches at LHC. *Phys Lett*. (2017) **B764**:126–34. doi: 10.1016/j.physletb.2016.11.011
586. Greljo A, Marzocca D. High-p_T dilepton tails and flavor physics. *Eur Phys J*. (2017) **C77**:548. doi: 10.1140/epjc/s10052-017-5119-8
587. Schmaltz M, Zhong YM. The leptoquark Hunter's guide: large coupling. *J High Energy Phys*. (2018). doi: 10.1007/JHEP01(2019)132
588. Mandal T, Mitra S, Raz S. $R_{D^{(*)}}$ in minimal leptoquark scenarios: impact of interference on the exclusion limits from LHC data. *Phys Rev D*. (2018) **99**:055028. doi: 10.1103/PhysRevD.99.055028
589. Greljo A, Martin Camalich J, Ruiz-Álvarez JD. The mono-tau menace: from B decays to high-p_T Tails. *Phys Rev Lett*. (2018) **122**:131803. doi: 10.1103/PhysRevLett.122.131803

590. Bansal S, Capdevilla RM, Delgado A, Kolda C, Martin A, Raj N. Hunting leptoquarks in monolepton searches. *Phys Rev D*. (2018) **98**:015037. doi: 10.1103/PhysRevD.98.015037
591. Vignaroli N. Seeking LQs in the $t\bar{t}$ plus missing energy channel at the high-luminosity LHC. *Phys Rev D*. (2018) **99**:035021. doi: 10.1103/PhysRevD.99.035021
592. Glashow SL, Iliopoulos J, Maiani L. Weak interactions with lepton-hadron symmetry. *Phys Rev*. (1970) **D2**:1285–92. doi: 10.1103/PhysRevD.2.1285
593. Petcov ST. The Processes mu –> e Gamma, mu –> e e anti-e, Neutrino' –> Neutrino gamma in the Weinberg-Salam Model with Neutrino Mixing. *Sov J Nucl Phys*. (1977) **25**:340.
594. Cheng TP, Li LF. Nonconservation of separate mu - lepton and e - lepton numbers in gauge theories with v+a currents. *Phys Rev Lett*. (1977) **38**:381. doi: 10.1103/PhysRevLett.38.381
595. Bilenky SM, Petcov ST, Pontecorvo B. Lepton Mixing, mu –> e + gamma Decay and Neutrino Oscillations. *Phys Lett*. (1977) **67B**:309. doi: 10.1016/0370-2693(77)90379-3
596. Kuno Y, Okada Y. Muon decay and physics beyond the standard model. *Rev Mod Phys*. (2001) **73**:151–202. doi: 10.1103/RevModPhys.73.151
597. Abada A, Krauss ME, Porod W, Staub F, Vicente A, Weiland C. Lepton flavor violation in low-scale seesaw models: SUSY and non-SUSY contributions. *J High Energy Phys*. (2014) **11**:048. doi: 10.1007/JHEP11(2014)048
598. Bernabeu J, Santamaria A, Vidal J, Mendez A, Valle JWF. Lepton Flavor Nonconservation at High-Energies in a Superstring Inspired Standard Model. *Phys Lett*. (1987) **B187**:303–8. doi: 10.1016/0370-2693(87)91100-2
599. Ilakovac A, Pilaftsis A. Flavor violating charged lepton decays in seesaw-type models. *Nucl Phys*. (1995) **B437**:491. doi: 10.1016/0550-3213(94)00567-X
600. Deppisch F, Kosmas TS, Valle JWF. Enhanced mu- - e- conversion in nuclei in the inverse seesaw model. *Nucl Phys*. (2006) **B752**:80–92. doi: 10.1016/j.nuclphysb.2006.06.032
601. Alonso R, Dhen M, Gavela MB, Hambye T. Muon conversion to electron in nuclei in type-I seesaw models. *J High Energy Phys*. (2013) **01**:118. doi: 10.1007/JHEP01(2013)118
602. Barry J, Rodejohann W. Lepton number and flavour violation in TeV-scale left-right symmetric theories with large left-right mixing. *J High Energy Phys*. (2013) **09**:153. doi: 10.1007/JHEP09(2013)153
603. Vicente A. Lepton flavor violation beyond the MSSM. *Adv High Energy Phys*. (2015) **2015**:686572. doi: 10.1155/2015/686572
604. Grinstein B, Cirigliano V, Isidori G, Wise MB. Grand Unification and the Principle of Minimal Flavor Violation. *Nucl Phys*. (2007) **B763**:35–48. doi: 10.1016/j.nuclphysb.2006.11.005
605. Ciuchini M, Masiero A, Paradisi P, Silvestrini L, Vempati SK, Vives O. Soft SUSY breaking grand unification: Leptons versus quarks on the flavor playground. *Nucl Phys*. (2007) **B783**:112–42. doi: 10.1016/j.nuclphysb.2007.05.032
606. Hisano J, Moroi T, Tobe K, Yamaguchi M. Lepton flavor violation via right-handed neutrino Yukawa couplings in supersymmetric standard model. *Phys Rev*. (1996) **D53**:2442–59. doi: 10.1103/PhysRevD.53.2442
607. Arganda E, Herrero MJ. Testing supersymmetry with lepton flavor violating tau and mu decays. *Phys Rev*. (2006) **D73**:055003. doi: 10.1103/PhysRevD.73.055003
608. Hirsch M, Joaquim FR, Vicente A. Constrained SUSY seesaws with a 125 GeV Higgs. *J High Energy Phys*. (2012) **11**:105. doi: 10.1007/JHEP11(2012)105
609. Rossi A. Supersymmetric seesaw without singlet neutrinos: Neutrino masses and lepton flavor violation. *Phys Rev*. (2002) **D66**:075003. doi: 10.1103/PhysRevD.66.075003
610. Deppisch F, Valle JWF. Enhanced lepton flavor violation in the supersymmetric inverse seesaw model. *Phys Rev*. (2005) **D72**:036001. doi: 10.1103/PhysRevD.72.036001
611. Hirsch M, Valle JWF, Porod W, Romao JC, Villanova del Moral A. Probing minimal supergravity in type I seesaw with lepton flavour violation at the LHC. *Phys Rev*. (2008) **D78**:013006. doi: 10.1103/PhysRevD.78.013006
612. Esteves JN, Romao JC, Hirsch M, Staub F, Porod W. Supersymmetric type-III seesaw: lepton flavour violating decays and dark matter. *Phys Rev*. (2011) **D83**:013003. doi: 10.1103/PhysRevD.83.013003
613. Dreiner HK, Kramer M, O'Leary B. Bounds on R-parity violating supersymmetric couplings from leptonic and semi-leptonic meson decays. *Phys Rev*. (2007) **D75**:114016. doi: 10.1103/PhysRevD.75.114016
614. de Gouvea A, Lola S, Tobe K. Lepton flavor violation in supersymmetric models with trilinear R-parity violation. *Phys Rev*. (2001) **D63**:035004. doi: 10.1103/PhysRevD.63.035004
615. Arhrib A, Cheng Y, Kong OCW. Comprehensive analysis on lepton flavor violating Higgs boson to $\mu^{\mp}\tau^{\pm}$ decay in supersymmetry without *R* parity. *Phys Rev*. (2013) **D87**:015025. doi: 10.1103/PhysRevD.87.015025
616. Romao JC, Rius N, Valle JWF. Supersymmetric signals in muon and τ decays. Nucl Phys. 1991) **B363**:369–84. doi: 10.1016/0550-3213(91)80025-H
617. Hirsch M, Vicente A, Meyer J, Porod W. Majoron emission in muon and tau decays revisited. *Phys Rev*. (2009) **D79**:055023. doi: 10.1103/PhysRevD.79.079901
618. Raidal M, van der Schaaf A, Bigi I, Mangano ML, Semertzidis Y, Abel S, et al. Flavour physics of leptons and dipole moments. *Eur Phys J*. (2008) **C57**:13–182. doi: 10.1140/epjc/s10052-008-0715-2
619. Abada A, Toma T. Electric dipole moments of charged Leptons with sterile fermions. *J High Energy Phys*. (2016) **02**:174. doi: 10.1007/JHEP02(2016)174
620. Dimopoulos S, Hall LJ. Electric dipole moments as a test of supersymmetric unification. *Phys Lett*. (1995) **B344**:185–92. doi: 10.1016/0370-2693(94)01572-T
621. Romanino A, Strumia A. Electron and muon electric dipoles in supersymmetric scenarios. *Nucl Phys*. (2002) **B622**:73–94. doi: 10.1016/S0550-3213(01)00607-1
622. Jung M, Pich A. Electric dipole moments in two-higgs-doublet models. *J High Energy Phys*. (2014) **04**:076. doi: 10.1007/JHEP04(2014)076
623. Stockinger D. The muon magnetic moment and supersymmetry. *J Phys*. (2007) **G34**:R45–92. doi: 10.1088/0954-3899/34/2/R01
624. Dekens W, De Vries J, Jung M, Vos KK. The phenomenology of electric dipole moments in models of scalar leptoquarks. *J High Energy Phys*. (2018) **01**:069. doi: 10.1007/JHEP01(2019)069
625. Fuyuto K, Ramsey-Musolf M, Shen T. Electric dipole moments from CP-Violating scalar leptoquark interactions. *Phys Lett*. (2019) **B788**:52–7. doi: 10.1016/j.physletb.2018.11.016
626. Baldini AM, Bao Y, Baracchini E, Bemporad C, Berg F, Biasotti M, et al. Search for the lepton flavour violating decay $\mu^+ \rightarrow e^+\gamma$ with the full dataset of the MEG experiment. *Eur Phys J*. (2016) **C76**:434. doi: 10.1140/epjc/s10052-016-4271-x
627. Aubert B, Karyotakis Y, Lees JP, Poireau V, Prencipe E, Prudent X, et al. Searches for Lepton Flavor Violation in the Decays $\tau^{+-} \rightarrow e^{+-}gamma$ and $\tau^{+-} \rightarrow \mu^{+-}gamma$. *Phys Rev Lett*. (2010) **104**:021802. doi: 10.1103/PhysRevLett.104.021802
628. Hayasaka K, Abe K, Adachi I, Anipko HAD, Arinstein K, et al. New Search for tau $->$ mu gamma and tau $->$ e gamma Decays at Belle. *Phys Lett*. (2008) **B666**:16–22. doi: 10.1016/j.physletb.2008.06.056
629. Bellgardt U, Otter G, Eichler R, Felawka L, Niebuhr C, Walter HK, et al. Search for the Decay mu+ $---->$ e+ e+ e-. *Nucl Phys*. (1988) **B299**:1–6. doi: 10.1016/0550-3213(88)90462-2
630. Lees JP, Poireau V, Prencipe E, Tisserand V, Tico JG, Grauges E, et al. Limits on tau Lepton-Flavor Violating Decays in three charged leptons. *Phys Rev*. (2010) **D81**:111101. doi: 10.1103/PhysRevD.81.111101
631. Hayasaka K, Inami K, Miyazaki Y, Arinstein K, Aulchenko V, Aushev T, et al. Search for Lepton Flavor Violating Tau Decays into Three Leptons with 719 Million Produced Tau+Tau- Pairs. *Phys Lett*. (2010) **B687**:139–43. doi: 10.1016/j.physletb.2010.03.037
632. Aad G, Abbott B, Abdallah J, Abdinov O, Aben R, Abolins M, et al. Probing lepton flavour violation via neutrinoless $\tau \longrightarrow 3\mu$ decays with the ATLAS detector. *Eur Phys J*. (2016) **C76**:232. doi: 10.1140/epjc/s10052-016-4041-9
633. Aaij R, Beteta CA, Adeva B, Adinolfi M, Affolder A, Ajaltouni Z, et al. Search for the lepton flavour violating decay $\tau^- \rightarrow \mu^-\mu^+\mu^-$. *J High Energy Phys*. (2015) **02**:121. doi: 10.1007/JHEP02(2015)121
634. Kaulard J, Dohmen C, Haan H, Honecker W, Junker D, Otter G, et al. Improved limit on the branching ratio of $\mu -> e+$ conversion on titanium. *Phys Lett*. (1998) **B422**:334–8. doi: 10.1016/S0370-2693(97)01423-8

635. Honecker W, Dohmen C, Haan H, Junker D, Otter G, Starlinger M, et al. Improved limit on the branching ratio of μ → e conversion on lead. *Phys Rev Lett*. (1996) **76**:200–3. doi: 10.1103/PhysRevLett.76.200
636. Bertl WH, Rosenbaum F, Ryskulov NM, Engfer R, Hermes EA, Kurz G, et al. A Search for muon to electron conversion in muonic gold. *Eur Phys J*. (2006) **C47**:337–46. doi: 10.1140/epjc/s2006-02582-x
637. Andreev V, Ang DG, DeMille D, Doyle JM, Gabrielse G, Haefner J, et al. Improved limit on the electric dipole moment of the electron. *Nature*. (2018) **562**:355–60. doi: 10.1038/s41586-018-0599-8
638. Bennett GW, Bousquet B, Brown HN, Bunce G, Carey RM, Cushman P, et al. An Improved Limit on the Muon Electric Dipole Moment. *Phys Rev*. (2009) **D80**:052008. doi: 10.1103/PhysRevD.80.052008
639. Inami K, Abe K, Abe R, Abe T, Adachi I, Aihara H, et al. Search for the electric dipole moment of the tau lepton. *Phys Lett*. (2003) **B551**:16–26. doi: 10.1016/S0370-2693(02)02984-2
640. Hanneke D, Fogwell S, Gabrielse G. New measurement of the electron magnetic moment and the fine structure constant. *Phys Rev Lett*. 2008) **100**:120801. doi: 10.1103/PhysRevLett.100.120801
641. Bennett GW, Bousquet B, Brown HN, Bunce G, Carey RM, Cushman P, et al. Final report of the muon E821 anomalous magnetic moment measurement at BNL. *Phys Rev*. (2006) **D73**:072003. doi: 10.1103/PhysRevD.73.072003
642. Blondel A, Bravar A, Pohl M, Bachmann S, Berger N, Kiehn M, et al. Research proposal for an experiment to search for the decay $\mu \rightarrow eee$. *arXiv:1301.6113* (2013).
643. Kurup A. The cOherent muon to electron transition (COMET) experiment. *Nucl Phys Proc Suppl*. (2011) **218**:38–43. doi: 10.1016/j.nuclphysbps.2011.06.008
644. Kutschke RK. The Mu2e Experiment at Fermilab. In: *Proceedings, 31st International Conference on Physics in collisions (PIC 2011)*. Vancouver, BC. (2011). Available online at: http://lss.fnal.gov/archive/2011/conf/fermilab-conf-11-887-cd.pdf.
645. Chapelain A. The Muon g-2 experiment at Fermilab. *EPJ Web Conf*. (2017) **137**:08001. doi: 10.1051/epjconf/201713708001
646. Furry WH. On transition probabilities in double beta-disintegration. *Phys Rev*. (1939) **56**:1184–93. doi: 10.1103/PhysRev.56.1184
647. Agostini M, Allardt M, Bakalyarov AM, Balata M, Barabanov I, Baudis L, et al. Background-free search for neutrinoless double-β decay of ^{76}Ge with GERDA. *Nature*. (2017) **544**:47. doi: 10.1038/nature21717
648. Gando A, Gando Y, Hachiya T, Hayashi A, Hayashida S, Ikeda H, et al. Search for majorana neutrinos near the inverted mass hierarchy region with kamLAND-zen. *Phys Rev Lett*. (2016) **117**:082503. doi: 10.1103/PhysRevLett.117.082503
649. Schechter J, Valle JWF. Neutrinoless double beta decay in SU(2) x U(1) theories. *Phys Rev*. (1982) **D25**:2951. doi: 10.1103/PhysRevD.25.2951
650. Nieves JF. Dirac and pseudodirac neutrinos and neutrinoless double beta decay. *Phys Lett*. (1984) **147B**:375–9. doi: 10.1016/0370-2693(84)90136-9
651. Takasugi E. Can the neutrinoless double beta decay take place in the case of dirac neutrinos? *Phys Lett*. (1984) **149B**:372–6. doi: 10.1016/0370-2693(84)90426-X
652. Pas H, Hirsch M, Klapdor-Kleingrothaus HV, Kovalenko SG. Towards a superformula for neutrinoless double beta decay. *Phys Lett*. (1999) **B453**:194–8. doi: 10.1016/S0370-2693(99)00330-5
653. Pas H, Hirsch M, Klapdor-Kleingrothaus HV, Kovalenko SG. A Superformula for neutrinoless double beta decay. 2. The Short range part. *Phys Lett*. (2001) **B498**:35–9. doi: 10.1016/S0370-2693(00)01359-9
654. Deppisch FF, Graf L, Harz J, Huang WC. Neutrinoless double beta decay and the baryon asymmetry of the universe. *Phys Rev*. (2018) **D98**:055029. doi: 10.1103/PhysRevD.98.055029
655. Cirigliano V, Dekens W, de Vries J, Graesser ML, Mereghetti E. A neutrinoless double beta decay master formula from effective field theory. *J High Energy Phys*. (2018) **12**:097. doi: 10.1007/JHEP12(2018)097
656. Graf L, Deppisch FF, Iachello F, Kotila J. Short-range neutrinoless double beta decay mechanisms. *Phys Rev*. (2018) **D98**:095023. doi: 10.1103/PhysRevD.98.095023
657. Deppisch FF, Hirsch M, Pas H. Neutrinoless double beta decay and physics beyond the standard model. *J Phys*. (2012) **G39**:124007. doi: 10.1088/0954-3899/39/12/124007
658. Hirsch M, Klapdor-Kleingrothaus HV, Kovalenko SG. New low-energy leptoquark interactions. *Phys Lett*. (1996) **B378**:17–22. doi: 10.1016/0370-2693(96)00419-4
659. Hirsch M, Klapdor-Kleingrothaus HV, Kovalenko SG. New leptoquark mechanism of neutrinoless double beta decay. *Phys Rev*. (1996) **D54**:R4207–10. doi: 10.1103/PhysRevD.54.R4207
660. Mohapatra RN. New contributions to neutrinoless double beta decay in supersymmetric theories. *Phys Rev*. (1986) **D34**:3457–61. doi: 10.1103/PhysRevD.34.3457
661. Hirsch M, Klapdor-Kleingrothaus HV, Kovalenko SG. New constraints on R-parity broken supersymmetry from neutrinoless double beta decay. *Phys Rev Lett*. (1995) **75**:17–20. doi: 10.1103/PhysRevLett.75.17
662. Hirsch M, Klapdor-Kleingrothaus HV, Kovalenko SG. Supersymmetry and neutrinoless double beta decay. *Phys Rev*. (1996) **D53**:1329–1348. doi: 10.1103/PhysRevD.53.1329
663. Hirsch M, Klapdor-Kleingrothaus HV, Kovalenko SG. On the SUSY accompanied neutrino exchange mechanism of neutrinoless double beta decay. *Phys Lett*. (1996) **B372**:181–6. doi: 10.1016/0370-2693(96)00050-0
664. Pas H, Hirsch M, Klapdor-Kleingrothaus HV. Improved bounds on SUSY accompanied neutrinoless double beta decay. *Phys Lett*. (1999) **B459**:450–4. doi: 10.1016/S0370-2693(99)00711-X

Conflict of Interest Statement: The authors declare that the research was conducted in the absence of any commercial or financial relationships that could be construed as a potential conflict of interest.

frontiers in Physics

MINI REVIEW
published: 25 June 2019
doi: 10.3389/fphy.2019.00090

Decoding the Nature of Dark Matter at Current and Future Experiments

Alexander Belyaev [1,2]*

[1] School of Physics and Astronomy, University of Southampton, Southampton, United Kingdom, [2] Rutherford Appleton Laboratory, Particle Physics Department, Didcot, United Kingdom

Determination of the nature of Dark Matter (DM) is one of the most fundamental problems of particle physics and cosmology. If DM is light enough and interacts with Standard Model particles directly or via some mediators with a strength beyond the gravitational one, it can be probed at particle accelerators or in complementary direct and indirect DM searches in non-collider experiments. In the absence of such signals at present we can prepare ourselves for its discovery and identification. Generic signature from DM produced in particles collisions is missing transverse energy, MET, originating from DM particles escaping detector. Using effective field theory approach one can show that, depending on the structure and DM spin, effective operators have different MET distributions. This provides potential to distinguish certain classes of effective field theory (EFT) operators and related spin of DM at the LHC. This observation can be directly applied to theories beyond EFT paradigm as we demonstrate for Supersymmetry and inert two Higgs doublet model (i2HDM) as two examples. At the same time direct and indirect DM searches strongly complement collider searches for DM with large masses and pointing that collider and non-collider DM searches have unique power to probe the nature of Dark Matter. We also highlight prospects of new collider signature from DM such as disappearing charge tracks which are characteristic for wide class of DM theories. Finally, we advocate the importance of the joint framework which would join efforts of HEP community and allow to effectively identify the underlying theory of DM.

Keywords: dark matter, large hadron collider, DM direct detection, DM indirect detection, BSM

OPEN ACCESS

Edited by:
António Pestana Morais,
University of Aveiro, Portugal

Reviewed by:
Zhenbin Wu,
University of Illinois at Chicago, United States
Bhupal Dev,
Washington University in St. Louis, United States
Narendra Sahu,
Indian Institute of Technology Hyderabad, India

***Correspondence:**
Alexander Belyaev
a.belyaev@soton.ac.uk

Specialty section:
This article was submitted to High-Energy and Astroparticle Physics, a section of the journal Frontiers in Physics

Received: *20 December 2018*
Accepted: *03 June 2019*
Published: *25 June 2019*

Citation:
Belyaev A (2019) Decoding the Nature of Dark Matter at Current and Future Experiments. Front. Phys. 7:90. doi: 10.3389/fphy.2019.00090

1. INTRODUCTION

Understanding the nature of Dark Matter (DM) is one of the greatest puzzles of modern particle physics and cosmology. Although overwhelming observational evidences from galactic to cosmological scales point to the existence of DM [1–3], after decades of experimental effort only its gravitational interaction has been experimentally confirmed. Currently, no information is available on the DM properties, such as its spin, mass, interactions other than gravitational, symmetry responsible for its stability, number of states associated to it, and possible particles that would mediate the interactions between DM and the standard model (SM) particles.

If DM is light enough and interacts with SM particles directly or via some mediators with a strength beyond the gravitational one, its elusive nature can be detected or constrained in different ways: (a) from direct production at colliders, resulting in a signature exhibiting an observed SM object, such as jet, Higgs, Z, W, photon, or top-quark(s) that recoils against the missing energy from the DM pair [4–8]; (b) via the relic density constraint obtained through the observations

of cosmic microwave background (CMB) anisotropies, such as those of WMAP and PLANCK collaborations [1, 9, 10]; (c) from DM direct detection (DD) experiments, which are sensitive to elastic spin independent (SI) or spin dependent (SD) DM scattering off nuclei [11–14]; (d) from DM indirect detection searches, that look for SM particles produced in the decay or annihilation of DM present in the cosmos, both with high energy observables (gamma-rays, neutrinos, charge cosmic rays) produced in the local Universe [15–20], and by studying the effects of energy produced by DM annihilation in the early universe on the properties of the CMB spectrum [1, 21, 22].

It is clear that decoding the nature of DM requires the respective signal at least in one of the search experiments. We do not have one yet. However, even without having the signal at the moment we can already conclude on what kind of DM models are excluded. Moreover, by exploring different signatures of one particular model, their correlation and interplay we can prepare ourselves to discovery of DM and their identification.

2. CONTACT INTERACTIONS

Let us start our discussion with the three simplest scenarios for the DM particles: complex scalars (ϕ), Dirac fermions (χ), and complex vectors (V_μ) within the effective field theory (EFT) approach. In the EFT approach we parametrize the DM interactions with the SM quarks and gluons with the effective coupling and the scale describing operators of dimension six or five. In **Table 1** we have summarized a minimal set of independent dimension-5 and dimension-6 operators for complex scalar, Dirac fermion, and complex vector DM coupling to quarks and gluons, adopting the widely used notations of Goodman et al. [23], Kumar et al. [24], and Belyaev et al. [25]. Since different operators have different energy behavior and respective different invariant mass distributions: typically softer for majority operators with scalar DM, intermediate for fermion DM and the hardest for vector DM and because of relation of $M_{\rm inv}(DM, DM)$ and $\boldsymbol{E}_{\rm T}^{\rm miss}$ slope one can distinguish several operators and related underlying theories using the shape of the $\boldsymbol{E}_{\rm T}^{\rm miss}$ signal: C1-C2,C5-C6,D9-D10,V1-V2,V3-V4,V5-V6, and V11-12 pairs among each other [25].

Notice the presence of the coupling g_* in the definition of the effective operators, which we insert according to the Naive Dimensional Analysis [26]. Moreover, for the vector DM case we choose the parametrization suggested in Belyaev et al. [25] that takes into account the high energy behavior of the scattering amplitudes that are enhanced by an energy factor $(E/m_{\rm DM})$ for every longitudinal vector DM polarization. These operators are gauge invariant and provides the minimal and simplistic description of underlying theory of DM. The scale Λ is related to the mass of the mediator, while coupling g^* is related to the product of DM and SM couplings to the mediator.

These operators provide monojet-signature, the shapes of $\boldsymbol{E}_{\rm T}^{\rm miss}$ distributions for which is presented in **Figure 1** from Belyaev et al. [25] for DM mass of 10 GeV. One can observe a big difference in $\boldsymbol{E}_{\rm T}^{\rm miss}$ shapes of the groups of the operators, primarily split into groups of operators with scalar, femion and vector DM. The origin of the different $\boldsymbol{E}_{\rm T}^{\rm miss}$ shapes from different operators can be related to a combination of effects. First, for a fixed Lorentz structure of the SM part of the EFT operators, the same invariant mass distribution of the DM pair, $M_{\rm inv}(DM, DM)$, uniquely defines the shape of the $\boldsymbol{E}_{\rm T}^{\rm miss}$ distribution. Moreover, with the increase of $M_{\rm inv}(DM, DM)$, the $\boldsymbol{E}_{\rm T}^{\rm miss}$ shape falls less and less steeply (again, for a given SM component of the EFT operator).

It was found in Belyaev et al. [25] that the reason why the bigger invariant mass of DM is correlated with flatter $\boldsymbol{E}_{\rm T}^{\rm miss}$ behavior is related to phase space and parton density effects: when $M_{\rm inv}(DM, DM)$ is small, the radiation of a high p_T jet will "cost" a *large relative shift in x*, the transferred momentum of the parton, leading to a rapidly falling $\boldsymbol{E}_{\rm T}^{\rm miss}$ distribution; on the contrary, when $M_{\rm inv}(DM, DM)$ is large, the radiation of a high p_T jet will "cost" a *small relative shift in x*, which will lead to a more slowly falling $\boldsymbol{E}_{\rm T}^{\rm miss}$ distribution in comparison to the first case.

Therefore if one theory predicts higher values of the invariant mass of DM-pair, $M(DM, DM)$, than the other theory, one expects the flatter $\boldsymbol{E}_{\rm T}^{\rm miss}$ distribution for the first one. In **Figure 2** we present $M(DM, DM)$ distributions for all EFT operators in **Table 1** where one clearly observes that the mean values of $M(DM, DM)$ distributions for vector DM operators are larger than those for most of fermion DM operators which are in their turn have higher mean value of $M(DM, DM)$ than most of scalar DM operators. Now we can see the connection of $M(DM, DM)$ distributions shape and the slope of the $\boldsymbol{E}_{\rm T}^{\rm miss}$ which was presented in **Figure 1**.

One should stress that non-collider DM searches play an important complementary role in probing DM parameter space. As an example in **Figure 3** (left) we present the non-collider constraints for the operators D2, which exhibit pseudo-scalar interactions of fermion Dirac DM with quarks.

One can see that even for momentum-suppressed operator D2 (because of its pseudo-scalar nature) DM DD constraints from Xenon [28] play an important role which is comparable to collider constraints, presented in **Figure 3** (right). It is important to stress that both LHC and DM DD searches set an upper limit on value of Λ. The LHC limit is of the order of 1 TeV for present LHC data while DM DD searches the limit strongly depend on the operator. For example for non-suppressed operators conserving parity the limit on Λ is about 3 orders of magnitude above the LHC one. On the other hand LHC limit is beyond DM DD searches for operators with suppressed elastic scattering cross sections on the nuclei (C2,C4,C6,D2,D3,D4,D6-10,V2,V4-V10). Moreover, for operators with pseudo-vector currents which have suppressed DM DD rates, one should take into account effect of their running from TeV energy scale at the LHC down to low energy scale at DM DD experiments, due to which an operator acquires non-negligible vector component [29–31].

3. BEYOND EFT

The analysis of $\boldsymbol{E}_{\rm T}^{\rm miss}$ shape presented here can be applied to different scenarios, beyond the EFT approach in general, where the DM mediator is not produced on-the-mass-shell, such as the

TABLE 1 | Minimal basis of dimension 5 and 6 operators for complex scalar DM (ϕ), Dirac fermion DM (χ) or complex vector DM (V^μ) interacting with SM quarks (q) or gluons.

Complex Scalar DM	
$\frac{g_*^2}{\Lambda}\phi^\dagger\phi\bar{q}q$	[C1]
$\frac{g_*^2}{\Lambda}\phi^\dagger\phi\bar{q}i\gamma^5 q$	[C2]
$\frac{g_*^2}{\Lambda^2}\phi^\dagger i\overleftrightarrow{\partial_\mu}\phi\bar{q}\gamma^\mu q$	[C3]
$\frac{g_*^2}{\Lambda^2}\phi^\dagger i\overleftrightarrow{\partial_\mu}\phi\bar{q}\gamma^\mu\gamma^5 q$	[C4]
$\frac{g_*^2}{\Lambda^2}\phi^\dagger\phi G^{\mu\nu}G_{\mu\nu}$	[C5]
$\frac{g_*^2}{\Lambda^2}\phi^\dagger\phi\tilde{G}^{\mu\nu}G_{\mu\nu}$	[C6]
Dirac Fermion DM	
$\frac{g_*^2}{\Lambda^2}\bar{\chi}\chi\bar{q}q$	[D1]
$\frac{g_*^2}{\Lambda^2}\bar{\chi}i\gamma^5\chi\bar{q}q$	[D2]
$\frac{g_*^2}{\Lambda^2}\bar{\chi}\chi\bar{q}i\gamma^5 q$	[D3]
$\frac{g_*^2}{\Lambda^2}\bar{\chi}\gamma^5\chi\bar{q}\gamma^5 q$	[D4]
$\frac{g_*^2}{\Lambda^2}\bar{\chi}\gamma^\mu\chi\bar{q}\gamma_\mu q$	[D5]
$\frac{g_*^2}{\Lambda^2}\bar{\chi}\gamma^\mu\gamma^5\chi\bar{q}\gamma_\mu q$	[D6]
$\frac{g_*^2}{\Lambda^2}\bar{\chi}\gamma^\mu\chi\bar{q}\gamma_\mu\gamma^5 q$	[D7]
$\frac{g_*^2}{\Lambda^2}\bar{\chi}\gamma^\mu\gamma^5\chi\bar{q}\gamma_\mu\gamma^5 q$	[D8]
$\frac{g_*^2}{\Lambda^2}\bar{\chi}\sigma^{\mu\nu}\chi\bar{q}\sigma_{\mu\nu}q$	[D9]
$\frac{g_*^2}{\Lambda^2}\bar{\chi}\sigma^{\mu\nu}i\gamma^5\chi\bar{q}\sigma_{\mu\nu}q$	[D10]

Complex Vector DM	
$\frac{g_*^2 m_{\rm DM}^2}{\Lambda^3}V_\mu^\dagger V^\mu\bar{q}q$	[V1]
$\frac{g_*^2 m_{\rm DM}^2}{\Lambda^3}V_\mu^\dagger V^\mu\bar{q}i\gamma^5 q$	[V2]
$\frac{g_*^2 m_{\rm DM}^2}{2\Lambda^4}i(V_\nu^\dagger\partial_\mu V^\nu - V^\nu\partial_\mu V_\nu^\dagger)\bar{q}\gamma^\mu q$	[V3]
$\frac{g_*^2 m_{\rm DM}^2}{2\Lambda^4}(V_\nu^\dagger\partial_\mu V^\nu - V^\nu\partial_\mu V_\nu^\dagger)\bar{q}i\gamma^\mu\gamma^5 q$	[V4]
$\frac{g_*^2 m_{\rm DM}^2}{\Lambda^3}V_\mu^\dagger V_\nu\bar{q}i\sigma^{\mu\nu}q$	[V5]
$\frac{g_*^2 m_{\rm DM}^2}{\Lambda^3}V_\mu^\dagger V_\nu\bar{q}\sigma^{\mu\nu}\gamma^5 q$	[V6]
$\frac{g_*^2 m_{\rm DM}}{2\Lambda^3}(V_\nu^\dagger\partial^\nu V_\mu + V_\nu\partial^\nu V_\mu^\dagger)\bar{q}\gamma^\mu q$	[V7P]
$\frac{g_*^2 m_{\rm DM}^2}{2\Lambda^4}(V_\nu^\dagger\partial^\nu V_\mu - V_\nu\partial^\nu V_\mu^\dagger)\bar{q}i\gamma^\mu q$	[V7M]
$\frac{g_*^2 m_{\rm DM}}{2\Lambda^3}(V_\nu^\dagger\partial^\nu V_\mu + V_\nu\partial^\nu V_\mu^\dagger)\bar{q}\gamma^\mu\gamma^5 q$	[V8P]
$\frac{g_*^2 m_{\rm DM}^2}{2\Lambda^4}(V_\nu^\dagger\partial^\nu V_\mu - V_\nu\partial^\nu V_\mu^\dagger)\bar{q}i\gamma^\mu\gamma^5 q$	[V8M]
$\frac{g_*^2 m_{\rm DM}}{2\Lambda^3}\epsilon^{\mu\nu\rho\sigma}(V_\nu^\dagger\partial_\rho V_\sigma + V_\nu\partial_\rho V_\sigma^\dagger)\bar{q}\gamma_\mu q$	[V9P]
$0.5\frac{g_*^2 m_{\rm DM}}{2\Lambda^3}\epsilon^{\mu\nu\rho\sigma}(V_\nu^\dagger\partial_\rho V_\sigma - V_\nu\partial_\rho V_\sigma^\dagger)\bar{q}i\gamma_\mu q$	[V9M]
$\frac{g_*^2 m_{\rm DM}}{2\Lambda^3}\epsilon^{\mu\nu\rho\sigma}(V_\nu^\dagger\partial_\rho V_\sigma + V_\nu\partial_\rho V_\sigma^\dagger)\bar{q}\gamma_\mu\gamma^5 q$	[V10P]
$\frac{g_*^2 m_{\rm DM}}{2\Lambda^3}\epsilon^{\mu\nu\rho\sigma}(V_\nu^\dagger\partial_\rho V_\sigma - V_\nu\partial_\rho V_\sigma^\dagger)\bar{q}i\gamma_\mu\gamma^5 q$	[V10M]
$\frac{g_*^2 m_{\rm DM}^2}{\Lambda^4}V_\mu^\dagger V^\mu G^{\rho\sigma}G_{\rho\sigma}$	[V11]
$\frac{g_*^2 m_{\rm DM}^2}{\Lambda^4}V_\mu^\dagger V^\mu\tilde{G}^{\rho\sigma}G_{\rho\sigma}$	[V12]

Here we denote the field strength tensor of the gluons as $G^{\mu\nu}$ and its dual as $\tilde{G}^{\mu\nu}$.

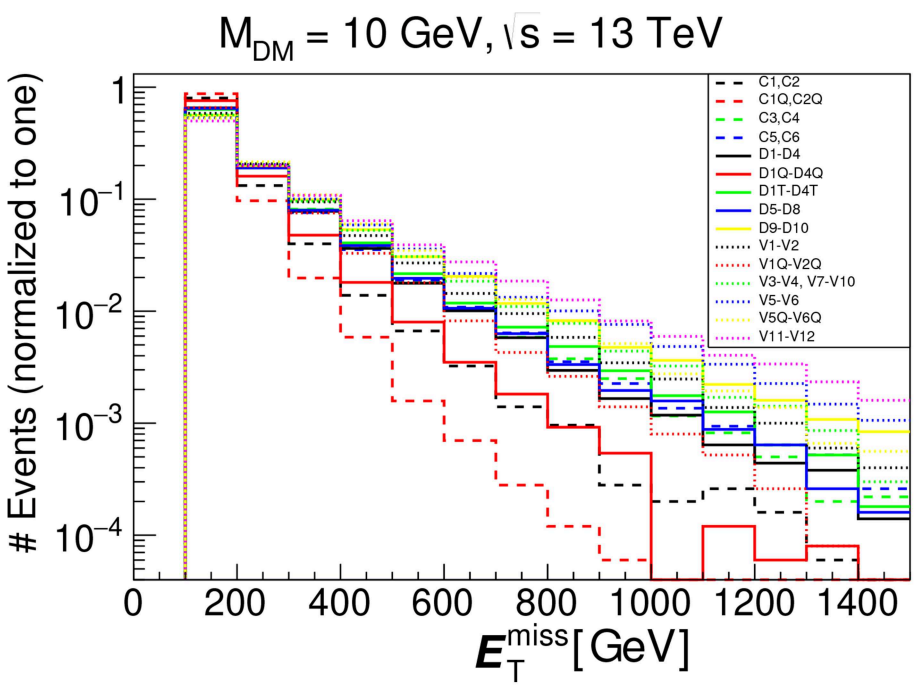

FIGURE 1 | $E_{\rm T}^{\rm miss}$ parton level distributions for a representative subset of the EFT operators from **Table 1** for 13 TeV LHC energy and $M_{\rm DM} = 10$ GeV.

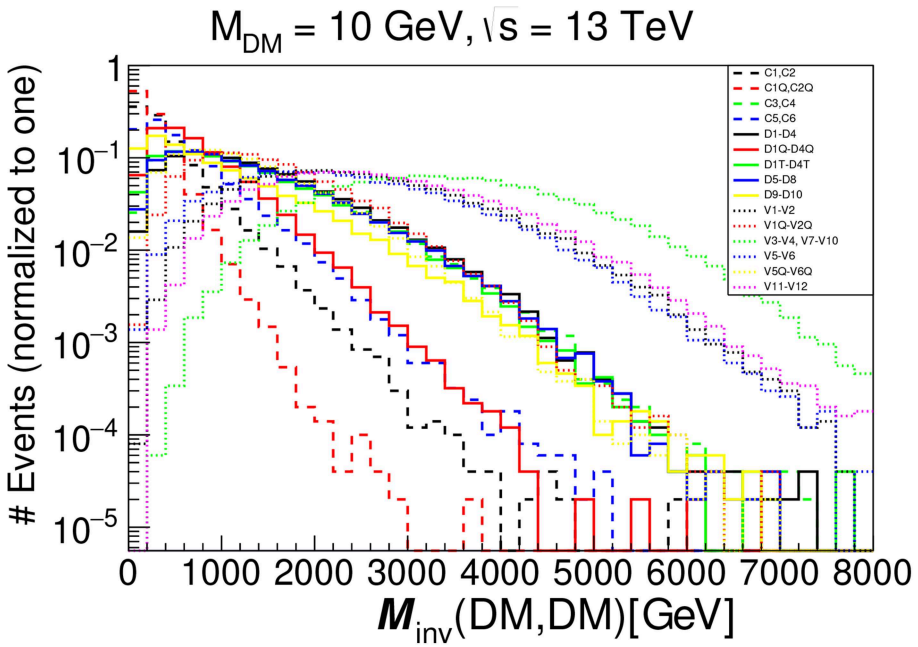

FIGURE 2 | Invariant mass of DM pair distributions normalized to unity for EFT operators in **Table 1** for 13 TeV LHC energy, $M_{\rm DM} = 10$ GeV and $p_{T\,jet} \geq 100$ GeV cut applied.

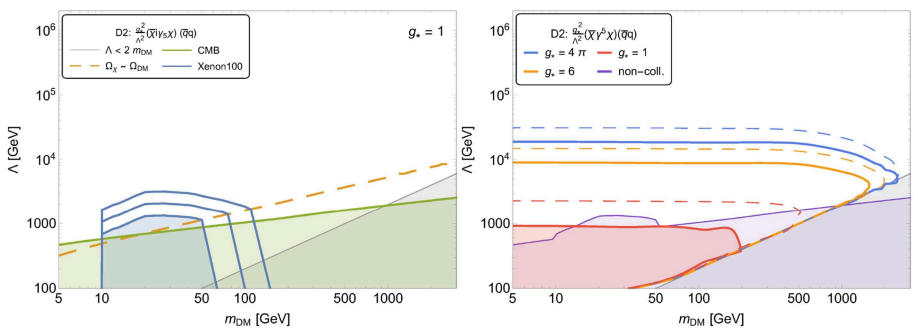

FIGURE 3 | (Left) Non-collider constraints on D2 operator with fermion DM: (i) SI DM DD searches (shaded blue region below the lowest blue contour), (ii) constraints from relic density (above the yellow dashed line), (iii) constraints from the CMB (shaded green area), and (iv) constraints from the validity of the EFT ($\Lambda > 2m_{DM}$). **(Right)** LHC monojet constraints on D2 EFT operator. The area inside the red, orange and blue solid curves is excluded by current LHC data at 95% CL for $g_\star = 1$, 6, and 4π, respectively. The projected LHC limits for 300 fb^{-1} are indicated by dashed thin lines. The combined exclusion regions from CMB and DM DD searches for $g_\star = 1$ are given by the light-purple area. See details and complete set of plots in Belyaev et al. [27].

case of t-channel mediator or mediators with mass below $2M_{DM}$, where the $M_{\rm inv}(DM, DM)$ is not fixed. This case covers a wide range of theories.

As an example in **Figure 4** (left) the normalized shape for $\boldsymbol{E}_{\rm T}^{\rm miss}$ distribution from $pp \rightarrow \chi_1^+\chi_1^-/\chi_1^\pm\chi_1^0 \rightarrow \chi_1^0\chi_1^0 +$ soft leptons/jets Minimal Supersymmetric Model(MSSM) signal and its dominant irreducible background $Z + jet \rightarrow \nu\bar{\nu} + jet$ (Zj) is presented for LHC@13TeV [32]. The model parameter space in the compressed chargino-neutralino scenario driven by small μ parameter is essentially characterized only by DM (χ_1^0) and chargino (χ_1^+) masses and mildly depends on the value of tan β.

In the **Figure 4** (right) we present $\boldsymbol{E}_{\rm T}^{\rm miss}$ from h_1h_2j inert two Higgs doublet model (i2HDM) signal alongside the estimated (by CMS) experimental background for $\sqrt{s} = 13$ TeV. The parameter space of the model, details of which can be found for example in Belyaev et al. [33], is characterized by DM mass (h_1), the mass of the second neutral scalar (h_2), the mass of the charged scalar (h^+) and the DM-Higgs boson coupling. However, the h_1h_2j production cross section depends only on two parameters– h_1 and h_2 masses in analogy to the above SUSY scenario. An important feature of the signal vs. background shapes in these completely different theory cases is that the background falls more rapidly with $\boldsymbol{E}_{\rm T}^{\rm miss}$, and the difference in the slope with

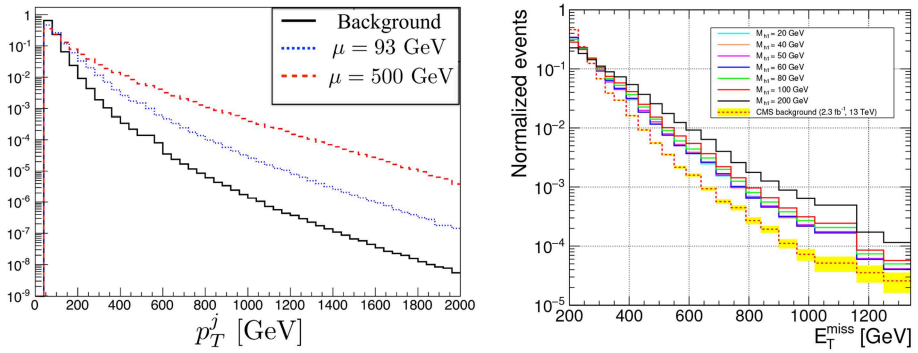

FIGURE 4 | (Left) Normalized signal (dotted blue and dashed red) and Zj background (solid black) parton-level p_T^j distributions for the 13 TeV LHC for the NSUSY scenario: normalized signal and Zj background distributions. See details in Barducci et al. [32]. **(Right)** Normalized $\boldsymbol{E}_{\mathrm{T}}^{\mathrm{miss}}$ from h_1h_2j i2HDM signal vs. background for $\sqrt{s} = 13$ TeV. See details in Belyaev et al. [33].

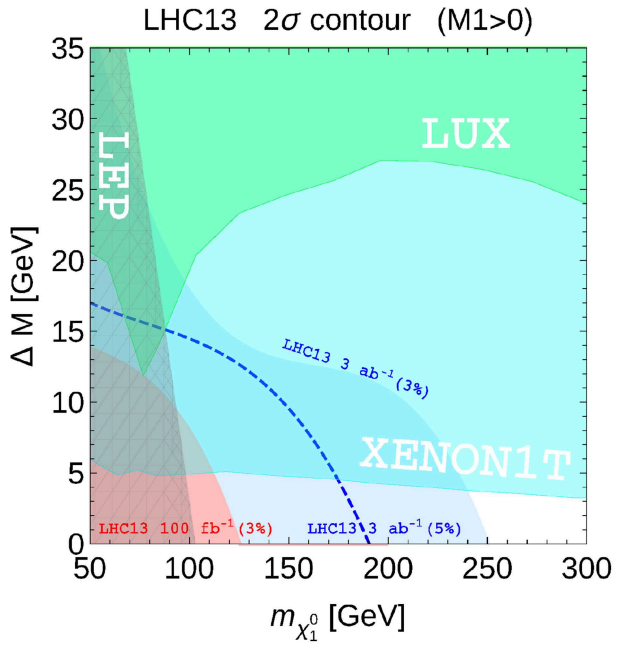

FIGURE 5 | Exclusion contour lines for the 13 TeV LHC at the end of the LHC Run2 (light red region) and of the HL-LHC (light blue region). The region excluded by LUX and Xenon1T are also shown, together with the LEP limit. See details in Barducci et al. [32].

respect to the signal is bigger for higher DM mass. This behavior has the same explanation as for EFT study case above—it is related to the bigger invariant mass of the invisible system for the signal—$M(DM, DM)$ than for the background—M_Z. This feature is very instrumental to increase signal-to-background ratio (S/B) (which is typically below 1% for low $\boldsymbol{E}_{\mathrm{T}}^{\mathrm{miss}}$ cuts) by increasing the value of $\boldsymbol{E}_{\mathrm{T}}^{\mathrm{miss}}$ or by performing the signal-background shape analysis [33].

The role of non-collider DM searches is also crucial in case of these two complete and consistent models. And an example in **Figure 5** we present the projected LHC reach for MSSM monojet signal in the $\Delta M = m_{\chi_1^+} - m_{\chi_1^0}$, $M_{DM} = m_{\chi_1^0}$ parameter space together with LUX and Xenon1T DM DD exclusion [32]. One can see that LHC would be able cover neutralino DM mass only below 250 GeV (with the assumption that S/B of the order of 3% will be under control) even with 3 ab^{-1} total integrated luminosity. But coverage of this region is important as well as LHC-Xenon1T complementarity: LHC will be able to cover the region inaccessible by Xenon1T in small ΔM region, while Xenon1T is able to cover m_{DM} well beyond the LHC reach for $\Delta M > 3 - 5$ GeV. In case of i2HDM model collider sensitivity with mono-jet signature is even more limited because of the lower production rates of the scalar DM, h_1, or its inert partners (h_2 and h^+) and expected LHC reach is below 100 GeV for M_{h1}.

4. BEYOND MONO-X SIGNATURE

While mono-X (with X being jet, γ, Z, H, t etc.) DM signatures at colliders are the most general ones, their rates are typically very low (usually at the percent level or even lower). Besides several other interesting but model-specific DM signature studies, one should stress one signature which can be also considered as quite generic one. In case when DM, D^0, is embedded into electroweak multiplet and its mass split from the charged odd particle(s), D^+, is generated only radiatively (preserving gauge invariance), the one can find that the value of this mass split is of the order of 0.2 GeV. In this case D^+ has a very small width and respectively large life-time. D^+ being long lived particle (LLP) dominantly decays into DM and very soft pion: $D^+ \to D^0\pi^0$. Production of D^+ in pairs or in association with DM leads then to the typical signature from charged LLP: disappearing charged track (DCT) as soon as the track from LLP is long enough (from few cm to a meter). In case of such signature the S/B ratio is much higher than in case of mono-jet signal and therefore, substantially bigger DM masses can be probed with charged LLPs from DM sector [34–36]. As an example, we would like to present here results for the minimal vector triplet DM

(V^0) model [36] which predicts the right amount of DM for M_{DM} in the 3-4 TeV range depending on DM coupling to the Higgs boson.

In this model the SM is supplemented by a new massive vector boson V_μ in the adjoint representation of $SU(2)_L$, e.g., by two new massive vector particles: V^0 and $V^\pm$. If V_μ transforms homogeneously (*i.e.*, $V_\mu \rightarrow g_L^\dagger V_\mu g_L$ where $g_L \in SU(2)_L$) and Z_2 symmetry is imposed (which links the quartic V coupling to the gauge coupling constant and makes theory unitary is unitary before EW symmetry breaking and in the absence of the Higgs boson as found in Zerwekh [37]) then Lagrangian can be written as:

$$\mathcal{L} = \mathcal{L}_{SM} - Tr\left\{D_\mu V_\nu D^\mu V^\nu\right\} + Tr\left\{D_\mu V_\nu D^\nu V^\mu\right\} - \frac{g^2}{2} Tr\left\{\left[V_\mu, V_\nu\right]\left[V^\mu, V^\nu\right]\right\}$$

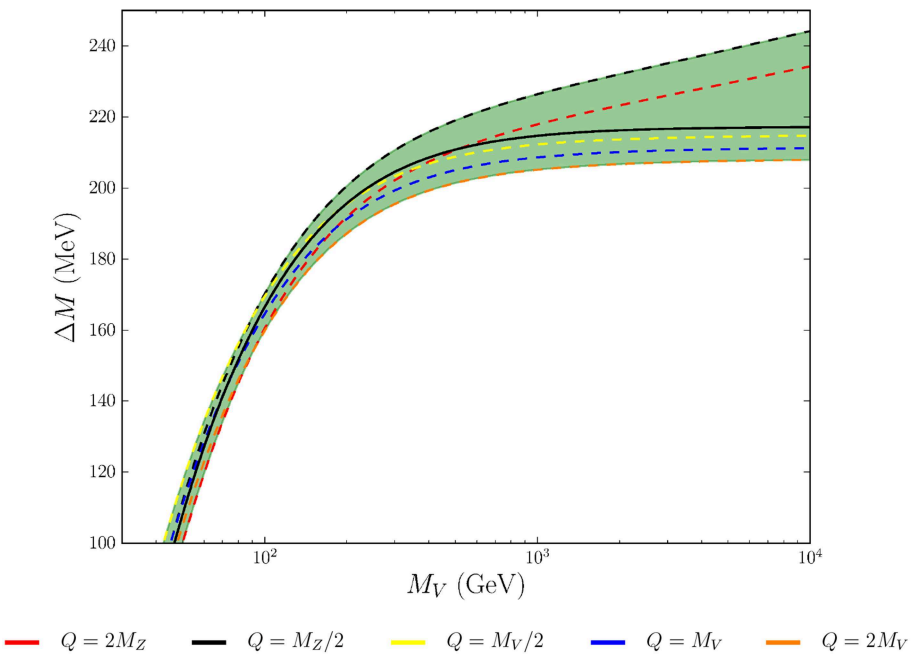

FIGURE 6 | The one-loop radiatively induced mass splitting between the charged and neutral components of the vector DM. The solid lines represent ΔM computed at fixed values of the renormalization scale Q. The shaded green band indicates the range of values obtained by varying Q continuously between $\min\{M_V/2, M_Z/2\}$ and $\max\{2M_V, 2M_Z\}$ and thus constitutes an estimate of the uncertainty on ΔM. The solid black line is the one-loop mass splitting, with all higher order terms truncated [36].

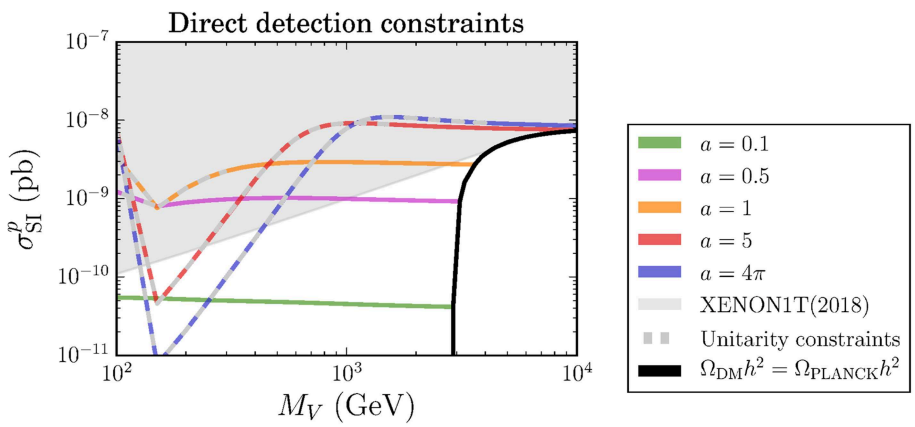

FIGURE 7 | Spin-independent cross-section for V^0-nucleon elastic scattering as a function of M_V and for representative values of a. The continuous black curve represents the elastic cross-section computed with the values of M_V and a that saturate the measured DM relic density. The gray dashing highlights the parameter space where perturbative unitarity loss occurs at too low scale. See details in Belyaev et al. [36].

$$-igTr\left\{W_{\mu\nu}\left[V^{\mu},V^{\nu}\right]\right\}+\tilde{M}^{2}Tr\{V_{\nu}V^{\nu}\}$$
$$+a\left(\Phi^{\dagger}\Phi\right)Tr\{V_{\nu}V^{\nu}\}$$

where $D_{\mu}=\partial_{\mu}-ig\left[W_{\mu},\right]$ is the usual $SU(2)_L$ covariant derivative in the adjoint representation and $\mathcal{L}_{SM}$ represents the SM Lagrangian. The main difference with respect to the model in Zerwekh [37] is that the $SU(2)_L$ symmetry is broken by the Higgs mechanism and the associated gauge bosons have mass. We thus allow for a coupling of V to the Higgs scalar field Φ. Due to the Z_2 symmetry the neutral new vector boson, V^0 is stable and therefore is the perfect DM candidate. The mass split, ΔM, between V^0 and $V^{\pm}$ is generated radiatively and its value is just above the pion mass which makes $V^{\pm}$ long lived. In **Figure 6** we present ΔM as a function of M_V, which was calculated in Belyaev et al. [36].

In **Figure 7** we present results for spin-independent cross-section for V^0-nucleon elastic scattering as a function of M_V and for representative values of a. It is very important to note that Xenon1T experiment combined with DM relic density constraints excludes DM mass above 4 TeV.

At the same time the production rate σ_{eff} for $\sigma(pp\rightarrow V^{\pm}V^{0})+2\sigma(pp\rightarrow V^{+}V^{-})$ process which leads to the disappearing charge track signatures (that is why $pp\rightarrow V^{+}V^{-}$ process comes with coefficient 2 which is equal to the number of disappearing charged tracks it provides) are high enough to probe this process at colliders. In particular, the current LHC@13TeV limit on M_V is about 1.4 TeV as one can see from **Figure 8**. Moreover, one can also see from this figure that 100 TeV collider will be able to exclude DM mass below 4 TeV, thus allowing to probe the entire parameter space of the model.

One should also note that in case of i2HDM, DCT signature also allows to substantially enhance LHC potential and probe DM mass upto about 500 GeV [34] which is much higher than 100 GeV—the maximum DM mass which can be probed via mono-jet signature.

5. TOWARD DECODING FRAMEWORK

There is no framework at the moment which can solve the reverse engineering task—the task of decoding the nature of DM. It is not surprising why—we are all eagerly looking for the signal first of all and busy with the interpreting and exploring our own models. The huge amount of work has been done on the model building, phenomenology and experimental searches as well as on building different tools, examples of which has been given above. And there is really huge potential of combining different methods and signatures to probe different models. What is missing is the framework which joins all these pieces in one tool which would help us to decode underlying theory, in particular its part related to DM. The task of decoding of the whole underlying theory sounds probably too ambitious to the author, while decoding of its DM part sound more realistic since it contain specific and possibly much smaller piece of the theory. This framework requires the database of models, database of various signatures and set of tools which will be able to effectively explore not only parameter space of each particular model, but also the *model parameter space* and compare predicted signatures with the observed ones. Such a framework would allow objectively judge about preferred model or set of models which would fit signal best of all. An example of the prototype of such a framework actually already exists in the form of High Energy Physics Model Data

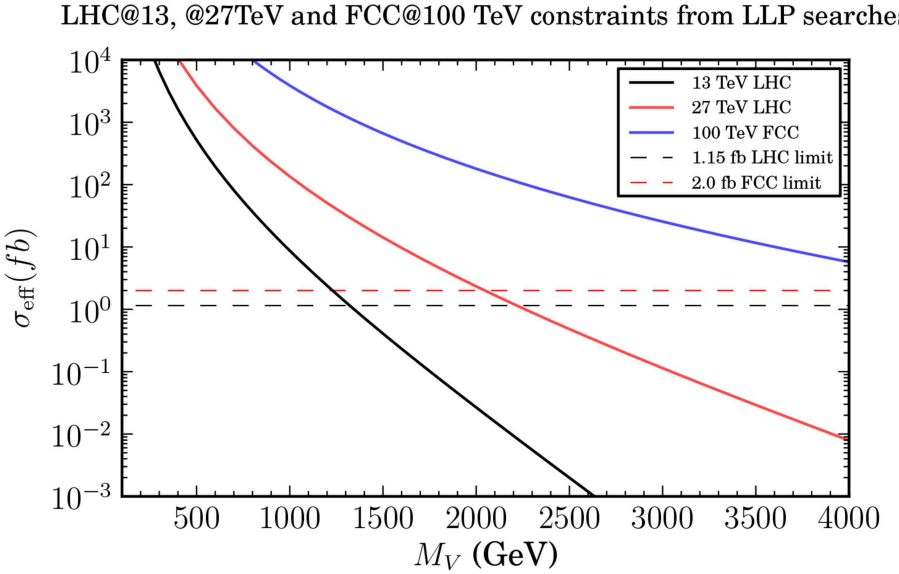

FIGURE 8 | The effective cross-sections $\sigma_{eff}=\sigma(pp\rightarrow V^{\pm}V^{0})+2\sigma(pp\rightarrow V^{+}V^{-})$ at leading order for the vector isotriplet model for 13 and 27 TeV LHC energies and for a 100 TeV future collider. The dashed lines corresponds to collider sensitivity. See details in Belyaev et al. [36].

Base (HEPMDB) (https://hepmdb.soton.ac.uk) [38], created at Southampton University in 2011. At the moment HEPMDB is created as a web-server accessible to everybody and is able to:

1. collect HEP models for all multipurpose Matrix Element (ME) generators in the form of Feynman rules and parameters written in the format specific for a given package;
2. collect models' sources which can be used to generate HEP models for various ME generators using FeynRules [39] or LanHEP [40];
3. allow users to perform simulations for their own models or models available at HEPMDB using the full power of the High Performance Computing (HPC) IRIDIS cluster standing behind the HEPMDB itself. Connection to HPC cluster is one of the key features of the HEPMDB: it provides a web interface to various ME generators (CalcHEP[41], Madgraph [42], and Whizard [43]) which can then also be run directly on the HPC cluster avoiding problems related to installing the actual software, which can sometimes be quite cumbersome;
4. collect simulated events and plot distributions using web interface.

Though the signature database at HEPMDB is at the development stage, users can indicate some essential features of the signatures which model can provide, such as presence of resonance, $\boldsymbol{E}_{\mathrm{T}}^{\mathrm{miss}}$ etc. The next step of development of HEPMDB will include an addition of various packages to event analysis. Probably the most important feature of HEPMDB is that it can be developed by the whole HEP community—any registered user can add his/her own model and signature which would be used for identification of underlying theory when the experimental signal will be observed.

6. CONCLUSIONS

In the absence of DM signal we can still do a lot—we can prepare ourselves for its discovery and identification. $\boldsymbol{E}_{\mathrm{T}}^{\mathrm{miss}}$ shape is quite instrumental in understanding the underlying theory at colliders, while direct and indirect DM searches are very powerful in complementing collider searches especially in the parameter space with large DM mass. We also advocate the usage of new DM signatures such as disappearing charge tracks which allows to substantially extend collider exploration of large DM mass. Moreover, we would like to stress the crucial role of 100 TeV *pp* collider which is likely to exclude substantial amount of thermal DM models. We show that collider and non-collider DM searches have a unique power to decode the nature of Dark Matter on the examples of several appealing DM theories. Such complementarity and usage of different signatures would allow us to decode the nature of DM, signals from which we are expecting in the near future. Finally, we advocate the importance of the framework which would combine the experience of HEP community and would allow to identify effectively the underlying theory of DM from the experimental signal which we will hopefully observe in the near future.

AUTHOR CONTRIBUTIONS

The author confirms being the sole contributor of this work and has approved it for publication.

ACKNOWLEDGMENTS

AB acknowledges partial support from the STFC grant ST/L000296/1 and Soton-FAPESP grant. AB also thanks the NExT Institute and Royal Society International Exchange grant IE150682.

REFERENCES

1. Ade PAR, Aghanim N, Arnaud M, Ashdown M, Aumont J, Baccigalupi C, et al. Planck 2015 results. XIII. Cosmological parameters. *Astron Astrophys.* (2016) **594**:A13. doi: 10.1051/0004-6361/201525830
2. Blumenthal GR, Faber SM, Primack JR, Rees MJ. Formation of galaxies and large scale structure with cold dark matter. *Nature* (1984) **311**:517–25. doi: 10.1038/311517a0
3. Bullock JS, Kolatt TS, Sigad Y, Somerville RS, Kravtsov AV, Klypin AA, et al. Profiles of dark haloes. Evolution, scatter, and environment. *Mon Notices R Astron Soc.* (2001) **321**:559–75. doi: 10.1046/j.1365-8711.2001.04068.x
4. Aaboud M, Aad G, Abbott B, Abdinov O, Abeloos B, Abidi SH, et al. Search for dark matter and other new phenomena in events with an energetic jet and large missing transverse momentum using the ATLAS detector. *J High Energy Phys.* (2018) **1**:126. doi: 10.1007/JHEP01
5. CMS Collaboration. Search for new physics in final states with an energetic jet or a hadronically decaying W or Z boson using 35.9 fb^{-1} of data at $\sqrt{s} = 13$ TeV CMS-PAS-EXO-16-048 (2017).
6. ATLAS Collaboration. *Search for Dark Matter in Events with a Hadronically Decaying Vector Boson and Missing Transverse Momentum in pp Collisions at* $\sqrt{s} = 13$ *TeV with the ATLAS Detector* ATLAS-CONF-2018-005 (2018).
7. ATLAS Collaboration. Search for Dark Matter at p $\sqrt{s} = 13$ in final states containing an energetic photon and large missing transverse momentum with the ATLAS detector. *Eur Phys J.* (2017) **C77**:393. doi: 10.1140/epjc/s10052-017-4965-8
8. CMS Collaboration. Search for dark matter produced in association with a single top quark or a top quark pair in proton-proton collisions at $\sqrt{s} = 13$ TeV. *J High Energy Phys.* (2019) **3**:141. doi: 10.1007/JHEP03(2019)141
9. Hinshaw G, Larson D, Komatsu E, Spergel DN, Bennett CL, Dunkley J, et al. Nine-Year wilkinson microwave anisotropy probe (WMAP) observations: cosmological parameter results. *Astrophys J Suppl.* (2013) **208**:19. doi: 10.1088/0067-0049/208/2/19
10. Aghanim N, Akrami Y, Ashdown M, Aumont J, Baccigalupi C, Ballardini M, et al. Planck 2018 results. VI. Cosmological parameters. arXiv:1807.06209 (2018).
11. Goodman MW, Witten E. Detectability of certain dark matter candidates. *Phys Rev.* (1985) **D31**:3059–63. doi: 10.1103/PhysRevD.31.3059

12. Aprile E, Aalbers J, Agostini F, Alfonsi M, Amaro FD, Anthony M, et al. First dark matter search results from the XENON1T experiment. *Phys Rev Lett.* (2017) **119**:181301. doi: 10.1103/PhysRevLett.119.181301
13. Akerib DS, Alsum S, Araújo HM, Bai X, Bailey AJ, Balajthy J, et al. Results from a search for dark matter in the complete LUX exposure. *Phys Rev Lett.* (2017) **118**:021303. doi: 10.1103/PhysRevLett.118.021303
14. Cui X, Abdukerim A, Chen W, Chen X, Chen Y, Dong B, et al. Dark matter results from 54-Ton-Day exposure of PandaX-II experiment. *Phys Rev Lett.* (2017) **119**:181302. doi: 10.1103/PhysRevLett.119.181302
15. Slatyer TR. TASI Lectures on Indirect Detection of Dark Matter. In: *Theoretical Advanced Study Institute in Elementary Particle Physics: Anticipating the Next Discoveries in Particle Physics (TASI 2016).* Boulder, CO (2017).
16. Ackermann M, Albert AM, Anderson B, Atwood WB, Baldini L, Barbiellini G, et al. Searching for dark matter annihilation from milky way dwarf spheroidal galaxies with six years of Fermi large area telescope data. *Phys Rev Lett.* (2015) **115**:231301. doi: 10.1103/PhysRevLett.115.231301
17. Zitzer B. A Search for Dark Matter from Dwarf Galaxies using VERITAS. *The 34th International Cosmic Ray Conference.* ICRC2015 (2016).
18. Ahnen ML, Ansoldi S, Antonelli LA, Antoranz P, Babic A, Banerjee B, et al. Limits to dark matter annihilation cross-section from a combined analysis of MAGIC and Fermi-LAT observations of dwarf satellite galaxies. *J Cosmol Astropart Phys.* (2016) **1602**:039. doi: 10.1088/1475-7516/2016/02/039
19. Abdallah H, Abramowski A, Aharonian F, Ait Benkhali F, Akhperjanian AG, Angüner E, et al. Search for dark matter annihilations towards the inner Galactic halo from 10 years of observations with H.E.S.S. *Phys Rev Lett.* (2016) **117**:111301. doi: 10.1103/PhysRevLett.117.111301
20. Abramowski A, Acero F, Aharonian F, Akhperjanian AG, Anton G, Balenderan S, et al. Search for photon-linelike signatures from dark matter annihilations with H.E.S.S. *Phys Rev Lett.* (2013) **110**:041301. doi: 10.1103/PhysRevLett.110.041301
21. Galli S, Iocco F, Bertone G, Melchiorri A. CMB constraints on Dark Matter models with large annihilation cross-section. *Phys Rev.* (2009) **D80**:023505. doi: 10.1103/PhysRevD.80.023505
22. Galli S, Iocco F, Bertone G, Melchiorri A. Updated CMB constraints on Dark Matter annihilation cross-sections. *Phys Rev.* (2011) **D84**:027302. doi: 10.1103/PhysRevD.84.027302
23. Goodman J, Ibe M, Rajaraman A, Shepherd W, Tait TM, Yu H-B. Constraints on dark matter from colliders. *Phys Rev.* (2010) **D82**:116010. doi: 10.1103/PhysRevD.82.116010.
24. Kumar J, Marfatia D, Yaylali D. Vector dark matter at the LHC. *Phys Rev.* (2015) **D92**:095027. doi: 10.1103/PhysRevD.92.095027
25. Belyaev A, Panizzi L, Pukhov A, Thomas M. Dark Matter characterization at the LHC in the Effective Field Theory approach. *J High Energy Phys.* (2017) **4**:110. doi: 10.1007/JHEP04(2017)110
26. Contino R, Falkowski A, Goertz F, Grojean C, Riva F. On the validity of the effective field theory approach to SM precision tests. *J High Energy Phys.* (2016) **7**:144. doi: 10.1007/JHEP07(2016)144
27. Belyaev A, Bertuzzo E, Caniu Barros C, Eboli O, Grilli Di Cortona G, Iocco F, et al. Interplay of the LHC and non-LHC Dark Matter searches in the Effective Field Theory approach. *Phys Rev.* (2019) **D99**:015006. doi: 10.1103/PhysRevD.99.015006
28. Aprile E, Aalbers J, Agostini F, Alfonsi M, Althueser L, Amaro FD, et al. Dark matter search results from a one Ton-year exposure of XENON1T. *Phys Rev Lett.* (2018) **121**:111302. doi: 10.1103/PhysRevLett.121.111302
29. Hill RJ, Solon MP. Universal behavior in the scattering of heavy, weakly interacting dark matter on nuclear targets. *Phys Lett.* (2012) **B707**:539–45. doi: 10.1016/j.physletb.2012.01.013
30. Frandsen MT, Haisch U, Kahlhoefer F, Mertsch P, Schmidt-Hoberg K. Loop-induced dark matter direct detection signals from gamma-ray lines. *J Cosmol Astropart Phys.* (2012) **1210**:033. doi: 10.1088/1475-7516/2012/10/033
31. Vecchi L. WIMPs and Un-Naturalness. arXiv:1312.5695 (2013).
32. Barducci D, Belyaev A, Bharucha AKM, Porod W, Sanz V. Uncovering natural supersymmetry via the interplay between the LHC and direct dark matter detection. *J High Energy Phys.* (2015) **7**:066. doi: 10.1007/JHEP07(2015)066.
33. Belyaev A, Fernandez Perez Tomei TR, Mercadante PG, Moon CS, Moretti S, Novaes SF, et al. Advancing LHC probes of dark matter from the inert two-Higgs-doublet model with the monojet signal. *Phys Rev.* (2019) **D99**:015011. doi: 10.1103/PhysRevD.99.015011
34. Belyaev A, Cacciapaglia G, Ivanov IP, Rojas-Abatte F, Thomas M. Anatomy of the inert two higgs doublet model in the light of the LHC and non-LHC dark matter searches. *Phys Rev.* (2018) **D97**:035011. doi: 10.1103/PhysRevD.97.035011
35. Mahbubani R, Schwaller P, Zurita J. Closing the window for compressed Dark Sectors with disappearing charged tracks. *J High Energy Phys.* (2017) **6**:119. doi: 10.1007/JHEP06(2017)119
36. Belyaev A, Cacciapaglia G, Mckay J, Marin D, Zerwekh AR. Minimal Spin-one Isotriplet Dark Matter. Phys. Rev. (2019) **D99**:115003. doi: 10.1103/PhysRevD.99.115003
37. Zerwekh AR. On the quantum chromodynamics of a massive vector field in the adjoint representation. *Int J Mod Phys.* (2013) **A28**:1350054. doi: 10.1142/S0217751X13500541
38. Bondarenko M, Belyaev A, Blandford J, Basso L, Boos E, Bunichev V, et al. *High Energy Physics Model Database: Towards Decoding of the Underlying Theory (within Les Houches 2011: Physics at TeV Colliders New Physics Working Group Report*) (2012).
39. Alloul A, Christensen ND, Degrande C, Duhr C, Fuks B. FeynRules 2.0 - A complete toolbox for tree-level phenomenology. *Comput Phys Commun.* (2014) **185**:2250–300. doi: 10.1016/j.cpc.2014.04.012
40. Semenov A. *LanHEP - A Package for Automatic Generation of Feynman Rules From the Lagrangian*. Updated version 3.1. arXiv:1005.1909 (2010).
41. Belyaev A, Christensen ND, Pukhov A. CalcHEP 3.4 for collider physics within and beyond the Standard Model. *Comput Phys Commun.* (2013) **184**:1729–69. doi: 10.1016/j.cpc.2013.01.014
42. Alwall J, Herquet M, Maltoni F, Mattelaer O, Stelzer T. MadGraph 5: Going Beyond. *J High Energy Phys.* (2011) **06**:128. doi: 10.1007/JHEP06(2011)128
43. Kilian W, Ohl T, Reuter J. WHIZARD: Simulating Multi-Particle Processes at LHC and ILC. *Eur Phys J.* (2011) **C71**:1742. doi: 10.1140/epjc/s10052-011-1742-y

Conflict of Interest Statement: The author declares that the research was conducted in the absence of any commercial or financial relationships that could be construed as a potential conflict of interest.

frontiers in Physics

REVIEW
published: 20 September 2019
doi: 10.3389/fphy.2019.00135

The Multiple Point Principle and Extended Higgs Sectors

*John McDowall and David J. Miller**

SUPA, School of Physics and Astronomy, University of Glasgow, Glasgow, United Kingdom

The Higgs boson quartic self-coupling in the Standard Model appears to become zero just below the Planck scale, with interesting implications to the stability for the Higgs vacuum at high energies. We review the *Multiple Point Principle* that suggests the quartic self-coupling should vanish exactly at the Planck scale. Although this vanishing is not consistent with the Standard Model, we investigate Higgs sectors extended with additional states to test whether one may satisfy the high scale boundary condition while maintaining the observed Higgs mass. We also test these scenarios to ensure the stability of the vacuum at all energies below the Planck scale and confront them with experimental results from the LHC and Dark Matter experiments.

Keywords: Higgs boson, beyond the standard model, extended Higgs sectors, renormalization group, multiple point principle, dark matter

OPEN ACCESS

Edited by:
António Pestana Morais, University of Aveiro, Portugal

Reviewed by:
Rui Ribeiro Santos, Instituto Superior de Engenharia de Lisboa, Portugal
Bhupal Dev, Washington University in St. Louis, United States

***Correspondence:**
David J. Miller
david.j.miller@glasgow.ac.uk

Specialty section:
This article was submitted to High-Energy and Astroparticle Physics, a section of the journal Frontiers in Physics

Received: *17 December 2018*
Accepted: *04 September 2019*
Published: *20 September 2019*

Citation:
McDowall J and Miller DJ (2019) The Multiple Point Principle and Extended Higgs Sectors. Front. Phys. 7:135. doi: 10.3389/fphy.2019.00135

1. INTRODUCTION

It is widely believed that investigations of the Higgs boson and the resulting breaking of Electroweak Symmetry provide the best opportunity for finding new physics beyond the Standard Model (SM). In part, this is because the Higgs boson is the most recently discovered fundamental particle [1], and investigations of its properties are still underway (though so far no significant deviation from the SM has been observed [2–5]). This view is reinforced by the required relative smallness of the Higgs boson mass and its related *hierarchy problem*. Since the SM Higgs boson mass is unprotected by any symmetries, it should have large quantum corrections of magnitude comparable to the scale of new physics. To restore a physical Higgs mass of order the Electroweak scale one must *fine-tune* to ensure the unnatural cancelation of the bare Higgs mass with its corrections. Provided there is new physics of some type beyond the SM (a reasonable assumption, given its large number of problems and omissions) this is a genuine and very real issue that must be addressed.

The combined ATLAS and CMS value of the Higgs mass [2], $m_h = 125.09 \pm 0.23$ GeV, raises further questions. This is a challenging value for both supersymmetry and composite Higgs models, requiring a significant tuning of parameters or a non-minimal field content [6–8], making it difficult to motivate any particular models and unclear which direction to head next. However, this particular mass has another reason for being peculiar—it is just the right value to allow the Higgs potential to be *metastable* at high energies [6].

As usual for a parameter of a Quantum Field Theory, the Higgs quartic coupling λ evolves with energy according to the Renormalization Group (RG) and is pulled downwards at higher energies by the large top-quark mass. If it were to run to negative values the potential may become unstable and the correct pattern of Electroweak Symmetry breaking is lost. Indeed, requiring absolute stability of the vacuum up to the Planck scale $M_{\rm Pl}$, i.e., $\lambda(M_{\rm Pl}) \geq 0$, places a limit on the top mass [6],

$$m_t < 171.36 \pm 0.46 \text{ GeV}, \tag{1}$$

which is in tension with the current experimental value by about $2.6\,\sigma$. **Figure 1A** shows the quartic coupling dependence on renormalization scale μ, and the $3\,\sigma$ uncertainties that arise from the uncertainties in the top-quark mass m_t and the strong coupling constant α_s. The quartic coupling turns negative at an energy scale of $\mu \sim 10^{10}$ GeV, though a stable potential is not ruled out due to the uncertainties. However, a very small negative value is not a catastrophe, since the vacuum may still be *metastable* with a lifetime much longer than the age of the universe. That nature should choose this metastable vacuum is intriguing. Why does the quartic coupling become so very nearly zero right at the Planck scale?

We may gain further insight by examining the beta-function of the quartic coupling, shown in **Figure 1B**. As indicated already in **Figure 1A**, the running of λ flattens out at high energies, i.e., $\beta_\lambda(M_{\rm Pl}) \approx 0$ too. We stress that in the SM this is *not* an ultraviolet fixed-point since λ would continue to evolve if we increased the energy further. However, if some new physics theory takes over above the Planck scale, then the SM running becomes irrelevant and we must instead consult the new theory. If this new theory sets $\lambda = \beta_\lambda = 0$ at the Planck scale we may recover a low energy phenomenology very similar to what we observe, modulo the slight deviation in the Higgs mass.

In this article, we will review one proposed high scale possibility, the *Multiple Point Principle* (MPP) [10]. Although this is not compatible with the SM running, it provides a Higgs mass prediction that is curiously close to the measured value. We will then examine several theories with extended Higgs sectors to see if they alter the running sufficiently to provide the correct Higgs mass. For recent investigations of alternative high scale boundary conditions at $M_{\rm Pl}$ (see for example [11–16]).

2. THE MULTIPLE POINT PRINCIPLE IN THE SM

The Multiple Point Principle (MPP) asserts that nature chooses the Higgs potential parameters so that different phases of electroweak symmetry breaking may coexist. This is analagous to how ice, water and vapor may coexist for specific values of temperature and pressure near water's triple-point. Since the two phases must be energetically comparable in order to coexist, this means that the potential should have at least two degenerate vacua, that is an additional vacuum degenerate with the usual Electroweak vacuum.

The authors of this principle argue in Froggatt and Nielsen [10] that this is rather natural if we consider *extensive* variables constrained by some new physics theory at high energies, as long as the system has a rather strong first order phase transition. Again we may use the analogy of water and note that slush (in which ice and liquid water coexist) is present for a (relatively) wide range of extensive variables (in this case temperature and pressure) due to the existence of a first order phase transition. Returning to the Higgs potential, a possible *extensive* quantity could be $\langle|\phi|^2\rangle$. If this were set by some new physics theory at the Planck scale with a strong first order phase transition, it would be rather likely to find $\langle|\phi|^2\rangle \sim M_{\rm Pl}^2$, leading to a second degenerate vacuum at the Planck Scale. In essence, this principle is relying on a rather flat distribution of *extensive* parameter space set at the Planck scale matching to a rather peaked distribution of *intensive* parameters (i.e., the usual Higgs potential parameters) due to a strong first-order phase transition, which in turn leads to a second degenerate vacuum [17].

We should note that what this Planck scale theory could be is still unknown, and Froggatt and Nielsen [10] makes no attempt to describe one, using only general principles to support the assertion. Also, we note that this provides no explanation of why the Planck scale is so much bigger than the electroweak scale. Nevertheless, the constraints on the Higgs parameters does provide a *prediction* of the Higgs boson mass that can be compared with experiment, and we further note that this prediction was first made long before the Higgs boson discovery.

The one-loop Coleman-Weinberg effective potential [18] can be written,

$$V_{\rm eff} = -\mu^2(\mu)\phi^2 + \frac{1}{4}\lambda\,(\mu)\,\phi^4(\mu) + \frac{1}{16\pi^2}V_1, \qquad (2)$$

where V_1 takes the schematic form $V_1 \sim \phi^2 \log\left(\phi^2/\mu^2\right)$. For a more explicit form see, for example, Jegerlehner et al. [19]. We see that at one-loop, in addition to the new logarithmic contribution, the parameters μ and λ become energy dependent. For low field values (and low energies) this reproduces the usual "wine-bottle" potential of the Higgs mechanism, but for higher field values, the logarithm pulls the potential back down. Eventually the ϕ^4 terms becomes dominant and the potential will remain stable at the Planck scale if $\lambda(M_{\rm Pl}) > 0$. However, the additional structure causes a second minimum very close to the Planck scale. This is schematically depicted in **Figure 2**. In the SM, taking the measured central values of the Higgs potential parameters, the second vacuum is of slightly lower energy than the Electroweak vacuum, causing the potential to be metastable. The MPP posits that the two minima should be degenerate.

For high field values the effective potential is dominated by its quadratic term, $V_{\rm eff} \approx \lambda\,(\mu)\,\phi^4$, so the second minima at the Planck scale requires

$$\left.\frac{dV_{\rm eff}}{d\phi}\right|_{\phi=M_{\rm Pl}} \approx \lambda\,(\mu)\,\phi^3 + \frac{1}{4}\beta_\lambda\,(\mu)\,\phi^4 = 0. \qquad (3)$$

We see that the MPP is satisfied if $\lambda(M_{\rm Pl}) = \beta_\lambda(M_{\rm Pl}) = 0$.

Applying this boundary condition, the MPP hypothesis gave an early prediction [10] of the Higgs mass $m_h = 135 \pm 9$ GeV, which is remarkably good considering it was made 17 years before the discovery of the Higgs boson, and they simultaneously predicted the top-quark mass (finding 173 ± 5 GeV) in the same year it was discovered. A more recent calculation using the measured top-quark mass and newer determinations of e.g., α_s, gave $m_h = 129 \pm 1.5$ GeV [6]. Although this is slightly too high to be compatible with our by now very accurate Higgs mass measurement, it is still rather remarkable.

Figure 3A shows contours corresponding to the boundary conditions $\lambda(M_{\rm Pl}) = 0$ and $\beta_\lambda\,(M_{Pl}) = 0$ in the $m_h - m_t$ plane, and we see that a slightly heavier Higgs is needed for both

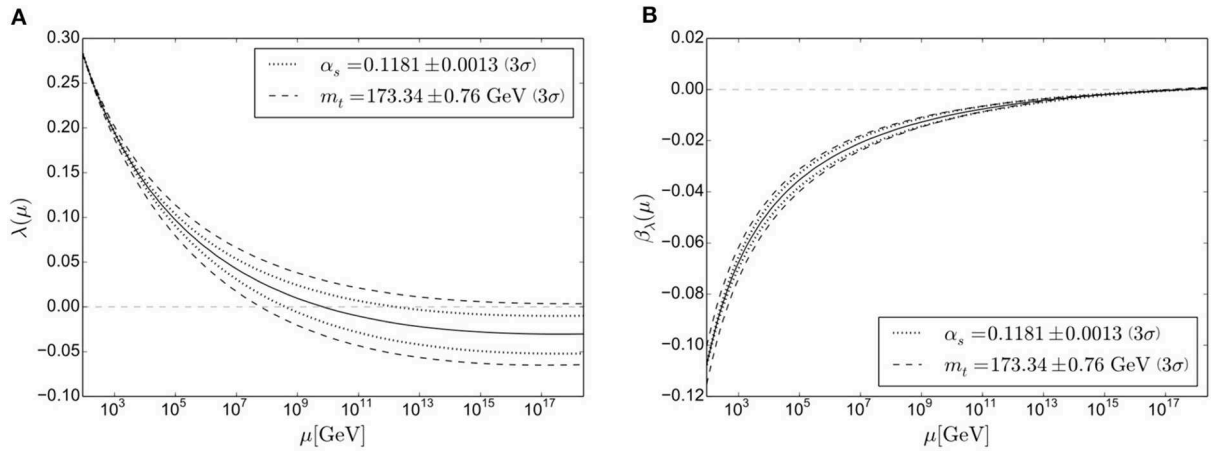

FIGURE 1 | (A) Three-loop running of the SM Higgs quartic coupling λ and **(B)** its β function with 3σ uncertainties from the top pole mass m_t (dashed) and the strong coupling constant α_S (dotted). These plots originally appeared in McDowall and Miller [9].

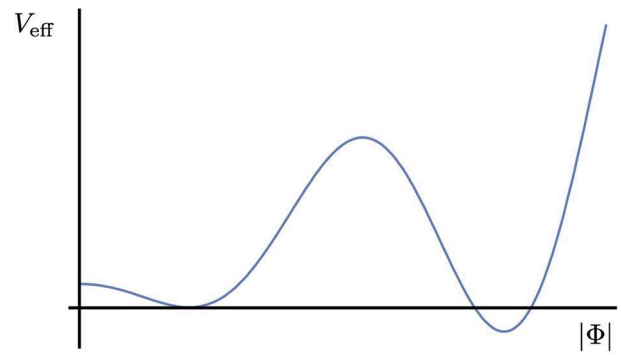

FIGURE 2 | A schematic depiction of the one-loop effective potential in the SM. This is intended only to present a general picture of the minima and is not to scale.

conditions to be satisfied. These contours are calculated using three-loop SM RG equations; the Higgs mass is calculated to two-loop order, while the top mass additionally contains three-loop QCD corrections. This plot is in agreement with the similar plot in Degrassi et al. [11], but we used a different value of the uncertainty in the strong coupling constant $\alpha_s\,(M_Z) = 0.1181 \pm 0.0013$ to reflect more recent estimates [20]. We also use the reduced Planck scale $M_{\text{Pl}} = 2.4 \times 10^{18}$ GeV as our scale at which these boundary conditions are set. **Figure 3A** shows that $\lambda\,(M_{\text{Pl}}) = 0$ can be satisfied with an acceptable value of m_h for a top mass 171 GeV $\lesssim m_t \lesssim$ 174 GeV, and although the corresponding value of $\beta_\lambda\,(M_{\text{Pl}})$ is not zero, it is extremely small.

Note that we have required that these boundary conditions be satisfied at M_{Pl}, but if the theory that dictates the appearance of a second minimum were to become active at a lower energy scale, these boundary conditions would need to be altered. **Figure 3B** shows the $m_h - m_t$ plane with points that satisfy both boundary conditions $\lambda = \beta_\lambda = 0$ simultaneously at different UV scales. The green region corresponds to a 1 σ uncertainty in α_s. We see it is possible to obtain a Higgs mass that is within experimental limits by applying these boundary conditions at approximately 5×10^{17} GeV. It's interesting to note that this is a scale of importance in string scenarios (see e.g., [21, 22]).

As one approaches the Planck Scale, one might expect gravity to become significant and contribute to the RGE running of couplings. The study of these effects has caused some confusion in the literature. An initial calculation of the effect on the running of gauge couplings [23], using a quantized Einstein-Hilbert action as an effective field theory below the Planck scale, showed that this alters the gauge couplings sufficiently to render them asymptotically free. However, this calculation was disputed [24, 25] on the grounds that the derived result is gauge-dependent and therefore unreliable; a calculation performed with a different gauge choice (the harmonic gauge) instead revealed the contributions to be exactly zero. A recalculation was then done using the gauge-invariant background field method [26, 27] and found a result in support of the original claim that the gauge coupling is rendered asymptotically free, though with a modified β-function. Also see He et al. [28] and Daum et al. [29] for alternative calculations. Calculations have also been performed to asses the affect on the quartic Higgs self-coupling relevant to the MPP [30, 31]. These two calculations disagree on the sign of the gravitational contributions to Yukawa couplings, but the corrections to the predicted Higgs mass are small; they predict a Higgs mass of "approximately 130 GeV" and "$\gtrsim$ 131.5 GeV," neither of which are differing very far from the earlier prediction of 129 ± 1.5 GeV [6] and remain incompatible with the SM. See also Branchina et al. [32] for a discussion of the effect on the electroweak vacuum of Planck suppressed operators.

3. A REAL SINGLET EXTENSION

The simplest extension to the Higgs sector is to include an extra real singlet S, with potential,

$$V(\Phi, S) = \mu^2 \Phi^\dagger \Phi + m_S^2 S^2 + \lambda \left(\Phi^\dagger \Phi\right)^2 + \lambda_S S^4 + k_2 \Phi^\dagger \Phi S^2, \tag{4}$$

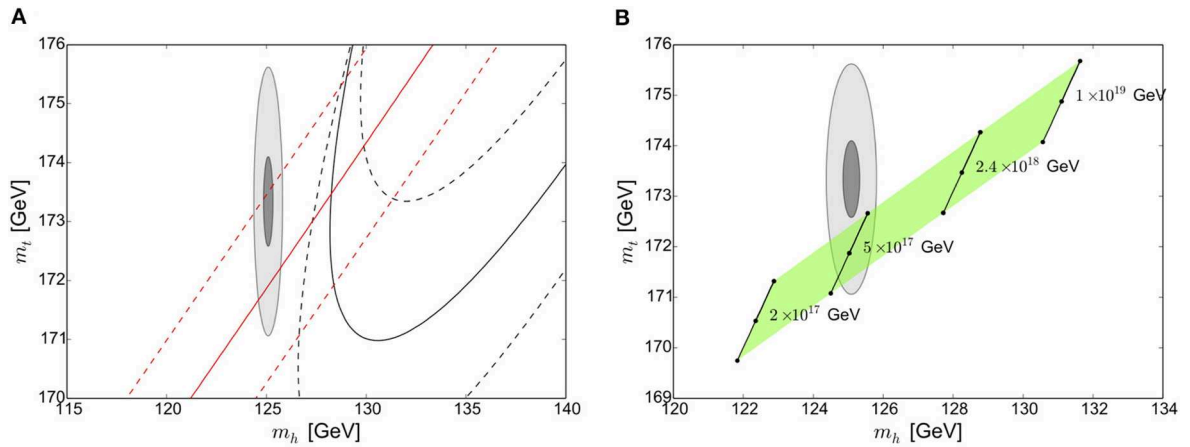

FIGURE 3 | (A) $\lambda\,(M_{Pl}) = 0$ (red) and $\beta_\lambda\,(M_{Pl}) = 0$ (black) contours in the $m_h - m_t$ plane. The dashed lines show $3\,\sigma$ variations in $\alpha_S\,(M_Z) = 0.1181 \pm 0.0013$. **(B)** Mass values that satisfy both boundary conditions at various UV scales. The green region corresponds to a $1\,\sigma$ uncertainty in α_S. Ellipses show the experimentally allowed values of m_t and m_h with $1\,\sigma$ (dark gray) and $3\,\sigma$ (light gray) uncertainty. These plots originally appeared in McDowall and Miller [9].

where a Z_2 symmetry, under which the new scalar is odd, has been used to eliminate terms odd in S [see [33] for a discussion of this model]. During electroweak symmetry breaking, the real singlet field can acquire a non-zero vacuum expectation value (vev) v_S alongside the SM Higgs. The usual Higgs scalar may then mix with the new singlet, though this mixing should not be too strong if we want to avoid LHC constraints. The singlet mass m_S is fixed by the tadpole equation minimizing the potential, analagous to the fixing of μ using the vev v. This leaves the parameters λ, λ_S, k_2, and v_S. We refer to this as the "broken phase." Alternatively, if the new scalar does not acquire a vev (i.e., $v_S = 0$) the tadpole equation becomes trivial and cannot be used to remove m_S. Therefore we have parameters λ, λ_S, k_2, and m_S. Now the scalars do not mix, and the new scalar may be a Dark Matter candidate, so we refer to this as the "Dark Matter phase."

This real singlet model has been investigated in the context of the MPP in Haba et al. [34–36], Hamada et al. [37], and Kawana [38, 39], with varying results. Haba et al. [34] investigated the model in the Dark Matter phase for the MPP as well as the Veltman condition [40]. They found that both boundary conditions could be accommodated (separately) with a 126 GeV Higgs boson, while simultaneously providing the correct DM relic density. An alternative approach was taken in Haba et al. [35, 36] where the MPP was instead imposed on the real singlet model with the addition of an extra right-handed neutrino. Again, the MPP could be made compatible with a 126 GeV Higgs boson provided the scalar mass fell between approximately 850–1,400 GeV and the right-handed neutrino remained very heavy (of order 10^{14} GeV). The MPP can instead be imposed at the "string scale" of 10^{17} GeV in order to facilitate Higgs inflation, which results in somewhat lighter DM at around $400 - 470$ GeV [37]. Kawana [38] includes three additional right-handed neutrinos (one for each generation) at 10^{13} GeV and instead of fixing the MPP condition at $M_{\rm Pl}$ allows the boundary condition energy scale to shift, insisting only that $\lambda = \beta_\lambda = 0$ at a single scale. Similarly to the other analyses this finds the DM mass must be of order 770–1,050 GeV. Finally, Kawana [39] investigates a gauged B-L model, and claim that this can accommodate an MPP condition applied at 10^{17} GeV, as well as Higgs inflation, by tuning the coupling of the Higgs boson to the new scalar.

We see that applying the Planck scale MPP to the real singlet model requires $\lambda = \lambda_S = k_2 = \beta_\lambda = \beta_{\lambda_S} = \beta_{k_2} = 0$. However, this constraint will immediately decouple the new scalar state, and the couplings will not be regenerated by renormalization group running. In other words we revert back to the SM. This seems a serious barrier to the MPP, but is not quite as bad as it appears. Firstly, the MPP itself is somewhat imprecise—the strong first order phase transition made the particular choice of parameters *more likely* but some wriggle-room in these parameters is not unreasonable. (How much wriggle-room is appropriate depends on the UV theory of course.) Furthermore, our calculations themselves are imprecise and include uncertainties. We truncate our β-functions at two-loops and apply approximations to find the MPP solutions themselves. Therefore, it is more appropriate to ask if the MPP constraints can be approximately applied, i.e., λ, λ_S, k_2, β_λ, β_{λ_S}, and β_{k_2} should be "small."

To investigate if small parameters are compatible with the low energy observations we fix all the quartic scalar couplings at M_{Pl}. We perform a scan over Planck scale parameters, allowing λ, λ_S, and $|\kappa_2|$ to vary between 0 and 1. We also allow v_S or m_S to vary between zero and 2 TeV in the broken or Dark Matter phases, respectively. We use SARAH 4.12.2 [41] to calculate the two-loop β functions as well as the mass matrices, tadpole equations, vertices and loop corrections we need to calculate mass spectra at low energies; and FlexibleSUSY 2.0.1 [42–45] is used to build the spectrum generator needed to get the mass spectrum for each point.

Valid parameter choices must result in a vacuum that is bounded from below up to M_{Pl}, so we also require, at all scales,

the vacuum stability conditions,

$$\lambda, \lambda_S \geq 0, \qquad \sqrt{\lambda \lambda_S} + k_2 \geq 0. \tag{5}$$

We also require dimensionless couplings remain perturbative up to M_{Pl}, so,

$$\lambda, \lambda_S, k_2 \leq \sqrt{4\pi}. \tag{6}$$

We further check vacuum stability using Vevacious [46] which minimizes the one-loop effective potential and checks that it is indeed the global minimum. We also require that one of the two scalars of the model is a valid SM Higgs, with mass in the range 124.7 GeV $\leq m_{h,H} \leq$ 127.1 GeV. We allow for a wider range of Higgs masses than the experimental uncertainty as an estimate of the theoretical uncertainty associated with the calculation of the mass spectrum.

These constraints already invalidate much of the parameter space, but we must also apply experimental constraints from the LHC, LEP, and Tevatron to ensure they are phenomenologically viable. To this end, we employ HiggsBounds [47] and HiggsSignals [48], and further use sHDECAY [49–51] to calculate the total widths and branching ratios for each parameter choice.

In the Dark Matter phase we must also include constraints from the dark matter, using micrOMEGAS [52] to calculate the relic density to compare with the combined WMAP [53] and Planck [54] result,

$$\Omega h^2 = 0.1199 \pm 0.0027. \tag{7}$$

A point is excluded if the calculated relic density is greater than $\Omega h^2 + 3\sigma$ to ensure that a DM candidate does not overclose the universe, but we allow for the possibility that there may be some other contributions to the relic density which we are not taking into account. We also include constraints from dark matter direct detection that place limits on the spin independent cross section of weakly interacting massive particles (WIMPs) on nucleons. The strongest of those constraints comes from the LUX experiment [55].

We present the results of the analysis of the broken phase in **Figure 4**, where we see lots of parameter choices pass the theoretical and experimental constraints, although only a few of these obey the MPP criterion of the quartic couplings being small. We are interested in points that fall in the lower left corner of **Figures 4A–C** as well as those to the left in **Figure 4D**. To further aid in the discrimination of small values we have colored red those points for which $\beta_\lambda < 0.0009$, $\beta_{\lambda_S} < 0.019$, and $\beta_{k_2} < 0.0045$, which is an estimate of the truncation error in their high scale values as estimated by the difference between the one and two loop Renormalization Group running.

These reasonably numerous red points indicate parameter choices for which there is indeed a second approximately degenerate vacuum at the Planck scale, that provide the correct Higgs boson mass and conform to all low energy observations. This remarkable result need not have been the case. Unfortunately we have also lost predictive power. The SM Higgs mass is fixed by our constraints, so not a prediction and the new Higgs mass can take on a rather wide range of values between 200 GeV and 2 TeV.

It is much more difficult to accommodate the MPP in the Dark Matter phase, as can bee seen in **Figure 5**, which is in part due to the extra constraint from Dark Matter which considerably reduces the acceptable points. We do see parameter choices that evade all constraints with very small values of the β-functions (red points) but these often have rather large values of the quartic couplings. This is especially true for κ_2 but is also true, to a lesser degree, for λ.

4. A COMPLEX SINGLET EXTENSION

We may complicate the model only slightly be promoting our new singlet to a complex field, $\mathbb{S} = S_1 + iS_2$, and consider a potential of the form [33, 50, 56–60]

$$V = \frac{\mu^2}{2} H^\dagger H + \frac{\lambda}{4}\left(H^\dagger H\right)^2 + \frac{\delta}{2}\left(H^\dagger H\right)|\mathbb{S}|^2 + \frac{b_2}{2}|\mathbb{S}|^2 + \frac{d_2}{4}|\mathbb{S}|^4 + \left(\frac{b_1}{4}\mathbb{S}^2 + a_1\mathbb{S} + c.c\right). \tag{8}$$

For computational convenience we define

$$b_\pm = \frac{1}{2}\left(b_2 \pm b_1\right), \tag{9}$$

which function as the (squared) masses if the model is recast as two real scalar fields. The complex singlet field may acquire a non-zero vev for its real, and possibly imaginary, part. If both real and imaginary parts acquire non-zero vevs,

$$\mathbb{S} = \frac{1}{\sqrt{2}}\left[v_{s_1} + s_1 + i\left(v_{s_2} + s_2\right)\right], \tag{10}$$

we again call this the "broken phase" following our earlier nomenclature (introduced in [59]). Therefore, in addition to the bilinear terms μ^2 and $b_\pm$ which are fixed via the electroweak vacuum minimization conditions, the model is described by

$$\lambda, \quad d_2, \quad \delta, \quad v_{s_1}, \quad v_{s_2}, \quad a_1. \tag{11}$$

In this phase, all three scalar field fluctuations h, s_1 and s_2 mix.

In contrast, if the vev of the imaginary part remains zero, the second electroweak vacuum minimization condition (for S_2) is trivial and b_- becomes a free parameter. In this case the input parameters are

$$\lambda, \quad d_2, \quad \delta, \quad v_{s_1}, \quad b_-, \quad a_1. \tag{12}$$

Now we find ourselves in the "dark matter phase," where mixing is allowed between h and the real part of the complex singlet field s_1. The imaginary part s_2 does not mix and is a dark matter candidate kept stable by the symmetry $S_2 \to -S_2$.

The numerical analysis of this model follows closely with that of the real singlet extension discussed above. We scan over λ, d_2, and δ, allowing them to vary between 0 and 0.5; v_{s_1} and v_{s_2}, if present, are allowed to take values up to 2 TeV; b_- has

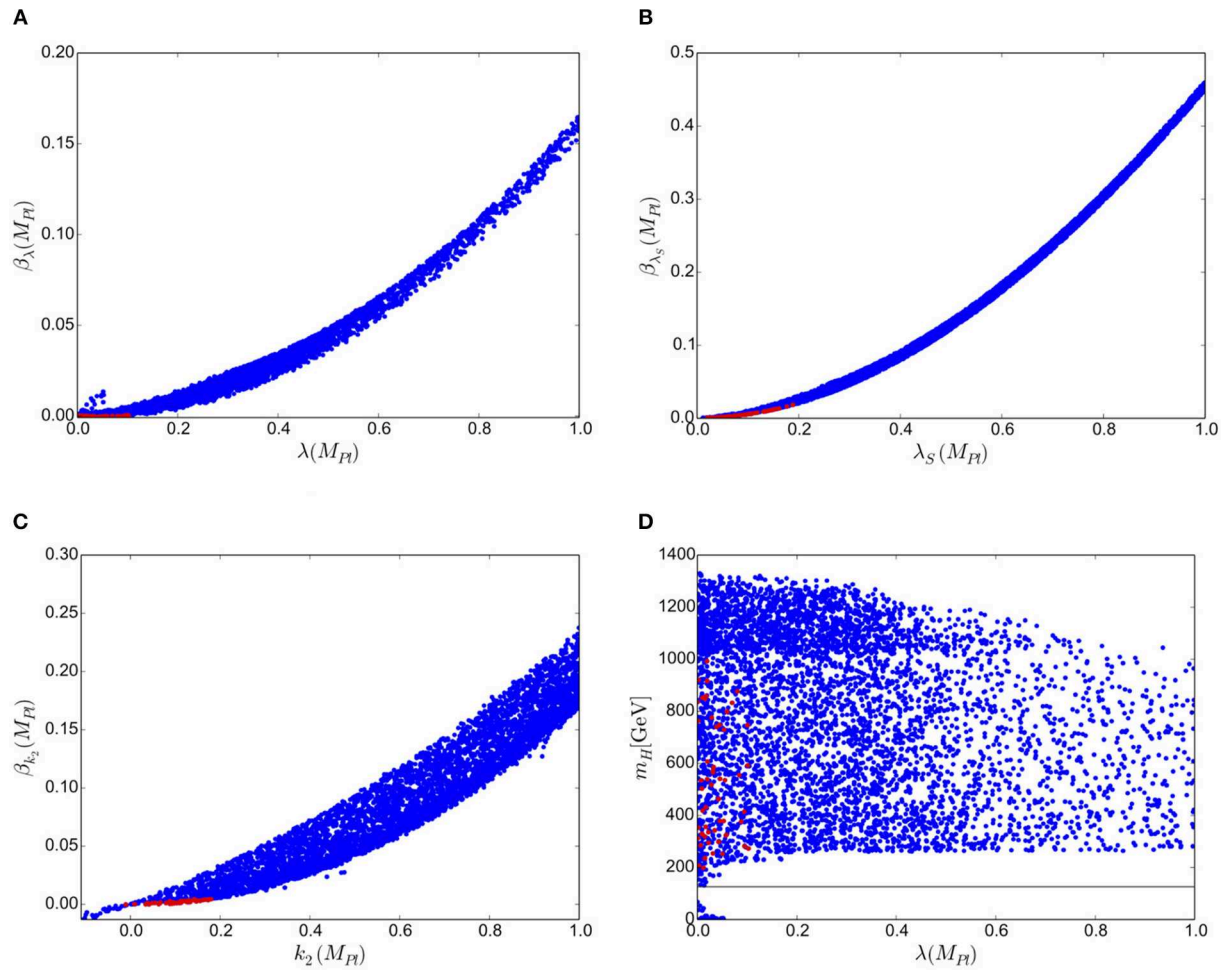

FIGURE 4 | Values of **(A)** $\lambda(M_{\rm Pl})$, **(B)** $\lambda_S(M_{\rm Pl})$ and **(C)** $\lambda(M_{\rm Pl})$ compared to their respective β-functions in the broken phase. All points pass theoretical and experimental constraints. Red points further obey $\beta_\lambda < 0.0009$, $\beta_{\lambda_S} < 0.019$, $\beta_{k_2} < 0.0045$ at M_{Pl}. Also shown **(D)** is the mass of the additional Higgs for values of $\lambda(M_{\rm Pl})$.

dimension mass^2 and is allowed to range to 10^5 GeV^2. Finally a_1, with dimension mass^3 and is allowed up to 10^8 GeV^3.

We make use of SARAH and FlexibleSUSY again (though slightly older versions, 4.9.3 and 1.6.1, respectively). Constraints on vacuum stability and perturbativity are again applied; in this case stability requires [58]

$$\lambda, d_2 \geq 0, \qquad \delta + \sqrt{\lambda d_2} \geq 0. \tag{13}$$

The global minimum is ensured with Vevacious. Finally, we allowed the same Higgs mass range as before and apply experimental constraints using HiggsBounds, and HiggsSignals [48], and sHDECAY. MicrOMEGAS is used to provide constraints from Dark Matter in the Dark Matter phase. For further details of this analysis (see [9]).

We are in principle interested in the high scale constraints $\lambda = \beta_\lambda = 0$, $d_2 = \beta_{d_2} = 0$ and $\delta = \beta_\delta = 0$. However, similar to the real scalar case, we note that setting δ to zero at $M_{\rm Pl}$ decouples the extra scalars from the SM, and since $\beta_\delta = 0$ for this choice, δ remains zero at all scales and the new scalars are unobservable. We are therefore forced to only consider δ "small." The situation for d_2 is slightly more subtle—for non-zero values of δ, we cannot set d_2 exactly to zero at $M_{\rm Pl}$ since it is immediately driven negative by RG running and the vacuum destabilizes according to (13). So again, we are forced to only consider d_2 "small" at the Planck scale and indeed must keep it large enough at $M_{\rm Pl}$ to stop it running negative. Fortunately this is not too onerous, and stability is still viable with d_2 as small as 0.005 at the Planck scale, but it is not really clear how large we should permit this to be and still regard the MPP as "approximately valid."

In the broken phase, we now have three neutral scalars that mix. One must provide the SM Higgs, while we will call the other two $m_{h_{\rm Light}}$ and $m_{h_{\rm Heavy}}$. Obviously $m_{h_{\rm Light}} < m_{h_{\rm Heavy}}$, but that $h_{\rm Light}$ may still be heavier than the SM-like Higgs, or correspondingly $h_{\rm Heavy}$ may be lighter. We note that these new states may be considerably lighter than the discovered Higgs mass as long as the component from the doublet is not too large, leaving it relatively decoupled.

This time we will look first at surviving scenarios in the $m_{h_{Light}} - m_{h_{Heavy}}$ plane, with small values of λ and β_λ at the high

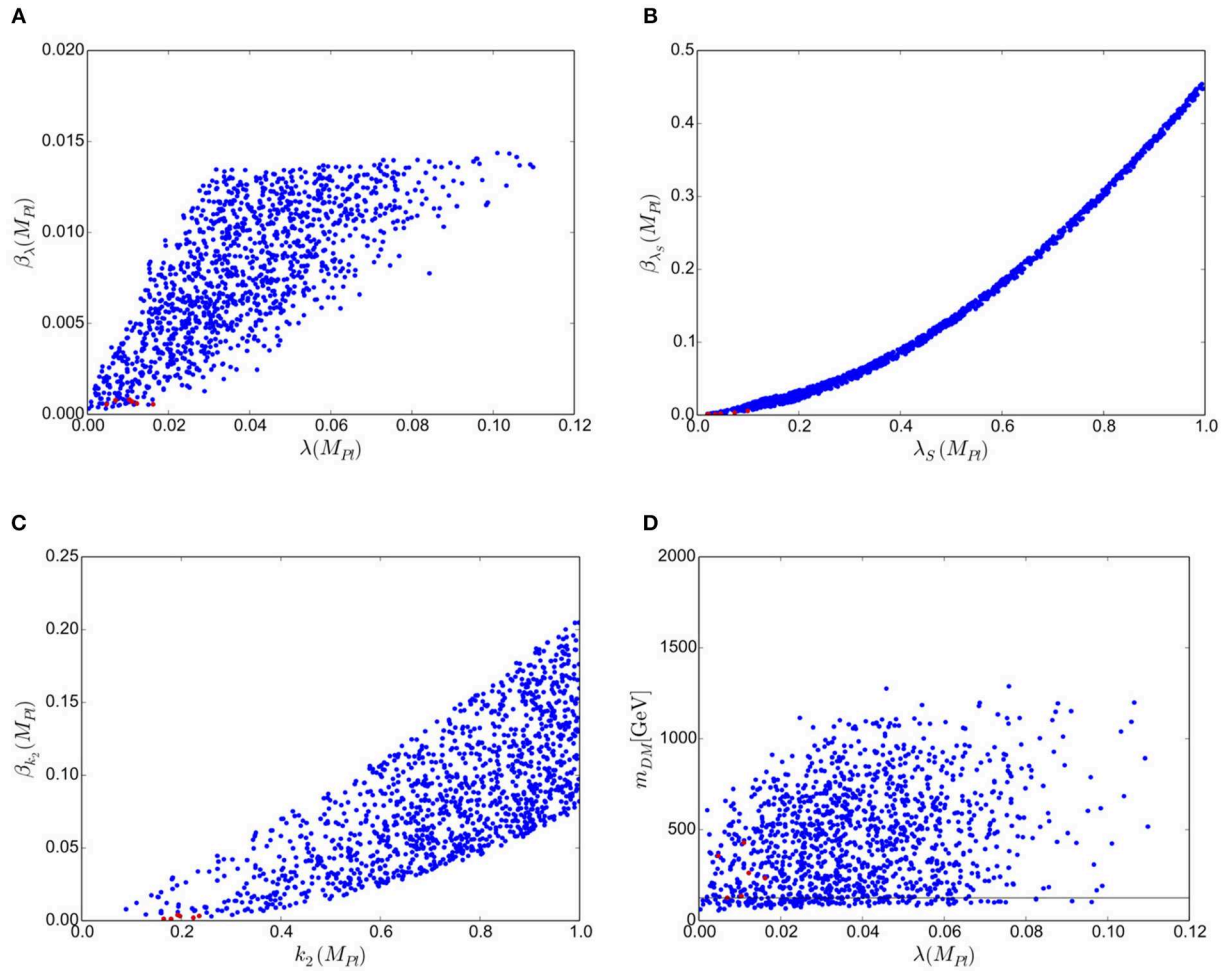

FIGURE 5 | Values of **(A)** $\lambda(M_{\mathrm{Pl}})$, **(B)** $\lambda_S(M_{\mathrm{Pl}})$ and **(C)** $\lambda(M_{\mathrm{Pl}})$ compared to their respective β-functions in the Dark Matter phase. All points pass theoretical and experimental constraints. Red points further obey $\beta_\lambda < 0.0009$, $\beta_{\lambda_S} < 0.019$, $\beta_{k_2} < 0.0045$ at M_{Pl}. Also shown **(D)** is the mass of the additional scalar for values of $\lambda(M_{\mathrm{Pl}})$.

scale. In **Figure 6A** we see scenarios that survive all theoretical and experimental constraints. For clarity of the plot, we restrict our points to those with $\lambda < 0.067$ and $\beta_{\lambda,\delta,d_2} < 0.05$ at M_{Pl}. Points shown in red have been further restricted to have exceptionally small values of $\beta_\lambda < 0.00005$, which is the appropriate truncation error arising from the RG running. Corresponding restrictions on β_δ and β_{d_2} would be $\beta_\delta < 0.00025$ and $\beta_{d_2} < 0.001$, but unfortunately we find if we apply these then no points survive.

However, we are reluctant to declare the MPP incompatible with the complex singlet extension. These restrictions on the β-functions are exceedingly severe and may be too strong. Without knowing the form of the UV completion, we don't know the size of any possible threshold corrections that might arise was we approach the Planck scale, so really don't know how much deviation from zero we should allow in our boundary conditions. To allow some extra slack, we can somewhat arbitrarily relax our boundary condition β-function cut-offs to ten times the truncation error. We now find some points survive and plot these in **Figure 6B**. Notice that a small number of points survive that have the SM Higgs as the heaviest of the three scalars.

In the dark matter phase only two of the three scalars are allowed to mix, with the third becoming a dark matter candidate. We call the non-SM-like Higgs h_{New} whilst the DM scalar is h_{DM}. **Figure 7A** examines these extra scalar masses when we restrict λ and β_λ to be consistent with zero. Again, for clarity of the plot, we show only points with $\beta_\lambda < 0.05$ in blue before demonstrating the effect of the constraint $\beta_\lambda < 0.00005$ in red. It is interesting to note that no points with $m_{h_{New}} < m_{h_{SM}}$ survive the stronger constraint on β_λ, and the majority of the points that do survive have almost degenerate masses of $m_{h_{New}}$ and $m_{h_{DM}}$. The tree level masses of $m_{h_{New}}$ ($m_{h_{DM}}$) have a linear dependence on a_1 (b_-) which appears to dominate when both of the additional scalars are heavier than the SM Higgs.

Figure 7A might suggest that small values of the β functions at the Planck scale correlates with a small mass difference

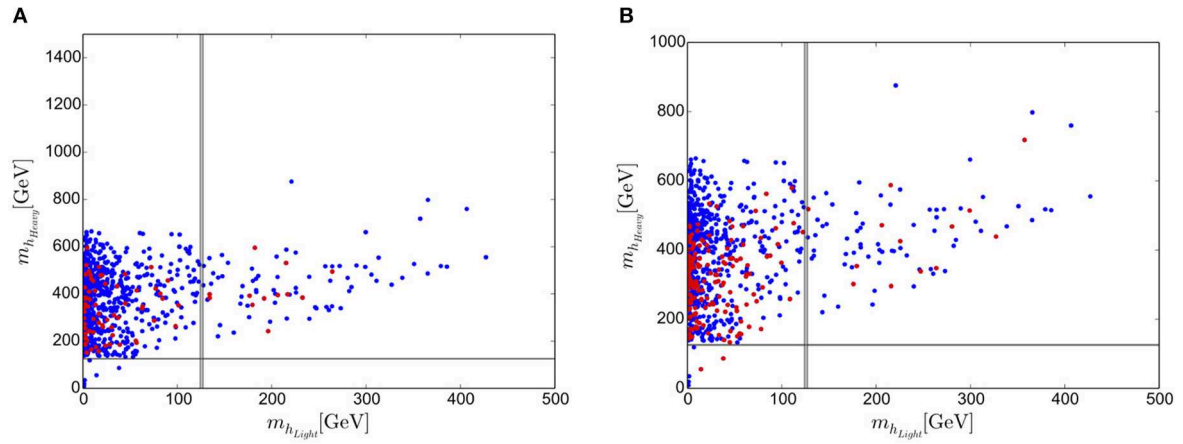

FIGURE 6 | Values of $m_{h_{Light}}$ and $m_{h_{Heavy}}$ in the broken phase. All points obey $\lambda < 0.067$ and $\beta_{\lambda,\delta,d_2} < 0.05$ at $M_{\rm Pl}$. The gray bands highlight the SM Higgs mass range. **(A)** Red points obey the more restrictive condition $\beta_\lambda < 0.00005$. **(B)** Red points obey $\beta_\lambda < 0.0005$, $\beta_\delta < 0.0025$ and $\beta_{d_2} < 0.01$. These plots originally appeared in McDowall and Miller [9].

$\Delta m = |m_{h_{New}} - m_{h_{DM}}|$. However, while 80% of the points that pass through the constraint $\lambda < 0.067, \beta_\lambda < 0.00005$ result in $\Delta m < 40$ GeV, so do 67% of the points that don't. This tendency toward degeneracy is a feature of all of the points that satisfy the theoretical constraints. These points exhibit small values of the soft $U(1)$ breaking parameters a_1 and b_1, forcing a small Δm [50]. It is interesting to note that many points in the degenerate mass region can completely account for the dark matter relic density. The degeneracy opens up co-annihilation channels involving both $m_{h_{DM}}$ and $m_{h_{New}}$ that enter the relic density calculation [61, 62]. These new channels help bring down the relic density to within the 3σ range.

As in the broken phase, no DM phase points survive when the severe truncation error cut-offs are applied simultaneously with the experimental constraints. However, we see scenarios survive if we relax the constraints by a factor of 10. These scenarios are shown in **Figure 7B**.

5. THE TWO HIGGS DOUBLET MODEL

Finally we will examine models with two Higgs doublets to see if they are compatible with the MPP. The most general potential of the Two Higgs Doublet Model (2HDM) (see [63] for a useful review) is,

$$\begin{aligned} V(H_1,H_2) &= m_{11}^2 H_1^\dagger H_1 + m_{22}^2 H_2^\dagger H_2 - \left(m_{12}^2 H_1^\dagger H_2 + c.c\right) \\ &+\lambda_1 \left(H_1^\dagger H_1\right)^2 + \lambda_2 \left(H_2^\dagger H_2\right)^2 + \lambda_3 \left(H_1^\dagger H_1\right)\left(H_2^\dagger H_2\right) \\ &+\lambda_4 \left(H_1^\dagger H_2\right)\left(H_2^\dagger H_1\right) + \left(\frac{\lambda_5}{2}\left(H_1^\dagger H_2\right)^2\right. \\ &\left.+\lambda_6 \left(H_1^\dagger H_1\right)\left(H_1^\dagger H_2\right) + \lambda_7 \left(H_2^\dagger H_2\right)\left(H_1^\dagger H_2\right) + c.c\right), \end{aligned} \tag{14}$$

where the two Higgs-doublets themselves are given by,

$$H_n = \begin{pmatrix} \chi_n^+ \\ \left(H_n^0 + iA_n^0\right)/\sqrt{2} \end{pmatrix}, \quad n = 1, 2. \tag{15}$$

The parameters m_{11}^2, m_{22}^2 and $\lambda_{1,2,3,4}$ are real, whilst m_{12}^2 and $\lambda_{5,6,7}$ can in principle be complex and induce CP violation. During electroweak symmetry breaking the neutral components of the Higgs fields, H_n^0, develop vacuum expectation values (vevs) $\langle H_n^0 \rangle = v_n/\sqrt{2}$. The relationship to the SM vev $v = \sqrt{v_1^2 + v_2^2} = 246$ GeV is determined by the Fermi constant but the ratio of the vevs, $\tan\beta = v_2/v_1$, is a free parameter. The physical scalar sector of the model includes two neutral scalar Higgs h and H, a pseudoscalar Higgs A and the charged Higgs $H^\pm$.

It's clear that the 2HDM potential is considerably more complicated than its Standard Model counterpart, so it's common to employ additional global symmetries to increase the predictivity of the model. There are only six possible types of global symmetry that have a distinctive effect on the potential [64, 65]. The 2HDM has been considered for suitability of the MPP in Froggatt et al. [66, 68–70], Laperashvili [67], and McDowall and Miller [71], though all but the last of these predate the Higgs discovery so could not be confronted with the measured Higgs mass. Froggatt et al. [70] is notable in that it shows that the MPP itself may be used as a mechanism for suppressing CP-violation and Flavor Changing Neutral Currents (FCNCs).

In McDowall and Miller [71] we took the more usual route of implementing a $\mathbb{Z}_2$ symmetry to forbid FCNCs by allowing only one type of fermion to couple to one Higgs doublet. This requirement sets λ_6, λ_7 and m_{12} to zero. Following McDowall and Miller [71]'s treatment, we may then softly break this $\mathbb{Z}_2$ by re-introducing a (real) non-zero m_{12}. We will restrict ourselves to a Type-II model where up-type quarks and leptons couple to the first Higgs-doublet and down-type quarks to the second Higgs-doublet, though we note that the most significant effect of the Yukawa sector comes from which doublet the top-quark couples

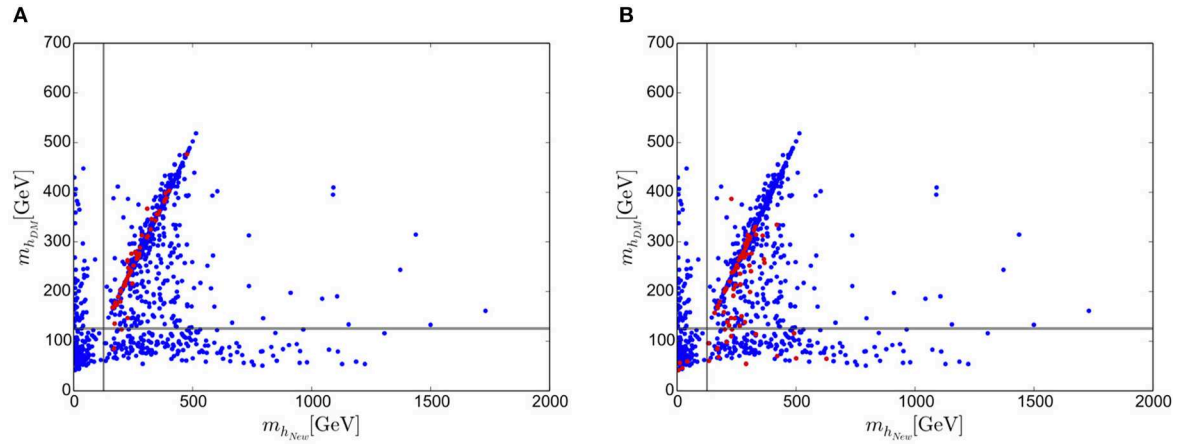

FIGURE 7 | Values of $m_{h_{Light}}$ and $m_{h_{Heavy}}$ in the DM phase. All points obey $\lambda < 0.067$ and $\beta_{\lambda,\delta,d_2} < 0.05$ at $M_{\rm Pl}$. The gray bands highlight the SM Higgs mass range. **(A)** Red points obey the more restrictive condition $\beta_\lambda < 0.00005$. **(B)** Red points obey $\beta_\lambda < 0.0005$, $\beta_\delta < 0.0025$ and $\beta_{d_2} < 0.01$. These plots originally appeared in McDowall and Miller [9].

to, so results for other 2HDM Yukawa assignments would be very similar to those for Type-II.

For each parameter point the model is described by the bilinear terms m_{11} and m_{22}, which are replaced by M_Z and $\tan\beta$ by applying the electroweak vacuum minimization conditions, as well as the additional input parameters, m_{12} and $\lambda_i(M_{\rm Pl})$ with $i = 1\ldots5$. As previously we use SARAH to calculate the two-loop β functions, which are used by FlexibleSUSY to run the couplings between M_Z and $M_{\rm Pl}$.

We also consider a simpler model, the Inert Doublet Model (IDM), where we introduce an additional unbroken $\mathbb{Z}_2$ symmetry, under which the new doublet has odd parity but all other fields are even (see [72] for a useful review). The scalar sector now consists of the SM Higgs field H and an inert doublet Φ, with mixing between the two forbidden by the new symmetry. The inert doublet does not couple to any of the SM fields and does not gain a vacuum expectation value.

The potential is,

$$\begin{aligned} V(H,\Phi) = {} & m_{11}^2 H^\dagger H + m_{22}^2 \Phi^\dagger\Phi + \lambda_1\left(H^\dagger H\right)^2 + \lambda_2\left(\Phi^\dagger\Phi\right)^2 \\ & + \lambda_3\left(H^\dagger H\right)\left(\Phi^\dagger\Phi\right) + \lambda_4\left(H^\dagger\Phi\right)\left(\Phi^\dagger H\right) \\ & + \left(\frac{\lambda_5}{2}\left(H^\dagger\Phi\right)^2 + c.c\right). \end{aligned} \tag{16}$$

Once again the quartic coupling can have complex values, but we will focus on the real-valued case. Note that now the mixing term proportional to m_{12}^2 is absent. During electroweak symmetry breaking the neutral component of the SM Higgs doublet acquires a vacuum expectation value $v = 246\,\text{GeV}$. The neutral Higgs h corresponds to the SM Higgs boson whilst H, A, and $H^\pm$ are inert scalars. The lightest of these is stable thanks to the $\mathbb{Z}_2$ symmetry and, assuming it is one of the neutral scalars H or A, it is a potential Dark Matter (DM) candidate [73, 74].

As in the previous case, the mass term associated with the SM Higgs doublet m_{11}^2 is fixed via the electroweak minimization conditions, but now we don't have a second vev to fix m_{22}^2, which must remain an input. Our input parameters are therefore m_{22} and $\lambda_i(M_{\rm Pl})$ with $i = 1\ldots5$. As in the Type-II model, we use SARAH and FlexibleSUSY to calculate the mass spectrum and to run couplings between the low and high scales of interest.

Valid points in our parameter space scan must be perturbative up to the Planck scale. For the Higgs quartic couplings this requires them to satisfy $\lambda_i < \sqrt{4\pi}$ up to M_{Pl}. We require points that are bounded from below at all scales up to M_{Pl} [75]. To that end we check if the boundedness conditions [63],

$$\begin{aligned} \lambda_1, \lambda_2 &> 0, \\ \lambda_3 &> -2\sqrt{\lambda_1\lambda_2}, \\ \lambda_3 + \lambda_4 - |\lambda_5| &> -2\sqrt{\lambda_1\lambda_2}, \end{aligned} \tag{17}$$

are met at all scales [76, 77].

The goal for the MPP is to have an additional minimum at $M_{\rm Pl}$, degenerate with the electroweak minimum,. This is naively satisfied if all of the quartic couplings are zero at $M_{\rm Pl}$, i.e., $\lambda_i = 0, i = 1\ldots5$. However, the RG running of λ_1 and λ_2 results in an unstable vacuum configuration [66–69]. It is also possible for degenerate vacua to exist within the 2HDM if we relax the condition $\lambda_i = 0$. Specifically, by allowing λ_1, λ_2, λ_3, and λ_4 to be non-zero at $M_{\rm Pl}$, the following conditions [66] are consistent with the implementation of the MPP at $M_{\rm Pl}$;

$$\begin{aligned} \lambda_5(M_{\rm Pl}) &= 0 \\ \lambda_4(M_{\rm Pl}) &< 0 \\ \tilde{\lambda}(M_{\rm Pl}) = \sqrt{\lambda_1\lambda_2} + \lambda_3 + \min(0,\lambda_4) &= 0 \\ \beta_{\tilde{\lambda}}(M_{\rm Pl}) &= 0. \end{aligned} \tag{18}$$

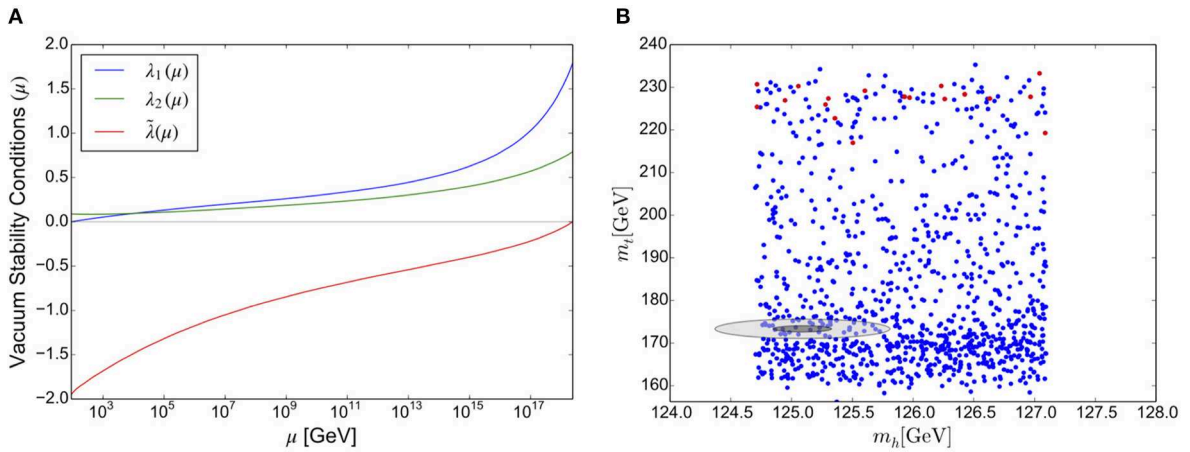

FIGURE 8 | (A) Example running of λ_1, λ_2, and $\tilde{\lambda}$ for a point that provides valid masses for the SM Higgs and the top quark in the Type-II Two Higgs Doublet Model. Boundedness from below and vacuum stability requires that all three couplings are positive at all scales. **(B)** Results of our Multiple Point Principle scan in the $m_h - m_t$ plane of the Type-II Two Higgs Doublet Model. The blue points provide valid SM higgs masses whilst the red points also pass the vacuum stability conditions at all scales. The ellipses show the experimentally allowed values of m_t and m_h at $1\,\sigma$ (dark gray) and $3\,\sigma$ (light gray) uncertainty. These plots originally appeared in McDowall and Miller [71].

To investigate whether these MPP conditions in the Type-II 2HDM are consistent with the current experimental constraints on the SM Higgs mass m_h and the top-quark mass m_t, we generated points in the parameter space, applying the theoretical constraint of vacuum stability at all scales. **Figure 8A** shows an example of the running of λ_1, λ_2 and $\tilde{\lambda}$ for a point that results in experimentally valid values of the SM Higgs mass and the top-quark mass, and is also consistent with the MPP conditions of (18). Vacuum stability requires that all of these couplings remain greater than zero at all scales, but the negative running of $\tilde{\lambda}$ pulls it to negative values.

Figure 8B shows an investigation of the $m_h - m_t$ plane, where we temporarily suspend vacuum stability to demonstrate the effect. We see plenty of valid points in blue, where vacuum stability is not required. However, the points that satisfy the vacuum stability conditions, highlighted in red, have larger values of the top Yukawa y_t which positively contribute to the running of the quartic couplings. The larger required y_t corresponds to a top mass in the range $220 \lesssim m_t \lesssim 230\,\text{GeV}$ which is not compatible with current experimental bounds on the top-quark mass.

These MPP constraints also apply to the Inert Doublet Model. We examined the IDM parameter space as we did for the Type-II 2HDM, applying the MPP conditions at M_{Pl} and requiring valid points to be stable up to the Planck scale and to have a SM Higgs candidate.

Figure 9 shows the running of the quartic couplings λ_1, λ_2, and $\tilde{\lambda}$ for an example point in our scan that provided a valid SM Higgs and top mass. As in the Type-II model, a stable vacuum requires all three of these couplings to be positive at all scales. Clearly this point fails our vacuum stability test, and unfortunately it is representative of the other points in our scan. We found *no points* that could simultaneously satisfy the constraints of perturbativity, vacuum stability and the requirement of a realistic SM mass spectrum. Specifically, there are points that provide valid SM Higgs and top masses, but all of these points fail the condition $\tilde{\lambda} > 0$. In fact, we found no points that could satisfy the MPP conditions outlined in (18) that remained stable up to the Planck scale, regardless of their Higgs or top masses. This therefore suggests that the multiple point principle cannot be implemented successfully in the Inert Doublet Model.

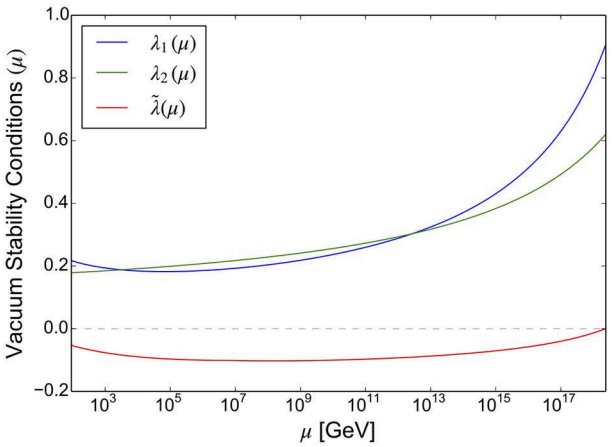

FIGURE 9 | Example running of λ_1, λ_2, and $\tilde{\lambda}$ for a point that provides valid masses for the SM Higgs and the top quark in the Inert Doublet Model. Boundedness from below and vacuum stability requires that all three couplings are positive at all scales. This plot originally appeared in McDowall and Miller [71].

6. MORE EXOTIC MODELS

The MPP has also been applied to several other models of new physics, of varying degrees of complexity. For example, Hamada

and Kawana [78] consider one of the more minimal extensions by including either a Majorana fermion triplet or a real scalar triplet, and in both cases were able to find good agreement with the MPP by keeping the new states rather heavy (of order 10^{16} GeV for the fermion triplet and slightly higher for the scalar).

Bennett et al. [79] studies what the authors term an "anti-GUT" within the context of the SM. This is a model where each generation comes with a full complement of the SM gauge groups, augmented with an additional local $U(1)$, so that the full group (at high energies) is $[SU(3) \times U(2) \times U(1)]^3 \times U(1)$. The resulting Higgs mass prediction is 139 ± 16 GeV, though the uncertainty in this prediction would no doubt be significantly reduced with more modern inputs, and they also find reasonable agreement with the SM Yukawa couplings.

Another proposed alternative is to mix a fundamental scalar with the scalar bound states of a new strongly interacting gauge symmetry [80]. This allows for the dynamical generation of the Higgs mass, with a classically scale invariant theory satisfying the MPP condition. They predict new scalar states at approximately 300 GeV as well as a new gauge boson coupling to the SM fermions.

The MPP may also be used to constrain theories with extra dimensions. Hamada and Shiu [81] examines the SM compactified at high scales onto S^1 and T^1, additionally applying the MPP. They find this constrains the neutrinos in the model to have Dirac masses, with the lightest of order $1 - 10$ meV. This would prevent neutrinoless double-beta decay and have interesting cosmological consequences.

An more exotic suggestion comes from the original authors of the MPP: the existence of a bound state made of six top-quarks and six anti-top-quarks [82–87]. They postulate a new phase different from and degenerate with the standard electroweak Higgs phase, caused by the condensation of this new top-anti-top bound state. They claim this bound state arises from the exchange of Higgs bosons due to the large top Yukawa coupling. Therefore the MPP is extended to insist on not just two, but three degenerate vacua: two at low energies and one at the Planck scale. The authors also claim that the extra energy density of this new bound state provides a solution for the cosmological constant problem.

7. SUMMARY AND CONCLUSIONS

The measured value of the Higgs boson mass implies that, if the SM is true to high scales, the Higgs quartic coupling and its β-function are intriguingly close to zero at the Planck scale. Indeed, their values imply that the SM vacuum is metastable, with a slightly deeper vacuum at the Planck scale.

One suggested explanation for this is the *Multiple Point Principle*. By considering *extensive* variables, nature tends to choose Higgs parameters so that different phases of Electroweak symmetry breaking may coexist. This predicts a second degenerate vacuum at the Planck scale, rather similar to that implied by the Higgs measurements. An analysis of the MPP in the SM provides a prediction of the Higgs mass, $m_h = 129 \pm 1.5$ Gev which is slightly above the measured value. It is therefore interesting to ask how extensions to the SM might change this picture, especially since we do expect new physics to appear well before the Planck scale. In this paper, we have reviewed the compatibility of the MPP with simple Higgs sector extensions, considering both extra scalars and doublets.

We began our review of extended models by considering an additional real scalar field, in both the broken and Dark Matter phases. We had to weaken the MPP constraints somewhat in order to prevent the extra states from decoupling, but found promising results. These real scalar extensions were both compatible with the (relaxed) MPP, though working scenarios in the Dark Matter case were rare due to the additional Dark Matter constraints. Unfortunately the MPP didn't prove very predictive because it left us with a wide range of allowed additional scalar masses.

The next extension we considered was an extra complex singlet, where again we had to relax the MPP condition in order to prevent decoupling. We also found that we were unable to keep the parameter d_2 very small at the Planck scale since it tended to run negative, destabilizing the vacuum. Furthermore, our constraints setting the β-functions for the Higgs parameters to zero could not all be accommodated simultaneously while keeping viable low energy phenomenology. However, relaxing these constraints somewhat did again yield scenarios that are stable, evade experimental constraints, have the correct Higgs mass, and in the Dark Matter phase, provide the correct relic density.

Finally we investigated the Type-II Two Higgs Doublet Model and the Inert Doublet Model. Models with a second Higgs doublet have much more flexibility in their scalar potential, which one might expect gives them more freedom to accommodate the boundary conditions of the MPP. However, we found that both the Type-II 2HDM and the IDM cannot satisfy the conditions required at the Planck scale by the MPP. Specifically, we found no points in either model's parameter space that was consistent with the MPP whilst also having a valid SM Higgs, an experimentally acceptable top quark mass, and a stable vacuum. In the Type-II case we found that a stable vacuum would require a top mass on the order of 230 GeV, whilst in the Inert case we found no points at all that could meet our theoretical requirements. The results of our analysis would suggest that the Multiple Point Principle is not compatible with the Two Higgs Doublet Models that we investigated.

In general it seems rather difficult to accommodate an *exact* MPP in any of these models. There are several possible explanations for this. Firstly the MPP conditions may only hold approximately. The original conjecture that there should be a second degenerate vacuum at the Planck scale was itself based on general arguments, and may be realized with some slight modifications. Indeed, one might expect threshold corrections for the new theory to become significant as we approach the Planck scale, slightly modifying the RG running. Secondly, we do expect new physics before the Planck scale to solve the many deficiencies of the SM. It could be that this new physics alters the Higgs running sufficiently to allow the MPP to hold more exactly. It would be interesting to examine the SM Higgs sector with alternative additions, such as vector-like fermions. Finally, the literature thus far has entirely neglected finite temperature effects in

the study of the MPP. Such effects could very well alter the vacuum structure.

Ultimately the question remains, is the peculiar behavior of the SM Higgs potential at the Planck scale a coincidence or a sign of new physics?

AUTHOR CONTRIBUTIONS

The text of this review was written by DM. The research itself was performed jointly by DM and JM, with DM taking a lead role as supervisor.

FUNDING

DM acknowledges partial support from the STFC grants ST/L000446/1 and ST/P000746/1.

ACKNOWLEDGMENTS

The authors would like to thank Peter Athron for invaluable help with FlexibleSUSY; as well as Karl Nordstrom, António Morais, and David Sutherland for useful discussions.

REFERENCES

1. Aad G, Abajyan T, Abbott B, Abdallah J, Abdel Khalek S, Abdelalim AA, et al. Observation of a new particle in the search for the Standard Model Higgs boson with the ATLAS detector at the LHC. *Phys. Lett.* (2012) **B716**:1–29. doi: 10.1016/j.physletb.2012.08.020
2. Aad G, Abbott B, Abdallah J, Abdinov O, Aben R, Abolins M, et al. Combined measurement of the Higgs Boson Mass in *pp* collisions at $\sqrt{s} = 7$ and 8 TeV with the ATLAS and CMS experiments. *Phys Rev Lett.* (2015) **114**:191803. doi: 10.1103/PhysRevLett.114.191803
3. Khachatryan V, Sirunyan AM, Tumasyan A, Adam W, Bergauer T, Dragicevic M, et al. Constraints on the spin-parity and anomalous HVV couplings of the Higgs boson in proton collisions at 7 and 8 TeV. *Phys Rev D.* (2015) **92**:012004. doi: 10.1103/PhysRevD.92.012004
4. Khachatryan V, Sirunyan AM, Tumasyan A, Adam W, Bergauer T, Dragicevic M, et al. Precise determination of the mass of the Higgs boson and tests of compatibility of its couplings with the standard model predictions using proton collisions at 7 and 8 TeV. *Eur Phys J C.* (2015) **75**:212. doi: 10.1140/epjc/s10052-015-3351-7
5. Aad G, Abbott B, Abdallah J, Abdinov O, Aben R, Abolins M, et al. Measurements of the Higgs boson production and decay rates and coupling strengths using pp collision data at $\sqrt{s} = 7$ and 8 TeV in the ATLAS experiment. *Eur Phys J C.* (2016) **76**:6. doi: 10.1140/epjc/s10052-015-3769-y
6. Buttazzo D, Degrassi G, Giardino PP, Giudice GF, Sala F, Salvio A, et al. Investigating the near-criticality of the Higgs boson. *J High Energy Phys.* (2013) **12**:089. doi: 10.1007/JHEP12(2013)089
7. Craig N. The state of supersymmetry after run I of the LHC. *arXiv: 1309.0528 [Preprint]* (2013).
8. Ross GG, Schmidt-Hoberg K, Staub F. Revisiting fine-tuning in the MSSM. *J High Energy Phys.* (2017) **03**:021. doi: 10.1007/JHEP03(2017)021
9. McDowall J, Miller DJ. High scale boundary conditions with an additional complex singlet. *Phys Rev D.* (2018) **97**:115042. doi: 10.1103/PhysRevD.97.115042
10. Froggatt CD, Nielsen HB. Standard model criticality prediction: top mass 173 +- 5-GeV and Higgs mass 135 +- 9-GeV. *Phys Lett B.* (1996) **368**:96–102. doi: 10.1016/0370-2693(95)01480-2
11. Degrassi G, Di Vita S, Elias-Miro J, Espinosa JR, Giudice GF, Isidori G, et al. Higgs mass and vacuum stability in the standard model at NNLO. *J High Energy Phys.* (2012) **08**:098. doi: 10.1007/JHEP08(2012)098
12. Holthausen M, Lim KS, Lindner M. Planck scale Boundary Conditions and the Higgs Mass. *J High Energy Phys.* (2012) **02**:037. doi: 10.1007/JHEP02(2012)037
13. Iacobellis G, Masina I. Stationary configurations of the Standard Model Higgs potential: electroweak stability and rising inflection point. *Phys Rev D.* (2016) **94**:073005. doi: 10.1103/PhysRevD.94.073005
14. Eichhorn A, Scherer MM. Planck scale, Higgs mass, and scalar dark matter. *Phys Rev D.* (2014) **90**:025023. doi: 10.1103/PhysRevD.90.025023
15. Khan N, Rakshit S. Study of electroweak vacuum metastability with a singlet scalar dark matter. *Phys Rev D.* (2014) **90**:113008. doi: 10.1103/PhysRevD.90.113008
16. Helmboldt AJ, Humbert P, Lindner M, Smirnov J. Minimal conformal extensions of the Higgs sector. *J High Energy Phys.* (2017) **07**:113. doi: 10.1007/JHEP07(2017)113
17. Bennett DL. Multiple point criticality, nonlocality, and fine tuning in fundamental physics: predictions for gauge coupling constants gives alpha**−1 = 136.8 +− 9. *arXiv:hep-ph/9607341 [Preprint]* (1996).
18. Coleman SR, Weinberg EJ. Radiative corrections as the origin of spontaneous symmetry breaking. *Phys Rev D.* (1973) **7**:1888–910. doi: 10.1103/PhysRevD.7.1888
19. Jegerlehner F, Kalmykov MYu, Kniehl BA. Self-consistence of the Standard Model via the renormalization group analysis. *J Phys Conf Ser.* (2015) **608**:012074. doi: 10.1088/1742-6596/608/1/012074
20. Bethke S, Dissertori G, Salam GP. *Particle Data Group Review on Quantum Chromodynamics* (2015). Available online at: http://pdg.lbl.gov/2015/reviews/rpp2015-rev-qcd.pdf
21. Ginsparg PH. Gauge and gravitational couplings in four-dimensional string theories. *Phys Lett B.* (1987) **197**:139–43. doi: 10.1016/0370-2693(87)90357-1
22. Witten E. Strong coupling expansion of Calabi-Yau compactification. *Nucl Phys B.* (1996) **471**:135–58. doi: 10.1016/0550-3213(96)00190-3
23. Robinson SP, Wilczek F. Gravitational correction to running of gauge couplings. *Phys Rev Lett.* (2006) **96**:231601. doi: 10.1103/PhysRevLett.96.231601
24. Pietrykowski AR. Gauge dependence of gravitational correction to running of gauge couplings. *Phys Rev Lett.* (2007) **98**:061801. doi: 10.1103/PhysRevLett.98.061801
25. Toms DJ. Quantum gravity and charge renormalization. *Phys Rev D.* (2007) **76**:045015. doi: 10.1103/PhysRevD.76.045015
26. Toms DJ. Quantum gravitational contributions to quantum electrodynamics. *Nature.* (2010) **468**:56–9. doi: 10.1038/nature09506
27. Mackay PT, Toms DJ. Quantum gravity and scalar fields. *Phys Lett B.* (2010) **684**:251–5. doi: 10.1016/j.physletb.2009.12.032
28. He HJ, Wang XF, Xianyu ZZ. Gauge-invariant quantum gravity corrections to gauge couplings via Vilkovisky-DeWitt method and gravity assisted gauge unification. *Phys Rev D.* (2011) **83**:125014. doi: 10.1103/PhysRevD.83.125014
29. Daum JE, Harst U, Reuter M. Running gauge coupling in asymptotically safe quantum gravity. *J High Energy Phys.* (2010) **01**:084. doi: 10.1007/JHEP01(2010)084
30. Haba N, Kaneta K, Takahashi R, Yamaguchi Y. Gravitational effects on vanishing Higgs potential at the Planck scale. *Phys Rev D.* (2015) **91**:016004. doi: 10.1103/PhysRevD.91.016004
31. Wang F, Liu GL, Wu K. Bounds on higgs and top quark masses from the other degenerate vacua near the planck scale with gravitational contributions. *Sci China Phys Mech Astron.* (2018) **61**:091011. doi: 10.1007/s11433-017-9179-1
32. Branchina V, Contino F, Pilaftsis A. Protecting the stability of the electroweak vacuum from Planck-scale gravitational effects. *Phys Rev D.* (2018) **98**:075001. doi: 10.1103/PhysRevD.98.075001
33. Robens T, Stefaniak T. Status of the Higgs singlet extension of the standard model after LHC Run 1. *Eur Phys J C.* (2015) **75**:104. doi: 10.1140/epjc/s10052-015-3323-y
34. Haba N, Kaneta K, Takahashi R. Planck scale boundary conditions in the standard model with singlet scalar dark matter. *J High Energy Phys.* (2014) **04**:029. doi: 10.1007/JHEP04(2014)029

35. Haba N, Ishida H, Kaneta K, Takahashi R. Vanishing Higgs potential at the Planck scale in a singlet extension of the standard model. *Phys Rev D.* (2014) **90**:036006. doi: 10.1103/PhysRevD.90.036006
36. Haba N, Ishida H, Okada N, Yamaguchi Y. Multiple-point principle with a scalar singlet extension of the Standard Model. *PTEP.* (2017) **2017**:013B03. doi: 10.1093/ptep/ptw186
37. Hamada Y, Kawai H, Oda Ky. Predictions on mass of Higgs portal scalar dark matter from Higgs inflation and flat potential. *J High Energy Phys.* (2014) **07**:026. doi: 10.1007/JHEP07(2014)026
38. Kawana K. Multiple point principle of the standard model with scalar singlet dark matter and right handed neutrinos. *PTEP.* (2015) **2015**:023B04. doi: 10.1093/ptep/ptv006
39. Kawana K. Multiple point principle of the gauged B-L model. In: *2nd Toyama International Workshop on Higgs as a Probe of New Physics (HPNP2015), Japan, February 11–15, 2015*. Toyama (2015).
40. Veltman MJG. The infrared - ultraviolet connection. *Acta Phys Polon B.* (1981) **12**:437.
41. Staub F. SARAH 4: a tool for (not only SUSY) model builders. *Comput Phys Commun.* (2014) **185**:1773–90. doi: 10.1016/j.cpc.2014.02.018
42. Athron P, Bach M, Harries D, Kwasnitza T, Park JH, Stöckinger D, et al. FlexibleSUSY 2.0: extensions to investigate the phenomenology of SUSY and non-SUSY models. *Comput Phys Commun.* (2018) **230**:145–217. doi: 10.1016/j.cpc.2018.04.016
43. Athron P, Park Jh, Stockinger D, Voigt A. FlexibleSUSY - A spectrum generator generator for supersymmetric models. *Comput Phys Commun.* (2015) **190**:139–72. doi: 10.1016/j.cpc.2014.12.020
44. Allanach BC. SOFTSUSY: a program for calculating supersymmetric spectra. *Comput Phys Commun.* (2002) **143**:305–31. doi: 10.1016/S0010-4655(01)00460-X
45. Allanach BC, Athron P, Tunstall LC, Voigt A, Williams AG. Next-to-minimal SOFTSUSY. *Comput Phys Commun.* (2014) **185**:2322–39. doi: 10.1016/j.cpc.2014.04.015
46. Camargo-Molina JE, O'Leary B, Porod W, Staub F. **Vevacious**: a tool for finding the global minima Of one-loop effective potentials with many scalars. *Eur Phys J C.* (2013) **73**:2588. doi: 10.1140/epjc/s10052-013-2588-2
47. Bechtle P, Brein O, Heinemeyer S, Stal O, Stefaniak T, Weiglein G, et al. HiggsBounds – 4: improved tests of extended higgs sectors against exclusion bounds from LEP, the tevatron and the LHC. *Eur Phys J C.* (2014) **74**:2693. doi: 10.1140/epjc/s10052-013-2693-2
48. Bechtle P, Heinemeyer S, Stal O, Stefaniak T, Weiglein G. *HiggsSignals*: confronting arbitrary Higgs sectors with measurements at the Tevatron and the LHC. *Eur Phys J C.* (2014) **74**:2711. doi: 10.1140/epjc/s10052-013-2711-4
49. Costa R, Mühlleitner M, Sampaio MOP, Santos R. Singlet extensions of the standard model at LHC run 2: benchmarks and comparison with the NMSSM. *J High Energy Phys.* (2016) **06**:034. doi: 10.1007/JHEP06(2016)034
50. Coimbra R, Sampaio MOP, Santos R. ScannerS: constraining the phase diagram of a complex scalar singlet at the LHC. *Eur Phys J C.* (2013) **73**:2428. doi: 10.1140/epjc/s10052-013-2428-4
51. Butterworth JM, Arbey A, Basso L, Belov S, Bharucha A, Braam F, et al. The tools and Monte Carlo working group summary report from the Les Houches 2009 workshop on TeV colliders. In: *Physics at TeV Colliders. Proceedings, 6th Workshop, dedicated to Thomas Binoth, June 8–26, 2009.* Les Houches (2010). Available online at: https://inspirehep.net/record/848006
52. Bélanger G, Boudjema F, Pukhov A, Semenov A. micrOMEGAs4.1: two dark matter candidates. *Comput Phys Commun.* (2015) **192**:322–9. doi: 10.1016/j.cpc.2015.03.003
53. Hinshaw G, Larson D, Komatsu E, Spergel DN, Bennett CL, Dunkley J, et al. Nine-year Wilkinson microwave anisotropy probe (WMAP) observations: cosmological parameter results. *Astrophys J Suppl.* (2013) **208**:19. doi: 10.1088/0067-0049/208/2/19
54. Ade PAR, Aghanim N, Arnaud M, Ashdown M, Aumont J, Baccigalupi C, et al. Planck 2015 results. XIII. Cosmological parameters. *Astron Astrophys.* (2016) **594**:A13. doi: 10.1051/0004-6361/201525830
55. Akerib DS, Alsum S, Araújo HM, Bai X, Bailey AJ, Balajthy J, et al. Results from a search for dark matter in the complete LUX exposure. *Phys Rev Lett.* (2017) **118**:021303. doi: 10.1103/PhysRevLett.118.021303
56. Barger V, Langacker P, McCaskey M, Ramsey-Musolf M, Shaughnessy G. Complex singlet extension of the standard model. *Phys Rev D.* (2009) **79**:015018. doi: 10.1103/PhysRevD.79.015018
57. Barger V, McCaskey M, Shaughnessy G. Complex scalar dark matter vis-à-vis CoGeNT, DAMA/LIBRA and XENON100. *Phys Rev D.* (2010) **82**:035019. doi: 10.1103/PhysRevD.82.035019
58. Gonderinger M, Lim H, Ramsey-Musolf MJ. Complex scalar singlet dark matter: vacuum stability and phenomenology. *Phys Rev D.* (2012) **86**:043511. doi: 10.1103/PhysRevD.86.043511
59. Costa R, Morais AP, Sampaio MOP, Santos R. Two-loop stability of a complex singlet extended Standard Model. *Phys Rev D.* (2015) **92**:025024. doi: 10.1103/PhysRevD.92.025024
60. Muhlleitner M, Sampaio MOP, Santos R, Wittbrodt J. Phenomenological comparison of models with extended Higgs sectors. *J. High Energ. Phys.* (2017) **2017**:132. doi: 10.1007/JHEP08(2017)132
61. Baker MJ, Brod J, El Hedri S, Kaminska A, Kopp J, Liu J, et al. The coannihilation codex. *J High Energy Phys.* (2015) **12**:120. doi: 10.1007/JHEP12(2015)120
62. Ghorbani K, Ghorbani H. Scalar split WIMPs in future direct detection experiments. *Phys Rev D.* (2016) **93**:055012. doi: 10.1103/PhysRevD.93.055012
63. Branco GC, Ferreira PM, Lavoura L, Rebelo MN, Sher M, Silva JP. Theory and phenomenology of two-Higgs-doublet models. *Phys Rept.* (2012) **516**:1–102. doi: 10.1016/j.physrep.2012.02.002
64. Ivanov IP. Minkowski space structure of the Higgs potential in 2HDM. *Phys Rev D.* (2007) **75**:035001. [Erratum: Phys. Rev. D76, 039902(2007)]. doi: 10.1103/PhysRevD.76.039902
65. Ferreira P, Haber HE, Santos E. Preserving the validity of the Two-Higgs Doublet Model up to the Planck scale. *Phys Rev D.* (2015) **92**:033003. doi: 10.1103/PhysRevD.92.033003
66. Froggatt CD, Laperashvili LV, Nevzorov RB, Nielsen HB, Sher M. The two Higgs doublet model and the multiple point principle. In: *Bled Workshops in Physics*. Vol. 5 (2004). p. 28–39.
67. Laperashvili LV. The Multiple point principle and Higgs bosons. *Phys Part Nucl.* (2005) **36**:S38–40.
68. Froggatt CD, Laperashvili L, Nevzorov R, Nielsen HB, Sher M. Implementation of the multiple point principle in the two-Higgs doublet model of type II. *Phys Rev D.* (2006) **73**:095005. doi: 10.1103/PhysRevD.73.095005
69. Froggatt CD, Nevzorov R, Nielsen HB, Thompson D. Fixed point scenario in the Two Higgs Doublet Model inspired by degenerate vacua. *Phys Lett B.* (2007) **657**:95–102. doi: 10.1016/j.physletb.2007.10.010
70. Froggatt CD, Nevzorov R, Nielsen HB. Multiple point principle as a mechanism for the suppression of FCNC and CP-violation phenomena in the 2HDM. In: *SUSY 2007 Proceedings, 15th International Conference on Supersymmetry and Unification of Fundamental Interactions, July 26 - August 1, 2007, Karlsruhe, Germany* (2007). p. 710–3. Available online at: http://inspirehep.net/record/792568
71. McDowall J, Miller DJ. High scale boundary conditions in models with two higgs doublets. *Phys Rev D.* (2019) **100**:015018. doi: 10.1103/PhysRevD.100.015018
72. Ilnicka A, Krawczyk M, Robens T. Inert doublet model in light of LHC Run I and astrophysical data. *Phys Rev D.* (2016) **93**:055026. doi: 10.1103/PhysRevD.93.055026
73. Datta A, Ganguly N, Khan N, Rakshit S. Exploring collider signatures of the inert Higgs doublet model. *Phys Rev D.* (2017) **95**:015017. doi: 10.1103/PhysRevD.95.015017
74. Khan N, Rakshit S. Constraints on inert dark matter from the metastability of the electroweak vacuum. *Phys Rev D.* (2015) **92**:055006. doi: 10.1103/PhysRevD.92.055006
75. Chowdhury D, Eberhardt O. Global fits of the two-loop renormalized Two-Higgs-Doublet model with soft Z_2 breaking. *J High Energy Phys.* (2015) **11**:052. doi: 10.1007/JHEP11(2015)052
76. Sher M. Electroweak Higgs potentials and vacuum stability. *Phys Rept.* (1989) **179**:273–418. doi: 10.1016/0370-1573(89)90061-6

77. Chataignier L, Prokopec T, Schmidt MG, Swiezewska B. Single-scale renormalisation group improvement of multi-scale effective potentials. *J High Energy Phys.* (2018) **03**:014. doi: 10.1007/JHEP03(2018)014
78. Hamada Y, Kawana K. Vanishing Higgs potential in minimal dark matter models. *Phys Lett B.* (2015) **751**:164–70. doi: 10.1016/j.physletb.2015.10.006
79. Bennett DL, Nielsen HB, Froggatt CD. Standard model parameters from the multiple point principle and anti-GUT. In: *Recent developments in nonperturbative quantum field theory. Proceedings, APCTP-ICTP Joint International Conference, Seoul, May 26-30, 1997* (1997). p. 362–93.
80. Haba N, Yamada T. Multiple-point principle realized with strong dynamics. *Phys Rev D.* (2017) **95**:115015. doi: 10.1103/PhysRevD.95.115015
81. Hamada Y, Shiu G. Weak gravity conjecture, multiple point principle and the standard model landscape. *J High Energy Phys.* (2017) **11**:043. doi: 10.1007/JHEP11(2017)043
82. Froggatt CD, Laperashvili LV, Nielsen HB. The fundamental-weak scale hierarchy in the standard model. *Phys Atom Nucl.* (2006) **69**:67–80. doi: 10.1134/S1063778806010108
83. Froggatt CD, Nielsen HB, Laperashvili LV. Hierarchy-problem and a bound state of 6 t and 6 anti-t. *Int J Mod Phys A.* (2005) **20**:1268–75. doi: 10.1142/S0217751X0502416X
84. Das CR, Froggatt CD, Laperashvili LV, Nielsen HB. New bound states of heavy quarks at LHC and tevatron. *Int J Mod Phys A.* (2011) **26**:2503–21. doi: 10.1142/S0217751X11053420
85. Laperashvili LV, Nielsen HB, Das CR. New results at LHC confirming the vacuum stability and multiple point principle. *Int J Mod Phys A.* (2016) **31**:1650029. doi: 10.1142/S0217751X16500299
86. Laperashvili LV, Nielsen HB, Froggatt CD, Sidharth BG, Das CR. New resonances at LHC are possible. Multiple point principle and new bound states in the standard model. *arXiv:1703.01757 [Preprint]* (2017).
87. Nielsen HFB, Bennett DL, Das CR, Froggatt CD, Laperashvili LV. F(750), we miss you as a bound state of 6 top and 6 antitop quarks, multiple point principle. *PoS.* (2017) **CORFU2016**:050. doi: 10.22323/1.292.0050

Conflict of Interest Statement: The authors declare that the research was conducted in the absence of any commercial or financial relationships that could be construed as a potential conflict of interest.

frontiers in Physics

HYPOTHESIS AND THEORY
published: 10 March 2020
doi: 10.3389/fphy.2020.00039

A Guidebook to Hunting Charged Higgs Bosons at the LHC

Abdesslam Arhrib[1], *Rachid Benbrik*[2*], *Hicham Harouiz*[2], *Stefano Moretti*[3] and *Abdessamad Rouchad*[2]

[1] Faculté des Sciences et Techniques, Abdelmalek Essaadi University, Tangier, Morocco, [2] Laboratoire de Physique Fondamentale et Appliquée–Safi, Faculté Polydisciplinaire de Safi, Safi, Morocco, [3] School of Physics and Astronomy, University of Southampton, Southampton, United Kingdom

We perform a comprehensive global analysis in the Minimal Supersymmetric Standard Model (MSSM) as well as in the 2-Higgs Doublet Model (2HDM) of the production and decay mechanisms of charged Higgs bosons ($H^{\pm}$) at the Large Hadron Collider (LHC). We start from accounting for the most recent experimental results (SM-like Higgs boson signal strengths and search limits for new Higgs boson states obtained at Run-1 and -2 of the LHC and previous colliders), from (both direct and indirect) searches for supersymmetric particles as well as from flavor observables (from both e^+e^- factories and hadron colliders). We then present precise predictions for $H^{\pm}$ cross sections and decay rates in different reference scenarios of the two aforementioned models in terms of the parameter space currently available, specifically, mapped over the customary ($m_{A,H^{\pm}}$, tan β) planes. These include the m_h^{mod+} and hMSSM configurations of the MSSM and the 2HDM Type-I, -II, -X, and -Y for which we also enforce theoretical constraints, such as vacuum stability, perturbativity, and unitarity. We also define specific Benchmark Points (BPs) which are always close to (or coinciding with) the best fits of the theoretical scenarios to experimental data. We finally briefly discuss the ensuing phenomenology for the purpose of aiding future searches for such charged Higgs boson states.

Keywords: beyond standard model, Higgs physics, charged Higgs, 2HDM, MSSM, LHC

OPEN ACCESS

Edited by:
Frank Franz Deppisch, University College London, United Kingdom

Reviewed by:
Athanasios Dedes, University of Ioannina, Greece
Yuval Grossman, Cornell University, United States

***Correspondence:**
Rachid Benbrik
r.benbrik@uca.ac.ma

Specialty section:
This article was submitted to High-Energy and Astroparticle Physics, a section of the journal Frontiers in Physics

Received: *29 March 2019*
Accepted: *12 February 2020*
Published: *10 March 2020*

Citation:
Arhrib A, Benbrik R, Harouiz H, Moretti S and Rouchad A (2020) A Guidebook to Hunting Charged Higgs Bosons at the LHC. Front. Phys. 8:39. doi: 10.3389/fphy.2020.00039

1. INTRODUCTION

The Higgs boson discovery of 2012 [1–4] at the CERN Large Hadron Collider (LHC) has led to the confirmation of the Standard Model (SM) as the proper theory of the Electro-Weak (EW) scale. However, there is much evidence that the SM is not appropriate at all scales, rather it should be viewed as an effective low-energy realization of a more complete and fundamental theory on setting beyond the EW regime. Among the many proposals for the latter, one can list theories with some new symmetry, e.g., Supersymmetry (SUSY), or an enlarged particle content (e.g., in the Higgs sector), or both. Following the aforementioned discovery, no new particle has however been seen at the LHC, implying that new physics at the EW scale should be weakly interacting or that strongly interacting particles, if present, should lead to signatures involving soft decay products or in channels with overwhelming (ir)reducible backgrounds. We shall adopt here the first assumption.

Many SM extensions possess in their spectra additional neutral and/or charged Higgs states. Amongst these, SUSY [5] is indeed considered the most appealing one as it addresses several shortcomings of the SM, including the problem of the large hierarchy between the EW and Planck

scales as well as the dark matter puzzle. While the search for SUSY was unsuccessful during the first LHC run, the increase in the Center-of-Mass (CM) energy of the machine from 8 to 13 TeV plus the additional luminosity of the second run are improving greatly the sensitivity to the new superparticles which are predicted. While the jury is still out on these, we remind here the reader that SUSY also requires at least two Higgs doublets for a successful EW Symmetry Breaking (EWSB) pattern. For exactly two such fields, yielding the so-called Minimal Supersymmetric Standard Model (MSSM), also having the same gauge group structure of the SM, one obtains four physical Higgs particles, in addition to the discovered SM-like one with the observed mass of 125 GeV. In fact, the same Higgs mass spectrum also belongs to a generic 2-Higgs Doublet Model (2HDM), i.e., one not originating from SUSY. In neither case, though, there exists a precise prediction of the typical masses of the new Higgs states, though we know already that the MSSM allows for one to be lighter than the 125 GeV state in a very small region of parameter space [6], whereas the 2HDM generally does so over a significantly larger expanse of it [7, 8]. Either way, the presence of extra physical Higgs boson states alongside the SM-like one is thus one of the characteristics of Beyond the SM (BSM) physics, whether within SUSY or otherwise. Hence, looking for these additional states in various production and decay channels over a wide range of kinematic regimes is an important part of the physics programme of the multi-purpose LHC experiments, ATLAS, and CMS. Specifically, the discovery of a (singly) charged Higgs boson would point to a likely additional Higgs doublet (or a Higgs field with higher representation, such as triplet). Hence, we concentrate on this Higgs state here.

The two Higgs doublet fields pertaining to the MSSM are required to break the EW symmetry and to generate the isospin-up and -down type fermions as well as the $W^\pm$ and Z boson masses [9–11]. The Higgs spectrum herein is given by the following states: two charged $H^\pm$'s, a CP-odd A and two CP-even Higgses h and H, with $m_h < m_H$ (conventionally, wherein h is the SM-like Higgs state). The tree-level phenomenology of the Higgs sector of the MSSM is described entirely by two input parameters, one Higgs mass (that can be taken to be that of the CP-odd Higgs state, m_A) and the ratio $\tan\beta$ of the Vacuum Expectation Values (VEVs) of the two Higgs doublet fields. Note that one of the most powerful prediction of SUSY is the existence of a light Higgs boson that could be produced at colliders. In the MSSM, at the tree-level, the light CP-even h is predicted to be lighter than the Z boson. However, it is well-known that loop effects could raise the h mass upper bound to 135 GeV for a large soft breaking trilinear parameter, A_t, and/or a heavy scalar top [12–22]. After the Higgs boson discovery at the LHC, MSSM benchmark scenarios have been refined to match the experimental data and to reveal characteristic features of certain regions of the parameter space [23–25]. Of the many MSSM frameworks presented in literature, we consider in this work the so-called $m_h^{\rm mod+}$ [24] and hMSSM [26–30] ones, which will be described in the coming section. As for the 2HDM, one ought to specify the Yukawa sector, in order to proceed to study phenomenologically its manifestations. While SUSY enforces this in the form of a so-called Type-II, this is only one of four Ultra-Violet (UV) complete realizations of a generic 2HDM, the others been termed Type-I, -X, and -Y. The difference between these four scenarios is the way the fermionic masses are generated. We define as Type-I the model where only one doublet couples to all fermions, Type-II is the scenario where one doublet couples to up-type quarks and the other to down-type quarks and leptons, the Type-X is the model where one doublet couples to all quarks and the other to all leptons while a Type-Y is built such that one doublet couples to up-type quarks and to leptons and the other to down-type quarks. In all such cases, the number of free parameters at tree-level is seven to start with, hence it becomes more cumbersome than in SUSY to map experimental results onto theoretical constraints. Yet, in virtue of the fact that a 2HDM is the simplest realization of a BSM scenario based solely on doublet Higgs fields, its study is vigorously being pursued experimentally.

So far, the non-observation of any Higgs signal events in direct searches above and beyond those of the SM-like Higgs state constrains the parameter space of the underlying physics model. Specifically, in the case of the $H^\pm$ boson, wherein the relevant phenomenological parameters are $m_{H^\pm}$ and $\tan\beta$ in whatever scenario, one can pursue the study of its production and decay modes in a model independent way, which results can *a posteriori* be translated to exclude the relevant parameter space in a given scenario (whether it be the MSSM, 2HDM, or something else). This recasting is conveniently done on the $(m_A, \tan\beta)$ and $(m_{H^\pm}, \tan\beta)$ planes for the MSSM and 2HDM, respectively, so that we will map our findings in the same way.

At hadron colliders, there exists many production modes for charged Higgs bosons which are rather similar in the MSSM and 2HDM. For a light charged Higgs, i.e., with mass $m_{H^\pm} + m_b < m_t$, its production comes mainly from top decay. At the LHC, the production of top quark pairs proceeds via Quantum Chromo-Dynamics (QCD) interactions and, when kinematically allowed, one top could decay into a charged Higgs state and a bottom quark in a competition with the SM decay into a $W^\pm$ boson and again a bottom quark. Therefore, the complete $H^\pm$ production mechanism $q\bar{q}, gg \to t\bar{t} \to t\bar{b}H^-$ provides the main source of light charged Higgs bosons at the LHC and offers a much more copious signature than any other form of direct production. After crossing the top-bottom threshold, i.e., when $m_{H^\pm} + m_b > m_t$, a charged Higgs (pseudo)scalar can be produced through the process $gb \to tH^-$ [31–34]. In fact, these two mechanisms can be simultaneously captured via the process $gg \to t\bar{b}H^-$ [35, 36], which again makes it clear that one should expect large $H^\pm$ cross sections induced by QCD interactions also in the heavy $H^\pm$ mass range[1].

In the MSSM, and also in a variety of 2HDM Types, light charged Higgs bosons would decay almost exclusively into a (hadronic or leptonic) τ lepton and its associated neutrino for $\tan\beta \gtrsim 1$. When the top-bottom channel is kinematically open, then $H^+ \to t\bar{b}$ would compete with $H^\pm \to hW^\pm, HW^\pm, AW^\pm$ decays as well as various SUSY channels in the MSSM. In the latter, $H^+ \to t\bar{b} \to b\bar{b}W^+$ is the dominant channel and the bosonic decays $H^\pm \to hW^\pm, HW^\pm, AW^\pm$ (also yielding $b\bar{b}W^+$

[1]For a complete review on charged Higgs production modes, see Akeroyd et al. [34].

final states) are subleading. In the 2HDM, if none of these bosonic decays is open, then $H^+ \to t\bar{b}$ is the dominant mode. At the LHC Run-1, lighter charged Higgs bosons were probed in the decay channels $\tau\nu$ [37, 38], cs [39, 40] and also cb [41]. No excess was observed and model independent limits are set on the following product of Branching Ratios (BRs): BR($t \to H^+b$) × BR($H^+ \to \tau\nu$). At Run-2, mainly the decay modes $\tau\nu$ [42, 43] and tb [44] are explored in the mass range $m_{H^\pm} = 200$–1,000 GeV, in the latter mode using multi-jet final states with one electron or muon from the top quark decay. No significant excess above the background-only hypothesis has been observed and upper limits are set on the $pp \to tbH^\pm$ production cross section times BR($H^\pm \to tb$). Several interpretations of these limits have eventually been given in benchmark scenarios of the MSSM, including those mentioned above. Note that current ATLAS and CMS bounds are significantly weakened in the 2HDM once the exotic decay channels into a lighter neutral Higgs, e.g., $H^\pm \to hW^\pm$ or $H^\pm \to AW^\pm$, are open. This scenario could also happen in the MSSM if one of the SUSY decay channels of charged Higgs bosons are open (such as into chargino-neutralino pairs). In the 2HDM, the possibility of producing a light charged Higgs boson from top decay with a subsequent step $H^\pm \to hW^\pm$ or $H^\pm \to AW^\pm$ was studied in Arhrib et al. [45] and it was shown that it can lead to sizable cross sections at low $\tan\beta$. We stress here that there exist several recent analyses dedicated to 2HDM phenomenology [34, 46, 47] that we consulted. However, unlike Akeroyd et al. [34], Arbey et al. [46], and Bernon et al. [47] only concentrates on neutral Higgs phenomenology and discuss the charged Higgs contribution only to flavor physics observables without singling out the relevant charged Higgs production and decay channels at the LHC, which is indeed one of the aims of this analysis.

In this paper, we analyze the allowed $\sigma(pp \to t\bar{b}H^+ + \text{c.c.}) \times \text{BR}(H^\pm \to \text{anything})$ rates by taking into account both theoretical and experiments constraints on the underlying BSM model, the latter including the latest ATLAS and CMS results for SM-Higgs (h) and other Higgs (H, A, H^+) searches with the full set of 36.5 fb^{-1} data collected in the second LHC phase. We will then interpret these results under the proposed scenarios to quantify the magnitude of the available parameter space to be covered by future LHC analyses. In doing so, we will extract several Benchmarks Points (BPs) that could lead to detectable signals, all of which are consistent with the best fit regions in both the MSSM and 2HDM.

The paper is organized as follows. In the second section we review the MSSM and introduce the benchmark scenarios that we will discuss. The 2HDM, with its parameterizations and Yukawa textures, is described in the third section. The fourth section is devoted to a discussion of the theoretical and experimental constraints used in our study. Results and discussions for the MSSM and 2HDM are presented in the fifth section and we finish with our conclusions.

2. THE MSSM

In the MSSM, due to the holomorphy of the superpotential, one introduce two Higgs doublets $\Phi_{1,2}$ in order to give masses to up-type quarks as well as down-type quarks and leptons, respectively. Both Higgs fields acquire VEVs, denoted by $v_{1,2}$. After EWSB takes place, the spectrum of the model contains the aforementioned Higgs states: h, H, A and $H^\pm$. The MSSM Higgs sector is parameterized at tree-level by $\tan\beta = v_2/v_1$, and e.g., the CP-odd mass m_A. One of the interesting features of the MSSM is the prediction, at the tree-level, of a light CP-even Higgs h with a mass $m_h \leq m_Z$. However, such tree-level prediction is strongly modified by radiative corrections at one- and two-loop level [12–21]. It has been shown in Degrassi et al. [22], on the one hand, that the loop effects can make the light CP-even mass m_h reach a value of 135 GeV and, on the other hand, that the theoretical uncertainties due to unknown high order effects can be of the order of 3 GeV. In fact, these large loop effects are welcome in order to shift the light CP-even Higgs mass to the measured experimental value $m_h \approx 125$ GeV. Note also that the loop effects will modify not only the tree-level Higgs mass relations but also the Higgs self-couplings and the Higgs coupling to SUSY particles. Therefore, beside the tree-level parameters $\tan\beta$ and m_A, the top quark mass and the associated squark masses and their soft SUSY breaking parameters enter through radiative corrections [12–21, 48, 49]. In fact, when trying to push the light CP-even mass from m_Z to 125 GeV through loop effects, one needs to introduce a large SUSY scale with large soft trilinear parameter A_t. Such a large SUSY scale puts automatically the SUSY spectrum at the TeV scale, which is consistent with negative searches for SUSY particles at the LHC.

To compute the masses and couplings of Higgs bosons in a given point of the MSSM parameter space we use the code FeynHiggs [50, 51] for the m_h^{mod+} scenario and the program HDECAY for the hMSSM case [52, 53]. Both codes include the full one-loop and a large part of the dominant two-loop corrections to the neutral Higgs masses. Since the theoretical uncertainty on the Higgs mass calculation in the FeynHiggs code has been estimated to be of the order of 3 GeV, we consider as phenomenologically acceptable the points in the MSSM parameter space where FeynHiggs predicts the existence of a scalar state with mass between 122.5 and 128.5 GeV and with approximately SM-like couplings to gauge bosons and fermions. In addition to the tree-level scalar potential parameters, $\tan\beta$ and m_A, when taking into account high order corrections, the MSSM parameters most relevant to the prediction of the masses and production cross sections of the Higgs bosons are: the soft SUSY-breaking masses for the stop and sbottom squarks, which, for simplicity, we assume all equal to a common mass parameter M_{SUSY}, the soft SUSY-breaking gluino mass $m_{\tilde{g}}$, the soft SUSY-breaking Higgs-squark-squark couplings A_t and A_b, the superpotential Higgs(ino)-mass parameter μ and the left-right mixing terms in the stop and sbottom mass matrices (divided by m_t and m_b)

$$X_t = A_t - \mu \cot\beta, \qquad X_b = A_b - \mu \tan\beta, \tag{1}$$

respectively. Since the (approximate) two-loop calculation of the Higgs masses implemented in FeynHiggs and the Next-to-Leading Order (NLO) calculation of QCD corrections to the production cross section implemented in SusHi [54, 55] employ

the same renormalization (on-shell) scheme, the input values of the soft SUSY-breaking parameters can be passed seamlessly from the Higgs mass to the cross section calculations.

In the light of the latest LHC data on the discovered Higgs-like boson, and given the fact that the MSSM contains many independent parameters which makes it a fastidious task to perform a full scan, there have been many studies which lead to several benchmarks that could fit the observed Higgs boson as well as be tested at the future LHC with higher luminosity [24, 26–29]. As intimated already, in this study, we will concentrate on two of these benchmark scenarios: the $m_h^{\rm mod+}$ and hMSSM ones, which we will describe hereafter.

2.1. The $m_h^{\rm mod+}$ Scenario

The $m_h^{\rm mod+}$ scenario is a modification of the time-honored $m_h^{\rm max}$ scenario (also called maximal mixing scenario), which was originally defined to give conservative exclusion bounds on $\tan\beta$ in the context of Higgs boson searches at LEP [56]. The $m_h^{\rm max}$ scenario was introduced in order to maximize the value of m_h by incorporating large radiative correction effects for a large $m_A >> m_Z$ mass, fixed value of $\tan\beta > 8$ and large SUSY scale of the order 1 TeV. However, this scenario predicts m_h to be much higher than the observed Higgs boson mass, due to the large mixing in the scalar top sector.

Hence, the maximal mixing scenario has been modified, by reducing the amount of scalar top mixing, such that the mass of the lightest Higgs state, m_h, is compatible with the mass of the observed Higgs boson within ± 3 GeV in a large fraction of the considered parameter space. In fact, modifications of the $m_h^{\rm max}$ scenario can be done in two ways depending on the sign of $(A_t - \mu\cot\beta)/M_{\rm SUSY}$, leading to an $m_h^{\rm mod-}$ and $m_h^{\rm mod+}$ [24]. It has been demonstrated in Carena et al. [24] that when $m_h^{\rm mod+}$ is confronted with LHC data, there is a substantial region in the plane $(m_A, \tan\beta)$ with $\tan\beta > 7$ for which the light CP-even Higgs mass is in a good agreement with the measured one at the LHC, hence our choice of this scenario.

The SUSY input parameters in this scenario are fixed as[2]

$$\begin{gathered} M_{Q_3} = M_{U_3} = M_{D_3} = 1.5\ \text{TeV}, \quad M_{L_3} = M_{E_3} = 2\ \text{TeV}, \\ \mu = 200\ \text{GeV},\ M_1 = 100\ \text{GeV},\ M_2 = 200\ \text{GeV},\ m_{\tilde g} = 1.5\ \text{TeV}, \\ X_t = 2M_{\rm SUSY} = 1\ \text{TeV}, \quad A_b = A_\tau = A_t, \end{gathered} \tag{2}$$

where $M_{\rm SUSY}$ is the aforementioned SUSY mass scale.

2.2. The hMSSM Scenario

In the previous scenario, one need to input $\tan\beta$, m_A and also the other SUSY parameters to get the Higgs and SUSY (mass and coupling) spectrum. Taking into account the theoretical uncertainty of the order 3 GeV on the Higgs mass, which could originate from unknown high order loop effects, a light CP-even Higgs boson with a mass in the range [122, 128] GeV would be an MSSM candidate for the observed Higgs-like particle. However, plenty of points on the $(m_A, \tan\beta)$ plane would correspond to one configuration of m_h mass. To avoid this situation, the hMSSM benchmark was introduced [26–29]. In this scenario, the light CP-even Higgs state is enforced to be $\sim$125 GeV while setting the SUSY mass scale $M_{\rm SUSY}$ to be rather high (i.e., $>$ 1 TeV) in order to explain the non-observation of any SUSY particle at colliders. The hMSSM setup thus describes the MSSM Higgs sector in terms of just m_A and $\tan\beta$, exactly like for tree-level predictions, given the experimental knowledge of m_Z and m_h. In this scenario, therefore, the dominant radiative corrections would be fixed by the measured experimental value of m_h which in turn fixes the SUSY scale [26–29]. It defines a largely model-independent scenario, because the predictions of the properties of the MSSM Higgs bosons do not depend on the details of the SUSY sector, somewhat unlike the previous case, wherein squark masses are fine-tuned to obtain $m_h \approx 125$ GeV.

The SUSY input parameters in this scenario are similar to the previous one, Equation (2), except that we take $X_t = 2M_{\rm SUSY} = 2$ TeV.

2.3. Setup

Both scenarios introduced above are characterized by relatively large values of the ratio $X_t/M_{\rm SUSY}$, ensuring that the MSSM mass of the SM-like Higgs state falls within the required range without the need for an extremely heavy stop. In addition, the masses of the gluino and first two generation squarks are set to 1.5 TeV, large enough to evade the current ATLAS and CMS limits stemming from SUSY searches [57–61]. We vary the parameters $\tan\beta$ and m_A within the following ranges:

$$0.5 \le \tan\beta \le 15, \qquad 90\ \text{GeV} \le m_A \le 1\ \text{TeV}. \tag{3}$$

The soft trilinear term A_t is set to be equal to A_b. Due to the smallness of the light quarks masses, the left-right mixing of the first two generation squarks is neglected. The gaugino mass parameters M_1, M_2 and the soft SUSY-breaking gluino mass $m_{\tilde g}$ are all related through Renormalization Group Equation (RGE) running to some common high scale $m_{1/2}$ soft term which yields the relations $m_{\tilde g} \approx 3.5M_2$ and $M_1 \approx 0.5M_2$. In our analysis, we assume Grand Unified Theory (GUT) relations only between M_1 and M_2 while M_2 and $m_{\tilde g}$ are taken independent from each other. Finally, the soft SUSY-breaking parameters in the slepton sector have a very small impact on the predictions for the Higgs masses and production cross sections, therefore we do not report on them here.

3. THE 2HDM

In this section, we define the scalar potential and the Yukawa sector of the general 2HDM. The most general scalar potential which is $SU(2)_L \otimes U(1)_Y$ invariant is given by [62, 63]

$$\begin{aligned} V(\Phi_1,\Phi_2) =\ & m_1^2\Phi_1^\dagger\Phi_1 + m_2^2\Phi_2^\dagger\Phi_2 - (m_{12}^2\Phi_1^\dagger\Phi_2 + \text{h.c}) \\ & + \tfrac{1}{2}\lambda_1(\Phi_1^\dagger\Phi_1)^2 + \tfrac{1}{2}\lambda_2(\Phi_2^\dagger\Phi_2)^2 \\ & + \lambda_3(\Phi_1^\dagger\Phi_1)(\Phi_2^\dagger\Phi_2) + \lambda_4(\Phi_1^\dagger\Phi_2)(\Phi_1^\dagger\Phi_2) \end{aligned}$$

[2]Notice that this $m_h^{\rm mod+}$ configuration is compliant with the theoretical and experimental constraints discussed below, including Dark Matter (DM) ones. So is the case for the hMSSM configuration below.

$$+\left[\frac{\lambda_5}{2}(\Phi_1^\dagger\Phi_2)^2+\text{H.c.}\right]. \quad (4)$$

The complex (pseudo)scalar doublets Φ_i ($i = 1,2$) can be parameterized as

$$\Phi_i(x)=\begin{pmatrix}\phi_i^+(x)\\ \frac{1}{\sqrt{2}}\left[v_1+\rho_1(x)+i\eta_1(x)\right]\end{pmatrix}, \quad (5)$$

with $v_{1,2} \geq 0$ being the VEVs satisfying $v = \sqrt{v_1^2+v_2^2}$, with $v = 246.22$ GeV. Hermiticity of the potential forces $\lambda_{1,2,3,4}$ to be real while λ_5 and m_{12}^2 can be complex. In this work we choose to work in a CP-conserving potential where both VEVs are real and so are also λ_5 and m_{12}^2.

After EWSB, three of the eight degrees of freedom in the Higgs sector of the 2HDM are eaten by the Goldstone bosons ($G^\pm$ and G) to give masses to the longitudinal gauge bosons ($W^\pm$ and Z). The remaining five degrees of freedom become the aforementioned physical Higgs bosons. After using the minimization conditions for the potential together with the $W^\pm$ boson mass requirement, we end up with seven independent parameters which will be taken as

$$m_h\,, m_H\,, m_A\,, m_{H^\pm}\,, \alpha\,, \tan\beta\,, m_{12}^2, \quad (6)$$

where, as usual, $\tan\beta \equiv v_2/v_1$ and β is also the angle that diagonalizes the mass matrices of both the CP-odd and charged Higgs sector while the angle α does so in the CP-even Higgs sector.

The most commonly used versions of a CP-conserving 2HDM are the ones that satisfy a discrete Z_2 symmetry $\Phi_i \to (-1)^{i+1}\Phi_i$ ($i = 1,2$), that, when extended to the Yukawa sector, guarantees the absence of Flavor Changing Neutral Currents (FCNCs). Such a symmetry would also require $m_{12}^2 = 0$, unless we tolerate a soft violation of this by the dimension two term m_{12}^2 (as we do here). The Yukawa Lagrangian can then be written as

$$-\mathcal{L}_Y = \bar{Q}_L(Y_1^d\Phi_1+Y_2^d\Phi_2)d_R+\bar{Q}_L(Y_1^u\tilde{\Phi}_1+Y_2^u\tilde{\Phi}_2)u_R +\bar{L}_L(Y_1^l\Phi_1+Y_2^l\Phi_2)l_R+\text{H.c.}, \quad (7)$$

where $Q_L^T = (u_L, d_L)$ and $L_L^T = (l_L, l_L)$ are the left-handed quark doublet and lepton doublet, respectively, the Y_k^f's ($k = 1,2$ and $f = u,d,l$) denote the 3×3 Yukawa matrices and $\tilde{\Phi}_k = i\sigma_2\Phi_k^*$ ($k = 1,2$). The mass matrices of the quarks and leptons are a linear combination of Y_1^f and Y_2^f, $Y_{1,2}^{d,l}$ and $Y_{1,2}^u$. Since they cannot be diagonalized simultaneously in general, neutral Higgs Yukawa couplings with flavor violation appear at tree-level and contribute significantly to FCNC processes, such as $\Delta M_{K,B,D}$ as well as $B_{d,s} \to \mu^+\mu^-$ mediated by neutral Higgs exchanges. To avoid having those large FCNC processes, one known solution is to extend the Z_2 symmetry to the Yukawa sector. When doing so, we ended up with the already discussed four possibilities regarding the Higgs bosons couplings to fermions [63].

TABLE 1 | Yukawa couplings in terms of the standard κ coefficients, in turn expressed as function of the angles α and β, in the four 2HDM Types.

	κ_u^h	κ_d^h	κ_l^h	κ_u^H	κ_d^H	κ_l^H	κ_u^A	κ_d^A	κ_l^A
Type-I	c_α/s_β	c_α/s_β	c_α/s_β	s_α/s_β	s_α/s_β	s_α/s_β	c_β/s_β	$-c_\beta/s_\beta$	$-c_\beta/s_\beta$
Type-II	c_α/s_β	$-s_\alpha/c_\beta$	$-s_\alpha/c_\beta$	s_α/s_β	c_α/c_β	c_α/c_β	c_β/s_β	s_β/c_β	s_β/c_β
Type-X	c_α/s_β	c_α/s_β	$-s_\alpha/c_\beta$	s_α/s_β	s_α/s_β	c_α/c_β	c_β/s_β	$-c_\beta/s_\beta$	s_β/c_β
Type-Y	c_α/s_β	$-s_\alpha/c_\beta$	c_α/s_β	s_α/s_β	c_α/c_β	s_α/s_β	c_β/s_β	s_β/c_β	$-c_\beta/s_\beta$

Here, the shorthand notation $c_x \equiv \cos x$ and $s_x \equiv \sin x$ is used.

After EWSB, the Yukawa Lagrangian can be expressed in the mass eigenstate basis as follows [64, 65]:

$$\mathcal{L}_Y = -\sum_{f=u,d,\ell}\frac{m_f}{v}\left(\kappa_f^h\bar{f}fh+\kappa_f^H\bar{f}fH-i\kappa_f^A\bar{f}\gamma_5fA\right) -\left(\frac{\sqrt{2}V_{ud}}{v}\bar{u}\left(m_u\kappa_u^AP_L+m_d\kappa_d^AP_R\right)dH^+ +\text{H.c.}\right). \quad (8)$$

We give in **Table 1** the values of the Yukawa couplings κ_f^ϕ ($\phi = h,H,A$), i.e., the Higgs boson interactions normalized to the SM vertices introduced in David et al. [66], in the four 2HDM Types. The couplings of h and H to gauge bosons $W^\pm, Z$ are proportional to $\sin(\beta-\alpha)$ and $\cos(\beta-\alpha)$, respectively. Since these are gauge couplings, they are the same for all Yukawa types. As we are considering the scenario where the lightest neutral Higgs state is the 125 GeV scalar, the SM-like Higgs boson h is recovered when $\cos(\beta-\alpha) \approx 0$. As one can see from **Table 1**, for all 2HDM Types, this is also the limit where the Yukawa couplings of the discovered Higgs boson become SM-like. The limit $\cos(\beta-\alpha) \approx 0$ seems to be favored by LHC data, except for the possibility of a wrong sign limit [67, 68], where the couplings to down-type quarks can have a relative sign to the gauge bosons ones, thus oppositely to those of the SM. Our benchmarks will focus on the SM-like limit where indeed $\cos(\beta-\alpha) \approx 0$.

We end this section by noticing that we have used the public program 2HDMC [69] to evaluate the 2HDM spectrum as well as the decay rates and BRs of all Higgs particles. We have used 2HDMC to also enforce the aforementioned theoretical constraints onto both BSM scenarios considered here.

4. THEORETICAL AND EXPERIMENTAL CONSTRAINTS

In order to perform a systematic scan over the parameter space of the two MSSM configurations and the four 2HDM Types, we take into account the following theoretical[3] and experimental constraints.

4.1. Theoretical Constraints

We list these here as itemized entries.

[3]Notice that, for the MSSM scenarios considered here, the (dynamically generated) scalar potential is stable in vacuum and does not induce perturbative unitarity violations.

- **Vacuum stability:** To ensure that the scalar potential is bounded from below, it is enough to assume that the quartic couplings should satisfy the following relations [70]:

$$\lambda_{1,2} > 0,\ \lambda_3 > -(\lambda_1\lambda_2)^{1/2} \text{ and } \lambda_3 + \lambda_4 - |\lambda_5| > -(\lambda_1\lambda_2)^{1/2}. \tag{9}$$

We also impose that the potential has a minimum that is compatible with EWSB. If this minimum is CP-conserving, any other possible charged or CP-violating stationary points will be a saddle point above the minimum [71]. However, there is still the possibility of having two coexisting CP-conserving minima. In order to force the minimum compatible with EWSB, one need to impose the following simple condition [72]:

$$m_{12}^2\left(m_{11}^2 - m_{22}^2\sqrt{\lambda_1/\lambda_2}\right)\left(\tan\beta - \sqrt[4]{\lambda_1/\lambda_2}\right) > 0. \tag{10}$$

Writing the minimum conditions as

$$\begin{aligned} m_{11}^2 + \frac{\lambda_1 v_1^2}{2} + \frac{\lambda_3 v_2^2}{2} &= \frac{v_2}{v_1}\left[m_{12}^2 - (\lambda_4+\lambda_5)\frac{v_1 v_2}{2}\right], \\ m_{22}^2 + \frac{\lambda_2 v_2^2}{2} + \frac{\lambda_3 v_1^2}{2} &= \frac{v_1}{v_2}\left[m_{12}^2 - (\lambda_4+\lambda_5)\frac{v_1 v_2}{2}\right], \end{aligned} \tag{11}$$

allows us to express m_{11}^2 and m_{22}^2 in terms of the soft Z_2 breaking term m_{12}^2 and the quartic couplings λ_{1-5}.

- **Perturbative unitarity:** Another important theoretical constraint on the (pseudo)scalar sector of the 2HDM is the perturbative unitarity requirement. We require that the S-wave component of the various (pseudo)scalar scattering amplitudes of Goldstone and Higgs states remains unitary. Such a condition implies a set of constraints that have to be fulfilled and are given by [73, 74]

$$|a_\pm|, |b_\pm|, |c_\pm|, |f_\pm|, |e_{1,2}|, |f_1|, |p_1| < 8\pi, \tag{12}$$

where

$$\begin{aligned} a_\pm &= \frac{3}{2}(\lambda_1+\lambda_2) \pm \sqrt{\frac{9}{4}(\lambda_1-\lambda_2)^2 + (2\lambda_3+\lambda_4)^2}, \\ b_\pm &= \frac{1}{2}(\lambda_1+\lambda_2) \pm \frac{1}{2}\sqrt{(\lambda_1-\lambda_2)^2 + 4\lambda_4^2}, \\ c_\pm &= \frac{1}{2}(\lambda_1+\lambda_2) \pm \frac{1}{2}\sqrt{(\lambda_1-\lambda_2)^2 + 4\lambda_5^2}, \\ e_1 &= \lambda_3 + 2\lambda_4 - 3\lambda_5, & e_2 &= \lambda_3 - \lambda_5, \\ f_+ &= \lambda_3 + 2\lambda_4 + 3\lambda_5, & f_- &= \lambda_3 + \lambda_5, \\ f_1 &= \lambda_3 + \lambda_4, & p_1 &= \lambda_3 - \lambda_4. \end{aligned} \tag{13}$$

- **EW precision observables (EWPOs):** The additional neutral and charged (pseudo)scalars, beyond the SM-like Higgs state, contribute to the gauge bosons vacuum polarization through their coupling to gauge bosons. In particular, the universal parameters S, T, and U provide constraints on the mass splitting between the heavy states m_H, $m_{H^\pm}$, and m_A in the scenario in which h is identified with the SM-like Higgs state. The general expressions for the parameters S, T, and U in 2HDMs can be found in Kanemura et al. [75]. To derive constraints on the scalar spectrum we consider the following values for S, T, and U:

$$\Delta S = 0.05 \pm 0.11, \quad \Delta T = 0.09 \pm 0.13, \quad \Delta U = 0.01 \pm 0.11, \tag{14}$$

while using the corresponding covariance matrix given in Baak et al. [76]. The χ^2 function is then expressed as

$$\chi^2 = \sum_{i,j}(X_i - X_i^{\rm SM})(\sigma^2)_{ij}^{-1}(X_j - X_j^{\rm SM}), \tag{15}$$

with correlation factor +0.91.

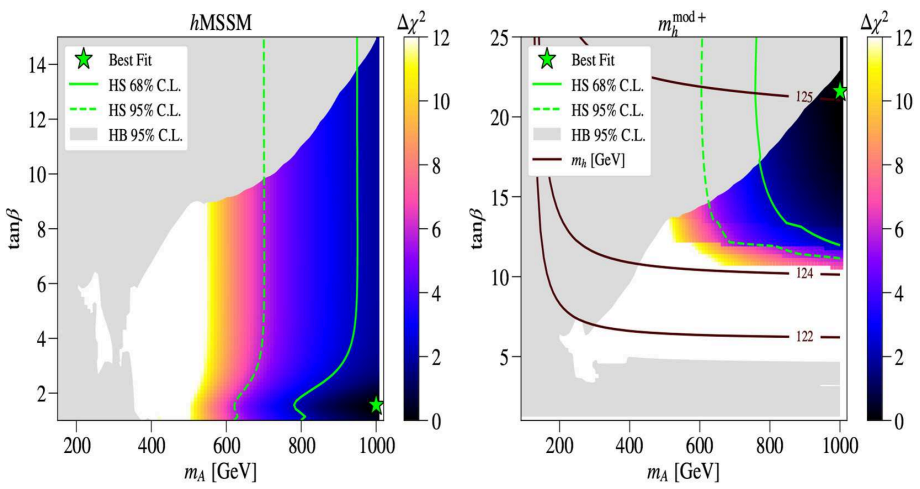

FIGURE 1 | The allowed regions on the $(m_A, \tan\beta)$ plane in hMSSM **(left)** and $m_h^{\rm mod+}$ **(right)**. The cyan lines in the right plot are level curves for the SM-like Higgs mass. By definition, in the hMSSM, m_h is fixed at 125 GeV. The best fit points are marked by green stars.

The aforementioned 2HDMC program allows us to check most of the above theoretical constraints, such as perturbative unitarity, boundedness from below of the scalar potential as well as EWPOs (S, T, and U), which are all turned on during the calculation, and can be adapted to the MSSM as well.

4.2. Experimental Constraints

The parameter space of our benchmark scenarios is already partially constrained by the limits obtained from various searches for additional Higgs bosons at the LHC and elsewhere as well as the requirement that one of the neutral scalar states should match the properties of the observed SM-like Higgs boson. We evaluate the former constraints with the code HiggsBounds [77–80] and the latter with the code HiggsSignals [81]. We stress, however, that our study of the existing constraints cannot truly replace a dedicated analysis of the proposed benchmark scenarios by ATLAS and CMS, which alone would be able to combine the results of different searches taking into account all correlations. In this section we briefly summarize the relevant features of HiggsBounds and HiggsSignals used in our study.

4.2.1. Collider Constraints

The code HiggsBounds tests each parameter point for 95% Confidence Level (CL) exclusion from Higgs searches at the LHC as well as LEP and Tevatron. First, the code determines the most sensitive experimental search available, as judged by the expected limit, for each additional Higgs boson in the model. Then, only the selected channels are applied to the model, i.e., the predicted signal rate for the most sensitive search of each additional Higgs boson is compared to the observed upper limit. In the case the prediction exceeds the limit, the parameter point is regarded as excluded. For more details on the procedure, the reader can see Bechtle et al. [80].

Among the searches that are relevant in constraining our scenarios for charged Higgs studies, the version we have used, 5.2.0beta, of HiggsBounds includes the following.

- ATLAS [82] and CMS [83] searches for heavy Higgs bosons decaying to $\tau^+\tau^-$ pairs using about 36 fb^{-1} of Run-2 data as well as the CMS results from Run-1 [84].
- Searches at Run-1 and Run-2 by ATLAS [85, 86] and CMS [40, 87] for a heavy scalar decaying to a Z boson pair, $H \to ZZ$.
- Searches at Run-1 and Run-2 by ATLAS [88] and CMS [89, 90] for a heavy scalar decaying to a pair of 125 GeV SM-like Higgs scalars, $H \to hh$.
- Searches at Run-1 by ATLAS [91] and CMS [92] for the 125 GeV scalar decaying to a pair of lighter pseudoscalars, $h \to AA$.
- Searches at Run-1 by ATLAS [93] and CMS [94] for a heavy pseudoscalar decaying to a Z boson and the 125 GeV scalar, $A \to Zh$.

By comparing these results with the predictions of SusHi, FeynHiggs, and 2HDMC for the production cross sections and decay BRs of the additional neutral Higgs bosons, HiggsBounds reconstructs the 95% CL exclusion contours for our benchmark scenarios. In the MSSM and 2HDM Type II, these constraints are typically stronger for large values of $\tan\beta$, due to an enhancement of the production cross section of the heavier Higgs bosons in bottom-quark annihilation (in that case the most relevant searches are those for the decay to a $\tau^+\tau^-$ pair). However, this is not generally true in the other 2HDM Types. HiggsBounds also contains the available constraints from searches for a charged Higgs boson by ATLAS and CMS. Most relevant in our scenarios are the constraints on the production of a light charged Higgs via top quark decay, $t \to H^+b$, with subsequent decay $H^+ \to \tau^+\nu$ [37, 38, 43, 95], as well as top-quark associated $H^\pm$ production, with subsequent decays to the $\tau\nu$ [37, 38, 43, 95] and/or tb [38, 44, 96] channels.

In order to estimate the theoretical uncertainty in our determination of the excluded regions, we rely on the

TABLE 2 | Benchmark points for the *h*MSSM and $m_h^{\text{mod+}}$ scenarios.

Parameters	*h*MSSM	$m_h^{\text{mod+}}$
MSSM inputs		
$\tan\beta$	1.804	5.9495
μ (GeV)	200	200
M_2 (GeV)	200	200
$m_{\tilde{g}}$ (GeV)	1,500	1,500
$A_t = A_b = A_\tau$ (GeV)	2,110.9	1,533.6
$M_{Q_{1,2}} = M_{U_{1,2}} = M_{D_{1,2}}$ (GeV)	1,500	1,500
$M_{Q_3} = M_{U_3} = M_{D_3}$ (GeV)	1,000	1,000
$M_{L_{1,2}} = M_{E_{1,2}}$ (GeV)	500	500
$M_{L_3} = M_{E_3}$ (GeV)	1,000	1,000
Masses in GeV		
M_{h^0}	125	118.45
M_{H^0}	504.23	222.35
M_{A^0}	493.43	218.69
M_{H^+}	499.94	232.91
$M_{\tilde{b}_1}$	1,109.7	1,000
$M_{\tilde{b}_2}$	3,041.3	1,002
$M_{\tilde{t}_1}$	990.91	876.49
$M_{\tilde{t}_2}$	1,230.4	1,134.8
$M_{\tilde{\tau}_1}$	999	1,000.7
$M_{\tilde{\tau}_2}$	1,002.1	1,001.3
$M_{\tilde{\chi}_1^0}$	74.736	84.302
$M_{\tilde{\chi}_2^0}$	139.94	147.15
$M_{\tilde{\chi}_4^0}$	282.57	271.82
$M_{\tilde{\chi}_1^+}$	123.97	139.89
$M_{\tilde{\chi}_2^+}$	278.48	270.84
Total decay width in GeV		
$\Gamma(H^+)$	6.7338	0.16321
***BR*($H^+ \to XY$) in %**		
$BR(H^+ \to \tilde{\chi}_1^0\tilde{\chi}_1^+)$	–	27.93
$BR(H^+ \to \tau^+\nu_\tau)$	0.05	10.1
$BR(H^+ \to W^+h^0)$	1.04	4.08
$BR(H^+ \to bt)$	98.74	57.65
Cross sections in pb		
$\sigma(pp \to tH^+ + \text{c.c.})$	0.246	0.204

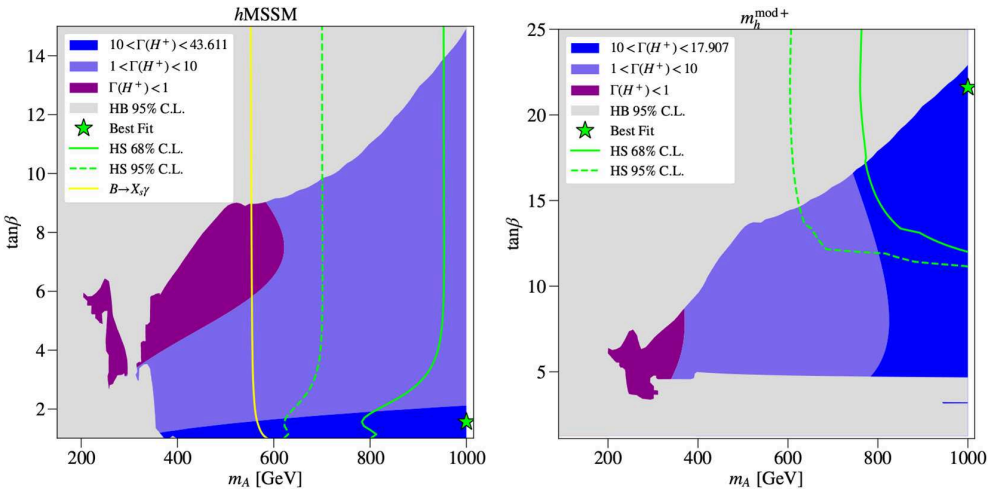

FIGURE 2 | Total charged Higgs boson width (in GeV) mapped on the $(m_A, \tan\beta)$ plane in hMSSM **(left)** and $m_h^{\text{mod+}}$ **(right)**. The units of $\Gamma_{H^\pm}$ in the legends are intended in GeV. The best fit points are marked by green stars.

uncertainty estimates for the gluon-fusion and bottom-quark annihilation cross sections. The most conservative (i.e., weakest) determination of the exclusion region is obtained by taking simultaneously the lowest values in the uncertainty range for both production processes of each of the heavier Higgs bosons, while the least conservative (i.e., strongest) determination is obtained by taking simultaneously the highest values in the uncertainty range.

With the use of the code HiggsSignals, we test the compatibility of our scenarios with the observed SM-like Higgs signals, by comparing the predictions of SusHi, FeynHiggs, and 2HDMC for the signal strengths of Higgs production and decay in a variety of channels against ATLAS and CMS measurements. The version we have used, 2.2.0beta, of HiggsSignals includes all the combined ATLAS and CMS results from Run-1 of the LHC [97] as well as all the available ATLAS [98–104] and CMS limits from Run-2 [105–113].

4.2.2. DM Constraints

These have naturally been enforced only in the MSSM case, by using the program micrOMEGAs version 5.0.9 [114][4]. Such a code calculates the properties of DM in terms of its relic density as well as its direct and indirect detection rates. For the two MSSM scenarios considered here, the DM candidate, i.e., the Lightest Supersymmetric Particle (LSP), is the lightest neutralino. We require that the outcome of the calculation of the relic density should be in agreement with the latest Planck measurement [115].

5. NUMERICAL RESULTS

In this section, we present our findings for the MSSM and 2HDM in turn.

[4]https://lapth.cnrs.fr/micromegas/

5.1. MSSM Results

In the hMSSM scenario, all superparticles are chosen to be rather heavy so that production and decays of the MSSM Higgs bosons are only mildly affected by their presence due to the decoupling properties of SUSY. In particular, the loop-induced SUSY contributions to the couplings of the light CP-even scalars are small and the heavy Higgs bosons with the masses even up to 2 TeV decay only to SM particles. Therefore, the phenomenology of this scenario at the LHC resembles that of a 2HDM Type-II with MSSM-inspired Higgs couplings and mass relations.

The masses of the third generation squarks and that of the gluino are safely above the current bounds from direct searches at the LHC, as intimated. Specifically, we refer to CMS Collaboration [116, 117], ATLAS Collaboration [118–120], CMS Collaboration [121–123] for the scalar top quarks, CMS Collaboration [116, 117] and ATLAS Collaboration [116, 117, 124–126] for the scalar bottom quarks and CMS Collaboration [117], ATLAS Collaboration [125, 127, 128], and CMS Collaboration [129] for the gluino. The value chosen for X_t is close to the one for which the maximal value of m_h is obtained. The $m_h^{\text{mod+}}$ scenario is very similar to the hMSSM one except the fact that we take $X_t = 2M_{\text{SUSY}} = 1$ TeV.

In **Figure 1** the allowed regions on the $(m_A, \tan\beta)$ plane are depicted for various $\Delta\chi^2$, wherein the left and right panel are, respectively, for the hMSSM and $m_h^{\text{mod+}}$ scenarios. For the hMSSM and $\Delta\chi^2 \leq 12$, one can see that m_A should be heavier than about 400 GeV. In the case of $m_A \approx 400 - 600$ GeV, $\tan\beta$ should be in the range $[1, 9]$ while for m_A around 1 TeV $\tan\beta$ is in the range $[1, 15]$. The dashed (solid) line represents the 95% (68%) CL obtained by the HiggsSignals fit and the best fit point is located at $m_A \approx 1$ TeV and $\tan\beta \approx 2$. For the $m_h^{\text{mod+}}$ scenario, the situation is quite different. In order to accommodate $m_h \approx 125$ GeV, one needs $\tan\beta > 10$. Similarly to the left panel, also in the right one the dashed(solid) line represents the 95% (68%) CL obtained by the HiggsSignals fit and the best fit point is

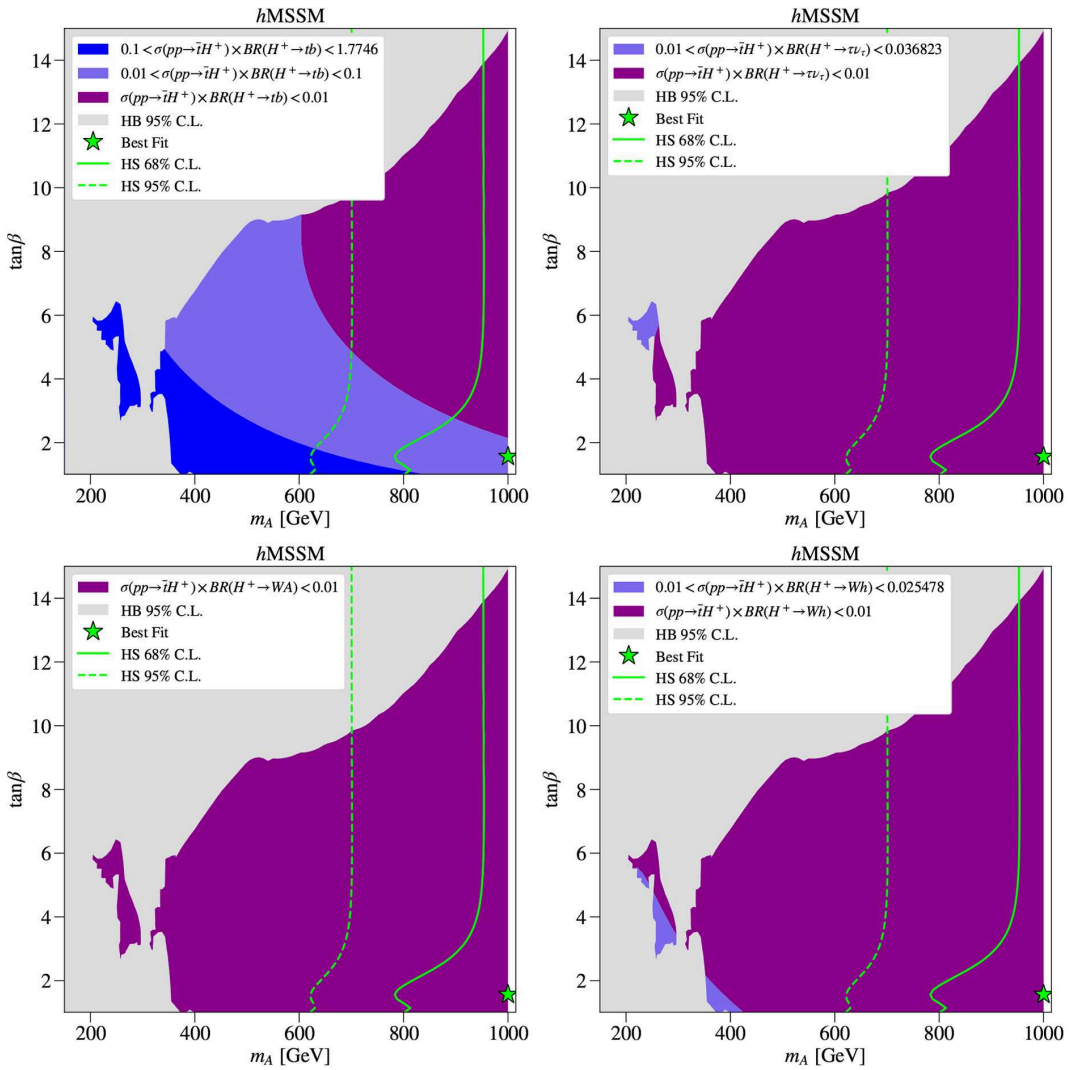

FIGURE 3 | The $\sigma(pp \to tH^- + \text{c.c.}) \times \text{BR}(H^\pm \to XY)$ rate (in pb) at $\sqrt{s}$=14 TeV in the hMSSM scenario, for $XY \equiv tb$ **(top left)**, $XY \equiv \tau\nu$ **(top right)**, $XY \equiv AW^\pm$ **(bottom left)**, and $XY \equiv hW^\pm$ **(bottom right)**. Notice that c.c. channels are included. The best fit points are marked by green stars.

located at $m_A \approx 1$ TeV and $\tan\beta \approx 20$. For this scenario and for $\Delta\chi^2 < 12$, all $\tan\beta \leq 10$ are excluded. Note that after imposing DM constraints onto the best fit analysis, we observe that the best fit points for both the hMSSM and $m_h^{\text{mod}+}$ scenarios move to somewhat lighter values of the charged Higgs boson mass. The BPs given in **Table 2** account for this effect.

In **Figure 2** we present the total width of the charged Higgs boson, again, over the $(m_A, \tan\beta)$ plane, for both hMSSM (left) and $m_h^{\text{mod}+}$ (right). As one can see from the left panel, the total width for the hMSSM case is largest for $\tan\beta \leq 3$, which is when $\Gamma_{H^\pm} \approx 7 - 10$ GeV, while for $\tan\beta \geq 5$ the width drops to 1–3 GeV. This effect can be attributed to the fact that the total width is fully dominated by $H^+ \to t\bar{b}$, whenever this channel is open, in which the top effect is more pronounced for low $\tan\beta$. In this case, $H^+ \to \tau\nu$ is subleading and also the decay modes $H^+ \to \tilde{\chi}_i^+ \tilde{\chi}_j^0$ are suppressed. In the case of $m_h^{\text{mod}+}$, since small $\tan\beta$ is not allowed, the total charged Higgs boson width is generally smaller than in the hMSSM case, as a consequence of the fact that $H^+ \to t\bar{b}$ is therefore smaller in this scenario. The maximal total width is here obtained for $m_A \approx 1$ TeV and a large $\tan\beta \approx 20$. In the $m_h^{\text{mod}+}$ scenario, the decay $H^+ \to \tilde{\chi}_2^+ \tilde{\chi}_2^0$ could have a significant BR, reaching 30%. Hence, the $H^\pm$ is always rather narrow, whichever its mass. In fact, owing to the degeneracy between m_A and $m_{H^\pm}$ in the MSSM, as dictated by h data, a remarkable result is that in the minimal SUSY scenario a charged Higgs boson is essentially always heavier than the top quark.

In **Figure 3** we show the production cross section for single charged Higgs boson production in association with a top quark (as appropriate for the $m_{H^\pm} > m_t$ case) times the BR of H^+ into a specific final state for both the hMSSM and $m_h^{\text{mod}+}$ scenarios using Prospino [130–132]. In fact, as we have seen previously, the total width of the charged Higgs state is rather small in both cases, in relation to the mass, so that one can use the Narrow

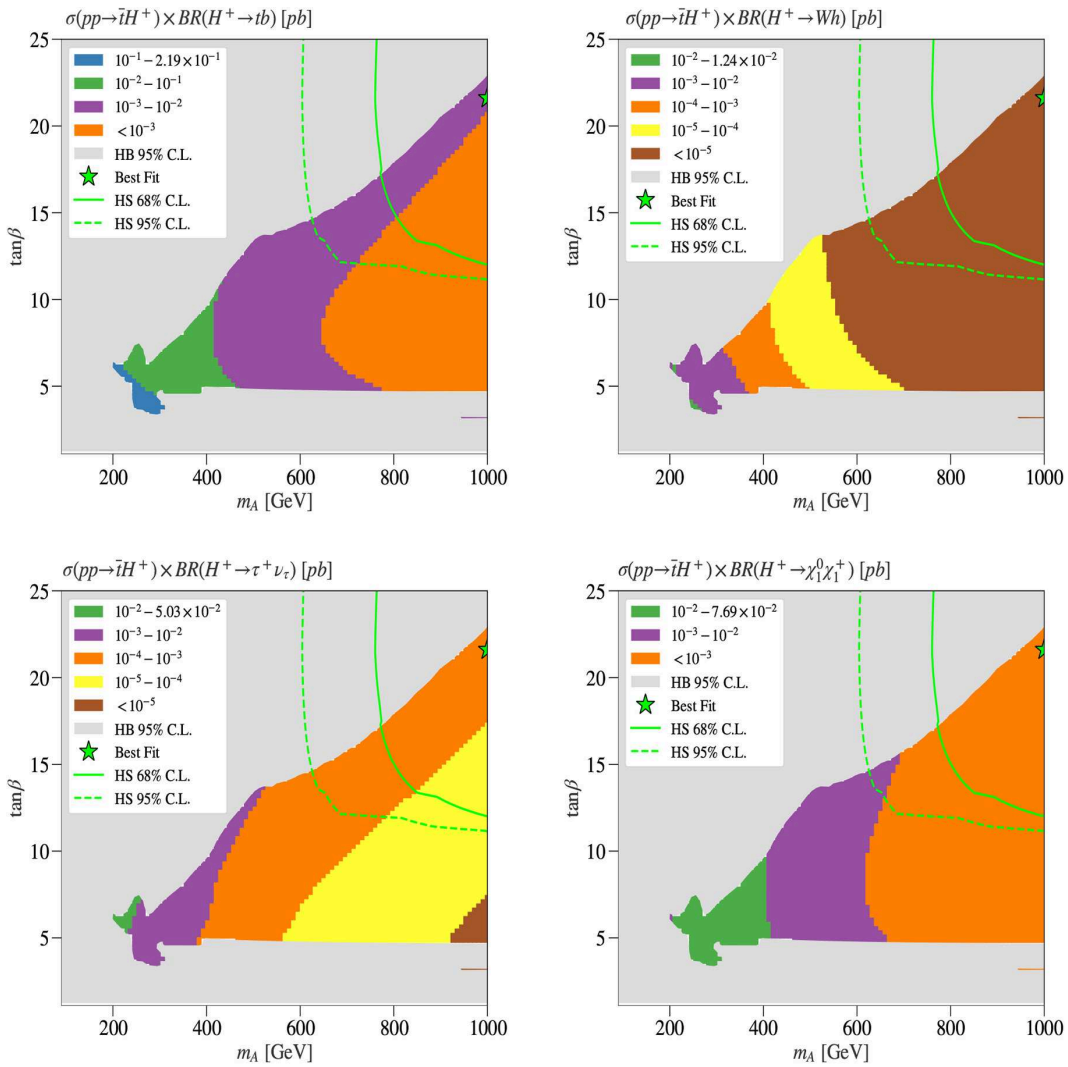

FIGURE 4 | The $\sigma(pp \to tH^- + \text{c.c.}) \times \text{BR}(H^\pm \to XY)$ rate (in pb) at $\sqrt{s}$=14 TeV in the $m_h^{\text{mod+}}$ scenario, for $XY \equiv tb$ **(top left)**, $XY \equiv W^\pm h$ **(top right)**, $XY \equiv \tau\nu$ **(bottom left)**, and $XY \equiv \tilde{\chi}_1^0\tilde{\chi}_1^+$ **(bottom right)**. Notice that c.c. channels are included. The best fit points are marked by green stars.

TABLE 3 | Allowed range of variation for the free parameters of all 2HDM types.

m_h (GeV)	m_H (GeV)	m_A (GeV)	$m_{H^\pm}$ (GeV)	α	β	m_{12}^2 (GeV^2)
125	$[m_{H^\pm}; 1000]$	$[90; m_{H^\pm}]$	[90; 1000]	$[\pi/5; \pi/2]$	$[-\pi/2; \pi/2]$	$m_A^2 \tan\beta/(1+\tan^2\beta)$

TABLE 4 | Experimental results of flavor observables combined by the PDG and/or HFAG collaborations in Amhis et al. [134] and Olive et al. [135].

Observable	Experimental result	SM contribution	Combined at 1σ
BR($B \to \tau\nu$)	$(1.14 \pm 0.22) \times 10^{-4}$ [134]	$(0.78 \pm 0.07) \times 10^{-4}$	0.23×10^{-4}
BR($B_s^0 \to \mu^+\mu^-$)	$(2.8 \pm 0.7) \times 10^{-9}$ [136]	$(3.66 \pm 0.28) \times 10^{-9}$	0.75×10^{-9}
BR($B_d^0 \to \mu^+\mu^-$)	$(3.9 \pm 1.5) \times 10^{-10}$ [136]	$(1.08 \pm 0.13) \times 10^{-10}$	1.50×10^{-10}
BR($\overline{B} \to X_s\gamma)_{E_\gamma > 1.6\,\text{GeV}}$	$(3.43 \pm 0.22) \times 10^{-4}$ [134]	$(3.36 \pm 0.24) \times 10^{-4}$	0.32×10^{-4}
ΔM_s	(17.757 ± 0.021) ps^{-1} [134, 135]	(18.257 ± 1.505) ps^{-1}	1.5 ps^{-1}
ΔM_d	(0.510 ± 0.003) ps^{-1} [134, 135]	(0.548 ± 0.075) ps^{-1}	0.075 ps^{-1}

As for BR($B_q^0 \to \mu^+\mu^-$), the combined results from the LHCb and CMS collaborations are shown as in Archilli [136].

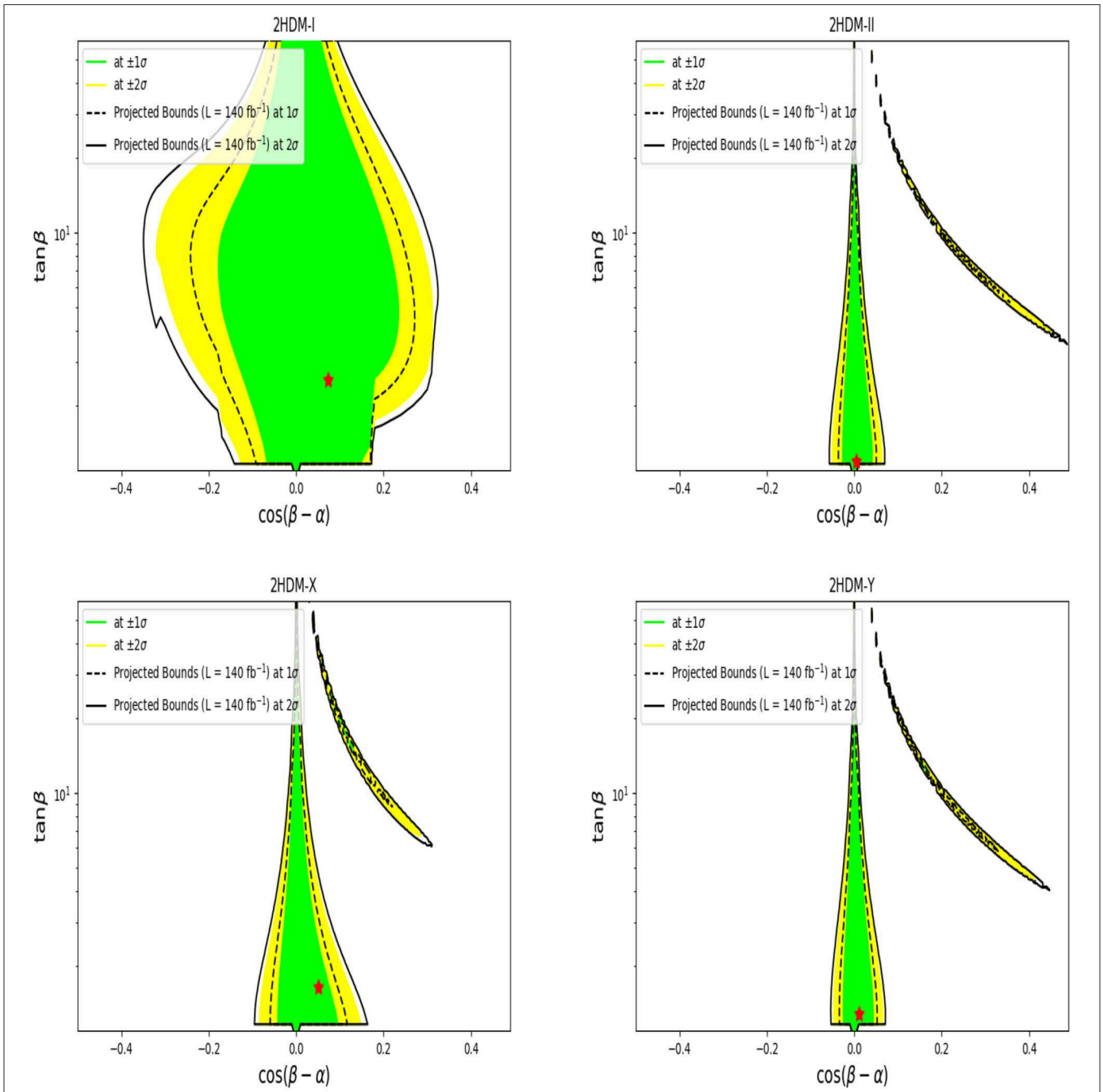

FIGURE 5 | Direct constraints from null heavy Higgs searches at the LHC on the parameter space of the 2HDM Type-I **(top left)**, Type-II **(top right)**, Type-X **(bottom left)**, and Type-Y **(bottom right)** mapped on the (α, β) plane. The colors indicate compatibility with the observed Higgs signal at 1σ (green), 2σ (yellow) around the best fit points (red stars).

Width Approximation (NWA) to estimate such a cross section (which we have done here). In the top-left(top-right) panel of **Figure 3**, we show the size of the cross section of $\sigma(pp \to tH^- + \text{c.c.}) \times \text{BR}(H^\pm \to tb)(\sigma(pp \to tH^- + \text{c.c.}) \times \text{BR}(H^\pm \to \tau\nu))$, given in pb.

For the hMSSM scenario, one can see that in the tb channel the largest cross section (more than 0.1 pb) is reached for small $\tan\beta < 3$. There is also a wide region with $m_{H^\pm} \in [400, 600]$ GeV and $\tan\beta < 10$ where the cross section is still rather important: between 10^{-3} and 0.1 pb. As for the $\tau\nu$ channel, the cross section is maximized when $\tan\beta$ is in the range $[4, 9]$ and the largest cross section is seen around 10^{-3} pb. However, amongst the bosonic channels, $H^\pm \to W^\pm A$ is hopeless because $\text{BR}(H^\pm \to W^\pm A)$ is very suppressed while $H^\pm \to W^\pm h$ can have a rate that is close to 10^{-2} pb for small $\tan\beta \approx 1$. Note that, for completeness, we have also drawn the exclusion region due to

TABLE 5 | The best fit points in the 2HDM Type-I, -II, -X, and -Y.

Parameters	Type-I	Type-II	Type-X	Type-Y
(α, β)	$(-0.30107, 1.19645)$	$(-0.77474, 0.791554)$	$(-0.49444, 1.02543)$	$(-0.64861, 0.91044)$
$(\cos(\beta-\alpha), \tan\beta)$	(0.07321, 2.54535)	(0.00450, 1.01239)	(0.05090, 1.64813)	(0.01175, 1.28754)
$(m_{H^\pm}, \Gamma_{H^\pm})$ (GeV)	$(178, 1.4\times10^{-2})$	(592, 25.2)	(493, 7.63)	(631, 16.8)
(m_A, m_H) (GeV)	(97.71, 212)	(512, 694)	(412, 509)	(550, 652)
BR($H^\pm \to \tau\nu$)	0.4%	–	0.03%	–
BR($H^\pm \to AW^\pm$)	55.2%	0.05%	0.18%	0.08%
BR($H^\pm \to hW^\pm$)	0.01%	0.04%	0.9%	0.06%
BR($H^\pm \to tb$)	44.1%	99.7%	98.6%	99.6%
$\sigma(pp \to \bar{t}H^+ + \text{c.c.})$ (fb)	1570	434	308	214

The decay width $\Gamma_{H^\pm}$, cross sections $\sigma(pp \to tH^- + \text{c.c.})$ as well as relevant decay BRs for the charged Higgs state are listed, for which values smaller than 10^{-4} are neglected. We have fixed $m_h = 125$ GeV and $m_{12}^2 = m_A^2 \sin\beta\cos\beta$.

BR($\overline{B} \to X_s\gamma$), even though we can always assume some kind of flavor violation that takes place in the MSSM and can bring the BR($\overline{B} \to X_s\gamma$) to a correct value. In terms of $\sigma(pp \to tH^- + \text{c.c.}) \times \text{BR}(H^\pm \to XY)$ for the $m_h^{\text{mod+}}$ scenario, the situation is worse. The best channels are $H^+ \to t\bar{b}$ and $H^+ \to \tilde{\chi}_1^+\tilde{\chi}_1^0$ with the maximum cross section in the allowed region being between 10^{-3} and 10^{-2} pb for charged Higgs boson masses in the range 400–600 GeV, as can be seen from **Figure 4**.

We conclude this section by presenting in **Table 2** two BPs, one each for the $m_h^{\text{mod+}}$ and hMSSM scenarios, to aid future analyses of Run-2 (and possibly Run-3) data from the LHC. Notice that these BPs do not correspond to the best fit points in these two MSSM configurations, as the latter would yield too small cross sections[5], owing to the very large charged Higgs mass involved (of order 1 TeV). Yet, the BPs presented correspond to rather large values of $m_{H^\pm}$, as dictated by the compatibility tests of the $m_h^{\text{mod+}}$ and hMSSM scenarios with current datasets, still giving production and decay rates (in one or more channels) potentially testable in the near future.

5.2. 2HDM Results

We now move on to discuss the 2HDM. In this scenario, we consider h as being again the 125 GeV SM-like Higgs and vary the other six parameters as indicated in **Table 3**. When performing the scan over the 2HDM parameter space, other than taking into account the usual LHC, Tevatron and LEP bounds (as implemented in HiggsBounds and HiggsSignals) as well as the theoretical ones (as implemented in 2HDMC), we also have to consider flavor observables. In fact, unlike the MSSM, where potentially significant contributions to (especially) B-physics due to the additional Higgs states entering the 2HDM beyond the SM-like one can be canceled by the corresponding sparticle effects (and besides, are generally small because of the rather heavy H, A, and $H^\pm$ masses), the 2HDM has to be tested against a variety of such data. The B-physics observables that we have considered to that effect are listed in **Table 4**. We have computed the 2HDM predictions for these in all 2HDM Types using our own implementation, which output in fact agrees with the one from SuperIso [137] (when run in 2HDM mode).

Based on such constrained scans, we first illustrate in **Figure 5**, on the $(\cos(\beta-\alpha), \tan\beta)$ plane, the best fit points for the four 2HDM Types. Herein, are also shown the compatibility regions with the observed Higgs signal at the 1σ (green) and 2σ (yellow) level. The details of the best fit points herein (red stars) are given in **Table 5** together with the values of the following observables: the total charged Higgs width $\Gamma_{H^\pm}$, $\sigma(pp \to tH^- + \text{c.c.})$, BR($H^\pm \to \tau\nu$), BR($H^\pm \to tb$), BR($H^\pm \to AW^\pm$), and BR($H^\pm \to hW^\pm$). Note that in the 2HDM Type-II and -Y, the best fit point is located at a charged Higgs mass around 600 GeV because of the $\overline{B} \to X_s\gamma$ constraints while in the 2HDM Type-I and- X one can fit data with a rather light charged Higgs state.

In **Figures 6–9**, we show (in gray) over the $(m_{H^\pm}, \tan\beta)$ plane the 95% CL exclusion region from the non-observation of the additional Higgs states for 2HDM Type-I(-II)[-X]{-Y}. In all these plots, we also draw (as a solid yellow line) the 95% CL exclusion from BR($\overline{B} \to X_s\gamma$) together with a solid green line representing the 1σ compatibility with the Higgs signals observed at the LHC. As a green star, we also give the best fit point to these data over the available parameter space for all Types (these are the same as the red stars in the previous figure). It is clear from these plots that, in the 2HDM-I and -X, one can still have relatively light charged Higgs states (of the order 100–200 GeV in mass) that are consistent with all aforementioned data, crucially including B-physics observables. In addition, such light charged Higgs does not affect too much the rate of $h \to \gamma\gamma$ which is strongly dominated by the $W^\pm$ loops while the charged Higgs loops are subleading. In the case of the 2HDM Type-II and -Y, the BR($\overline{B} \to X_s\gamma$) constraint pushes the charged Higgs boson mass to be higher than 580 GeV. (Note that, in the 2HDM Type-II, it is clear that, like for the MSSM case, large $\tan\beta$ is excluded mainly from $H, A \to \tau^+\tau^-$ as well as from $H^+ \to \tau\nu$ searches at the LHC). However, for 2HDM Type-X, one can see that light charged Higgs states, with $m_{H^\pm} \leq 170$ GeV, are excluded for all $\tan\beta$'s and this is due to charged Higgs searches failing to detect $H^\pm \to \tau\nu$.

We now discuss the size of the charged Higgs production cross section times its BRs in decay channels, such as

[5]Probably accessible only at the High-Luminosity LHC [133].

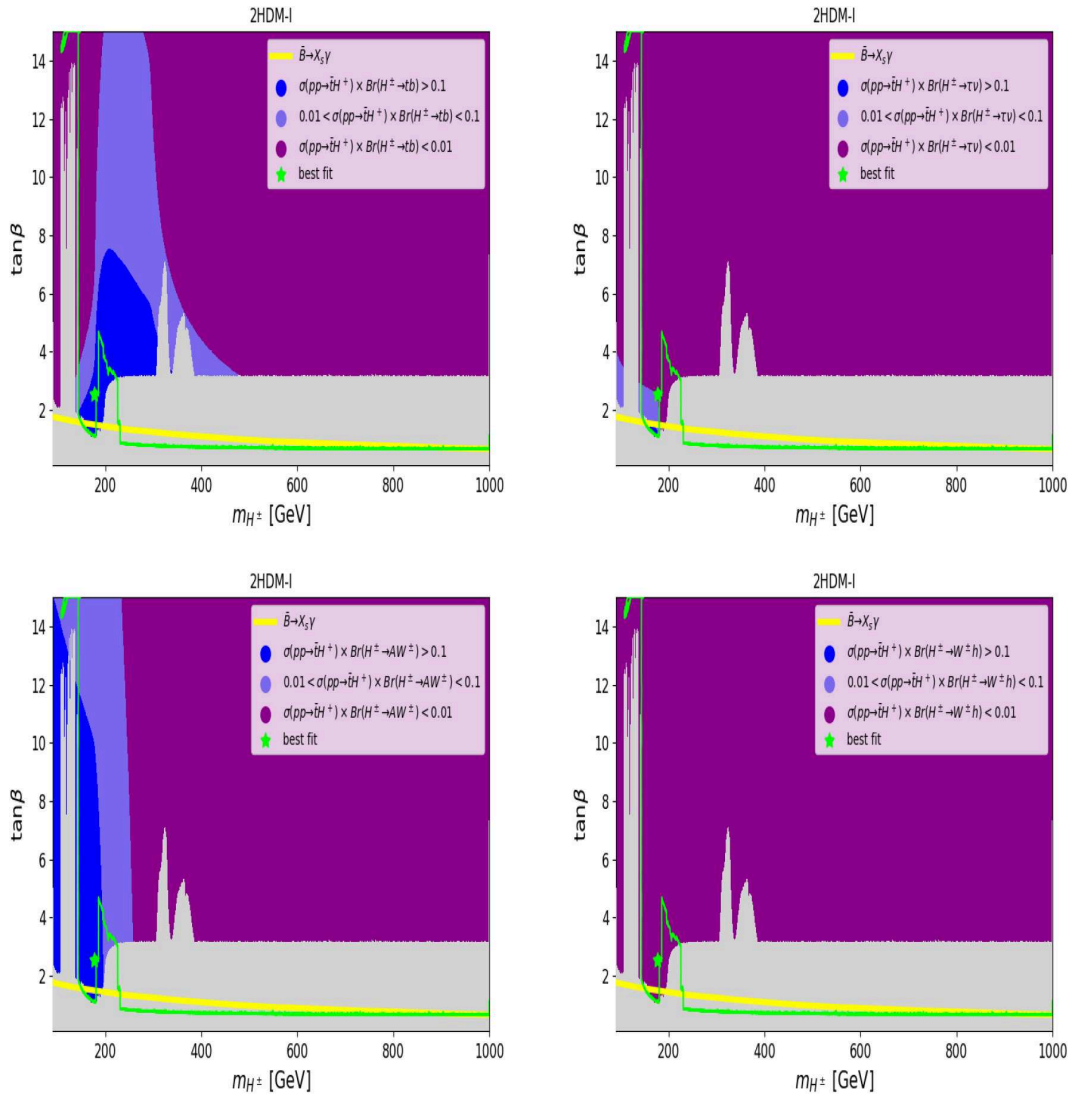

FIGURE 6 | The $\sigma(pp \to tH^- + \text{c.c.}) \times \text{BR}(H^\pm \to XY)$ rate (in pb) at $\sqrt{s}$=14 TeV in the 2HDM Type-I, for $XY \equiv tb$ **(top left)**, $XY \equiv \tau\nu$ **(top right)**, $XY \equiv AW^\pm$ **(bottom left)**, and $XY \equiv hW^\pm$ **(bottom right)**. Exclusion bounds at 95% CL from the non-observation of the additional Higgs states are overlaid in gray. The green contour indicates compatibility with the observed Higgs signal at 68% CL and the best fit (benchmark) points are marked by green stars. The solid yellow line contours are the boundary of 95% CL exclusion from $\overline{B} \to X_s\gamma$ measurements. The maximum of the cross section $\sigma(pp \to tH^- + \text{c.c.}) \times \text{BR}(H^\pm \to XY)$ is 3.1 and 1.83 pb for $XY \equiv AW^\pm$, tb, respectively.

$H^+ \to \tau\nu, t\bar{b}, AW^\pm$ and $hW^\pm$. In **Figure 6** (top-left panel) we illustrate the values of $\sigma(pp \to tH^- + \text{c.c.}) \times \text{BR}(H^\pm \to tb)$ (in pb) where we can see that it is possible tohave a production times decay rate in the range 0.01 to 0.2 pb for $1 \leq \tan\beta \leq 6$ and 180 GeV $< m_{H^\pm} <$ 300 GeV. This could lead to more than thousands raw $t\bar{t}b$ signal events for 100 fb^{-1} luminosity. In the case of $H^\pm \to \tau\nu$ and $H^\pm \to hW^\pm$, which are suppressed, respectively, by $1/\tan\beta$ and $\cos(\beta - \alpha) \approx 0$, the rate is much smaller than for the tb mode. In contrast, since the coupling $H^\pm W^\mp A$ is a gauge coupling without any suppression factor, when $H^\pm \to AW^\pm$ is open, it may dominate over the $H^\pm \to tb$ channel. One can see from **Figure 6** (bottom-left panel) that, for 100 GeV $< m_{H^\pm} <$ 220 GeV and for $1 \leq \tan\beta \leq 14$, the corresponding rate for $\sigma(pp \to tH^- + \text{c.c.}) \times \text{BR}(H^\pm \to AW^\pm) \geq 0.01$ pb. This could lead to an interesting final state bW^+W^-A where one $W^\pm$ could decay leptonically, hence offering a clean trigger. The decay $H^\pm \to hW^\pm$ is essentially inaccessible, see **Figure 6** (bottom-right panel).

In the case of 2HDM Type-II and -Y, as one can see from **Figures 7**, **9**, respectively, there is a wide region over the $(m_{H^\pm}, \tan\beta)$ plane where the rate for $\sigma(pp \to tH^- + \text{c.c.}) \times \text{BR}(H^\pm \to tb)$ is rather sizable for both moderate ($m_{H^\pm} \leq 300$ GeV) and heavy (otherwise) charged Higgs masses (top-left panel). However, if one takes into account the $\overline{B} \to X_s\gamma$ constraint, then $m_{H^\pm}$ is required to be much heavier than 580 GeV (as already discussed), which makes

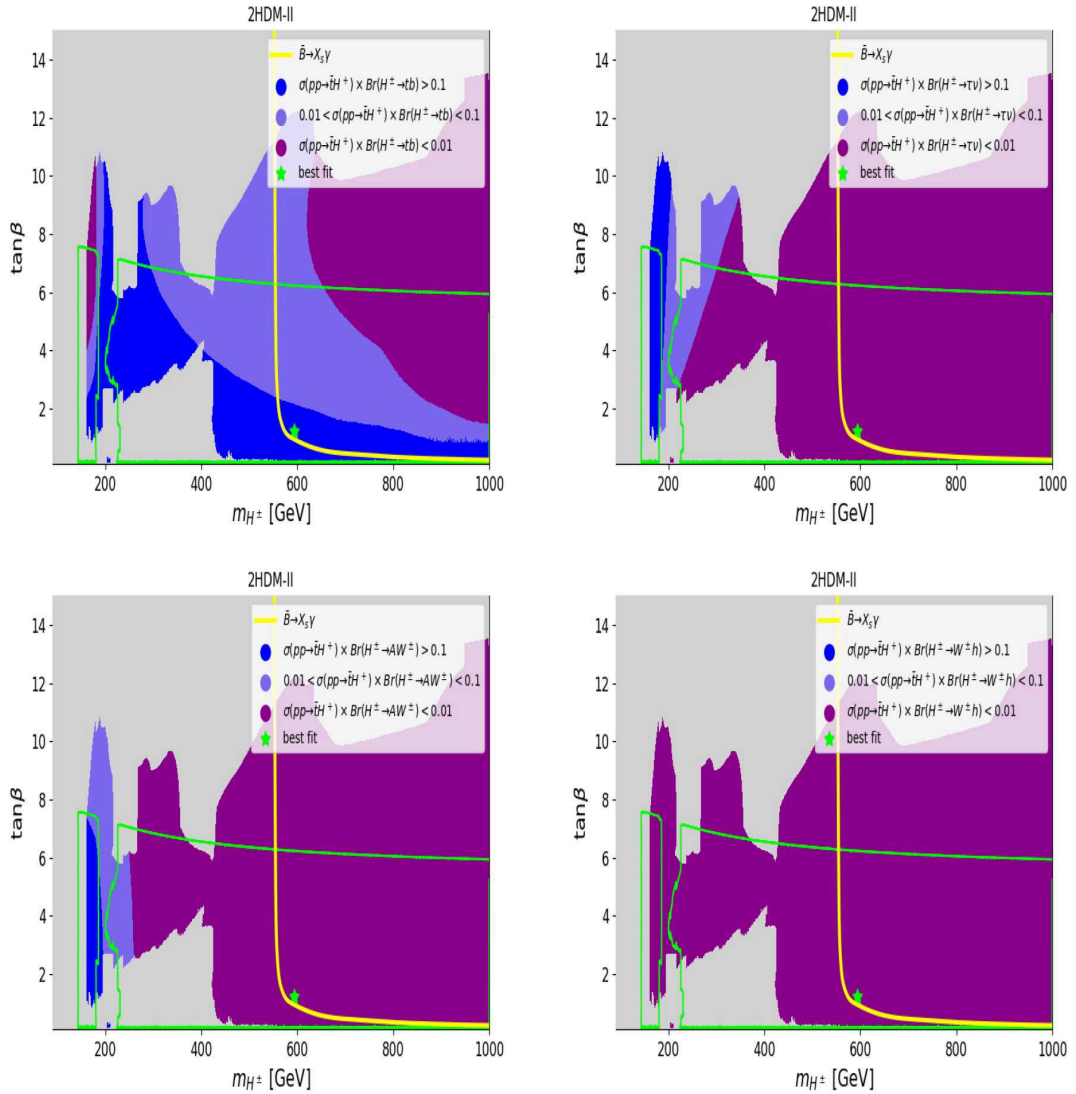

FIGURE 7 | The $\sigma(pp \to tH^- + \text{c.c.}) \times \text{BR}(H^\pm \to XY)$ rate (in pb) at $\sqrt{s}$=14 TeV in the 2HDM Type-II, for $XY \equiv tb$ **(top left)**, $XY \equiv \tau\nu$ **(top right)**, $XY \equiv AW^\pm$ **(bottom left)**, and $XY \equiv hW^\pm$ **(bottom right)**. The maximum of the cross section $\sigma(pp \to tH^- + \text{c.c.}) \times \text{BR}(H^\pm \to XY)$ is 2.3 and 1.38 pb for $XY \equiv AW^\pm$, tb, respectively. The color coding is the same as in **Figure 6**.

the rate $\sigma(pp \to tH^- + \text{c.c.}) \times \text{BR}(H^\pm \to tb) \geq 0.1$ pb only for $\tan\beta < 1.5$. All the other channels (in the three remaining panels) have smaller production times decay rates.

The 2HDM Type-X is depicted in **Figure 8**, wherein the usual production times BR rates are shown. The top-right panel is again for the $H^+ \to t\bar{b}$ channel, which exhibits a potentially interesting cross section ($\geq$ 1 fb) in the $H^+ \to t\bar{b}$ channel for both a light charged Higgs mass (around 200 GeV) and a heavy one (around 420 GeV). In the case of the $\tau\nu$ channel (top-right panel), one can get sizable rates for $\sigma(pp \to tH^- + \text{c.c.}) \times \text{BR}(H^\pm \to \tau\nu)$ for a charged Higgs mass around 200 GeV and $\tan\beta \geq 2$.

In all 2HDM Types, we elect the best fit points to also be the BPs amenable to experimental tests by ATLAS and CMS.

6. CONCLUSIONS

We have studied charged Higgs boson phenomenology in both the MSSM and 2HDM, the purpose being to define BPs amenable to phenomenological investigation already with the full Run-1 and -2 datasets and certainly accessible with the Run-3 one of the LHC. They have been singled out following the enforcement of the latest theoretical and experimental constraints, so as to be entirely up-to-date. Furthermore, they have been defined with the intent of increasing sensitivity of dedicated (model-dependent) $H^\pm$ searches to some of the most probable parameter space configurations of either scenario. With this in mind, we have listed in two tables their input and output values, the former in terms of the fundamental parameters of the model concerned and the latter in terms of key observables (like,

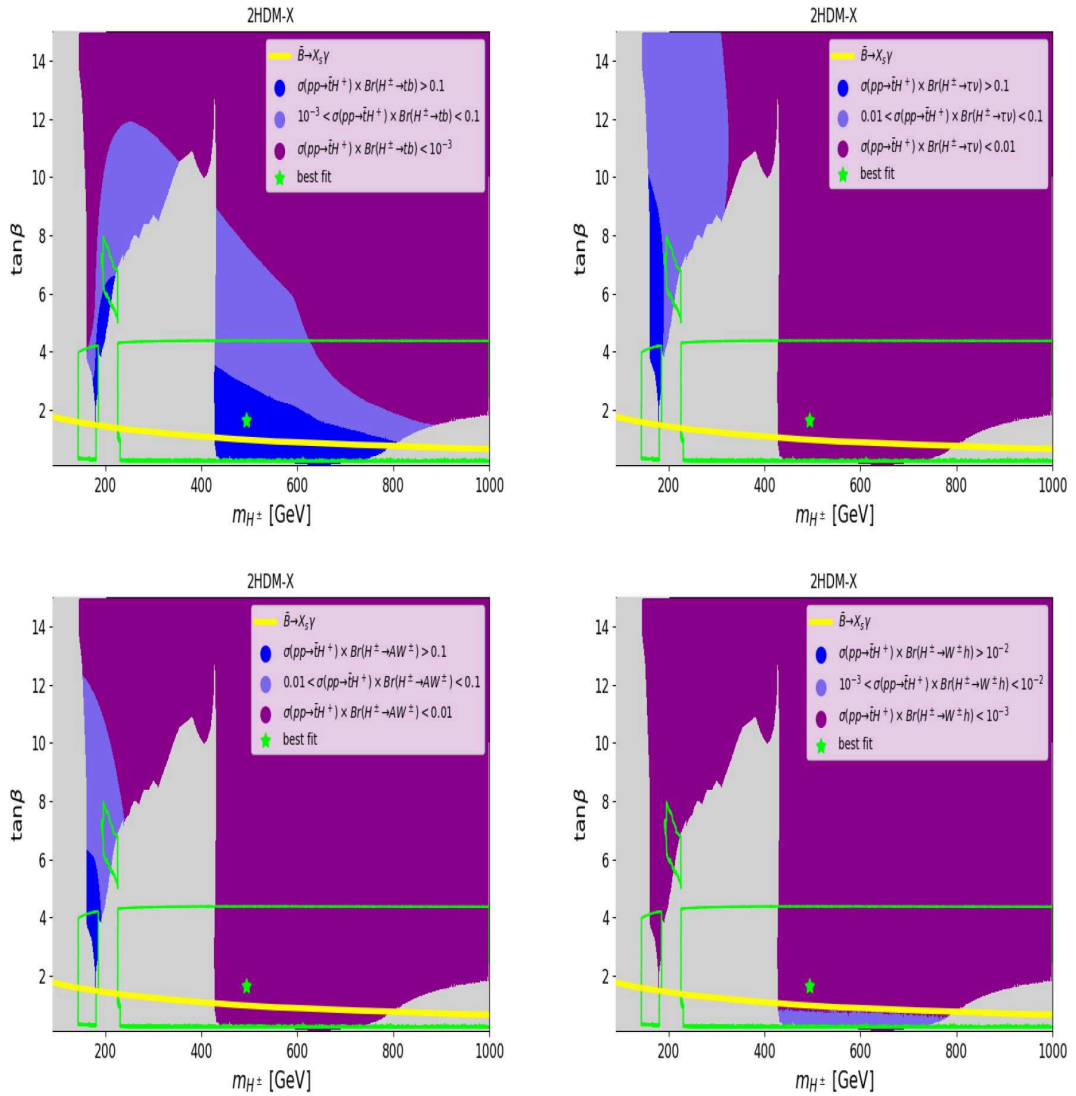

FIGURE 8 | The $\sigma(pp \to tH^- + \text{c.c.}) \times \text{BR}(H^\pm \to XY)$ rate (in pb) at $\sqrt{s}$=14 TeV in the 2HDM Type-X, for $XY \equiv tb$ **(top left)**, $XY \equiv \tau\nu$ **(top right)**, $XY \equiv AW^\pm$ **(bottom left)**, and $XY \equiv hW^\pm$ **(bottom right)**. The maximum of the cross section $\sigma(pp \to tH^- + \text{c.c.}) \times \text{BR}(H^\pm \to XY)$ is 2.3 and 1.23 pb for $XY \equiv AW^\pm$, tb, respectively. The color coding is the same as in **Figure 6**.

e.g., physical masses and couplings, production cross sections and decay BRs). We have also specified which numerical tools we have used to produce all such an information, including their settings.

For the MSSM we have concentrated on two popular scenarios, i.e., the hMSSM and $m_h^{\text{mod}+}$ ones. It was found that the hMSSM case still possesses a rather large available parameter space, here mapped over the $(m_A, \tan\beta)$ plane, while the $m_h^{\text{mod}+}$ one is instead much more constrained. In terms of the largest production and decay rates, in the hMSSM scenario one finds that the most copious channels, assuming $pp \to tH^- + \text{c.c.}$ production, are via the decay $H^+ \to t\bar{b}$ followed by $H^+ \to \tau\nu$ whereas for the $m_h^{\text{mod}+}$ scenario the decay modes $H^+ \to t\bar{b}$ and $H^+ \to \tilde{\chi}_1^+\tilde{\chi}_0$ offer the largest rates. In both cases, only $m_{H^\pm} > m_t$ values are truly admissible by current data.

Within the 2HDM, we have looked at the four standard Yukawa setups, known as Type-I, -II, -X, and -Y. Because of $\overline{B} \to X_s\gamma$ constraints, the profile of a charged Higgs in the 2HDM Type-II and -Y is a rather heavy one, with a mass required to be more than 580 GeV. While this puts an obvious limit to LHC sensitivity owing to a large phase space suppression in production, we have emphasized that $H^\pm \to b\bar{b}W^\pm$ channels should be searched for, with intermediate contributions from the $AW^\pm$ and tb modes (including their interference [138]), alongside $H^\pm \to \tau\nu$. In the case of the 2HDM Type-I and -X, a much lighter charged Higgs state is still allowed by data, in fact, even with a mass below that of the top quark. While the configuration $m_{H^\pm} < m_t$ is best probed by using $t\bar{t}$ production and decays into $\tau\nu$, the complementary mass region, i.e., $m_{H^\pm} > m_t$ (wherein $pp \to tH^- + \text{c.c.}$ is the production mode), may well

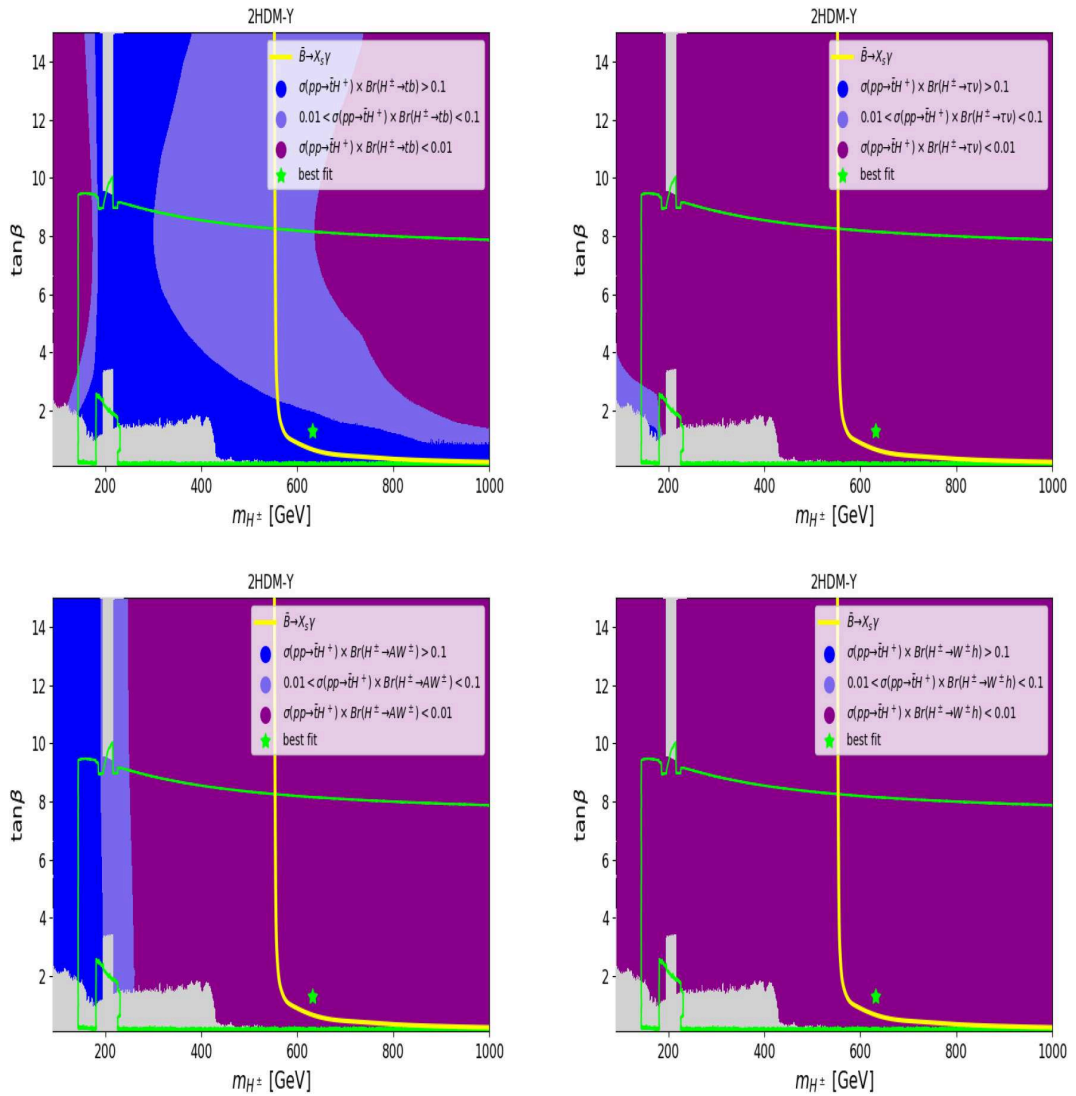

FIGURE 9 | The $\sigma(pp \to tH^- + \text{c.c.}) \times \text{BR}(H^\pm \to XY)$ rate (in pb) at $\sqrt{s}$=14 TeV in the 2HDM Type-Y, for $XY \equiv tb$ **(top left)**, $XY \equiv \tau\nu$ **(top right)**, $XY \equiv AW^\pm$ **(bottom left)**, and $XY \equiv hW^\pm$ **(bottom right)**. The maximum of the cross section $\sigma(pp \to tH^- + \text{c.c.}) \times \text{BR}(H^\pm \to XY)$ is 3.54 and 1.85 pb for $XY \equiv AW^\pm$, tb, respectively. The color coding is the same as in **Figure 6**.

be accessible via a combination of $H^+ \to t\bar{b}$ and $H^\pm \to AW^\pm$ (in Type-I) plus $H^\pm \to \tau\nu$ (in Type-X).

DATA AVAILABILITY STATEMENT

The datasets analysed in this study can be found in the HiggsBounds repository: https://higgsbounds.hepforge.org.

AUTHOR'S NOTE

Since the original submission of this paper, several new experimental analyses have been carried out by ATLAS and CMS using the full Run-2 data sample of $\approx$ 139 fb^{-1}. Some of these, covering both measurements of the SM-like Higgs Boson and the search for new (pseudo)scalar Higgs states, both charged and neutral, have been captured by the latest versions of HiggsBounds and HiggsSignals, HiggsBounds-5.3.2beta and HiggsSignals-2.2.3beta, respectively. Likewise, further analyses by LHCb of flavor observables have been carried out since and most of these have been captured by the latest version of SuperIso. Hence, we have repeated our scans using all such tools and found negligible differences between our original results and the new ones. Further, we have investigated which ones of the full Run-2 data set analyses were not incorporated in the above codes and found that their *ad-hoc* application to our analysis did not change our results either.

AUTHOR CONTRIBUTIONS

All authors listed have made a substantial, direct and intellectual contribution to the work, and approved it for publication.

FUNDING

AA, RB, and SM were supported by the grant H2020-MSCA-RISE-2014 no. 645722 (NonMinimalHiggs). This work was also supported by the Moroccan Ministry of Higher Education and Scientific Research MESRSFC and CNRST: Project PPR/2015/6. SM was supported in part through the NExT. Institute and the STFC CG ST/L000296/1.

ACKNOWLEDGMENTS

For the avoidance of doubt, we acknowledge that this paper has already been submitted to a public database as https://arxiv.org/abs/1810.09106.

REFERENCES

1. ATLAS Collaboration. Observation of a new particle in the search for the standard model Higgs Boson with the ATLAS detector at the LHC. *Phys Lett B.* (2012) **716**:1–29. doi: 10.1016/j.physletb.2012.08.020
2. ATLAS Collaboration. Measurements of Higgs Boson production and couplings in Diboson final states with the ATLAS detector at the LHC. *Phys Lett B.* (2013) **726**:88–119. doi: 10.1016/j.physletb.2013.08.010
3. CMS Collaboration. Observation of a New Boson at a mass of 125 GeV with the CMS experiment at the LHC. *Phys Lett B.* (2012) **716**:30. doi: 10.1016/j.physletb.2012.08.021
4. CMS Collaboration. Observation of a New Boson with Mass Near 125 GeV in *pp* Collisions at $\sqrt{s}$ = 7 and 8 TeV. *JHEP.* (2013) **1306**:081. doi: 10.1007/JHEP06(2013)081
5. Martin SP. A supersymmetry primer. *Adv Ser Direct High Energy Phys.* (2010) **21**:1. doi: 10.1142/9789812839657_0001
6. Bagnaschi E, Bahl H, Fuchs E, Hahn T, Heinemeyer S, Liebler S, et al. MSSM Higgs Boson searches at the LHC: benchmark scenarios for run 2 and beyond. *Eur Phys J C.* (2019) **79**:617. doi: 10.1140/epjc/s10052-019-7114-8
7. ATLAS Collaboration. Updated coupling measurements of the Higgs Boson with the ATLAS detector using up to 25 fb^{-1} of proton-proton collision data. In: *49th Rencontres de Moriond on Electroweak Interactions and Unified Theories*. La Thuile.
8. CMS Collaboration. Precise determination of the mass of the Higgs Boson and tests of compatibility of its couplings with the standard model predictions using proton collisions at 7 and 8 TeV. *Eur Phys J C.* (2015) **75**:212. doi: 10.1140/epjc/s10052-015-3351-7
9. Gunion JF, Haber HE, Kane GL, Dawson S. The Higgs Hunter's guide. *Front Phys.* (2000) **80**:1–404.
10. Carena M, Haber HE. Higgs Boson theory and phenomenology. *Prog Part Nucl Phys.* (2003) **50**:63–152. doi: 10.1016/S0146-6410(02)00177-1
11. Djouadi A. The anatomy of electro-weak symmetry breaking. II. The Higgs Bosons in the minimal supersymmetric model. *Phys Rept.* (2008) **459**:1–241. doi: 10.1016/j.physrep.2007.10.005
12. Okada Y, Yamaguchi M, Yanagida T. Upper bound of the lightest Higgs Boson mass in the minimal supersymmetric standard model. *Prog Theor Phys.* (1991) **85**:1. doi: 10.1143/ptp/85.1.1
13. Ellis JR, Ridolfi G, Zwirner F. Radiative corrections to the masses of supersymmetric Higgs Bosons. *Phys Lett B.* (1991) **257**:83.
14. Haber HE, Hempfling R. Can the mass of the lightest Higgs boson of the minimal supersymmetric model be larger than m(Z)? *Phys Rev Lett* (1991) **66**:1815.
15. Carena M, Espinosa JR, Quiros M, Wagner CEM. Analytical expressions for radiatively corrected Higgs masses and couplings in the MSSM. *Phys Lett B.* (1995) **355**:209.
16. Haber HE, Hempfling R, Hoang AH. Approximating the radiatively corrected Higgs mass in the minimal supersymmetric model. *Z Phys C.* (1997) **75**:539.
17. Heinemeyer S, Hollik W, Weiglein G. The Masses of the neutral CP—even Higgs bosons in the MSSM: accurate analysis at the two-loop level. *Eur Phys J C.* (1999) **9**:343.
18. Degrassi G, Slavich P, Zwirner F. On the neutral Higgs boson masses in the MSSM for arbitrary stop mixing. *Nucl Phys B.* (2001) **611**:403. doi: 10.1016/S0550-3213(01)00343-1
19. Brignole A, Degrassi G, Slavich P, Zwirner F. On the two-loop sbottom corrections to the neutral Higgs boson masses in the MSSM. *Nucl Phys B.* (2002) **643**:79. doi: 10.1016/S0550-3213(02)00748-4
20. Brignole A, Degrassi G, Slavich P, Zwirner F. On the O(alpha(t)**2) two-loop corrections to the neutral Higgs boson masses in the MSSM. *Nucl Phys B* (2002) **631**:195. doi: 10.1016/S0550-3213(02)00184-0
21. Harlander RV, Kant P, Mihaila L, Steinhauser M. Higgs boson mass in supersymmetry to three loops. *Phys Rev Lett.* (2008) **100**:191602. doi: 10.1103/PhysRevLett.100.191602
22. Degrassi G, Heinemeyer S, Hollik W, Slavich P, Weiglein G. Towards high precision predictions for the MSSM Higgs sector. *Eur Phys J C.* (2003) **28**:133. doi: 10.1140/epjc/s2003-01152-2
23. Carena M, Heinemeyer S, Wagner CEM, Weiglein G. MSSM Higgs boson searches at the Tevatron and the LHC: impact of different benchmark scenarios. *Eur Phys J C.* (2006) **45**:797. doi: 10.1140/epjc/s2005-02470-y
24. Carena M, Heinemeyer S, Stål O, Wagner CEM, Weiglein G. MSSM Higgs Boson searches at the LHC: benchmark scenarios after the discovery of a Higgs-like particle. *Eur Phys J C.* (2013) **73**:2552. doi: 10.1140/epjc/s10052-013-2552-1
25. Carena M, Heinemeyer S, Wagner CEM, Weiglein G. Suggestions for benchmark scenarios for MSSM Higgs boson searches at Hadron colliders. *Eur Phys J C.* (2003) **26**:601. doi: 10.1140/epjc/s2002-01084-3
26. Djouadi A, Maiani L, Moreau G, Polosa A, Quevillon J, Riquer V. The post-Higgs MSSM scenario: Habemus MSSM? *Eur Phys J C.* (2013) **73**:2650. doi: 10.1140/epjc/s10052-013-2650-0
27. Maiani L, Polosa AD, Riquer V. Probing minimal supersymmetry at the LHC with the Higgs Boson masses. *New J Phys.* (2012) **14**:073029. doi: 10.1088/1367-2630/14/7/073029
28. Maiani L, Polosa AD, Riquer V. Heavier Higgs particles: indications from minimal supersymmetry. *Phys Lett B.* (2012) **718**:465. doi: 10.1016/j.physletb.2012.10.041
29. Djouadi A, Quevillon J. The MSSM Higgs sector at a high M_{SUSY}: reopening the low tanβ regime and heavy Higgs searches. *JHEP.* (2013) **1310**:028. doi: 10.1007/JHEP10(2013)028
30. Bagnaschi E, Frensch F, Heinemeyer S, Lee G, Liebler S, Muhlleitner M, et al. *Benchmark scenarios for low* tanβ *in the MSSM*. LHCHXSWG-2015-002. (2015).
31. Barger VD, Phillips RJN, Roy DP. Heavy charged Higgs signals at the LHC. *Phys Lett B.* (1994) **324**:236.
32. Gunion JF, Haber HE, Paige FE, Tung WK, Willenbrock SSD. Neutral and charged Higgs detection: heavy quark fusion, top quark mass dependence and rare decays. *Nucl Phys B.* (1987) **294**:621.
33. Diaz-Cruz JL, Sampayo OA. Contribution of gluon fusion to the production of charged Higgs at Hadron colliders. *Phys Rev D.* (1994) **50**:6820.
34. Akeroyd AG, Aoki M, Arhrib A, Basso L, Ginzburg IF, Guedes R, et al. Prospects for charged Higgs searches at the LHC. *Eur Phys J C.* (2017) **77**:276. doi: 10.1140/epjc/s10052-017-4829-2
35. Borzumati F, Kneur JL, Polonsky N. Higgs-Strahlung and R-parity violating slepton-Strahlung at Hadron colliders. *Phys Rev D.* (1999) **60**:115011.

36. Guchait M, Moretti S. Improving the discovery potential of charged Higgs bosons at Tevatron run II. *JHEP.* (2002) **0201**:001. doi: 10.1088/1126-6708/2002/01/001
37. ATLAS Collaboration. Search for charged Higgs Bosons decaying via $H^{\pm} \to \tau^{\pm}\nu$ in fully hadronic final states using *pp* collision data at $\sqrt{s} = 8$ TeV with the ATLAS detector. *JHEP.* (2015) **1503**:088 doi: 10.1007/JHEP03(2015)088
38. CMS Collaboration. Search for a charged Higgs boson in pp collisions at $\sqrt{s} = 8$ TeV. *JHEP.* (2015) **1511**:018. doi: 10.1007/JHEP11(2015)018
39. ATLAS Collaboration. Search for a light charged Higgs boson in the decay channel $H^{+} \to c\bar{s}$ in $t\bar{t}$ events using pp collisions at $\sqrt{s}$ = 7 TeV with the ATLAS detector. *Eur Phys J C.* (2013) **73**:2465. doi: 10.1140/epjc/s10052-013-2465-z
40. CMS Collaboration. Search for a light charged Higgs boson decaying to $c\bar{s}$ in pp collisions at $\sqrt{s} = 8$ TeV. *JHEP.* (2015) **1512**:178. doi: 10.1007/JHEP12(2015)178
41. CMS Collaboration. Search for Charged Higgs boson to $c\bar{b}$ in lepton+jets channel using top quark pair events.
42. ATLAS Collaboration. Search for charged Higgs bosons produced in association with a top quark and decaying via $H^{\pm} \to \tau\nu$ using *pp* collision data recorded at $\sqrt{s} = 13$ TeV by the ATLAS detector. *Phys Lett B.* (2016) **759**:555. doi: 10.1016/j.physletb.2016.06.017
43. CMS Collaboration. Search for charged Higgs bosons with the $H^{\pm} \to \tau^{\pm}\nu_{\tau}$ decay channel in the fully hadronic final state at $\sqrt{s} = 13$ TeV. *CMS-PAS-HIG-16-031*. (2016).
44. ATLAS Collaboration. Search for charged Higgs bosons in the $H^{\pm} \to tb$ decay channel in *pp* collisions at $\sqrt{s} = 13$ TeV using the ATLAS detector. *ATLAS-CONF-2016-089*. (2016).
45. Arhrib A, Benbrik R, Moretti S. Bosonic decays of charged Higgs Bosons in a 2HDM type-I. *Eur Phys J C.* (2017) **77**:621. doi: 10.1140/epjc/s10052-017-5197-7
46. Arbey A, Mahmoudi F, Stal O, Stefaniak T. Status of the charged Higgs Boson in two Higgs doublet models. *Eur Phys J C.* (2018) **78**:182. doi: 10.1140/epjc/s10052-018-5651-1
47. Bernon J, Gunion JF, Haber HE, Jiang Y, Kraml S. Scrutinizing the alignment limit in two-Higgs-doublet models: m_h=125 GeV. *Phys Rev D.* (2015) **92**:075004. doi: 10.1103/PhysRevD.92.075004
48. Heinemeyer S, Hollik W, Weiglein G. QCD corrections to the masses of the neutral CP—even Higgs bosons in the MSSM. *Phys Rev D.* (1998) **58**:091701.
49. Heinemeyer S, Hollik W, Weiglein G. Precise prediction for the mass of the lightest Higgs Boson in the MSSM. *Phys Lett B.* (1998) **440**:296.
50. Heinemeyer S, Hollik W, Weiglein G. FeynHiggs: a program for the calculation of the masses of the neutral CP even Higgs Bosons in the MSSM. *Comput Phys Commun.* (2000) **124**:76. doi: 10.1016/S0010-4655(99)00364-1
51. Hahn T, Heinemeyer S, Hollik W, Rzehak H, Weiglein G. FeynHiggs: a program for the calculation of MSSM Higgs-boson observables—version 2.6.5. *Comput Phys Commun.* (2009) **180**:1426. doi: 10.1016/j.cpc.2009.02.014
52. Djouadi A, Kalinowski J, Spira M. HDECAY: a program for Higgs boson decays in the standard model and its supersymmetric extension. *Comput Phys Commun.* (1998) **108**:56.
53. Djouadi A, Kalinowski J, Muehlleitner M, Spira M. HDECAY: twenty$_{++}$ years after. *Comput Phys Commun.* (2019) **238**:214. doi: 10.1016/j.cpc.2018.12.010
54. Harlander RV, Liebler S, Mantler H. SusHi: a program for the calculation of Higgs production in gluon fusion and bottom-quark annihilation in the Standard Model and the MSSM. *Comput Phys Commun.* (2013) **184**:1605. doi: 10.1016/j.cpc.2013.02.006
55. Harlander RV, Liebler S, Mantler H. SusHi Bento: beyond NNLO and the heavy-top limit. *Comput Phys Commun.* (2017) **212**:239. doi: 10.1016/j.cpc.2016.10.015
56. Heinemeyer S, Hollik W, Weiglein G. Constraints on tan Beta in the MSSM from the upper bound on the mass of the lightest Higgs Boson. *JHEP.* (2000) **0006**:009. doi: 10.1088/1126-6708/2000/06/009
57. ATLAS Collaboration. Search for strongly produced superpartners in final states with two same sign leptons with the ATLAS detector using 21 fb-1 of proton-proton collisions at sqrt(s) = 8 TeV. *ATLAS-CONF-2013-007*. (2013).
58. ATLAS Collaboration. Search for new phenomena in final states with large jet multiplicities and missing transverse momentum at $\sqrt{s}$=8 TeV proton-proton collisions using the ATLAS experiment. *JHEP.* (2013) **1310**:130. doi: 10.1007/JHEP10(2013)130
59. CMS Collaboration. Search for supersymmetry in hadronic final states with missing transverse energy using the variables α_T and b-quark multiplicity in pp collisions at $\sqrt{s} = 8$ TeV. *Eur Phys J C.* (2013) **73**:2568. doi: 10.1140/epjc/s10052-013-2568-6
60. CMS Collaboration. "Search for new physics in events with same-sign dileptons and jets in pp collisions at $\sqrt{s}$ = 8 TeV. *JHEP.* (2014) **1401**:163. doi: 10.1007/JHEP01(2014)163
61. CMS Collaboration. Search for new physics in the multijet and missing transverse momentum final state in proton-proton collisions at $\sqrt{s}$ = 8 TeV. *JHEP.* (2014) **1406**:055. doi: 10.1007/JHEP06(2014)055
62. Gunion JF, Haber HE. The CP conserving two Higgs doublet model: the approach to the decoupling limit. *Phys Rev D.* (2003) **67**:075019. doi: 10.1103/PhysRevD.67.075019
63. Branco GC, Lavoura L, Silva JP. CP violation. *Int Ser Monogr Phys.* (1999) **103**:1.
64. Gomez-Bock M, Noriega-Papaqui R. Flavor violating decays of the Higgs Bosons in the THDM-III. *J Phys G.* (2006) **32**:761. doi: 10.1088/0954-3899/32/6/002
65. Arhrib A, Benbrik R, Chen CH, Parry JK, Rahili L, Semlali S, et al. $R_{K^{(*)}}$ anomaly in type-III 2HDM. *arXiv [preprint].* arXiv:1710.05898.
66. David A, Denner A, Duehrssen M, Grazzini M, Grojean C, Passarino G, et al. LHC HXSWG interim recommendations to explore the coupling structure of a Higgs-like particle. *arXiv [preprint].* arXiv:1209.0040.
67. Ferreira PM, Gunion JF, Haber HE, Santos R. Probing wrong-sign Yukawa couplings at the LHC and a future linear collider. *Phys Rev D.* (2014) **89**:115003. doi: 10.1103/PhysRevD.89.115003
68. Ferreira PM, Guedes R, Sampaio MOP, Santos R. Wrong sign and symmetric limits and non-decoupling in 2HDMs. *JHEP.* (2014) **1412**:067. doi: 10.1007/JHEP12(2014)067
69. Eriksson D, Rathsman J, Stål O. 2HDMC: two-Higgs-doublet model calculator physics and manual. *Comput Phys Commun.* (2010) **181**:189. doi: 10.1016/j.cpc.2009.09.011
70. Deshpande NG, Ma E. Pattern of symmetry breaking with two Higgs doublets. *Phys Rev D.* (1978) **18**:2574.
71. Ferreira PM, Santos R, Barroso A. Stability of the tree-level vacuum in two Higgs doublet models against charge or CP spontaneous violation. *Phys Lett B.* (2004) **603**:219. doi: 10.1016/j.physletb.2004.10.022
72. Barroso A, Ferreira PM, Ivanov IP, Santos R. Metastability bounds on the two Higgs doublet model. *JHEP.* (2013) **1306**:045. doi: 10.1007/JHEP06(2013)045
73. Akeroyd AG, Arhrib A, Naimi EM. Note on tree-level unitarity in the general two Higgs doublet model. *Phys Lett B.* (2000) **490**:119. doi: 10.1016/S0370-2693(00)00962-X73
74. Kanemura S, Kubota T, Takasugi E. Lee-Quigg-Thacker bounds for Higgs boson masses in a two doublet model. *Phys Lett B.* (1993) **313**:155.
75. Kanemura S, Kikuchi M, Yagyu K. Fingerprinting the extended Higgs sector using one-loop corrected Higgs boson couplings and future precision measurements. *Nucl Phys B.* (2015) **896**:80. doi: 10.1016/j.nuclphysb.2015.04.015
76. Baak M, Cuth J, Haller J, Hoecker A, Kogler R, Moenig K, et al. The global electroweak fit at NNLO and prospects for the LHC and ILC. *Eur Phys J C.* (2014) **74**:3046. doi: 10.1140/epjc/s10052-014-3046-5
77. Bechtle P, Brein O, Heinemeyer S, Weiglein G, Williams KE. HiggsBounds: confronting arbitrary Higgs sectors with exclusion bounds from LEP and the tevatron. *Comput Phys Commun.* (2010) **181**:138. doi: 10.1016/j.cpc.2009.09.003
78. Bechtle P, Brein O, Heinemeyer S, Weiglein G, Williams KE. HiggsBounds 2.0.0: confronting neutral and charged Higgs sector predictions with exclusion bounds from LEP and the tevatron. *Comput Phys Commun.* (2011) **182**:2605. doi: 10.1016/j.cpc.2011.07.015
79. Bechtle P, Brein O, Heinemeyer S, Ståll O, Stefaniak T, Weiglein G, et al. HiggsBounds − 4: improved tests of extended Higgs sectors against exclusion bounds from LEP, the tevatron and the LHC. *Eur Phys J C.* (2014) **74**:2693. doi: 10.1140/epjc/s10052-013-2693-2

80. Bechtle P, Heinemeyer S, Stål O, Stefaniak T, Weiglein G. Applying exclusion likelihoods from LHC searches to extended Higgs sectors. *Eur Phys J C.* (2015) **75**:421. doi: 10.1140/epjc/s10052-015-3650-z
81. Bechtle P, Heinemeyer S, Stål O, Stefaniak T, Weiglein G. *HiggsSignals*: confronting arbitrary Higgs sectors with measurements at the tevatron and the LHC. *Eur Phys J C.* (2014) **74**:2711. doi: 10.1140/epjc/s10052-013-2711-4
82. ATLAS Collaboration. Search for additional heavy neutral Higgs and gauge bosons in the ditau final state produced in 36 fb^{-1} of *pp* collisions at $\sqrt{s}$ = 13 TeV with the ATLAS detector. *arXiv [Preprnt]*. arXiv:1709.07242.
83. CMS Collaboration. Search for additional neutral MSSM Higgs bosons in the $\tau\tau$ final state in proton-proton collisions at $\sqrt{s} = 13$ TeV. *arXiv [Preprnt]*. arXiv:1803.06553.
84. CMS Collaboration. Search for additional neutral Higgs bosons decaying to a pair of tau leptons in *pp* collisions at $\sqrt{s}$ = 7 and 8 TeV. *CMS-PAS-HIG-14-029*. (2015).
85. ATLAS Collaboration. Search for an additional, heavy Higgs boson in the $H \to ZZ$ decay channel at $\sqrt{s} = 8$ TeV in *pp* collision data with the ATLAS detector. *Eur Phys J C.* (2016) **76**:45. doi: 10.1140/epjc/s10052-015-3820-z
86. ATLAS Collaboration. Search for heavy ZZ resonances in the $\ell^+\ell^-\ell^+\ell^-$ and $\ell^+\ell^-\nu\bar{\nu}$ final states using proton proton collisions at $\sqrt{s}$ = 13 TeV with the ATLAS detector. *Eur Phys J C.* (2018) **78**:293. doi: 10.1140/epjc/s10052-018-5686-3
87. CMS Collaboration. Search for a new scalar resonance decaying to a pair of Z bosons in proton-proton collisions at $\sqrt{s} = 13$ TeV. *JHEP.* (2018) **1806**:127. doi: 10.1007/JHEP06(2018)127
88. ATLAS Collaboration. Searches for Higgs boson pair production in the $hh \to bb\tau\tau, \gamma\gamma WW^*, \gamma\gamma bb, bbbb$ channels with the ATLAS detector. *Phys Rev D.* (2015) **92**:092004. doi: 10.1103/PhysRevD.92.092004
89. CMS Collaboration. Search for Higgs boson pair production in events with two bottom quarks and two tau leptons in proton proton collisions at $\sqrt{s}$ = 13 TeV. *Phys Lett B.* (2018) **778**:101. doi: 10.1016/j.physletb.2018.01.001
90. CMS Collaboration. Search for resonant and nonresonant Higgs boson pair production in the $b\bar{b}\ell\nu\ell\nu$ final state in proton-proton collisions at $\sqrt{s} = 13$ TeV. *JHEP.* (2018) **1801**:054. doi: 10.1007/JHEP01(2018)054
91. ATLAS Collaboration. Search for new phenomena in events with at least three photons collected in *pp* collisions at $\sqrt{s}$ = 8 TeV with the ATLAS detector. *Eur Phys J C.* (2016) **76**:210. doi: 10.1140/epjc/s10052-016-4034-8
92. CMS Collaboration. Search for light bosons in decays of the 125 GeV Higgs boson in proton-proton collisions at $\sqrt{s} = 8$ TeV. *JHEP.* (2017) **1710**:076. doi: 10.1007/JHEP10(2017)076
93. ATLAS Collaboration. Search for a CP-odd Higgs boson decaying to Zh in pp collisions at $\sqrt{s} = 8$ TeV with the ATLAS detector. *Phys Lett B.* (2015) **744**:163. doi: 10.1016/j.physletb.2015.03.054
94. CMS Collaboration. Search for a pseudoscalar boson decaying into a Z Boson and the 125 GeV Higgs Boson in $l^+l^-b\bar{b}$ final states. *Phys Lett B.* (2015) **748**:221. doi: 10.1016/j.physletb.2015.07.010
95. ATLAS Collaboration. Search for charged Higgs bosons decaying via $H^\pm \to \tau^\pm\nu_\tau$ in the τ+jets and τ+lepton final states with 36 fb^{-1} of *pp* collision data recorded at $\sqrt{s} = 13$ TeV with the ATLAS experiment. *JHEP.* (2018) **1809**:139. doi: 10.1007/JHEP09(2018)139
96. ATLAS Collaboration. Search for charged Higgs bosons in the $H^\pm \to tb$ decay channel in *pp* collisions at $\sqrt{s} = 8$ TeV using the ATLAS detector. *JHEP.* (2016) **1603**:127. doi: 10.1007/JHEP03(2016)127
97. ATLAS and CMS Collaborations. Measurements of the Higgs boson production and decay rates and constraints on its couplings from a combined ATLAS and CMS analysis of the LHC pp collision data at $\sqrt{s}$ = 7 and 8 TeV. *JHEP.* (2016) **1608**:045. doi: 10.1007/JHEP08(2016)045
98. ATLAS Collaboration. Measurements of the Higgs boson production cross section via Vector Boson Fusion and associated *WH* production in the $WW^* \to \ell\nu\ell\nu$ decay mode with the ATLAS detector at $\sqrt{s}$ = 13 TeV. *ATLAS-CONF-2016-112*. (2016).
99. ATLAS Collaboration. Measurement of gluon fusion and vector boson fusion Higgs boson production cross-sections in the $H \to WW^* \to e\nu\mu\nu$ decay channel in pp collisions at $\sqrt{s} = 13$ TeV with the ATLAS detector. *ATLAS-CONF-2018-004*. (2018).
100. ATLAS Collaboration. Evidence for the $H \to b\bar{b}$ decay with the ATLAS detector. *JHEP.* (2017) **1712**:024. doi: 10.1007/JHEP12(2017)024
101. ATLAS Collaboration. Measurement of the Higgs boson coupling properties in the $H \to ZZ^* \to 4\ell$ decay channel at $\sqrt{s}$ = 13 TeV with the ATLAS detector. *JHEP.* (2018) **1803**:095. doi: 10.1007/JHEP03(2018)095
102. ATLAS Collaboration. Evidence for the associated production of the Higgs boson and a top quark pair with the ATLAS detector. *Phys Rev D.* (2018) **97**:072003. doi: 10.1103/PhysRevD.97.072003
103. ATLAS Collaboration. Search for the standard model Higgs boson produced in association with top quarks and decaying into a $b\bar{b}$ pair in *pp* collisions at $\sqrt{s}$ = 13 TeV with the ATLAS detector. *Phys Rev D.* (2018) **97**:072016. doi: 10.1103/PhysRevD.97.072016
104. ATLAS Collaboration. Measurements of Higgs boson properties in the diphoton decay channel with 36 fb^{-1} of *pp* collision data at $\sqrt{s} = 13$ TeV with the ATLAS detector. *arXiv [Preprint]*. arXiv:1803.06553.
105. CMS Collaboration. Measurements of properties of the Higgs boson in the diphoton decay channel with the full 2016 data set. *CMS-PAS-HIG-16-040*. (2017).
106. CMS Collaboration. Measurements of properties of the Higgs boson decaying into the four-lepton final state in pp collisions at $\sqrt{s} = 13$ TeV. *JHEP.* (2017) **1711**:047. doi: 10.1007/JHEP11(2017)047
107. CMS Collaboration. Observation of the Higgs boson decay to a pair of τ leptons with the CMS detector. *Phys Lett B.* (2018) **779**:283. doi: 10.1016/j.physletb.2018.02.004
108. CMS Collaboration. Inclusive search for a highly boosted Higgs boson decaying to a bottom quark-antiquark pair. *Phys Rev Lett.* (2018) **120**:071802. doi: 10.1103/PhysRevLett.120.071802
109. CMS Collaboration. Evidence for the Higgs boson decay to a bottom quark antiquark pair. *Phys Lett B.* (2018) **780**:501. doi: 10.1016/j.physletb.2018.02.050
110. CMS Collaboration. Evidence for associated production of a Higgs boson with a top quark pair in final states with electrons, muons, and hadronically decaying τ leptons at $\sqrt{s} = 13$ TeV. *JHEP.* (2018) **1808**:066. doi: 10.1007/JHEP08(2018)066
111. CMS Collaboration. Search for $t\bar{t}H$ production in the all-jet final state in proton-proton collisions at $\sqrt{s} = 13$ TeV. *JHEP.* (2018) **1806**:101. doi: 10.1007/JHEP06(2018)101
112. CMS Collaboration. Search for $t\bar{t}H$ production in the $H \to b\bar{b}$ decay channel with leptonic $t\bar{t}$ decays in proton-proton collisions at $\sqrt{s} = 13$ TeV. *arXiv [Preprnt]*. arXiv:1804.03682.
113. CMS Collaboration. Measurements of properties of the Higgs boson decaying to a W boson pair in pp collisions at $\sqrt{s} = 13$ TeV. *arXiv [Preprnt]*. arXiv:1806.05246.
114. Belanger G, Boudjema F, Pukhov A, Semenov A. micrOMEGAs$_3$: a program for calculating dark matter observables. *Comput Phys Commun.* (2014) **185**:960. doi: 10.1016/j.cpc.2013.10.016
115. Planck Collaboration. Planck 2018 results. VI. Cosmological parameters. *arXiv [Preprnt]*. arXiv:1807.06209.
116. CMS Collaboration. Search for new phenomena with the M_{T2} variable in the all-hadronic final state produced in proton proton collisions at $\sqrt{s} = 13$ TeV. *Eur Phys J C.* (2017) **77**:710. doi: 10.1140/epjc/s10052-017-5267-x
117. CMS Collaboration. Search for natural and split supersymmetry in proton-proton collisions at $\sqrt{s} = 13$ TeV in final states with jets and missing transverse momentum. *JHEP.* (2018) **1805**:025. doi: 10.1007/JHEP05(2018)025
118. ATLAS Collaboration. Search for direct top squark pair production in final states with two leptons in $\sqrt{s} = 13$ TeV *pp* collisions with the ATLAS detector. *Eur Phys J C.* (2017) **77**:898. doi: 10.1140/epjc/s10052-017-5445-x
119. ATLAS Collaboration. Search for a scalar partner of the top quark in the jets plus missing transverse momentum final state at $\sqrt{s}$=13 TeV with the ATLAS detector. *JHEP.* (2017) **1712**:085. doi: 10.1007/JHEP12(2017)085
120. ATLAS Collaboration. Search for top-squark pair production in final states with one lepton, jets, and missing transverse momentum using 36 fb^{-1} of $\sqrt{s} = 13$ TeV pp collision data with the ATLAS detector. *JHEP.* (2018) **1806**:108. doi: 10.1007/JHEP06(2018)108
121. CMS Collaboration. Search for top squark pair production in pp collisions at $\sqrt{s} = 13$ TeV using single lepton events. *JHEP.* (2017) **1710**:019. doi: 10.1007/JHEP10(2017)019

122. CMS Collaboration. Search for direct production of supersymmetric partners of the top quark in the all-jets final state in proton-proton collisions at $\sqrt{s} = 13$ TeV. *JHEP.* (2017) **1710**:005. doi: 10.1007/JHEP10(2017)005
123. CMS Collaboration. Search for top squarks and dark matter particles in opposite-charge dilepton final states at $\sqrt{s} = 13$ TeV. *Phys Rev D.* (2018) **97**:032009. doi: 10.1103/PhysRevD.97.032009
124. ATLAS Collaboration. Search for dark matter and other new phenomena in events with an energetic jet and large missing transverse momentum using the ATLAS detector. *JHEP.* (2018) **1801**:126. doi: 10.1007/JHEP01(2018)126
125. ATLAS Collaboration. Search for supersymmetry in final states with two same-sign or three leptons and jets using 36 fb^{-1} of $\sqrt{s} = 13$ TeV pp collision data with the ATLAS detector. *JHEP.* (2017) **1709**:084. doi: 10.1007/JHEP09(2017)084
126. ATLAS Collaboration. Search for supersymmetry in events with b-tagged jets and missing transverse momentum in pp collisions at $\sqrt{s} = 13$ TeV with the ATLAS detector. *JHEP.* (2017) **1711**:195. doi: 10.1007/JHEP11(2017)195
127. ATLAS Collaboration. Search for squarks and gluinos in events with an isolated lepton, jets, and missing transverse momentum at $\sqrt{s} = 13$ TeV with the ATLAS detector. *Phys Rev D.* (2017) **96**:112010. doi: 10.1103/PhysRevD.96.112010
128. ATLAS Collaboration. Search for squarks and gluinos in final states with jets and missing transverse momentum using 36 fb^{-1} of $\sqrt{s} = 13$ TeV pp collision data with the ATLAS detector. *Phys Rev D.* (2018) **97**:112001. doi: 10.1103/PhysRevD.97.112001
129. CMS Collaboration. Search for supersymmetry in multijet events with missing transverse momentum in proton-proton collisions at 13 TeV. *Phys Rev D.* (2017) **96**:032003. doi: 10.1103/PhysRevD.96.032003
130. Dittmaier S, Kramer M, Spira M, Walser M. Charged-Higgs-Boson production at the LHC: NLO supersymmetric QCD corrections. *Phys Rev D.* (2011) **83**:055005. doi: 10.1103/PhysRevD.83.055005
131. Berger EL, Han T, Jiang J, Plehn T. Associated production of a top quark and a charged Higgs Boson. *Phys Rev D.* (2005) **71**:115012. doi: 10.1103/PhysRevD.71.115012
132. Beenakker W, Hopker R, Spira M. PROSPINO: a program for the production of supersymmetric particles in next-to-leading order QCD. *arXiv [Preprint].* arXiv: *HEP-PH/9611232.* (1996).
133. Gianotti F, Mangano ML, Virdee T, Abdullin S, Azuelos G, Ball A, et al. Physics potential and experimental challenges of the LHC luminosity upgrade. *Eur Phys J C.* (2005) **39**:293. doi: 10.1140/epjc/s2004-02061-6
134. Amhis Y, Banerjee S, Ben-Haim E, Blyth S, Bozek A, Bozzi C, et al. Averages of b-hadron, c-hadron, and τ-lepton properties as of summer 2014. *arXiv [Preprint].* arXiv:1412.7515.
135. Olive KA, Agashe K, Amsler C, Antonelli M, Arguin JF, Asner DM, et al. Review of particle physics. *Chin Phys C.* (2014) **38**:090001. doi: 10.1088/1674-1137/38/9/090001
136. Archilli F. $B_s^0 \to \mu^+\mu^-$ at LHC. *arXiv [Preprint].* arXiv:1411.4964.
137. Mahmoudi F. SuperIso v2.3: a program for calculating flavor physics observables in supersymmetry. *Comput Phys Commun.* (2009) **180**:1579. doi: 10.1016/j.cpc.2009.02.017
138. Arhrib A, Benbrik R, Moretti S, Santos R, Sharma P. Signal to background interference in $pp \to tH^- \to tW^-b\bar{b}$ at the LHC Run-II. *Phys Rev D.* (2018) **97**:075037. doi: 10.1103/PhysRevD.97.075037

Conflict of Interest: The authors declare that the research was conducted in the absence of any commercial or financial relationships that could be construed as a potential conflict of interest.

Advantages of publishing in Frontiers

OPEN ACCESS
Articles are free to read for greatest visibility and readership

FAST PUBLICATION
Around 90 days from submission to decision

HIGH QUALITY PEER-REVIEW
Rigorous, collaborative, and constructive peer-review

TRANSPARENT PEER-REVIEW
Editors and reviewers acknowledged by name on published articles

Frontiers
Avenue du Tribunal-Fédéral 34
1005 Lausanne | Switzerland

Visit us: www.frontiersin.org
Contact us: info@frontiersin.org | +41 21 510 17 00

REPRODUCIBILITY OF RESEARCH
Support open data and methods to enhance research reproducibility

DIGITAL PUBLISHING
Articles designed for optimal readership across devices

FOLLOW US
@frontiersin

IMPACT METRICS
Advanced article metrics track visibility across digital media

EXTENSIVE PROMOTION
Marketing and promotion of impactful research

LOOP RESEARCH NETWORK
Our network increases your article's readership